Alexey Shutov

Numerische Simulation des viskoplastischen Verhaltens metallischer Werkstoffe bei endlichen Deformationen

Alexey Shutov

Numerische Simulation des viskoplastischen Verhaltens metallischer Werkstoffe bei endlichen Deformationen

TECHNISCHE UNIVERSITÄT
CHEMNITZ

Universitätsverlag Chemnitz
2014

Impressum

Bibliografische Information der Deutschen Nationalbibliothek

Die Deutsche Nationalbibliothek verzeichnet diese Publikation in der Deutschen Nationalbibliografie; detaillierte bibliografische Angaben sind im Internet über http://dnb.d-nb.de abrufbar.

Zugl.: Chemnitz, Techn. Univ., Habil.-Schr., 2014

Technische Universität Chemnitz/Universitätsbibliothek
Universitätsverlag Chemnitz
09107 Chemnitz
http://www.tu-chemnitz.de/ub/univerlag

Herstellung und Auslieferung
Verlagshaus Monsenstein und Vannerdat OHG
Am Hawerkamp 31
48155 Münster
http://www.mv-verlag.de

ISBN 978-3-944640-28-0

http://nbn-resolving.de/urn:nbn:de:bsz:ch1-qucosa-151214

Numerische Simulation des viskoplastischen Verhaltens metallischer Werkstoffe bei endlichen Deformationen

Von der Fakultät für Maschinenbau der
Technischen Universität Chemnitz

genehmigte

Habilitationsschrift

zur Erlangung des akademischen Grades
Doktor (Russische Akademie der Wissenschaften) habilitatus
(Dr. habil.)

vorgelegt

von Doktor (Russische Akademie der Wissenschaften) Alexey Shutov
geboren am 29. Juli 1979 in Nowosibirsk
eingereicht am 16. Dezember 2013

Gutachter:
Prof. Dr.-Ing. habil. Jörn Ihlemann
Prof. Dr.-Ing. habil. Holm Altenbach
Prof. Dr.-Ing. habil. Alexander Lion

Tag der Verteidigung: 9. Mai 2014

Shutov, Alexey

Numerische Simulation des viskoplastischen Verhaltens metallischer Werkstoffe bei endlichen Deformationen

Habilitationsschrift an der Fakultät für Maschinenbau der Technischen Universität Chemnitz, Institut für Mechanik und Thermodynamik, Chemnitz, 2013

232	Seiten
65	Bilder
17	Tabellen
209	Literaturzitate

Referat

In den letzten Jahrzehnten hat sich auf dem Gebiet der phänomenologischen Metallplastizität eine schleichende Revolution vollzogen. Dank der gestiegenen Rechenleistung, in Kombination mit ausgereiften numerischen Algorithmen, sind viele technisch relevante Problemstellungen einer zuverlässigen numerischen Analyse zugänglich gemacht worden. Beispielsweise ermöglicht die Metallumformsimulation, als häufigste Anwendung der Plastizitätstheorie, eine Analyse des Eigenspannungszustandes und der Rückfederung in plastisch umgeformten Halbzeugen und Bauteilen. Solche Simulationen sind für die Planung energie- und ressourceneffizienter Herstellungsprozesse sowie für die Ausnutzung der plastischen Tragfähigkeitsreserven von großer Bedeutung. Die Crashtest-Simulation ist die zweithäufigste Anwendung, die in der Automobilindustrie und auch zunehmend im Flugzeugbau eingesetzt wird. Aus der Notwendigkeit, das Verhalten metallischer Werkstoffe auf Bauteilebene hinreichend genau zu beschreiben, resultiert die Motivation für eine breit angelegte Studie zur Materialmodellierung. Dabei führt die beträchtliche Anzahl unterschiedlicher Phänomene und Effekte, die berücksichtigt werden müssen, zu einer großen Vielfalt von Materialmodellen.

Da die Lösung komplizierter praktischer Probleme mit einem sehr großen numerischen Aufwand verbunden ist, wird der vorteilhafte phänomenologische Zugang bevorzugt. Bei der Konzeption von neuen phänomenologischen Materialmodellen müssen folgende Aspekte beachtet werden: die Genauigkeit bei der Beschreibung des Materialverhaltens; die Stabilität und Robustheit von zugehörigen numerischen Algorithmen; die numerische Effizienz; die zuverlässige Parameteridentifikation für einen möglichst großen Anwendbarkeitsbereich; die Anschaulichkeit und Einfachheit des Materialmodells. Im Allgemeinen stehen diese Anforderungen an ein "gutes Materialmodell" zwar in einem gewissen Widerspruch zueinander, bilden andererseits aber das Grundgerüst für eine systematische Studie. Obwohl sich die vorliegende Arbeit vordergründig an erfahrene Spezialisten im Bereich der Kontinuumsmechanik wendet, sind die darin präsentierten Modelle und Algorithmen auch für praktisch tätige Berechnungsingenieure von Interesse.

Schlagworte

Viskoplastizität, Metallplastizität, Endliche Deformationen, Bauschinger-Effekt, Kinematische Verfestigung, Formative Verfestigung, Numerische Integration, Finite-Elemente-Methode

Shutov, Alexey

Numerical simulation of viscoplastic behaviour of metallic materials at finite strains

Habilitation thesis at the Faculty of Mechanical Engineering of Chemnitz University of Technology, Institute of Mechanics and Thermodynamics, Chemnitz, 2013

232 pages
65 figures
17 tables
209 references

Abstract

In the last decades, a creeping revolution was taking place in the area of the phenomenological metal plasticity. Due to the increased computational power, combined with refined numerical algorithms, many of technically relevant problems are now available for the numerical analysis. In particular, the metal forming simulation is a typical application of the metal plasticity. It enables the analysis of the residual stresses and spring back phenomena in plastically deformed workpieces and components. Such analysis is advantageous for planning of energy and resource-efficient manufacturing and for exploitation of plastic reserves of bearing capacity. The crash test simulation is the second most common application of metal plasticity, highly celebrated in the automotive industry and gaining increasing popularity in the aircraft industry. The need for sufficiently accurate description of metal behaviour on the macroscale motivates wide-ranging studies on material modelling. The large number of different effects and phenomena contributes to the large manifold of material models.

The current work deals with the phenomenological approach, due to its great suitability for the solution of practical problems. The following aspects should be taken into account upon the construction of new phenomenological models: the accurate description of the material behaviour, the stability and robustness of the corresponding numerical algorithms, the numerical efficiency, the reliable parameter identification for a sufficiently large application area, the clearness and simplicity of the material models. In general, these requirements imposed on a "good material model" contradict each other. In this work, however, they are complimentary to each other and build a framework for a systematic study. Although this work is written primarily for experts on the continuum mechanics, the presented models and algorithms can be of interest for practically working engineers.

Key words

Viscoplasticity, Metal Plasticity, Finite Strains, Bauschinger Effect, Kinematic Hardening, Distortional Hardening, Numerical Integration, Finite Element Method

Vorwort und Danksagung

In dieser Schrift gebe ich einen Überblick über die wesentlichen Ergebnisse meiner Forschungsarbeit am Institut für Mechanik und Thermodynamik der TU Chemnitz seit meiner Einstellung als wissenschaftlicher Mitarbeiter im Jahre 2006. Die im Weiteren präsentierten Erkentnisse sind während der Bearbeitung des Teilprojekts "Materialgesetze und Identifikation" im Sonderforschungsbereich HALS (**H**ochfeste **A**luminiumbasierte **L**eichtbauwerkstoffe für **S**icherheitsbauteile) entstanden.

An dieser Stelle danke ich meinem Lehrer und Mentor Herrn Prof. i.R. Dr.-Ing. habil. Reiner Kreißig. Ohne seine wissenschaftliche Vorbereitung des Projekts und tatkräftige Unterstützung wäre diese Arbeit nicht möglich gewesen. Die Jahre in der Arbeitsgruppe Festkörpermechanik waren für mich eine Bereicherung und ich werde diese Zeit stets in guter Erinnerung behalten. Mein weiterer Dank gilt Herrn Prof. Dr.-Ing. habil. Jörn Ihlemann, dem Leiter der Professur Festkörpermechanik, für die vertrauensvolle Zusammenarbeit. Er hat mir die Lösung von vielen reizvollen Aufgaben der Mechanik übertragen. Seine Fähigkeit, viele hochbegabte und engagierte Mitarbeiter für die Professur Festkörpermechanik zu gewinnen, hat sich außerordentlich positiv ausgewirkt.

Ein herzlicher Dank gilt meinen Kollegen der TU Chemnitz für die gute Arbeitsatmosphäre und die gegenseitige Hilfe bei vielen wissenschaftlichen Fragestellungen und alltäglichen Problemen.

Shutov Alexey Valer'evich,
Chemnitz, 16. Dezember 2013

Inhaltsverzeichnis

KAPITEL 1

Zusammenfassung der publizierten Ergebnisse

1. Einleitung

Der Einsatz metallischer Werkstoffe für hochbeanspruchte Bauteile ist in vielen technischen Bereichen unabdingbar. Die allgemeine Verbreitung der Metalle ist auf deren günstige Eigenschaften zurückzuführen, wie der hohen Festigkeit, der guten Verformbarkeit sowie der Möglichkeit des Recyclings. Durch die ständige Entwicklung neuer Werkstoffe, wie zum Beispiel hochfeste nanostrukturierte Legierungen [**38, 8**] wird die praktische Bedeutung von Metallen auch weiterhin auf einem sehr hohen Niveau bleiben.

Die große Herausforderung bei der Entwicklung neuer Fertigungsprozesse liegt darin, eine erhöhte Ressourceneffizienz durch optimale Ausnutzung der Werkstoffeigenschaften zu erreichen. Für den praktischen Einsatz neuartiger Materialien soll zugleich der Mangel an Erfahrungen im Umgang mit diesen Werkstoffen überwunden werden. Diese zwei Ziele können nur unter Verwendung unterstützender Simulationen der Herstellungsprozesse und des Bauteilverhaltens erreicht werden. So werden mit Hilfe zahlreicher CAD-Systeme unterschiedliche Prozessschritte oder ganze Prozessketten virtuell nachgebildet und analysiert. Die Finite-Elemente-Methode (FEM) ist dabei wegen ihrer herausragenden Flexibilität und Robustheit zu einem Standardwerkzeug geworden. Für die numerischen Simulationen sind hierbei Materialmodelle erforderlich, die das mechanische Werkstoffverhalten möglichst genau auf makroskopischer Ebene beschreiben.

Die Materialmodellierung stellt ein wichtiges Bindeglied zwischen Materialwissenschaft, Kontinuumsmechanik und numerischer Mathematik dar. Zahlreiche Wechselwirkungen zwischen den geometrischen und physikalischen Nichtlinearitäten stellen besonders hohe Ansprüche an die Qualität der Modelle und der zugehörigen numerischen Algorithmen. In dieser Schrift wird der pragmatische phänomenologische Zugang zur Materialmodellierung wegen seiner besonderen Eignung zur Lösung praxisrelevanter Aufgaben favorisiert.

Die wesentlichen Ziele der vorliegenden Arbeit bestehen in:

(i) der Bereitstellung einer Palette von neuen phänomenologischen Modellen der Metallplastizität bei endlichen Deformationen,
(ii) deren numerischer Behandlung und dem Einbau in die Finite-Elemente-Methode,
(iii) der praktischen Nutzung von diesen Modellen bei der Identifikation der Materialparameter und der numerischen Lösung einiger ausgewählter Randwertaufgaben.

Die Zielgruppe dieser Schrift sind primär erfahrene Spezialisten auf dem Gebiet der Kontinuumsmechanik und Materialmodellierung. Der zwangsläufig beschränkte Umfang dieser Monografie erlaubt es nicht, die Grundlagen der Kontinuumsmechanik bei endlichen

Deformationen[1] ausführlich darzustellen. Der interessierte Leser muss deshalb auf entsprechende Lehrbücher verwiesen werden [**26, 19, 22, 18, 14, 11, 37, 1**]. Zum Einstieg in die Theorie der Elasto-Plastizität bei endlichen Deformationen sind die Monografien [**4, 21, 11, 13**] geeignet. Als mathematische Voraussetzungen werden an den Leser die Grundkenntnisse der linearen Algebra [**9**] und des klassischen Tensorformalismus [**35, 16**] gestellt. Zum Thema Numerik des inelastischen Materialverhaltens sei an dieser Stelle das grundlegende Handbuch von Simo und Hughes [**33**] genannt. Als Referenz für die allgemeine Technologie der nichtlinearen FEM kann eine Serie von Lehrbüchern herangezogen werden [**42, 3, 39**]. Die vorliegende Arbeit beschränkt sich auf jene Erkenntnisse, die gegenüber dem erreichten Stand der Forschung einen zusätzlichen Beitrag darstellen. Alle in dieser Schrift zusammengefassten Publikationen verkörpern eine thematische Einheit und werden kapitelweise angeordnet. Auf die Publikationen zu den gestaffelten Strategien der Parameteridentifikation [**27**], zum Konzept repräsentativer Richtungen [**7**], zur Versetzungskinetik unter nichtproportionaler Belastung [**32**], zur Numerik des Maxwell-Körpers [**31**] und zur qualitativen Analyse klassischer Plastizitätsmodelle [**30**] kann in dieser Schrift nicht eingegangen werden.

Die erzielten Ergebnisse werden in diesem Kapitel auf zweierlei Weise zusammengefasst: Zunächst wird auf den Ablauf eines Modellierungsprozesses am Beispiel eines typischen Modellierungszyklus eingegangen. Dabei werden die Zusammenhänge zwischen den einzelnen Modellierungsschritten hervorgehoben. Danach erfolgt die Darstellung der Hierarchie von Materialmodellen. Diese eignet sich besonders zur Erläuterung des modularen Aufbaus von Modellen.

2. Modellierungszyklus

Wie es bei vielen komplizierten Aufgaben üblich ist, erfolgt auch die Entwicklung von neuen Materialmodellen auf iterative Weise. Ein typischer Fall ist in Abbildung 1.1 schematisch in Form eines Modellierungszyklus dargestellt. Ausgehend von den bereits gesammelten Erkenntnissen und experimentellen Befunden wird die Realität zunächst idealisiert. Auf dieser Basis entsteht ein mathematisches Modell. Dieses Modell existiert in der Regel in Form von tensoriellen Gleichungssystemen, welche algebraische Gleichungen sowie Differential- oder Integralgleichungen enthalten. Die gesuchten Feldgrößen besitzen unendlich viele Freiheitsgrade. Im nächsten Schritt werden, basierend auf diesen Gleichungssystemen, numerische Algorithmen konstruiert. Alle Feldgrößen werden dabei mit diskreten Analogien angenähert. Die Evolutionsgleichungen werden zeitlich diskretisiert, die räumliche Diskretisierung erfolgt in der Regel mit der Methode der Finiten Elemente. Auf diese Weise entsteht ein System mit einer endlichen Anzahl von Freiheitsgraden. In dieser Arbeit wird ausführlich die Zeitdiskretisierung behandelt. Anschließend werden die Algorithmen in kommerzielle oder hauseigene FEM-Programme implementiert. Da die eigentliche Programmierung in der Regel mit einem großen Arbeitsaufwand und daraus resultierenden Fehlerquellen verbunden ist, müssen die entwickelten Programme ausgiebig getestet werden. Deshalb spielen die numerischen Tests in dieser Arbeit eine bedeutende Rolle. Im letzten Modellierungsschritt

---

[1] Der Begriff "endliche Deformation" wird in der Fachliteratur teils synonym mit dem Begriff "finite Deformation" oder sogar "große Deformation" verwendet (vgl. [**39**], Seite 2).

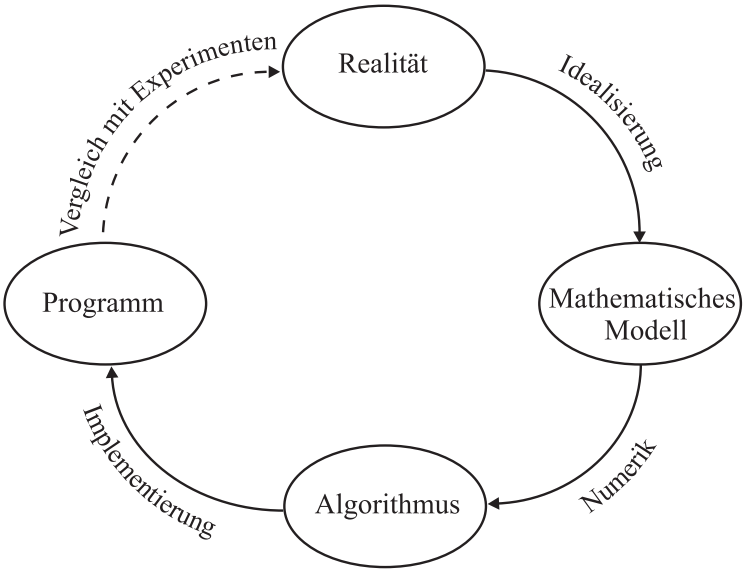

Abbildung 1.1. Typischer Modellierungszyklus.

erfolgen die Kalibrierung der Materialmodelle einschließlich der Identifikation der Materialparameter sowie die Validierung des Materialmodells durch Vergleich mit zusätzlichen experimentellen Daten. Kleinere korrigierende Rückkopplungsschleifen sind innerhalb dieses Zyklus ebenfalls möglich. So können beispielsweise bereits bei der Entwicklung von numerischen Algorithmen (Modellierungsschritt Numerik) einige Nachteile des Modells festgestellt werden, welche eine robuste Numerik unmöglich machen. Zu solchen Nachteilen zählen unter anderem verschiedene Singularitäten und Unstetigkeiten. Ein weiteres Beispiel ist die große Korrelation zwischen einzelnen Materialparametern. Das erschwert deren zuverlässige Identifikation. In manchen Fällen kann dieses Problem bereits durch eine äquivalente Umschreibung von konstitutiven Gleichungen gelöst werden.

2.1. Idealisierung. Der Idealisierungsschritt muss den allgemeinen Prinzipien der Materialmodellierung [**10**] genügen. Zu diesen zählen das Prinzip der materiellen Objektivität, das Prinzip des Determinismus, das Prinzip der lokalen Wirkung, das Prinzip der Basisinvarianz, das Prinzip der Dimensionsinvarianz sowie die Forderung nach thermodynamischer Konsistenz usw. Eine praktische Hilfestellung bei der Konzeption von Materialmodellen leistet auch das Prinzip der Dualen Variablen von Haupt und Tsakmakis [**12**]. Die Anwendung dieses Prinzips auf ein Modell mit kinematischer Verfestigung wird im Kapitel 2 diskutiert. Der heute bekannte Satz von allgemeinen Prinzipien reicht aber nicht aus, um automatisch die Plausibilität des Materialmodells zu garantieren [**10**]. Selbst bei Beachtung dieser Prinzipien besteht eine große Freiheit in der Konzeption von Materialmodellen.

In dieser Arbeit werden nur die sogenannten "einfachen" Materialien betrachtet (vgl. [**37**]). Hier hängt der aktuelle Wert des Cauchy'schen Spannungstensors $\mathbf{T}$ lediglich von der lokalen Geschichte des Deformationsgradienten $\mathbf{F}$ ab. Wenn der Ausgangszustand zum Zeitpunkt $t = 0$ mit einem Satz von inneren Variablen $\mathbf{Z}_0$ erfasst wird, erhält man

$$\mathbf{T}(t) = \mathbf{T}\Big(\big\{\mathbf{F}(\tau)\big\}_{0 \leq \tau \leq t}, \mathbf{Z}_0\Big). \tag{1.1}$$

Für alle Modelle wird in der vorliegenden Schrift die Erfüllung des Prinzips der materiellen Objektivität postuliert [**11**]. Somit lässt sich die Gleichung (1.1) in der reduzierten Form

$$\tilde{\mathbf{T}}(t) = \tilde{\mathbf{T}}\Big(\big\{\mathbf{C}(\tau)\big\}_{0\leq\tau\leq t}, \mathbf{Z}_0\Big) \tag{1.2}$$

darstellen, wobei $\tilde{\mathbf{T}}$ den 2. Piola-Kirchhoff-Tensor kennzeichnet und $\mathbf{C} = \mathbf{F}^{\mathrm{T}}\mathbf{F}$ für den rechten Cauchy-Green-Tensor steht. Es ist zu beachten, dass die Gleichung (1.2) der aktiven Interpretation des Objektivitätsprinzips entspricht, welche für metallische Werkstoffe durchaus legitim ist. Der Vorteil dieser Formulierung liegt darin, dass die nachgeschaltete Starrkörperdrehung "herausgefiltert" wird. An die Stelle der Geschichte des neundimensionalen Deformationsgradienten $\mathbf{F}$ tritt nun die Geschichte des sechsdimensionalen Tensors $\mathbf{C}$.

Bei allen in dieser Arbeit präsentierten Modellen wird die lokale Belastungsvorgeschichte des Materials auf eine pragmatische Weise mit einem Satz von inneren Variablen erfasst, der den aktuellen belastungsinduzierten Zustand des Materials kennzeichnet. Die dissipativen irreversiblen Vorgänge werden dabei mit Evolutionsgleichungen für die inneren Variablen beschrieben[2].

Im Rahmen der geometrisch nichtlinearen Elasto-Plastizität bietet sich ein weiteres einschränkendes Prinzip an. Es handelt sich um die Forderung der Invarianz beim isochoren Wechsel der Referenzkonfiguration [**29, 30**]. Es sei $\mathbf{F}_0$ ein beliebiger konstanter Tensor zweiter Stufe mit der Eigenschaft $\det \mathbf{F}_0 = 1$. Das Materialmodell (1.1) ist beim isochoren Wechsel der Referenzkonfiguration invariant, wenn ein neuer Satz $\mathbf{Z}_0^{\mathrm{new}} = \mathbf{Z}_0^{\mathrm{new}}(\mathbf{Z}_0, \mathbf{F}_0)$ existiert, sodass die folgende Invarianzbeziehung gilt:

$$\mathbf{T}\Big(\big\{\mathbf{F}(\tau)\big\}_{0\leq\tau\leq t}, \mathbf{Z}_0\Big) = \mathbf{T}\Big(\big\{\mathbf{F}^{\mathrm{new}}(\tau)\big\}_{0\leq\tau\leq t}, \mathbf{Z}_0^{\mathrm{new}}\Big), \quad \mathbf{F}^{\mathrm{new}}(\tau) := \mathbf{F}(\tau)\ \mathbf{F}_0^{-1}. \tag{1.3}$$

Das heißt mit anderen Worten: Die Referenzkonfiguration darf mit der Nebenbedingung, dass die Massendichte gleich groß bleibt, beliebig gewählt werden, die konstitutiven Gleichungen behalten trotzdem ihre ursprüngliche Form. Es lässt sich zeigen (vgl. Kapitel 10), dass die in dieser Schrift präsentierten Materialmodelle der genannten Invarianzbedingung genügen. Abgesehen davon, dass mit dieser Forderung mehrere alternative Zugänge zur Metallplastizität klassifiziert werden, hat die Invarianzeigenschaft auch praktische Vorteile: Bei der Simulation der mehrstufigen Metallumformung zieht ein Wechsel der Referenzkonfiguration lediglich eine Anpassung der Anfangsbedingungen für die tensorwertigen inneren Variablen nach sich (vgl. Kapitel 10). Da die Form der konstitutiven Gleichungen invariant ist, bleibt auch deren numerische Umsetzung vom Referenzwechsel unberührt. Von dieser Invarianz wird im Kapitel 4 (Abschnitt 3.2) und im Kapitel 8 (Appendix D) Gebrauch gemacht, um die mathematische Analyse von konstitutiven Gleichungen zu vereinfachen.

In der vorliegenden Schrift wird der konventionelle Zugang zur Metallplastizität verwendet. Dabei wird postuliert, dass für jedes Materialteilchen eine eindeutige Fließfläche im Spannungsraum existiert. Das Materialverhalten wird für alle Spannungszustände innerhalb der Fließfläche als hyperelastisch angenommen.

Das Prinzips der maximalen Dissipation wird häufig in der Literatur zur Metallplastizität postuliert [**11**]. Aus diesem Prinzip lassen sich die Konvexität der Fließfläche und die Normalenregel ableiten. In der vorliegenden Arbeit wird jedoch auf die zwingende Nutzung dieses Prinzips verzichtet. Trotzdem wird für alle Modelle die Konvexität der Fließfläche

---

[2] Fast alle bekannten Plastizitätsmodelle sind auf diesem Prinzip aufgebaut.

gewährleistet. Bei manchen Modellen besteht die Möglichkeit, zwischen der Normalenregel und der sogenannten radialen Fließregel zu wählen (vgl. Kapitel 8 und 9). Für viskose Werkstoffe wird die klassische Normalenregel insofern verallgemeinert, dass hier die Fließrichtung mit der Normale zur Fläche einer konstanten Überspannung zusammenfällt. Für konkrete Werkstoffe soll die Entscheidung zwischen der Normalenregel und der radialen Fließregel in Abhängigkeit von den verfügbaren Messdaten getroffen werden.

Die konzipierten Materialmodelle werden in dieser Schrift mit Hilfe von unterschiedlichen rheologischen Modellen veranschaulicht. Für jedes neue Modell wird eine entsprechende rheologische Analogie präsentiert. Diese rheologischen Analogien lassen sich auch für den Entwurf eines Grundgerüstes von Materialmodellen einsetzen. Im Allgemeinen kann die Nutzung von rheologischen Modellen als zu restriktiv erscheinen. Diese Vorgehensweise ist aber legitim, weil dabei gegen keine allgemeinen Prinzipien der Materialmodellierung verstoßen wird. In dieser Arbeit werden ebenfalls neue zweidimensionale rheologische Modelle konstruiert (vgl. Kapitel 8, 9). Sie ermöglichen eine besonders anschauliche Darstellung der kombinierten kinematisch-formativen Verfestigung.

Nach Lion [**20**] entspricht eine Reihenschaltung von rheologischen Modellen einer multiplikativen Zerlegung des Deformationsgradienten. Alle Materialmodelle in der vorliegenden Monografie werden dementsprechend aufgebaut[3]. Die multiplikative Plastizität ist in vielen Publikationen kritisch analysiert worden (vgl. Naghdi [**23**], Bertram [**4**], Xiao [**40**]). Der wichtigste Kritikpunkt besteht darin, dass die Zerlegung $\mathbf{F} = \mathbf{F}_{\mathrm{e}}\mathbf{F}_{\mathrm{p}}$ nur bis auf eine zwischengeschaltete Starrkörperdrehung eindeutig ist. Diese Mehrdeutigkeit spiegelt die Tatsache wider, dass die elastische Entlastung nur bis auf eine nachgeschaltete Starrkörperdrehung bestimmt ist. Wegen der Mehrdeutigkeit der multiplikativen Zerlegung werden in dieser Schrift nur solche Modelle entwickelt, bei denen der plastische Spin keinen Einfluss auf die Spannungsantwort hat. Dies ist immer dann der Fall, wenn elastische Eigenschaften als isotrop vorausgesetzt werden können (vgl. die Diskussion im Abschnitt 3.1).

Bei der Konzeption des Materialmodells ist offensichtlich zu beachten, dass der Idealisierungsschritt für den Erfolg des gesamten Modellierungszyklus entscheidend ist: So müssen für ein "gutes Modell" auch robuste und effiziente Algorithmen existieren. Dabei gilt die gleiche Aussage auch für die Identifizierbarkeit der Materialparameter. Die neuen Materialmodelle werden in den Kapiteln 2, 6, 7, 8 und 9 präsentiert.

2.2. Numerik. Sobald eine mathematische Formulierung des Materialmodells vorliegt, stellt sich die Frage nach der praktischen Bestimmung der Spannungsantwort. Da für dieses Problem im Allgemeinen keine geschlossene Lösung bekannt ist, müssen die entsprechenden Gleichungssysteme numerisch behandelt werden. Bei der Entwicklung von numerischen Algorithmen ist dafür zu sorgen, dass die günstigen Eigenschaften des ursprünglichen Gleichungssystems bei der numerischen Lösung vererbt bzw. ausgenutzt werden. Eine solche grundlegende Eigenschaft wie die Symmetrie von tensorwertigen inneren Variablen muss exakt eingehalten werden. In der Publikation von Dettmer und Reese [**6**] ist auf die Gefahr verwiesen worden, dass bei den klassischen impliziten Algorithmen die Symmetrie verletzt werden kann, wenn eine plastische Anisotropie vorliegt. Im Kapitel 2 wird für das Modell mit kinematischer

---

[3] Es existieren alternative Zugänge zur Konzeption von Materialgleichungen bei endlichen Deformationen, bei denen von rheologischen Modellen ausgegangen wird (vgl. [**25**]).

Verfestigung mathematisch bewiesen, dass die klassischen impliziten Diskretisierungsverfahren wie das Euler-Rückwärts-Verfahren oder das exponentielle Verfahren *die Symmetrie nicht verletzen.* Somit entfällt die Notwendigkeit, neue, "nichtklassische" Zeitintegrationsverfahren aufgrund eines befürchteten Symmetrieverlustes zu entwickeln. Die automatische Erhaltung der Symmetrie wird im Kapitel 8 auch für Modelle mit formativer Verfestigung nachgewiesen. Geringfügige Modifikationen der klassischen Verfahren können aber sinnvoll werden, um deren Robustheit und numerische Effizienz zu vergrößen.

Im Kapitel 4 wird eine wichtige Eigenschaft der untersuchten Modelle der Viskoplastizität nachgewiesen: So tritt beim inelastischen Fließen eine exponentielle Stabilität gegenüber kleinen Störungen der Anfangswerte auf, wenn für gestörte Anfangsbedingungen die inelastische Inkompressibilität exakt eingehalten wird. Diese Stabilitätseigenschaft stellt eine starke Form des Prinzips des schwindenden Gedächtnisses dar: Kleine Störungen werden im Verlauf der plastischen Deformation "vergessen". Um von der exponentiellen Stabilität profitieren zu können, muss auch von den numerischen Algorithmen die inelastische Inkompressibilität exakt eingehalten werden. In diesem Falle wird die Akkumulation des numerischen Fehlers unterbunden. Solche Algorithmen werden in dieser Schrift als "geometrische Integratoren" bezeichnet, da die exakte Einhaltung der Inkompressibilität eine geometrische Interpretation zulässt. Jene Algorithmen, welche die Inkompressibilitätsbedingung verletzen, neigen dagegen zu einer Akkumulation des numerischen Fehlers mit zunehmender Zeit (vgl. Kapitel 4). Eine interessante Konsequenz besteht darin, dass alle impliziten, unbedingt stabilen Verfahren 1. Ordnung, die zugleich geometrische Integratoren darstellen, im Wesentlichen äquivalent sind. So wird in den Kapiteln 2 und 4 numerisch überprüft, dass das modifizierte Euler-Rückwärts-Verfahren und das exponentielle Verfahren im Sinne der Genauigkeit gleichwertig sind. Mathematisch gesehen ist für solche Verfahren der numerische Fehler kleiner als $C\Delta t$, wobei die Konstante C nicht von der Dauer des Prozesses abhängt, und Δt die Zeitschrittweite bezeichnet. Diese Tatsache bietet eine große Freiheit beim Aufbau problemspezifischer numerischer Algorithmen. Offensichtlich sollten die geometrischen Zeitintegratoren gegenüber alternativen Verfahren, bei denen die Inkompressibilität verloren geht, bevorzugt werden. Der Vorteil einer unterbundenen Fehlerakkumulation wird besonders bei Simulationen von plastischen Deformationen mit sehr großem aufsummierten Umformgrad (z. B. inkrementelle Umformung) deutlich.

Da die zugrunde liegenden konstitutiven Gleichungen der Viskoplastizität auf ein steifes Anfangswertproblem führen, spielen die impliziten, unbedingt stabilen Verfahren eine besonders große Rolle. Die in der Arbeit präsentierten Verfahren sind universell ausgelegt, so dass sowohl der geschwindigkeitsabhängige Fall der Viskoplastizität als auch der geschwindigkeitsunabhängige Fall der klassischen Plastizität einheitlich abgedeckt werden. Im geschwindigkeitsunabhängigen Fall ist der Übergang zwischen dem elastischen und dem plastischen Verhalten durch einen Knick im Spannungs-Dehnungs-Diagramm charakterisiert. Somit kann keine eindeutige Materialtangente definiert werden. Im Rahmen einer FEM-Simulation wirkt sich diese Unstetigkeit negativ auf das gesamte Konvergenzverhalten aus. Selbst bei Materialien, die keine nennenswerten viskosen Effekte aufweisen, wird deshalb empfohlen, eine geringfügige (fiktive) Viskosität als Regularisierungsparameter einzuführen. Für eine feste Zeitschrittweite Δt führt eine solche Regularisierung auf ein "glattes" Materialverhalten. Ein weiterer Aspekt ist die unsymmetrische Materialtangente, die für Modelle mit nichtlinearer kinematischer oder formativer Verfestigung auftritt. Diese Unsymmetrie muss im FEM-Programm berücksichtigt werden, indem eine unsymmetrische Steifigkeitsmatrix assembliert und numerisch behandelt wird.

Wie bereits erwähnt, weisen alle Modelle dieser Monografie eine konvexe Fließfläche auf. Diese Konvexität ist für die Stabilität des klassischen Radial-Return-Verfahrens erforderlich. Bei rein expliziter Integration der Evolutionsgleichungen kann theoretisch auf die Konvexität der Fließfläche verzichtet werden. Im Falle der expliziten Zeitintegration tritt jedoch das Problem auf, dass sich solche Verfahren nur für ausreichend kleine Zeitschrittweiten stabil verhalten. Die Ergebnisse aus dem vierten Kapitel sind im gleichen Maße auch für die explizite Zeitintegration gültig: Geometrische Integratoren sind gegenüber den alternativen Integratoren zu bevorzugen.

2.3. Implementierung. Die entwickelten numerischen Algorithmen müssen in Form von Computerprogrammen umgesetzt werden. In der vorliegenden Arbeit wird dazu konsequent ein koordinatenfreier Tensorformalismus herangezogen (vgl. Kapitel 3). Hier wird von der koordinatenfreien Natur der mechanischen Zusammenhänge und der dabei verwendeten Tensorrechnung profitiert. Im Rahmen der koordinatenfreien Tensorrechnung werden sowohl die Tensoren als auch die Tensoroperationen ohne Zuhilfenahme von Koordinaten definiert. Die Nutzung von Koordinaten ist damit nicht notwendig, aber auch nicht verboten. Ein wichtiger Vorteil der koordinatenfreien Vorgehensweise liegt an ihrer Universalität: Die Programme werden unabhängig vom eingesetzten Koordinatensystem geschrieben. Ein Wechsel des Koordinatensystems (beispielsweise ein Übergang von kartesischen zu krummlinigen Koordinaten) erfolgt, indem die konkreten Implementierungen des Tensorformalismus ausgetauscht werden. Ein weiterer Vorteil der koordinatenfreien Tensorrechnung liegt in der natürlichen Behandlung von Ableitungen nach einem symmetrischen Tensor 2. Stufe $\mathbf{X} \in Sym$ (vgl. Kapitel 3). Die formale koordinatenbasierte Darstellung von solchen Ableitungen durch eine Ableitungsmatrix (auch als Jakobi-Matrix bezeichnet) ist problematisch, weil einzelne Koordinaten von $\mathbf{X}$ miteinander verknüpft sind.

Alle Materialmodelle werden in dieser Schrift an die Lagrange'sche Beschreibungsweise angepasst. Für die implizite Zeitintegration im Rahmen der inkrementellen FEM-Strategie wird die Materialtangente benötigt. Die ebenfalls auf der Lagrange'schen Beschreibungsweise beruhende Benutzerschnittstelle Hypela2 von MSC.MARC erfordert die Kenntniss der Materialtangente als partielle Ableitung des 2. Piola-Kirchhoff'schen Spannungstensors $\tilde{\mathbf{T}}$ nach dem rechten Cauchy-Green-Tensor $\mathbf{C}$. Diese Tangente kann durch finite Differenzen angenähert werden (numerische Tangente). Obwohl diese Vorgehensweise sehr einfach ist, führen solche Berechnungen auf einen zusätzlichen numerischen Aufwand. Darüber hinaus enthalten numerische Tangenten einen Fehler, der deutlich größer ist als die Maschinengenauigkeit. Eine Alternative dazu ist die analytische Ableitung des gesamten algebraischen Systems der diskretisierten Materialgleichungen nach dem rechten Cauchy-Green-Tensor $\mathbf{C}$ (vgl. Kapitel 3). Da für manche Größen keine explizite Formel vorliegt, werden diese aus der Lösung des obigen Systems bestimmt. Deren Ableitung muss deshalb mit Hilfe des Satzes über die implizite Funktion berechnet werden. Die resultierende Tangente wird als analytische oder halbanalytische Tangente bezeichnet. Bei Nutzung der analytischen Tangente tritt eine quadratische Konvergenz der FEM-Lösung auf. Für eine zusätzliche Implementierung in FEM-Schnittstellen, die auf der Euler'schen Darstellungsweise basieren (z. B. ABAQUS oder

ANSYS), kann auf die Wrapper-Technologie von Ihlemann (2006) [**15**] zurückgegriffen werden. Sie gestattet die automatische Umrechnung eines numerisch umgesetzten Stoffgesetzes der einen Beschreibungsweise in die jeweils andere Beschreibungsweise des verwendeten FEM-Programms.

Um das Konvergenzverhalten bei der impliziten inkrementellen FEM-Lösung eines Randwertproblems zu verbessern, besteht die Möglichkeit, von der quasistatischen zu einer dynamischen Problemstellung überzugehen (vgl. Kapitel 10). Dies kann beispielsweise für Aufgaben mit Kontaktrandbedingungen wichtig werden. Die eingeführten Trägheitseffekte führen dann auf eine Art Dämpfung der numerischen Lösung. Um die eigentliche Lösung des quasistatischen Problems nicht zu stark zu verfälschen, sollen die eingeführten Trägheitskräfte relativ klein sein.

2.4. Vergleich mit Experimenten. Da der bekannte Satz von Prinzipien der Materialmodellierung allein nicht ausreicht, um die Plausibilität des Materialmodells nachzuweisen, muss eine zusätzliche Validierung des Modells durchgeführt werden. Im ersten Schritt reicht eine qualitative Analyse der Modellvorhersage aus (vgl. Kapitel 2). Dazu können typische einfache Versuche wie Zug, Druck oder Torsion mit physikalisch sinnvollen Materialparametern simuliert werden. Weist das simulierte Materialverhalten die erforderlichen Phänomene auf (z. B. isotrope und kinematische Verfestigung, Geschwindigkeitsabhängigkeit usw.), ist der Test bestanden.

Für die quantitative Analyse müssen die im Modell enthaltenen Materialparameter identifiziert werden. Auch die praktische Nutzung des Materialmodells erfordert natürlich die Kenntnis der Parameter des konkreten Werkstoffs. Die Parameteridentifikation erfolgt in der vorliegenden Arbeit durch die Minimierung eines Fehlerfunktionals, welches die gemittelte Abweichung zwischen den Messergebnissen und den dazugehörigen Modellvorhersagen widerspiegelt. Die eigentliche Minimierung des Fehlerfunktionals erfolgt mit dem gradientenbasierten Levenberg-Marquardt-Verfahren. An dieser Stelle ist anzumerken, dass der Erfolg einer Parameteridentifikation primär von der Vollständigkeit der Messdaten und der Güte der Anfangsnäherung abhängt. Für ein wohlgestelltes Optimierungsproblem muss unabhängig vom konkreten Optimierungsverfahren der gleiche Parametersatz identifiziert werden.

Das Kapitel 5 ist einigen wichtigen Problemen der Materialparameteridentifikation gewidmet. Dazu gehört die mögliche starke Korrelation zwischen den einzelnen Parametern und die Gefahr, dass der Optimierungsalgorithmus zu einem lokalen Minimum des Fehlerfunktionals konvergiert, welches vom globalen Minimum weit entfernt ist. Als ein Maß für die Korrelation zwischen den Parametern wird die so genannte Korrelationsmatrix verwendet. Im Kapitel 5 wird zudem eine Regularisierungsmethodik untersucht, die es ermöglicht, zusätzliche Informationen in den Optimierungsvorgang einzubringen. Dadurch wird die Wohlgestelltheit des Problems verbessert. Als Ergänzung zu diesen Regularisierungsmethoden können gestaffelte Strategien eingesetzt werden [**27**]. Das ist mit einer beträchtlichen Vereinfachung der Parameteridentifikation verbunden.

Eine Validierung des Materialmodells soll auf dem Vergleich mit zusätzlichen Messdaten beruhen, die bei der Parameteridentifikation noch nicht benutzt wurden. Somit wird die modellbasierte Extrapolation auf neue Belastungsfälle untersucht. Leider ist eine solche Validierung nur dann möglich, wenn ausreichend viele Messdaten vorliegen (vgl. Kapitel 6).

Es muss außerdem erwähnt werden, dass jeder Parametersatz nur einen bestimmten Anwendbarkeitsbereich besitzt. Die genauen Grenzen dieses Anwendbarkeitsbereichs sind in der Regel unbekannt. Eine Interpolation der Materialantwort "zwischen" den gegebenen Messergebnissen ist in der Regel mit deutlich kleineren Fehlern verbunden als eine Extrapolation. Als eine Faustregel wird deshalb empfohlen, den Modellvorhersagen für Belastungen mit einem akkumulierten plastischen Umformgrad s uneingeschränkt nur bis zum maximalen Umformgrad im Experiment zu vertrauen. Wenn also beispielsweise die Materialparameter aus Experimenten mit $s_{\max} < 0,5$ identifiziert wurden, sollten mit diesem Parametersatz keine Simulationen mit $s > 0,5$ durchgeführt werden. Obwohl die strikte Gewährleistung der Vorhersagegenauigkeit ein offenes Problem der phänomenologischen Materialmodellierung darstellt, ermöglicht die konsequente Ausnutzung der Modellierungsprinzipien in Kombination mit der experimentellen Validierung eine gute Genauigkeit für ein breites Spektrum der Belastungsfälle.

Eine systematische Abweichung der Simulationsergebnisse vom tatsächlichen Materialverhalten deutet darauf hin, dass bestimmte Phänomene im Modell falsch oder gar nicht berücksichtigt wurden. Falls diese Abweichung nicht toleriert werden kann, muss ein neuer Modellierungszyklus initiiert werden. Dadurch entsteht eine anwendungsbezogene Hierarchie von Materialmodellen.

3. Hierarchie von entwickelten Modellen

Alle Modelle wurden in der vorliegenden Schrift modular aufgebaut. In jedem Modell können bestimmte Module ein- oder ausgeschaltet werden. Eine Abschaltung von einzelnen Modulen kann beispielsweise dann sinnvoll sein, wenn bestimmte Effekte oder Phänomene nur schwach ausgeprägt sind und somit keinen signifikanten Einfluss auf die Simulationsergebnisse haben. Beim Hinzufügen von neuen Modulen entstehen neue Modelle mit einem größeren Anwendbarkeitsbereich. Die Hierarchie von Modellen ist in Abbildung 1.2 schematisch dargestellt.

3.1. Ausgangsmodell nach Simo und Miehe (1992). Im isothermen Fall enthalten alle Modelle der vorliegenden Monografie das klassische Viskoplastizitätsmodell nach Simo und Miehe (1992) [**34**] als einen Spezialfall. Dieses Modell beruht auf der klassischen multiplikativen Zerlegung des Deformationsgradienten $\mathbf{F}$ in einen elastischen Anteil $\mathbf{F}_{\mathrm{e}}$ und einen inelastischen Anteil $\mathbf{F}_{\mathrm{i}}$. In diesem Ausgangsmodell wird die freie Energiedichte als eine isotrope Funktion des elastischen Anteils postuliert. Damit das Materialmodell thermodynamisch widerspruchsfrei bleibt, wird das Materialverhalten im elastischen Bereich mit den Beziehungen der Hyperelastizität erfasst. Diese Art der Modellierung unterscheidet sich vorteilhaft von den Beziehungen der Hypoelastizität. Hier tritt eine unphysikalische Energiedissipation selbst im elastischen Bereich auf[4]. Die Fließbedingung stellt eine Verallgemeinerung der klassischen Fließbedingung von Huber-Mises auf den Fall von endlichen Deformationen dar. Dabei wird vorausgesetzt, dass im rein elastischen Zustand die Frobenius-Norm des

---

[4] Die einzige Ausnahme von dieser Regel stellt die Nutzung der so genannten logarithmischen Zeitableitung dar [**5**]. Es muss aber beachtet werden, dass die logarithmische Zeitableitung von der konkreten Wahl der Referenzkonfiguration abhängt [**30**].

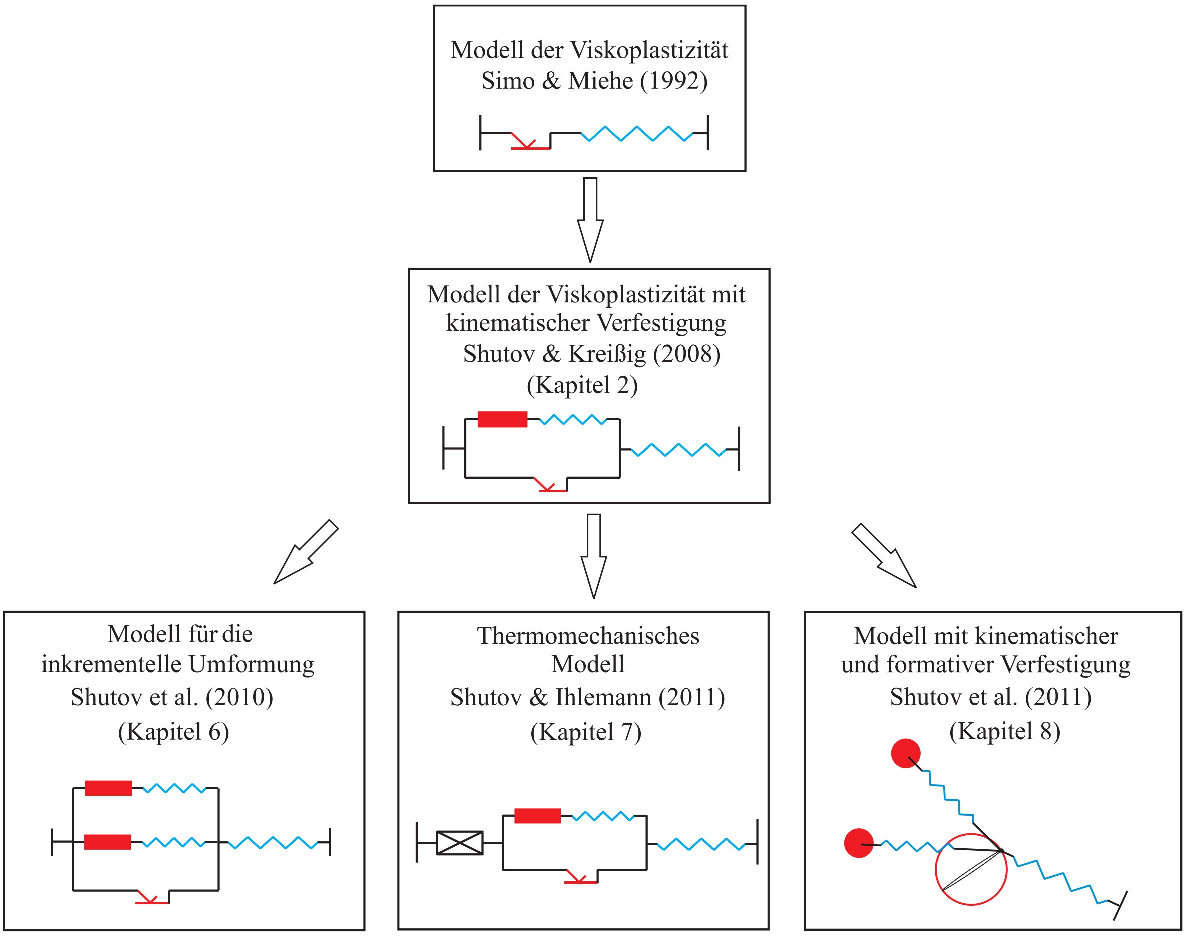

Abbildung 1.2. Hierarchie von Materialmodellen.

deviatorischen Anteils der Kirchhoff-Spannung $\boldsymbol{\tau}$ eine bestimmte Grenze unterschreitet[5]. Da alle Invarianten der Kirchhoff-Spannung mit den Invarianten der Mandel-Spannung übereinstimmen, kann diese Fließbedingung auch in Bezug auf die Mandel-Spannung formuliert werden. Eine solche Verallgemeinerung der klassischen Fließbedingung weist eine leichte Zug-Druck-Anisotropie auf. So ist die Cauchy-Zugfließspannung immer etwas kleiner als die Cauchy-Druckfließspannung.

Im Ausgangsmodell von Simo und Miehe (1992) genügt die plastische Fließregel dem Prinzip der maximalen Dissipation in folgender Form: Bei festgehaltener Richtung des plastischen Flusses (Richtung von $\mathrm{sym}(\dot{\mathbf{F}}_{\mathrm{i}}\mathbf{F}_{\mathrm{i}}^{-1})$) liefert der tatsächliche Mandel-Tensor ein Maximum der plastischen Dissipation über alle Mandel-Tensoren aus dem zulässigen (elastischen) Bereich.

Das inelastische Fließen ist inkompressibel ($\det \mathbf{F}_{\mathrm{i}} = 1$). Da die elastischen Eigenschaften des Ausgangsmodells als isotrop idealisiert werden, spielt der inelastische Spin

---

[5] So wie in der Literatur zur Plastizitätstheorie bei endlichen Deformationen üblich, wird im Modell von Simo und Miehe (1992) davon ausgegangen, dass die Kirchhoff-Spannung und nicht die Cauchy-Spannung ein natürliches Maß für die lokale Beanspruchung darstellt.

$\mathrm{skew}(\dot{\mathbf{F}}_\mathrm{i}\mathbf{F}_\mathrm{i}^{-1})$ keine Rolle. Aufgrund dessen ist die Fließregel sechsdimensional, und die numerische Behandlung des Materialmodells vereinfacht sich wesentlich[6]. Auf der Momentankonfiguration kann die Fließregel als eine Differentialgleichung in Bezug auf den elastischen linken Cauchy-Green-Tensor $\mathbf{B}_\mathrm{e} = \mathbf{F}_\mathrm{e}\mathbf{F}_\mathrm{e}^\mathrm{T}$ formuliert werden [**34**]. Dagegen wird die Fließregel auf der Referenzkonfiguration als eine gewöhnliche Differentialgleichung in Bezug auf den inelastischen rechten Cauchy-Green-Tensor $\mathbf{C}_\mathrm{i} = \mathbf{F}_\mathrm{i}^\mathrm{T}\mathbf{F}_\mathrm{i}$ dargestellt.

Die allgemeinen Prinzipien der Materialtheorie wie das Prinzip der materiellen Objektivität, das Prinzip des Determinismus und das Prinzip der lokalen Wirkung sind für das Ausgangsmodell erfüllt. Es ist thermodynamisch konsistent und seine konstitutiven Beziehungen sind invariant beim Wechsel der Referenzkonfiguration. Das Materialverhalten weist unter einfacher Scherung keine unphysikalischen Oszillationen auf. *In der vorliegenden Arbeit werden diese günstigen Eigenschaften bei allen Weiterentwicklungen vererbt.*

Die viskosen Eigenschaften werden im Ausgangsmodell mit einem Überspannungsansatz beschrieben. Dieser Ansatz wird auch bei allen Verallgemeinerungen des Modells benutzt. Nach dieser Regel hängt die Geschwindigkeit des inelastischen Fließens von der Überspannung ab, so dass größere Überspannungen einen schnelleren Fluss hervorrufen. Im Falle der formativen Verfestigung muss die Überspannung neu definiert werden (vgl. Kapitel 8 und 9), da hier die Form der Fließfläche zu berücksichtigen ist. In allen Modellen dieser Schrift wird der klassische Perzyna-Ansatz verwendet.

3.2. Modell der Viskoplastizität von Shutov und Kreißig (2008). Als erste Verallgemeinerung des Modells nach Simo und Miehe (1992) wird das Modell der Viskoplastizität von Shutov und Kreißig (2008) vorgestellt (vgl. Kapitel 2). Dieses Modell lässt die Berücksichtigung der nichtlinearen isotropen Verfestigung nach Voce und der nichtlinearen kinematischen Verfestigung nach Armstrong-Frederick zu[7]. Im Unterschied zum Ausgangsmodell von Simo und Miehe (1992) wird nun die Beschreibung des Bauschinger-Effekts möglich. Die für die Metallumformung wichtige Eigenspannungsanalyse und die Vorhersage der Rückfederung lassen sich nur mit Modellen dieser Klasse durchführen. Modelle ohne kinematische Verfestigung sind dagegen für solche Aufgaben ungeeignet. Da dieses Modell als Grundlage für alle weiteren Modelle dient (siehe Abbildung 1.2), wird es hier als "Basismodell" bezeichnet.

Die Beschreibung der modellspezifischen Kinematik beruht auf der doppelten multiplikativen Zerlegung des Deformationsgradienten (vgl. die Publikation von Lion [**20**]). Im Rahmen des Basismodells werden die elastischen Eigenschaften als isotrop vorausgesetzt. Das stellt für viele Materialien eine ausreichend genaue Näherung dar. Aus diesem Grunde spielen die inelastischen Spin-Tensoren keine Rolle und die Evolutionsgleichungen können in reduzierter Form benutzt werden. Das inelastische Fließen sowie die Gleichung für die nichtlineare kinematische Verfestigung sind dann sechsdimensional. Im Unterschied zu einigen alternativen Modellen der Plastizität mit kinematischer Verfestigung wird die Evolutionsgleichung nicht für den Rückspannungstensor formuliert. Stattdessen wird eine zusätzliche Fließregel (quasi auf der Mikrostrukturebene) eingeführt, die eine ähnliche mathematische

---

[6] Unter Berücksichtigung der Inkompressibilitätsbedingung kann die sechsdimensionale Fließregel theoretisch auf eine fünfdimensionale Fließregel reduziert werden.

[7] Die kinematische Verfestigung nach Armstrong-Frederick wird manchmal auch als Verfestigung nach Armstrong-Frederick-Kadashevich bezeichnet [**2, 17**]

Struktur wie die globale Fließregel besitzt. Diese Vorgehensweise bringt numerische Vorteile mit sich, weil beide Evolutionsgleichungen auf ähnlichen dimensionslosen Größen basieren und für beide Evolutionsgleichungen ähnliche Diskretisierungsverfahren eingesetzt werden können.

Obwohl das Modell lediglich vier Verfestigungsparameter enthält (zwei für die isotrope und zwei für die kinematische Verfestigung), wird das Verhalten einiger Al-Legierungen mit sehr guter Genauigkeit beschrieben (vgl. Kapitel 5). Für die Identifikation aller Verfestigungsparameter werden Versuche mit Belastungsumkehr benötigt.

Aufgrund der Invarianz beim Wechsel der Referenzkonfiguration ist dieses Modell besonders gut für die Simulation der mehrstufigen Metallumformung geeignet (vgl. Kapitel 10). Die durch die Vorstufen induzierte plastische Anisotropie des Materials ist zugleich die Ausgangsanisotropie der nächsten Stufe. Sie wird mit entsprechenden Anfangsbedingungen für relevante innere Variablen erfasst, was gleichwertig zur Einführung von Anfangsrückspannungen ist. Im Kapitel 10 wurde, basierend auf dem Wechsel der Referenzkonfiguration, eine einfache Transformationsregel hergeleitet. Diese ermöglicht die Bestimmung tensorwertiger Anfangsbedingungen bezogen auf die neue Referenzkonfiguration. Damit werden die Anfangsbedingungen unter Nutzung der Simulationsergebnisse der vorhergehenden Belastungsstufe formuliert. Der vorgeschlagene Zugang wurde anhand einer numerischen Simulation des Gleichkanal-Winkelpressens (ECAP) mit zylindrischem Halbzeug veranschaulicht. Die im Laufe eines ECAP-Durchgangs akkumulierte plastische Anisotropie wurde mit einer Serie von virtuellen Zugversuchen abgeschätzt. Dazu dienten virtuelle Versuche an Proben, die in unterschiedlichen Richtungen dem umgeformten Halbzeug entnommen wurden. Die Simulationsergebnisse stimmen qualitativ mit experimentellen Daten überein. Der Einfluss der plastischen Anisotropie auf die Halbzeugverdrehung innerhalb eines kreisförmigen Ausgangskanals wurde numerisch für die gängige Umformroute Bc abgeschätzt. Es konnte nachgewiesen werden, dass sogar eine sehr starke plastische Anisotropie nur eine geringe Verdrehung des Halbzeugs hervorruft.

Das phänomenologische Basismodell lässt eine ganze Reihe von Generalisierungen zu, wovon einige in den nächsten Abschnitten präsentiert werden.

3.3. Modell für die inkrementelle Umformung nach Shutov et al. (2010). Die Berücksichtigung des Bauschinger-Effekts ist für die meisten metallischen Werkstoffe im Falle einer nichtmonotonen Belastung erforderlich. Für einfache Belastungspfade mit einer geringen Anzahl von Umkehrpunkten ist der klassische Ansatz nach Armstrong-Frederick ausreichend, um die Spannungsantwort von einigen Al-Legierungen zu beschreiben (vgl. Kapitel 5). Eine große praktische Bedeutung haben die so genannten inkrementellen Umformverfahren. Als typische Beispiele seien hier das Bohrungsdrücken und die inkrementelle Blechumformung erwähnt. Im Falle einer inkrementellen Umformung mit vielen Umkehrpunkten kann sich das Basismodell als "zu grob" erweisen. Aus diesem Grunde wurde es, zwecks einer besseren Erfassung der belastungsinduzierten Anisotropie, verallgemeinert. Auf diese Weise ist ein spezielles Modell für die Simulation der inkrementellen Umformung entstanden (vgl. Kapitel 6).

Diese Verallgemeinerung besteht in der Einführung von zusätzlichen Rückspannungstensoren sowie in der Modifizierung der entsprechenden Evolutionsgleichungen. In Abbildung

1.2 ist dieses Modell schematisch für zwei Maxwell-Elemente dargestellt worden. Im einfachsten Fall operiert damit ein solches Modell mit zwei Rückspannungen: einer Rückspannung mit schneller Sättigung und kleinem Sättigungswert sowie einer weiteren Rückspannung mit etwas langsamerer Sättigung und größerem Sättigungswert. Die "schnelle" Rückspannung ist zusätzlich hilfreich, um den problematischen Knick im Spannungs-Dehnungs-Diagramm an der Fließgrenze zu verkleinern. Um Effekte wie die zyklische Ver- oder Entfestigung zu erfassen, wurde auch die Voce-Regel der isotropen Verfestigung modifiziert. So kann eine anfängliche Entfestigung in Kombination mit einer "verspäteten" Verfestigung simuliert werden. Im Kapitel 6 ist gezeigt worden, dass der einfache Ansatz mit nur zwei Rückspannungen ausreicht, um einen großen Satz von vielfältigen Messdaten abzudecken.

Da das Modell zwei identische modifizierte Maxwell-Elemente enthällt, ist es im Sinne der Parameteridentifikation sinnvoll, durch eine geeignete Anfangsnäherung einem Element die Rolle der "schnellen" und dem anderen jene der "langsamen" Rückspannung zuzuweisen. Dann bleibt die Korrelation zwischen entsprechenden Parametern schwach und eine robuste Parameteridentifikation ist bei ausreichender experimenteller Absicherung möglich (vgl. Kapitel 6).

Das modifizierte Materialmodell ist ebenfalls thermodynamisch konsistent und enthält das Basismodell als einen Spezialfall. Die Algorithmen und Konzepte des Basismodells können mit geringfügigen Modifikationen übernommen werden.

Eine alternative Erweiterung des Basismodells zur Erfassung des zyklischen Kriechens (ratcheting) wurde in [**41**] präsentiert.

3.4. Thermomechanisches Modell von Shutov und Ihlemann (2011). Es ist allgemein bekannt, dass plastische Verformungen mit einer lokalen Temperaturerhöhung infolge der Dissipation verbunden sind. Erhöhte Temperaturen beeinflussen wiederum das mechanische Verhalten des Materials. Um eine adäquate Simulation von thermomechanischen Vorgängen zu ermöglichen, wurde das Basismodell unter Berücksichtigung dieser Effekte verallgemeinert (vgl. Kapitel 7).

Zur Beschreibung der Kinematik wurde nun eine dreifache multiplikative Zerlegung des Deformationsgradienten eingeführt. Zusätzlich zur bereits untersuchten zweifachen Zerlegung (vgl. Kapitel 2) wird die Gesamtdeformation in einen isotropen thermischen Anteil $\mathbf{F}_\theta$ und einen mechanischen Anteil $\mathbf{F}_{\mathrm{M}}$ zerlegt. Eine solche dreifache Zerlegung wurde bereits in der Publikation von Lion [**20**] präsentiert.

Bei der Herleitung der Wärmeleitungsgleichung zur Beschreibung der Temperaturentwicklung konnte der klassische Taylor-Quinney-Ansatz (1934) [**36**] nicht benutzt werden, da dieser im Falle eines stark ausgeprägten Bauschinger-Effekts zu inkonsistenten Ergebnissen führt[8]. Stattdessen wurde in der vorliegenden Arbeit von der thermodynamischen Konsistenz des Basismodells Gebrauch gemacht und die Wärmeleitungsgleichung direkt aus der Energiebilanz abgeleitet. Dabei wurde die Berechnungsvorschrift für die plastische Dissipation auf einem natürlichen Wege erhalten, so dass auch im Falle eines starken Bauschinger-Effekts sinnvolle Simulationen ermöglicht wurden. Die abgeleitete Wärmeleitungsgleichung

---

[8] Diese Inkonsistenz liegt darin begründet, dass die plastische Spannungsleistung negative Werte annehmen kann. Der Taylor-Quinney-Ansatz wird in diesem Falle eine Abkühlung des plastisch umgeformten Materials vorhersagen.

berücksichtigt zudem den thermoelastischen Effekt, da dieser ebenfalls eine Folge der Energieerhaltung ist. Für die genauere Beschreibung der Materialerwärmung wurde eine zusätzliche Komponente der freien Energie eingeführt - die sogenannte abgetrennte freie Energie. Sie entspricht dem Anteil der Energie der Kristallgitterdefekte, der mit keinem Verfestigungsmechanismus in direkter Verbindung steht. Mit dieser konstitutiven Annahme konnte auf die Einführung von Korrekturfaktoren verzichtet werden. Diese Korrekturfaktoren sind sonst notwendig, um den überschätzten Temperaturanstieg künstlich zu verkleinern. Die Materialparameter, welche die zeitliche Entwicklung der abgetrennten Energie kennzeichnen, lassen sich nicht aus isothermen Spannungs-Dehnungs-Kurven bestimmen. Anhand von numerischen Simulationen ist gezeigt worden, dass die Entwicklung der abgetrennten Energie einen deutlichen Einfluss auf die Temperatur des Probekörpers hat (vgl. Kapitel 7). Die entsprechenden Materialparameter sind somit einer experimentellen Identifikation zugänglich, wenn Messdaten zur Temperaturentwicklung vorliegen. Da die zeitliche Entwicklung der abgetrennten freien Energie keinen Einfluss auf das isotherme Materialverhalten hat, tritt diese Komponente im isothermen Fall nicht auf (vgl. Kapitel 2, 6, 8, 9).

Mechanische Materialeigenschaften wie die Fließspannung und das Verfestigungsvermögen hängen nun von der Temperatur ab. Eine gleichmäßige Wärmeausdehnung wurde im Modell ebenfalls berücksichtigt. Das Modell ist thermodynamisch konsistent und enthält das Basismodell als Spezialfall.

3.5. Modelle mit kinematischer und formativer Verfestigung. Ein abrupter Wechsel der Belastungsrichtung ist für mehrstufige Umformprozesse typisch. Sogar bei einstufigen Umformprozessen wie dem Tiefziehen tritt ein Wechsel der Belastungsrichtung auf. Für solche Belastungsfälle wird in der Regel ein Modell benötigt, das eine vom Ellipsoid abweichende Fließfläche im Spannungsraum aufweist. Wenn das plastische Fließen mit der Normalenregel beschrieben wird, spielt die Form der Fließfläche eine besonders große Rolle. Mit dem Basismodell ist es lediglich möglich, eine isotrope Aufweitung und eine translatorische Verschiebung der elliptischen Fließfläche im Spannungsraum zu erfassen. Um diesen Nachteil zu beseitigen, wurde eine Reihe von Modellen mit einer kombinierten isotrop-kinematisch-formativen Verfestigung entwickelt (vgl. Kapitel 8 und 9). Im Unterschied zu vielen in der Literatur präsentierten Modellen werden in dieser Schrift keine sich mit der Zeit entwickelnden Tensoren vierter Stufe verwendet. Stattdessen wird die formative Verfestigung lediglich mit rückspannungsähnlichen Tensoren zweiter Stufe beschrieben. Da diese Tensoren die Ausrichtung der gekrümmten Fließfläche kennzeichnen, werden sie als "Direktoren" bezeichnet [**24**]. Die Evolutionsgleichungen für die Direktoren sind ähnlich jenen für die Rückspannungen aufgebaut. So kann von den bereits entwickelten und bewährten numerischen Algorithmen Gebrauch gemacht werden.

Im Kapitel 8 wird ein zweidimensionales rheologisches Modell der kombinierten kinematisch-formativen Verfestigung konstruiert. Diese rheologische Analogie führt auf eine Fließfläche in Form einer Pascal'schen Schnecke. Sowohl die Distorsion als auch die Ausrichtung der Fließfläche in Abhängigkeit vom Belastungsweg werden anschaulich mit dem rheologischen Modell beschrieben. Darauf aufbauend wird anschließend ein phänomenologisches Modell mit isotroper, kinematischer und formativer Verfestigung bei endlichen Deformationen konzipiert. Neben der Normalenregel wird auch die radiale Fließregel untersucht. Beide Fließregeln führen auf ein thermodynamisch konsistentes Materialmodell. Trotz der

Formänderung der Fließfläche bleibt deren Konvexität stets erhalten. Die konstitutiven Gleichungen werden zuerst auf fiktiven Zwischenkonfigurationen formuliert. Hier erfolgt auch der Beweis der thermodynamischen Konsistenz. Für die numerische Behandlung werden die Gleichungen in die Referenzkonfiguration zurückgezogen.

Im Kapitel 9 wird ein weiteres zweidimensionales rheologisches Modell vorgeschlagen, mit dem im Gegensatz zum Kapitel 8 eine beliebige symmetrische Distorsion der Fließfläche im Sättigungszustand exakt erfasst werden kann. Ein wesentlicher Bestandteil dieses rheologischen Modells ist die Annahme einer prozessabhängigen Reibkraft im St.-Venant-Element. Diese Annahme ist in einer Versetzungsimmobilisierung bei monotoner Belastung in Kombination mit einer Versetzungsremobilisierung kurz nach dem Belastungswechsel begründet. Aufbauend auf dieser rheologischen Analogie wird ein thermodynamisch konsistentes Materialmodell konstruiert, mit dem sich die bei Al-Legierungen und Stählen experimentell beobachtbare starke Verkrümmung der Fließfläche in der Belastungsrichtung und eine entsprechende Abplattung entgegen der Belastungsrichtung simulieren lassen. Zusätzlich zum Satz von Materialparametern wird nun eine Materialfunktion benötigt. Diese Materialfunktion entspricht der Geometrie der gesättigten Fließläche. Dabei entwickelt sich die Fließfläche stetig und bleibt glatt sowie konvex. Das ist wiederum für die Stabilität von numerischen Algorithmen von großer Bedeutung.

4. Abschließende Bemerkungen und Ausblick

In dieser Schrift wurde die phänomenologische Materialmodellierung unter Verwendung von Stoffgesetzen der multiplikativen Plastizität weiterentwickelt. Der multiplikative Zugang stellt eine sich intensiv entwickelnde Forschungsrichtung dar, zu der neue Erkenntnisse in der vorliegenden Schrift präsentiert wurden. Beispielsweise wurde für das viskoplastische Modell (vgl. Kapitel 4) eine exponentielle Stabilität nachgewiesen. Diese Eigenschaft bringt für die numerische Integration den Vorteil mit sich, dass der numerische Fehler mit zunehmender Zeit nicht akkumuliert wird. Eine weitere Erkenntnis besteht in der Invarianz des Basismodells beim Wechsel der Referenzkonfiguration. Aus praktischer Sicht ist diese Invarianz für die Simulation der mehrstufigen Umformung vorteilhaft (vgl. Kapitel 10). Darüber hinaus lässt sich die Invarianzeigenschaft auch als eine verallgemeinerte Symmetrie der konstitutiven Gleichungen interpretieren [**30**]. Da alle Modelle in dieser Schrift thermodynamisch widerspruchsfrei sind, kann mathematisch exakt nachgewiesen werden, dass die Energie bei beliebiger zyklischer Belastung im stationären Zustand verbraucht und nicht freigesetzt wird. Die weitere Konsequenz der thermodynamischen Zulässigkeit liegt auch darin, dass eine konsistente Verallgemeinerung der Modelle auf den thermomechanischen Fall möglich ist (vgl. Kapitel 7). Die Präzisierung der Ansätze für die Energiespeicherung wird aber weitere experimentelle Untersuchungen zur Temperaturentwicklung bei nichtmonotoner Belastung erfordern.

Für das Basismodell wurden effiziente und robuste numerische Algorithmen konstruiert. Dank der Ähnlichkeit der Modellierungsansätze können diese numerischen Verfahren mit minimalem Aufwand auf neue erweiterte Modelle angepasst werden. Die Entwicklung von numerischen Algorithmen ist aber noch nicht komplett abgeschlossen. Unter anderem soll die Suche nach expliziten Lösungsformeln für implizite Zeitintegration weiter fortgesetzt werden. Wie es am Beispiel des Maxwell-Körpers gezeigt wurde [**31**], lässt sich sogar für komplizierte nichtlineare Gleichungssysteme eine einfache explizite Lösung finden, wenn von der konkreten Struktur des Materialmodells Gebrauch gemacht wird. Um von der exponentiellen Stabilität der Lösung profitieren zu können, müssen die numerischen Algorithmen die Inkompressibilitätsbedingung exakt erfüllen (vgl. Kapitel 4). Von besonderem Interesse sind solche Algorithmen, bei denen auch die Invarianz beim Wechsel der Referenzkonfiguration exakt eingehalten wird [**31**].

Wie in der Arbeit [**7**] gezeigt wurde, kann der multiplikative Zugang mit anderen Konzepten der Materialmodellierung erfolgreich gekoppelt werden. So ist das Basismodell in der Lage in Kombination mit dem Konzept repräsentativer Richtungen eine formative Verfestigung auf eine realistische Art zu erfassen.

Die in der Schrift präsentierten rheologischen Modelle der formativen Verfestigung (vgl. Kapitel 8 und 9) haben sich als ein flexibles Instrument der Materialmodellierung erwiesen. Mit den rheologischen Schaltbildern werden die wichtigen Modellierungsannahmen anschaulich erklärt. Solche Betrachtungen vereinfachen die Modellkonzeption, da die rheologischen Modelle konsistent in Ansätze der multiplikativen Elastoplastizität umgewandelt werden können. Der rheologische Zugang lässt auch eine Weiterentwicklung für eine noch bessere Beschreibung des Verfestigungsverhaltens zu [**28**].

Um den Anwendungsbereich existierender phänomenologischer Modelle noch weiter zu vergrößern, können mikrostrukturelle Betrachtungen explizit herangezogen werden. So wird in der Arbeit [**32**] das Basismodell mit einem fortgeschrittenen Modell der Versetzungskinetik gekoppelt. Als Ergebnis ist ein neues mikrostrukturbasiertes Modell entstanden, welches großes Potential für die numerische Untersuchung der Mikrostrukturentwicklung bei hochgradiger plastischer Deformation verspricht.

Literaturverzeichnis

[1] H. Altenbach, Kontinuumsmechanik: Einführung in die materialunabhängigen und materialabhängigen Gleichungen, Springer, 2012.

[2] P. J. Armstrong, C. O. Frederick, A mathematical representation of the multiaxial Bauschinger effect, Technical Report RD/B/N731, G.E.G.B, 1966.

[3] K. J. Bathe, Finite Element Procedures, Prentice Hall, 2nd edition, 1995.

[4] A. Bertram, Elasticity and Plasticity of Large Deformations, Springer, 2005.

[5] O.T. Bruhns, H. Xiao, A. Meyers, Self-consistent Eulerian type elasto-plasticity models based upon the logarithmic stress rate, International Journal of Plasticity, **36** 5 (1999) 479–520.

[6] W. Dettmer, S. Reese, On the theoretical and numerical modelling of Armstrong-Frederick kinematic hardening in the finite strain regime, Computer Methods in Applied Mechanics and Engineering, **193** (2004) 87–116.

[7] M. Freund, A. V. Shutov, J. Ihlemann, Simulation of distortional hardening by generalizing a uniaxial model of finite strain viscoplasticity. International Journal of Plasticity, **36** (2012) 113–129.

[8] P. Frint, M. Hockauf, T. Halle, G. Strehl, T. Lampke, M.F.-X. Wagner, Microstructural features and mechanical properties after industrial scale ECAP of an Al–6060 alloy. Materials Science Forum, **667-669** (2011) 1153–1158.

[9] P. R. Halmos, Finite-dimensional vector spaces, Princeton University Press, 2001.

[10] P. Haupt, Konzepte der Materialtheorie. Technische Mechanik, **16** 1 (1996) 13–22.

[11] P. Haupt, Continuum Mechanics and Theory of Materials, 2nd edition, Springer, 2002.

[12] P. Haupt, Ch. Tsakmakis, On the application of dual variables in continuum mechanics, Continuum Mechanics and Thermodynamics **1** (1989) 165–196.

[13] K. Hashiguchi, Y. Yamakawa, Introduction to Finite Strain Theory for Continuum Elasto-Plasticity, Wiley, 2012.

[14] G. A. Holzapfel, Nonlinear Solid Mechanics: A Continuum Approach for Engineering, Wiley, 2000.

[15] J. Ihlemann, Beobachterkonzepte und Darstellungsformen der nichtlinearen Kontinuumsmechanik. Habilitationsschrift, Leibniz Universität Hannover, 2006.

[16] M. Itskov, Tensor Algebra and Tensor Analysis for Engineers: With Applications to Continuum Mechanics, Springer, 2007.

[17] Û. I. Kadaševič: O različnyh variantah tenzorno-linejnyh sootnoshenij v teorii plastičnosti [In Russian]. Issledovaniâ po uprugosti i plastičnosti, **6** (1967) 39–45.

[18] S. N. Korobeinikov, Nonlinear Deformation of Solids [in Russian], Izd. Sib. Otd. Ross. Akad. Nauk, Novosibirsk, 2000.

[19] R. Kreißig, Einführung in die Plastizitätstheorie. Mit technischen Anwendungen, Hanser Fachbuchverlag, 1992.

[20] A. Lion, Constitutive modelling in finite thermoviscoplasticity: a physical approach based on nonlinear rheological elements, International Journal of Plasticity, **16** (2000) 469–494.

[21] J. Lubliner, Plasticity Theory, Macmillan Publishing, 1990.

[22] J. E. Marsden, T. J. Hughes, Mathematical Foundations of Elasticity, Dover Publications Inc., 1994.

[23] P. Naghdi, A critical review of the state of finite plasticity, Journal of Applied Mathematics and Physics, **41** (1990) 315–394.

[24] M. Ortiz, E. P. Popov, Distortional hardening rules for metal plasticity. J. Engng Mech., **109** (1983) 1042–1058.

[25] W. A. Palmow, Rheologische Modelle für Materialien bei endlichen Deformationen. Technische Mechanik, **4** (1984) 20–31.

[26] L. I. Sedov, Foundations of the non-linear mechanics of continua, Pergamon Press, 1966.

[27] A. V. Shutov, K. Hockauf, T. Halle, R. Kreißig, L.W. Meyer, Experimentelle und phänomenologische Beschreibung des mechanischen Verhaltens der Aluminiumlegierung EN AW-7075 nach großer plastischer Vorverformung, Materialwissenschaft und Werkstofftechnik, **40** 7 (2009) 551–558.

[28] A.V. Shutov, J. Ihlemann, On the phenomenological modelling of yield surface distortion (2013). http://arxiv.org/abs/1309.3091

[29] A. V. Shutov, J. Ihlemann, On the absence of a preferred configuration in constitutive relations of finite strain elasto-plasticity. PAMM, **13** (2013) 141–142.

[30] A. V. Shutov, J. Ihlemann, Analysis of some basic approaches to finite strain elasto-plasticity in view of reference change. International Journal of Plasticity (2014), http://dx.doi.org/10.1016/j.ijplas.2014.07.004

[31] A. V. Shutov, R. Landgraf, J. Ihlemann, An explicit solution for implicit time stepping in multiplicative finite strain viscoelasticity. Computer Methods in Applied Mechanics and Engineering, **256** (2013) 213–225.

[32] C. B. Silbermann, A. V. Shutov, J. Ihlemann, Modeling the evolution of dislocation populations under non-proportional loading. International Journal of Plasticity, **55** (2014) 58–79.

[33] J. C. Simo, T. J. R. Hughes, Computational Inelasticity, Springer, 1998.

[34] J. C. Simo, C. Miehe, Associative coupled thermoplasticity at finite strains: formulation, numerical analysis and implementation. Computer Methods in Applied Mechanics and Engineering, **98** (1992) 41–104.

[35] I. S. Sokolnikoff, Tensor Analysis: Theory and Applications to Geometry and Mechanics of Continua, Wiley, 1964.

[36] G. Taylor, M. Quinney, The latent energy remaining in a metal after cold working. Proceedings of the Royal Society of London A, **143** (1934) 307–326.

[37] C. Truesdell, W. Noll, The Non-Linear Field Theories of Mechanics, 3rd ed., Springer, 2004.

[38] S. Wagner, H. Podlesak, S. Siebeck, D. Nestler, M.F.-X. Wagner, B. Wielage, M. Hockauf, Effect of ECAP and heat treatment on microstructure and mechanical properties of a SiC reinforced Al–Cu alloy. Materialwissenschaft und Werkstofftechnik, **143**(9) (2010) 704–710.

[39] P. Wriggers, Nichtlineare Finite-Element-Methoden, Springer, 2001.

[40] H. Xiao, O. T. Bruhns, A. Meyers, Elastoplasticity beyond small deformations, Acta Mechanica, **182** (2006) 31–111.

[41] Y. Zhu, G. Kang, Q. Kan, C. Yu, J. Ding, An extended cyclic plasticity model at finite deformations describing the Bauschinger effect and ratchetting behaviour. Proceedings of 13th International Conference on Fracture (2013).

[42] O. C. Zienkiewicz, R. L. Taylor, The Finite Element Method, Volume 2: Solid Mechanics, Butterworth-Heinemann, 2000.

KAPITEL 2

Finite strain viscoplasticity with nonlinear kinematic hardening: phenomenological modeling and time integration

A.V. Shutov,[1] R.Kreißig

Institute of Mechanics and Thermodynamics, Chemnitz University of Technology,
Str. d. Nationen 62, D-09111 Chemnitz, Germany

Abstract: *This article deals with a viscoplastic material model of overstress type. The model is based on a multiplicative decomposition of the deformation gradient into elastic and inelastic part. An additional multiplicative decomposition of inelastic part is used to describe a nonlinear kinematic hardening of Armstrong-Frederick type.*

Two implicit time-stepping methods are adopted for numerical integration of evolution equations, such that the plastic incompressibility constraint is exactly satisfied. The first method is based on the tensor exponential. The second method is a modified Euler-Backward method. Special numerical tests show that both approaches yield similar results even for finite inelastic increments.

The basic features of the material response, predicted by the material model, are illustrated with a series of numerical simulations.

Keywords: viscoplasticity; finite strains; kinematic hardening; inelastic incompressibility; integration algorithm; material testing.
AMS Subject Classification: 74C20; 74S05.

Nomenclature

$\mathbf{F}$	deformation gradient
$\mathbf{F}_{\mathrm{i}}$	inelastic part of the deformation gradient
$\hat{\mathbf{F}}_{\mathrm{e}}$	elastic part of the deformation gradient
$\mathbf{F}_{\mathrm{ii}}$	dissipative part of $\mathbf{F}_{\mathrm{i}}$
$\check{\mathbf{F}}_{\mathrm{ie}}$	energy storage part of $\mathbf{F}_{\mathrm{i}}$
$\mathcal{K}$	current configuration
$\tilde{\mathcal{K}}$	reference configuration

---

[1] Corresponding author. alexey.v.shutov@gmail.com
web: http://sites.google.com/site/materialmodeling

This chapter is reproduced from the paper: A. V. Shutov, R. Kreißig: Finite strain viscoplasticity with nonlinear kinematic hardening: phenomenological modeling and time integration. Computer Methods in Applied Mechanics and Engineering. 2008. 197. 2015-2029. Copyright Elsevier. Reproduced with permission.

$\hat{\mathcal{K}}$	stress-free intermediate configuration
$\check{\mathcal{K}}$	intermediate configuration of microstructure
$\mathbf{C}$	right Cauchy-Green tensor (see (2.5))
$\mathbf{C}_{\mathrm{i}}$	inelastic right Cauchy-Green tensor (see $(2.6)_1$)
$\mathbf{C}_{\mathrm{ii}}$	inelastic right Cauchy-Green tensor of microstructure (see $(2.6)_2$)
$\hat{\mathbf{C}}_{\mathrm{e}}$	elastic right Cauchy-Green tensor (see $(2.7)_1$)
$\check{\mathbf{C}}_{\mathrm{ie}}$	elastic right Cauchy-Green tensor of microstructure (see $(2.7)_2$)
$\mathbf{E}$	Green strain tensor
$\mathbf{\Gamma}$	Almansi strain tensor
$\mathbf{T}$	Cauchy stress tensor
$\mathbf{S}$	weighted Cauchy tensor (Kirchhoff tensor) (see (2.16))
$\hat{\mathbf{S}}$, $\tilde{\mathbf{T}}$	2nd Piola-Kirchhoff tensors operating on $\hat{\mathcal{K}}$, $\tilde{\mathcal{K}}$, respectively (see (2.17))
$\check{\mathbf{X}}$, $\hat{\mathbf{X}}$, $\tilde{\mathbf{X}}$	backstress tensors operating on $\check{\mathcal{K}}$, $\hat{\mathcal{K}}$ and $\tilde{\mathcal{K}}$, respectively (see (2.20))
$\hat{\mathbf{\Sigma}}$	the driving force for inelastic flow (see $(2.35)_1$)
$\check{\mathbf{\Xi}}$	the driving force for inelastic flow of microstructure (see $(2.35)_2$)
$\mathbf{1}$	second-rank identity tensor
$\mathbf{M}^*, \mathbf{M}_*$	covariant pull-back and push-forward (see (2.3))
$(\mathbf{M}^{-\mathrm{T}})^*, (\mathbf{M}^{-\mathrm{T}})_*$	contravariant pull-back and push-forward (see (2.4))
$\mathbf{A} \cdot \mathbf{B} = \mathbf{AB}$	product (composition) of two second-rank tensors
$\mathbf{A} : \mathbf{B}$	scalar product of two second-rank tensors (see (2.19))
$\lVert\mathbf{A}\rVert$	l_2 norm of a second-rank tensor (Frobenius norm) (see $(2.38)_1$)
$\lVert\mathbf{A}\rVert^*$	induced norm of a second-rank tensor (spectral norm) (see (2.69))
Sym	space of symmetric second-rank tensors
$(\cdot)^{\mathrm{D}}$	deviatoric part of a tensor (see $(2.38)_2$)
$(\cdot)^{\mathrm{T}}$	transposition of a tensor
$(\cdot)^{-\mathrm{T}}$	inverse of transposed
$\mathrm{tr}(\cdot)$	trace of a second-order tensor
$\overset{\triangle}{(\cdot)}$	covariant Oldroyd rate with respect to $\hat{\mathcal{K}}$ (see $(2.12)_1$)
$\overset{\diamond}{(\cdot)}$	covariant Oldroyd rate with respect to $\check{\mathcal{K}}$ (see $(2.12)_2$)
$\overline{(\cdot)}$	unimodular part of a tensor (see (2.26))
$\mathrm{sym}(\cdot)$	symmetric part of a tensor (see (2.15))
$\mathrm{skew}(\cdot)$	skew-symmetric part of a tensor (see $(2.66)_2$)
$\langle x \rangle$	MacCauley bracket (see $(2.39)_3$)
ψ	specific free energy
K	initial yield stress
R	isotropic hardening
s	inelastic arc length
s_{d}	dissipative part of s
s_{e}	energy storage part of s (see (2.22))
λ_{i}	proportionality factor (inelastic multiplier) (see $(2.39)_1$)
f	overstress (see $(2.39)_2$)
$\mathfrak{F}$	norm of the driving force (see (2.52))
ξ	incremental inelastic parameter (see (2.77))

ρ_{R}	mass density in the reference configuration
k	bulk modulus (see (2.24))
μ	shear modulus (see (2.24))
c	bulk modulus of microstructure (see $(2.25)_1$)
γ	hardening modulus (see $(2.25)_2$)
ε	technical strain (see $(2.92)_1$)
ϕ	shear strain (see $(2.93)_1$)
σ, τ	axial and shear stresses, respectively

1. Introduction

New materials, such as ultrafine-grained-aluminium (see the papers [**15, 28**]), are of special interest for many practical applications. To promote the innovation of the new materials, the robust numerical simulation of the material response is required. It is desirable to have a phenomenological description of the material which on the one hand takes important phenomena into account, and on the other hand enables stable numerical computations.

In this paper we investigate the simulation of rate-dependent material behavior with equilibrium hysteresis effect (for the general introduction to the theory of viscoplasticity see, for example, [**33, 23, 12**]).

The Bauschinger effect is observed in most metals under non-monotonic loading. The most popular approach to describe the Bauschinger effect was proposed by Armstrong and Frederick [**2**] in 1966. Application of the Armstrong-Frederick hardening concept within the framework of Perzyna type viscoplasticity (see [**33**]) yields the classical material model of overstress type (see [**3, 23**]). This model has the advantage that it admits simple rheological interpretation (see fig. 2.1.a). Such phenomena as creep, relaxation and nonlinear kinematic hardening are taken into account by the model. Simple modification of this model is possible to include isotropic hardening as well [2].

Several strategies can be adopted for the generalization of this model to finite strains (see, for example, [**6, 38, 26, 37, 24, 13, 31**]). Some of the generalizations were analyzed numerically in [**5**]. Following the elegant approach of Lion [**24**], we use the rheological interpretation (fig. 2.1.a) of the classical model to construct its finite-strain counterpart.

The specific modeling assumptions adopted in this paper are as follows:

- Multiplicative decomposition of the deformation gradient into elastic and inelastic part: $\mathbf{F} = \hat{\mathbf{F}}_{\mathrm{e}}\mathbf{F}_{\mathrm{i}}$ [**21, 22**].
- Multiplicative decomposition of the inelastic part into energy storage part and dissipative part: $\mathbf{F}_{\mathrm{i}} = \check{\mathbf{F}}_{\mathrm{ie}}\mathbf{F}_{\mathrm{ii}}$ [**24, 13**].
- Free energy is a sum of appropriate isotropic strain energy functions [**24, 13**].

The resulting material model takes both kinematic and isotropic hardening into account. The thermodynamic consistency is proved.

The purpose of the present paper is threefold. First, we formulate the material model under consideration. In particular, we transform the constitutive equations to the reference

---

[2] The diagram in fig. 2.1.a provides insight into the rheological modeling of kinematic hardening. To the best of our knowledge, there is no simple rheological diagram of viscoplastic material with isotropic hardening.

configuration in order to simplify the numerical treatment. Next, two implicit schemes for the numerical integration of evolution equations are developed. Finally, we analyse numerically the basic properties of the material response, predicted by the model.

A global *implicit* time stepping procedure in the context of displacement based FEM requires a proper stress algorithm (local integration algorithm) [**40**]. Such algorithm provides the stresses and the consistent tangent operator as a function of the strain history locally at each integration point. A set of internal variables is used in this paper to describe the history dependence, and the stress algorithm includes *implicit* integration of a system of differential (evolution) and algebraic equations.

Two most popular implicit schemes for integration of inelastic strains in the context of viscoplasticity/plasticity are:

- *Backward-Euler scheme*, also referred as *implicit Euler scheme* (see, for example, [**10, 35, 36, 13, 5**]).
- *Exponential scheme*, also referred as *Euler scheme with exponential map* (see, for example, [**39, 29, 30, 5**]).

The exponential scheme is advantageous since it retains the inelastic incompressibility even for finite time steps. Thus, an important geometric property of the solution is automatically preserved. Moreover, the numerical error of Euler-Backward method, related to the violation of incompressibility, *tends to accumulate over time* (see, for example, [**5, 14**]). Therefore, even for small time steps, the numerical solution deviates from the exact solution after some period of time.

Helm [**14**] modified the classical Euler-Backward scheme, using a projection on the group of unimodular tensors, to enforce the incompressibility of inelastic flow.

In this work we implement in a uniform manner both modified Euler-Backward method (MEBM) and the exponential method (EM). Both methods result in a nonlinear system of equations with respect to strain-like internal variables $\mathbf{C}_{\mathrm{i}} = \mathbf{F}_{\mathrm{i}}^{\mathrm{T}}\mathbf{F}_{\mathrm{i}}$, $\mathbf{C}_{\mathrm{ii}} = \mathbf{F}_{\mathrm{ii}}^{\mathrm{T}}\mathbf{F}_{\mathrm{ii}}$ and $\xi = \lambda_{\mathrm{i}} \ \Delta t$.[3] This nonlinear system is split into two subproblems:
First subproblem: Finding $\mathbf{C}_{\mathrm{i}}, \mathbf{C}_{\mathrm{ii}}$ with a given ξ.
Second subproblem: Finding ξ, such that an incremental consistency condition is satisfied.
This adapted strategy is more robust than the straightforward application of a nonlinear solver to the original system of equations. At the same time, this approach is not limited by the special form of the free energy, and finite elastic strains are likewise allowed. Moreover, the stress algorithms are applicable in the limiting case of rate-independent plasticity (as viscosity tends to zero).

Although the material response is anisotropic, it is shown that MEBM as well as EM *exactly preserve the symmetry* of $\mathbf{C}_{\mathrm{i}}$ and $\mathbf{C}_{\mathrm{ii}}$. Furthermore, the accuracy and robustness of both integration algorithms is verified with the help of special numerical tests. Both methods provide similar results with almost the same integration error. A common feature of MEBM and EM is that the numerical error is not accumulated over time.

The phenomenological description of each specific material can be schematically subdivided into three steps:

- Material testing, such that the important phenomena make themselves evident.

---

[3] $\xi \geq 0$ is an incremental inelastic parameter, defined by (2.77).

- Choosing an appropriate phenomenological model, that reproduces qualitatively the experimental data.
- Parameter identification, using the experimental data.

To illustrate the basic characteristics of the material model we simulate a series of material testing experiments. These experiments are uniaxial tension and torsion under monotonic and cyclic loading. In particular, we conclude that the material model can be used (after a proper parameter identification) to describe the mechanical response of an aluminium alloy processed by ECA-pressing [**15, 28**].

Throughout this article, bold-faced symbols denote first- and second-rank tensors in $\mathbb{R}^3$. Expression $a := b$ means a is defined to be another name for b.

2. Material model of finite strain viscoplasticity

The material model is motivated by the rheological diagram in fig. 2.1.a. This diagram takes the kinematic hardening of Armstrong-Frederick type into account (for the sake of simplicity the isotropic hardening is omitted in the diagram). The total inelastic strains and the inelastic strains of microstructure are used as internal variables. The evolution of these quantities is closely related to the energy dissipation during the inelastic processes. Besides, additional real-valued strain-like internal variables are introduced in order to describe the nonlinear isotropic hardening.

2.1. Kinematics. For a fixed time instant $t \geq 0$ let $\mathcal{K} \subset \mathbb{R}^3$ be a current configuration occupied by the solid. Suppose $\tilde{\mathcal{K}} \subset \mathbb{R}^3$ is the reference configuration, which uniquely designates the material points. Let us consider the classical multiplicative decomposition of the deformation gradient $\mathbf{F}$ into *elastic part* $\hat{\mathbf{F}}_{\mathrm{e}}$ and *inelastic part* $\mathbf{F}_{\mathrm{i}}$ [**21, 22**]

$$\mathbf{F} = \hat{\mathbf{F}}_{\mathrm{e}}\mathbf{F}_{\mathrm{i}}. \tag{2.1}$$

The mechanical justification of (2.1) uses the idea of the local (within a neighborhood of the material point) elastic unloading. The multiplicative decomposition (2.1) implements the *stress-free intermediate configuration* $\hat{\mathcal{K}}$ (see fig. 2.1.b).

A second multiplicative decomposition is introduced in order to simulate a nonlinear kinematic hardening of Armstrong-Frederick type. Following Lion [**24**], we decompose the inelastic part $\mathbf{F}_{\mathrm{i}}$ into *energy storage part* $\check{\mathbf{F}}_{\mathrm{ie}}$ and *dissipative part* $\mathbf{F}_{\mathrm{ii}}$

$$\mathbf{F}_{\mathrm{i}} = \check{\mathbf{F}}_{\mathrm{ie}}\mathbf{F}_{\mathrm{ii}}. \tag{2.2}$$

The energy storage part $\check{\mathbf{F}}_{\mathrm{ie}}$ describes the heterogeneity of elastic strains associated with the energy storage on the microscale. The dissipative part $\mathbf{F}_{\mathrm{ii}}$ can be attributed to slip processes on the microscale (see [**24, 13**] for details). Decomposition (2.2) implements the *intermediate configuration of microstructure*[4] $\check{\mathcal{K}}$ (see fig. 2.1.b). The commutative diagram in fig. 2.1.b summarizes the multiplicative decompositions (2.1) and (2.2).

In this paper we deal with second-order tensors, which operate on configurations $\mathcal{K}$, $\tilde{\mathcal{K}}$, $\hat{\mathcal{K}}$, $\check{\mathcal{K}}$. Pull-back (push-forward) operations describe the transformation of tensor fields during the change of configurations. Let $\mathbf{M} \in \left\{\mathbf{F}, \mathbf{F}_{\mathrm{i}}, \mathbf{F}_{\mathrm{ii}}, \hat{\mathbf{F}}_{\mathrm{e}}, \check{\mathbf{F}}_{\mathrm{ie}}\right\}$ be a linear transformation

---

[4] In [**24**] the similar configuration is called the *intermediate configuration of kinematic hardening.*

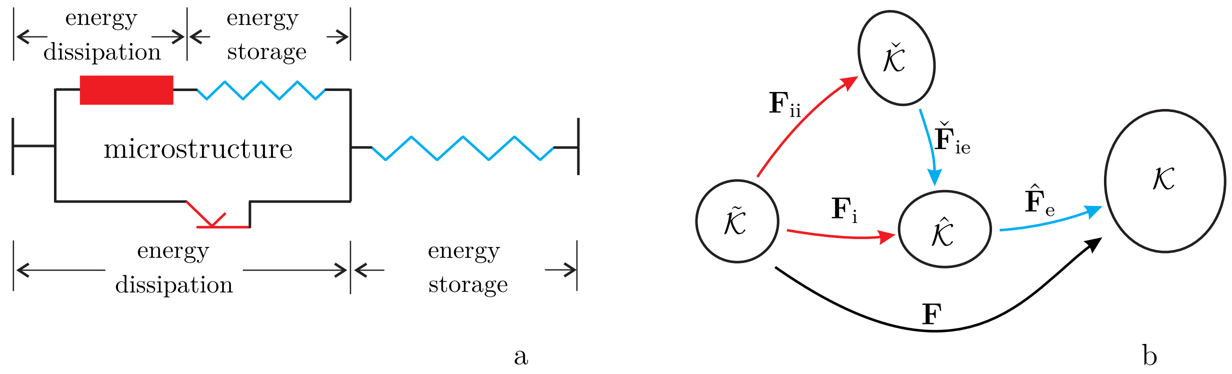

Figure 2.1. Rheological model (a) and a commutative diagram (b) showing corresponding configurations with transformations of material line elements.

of material line elements on two different configurations. We define corresponding *pull-back and push-forward of covariant tensor field* by

$$\mathbf{M}^{*}(\cdot) := \mathbf{M}^{\mathrm{T}}(\cdot)\mathbf{M}, \quad \mathbf{M}_{*}(\cdot) := \mathbf{M}^{-\mathrm{T}}(\cdot)\mathbf{M}^{-1}. \tag{2.3}$$

Pull-back and push-forward of contravariant tensor field are given by

$$(\mathbf{M}^{-\mathrm{T}})^{*}(\cdot) = \mathbf{M}^{-1}(\cdot)\mathbf{M}^{-\mathrm{T}}, \quad (\mathbf{M}^{-\mathrm{T}})_{*}(\cdot) = \mathbf{M}(\cdot)\mathbf{M}^{\mathrm{T}}. \tag{2.4}$$

Thus, the right Cauchy-Green tensor is a covariant pull-back of identity tensor $\mathbf{1}$

$$\mathbf{C} := \mathbf{F}^{*}\mathbf{1} = \mathbf{F}^{\mathrm{T}}\mathbf{F}. \tag{2.5}$$

In the same manner, we define the inelastic right Cauchy-Green tensor $\mathbf{C}_{\mathrm{i}}$ and inelastic right Cauchy-Green tensor $\mathbf{C}_{\mathrm{ii}}$ of microstructure:

$$\mathbf{C}_{\mathrm{i}} := \mathbf{F}_{\mathrm{i}}^{*}\mathbf{1} = \mathbf{F}_{\mathrm{i}}^{\mathrm{T}}\mathbf{F}_{\mathrm{i}}, \quad \mathbf{C}_{\mathrm{ii}} := \mathbf{F}_{\mathrm{ii}}^{*}\mathbf{1} = \mathbf{F}_{\mathrm{ii}}^{\mathrm{T}}\mathbf{F}_{\mathrm{ii}}. \tag{2.6}$$

Further, the elastic right Cauchy-Green tensor $\hat{\mathbf{C}}_{\mathrm{e}}$ and the elastic right Cauchy-Green tensor $\check{\mathbf{C}}_{\mathrm{ie}}$ of microstructure are defined by

$$\hat{\mathbf{C}}_{\mathrm{e}} := \hat{\mathbf{F}}_{\mathrm{e}}{}^{*}\mathbf{1} = \hat{\mathbf{F}}_{\mathrm{e}}^{\mathrm{T}}\hat{\mathbf{F}}_{\mathrm{e}}, \quad \check{\mathbf{C}}_{\mathrm{ie}} := \check{\mathbf{F}}_{\mathrm{ie}}{}^{*}\mathbf{1} = \check{\mathbf{F}}_{\mathrm{ie}}^{\mathrm{T}}\check{\mathbf{F}}_{\mathrm{ie}}. \tag{2.7}$$

The tensors

$$\mathbf{E} := \frac{1}{2}(\mathbf{C} - \mathbf{1}), \quad \boldsymbol{\Gamma} := \mathbf{F}_{*}\mathbf{E} = \mathbf{F}^{-\mathrm{T}}\mathbf{E}\mathbf{F}^{-1}$$

are termed the Green strain tensor and the Almansi strain tensor, respectively. Basing on $\mathbf{E}$, we define a corresponding strain tensor $\hat{\boldsymbol{\Gamma}}$, which operates on $\hat{\mathcal{K}}$

$$\hat{\boldsymbol{\Gamma}} := (\mathbf{F}_{\mathrm{i}})_{*}\mathbf{E} = \mathbf{F}_{\mathrm{i}}^{-\mathrm{T}}\mathbf{E}\mathbf{F}_{\mathrm{i}}^{-1}.$$

Multiplicative decomposition (2.1) implements the additive decomposition of $\hat{\boldsymbol{\Gamma}}$:

$$\mathbf{F} = \hat{\mathbf{F}}_{\mathrm{e}}\mathbf{F}_{\mathrm{i}} \quad \Rightarrow \quad \hat{\boldsymbol{\Gamma}} = \hat{\boldsymbol{\Gamma}}_{\mathrm{i}} + \hat{\boldsymbol{\Gamma}}_{\mathrm{e}}, \tag{2.8}$$

where $\hat{\boldsymbol{\Gamma}}_{\mathrm{i}}$, $\hat{\boldsymbol{\Gamma}}_{\mathrm{e}}$ are the inelastic Almansi tensor and the elastic Green tensor, respectively

$$\hat{\boldsymbol{\Gamma}}_{\mathrm{i}} := \frac{1}{2}(\mathbf{1} - \mathbf{F}_{\mathrm{i}}^{-\mathrm{T}}\mathbf{F}_{\mathrm{i}}^{-1}), \quad \hat{\boldsymbol{\Gamma}}_{\mathrm{e}} := \frac{1}{2}(\hat{\mathbf{F}}_{\mathrm{e}}^{\mathrm{T}}\hat{\mathbf{F}}_{\mathrm{e}} - \mathbf{1}) = \frac{1}{2}(\hat{\mathbf{C}}_{\mathrm{e}} - \mathbf{1}). \tag{2.9}$$

Analogously, multiplicative decomposition (2.2) implements the additive decomposition of the pull-back of the inelastic Almansi tensor $\hat{\boldsymbol{\Gamma}}_{\mathrm{i}}$ to $\check{\mathcal{K}}$:

$$\check{\boldsymbol{\Gamma}}_{\mathrm{i}} := \check{\mathbf{F}}_{\mathrm{ie}}^{*}\hat{\boldsymbol{\Gamma}}_{\mathrm{i}} = \check{\mathbf{F}}_{\mathrm{ie}}^{\mathrm{T}}\hat{\boldsymbol{\Gamma}}_{\mathrm{i}}\check{\mathbf{F}}_{\mathrm{ie}},$$

$$\mathbf{F}_\mathrm{i} = \check{\mathbf{F}}_\mathrm{ie}\mathbf{F}_\mathrm{ii} \quad \Rightarrow \quad \check{\boldsymbol{\Gamma}}_\mathrm{i} = \check{\boldsymbol{\Gamma}}_\mathrm{ii} + \check{\boldsymbol{\Gamma}}_\mathrm{ie}, \tag{2.10}$$

where

$$\check{\boldsymbol{\Gamma}}_\mathrm{ii} := \frac{1}{2}(\mathbf{1} - \mathbf{F}_\mathrm{ii}^{-\mathrm{T}}\mathbf{F}_\mathrm{ii}^{-1}), \quad \check{\boldsymbol{\Gamma}}_\mathrm{ie} := \frac{1}{2}(\check{\mathbf{F}}_\mathrm{ie}^\mathrm{T}\check{\mathbf{F}}_\mathrm{ie} - \mathbf{1}) = \frac{1}{2}(\check{\mathbf{C}}_\mathrm{ie} - \mathbf{1}). \tag{2.11}$$

Finally, we define the inelastic pull-back of $\hat{\boldsymbol{\Gamma}}_\mathrm{i}$ to $\tilde{\mathcal{K}}$

$$\tilde{\boldsymbol{\Gamma}}_\mathrm{i} := \mathbf{F}_\mathrm{i}^*\hat{\boldsymbol{\Gamma}}_\mathrm{i}.$$

2.2. The concept of dual variables. The formalism of dual variables developed by Haupt and Tsakmakis [**11**] specifies the choice of stress and strain variables as well as their time derivatives. According to this concept, we introduce the covariant Oldroyd rates $\overset{\triangle}{(\cdot)}$, $\overset{\diamond}{(\cdot)}$ with respect to the stress-free configuration $\hat{\mathcal{K}}$ and the microstructural configuration $\check{\mathcal{K}}$, respectively,

$$\overset{\triangle}{(\cdot)} := \mathbf{F}_{\mathrm{i}*}\Big(\big(\mathbf{F}_\mathrm{i}^*(\cdot)\big)^{\cdot}\Big), \qquad \overset{\diamond}{(\cdot)} := \mathbf{F}_{\mathrm{ii}*}\Big(\big(\mathbf{F}_\mathrm{ii}^*(\cdot)\big)^{\cdot}\Big), \tag{2.12}$$

where $()^{\cdot}$ stands for material time derivative. The alternative representation of covariant Oldroyd derivatives is as follows

$$\overset{\triangle}{(\cdot)} = (\cdot)^{\cdot} + \hat{\mathbf{L}}_\mathrm{i}^\mathrm{T}(\cdot) + (\cdot)\hat{\mathbf{L}}_\mathrm{i}, \quad \overset{\diamond}{(\cdot)} = (\cdot)^{\cdot} + \check{\mathbf{L}}_\mathrm{ii}^\mathrm{T}(\cdot) + (\cdot)\check{\mathbf{L}}_\mathrm{ii}, \tag{2.13}$$
$$\hat{\mathbf{L}}_\mathrm{i} := \dot{\mathbf{F}}_\mathrm{i}\mathbf{F}_\mathrm{i}^{-1}, \quad \check{\mathbf{L}}_\mathrm{ii} := \dot{\mathbf{F}}_\mathrm{ii}\mathbf{F}_\mathrm{ii}^{-1}.$$

Relations (2.12) yield the inelastic deformation rates $\overset{\triangle}{\hat{\boldsymbol{\Gamma}}}_\mathrm{i}$ and $\overset{\diamond}{\check{\boldsymbol{\Gamma}}}_\mathrm{ii}$ as symmetric parts of $\hat{\mathbf{L}}_\mathrm{i}$ and $\check{\mathbf{L}}_\mathrm{ii}$, respectively:

$$\overset{\triangle}{\hat{\boldsymbol{\Gamma}}}_\mathrm{i} = \mathrm{sym}(\hat{\mathbf{L}}_\mathrm{i}), \quad \overset{\diamond}{\check{\boldsymbol{\Gamma}}}_\mathrm{ii} = \mathrm{sym}(\check{\mathbf{L}}_\mathrm{ii}), \tag{2.14}$$

where the symmetric part of a tensor is given by

$$\mathrm{sym}(\cdot) := \frac{1}{2}\Big((\cdot) + (\cdot)^\mathrm{T}\Big). \tag{2.15}$$

Let $\mathbf{T}$ be the Cauchy stress tensor. The weighted Cauchy tensor (or Kirchhoff stress tensor) is defined by

$$\mathbf{S} := (\det\mathbf{F})\mathbf{T}. \tag{2.16}$$

Now, we define the 2nd Piola-Kirchhoff tensors operating on $\hat{\mathcal{K}}$ and $\tilde{\mathcal{K}}$ using a contravariant pull-back of $\mathbf{S}$

$$\hat{\mathbf{S}} := \Big(\hat{\mathbf{F}}_\mathrm{e}^{-\mathrm{T}}\Big)^*\mathbf{S}, \quad \tilde{\mathbf{T}} := \Big(\mathbf{F}^{-\mathrm{T}}\Big)^*\mathbf{S} = \Big(\mathbf{F}_\mathrm{i}^{-\mathrm{T}}\Big)^*\hat{\mathbf{S}}. \tag{2.17}$$

The introduced stress and strain tensors form the following conjugate pairs: $(\mathbf{S}, \boldsymbol{\Gamma})$, $(\hat{\mathbf{S}}, \hat{\boldsymbol{\Gamma}})$, $(\tilde{\mathbf{T}}, \mathbf{E})$, such that the work and the stress power are invariant under the change of configuration:

$$\mathbf{S} : \boldsymbol{\Gamma} = \hat{\mathbf{S}} : \hat{\boldsymbol{\Gamma}} = \tilde{\mathbf{T}} : \mathbf{E}, \quad \hat{\mathbf{S}} : \overset{\triangle}{\hat{\boldsymbol{\Gamma}}} = \tilde{\mathbf{T}} : \dot{\mathbf{E}}. \tag{2.18}$$

Here ": " denotes the scalar product of two second-rank tensors

$$\mathbf{A} : \mathbf{B} \ := \mathrm{tr}(\mathbf{A} \cdot \mathbf{B}^\mathrm{T}). \tag{2.19}$$

Next, we denote by $\check{\mathbf{X}}$ the backstress tensor which operates on the intermediate configuration $\check{\mathcal{K}}$ of microstructure. This tensor can be interpreted as a generalized force, associated with strain measure $\check{\boldsymbol{\Gamma}}_\mathrm{i}$ and strain rate $\overset{\diamond}{\check{\boldsymbol{\Gamma}}}_\mathrm{i}$. According to the concept of dual variables, we define transformation rules for the backstress tensor, such that quantities $\check{\mathbf{X}} : \check{\mathbf{\Gamma}}_{\mathrm{i}}$ and $\check{\mathbf{X}} : \overset{\diamondsuit}{\check{\mathbf{\Gamma}}}_{\mathrm{i}}$ remain invariant under the change of configuration:

$$\tilde{\mathbf{X}} := \left(\mathbf{F}_{\mathrm{ii}}^{-\mathrm{T}}\right)^{*}\check{\mathbf{X}} = \mathbf{F}_{\mathrm{ii}}^{-1}\check{\mathbf{X}}\mathbf{F}_{\mathrm{ii}}^{-\mathrm{T}}, \quad \hat{\mathbf{X}} := \left(\check{\mathbf{F}}_{\mathrm{ie}}^{-\mathrm{T}}\right)_{*}\check{\mathbf{X}} = \check{\mathbf{F}}_{\mathrm{ie}}\check{\mathbf{X}}\check{\mathbf{F}}_{\mathrm{ie}}^{\mathrm{T}}, \tag{2.20}$$

$$\check{\mathbf{X}} : \check{\mathbf{\Gamma}}_{\mathrm{i}} = \hat{\mathbf{X}} : \hat{\mathbf{\Gamma}}_{\mathrm{i}} = \tilde{\mathbf{X}} : \tilde{\mathbf{\Gamma}}_{\mathrm{i}}, \quad \check{\mathbf{X}} : \overset{\diamondsuit}{\check{\mathbf{\Gamma}}}_{\mathrm{i}} = \hat{\mathbf{X}} : \overset{\triangle}{\hat{\mathbf{\Gamma}}}_{\mathrm{i}} = \tilde{\mathbf{X}} : \dot{\tilde{\mathbf{\Gamma}}}_{\mathrm{i}}. \tag{2.21}$$

The invariance relations (2.18) and (2.21) will be used in Section 2.4.

2.3. Free energy. The rheological model (fig. 2.1.a) motivates the additive split $\psi = \psi_{\mathrm{el}} + \psi_{\mathrm{kin}}$ of the stored energy into elastic part and a part, associated with the kinematic hardening.

In order to describe the energy storage due to the isotropic hardening, we introduce two real-valued internal variables of strain type: s and s_{d}. The first variable is the classical inelastic arc length, and s_{d} is interpreted as a dissipative part of s, such that

$$s_{\mathrm{e}} := s - s_{\mathrm{d}} \tag{2.22}$$

controls the energy storage associated with the isotropic hardening. Thus, we suppose that the free energy is given as a sum of isotropic functions (cf. [**24, 13**])

$$\psi = \psi(\hat{\mathbf{\Gamma}}_{\mathrm{e}}, \check{\mathbf{\Gamma}}_{\mathrm{ie}}, s_{\mathrm{e}}) = \psi_{\mathrm{el}}(\hat{\mathbf{\Gamma}}_{\mathrm{e}}) + \psi_{\mathrm{kin}}(\check{\mathbf{\Gamma}}_{\mathrm{ie}}) + \psi_{\mathrm{iso}}(s_{\mathrm{e}}), \tag{2.23}$$

where the tensors $\hat{\mathbf{\Gamma}}_{\mathrm{e}}$ and $\check{\mathbf{\Gamma}}_{\mathrm{ie}}$ are defined by $(2.9)_2$, $(2.11)_2$. Here, $\psi_{\mathrm{el}}(\hat{\mathbf{\Gamma}}_{\mathrm{e}})$ corresponds to the energy, stored due to macroscopic elastic deformations. The "inelastic" part $\psi_{\mathrm{kin}}(\check{\mathbf{\Gamma}}_{\mathrm{ie}}) + \psi_{\mathrm{iso}}(s_{\mathrm{e}})$ represents the energy, stored in the microstructure during the viscoplastic flow due to the heterogeneity of plastic deformation. The following special form of the free energy can be used (cf. [**13**])

$$\rho_{\mathrm{R}}\psi_{\mathrm{el}}(\hat{\mathbf{\Gamma}}_{\mathrm{e}}) = \frac{k}{2}\Big(\ln\sqrt{\det\hat{\mathbf{C}}_{\mathrm{e}}}\Big)^2 + \frac{\mu}{2}\Big(\mathrm{tr}\overline{\hat{\mathbf{C}}_{\mathrm{e}}} - 3\Big), \tag{2.24}$$

$$\rho_{\mathrm{R}}\psi_{\mathrm{kin}}(\check{\mathbf{\Gamma}}_{\mathrm{ie}}) = \frac{c}{4}\Big(\mathrm{tr}\overline{\check{\mathbf{C}}_{\mathrm{ie}}} - 3\Big), \quad \rho_{\mathrm{R}}\psi_{\mathrm{iso}}(s_{\mathrm{e}}) = \frac{\gamma}{2}\ (s_{\mathrm{e}})^2. \tag{2.25}$$

Here, $\rho_{\mathrm{R}} > 0$, $k > 0$, $\mu > 0$, $c > 0$, $\gamma \geq 0$ are material constants. The overline $\overline{(\cdot)}$ denotes the unimodular part of a tensor

$$\overline{\mathbf{A}} := (\det\mathbf{A})^{-1/3}\mathbf{A}\ . \tag{2.26}$$

Denote by $\dfrac{\partial\alpha(\mathbf{A})}{\partial\mathbf{A}}$ the derivative of a real-valued function α with respect to tensor-valued argument $\mathbf{A}$ such that

$$\alpha(\mathbf{A} + \Delta\mathbf{A}) - \alpha(\mathbf{A}) \underset{\Delta\mathbf{A}\to\mathbf{0}}{\approx} \frac{\partial\alpha(\mathbf{A})}{\partial\mathbf{A}} : \Delta\mathbf{A}. \tag{2.27}$$

Using this notation, we introduce formally the following potential relations for stresses $\hat{\mathbf{S}}$, $\check{\mathbf{X}}$ and for isotropic hardening R

$$\hat{\mathbf{S}} = \rho_{\mathrm{R}}\frac{\partial\psi_{\mathrm{el}}(\hat{\mathbf{\Gamma}}_{\mathrm{e}})}{\partial\hat{\mathbf{\Gamma}}_{\mathrm{e}}}, \quad \check{\mathbf{X}} = \rho_{\mathrm{R}}\frac{\partial\psi_{\mathrm{kin}}(\check{\mathbf{\Gamma}}_{\mathrm{ie}})}{\partial\check{\mathbf{\Gamma}}_{\mathrm{ie}}}, \quad R = \rho_{\mathrm{R}}\frac{\partial\psi_{\mathrm{iso}}(s_{\mathrm{e}})}{\partial s_{\mathrm{e}}}. \tag{2.28}$$

The physical meaning of these potential relations will be clear in subsequent sections. Namely, relations (2.28) in combination with evolution equations from Section 2.5 are sufficient to provide the thermodynamic consistency of the material response.

2.4. Clausius-Duhem inequality. The Clausius-Duhem inequality imposes an additional constraint on the material response, which states that the internal dissipation is always nonnegative. For isothermal processes the specific internal dissipation δ_{i} takes the form (see [**12**])

$$\delta_{\mathrm{i}} := \frac{1}{\rho_{\mathrm{R}}} \tilde{\mathbf{T}} : \dot{\mathbf{E}} - \dot{\psi} \geq 0. \tag{2.29}$$

Now, let us rewrite this expression, using relations of previous subsections. First, we note that $\hat{\mathbf{S}}$ and $\check{\mathbf{X}}$ are isotropic functions of $\hat{\mathbf{\Gamma}}_{\mathrm{e}}$ and $\check{\mathbf{\Gamma}}_{\mathrm{ie}}$, respectively. In particular, since $\hat{\mathbf{S}}$ and $\hat{\mathbf{\Gamma}}_{\mathrm{e}}$ commute, we have

$$\hat{\mathbf{S}} : \Big(\hat{\mathbf{L}}_{\mathrm{i}}^{\mathrm{T}} \hat{\mathbf{\Gamma}}_{\mathrm{e}} + \hat{\mathbf{\Gamma}}_{\mathrm{e}} \hat{\mathbf{L}}_{\mathrm{i}}\Big) \overset{(2.19)}{=} 2\Big(\hat{\mathbf{\Gamma}}_{\mathrm{e}} \hat{\mathbf{S}}\Big) : \hat{\mathbf{L}}_{\mathrm{i}} \overset{(2.14)_1}{=} 2\Big(\hat{\mathbf{\Gamma}}_{\mathrm{e}} \hat{\mathbf{S}}\Big) : \overset{\triangle}{\hat{\mathbf{\Gamma}}}_{\mathrm{i}}\, . \tag{2.30}$$

Further, note that

$$\hat{\mathbf{S}} : \overset{\triangle}{\hat{\mathbf{\Gamma}}} \overset{(2.8)}{=} \hat{\mathbf{S}} : \dot{\hat{\mathbf{\Gamma}}}_{\mathrm{e}} + \hat{\mathbf{S}} : \overset{\triangle}{\hat{\mathbf{\Gamma}}}_{\mathrm{i}} \overset{(2.13)_1}{=} \hat{\mathbf{S}} : \dot{\hat{\mathbf{\Gamma}}}_{\mathrm{e}} + \hat{\mathbf{S}} : \Big(\hat{\mathbf{L}}_{\mathrm{i}}^{\mathrm{T}} \hat{\mathbf{\Gamma}}_{\mathrm{e}} + \hat{\mathbf{\Gamma}}_{\mathrm{e}} \hat{\mathbf{L}}_{\mathrm{i}}\Big) + \hat{\mathbf{S}} : \overset{\triangle}{\hat{\mathbf{\Gamma}}}_{\mathrm{i}} \overset{(2.30)}{=} \hat{\mathbf{S}} : \dot{\hat{\mathbf{\Gamma}}}_{\mathrm{e}} + \Big(\hat{\mathbf{C}}_{\mathrm{e}} \hat{\mathbf{S}}\Big) : \overset{\triangle}{\hat{\mathbf{\Gamma}}}_{\mathrm{i}}\, . \tag{2.31}$$

In the same way, since $\check{\mathbf{X}}$ and $\check{\mathbf{\Gamma}}_{\mathrm{ie}}$ commute, we obtain from (2.10), $(2.13)_2$, $(2.14)_2$

$$\check{\mathbf{X}} : \overset{\diamond}{\check{\mathbf{\Gamma}}}_{\mathrm{i}} = \check{\mathbf{X}} : \dot{\check{\mathbf{\Gamma}}}_{\mathrm{ie}} + \Big(\check{\mathbf{C}}_{\mathrm{ie}} \check{\mathbf{X}}\Big) : \overset{\diamond}{\check{\mathbf{\Gamma}}}_{\mathrm{ii}}\, . \tag{2.32}$$

Thus, we obtain for the stress power

$$\begin{aligned} \hat{\mathbf{S}} : \overset{\triangle}{\hat{\mathbf{\Gamma}}} &\overset{(2.21)}{=} \hat{\mathbf{S}} : \overset{\triangle}{\hat{\mathbf{\Gamma}}} - \hat{\mathbf{X}} : \overset{\triangle}{\hat{\mathbf{\Gamma}}}_{\mathrm{i}} + \check{\mathbf{X}} : \overset{\diamond}{\check{\mathbf{\Gamma}}}_{\mathrm{i}} \\ &\overset{(2.31),(2.32)}{=} \hat{\mathbf{S}} : \dot{\hat{\mathbf{\Gamma}}}_{\mathrm{e}} + \Big(\hat{\mathbf{C}}_{\mathrm{e}} \hat{\mathbf{S}} - \hat{\mathbf{X}}\Big) : \overset{\triangle}{\hat{\mathbf{\Gamma}}}_{\mathrm{i}} + \check{\mathbf{X}} : \dot{\check{\mathbf{\Gamma}}}_{\mathrm{ie}} + \Big(\check{\mathbf{C}}_{\mathrm{ie}} \check{\mathbf{X}}\Big) : \overset{\diamond}{\check{\mathbf{\Gamma}}}_{\mathrm{ii}}\, . \end{aligned} \tag{2.33}$$

Hence, the internal dissipation takes the form

$$\begin{aligned} \delta_{\mathrm{i}} = \frac{1}{\rho_{\mathrm{R}}} \tilde{\mathbf{T}} : \dot{\mathbf{E}} - \dot{\psi} \overset{(2.18)_2}{=} \frac{1}{\rho_{\mathrm{R}}} \hat{\mathbf{S}} : \overset{\triangle}{\hat{\mathbf{\Gamma}}} - \dot{\psi} &\overset{(2.33)}{=} \Big(\frac{1}{\rho_{\mathrm{R}}} \hat{\mathbf{S}} - \frac{\partial \psi_{\mathrm{el}}}{\partial \hat{\mathbf{\Gamma}}_{\mathrm{e}}}\Big) : \dot{\hat{\mathbf{\Gamma}}}_{\mathrm{e}} + \Big(\frac{1}{\rho_{\mathrm{R}}} \check{\mathbf{X}} - \frac{\partial \psi_{\mathrm{kin}}}{\partial \check{\mathbf{\Gamma}}_{\mathrm{ie}}}\Big) : \dot{\check{\mathbf{\Gamma}}}_{\mathrm{ie}} \\ &+ \frac{1}{\rho_{\mathrm{R}}} \Big(\hat{\mathbf{C}}_{\mathrm{e}} \hat{\mathbf{S}} - \hat{\mathbf{X}}\Big) : \overset{\triangle}{\hat{\mathbf{\Gamma}}}_{\mathrm{i}} + \frac{1}{\rho_{\mathrm{R}}} \Big(\check{\mathbf{C}}_{\mathrm{ie}} \check{\mathbf{X}}\Big) : \overset{\diamond}{\check{\mathbf{\Gamma}}}_{\mathrm{ii}} - \frac{\partial \psi_{\mathrm{iso}}}{\partial s_{\mathrm{e}}}\, \dot{s}_{\mathrm{e}}. \end{aligned} \tag{2.34}$$

We abbreviate

$$\hat{\mathbf{\Sigma}} := \hat{\mathbf{C}}_{\mathrm{e}} \hat{\mathbf{S}} - \hat{\mathbf{X}}, \quad \check{\mathbf{\Xi}} := \check{\mathbf{C}}_{\mathrm{ie}} \check{\mathbf{X}}. \tag{2.35}$$

Finally, taking into account potential relations (2.28) and definition (2.22), we simplify (2.34) to obtain the Clausius-Duhem inequality in the form [5]

$$\rho_{\mathrm{R}} \delta_{\mathrm{i}} = \Big(\hat{\mathbf{\Sigma}} : \overset{\triangle}{\hat{\mathbf{\Gamma}}}_{\mathrm{i}} - R\, \dot{s}\Big) + \check{\mathbf{\Xi}} : \overset{\diamond}{\check{\mathbf{\Gamma}}}_{\mathrm{ii}} + R\, \dot{s}_{\mathrm{d}} \geq 0. \tag{2.36}$$

---

[5] In the case of kinematic hardening only ($R = 0$), the terms from the left-hand side of (2.36) have a simple rheological interpretation using fig. 2.1.b: the quantities $\hat{\mathbf{\Sigma}} : \overset{\triangle}{\hat{\mathbf{\Gamma}}}_{\mathrm{i}}$ and $\check{\mathbf{\Xi}} : \overset{\diamond}{\check{\mathbf{\Gamma}}}_{\mathrm{ii}}$ correspond to the energy dissipation in the friction element and in the viscoplastic element, respectively. The quantity $R\dot{s}_{\mathrm{d}} - R\dot{s}$ corresponds to the energy dissipation associated with the isotropic hardening.

2.5. Evolution equations. Following the standard procedure, we formulate the evolution equations for internal variables so that inequality (2.36) holds for arbitrary mechanical loadings (cf. [**24, 13**])

$$\overset{\triangle}{\hat{\mathbf{\Gamma}}}_{\mathrm{i}} := \lambda_{\mathrm{i}} \frac{\hat{\mathbf{\Sigma}}^{\mathrm{D}}}{\|\hat{\mathbf{\Sigma}}^{\mathrm{D}}\|}, \quad \overset{\diamond}{\check{\mathbf{\Gamma}}}_{\mathrm{ii}} := \lambda_{\mathrm{i}}\, \varkappa\, \check{\mathbf{\Xi}}^{\mathrm{D}}, \tag{2.37}$$

$$\dot{s} := \sqrt{\frac{2}{3}} \lambda_{\mathrm{i}}, \quad \dot{s}_{\mathrm{d}} := \frac{\beta}{\gamma} \dot{s} R,$$

$$\|\mathbf{A}\| := \sqrt{\mathbf{A} : \mathbf{A}}, \quad \mathbf{A}^{\mathrm{D}} := \mathbf{A} - \frac{1}{3} \mathrm{tr}(\mathbf{A}) \mathbf{1}, \tag{2.38}$$

where the inelastic multiplier λ_{i} is determined according to the Perzyna rule [**32**]

$$\lambda_{\mathrm{i}} := \frac{1}{\eta} \Big\langle \frac{1}{k_0} f \Big\rangle^{m}, \quad f := \|\hat{\mathbf{\Sigma}}^{\mathrm{D}}\| - \sqrt{\frac{2}{3}} \big[K + R \big], \quad \langle x \rangle := \max(x, 0). \tag{2.39}$$

Here, $\varkappa \geq 0$, $\eta \geq 0$, $m \geq 1$, $\beta \geq 0$, $K > 0$ are material parameters, $k_0 > 0$ is used to obtain a dimensionless term in the bracket.

Let us show that inequality (2.36) is fulfilled. For instance, we prove that the parenthetical term in (2.36) is nonnegative. Indeed,

$$\Big(\hat{\mathbf{\Sigma}} : \overset{\triangle}{\hat{\mathbf{\Gamma}}}_{\mathrm{i}} - R\, \dot{s} \Big) = \lambda_{\mathrm{i}} \Big(\|\hat{\mathbf{\Sigma}}^{\mathrm{D}}\| - \sqrt{\frac{2}{3}} R \Big) = \begin{cases} 0 & \text{if } \ f < 0 \ (\lambda_{\mathrm{i}} = 0) \\ \lambda_{\mathrm{i}} (f + \sqrt{\frac{2}{3}} K) & \text{if } \ f > 0 \ (\lambda_{\mathrm{i}} > 0) \end{cases} .$$

Therefore, the material model, defined in Sections 2.3 and 2.5, is *thermodynamically consistent.*

According to the evolution equations (2.37), the tensors $\hat{\mathbf{\Sigma}}^{\mathrm{D}}$ and $\check{\mathbf{\Xi}}^{\mathrm{D}}$ are termed *the driving force for inelastic flow* and *the driving force for inelastic flow of microstructure*, respectively. Note that both flows are incompressible. In fact,

$$(\mathrm{det} \mathbf{F}_{\mathrm{i}})^{\cdot} = (\mathrm{det} \mathbf{F}_{\mathrm{i}}) \ \mathrm{tr} \Big(\overset{\triangle}{\hat{\mathbf{\Gamma}}}_{\mathrm{i}} \Big) = 0, \quad (\mathrm{det} \mathbf{F}_{\mathrm{ii}})^{\cdot} = (\mathrm{det} \mathbf{F}_{\mathrm{ii}}) \ \mathrm{tr} \Big(\overset{\diamond}{\check{\mathbf{\Gamma}}}_{\mathrm{ii}} \Big) = 0. \tag{2.40}$$

Under appropriate initial conditions, it follows from (2.40) that

$$\mathrm{det} \mathbf{F}_{\mathrm{i}} = \mathrm{det} \mathbf{F}_{\mathrm{ii}} = \mathrm{det} \mathbf{C}_{\mathrm{i}} = \mathrm{det} \mathbf{C}_{\mathrm{ii}} = 1. \tag{2.41}$$

The inelastic flow takes place if the overstress f is positive. A case of rate-independent plasticity is covered by these evolution equations as viscosity η tends to zero.

2.6. Transformation to the reference configuration. A direct numerical treatment of Oldroyd derivatives in (2.37), formulated with respect to fictitious configurations $\hat{\mathcal{K}}$ and $\check{\mathcal{K}}$, is complicated. In this subsection we rewrite the material model in terms of strain-like internal variables $\mathbf{C}_{\mathrm{i}}$, $\mathbf{C}_{\mathrm{ii}}$, s, s_{d} such that the rate of $\mathbf{C}_{\mathrm{i}}$, $\mathbf{C}_{\mathrm{ii}}$ will be given by the material time derivatives $\dot{\mathbf{C}}_{\mathrm{i}}$, $\dot{\mathbf{C}}_{\mathrm{ii}}$. The transformation of the model includes:

- representation of the free energy ψ through $\mathbf{C}, \mathbf{C}_{\mathrm{i}}, \mathbf{C}_{\mathrm{ii}}, s, s_{\mathrm{d}}$.
- transformation of the potential relations for stresses.
- representation of $\|\hat{\mathbf{\Sigma}}^{\mathrm{D}}\|$ through $\mathbf{C}, \mathbf{C}_{\mathrm{i}}, \mathbf{C}_{\mathrm{ii}}$.
- transformation of the evolution equations.

2.6.1. *Representation of the free energy.* Let (J_1, J_2, J_3) be a full system of invariants of a second-rank tensor, defined by

$$J_1(\mathbf{A}) := \mathrm{tr}\ \mathbf{A}, \quad J_2(\mathbf{A}) := \frac{1}{2}\mathrm{tr}\ \mathbf{A}^2, \quad J_3(\mathbf{A}) := \frac{1}{3}\mathrm{tr}\ \mathbf{A}^3.$$

Then, using multiplicative decompositions (2.1), (2.2) and the property $\mathrm{tr}(\mathbf{AB}) = \mathrm{tr}(\mathbf{BA})$, it is easily proved that

$$J_k(\hat{\mathbf{C}}_{\mathrm{e}}) = J_k(\mathbf{C}{\mathbf{C}_{\mathrm{i}}}^{-1}), \quad J_k(\check{\mathbf{C}}_{\mathrm{ie}}) = J_k(\mathbf{C}_{\mathrm{i}}{\mathbf{C}_{\mathrm{ii}}}^{-1}), \quad k = 1, 2, 3. \tag{2.42}$$

Since ψ_{el} and ψ_{kin} are isotropic functions, it follows from (2.23), (2.42) that

$$\psi = \psi(\mathbf{C}, \mathbf{C}_{\mathrm{i}}, \mathbf{C}_{\mathrm{ii}}, s, s_{\mathrm{d}}) = \psi_{\mathrm{el}}(\mathbf{C}{\mathbf{C}_{\mathrm{i}}}^{-1}) + \psi_{\mathrm{kin}}(\mathbf{C}_{\mathrm{i}}{\mathbf{C}_{\mathrm{ii}}}^{-1}) + \psi_{\mathrm{iso}}(s - s_{\mathrm{d}}).$$

2.6.2. *Transformation of the potential relations for stresses.* Now we want to rewrite the potential relations $(2.28)_1$, $(2.28)_2$ in terms of tensors, which operate on the reference configuration $\mathcal{K}$. Recall that the following general relation holds (cf. equation (9.60) in [**12**])

$$\mathbf{A}^{\mathrm{T}} \frac{\partial \alpha(\mathbf{ABA}^{\mathrm{T}})}{\partial (\mathbf{ABA}^{\mathrm{T}})} \mathbf{A} = \frac{\partial \alpha(\mathbf{ABA}^{\mathrm{T}})}{\partial \mathbf{B}}\Big|_{\mathbf{A}=\mathrm{const}}. \tag{2.43}$$

In order to apply this relation, note that

$$\tilde{\mathbf{T}} \overset{(2.17)_2,(2.28)_1}{=} 2\rho_{\mathrm{R}} \mathbf{F}_{\mathrm{i}}^{-1} \frac{\partial \psi_{\mathrm{el}}(\hat{\mathbf{C}}_{\mathrm{e}})}{\partial \hat{\mathbf{C}}_{\mathrm{e}}} \mathbf{F}_{\mathrm{i}}^{-\mathrm{T}}, \quad \tilde{\mathbf{X}} \overset{(2.20)_1,(2.28)_2}{=} 2\rho_{\mathrm{R}} \mathbf{F}_{\mathrm{ii}}^{-1} \frac{\partial \psi_{\mathrm{kin}}(\check{\mathbf{C}}_{\mathrm{ie}})}{\partial \check{\mathbf{C}}_{\mathrm{ie}}} \mathbf{F}_{\mathrm{ii}}^{-\mathrm{T}}.$$

Moreover, it follows from $(2.6)_1$, (2.7) that

$$\hat{\mathbf{C}}_{\mathrm{e}} = \mathbf{F}_{\mathrm{i}}^{-\mathrm{T}} \mathbf{C} \mathbf{F}_{\mathrm{i}}^{-1}, \quad \check{\mathbf{C}}_{\mathrm{ie}} = \mathbf{F}_{\mathrm{ii}}^{-\mathrm{T}} \mathbf{C}_{\mathrm{i}} \mathbf{F}_{\mathrm{ii}}^{-1}.$$

Substituting $\mathbf{F}_{\mathrm{i}}^{-\mathrm{T}}, \mathbf{C}, \hat{\mathbf{C}}_{\mathrm{e}}$ and $\mathbf{F}_{\mathrm{ii}}^{-\mathrm{T}}, \mathbf{C}_{\mathrm{i}}, \check{\mathbf{C}}_{\mathrm{ie}}$ for $\mathbf{A}, \mathbf{B}, \mathbf{ABA}^{\mathrm{T}}$ in (2.43), we obtain

$$\tilde{\mathbf{T}} = 2\rho_{\mathrm{R}} \frac{\partial \psi_{\mathrm{el}}(\mathbf{C}{\mathbf{C}_{\mathrm{i}}}^{-1})}{\partial \mathbf{C}}\Big|_{\mathbf{C}_{\mathrm{i}}=\mathrm{const}}, \quad \tilde{\mathbf{X}} = 2\rho_{\mathrm{R}} \frac{\partial \psi_{\mathrm{kin}}(\mathbf{C}_{\mathrm{i}}{\mathbf{C}_{\mathrm{ii}}}^{-1})}{\partial \mathbf{C}_{\mathrm{i}}}\Big|_{\mathbf{C}_{\mathrm{ii}}=\mathrm{const}}. \tag{2.44}$$

Now let us show that $\mathbf{C}\tilde{\mathbf{T}}$ and $\mathbf{C}_{\mathrm{i}}\tilde{\mathbf{X}}$ are isotropic functions of $\mathbf{C}{\mathbf{C}_{\mathrm{i}}}^{-1}$ and $\mathbf{C}_{\mathrm{i}}{\mathbf{C}_{\mathrm{ii}}}^{-1}$, respectively. Toward this end we note that

$$\frac{\partial \alpha(\mathbf{AB}^{-1})}{\partial \mathbf{A}}\Big|_{\mathbf{B}=\mathrm{const}} = \frac{\partial \alpha(\mathbf{AB}^{-1})}{\partial (\mathbf{AB}^{-1})} \mathbf{B}^{-\mathrm{T}}, \quad \frac{\partial J_k(\mathbf{A})}{\partial \mathbf{A}} = (\mathbf{A}^{\mathrm{T}})^{k-1}, \quad k = 1, 2, 3. \tag{2.45}$$

Combining (2.44) and (2.45), we arrive at

$$\mathbf{C}\tilde{\mathbf{T}} = 2\rho_{\mathrm{R}} \sum_{k=1}^{3} \frac{\partial \psi_{\mathrm{el}}}{\partial J_k(\mathbf{C}{\mathbf{C}_{\mathrm{i}}}^{-1})} (\mathbf{C}{\mathbf{C}_{\mathrm{i}}}^{-1})^k, \quad \mathbf{C}_{\mathrm{i}}\tilde{\mathbf{X}} = 2\rho_{\mathrm{R}} \sum_{k=1}^{3} \frac{\partial \psi_{\mathrm{kin}}}{\partial J_k(\mathbf{C}_{\mathrm{i}}{\mathbf{C}_{\mathrm{ii}}}^{-1})} (\mathbf{C}_{\mathrm{i}}{\mathbf{C}_{\mathrm{ii}}}^{-1})^k.$$

If the special form (2.24), (2.25) of the free energy is used, then, taking into account incompressibility relations (2.41), we obtain

$$\tilde{\mathbf{T}} = k\ \ln \sqrt{\det(\mathbf{C})}\ \mathbf{C}^{-1} + \mu\ \mathbf{C}^{-1}(\overline{\mathbf{C}}\mathbf{C}_{\mathrm{i}}^{-1})^{\mathrm{D}}, \qquad \tilde{\mathbf{X}} = \frac{c}{2}\ \mathbf{C}_{\mathrm{i}}^{-1}(\mathbf{C}_{\mathrm{i}}\mathbf{C}_{\mathrm{ii}}^{-1})^{\mathrm{D}}. \tag{2.46}$$

Table 2.1. Summary of the material model

$$\boxed{\begin{array}{ll}
\dot{\mathbf{C}}_{\rm i} = 2\frac{\lambda_{\rm i}}{\mathfrak{F}}\Big(\mathbf{C}\tilde{\mathbf{T}} - \mathbf{C}_{\rm i}\tilde{\mathbf{X}}\Big)^{\rm D}\mathbf{C}_{\rm i}, & \mathbf{C}_{\rm i}|_{t=0} = \mathbf{C}^0_{\rm i},\ \det \mathbf{C}^0_{\rm i} = 1, \\
\dot{\mathbf{C}}_{\rm ii} = 2\lambda_{\rm i}\varkappa(\mathbf{C}_{\rm i}\tilde{\mathbf{X}}\Big)^{\rm D}\mathbf{C}_{\rm ii}, & \mathbf{C}_{\rm ii}|_{t=0} = \mathbf{C}^0_{\rm ii},\ \det \mathbf{C}^0_{\rm ii} = 1, \\
\dot{s} := \sqrt{\frac{2}{3}}\lambda_{\rm i}, \quad \dot{s}_{\rm d} := \frac{\beta}{\gamma}\dot{s}R, & s|_{t=0} = s^0,\ s_{\rm d}|_{t=0} = s^0_{\rm d}, \\
\tilde{\mathbf{T}} = 2\rho_{\rm R}\frac{\partial\psi_{\rm el}(\mathbf{C}{\mathbf{C}_{\rm i}}^{-1})}{\partial\mathbf{C}}\Big|_{\mathbf{C}_{\rm i}=\rm const}, & \tilde{\mathbf{X}} = 2\rho_{\rm R}\frac{\partial\psi_{\rm kin}(\mathbf{C}_{\rm i}{\mathbf{C}_{\rm ii}}^{-1})}{\partial\mathbf{C}_{\rm i}}\Big|_{\mathbf{C}_{\rm ii}=\rm const}, \\
R = \gamma s_{\rm e}, \quad s_{\rm e} = s - s_{\rm d}, & \\
\lambda_{\rm i} := \frac{1}{\eta}\Big\langle\frac{1}{k_0}f\Big\rangle^m, \quad f = \mathfrak{F} - \sqrt{\frac{2}{3}}\Big[K + R\Big], & \mathfrak{F} = \sqrt{\mathrm{tr}\Big[\Big(\mathbf{C}\tilde{\mathbf{T}} - \mathbf{C}_{\rm i}\tilde{\mathbf{X}}\Big)^{\rm D}\Big]^2}.
\end{array}}$$

2.6.3. *Representation of* $\|\hat{\mathbf{\Sigma}}^D\|$. First, let us note that

$$\mathrm{tr}\hat{\mathbf{\Sigma}} = \mathrm{tr}(\hat{\mathbf{C}}_{\rm e}\hat{\mathbf{S}} - \hat{\mathbf{X}}) = \mathrm{tr}(\mathbf{C}\tilde{\mathbf{T}} - \mathbf{C}_{\rm i}\tilde{\mathbf{X}}). \tag{2.47}$$

Moreover, we have

$$\|\hat{\mathbf{\Sigma}}^{\rm D}\|^2 = \hat{\mathbf{\Sigma}}^{\rm D} : \hat{\mathbf{\Sigma}}^{\rm D} = \Big[\Big(\mathbf{F}_{\rm i}^{-\rm T}\Big)^*\hat{\mathbf{\Sigma}}^{\rm D}\Big] : \Big[\Big(\mathbf{F}_{\rm i}\Big)^*\hat{\mathbf{\Sigma}}^{\rm D}\Big]. \tag{2.48}$$

Thus, since $\hat{\mathbf{\Sigma}}^{\rm D} \in Sym$, we obtain

$$\|\hat{\mathbf{\Sigma}}^{\rm D}\|^2 = \mathrm{tr}\Big\{\Big[\Big(\mathbf{F}_{\rm i}^{-\rm T}\Big)^*\hat{\mathbf{\Sigma}}^{\rm D}\Big]\Big[\Big(\mathbf{F}_{\rm i}\Big)^*\hat{\mathbf{\Sigma}}^{\rm D}\Big]\Big\}. \tag{2.49}$$

In order to use this relation, we compute the inelastic contravariant and covariant pull-back of $\hat{\mathbf{\Sigma}}^{\rm D}$

$$\Big(\mathbf{F}_{\rm i}^{-\rm T}\Big)^*\hat{\mathbf{\Sigma}}^{\rm D} = \mathbf{C}_{\rm i}^{-1}\mathbf{C}\tilde{\mathbf{T}} - \tilde{\mathbf{X}} - \mathrm{tr}\hat{\mathbf{\Sigma}}\ \mathbf{C}_{\rm i}^{-1} \overset{(2.47)}{=} \mathbf{C}_{\rm i}^{-1}\Big(\mathbf{C}\tilde{\mathbf{T}} - \mathbf{C}_{\rm i}\tilde{\mathbf{X}}\Big)^{\rm D}, \tag{2.50}$$

$$\Big(\mathbf{F}_{\rm i}\Big)^*\hat{\mathbf{\Sigma}}^{\rm D} = \mathbf{C}\tilde{\mathbf{T}}\mathbf{C}_{\rm i} - \mathbf{C}_{\rm i}\tilde{\mathbf{X}}\mathbf{C}_{\rm i} - \mathrm{tr}\hat{\mathbf{\Sigma}}\ \mathbf{C}_{\rm i} \overset{(2.47)}{=} \Big(\mathbf{C}\tilde{\mathbf{T}} - \mathbf{C}_{\rm i}\tilde{\mathbf{X}}\Big)^{\rm D}\mathbf{C}_{\rm i}. \tag{2.51}$$

Substituting (2.50) and (2.51) in (2.49) we obtain the norm of the driving force

$$\mathfrak{F} := \|\hat{\mathbf{\Sigma}}^{\rm D}\| = \sqrt{\mathrm{tr}\Big[\Big(\mathbf{C}\tilde{\mathbf{T}} - \mathbf{C}_{\rm i}\tilde{\mathbf{X}}\Big)^{\rm D}\Big]^2}. \tag{2.52}$$

2.6.4. *Transformation of the evolution equations.* Note that

$$\mathrm{tr}\ \check{\mathbf{\Xi}} = \mathrm{tr}\ (\check{\mathbf{C}}_{\rm ie}\check{\mathbf{X}}) = \mathrm{tr}(\mathbf{C}_{\rm i}\tilde{\mathbf{X}}). \tag{2.53}$$

Next, we compute the covariant pull-back of $\check{\mathbf{\Xi}}^{\rm D}$:

$$\Big(\mathbf{F}_{\rm ii}\Big)^*\check{\mathbf{\Xi}}^{\rm D} \overset{(2.53)}{=} \Big(\mathbf{C}_{\rm i}\tilde{\mathbf{X}}\Big)^{\rm D}\mathbf{C}_{\rm ii}. \tag{2.54}$$

Covariant pull-back of (2.37) yields

$$\dot{\mathbf{C}}_{\rm i} = 2\Big(\mathbf{F}_{\rm i}\Big)^*\overset{\triangle}{\hat{\mathbf{\Gamma}}}_{\rm i} \overset{(2.37)}{=} 2\frac{\lambda_{\rm i}}{\mathfrak{F}}\Big(\mathbf{F}_{\rm i}\Big)^*\hat{\mathbf{\Sigma}}^{\rm D}, \quad \dot{\mathbf{C}}_{\rm ii} = 2\Big(\mathbf{F}_{\rm ii}\Big)^*\overset{\diamond}{\check{\mathbf{\Gamma}}}_{\rm ii} \overset{(2.37)}{=} 2\lambda_{\rm i}\varkappa\Big(\mathbf{F}_{\rm ii}\Big)^*\check{\mathbf{\Xi}}^{\rm D}.$$

Combining this with (2.51) and (2.54), we obtain

$$\dot{\mathbf{C}}_{\rm i} = 2\frac{\lambda_{\rm i}}{\mathfrak{F}}\Big(\mathbf{C}\tilde{\mathbf{T}} - \mathbf{C}_{\rm i}\tilde{\mathbf{X}}\Big)^{\rm D}\mathbf{C}_{\rm i}, \quad \dot{\mathbf{C}}_{\rm ii} = 2\lambda_{\rm i}\varkappa\Big(\mathbf{C}_{\rm i}\tilde{\mathbf{X}}\Big)^{\rm D}\mathbf{C}_{\rm ii}. \tag{2.55}$$

The material model is summarized in table 2.1.

3. Integration algorithms

The exact solution of (2.55) has under proper initial conditions the following geometric property: $\mathbf{C}_{\mathrm{i}}, \mathbf{C}_{\mathrm{ii}}$ lie on the manifold $\mathbb{M}$, defined by

$$\mathbb{M} := \Big\{ \mathbf{B} \in Sym : \det\mathbf{B} = 1 \Big\}. \tag{2.56}$$

Hence, system (2.55) is a *system of differential equations on the manifold* (cf. the paper [**9**]). In this section we analyze two numerical schemes, such that the numerical solution lies exactly on $\mathbb{M}$.

3.1. Modified Euler-Backward and exponential scheme. Consider the Cauchy problem for a system of nonlinear ordinary differential equations

$$\dot{\mathbf{A}}(t) = \mathbf{f}(\mathbf{A}(t), t)\mathbf{A}(t), \quad \mathbf{A}(0) = \mathbf{A}^0, \quad \det(\mathbf{A}^0) = 1.$$

Suppose that the tensor-valued function $\mathbf{f}$ is sufficiently smooth, $\mathrm{tr}(\mathbf{f}(\mathbf{A}, t)) = 0$ and

$$\Big(\mathbf{f}(\mathbf{A}, t)\Big)^k \mathbf{A} \in Sym \quad \text{for all } \mathbf{A} \in Sym, \ k = 1, 2, 3, \dots \, . \tag{2.57}$$

Under such conditions the exact solution lies on $\mathbb{M}$.

Remark 1. Assumption (2.57) is nontrivial, since $\mathbf{f}(\mathbf{A}, t)$ is in general an anisotropic function of $\mathbf{A}$.

By ${}^n\mathbf{A}, {}^{n+1}\mathbf{A}$ denote numerical solutions respectively at t_n and t_{n+1}, $\Delta t := t_{n+1} - t_n$. Suppose that ${}^n\mathbf{A} \in \mathbb{M}$ is given. The classical Euler-Backward method (EBM) uses the equation with respect to the unknown ${}^{n+1}\mathbf{A}$:

$${}^{n+1}\mathbf{A} = \Big[\mathbf{1} - \Delta t \ \mathbf{f}({}^{n+1}\mathbf{A}, t_{n+1})\Big]^{-1} \, {}^n\mathbf{A}. \tag{2.58}$$

Recall that for small $\mathbf{B}$ [6]

$$\Big[\mathbf{1} - \mathbf{B}\Big]^{-1} = \mathbf{1} + \mathbf{B} + \mathbf{B}^2 + \mathbf{B}^3 + \dots \, . \tag{2.59}$$

The exponential method (EM) is based on the equation

$${}^{n+1}\mathbf{A} = \exp\Big(\Delta t \ \mathbf{f}({}^{n+1}\mathbf{A}, t_{n+1})\Big) \, {}^n\mathbf{A}, \tag{2.60}$$

where the tensor exponential is given by

$$\exp\Big(\mathbf{B}\Big) := \mathbf{1} + \mathbf{B} + \frac{1}{2!}\mathbf{B}^2 + \frac{1}{3!}\mathbf{B}^3 + \dots \, . \tag{2.61}$$

Let us show that *both methods yield a symmetric solution* ${}^{n+1}\mathbf{A}$ if assumption (2.57) is fulfilled. The idea of the proof is as follows. Substituting (2.59) for $\Big[\mathbf{1} - \Delta t \ \mathbf{f}({}^{n+1}\mathbf{A}, t_{n+1})\Big]^{-1}$ in (2.58), and (2.61) for $\exp\Big(\Delta t \ \mathbf{f}({}^{n+1}\mathbf{A}, t_{n+1})\Big)$ in (2.60), we have for both methods

$${}^{n+1}\mathbf{A} = \mathbf{K}({}^{n+1}\mathbf{A}), \tag{2.62}$$

$$\mathbf{K}(\mathbf{B}) := \Big(\mathbf{1} + \Delta t \ \mathbf{f}(\mathbf{B}, t_{n+1}) + \sum_{k=2}^{\infty} c_k \Big(\mathbf{f}(\mathbf{B}, t_{n+1})\Big)^k\Big) \, {}^n\mathbf{A}, \tag{2.63}$$

with some coefficients c_k. Next, let us consider an auxiliary problem

$$\mathbf{A}_{\mathrm{aux}} = \mathrm{sym}(\mathbf{K}(\mathbf{A}_{\mathrm{aux}})). \tag{2.64}$$

---

[6] The Neumann series (2.59) converges if $\|\mathbf{B}\|^* < 1$.

Here, the symmetrization operator $\mathrm{sym}(\cdot) = \frac{1}{2}\Big((\cdot)+(\cdot)^{\mathrm{T}}\Big)$ is used. Suppose $\mathbf{A}_{\mathrm{aux}}$ is a solution of (2.64). According to assumption (2.57), since $\mathbf{A}_{\mathrm{aux}}$ is symmetric, we obtain

$$\mathbf{A}_{\mathrm{aux}} \ {}^{n}\mathbf{A}^{-1} \ \mathbf{A}_{\mathrm{aux}} \in Sym, \quad \mathbf{K}(\mathbf{A}_{\mathrm{aux}}) \ {}^{n}\mathbf{A}^{-1} \ \mathbf{A}_{\mathrm{aux}} \in Sym. \tag{2.65}$$

Subtracting $(2.65)_1$ from $(2.65)_2$ and taking (2.64) into account, we arrive at

$$\mathrm{skew}\Big(\mathbf{K}(\mathbf{A}_{\mathrm{aux}})\Big) \ {}^{n}\mathbf{A}^{-1} \ \mathbf{A}_{\mathrm{aux}} \in Sym, \quad \mathrm{skew}(\cdot) := (\cdot) - \mathrm{sym}(\cdot). \tag{2.66}$$

Here skew$(\cdot)$ stands for the skew-symmetric part of a tensor. Thus, $(2.66)_1$ yields

$$\mathrm{skew}\Big(\mathrm{skew}\Big(\mathbf{K}(\mathbf{A}_{\mathrm{aux}})\Big) \ {}^{n}\mathbf{A}^{-1} \ \mathbf{A}_{\mathrm{aux}}\Big) = \mathbf{0}. \tag{2.67}$$

Adding $\mathrm{skew}\Big(\mathrm{skew}\Big(\mathbf{K}(\mathbf{A}_{\mathrm{aux}})\Big) \ \Big(\mathbf{1} - {}^{n}\mathbf{A}^{-1} \ \mathbf{A}_{\mathrm{aux}}\Big)\Big)$ to both sides of (2.67) and noting that skew skew$(\cdot)$ = skew$(\cdot)$, we obtain

$$\mathrm{skew}\Big(\mathbf{K}(\mathbf{A}_{\mathrm{aux}})\Big) = \mathrm{skew}\Big(\mathrm{skew}\Big(\mathbf{K}(\mathbf{A}_{\mathrm{aux}})\Big) \ \Big(\mathbf{1} - {}^{n}\mathbf{A}^{-1} \ \mathbf{A}_{\mathrm{aux}}\Big)\Big). \tag{2.68}$$

Denote by $\| \cdot \|^{*}$ the induced norm of a tensor

$$\|\mathbf{B}\|^{*} := \max_{\|\mathbf{x}\|_2=1} \|\mathbf{B}\mathbf{x}\|_2, \quad \|\mathbf{x}\|_2 := \sqrt{x_1^2 + x_2^2 + x_3^2}. \tag{2.69}$$

Then, for any tensors $\mathbf{B}_1$, $\mathbf{B}_2$ and $\mathbf{B}$

$$\|\mathbf{B}_1\mathbf{B}_2\|^{*} \leq \|\mathbf{B}_1\|^{*}\|\mathbf{B}_2\|^{*}, \quad \|\mathrm{skew}(\mathbf{B})\|^{*} \leq \|\mathbf{B}\|^{*}. \tag{2.70}$$

Note also that for small Δt

$$\|\mathbf{1} - {}^{n}\mathbf{A}^{-1} \ \mathbf{A}_{\mathrm{aux}}\|^{*} \leq \frac{1}{2}. \tag{2.71}$$

Taking the norm of both sides of (2.68) and using (2.70), (2.71), we have

$$\begin{aligned} \|\mathrm{skew}\Big(\mathbf{K}(\mathbf{A}_{\mathrm{aux}})\Big)\|^{*} &\overset{(2.68),(2.70)_2}{\leq} \Big\|\mathrm{skew}\Big(\mathbf{K}(\mathbf{A}_{\mathrm{aux}})\Big) \ \Big(\mathbf{1} - {}^{n}\mathbf{A}^{-1} \ \mathbf{A}_{\mathrm{aux}}\Big)\Big\|^{*} \\ &\overset{(2.70)_1}{\leq} \|\mathrm{skew}\Big(\mathbf{K}(\mathbf{A}_{\mathrm{aux}})\Big)\|^{*} \ \|\mathbf{1} - {}^{n}\mathbf{A}^{-1} \ \mathbf{A}_{\mathrm{aux}}\|^{*} \overset{(2.71)}{\leq} \frac{1}{2}\|\mathrm{skew}\Big(\mathbf{K}(\mathbf{A}_{\mathrm{aux}})\Big)\|^{*}. \end{aligned}$$

This implies that $\|\mathrm{skew}\Big(\mathbf{K}(\mathbf{A}_{\mathrm{aux}})\Big)\|^{*} = 0$. Therefore, $\mathbf{K}(\mathbf{A}_{\mathrm{aux}}) \in Sym$ and $\mathbf{A}_{\mathrm{aux}}$ is a solution of (2.62). In other words, equations (2.62) and (2.64) are *equivalent*. ■

This means that *no modifications of* (2.58) *and* (2.60) *are necessary* to ensure the symmetry of the solution ${}^{n+1}\mathbf{A}$. The reader will have no difficulty in showing that *the problem of conserving the symmetry does not occur* also for a system of equations of type (2.62), (2.63).

Therefore, the following modifications of equations (2.58) and (2.60) leave the corresponding original solutions unchanged:

$${}^{n+1}\mathbf{A} = \mathrm{sym}\Big\{\Big[\mathbf{1} - \Delta t \ \mathbf{f}({}^{n+1}\mathbf{A}, t_{n+1})\Big]^{-1} \ {}^{n}\mathbf{A}\Big\}, \tag{2.72}$$

$${}^{n+1}\mathbf{A} = \mathrm{sym}\Big\{\exp\Big(\Delta t \ \mathbf{f}({}^{n+1}\mathbf{A}, t_{n+1})\Big) \ {}^{n}\mathbf{A}\Big\}. \tag{2.73}$$

The advantage of the exponential method based on (2.60) or (2.73) is that the constraint $\det({}^{n+1}\mathbf{A}) = 1$ is exactly satisfied. In this paper we modify the right-hand side of (2.58) and (2.72), using the projection $\overline{(\cdot)} = (\det(\cdot))^{-1/3}(\cdot)$ on the group of unimodular tensors (cf. [**14**]):

$$ {}^{n+1}\mathbf{A} = \overline{\Big[\mathbf{1} - \Delta t\ \mathbf{f}({}^{n+1}\mathbf{A}, t_{n+1})\Big]^{-1}\ {}^{n}\mathbf{A}}, \tag{2.74} $$

$$ {}^{n+1}\mathbf{A} = \overline{\mathrm{sym}\Big\{\Big[\mathbf{1} - \Delta t\ \mathbf{f}({}^{n+1}\mathbf{A}, t_{n+1})\Big]^{-1}\ {}^{n}\mathbf{A}\Big\}}. \tag{2.75} $$

Let us remark that both (2.74) and (2.75) yield the same solution ${}^{n+1}\mathbf{A} \in \mathbb{M}$. Thus, the modified Euler-Backward (MEBM) is formulated by (2.74) or (2.75). Further, we notice that the exponential method (EM) (2.60) is equivalent to

$$ {}^{n+1}\mathbf{A} = \overline{\mathrm{sym}\Big\{\exp\Big(\Delta t\ \mathbf{f}({}^{n+1}\mathbf{A}, t_{n+1})\Big)\ {}^{n}\mathbf{A}\Big\}}. \tag{2.76} $$

Remark 2. We have a freedom in choosing between (2.74) and (2.75) for MEBM. Similarly, the EM can be based either on (2.60) or (2.76). In this paper we use symmetrized equations (2.75), (2.76). The reason is that these two equations can be formulated with respect to six real unknowns. At the same time equations (2.74), (2.60) are formulated with respect to nine independent real unknowns.

3.2. Adaptation of integration methods to the evolution equations. Suppose that the deformation gradient ${}^{n+1}\mathbf{F}$ at the time $t_{n+1} = t_n + \Delta t$ is known. Further, assume that the internal variables $\mathbf{C}_{\mathrm{i}}, \mathbf{C}_{\mathrm{ii}}, s, s_{\mathrm{d}}$ at the time t_n are given by ${}^{n}\mathbf{C}_{\mathrm{i}}, {}^{n}\mathbf{C}_{\mathrm{ii}}, {}^{n}s, {}^{n}s_{\mathrm{d}}$, respectively. In this subsection we formulate a system of equations for finding the internal variables at the time t_{n+1}.

First, we adopt the modified Euler-Backward scheme (2.75) and the exponential scheme (2.76) to the numerical integration of evolution equations (2.55). We stress that the right-hand sides in (2.55) satisfy requirements (2.57). For instance, let us check the evolution equation for $\mathbf{C}_{\mathrm{i}}$. Note that, since $\mathbf{C}\tilde{\mathbf{T}}$ and $\mathbf{C}_{\mathrm{i}}\tilde{\mathbf{X}}$ are isotropic functions of $\mathbf{C}{\mathbf{C}_{\mathrm{i}}}^{-1}$ and $\mathbf{C}_{\mathrm{i}}{\mathbf{C}_{\mathrm{ii}}}^{-1}$,

$$ 2\frac{\lambda_{\mathrm{i}}}{\mathfrak{F}}\Big(\mathbf{C}\tilde{\mathbf{T}} - \mathbf{C}_{\mathrm{i}}\tilde{\mathbf{X}}\Big)^{\mathrm{D}} = d_1\mathbf{1} + d_2\mathbf{C}\mathbf{C}_{\mathrm{i}}^{-1} + d_3(\mathbf{C}\mathbf{C}_{\mathrm{i}}^{-1})^2 + d_4\mathbf{C}_{\mathrm{i}}\mathbf{C}_{\mathrm{ii}}^{-1} + d_5(\mathbf{C}_{\mathrm{i}}\mathbf{C}_{\mathrm{ii}}^{-1})^2, $$

with some suitable $d_n \in \mathbb{R}$. It remains to check that

$$ (\mathbf{C}\mathbf{C}_{\mathrm{i}}^{-1})^k\mathbf{C}_{\mathrm{i}} \in Sym,\ (\mathbf{C}_{\mathrm{i}}\mathbf{C}_{\mathrm{ii}}^{-1})^k\mathbf{C}_{\mathrm{i}} \in Sym, \quad \text{for all } \mathbf{C}_{\mathrm{i}}, \mathbf{C}_{\mathrm{ii}} \in Sym,\ k = 1, 2, 3, \dots . $$

The evolution equations for s, s_{d} are discretized by implicit Euler scheme. For what follows it is convenient to introduce the incremental inelastic parameter

$$ \xi := \Delta t\ {}^{n+1}\lambda_{\mathrm{i}}. \tag{2.77} $$

Finally, we obtain the following system of equations with respect to the strain-like variables ${}^{n+1}\mathbf{C}_{\mathrm{i}}$, ${}^{n+1}\mathbf{C}_{\mathrm{ii}}$, ${}^{n+1}s$, ${}^{n+1}s_{\mathrm{d}}$, ξ.

$$ {}^{n+1}\mathbf{C}_{\mathrm{i}} - \overline{\mathrm{sym}\Big(\mathbf{K}_{\mathrm{i}}({}^{n+1}\mathbf{C}, {}^{n+1}\mathbf{C}_{\mathrm{i}}, {}^{n+1}\mathbf{C}_{\mathrm{ii}}, \xi)\Big)} = \mathbf{0}, \tag{2.78} $$

$$ {}^{n+1}\mathbf{C}_{\mathrm{ii}} - \overline{\mathrm{sym}\Big(\mathbf{K}_{\mathrm{ii}}({}^{n+1}\mathbf{C}_{\mathrm{i}}, {}^{n+1}\mathbf{C}_{\mathrm{ii}}, \xi)\Big)} = \mathbf{0}, \tag{2.79} $$

$$ \xi = \frac{\Delta t}{\eta}\Big\langle \frac{{}^{n+1}f}{k_0} \Big\rangle^m, \tag{2.80} $$

$$ {}^{n+1}s = {}^{n}s + \sqrt{\frac{2}{3}}\xi, \quad {}^{n+1}s_{\mathrm{d}} = {}^{n}s_{\mathrm{d}} + \frac{\beta}{\gamma}\sqrt{\frac{2}{3}}\xi\ {}^{n+1}R, \tag{2.81} $$

$$
{}^{n+1}R = \gamma({}^{n+1}s - {}^{n+1}s_{\mathrm{d}}), \quad {}^{n+1}f = {}^{n+1}\mathfrak{F} - \sqrt{\frac{2}{3}}(K + {}^{n+1}R), \tag{2.82}
$$

$$
{}^{n+1}\mathfrak{F} = \sqrt{\mathrm{tr}\Big[\big({}^{n+1}\mathbf{C}\ {}^{n+1}\tilde{\mathbf{T}} - {}^{n+1}\mathbf{C}_{\mathrm{i}}\ {}^{n+1}\tilde{\mathbf{X}}\big)^{\mathrm{D}}\Big]^2}, \tag{2.83}
$$

where the operators $\mathbf{K}_{\mathrm{k}},\ \mathrm{k} \in \{\mathrm{i}, \mathrm{ii}\}$ are defined by

$$
\mathbf{K}_{\mathrm{k}} := \begin{cases} \Big[\mathbf{1} - \mathbf{B}_{\mathrm{k}}\Big]^{-1}\ {}^{n}\mathbf{C}_{k} & \text{if MEBM is employed} \\ \exp\Big[\mathbf{B}_{\mathrm{k}}\Big]\ {}^{n}\mathbf{C}_{k} & \text{if EM is employed} \end{cases},
$$

$$
\mathbf{B}_{\mathrm{i}}({}^{n+1}\mathbf{C}, {}^{n+1}\mathbf{C}_{\mathrm{i}}, {}^{n+1}\mathbf{C}_{\mathrm{ii}}, \xi) := 2\frac{\xi}{{}^{n+1}\mathfrak{F}}\Big({}^{n+1}\mathbf{C}\ {}^{n+1}\tilde{\mathbf{T}} - {}^{n+1}\mathbf{C}_{\mathrm{i}}\ {}^{n+1}\tilde{\mathbf{X}}\Big)^{\mathrm{D}}, \tag{2.84}
$$

$$
\mathbf{B}_{\mathrm{ii}}({}^{n+1}\mathbf{C}_{\mathrm{i}}, {}^{n+1}\mathbf{C}_{\mathrm{ii}}, \xi) := 2\ \xi\ \varkappa\Big({}^{n+1}\mathbf{C}_{\mathrm{i}}\ {}^{n+1}\tilde{\mathbf{X}}\Big)^{\mathrm{D}}. \tag{2.85}
$$

Here ${}^{n+1}\tilde{\mathbf{T}}$, ${}^{n+1}\tilde{\mathbf{X}}$ are functions of ${}^{n+1}\mathbf{C}, {}^{n+1}\mathbf{C}_{\mathrm{i}}, {}^{n+1}\mathbf{C}_{\mathrm{ii}}$, given by (2.44) (or by (2.46) if the special form of ψ_{el}, ψ_{kin} is used).

3.3. Solution strategy. First, we exclude ${}^{n+1}s, {}^{n+1}s_{\mathrm{d}}$ from (2.81), $(2.82)_1$ (cf. [**14**]) to obtain

$$
{}^{n+1}R = R(\xi) := \frac{{}^{\mathrm{t}}R + \sqrt{\frac{2}{3}}\gamma\xi}{1 + \sqrt{\frac{2}{3}}\beta\xi}, \quad {}^{\mathrm{t}}R := \gamma({}^{n}s - {}^{n}s_{\mathrm{d}}). \tag{2.86}
$$

Next, substituting (2.83) and (2.86) in $(2.82)_2$, we represent ${}^{n+1}f$ as a function of ${}^{n+1}\mathbf{C}_{\mathrm{i}}$, ${}^{n+1}\mathbf{C}_{\mathrm{ii}}$, and ξ. Thus, the problem is reduced to system (2.78), (2.79), (2.80) with respect to ${}^{n+1}\mathbf{C}_{\mathrm{i}}, {}^{n+1}\mathbf{C}_{\mathrm{ii}}, \xi$.

In this paper we decompose the problem (2.78) — (2.80) as follows. The variables ${}^{n+1}\mathbf{C}_{\mathrm{i}}, {}^{n+1}\mathbf{C}_{\mathrm{ii}}$ are uniquely determined by system (2.78), (2.79) with a given ξ. Let us denote the corresponding solution by $\big(\mathbf{C}_{\mathrm{i}}({}^{n+1}\mathbf{C}, \xi), \mathbf{C}_{\mathrm{ii}}({}^{n+1}\mathbf{C}, \xi)\big)$. Substituting this solution in (2.83), we obtain a function $\mathfrak{F}({}^{n+1}\mathbf{C}, \xi)$.

If $\mathfrak{F}({}^{n+1}\mathbf{C}, 0) - \sqrt{\frac{2}{3}}(K + {}^{t}R) \leq 0$, then we put $\xi := 0$, ${}^{n+1}\mathbf{C}_{\mathrm{i}} := {}^{n}\mathbf{C}_{\mathrm{i}}$, ${}^{n+1}\mathbf{C}_{\mathrm{ii}} := {}^{n}\mathbf{C}_{\mathrm{ii}}$ (no inelastic flow occurs). Otherwise, ξ is computed using equation (2.80). Substituting $(2.82)_2$ for ${}^{n+1}f$ in (2.80), we obtain two alternative forms of the incremental consistency condition:

$$
H({}^{n+1}\mathbf{C}, \xi) := \frac{\eta\xi}{\Delta t} - \left(\frac{\mathfrak{F}({}^{n+1}\mathbf{C}, \xi) - \sqrt{\frac{2}{3}}(K + R(\xi))}{k_0}\right)^{m} = 0, \tag{2.87}
$$

$$
D({}^{n+1}\mathbf{C}, \xi) := \left(\frac{\eta\xi}{\Delta t}\right)^{1/m} - \frac{\mathfrak{F}({}^{n+1}\mathbf{C}, \xi) - \sqrt{\frac{2}{3}}(K + R(\xi))}{k_0} = 0. \tag{2.88}
$$

After the solution ξ is found, the values of ${}^{n+1}\mathbf{C}_{\mathrm{i}}$, ${}^{n+1}\mathbf{C}_{\mathrm{ii}}$ are given by $\mathbf{C}_{\mathrm{i}}({}^{n+1}\mathbf{C}, \xi)$, $\mathbf{C}_{\mathrm{ii}}({}^{n+1}\mathbf{C}, \xi)$. Finally, we update s and s_{d} using equations (2.81).

Remark 3. Solving system (2.80), $(2.82)_2$ with respect to ξ with a given $\mathfrak{F}$, it is possible to represent ξ as a function of ${}^{n+1}\mathbf{C}_{\mathrm{i}}, {}^{n+1}\mathbf{C}_{\mathrm{ii}}$, thus reducing the number of unknowns. On the other hand, for small η this approach will result in an ill-posed problem.

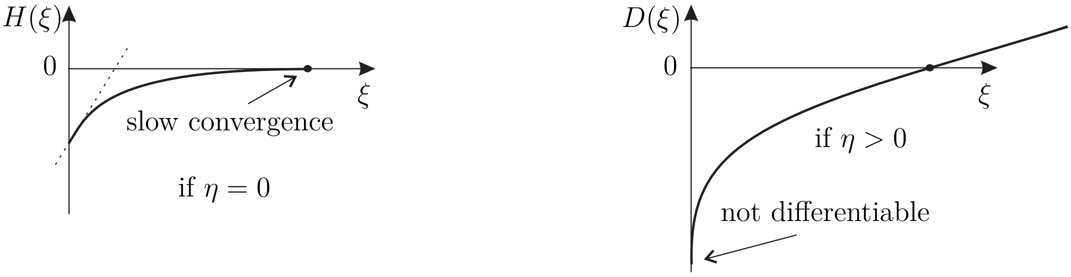

Figure 2.2. Finding ξ.

3.4. Numerical implementation. The Newton-Raphson method is used to compute $\big(\mathbf{C}_{\mathrm{i}}({}^{n+1}\mathbf{C},\xi), \mathbf{C}_{\mathrm{ii}}({}^{n+1}\mathbf{C},\xi)\big)$ from (2.78), (2.79). To this end, equations (2.78), (2.79) are linearized analytically using the coordinate-free tensor formalism proposed by Itskov (see [**16, 17**]).

Notice that the straightforward application of Newton's method to the solution of (2.87) or (2.88) is not trivial. Indeed, for $\eta = 0$, $m > 1$, the convergence of the Newton method for (2.87) fails to be quadratic since the first derivative is zero at the root (see fig. 2.2). At the same time, for $\eta > 0$, the initial approximation $\xi^{(0)} = 0$ can not be used to compute the solution of (2.88), since the function $D(\xi)$ is not differentiable at zero (see fig. 2.2). To overcome these difficulties, the first Newton iteration is performed using (2.87) with initial approximation $\xi^{(0)} = 0$, and the subsequent iterations are performed using (2.88).

The derivative $\dfrac{\partial \mathfrak{F}({}^{n+1}\mathbf{C},\xi)}{\partial \xi}$, required by the Newton method, is calculated using the implicit differentiation of (2.78), (2.79) with respect to ξ. An alternative strategy is to solve (2.88) with the help of a derivative-free iteration scheme like Pegasus method [**7**], [**20**]. This approach is reasonable being combined with a fixed-point iteration for finding $\big(\mathbf{C}_{\mathrm{i}}({}^{n+1}\mathbf{C},\xi), \mathbf{C}_{\mathrm{ii}}({}^{n+1}\mathbf{C},\xi)\big)$, such that no linearization of (2.78), (2.79) is required.

We implement the coordinate-free tensor formalism to obtain an analytical expression for the consistent tangent operator $\dfrac{\partial\, {}^{n+1}\tilde{\mathbf{T}}}{\partial\, {}^{n+1}\mathbf{C}}$. Using a special product $\mathbf{A} \times \mathbf{B}$ of two second-rank tensors and the composition $\mathbb{A}\,\mathbb{B}$ of two fourth-rank tensors (see definitions (2.6), (2.10) in [**17**]), it follows from (2.44) that

$$\frac{\partial\, {}^{n+1}\tilde{\mathbf{T}}}{\partial\, {}^{n+1}\mathbf{C}} = \frac{\partial \tilde{\mathbf{T}}({}^{n+1}\mathbf{C}, {}^{n+1}\mathbf{C}_{\mathrm{i}})}{\partial\, {}^{n+1}\mathbf{C}} + \frac{\partial \tilde{\mathbf{T}}({}^{n+1}\mathbf{C}, {}^{n+1}\mathbf{C}_{\mathrm{i}})}{\partial\, {}^{n+1}\mathbf{C}_{\mathrm{i}}} \frac{\partial\, {}^{n+1}\mathbf{C}_{\mathrm{i}}({}^{n+1}\mathbf{C})}{\partial\, {}^{n+1}\mathbf{C}},$$

$$\frac{\partial\, {}^{n+1}\mathbf{C}_{\mathrm{i}}({}^{n+1}\mathbf{C})}{\partial\, {}^{n+1}\mathbf{C}} = \frac{\partial \mathbf{C}_{\mathrm{i}}({}^{n+1}\mathbf{C},\xi)}{\partial\, {}^{n+1}\mathbf{C}} + \frac{\partial \mathbf{C}_{\mathrm{i}}({}^{n+1}\mathbf{C},\xi)}{\partial \xi} \times \frac{\partial \xi({}^{n+1}\mathbf{C})}{\partial\, {}^{n+1}\mathbf{C}},$$

$$\frac{\partial \xi({}^{n+1}\mathbf{C})}{\partial\, {}^{n+1}\mathbf{C}} = -\Big(\frac{\partial D({}^{n+1}\mathbf{C},\xi)}{\partial \xi}\Big)^{-1} \frac{\partial D({}^{n+1}\mathbf{C},\xi)}{\partial\, {}^{n+1}\mathbf{C}}.$$

The numerical computation of tensor exponential $\exp(\mathbf{B})$ is performed using Taylor power series expansion (2.61). The derivative of tensor exponential is computed by (see [**18**])

$$\frac{\partial \exp(\mathbf{B})}{\partial \mathbf{B}} = \sum_{n=1}^{\infty} \frac{1}{n!} \sum_{k=0}^{n-1} \mathbf{B}^{n-1-k} \otimes \mathbf{B}^{k}.$$

In general, this approach fails due to the roundoff errors, and more sophisticated techniques are required (see, for example, [**30, 18, 19, 25**]). We do not use these advanced techniques in this paper, since in the present calculations the argument of the exponential function is bounded. Indeed, if $\xi \leq 0.2$ then it follows from (2.84), (2.85) that

$$\|\mathbf{B}_{\mathrm{k}}\| \approx 2\xi \leq 0.4, \quad \mathrm{k} \in \{\mathrm{i}, \mathrm{ii}\}. \tag{2.89}$$

Therefore, the roundoff errors are negligible. Moreover, under condition (2.89), the truncated power series only with few terms yield exact results up to machine precision.

4. Numerical tests

Now we analyze the robustness and accuracy of the integration methods presented in Section 3. Toward this end, we simulate the material behaviour under strain controlled loading. The loading program in the time interval $t \in [0, 300]$ is defined by

$$\mathbf{F}(t) = \overline{\mathbf{F}'(t)} \quad \text{or} \quad \mathbf{F}(t) = \mathbf{F}'(t), \tag{2.90}$$

where $\mathbf{F}'(t)$ is a piecewise linear function of time t such that $\mathbf{F}'(0) = \mathbf{F}_1$, $\mathbf{F}'(100) = \mathbf{F}_2$, $\mathbf{F}'(200) = \mathbf{F}_3$, and $\mathbf{F}'(300) = \mathbf{F}_4$ with

$$\mathbf{F}_1 := \mathbf{1}, \ \mathbf{F}_2 := \begin{pmatrix} 2 & 0 & 0 \\ 0 & \dfrac{1}{\sqrt{2}} & 0 \\ 0 & 0 & \dfrac{1}{\sqrt{2}} \end{pmatrix}, \ \mathbf{F}_3 := \begin{pmatrix} 1 & 1 & 0 \\ 0 & 1 & 0 \\ 0 & 0 & 1 \end{pmatrix}, \ \mathbf{F}_4 := \begin{pmatrix} \dfrac{1}{\sqrt{2}} & 0 & 0 \\ 0 & 2 & 0 \\ 0 & 0 & \dfrac{1}{\sqrt{2}} \end{pmatrix}.$$

More precisely, we put

$$\mathbf{F}'(t) := \begin{cases} (1 - t/100)\mathbf{F}_1 + (t/100)\mathbf{F}_2 & \text{if } t \in [0, 100] \\ (2 - t/100)\mathbf{F}_2 + (t/100 - 1)\mathbf{F}_3 & \text{if } t \in (100, 200] \\ (3 - t/100)\mathbf{F}_3 + (t/100 - 2)\mathbf{F}_4 & \text{if } t \in (200, 300] \end{cases} .$$

Remark 4. In this section we test the numerical schemes under a variety of loading conditions, in particular, under non-proportional loading. In this connection, the loading programm does not have to be mechanically plausible.

The material parameters used in simulations are summarized in table 2.2.

Table 2.2. Material parameters

k [MPa]	μ [MPa]	c [MPa]	γ [MPa]
73500	28200	3500	460

K [MPa]	m [-]	η [s]	k_0 [Mpa]	$\varkappa$ [MPa^{-1}]	β [-]
270	3.6	$2 \cdot 10^6$	1	0.028	5

We put the following initial conditions on the internal variables

$$\mathbf{C}_{\mathrm{i}}|_{t=0} = \mathbf{1}, \quad \mathbf{C}_{\mathrm{ii}}|_{t=0} = \mathbf{1}, \quad s|_{t=0} = 0, \quad s_{\mathrm{d}}|_{t=0} = 0. \tag{2.91}$$

Only the uniform time stepping is used in this paper. The numerical solution obtained with extremely small time step ($\Delta t = 0.01$s) will be named the *exact solution.*

The coordinates of the Cauchy stress tensor $\mathbf{T}$ for loadings $(2.90)_1$ and $(2.90)_2$ are plotted respectively in figures 2.3 and 2.4. Note that $\det(\mathbf{F}) \equiv 1$ if $(2.90)_1$ is used, and no

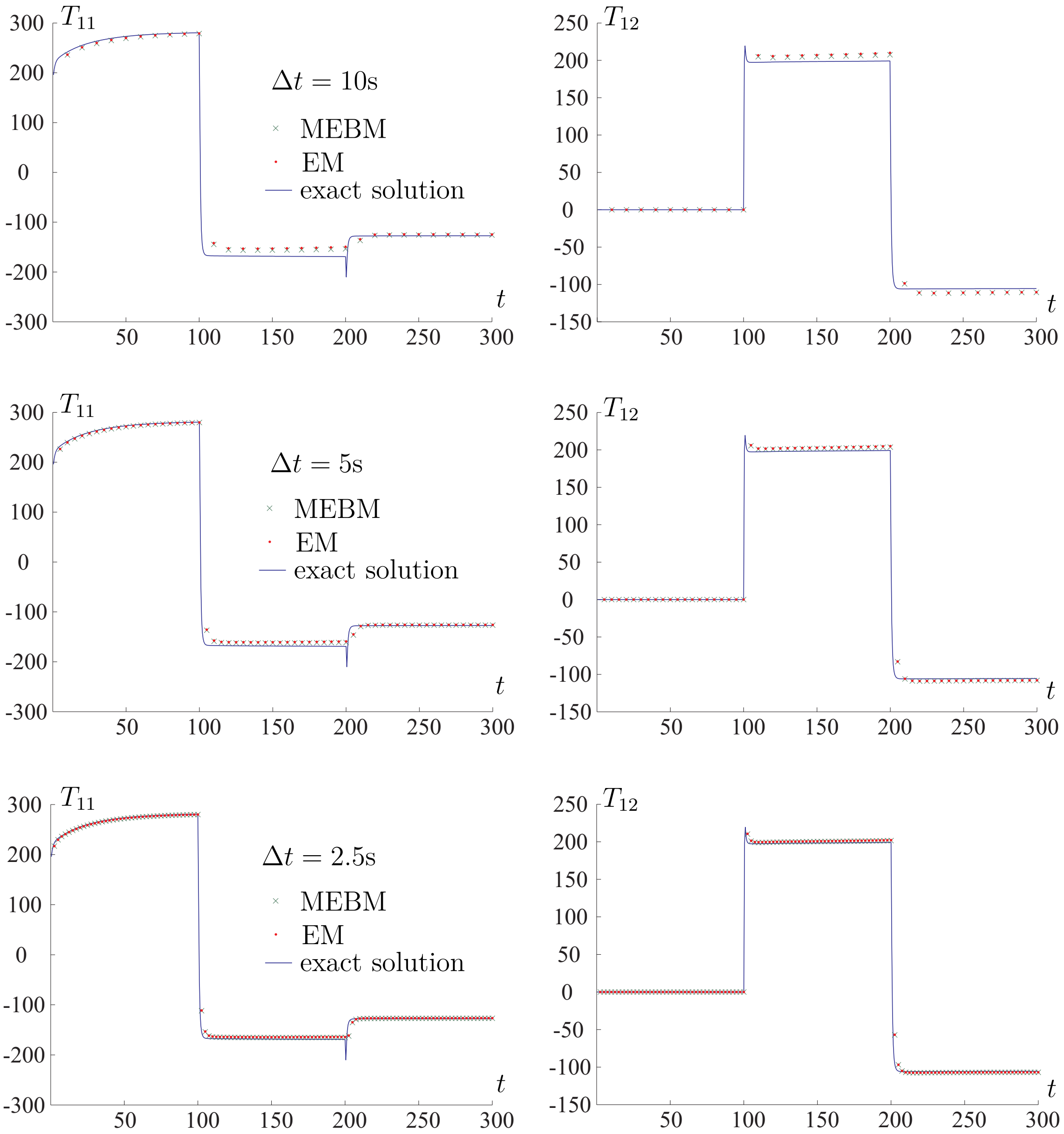

Figure 2.3. Accuracy test with small elastic strains (using $(2.90)_1$).

hydrostatic stress occurs. On the other hand, relation $(2.90)_2$ results in a large hydrostatic stress and a *finite elastic bulk strain.*

The numerical simulation shows that both MEBM and EM have a similar error. Both methods produce similar results even for big time steps $\Delta t = 10$ s when the inelastic increment ξ ranges up to about 17%. According to testing results, *none of algorithms prevail in accuracy.*

Both methods require nearly the same number of iterations to obtain a convergent solution of (2.78) — (2.80). The computation time is almost not affected by the choice of integration algorithm.

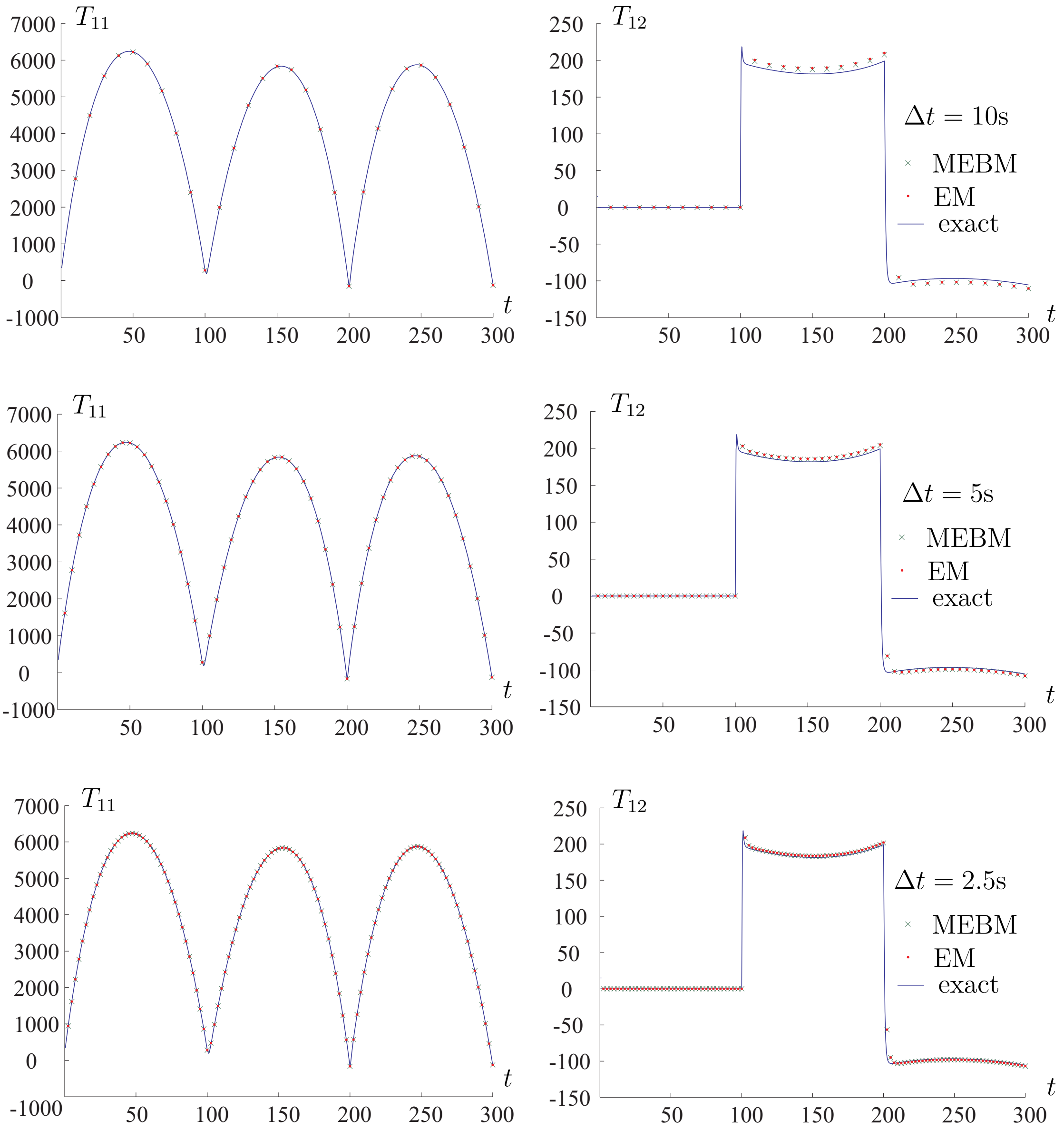

Figure 2.4. Accuracy test with finite elastic strains (using $(2.90)_2$).

5. Characterization of the material model

We investigate qualitatively the material response, predicted by the material model. The numerical computations simulate basic material testing experiments. Material parameters from table 2.2 and initial conditions (2.91) are used in this section.

5.1. Uniaxial testing. For uniaxial test we put

$$\mathbf{F} = \begin{pmatrix} 1+\varepsilon & 0 & 0 \\ 0 & \alpha & 0 \\ 0 & 0 & \alpha \end{pmatrix}, \quad T_{22} = T_{33} = 0. \tag{2.92}$$

The unknown α is determined using $(2.92)_2$. The technical stress $\sigma := \frac{A}{A_0} T_{11}$ is plotted in figure 2.5.a for various strain rates $\dot{\varepsilon}$. Here A, A_0 denote the current and initial cross sections, respectively. Although the material response is stable, the stress reduction is observed after

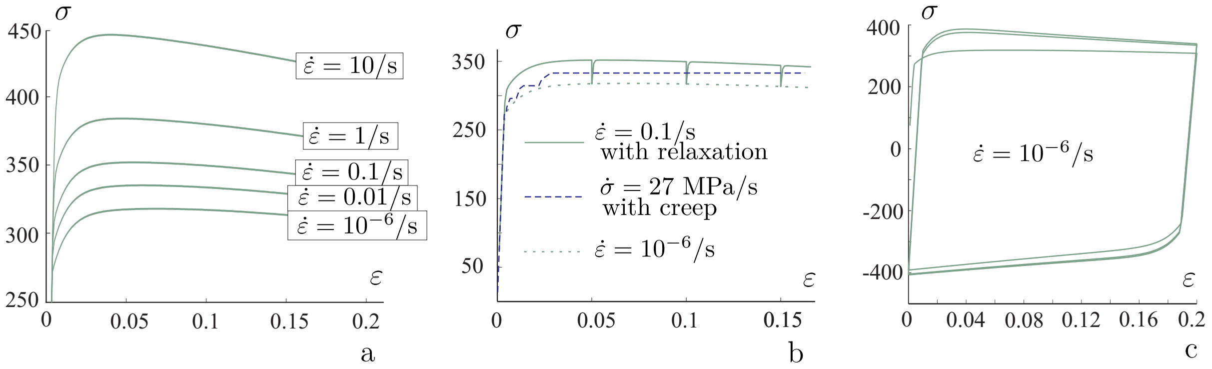

Figure 2.5. Uniaxial testing: monotonic loading (a), relaxation and creep (b), and cyclic loading (c).

the peak load in uniaxial monotonic test. The reason is the reduction of the cross-section. The equilibrium curve can be reached both by relaxation and creep (figure 2.5.b). In the simulation presented in figure 2.5.b each relaxation period lasts for 10 seconds. The creep time is 20 seconds. Therefore, the numerical experiment shows that it takes longer to reach equilibrium curve in the creep process than in the relaxation process. Finally, as indicated by the strain-controlled cyclic test (figure 2.5.c), the saturation is achieved after the isotropic hardening is accomplished.

5.2. Torsion testing. The cyclic torsion testing has much potential for providing information about the nonlinear hardening phenomena (see [**8**]). To simulate the torsion of constrained thin-walled tube we put

$$\mathbf{F} = \begin{pmatrix} 1 & \phi & 0 \\ 0 & 1 & 0 \\ 0 & 0 & \alpha \end{pmatrix}, \quad T_{33} = 0. \tag{2.93}$$

We consider a strain controlled torsion test with a given ϕ, $|\dot{\phi}| = 0.01/s$. The unknown α is determined using $(2.93)_2$. Denote by $\sigma := \dfrac{A}{A_0} T_{22}$ and $\tau := \dfrac{A}{A_0} T_{12}$ the axial and shear stresses, respectively.

The axial stress σ is exactly zero in geometric linear theory. But, in the case of finite strains, so-called second order effects can appear, leading to nonzero axial stress. For instance, the Poynting effect (see [**1**]) is observed during the torsion of cylindrical samples made of aluminium alloy. This effect consists in axial compression of constrained samples or axial elongation of unconstrained samples (see [**34**]). The axial and shear stresses are plotted in figure 2.6 for different forming increments. As may be seen from the figure, the Poynting effect is predicted by the material model.

Next, as indicated by figure 2.6, the maximal stresses are influenced by the forming increment. For smaller forming increment the isotropic hardening is accomplished on the early stage of the forming process, thus leading to higher maximal stresses. On the other hand, if the kinematic hardening is not accomplished within one forming increment, a somewhat different material response is possible. For instance, the maximal stresses under the cyclic loading can be smaller than the stresses under the monotonic loading. In order to demonstrate this effect, we perform the numerical simulation (see figure 2.7) with modified

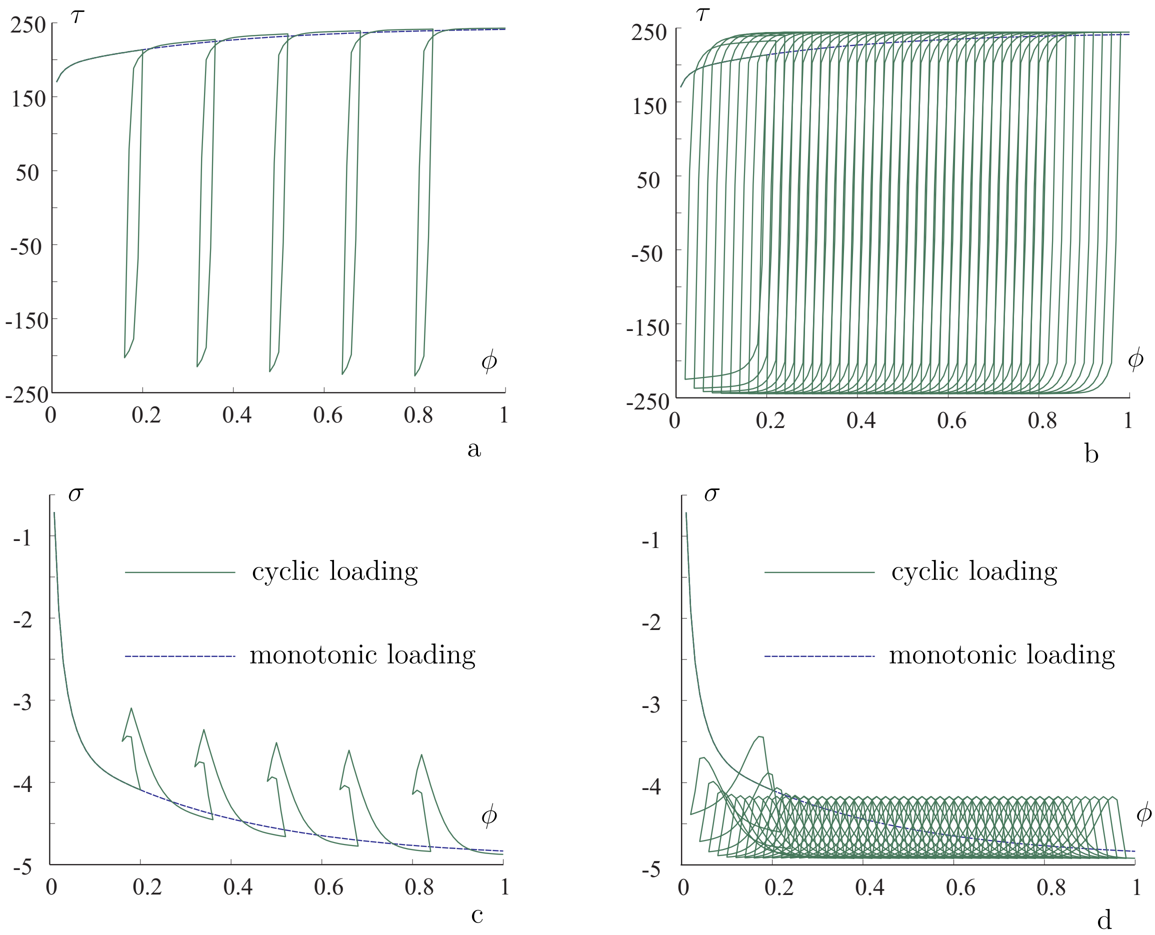

Figure 2.6. Torsion testing (material parameters from table 2.2): shear stress (a), (b), and axial stress (c), (d).

hardening parameters: $\varkappa := 0.0035\ \mathrm{MPa}^{-1}$, $c := 1500$ MPa, $\beta := 10$, $\gamma := 1800$ MPa. A similar effect was reported in [**27**] for 20MoCr24 steel alloy.

6. Discussion

The classical material model of viscoplasticity is modified in a thermodynamically consistent manner to incorporate finite elastic and inelastic strains. The model takes rate-dependence (relaxation, creep) and hysteresis effects (nonlinear kinematic and isotropic hardening) into account.

Although the material response is anisotropic, the symmetry of ${}^{n+1}\mathbf{C}_{\mathrm{i}}$ and ${}^{n+1}\mathbf{C}_{\mathrm{ii}}$ is a priori preserved by EBM, MEBM and EM. It is shown that *no symmetrization procedure is necessary.* Moreover, any symmetrization should leave the corresponding solutions unchanged. Both MEBM and EM have the advantage that the inelastic incompressibility constraint is exactly satisfied.

The most important properties of any stress algorithm are stability, accuracy, robustness, and universality. Under special assumptions on the potential functions ψ_{el} and ψ_{kin} it may be beneficial to optimize the solution procedure for system (2.78) — (2.85), thus reducing the computational effort. On the other hand, the computational efficiency of the integration algorithm becomes less important within the context of large scale FEM analysis

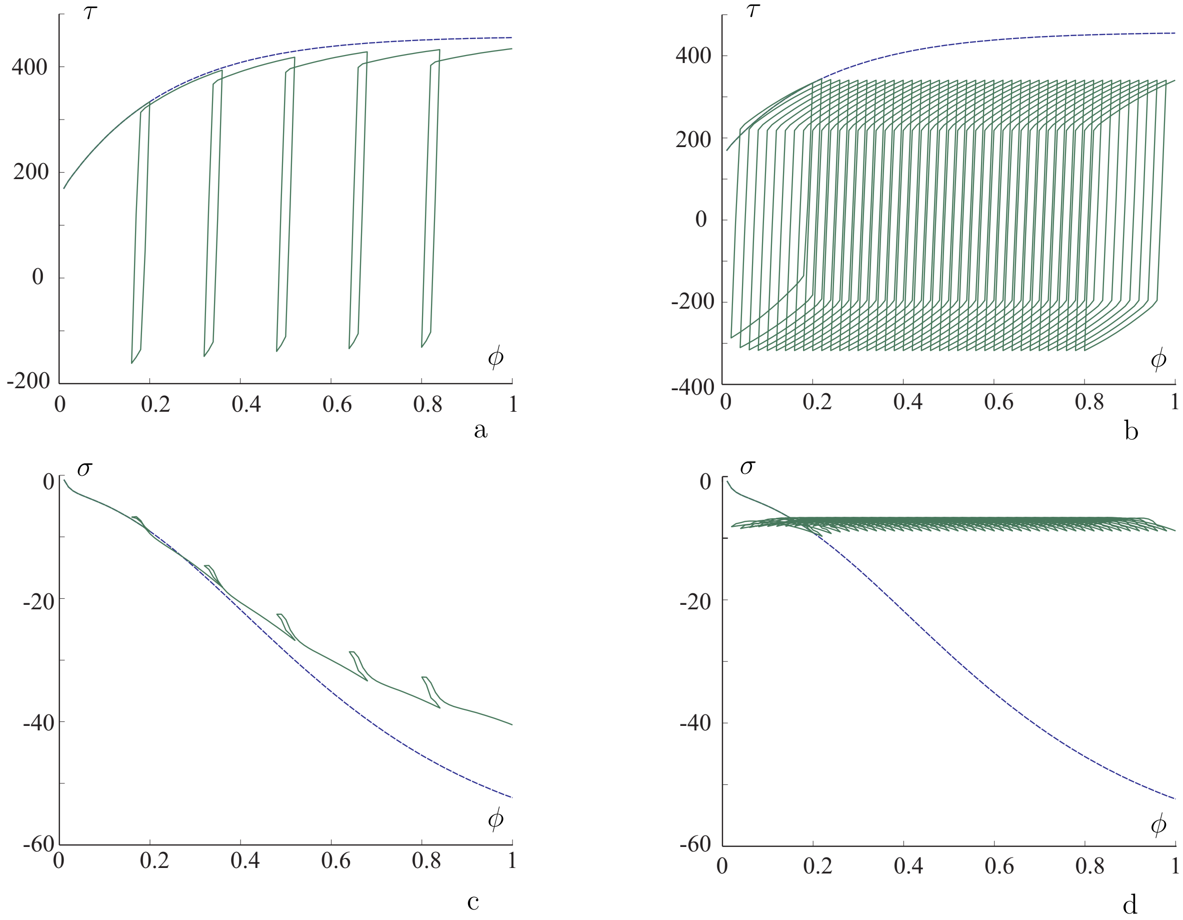

Figure 2.7. Torsion testing (modified material parameters): shear stress (a), (b), and axial stress (c), (d).

as the number of degrees of freedom grows large. The computational effort, required for the evaluation of stresses and tangential operator, is asymptotically negligible compared to the costs of solving the global linearized system of equations within the Newton-Raphson iterative procedure.

The material model reproduces qualitatively the experimental results [**15, 28**] for aluminium alloy processed by ECA-pressing. That means that the simulation was performed using physically reasonable material parameters (table 2.2). For more detailed modeling of kinematic hardening it is possible to introduce several Armstrong-Frederick terms, using a series of multiplicative decompositions of type (2.2). To complete the phenomenological description of the aluminium alloy, a proper parameter identification is required.

Acknowledgements

This research was supported by German National Science Foundation (DFG) within the collaborative research center SFB 692 "High-strength aluminium based light weight materials for reliable components". The authors are grateful to Dr. D. Helm and Dr. P. Neff for fruitful discussions.

Bibliography

[1] I. N. Andronov, N. P. Bogdanov, V. P. Vlasov, V. A. Likhachev, Laws governing the axial deformation of metals subjected to plastic torsion, Strength of Materials, 22, 7 (1990) 1046–1048.

[2] P. J. Armstrong, C. O. Frederick, A mathematical representation of the multiaxial Bauschinger effect, Technical Report RD/B/N731, G.E.G.B, 1966.

[3] J. L. Chaboche, G, Rousselier, On the Plastic and Viscoplastic Constitutive Equations, Part I: Rules Developed with Internal Variable Concept. Journal of Pressure Vessel Technology, ASME, 105 (1983) 153–158.

[4] J. Chaboche, Constitutive equations for cyclic plasticity and cyclic viscoplasticity, International Journal of Plasticity, 5 (1989) 247–302.

[5] W. Dettmer, S. Reese, On the theoretical and numerical modelling of Armstrong—Frederick kinematic hardening in the finite strain regime, Computer Methods in Applied Mechanics and Engineering, 193 (2004) 87—116.

[6] A. Dogui, F. Sidoroff, Kinematic hardening in large elastoplastic strain, Engineering Fracture Mechanics, 21, 4 (1985) 685–695.

[7] M. Dowell, P. Jarrat, The "Pegasus" method for computing the root of an equation, BIT Numerical Mathematics, 12 (1972) 503–508.

[8] U. J. Görke, A. Bucher, R. Kreißig, A study on kinematic hardening models for the simulation of cyclic loading in finite elasto-plasticity based on a substructure approach, In: Owen, D.R.J., Onate, E. and Suarez, B. (Eds.): Computational Plasticity: Fundamentals and Applications. Proceedings of COMPLAS VIII, CIMNE Barcelona, (2005) 723–726.

[9] E. Hairer, Geometric Integration of Ordinary Differential Equations on Manifolds, BIT Numerical Mathematics, 41, 5 (2001) 996–1007.

[10] S. Hartmann, G. Lührs, P. Haupt, An efficient stress algorithm with applications in viscoplasticity and plasticity, International Journal for Numerical Methods in Engineering, 40 (1997) 991–1013.

[11] P. Haupt, Ch. Tsakmakis, On the application of dual variables in continuum mechanics, Continuum Mechanics and Thermodynamics 1 (1989) 165–196.

[12] P. Haupt, Continuum Mechanics and Theory of Materials, 2nd edition, Springer, 2002.

[13] D. Helm, Formgedächtnislegierungen, experimentelle Untersuchung, phänomenologische Modellierung und numerische Simulation der thermomechanischen Materialeigenschaften, Universitätsbibliothek Kassel, 2001.

[14] D. Helm, Stress computation in finite thermoviscoplasticity. International Journal of Plasticity, 22 (2006) 1699–1721.

[15] M. Hockauf, L.W. Meyer, T. Halle, C. Kuprin, M. Hietschold, S. Schulze, L. Krüger, Mechanical properties and microstructural changes of ultrafine-grained AA6063T6 during high-cycle fatigue, International Journal of Materials Research, 10 (2006) 1392–1400.

[16] M. Itskov, On the theory of fourth-order tensors and their applications in computational mechanics, Computer Methods in Applied Mechanics and Engineering, 189 (2000) 419–438.

[17] M. Itskov, The derivative with respect to a tensor: some theoretical aspects and applications, ZAMM - Journal of Applied Mathematics and Mechanics, 82, 8 (2002) 535–544.

[18] M. Itskov, N. Aksel, A closed-form representation for the derivative of non-symmetric tensor power series, International Journal of Solids and Structures, 39 (2002) 5963–5978.

[19] M. Itskov, Computation of the exponential and other isotropic tensor functions and their derivatives, Computer Methods in Applied Mechanics and Engineering, 192 (2003) 3985–3999.

[20] R. F. King, An improved Pegasus method for root finding, BIT Numerical Mathematics, 13 (1973) 423–427.

[21] E. Kröner, Allgemeine Kontinuumstheorie der Versetzungen und Eigenspannungen, Archive for Rational Mechanics and Analysis, 4 (1960) 237–334.

[22] E. H. Lee, Elastic-plastic deformation at finite strains, Journal of Applied Mechanics, 91 (1969) 1–6.

[23] J. Lemaitre, J. L. Chaboche, Mechanics of solid materials, University Press, Cambridge, 1990.

[24] A. Lion, Constitutive modelling in finite thermoviscoplasticity: a physical approach based on nonlinear rheological elements, International Journal of Plasticity, 16 (2000) 469–494.

[25] J. Lu, Exact expansions of arbitrary tensor functions **F** and their derivatives, International Journal of Solids and Structures, 41 (2004) 337–349.

[26] G. Lührs, S. Hartmann, P. Haupt, On the numerical treatment of finite deformations in elastoviscoplasticity, Computer Methods in Applied Mechanics and Engineering, 144 (1997) 1-–21.

[27] W. Meyer, F. Hahn, R. Glass, A. Rackova, Werkstoffverhalten und Werkstofffluß bei der partiellen Massivumformung am Beispiel des Bohrungsdrückens, In: Sächsische Fachtagung Umformtechnik, 24 (1998) 1–16.

[28] L.W. Meyer, M. Hockauf, L. Krüger, I. Schneider, Compressive behaviour of ultrafine-grained AA6063T6 over a wide range of strains and strain rates, International Journal of Materials Research, (accepted for publication).

[29] C. Miehe, E. Stein, A canonical model of multiplicative elasto-plasticity: formulation and aspects of the numerical implementation, European Journal of Mechanics A/Solids, 11 (1992) 25–43

[30] C. Miehe, Exponential map algorithm for stress updates in anisotropic multiplicative elastoplasticity for single crystals, International Journal for Numerical Methods in Engineering, 39 (1996) 3367–3390.

[31] F. Mollica, K.R. Rajagopal, A.R. Srinivasa, The inelastic behavior of metals subject to loading reversal, International Journal of Plasticity, 17 (2001) 1119—1146.

[32] P. Perzyna. The constitutive equations for rate sensitive plastic materials, Quarterly of Applied Mathematics, 20 (1963) 321–331.

[33] P. Perzyna, Fundamental problems in visco-plasticity, G. Kuerti (Ed.), Advances in Applied Mechanics, vol. 9, Academic Press, New York, (1966) 243–377.

[34] J. H. Poynting, On pressure perpendicular to the shear planes in finite pure shear, and on the lengthening of loaded wires when twisted, Proceedings of the Royal Society of London. Series A, 82, 557 (1909) 546–559.

[35] J. Simo, T. Hughes, Computational inelasticity, Springer, 1998.

[36] J. Simo, C. Miehe, Associative coupled thermoplasticity at finite strains: formulation, numerical analysis and implementation, Computer Methods in Applied Mechanics and Engineering, 98 (1992) 41—104.

[37] B. Svendsen, S. Arndt, D. Klingbeil, R. Sievert, Hyperelastic models for elastoplasticity with nonlinear isotropic and kinematic hardening at large deformation, International Journal of Solids and Structures, 35 (1998) 3363—3389.

[38] Ch. Tsakmakis, Kinematic hardening rules in finite plasticity - Part I: A constitutive approach. Part II: Some examples, Continuum Mechanics and Thermodynamics, 8 (1996) 214–246.

[39] G. Weber, L. Annand, Finite deformation constitutive equations and a time integration procedure for isotropic, hyperelastic-viscoelastic solids, Computer Methods in Applied Mechanics and Engineering, 79 (1990) 173–202.

[40] O. C. Zienkiewicz, R. L. Taylor, The Finite Element Method, Volume 2: Solid Mechanics, Butterworth-Heinemann, 2000.

KAPITEL 3

Application of a coordinate-free tensor formalism to the numerical implementation of a material model

A.V. Shutov,[1] R.Kreißig

Institute of Mechanics and Thermodynamics, Chemnitz University of Technology,
Str. d. Nationen 62, D-09111 Chemnitz, Germany

Abstract: *We analyze a coordinate-free tensor setting in* $\mathbb{R}^3$ *within the context of the classical tensor analysis. To this end, we formulate in a basis-free manner the notions of second- and fourth-rank tensors in* $\mathbb{R}^3$*, and corresponding operations on tensors. Among the large number of different approaches to the tensor setting, we give the preference to the convenient ones, concerning the specific needs of computational solid mechanics.*

We use the well-known Fréchet derivative to define the derivative of a function with respect to its tensor argument in a natural way. Furthermore, such aspects as the derivative with respect to a symmetric tensor argument and its uniqueness are covered in this paper.

For the sake of completeness we present the coordinate representation of tensors and tensor operations. This representation is obtained in a straight-forward manner from the coordinate-free one. In particular, we elaborate the computation of the inverse of a fourth-rank tensor and the inverse of a linear transformation on the space of symmetric second-rank tensors.

The tensor formalism is applied to the analysis of a nonlinear system of differential and algebraic equations governing visoplastic material response. An implicit time-stepping algorithm is formulated and the numerical treatment of the algorithm is discussed.

Keywords: coordinate-free formalism, classical tensor analysis, material modeling, time-stepping scheme, analytical linearization, viscoplasticity.
MSC2000: 15A72; 53A45; 74C20; 74S05

Nomenclature

Lin	space of second-rank tensors
LinLin	space of fourth-rank tensors

---

[1] Corresponding author. alexey.v.shutov@gmail.com
web: http://sites.google.com/site/materialmodeling

This chapter is reproduced from the paper: A. V. Shutov, R. Kreißig: Application of a coordinate-free tensor formalism to the numerical implementation of a material model. Zeitschrift für Angewandte Mathematik und Mechanik (ZAMM). 2008. (88)11, 888-909. Copyright WILEY-VCH Verlag GmbH. Reproduced with permission.

$LinLin^{SS}$	subspace of $LinLin$ enjoying both minor symmetries (cf. (3.89))
$\mathscr{L}(V)$	space of linear transformations of vector space V into itself
$GL(V)$	group of invertible transformations of set V into itself
Sym, $Skew$	spaces of symmetric and skew-symmetric second-rank tensors, respectively (see (3.5))
sym	symmetric part of a tensor
$\mathbf{x}, \mathbf{y}, \mathbf{z}$	first-rank tensors (elements of $\mathbb{R}^3$)
$\mathbf{A}, \mathbf{B}, \mathbf{C}$	second-rank tensors
$\mathbb{A}, \mathbb{B}, \mathbb{C}$	fourth-rank tensors
$\mathcal{A}, \mathcal{B}, \mathcal{C}$	linear transformations of Sym into itself
$\mathbf{x} \cdot \mathbf{y}$	scalar product in $\mathbb{R}^3$
$\mathbf{A} : \mathbf{B}$	scalar product in Lin
$\mathbf{x} \otimes \mathbf{y}$	tensor product of two first-rank tensors (see (3.9))
$\mathbf{A} \otimes \mathbf{B}$	tensor product of two second-rank tensors (see (3.19))
$\mathbf{A} \odot \mathbf{B}$	product of two second-rank tensors (see (3.20))
$\mathbf{A} \cdot \mathbf{B} = \mathbf{AB}$	product (composition) of two second-rank tensors (see (3.6))
$\mathbb{A} : \mathbb{B} = \mathbb{AB}$	product (composition) of two fourth-rank tensors (see (3.17))
$\mathbf{A}^{\mathrm{T}}$	transposition of a second-rank tensor (see (3.3))
$\mathbf{A}^{\mathrm{D}}$	deviatoric part of a second-rank tensor
$\mathbf{A}^{-1}$	inverse of a second-rank tensor (see (3.7))
$\mathbb{A}^{\mathrm{T}}$, $\mathbb{A}^{\mathrm{ti}}$, $\mathbb{A}^{\mathrm{to}}$	transpositions of a fourth-rank tensors (see (3.14), (3.16))
$\mathbb{A}^{-1}$	inverse of a fourth-rank tensor (see (3.18))
$(\cdot)^R$, $(\cdot)^L$	argument rearrangements (see (3.21), (3.22))
$\overline{(\cdot)}$	projection on the group of unimodular tensors (see (3.122))
$\mathbb{P}$	deviatoric projection tensor (deviatoriser) (see (3.30))
$\mathbb{S}$	sym, treated as an element of $LinLin$ (symmetriser) (see (3.31))
$\mathfrak{L}(\mathcal{A})$	element of $LinLin^{SS}$ representing $\mathcal{A}$ (see (3.90))
$\mathfrak{R}(\mathbb{A})$	element of $\mathscr{L}(Sym)$ represented by $\mathbb{A} \in LinLin^{SS}$ (see (3.91))
$Df(x_0)(\Delta x)$	derivative of f at x_0 acting on Δx (see (3.32))
$\approx$, $\underset{\Delta x \to 0}{\approx}$	asymptotic equivalence
$\big[A; \mathcal{X}\big]$	matrix of a linear operator A with respect to a basis $\mathcal{X}$
$\{J_k\}_{k=1,2,3}$	system of invariants of a second-rank tensor (see (3.118))

1. Introduction

Recent trends in the field of computational mechanics are toward increased refinement of the material models being used. One of the major problems facing the researcher who is attempting to construct (and analyze) a new material model, as well as a corresponding numerical algorithm, is that the tensor calculations become more involved. To avoid tedious "index wrestling" in computations, more sophisticated description language is required than the language of coordinates.

In this paper we analyze such simple language using the underlying mechanical and mathematical concepts of invariance. Toward this end, we formulate consistently in coordinate-free manner the notions of second- and fourth-rank tensors in $\mathbb{R}^3$ and corresponding tensor operations. The resulting tensor formalism provides a basis for analysis of invariant functional relations among tensors making no appeal to coordinates. The advantage of this approach is that the coordinate-free setting is clearer than presentation based on coordinates. Definitions of tensor operations made in the basis-free manner are well posed in the sense that they are independent of the particular choice of coordinate system. Besides, the use of coordinates is complicated due to the variety of conventions governing coordinate representations, which is a possible source of confusion.

Nevertheless, the coordinates are widely used in the engineering literature since they are useful for computations. For this reason, we include a coordinate representation of tensors and tensor operations used in this paper. Note that coordinates play an *auxiliary role*, namely, they are used for the numerical implementation (construction) of corresponding data types and operations. The coordinate representation is obtained in a straight-forward manner by the decomposition of tensor relations into components [2].

We treat second- and fourth-rank tensors as linear transformations of an appropriate vector space into itself (for the general introduction to the theory of linear operators in finite dimensions see, for example, [**6**]). The application of this approach to continuum mechanics was advocated in [**3, 22, 30, 28, 11, 12, 2, 16, 15, 29**]. We consider the application of this coordinate-free concept to concrete problems of computational mechanics, but the concept is open to further extension. In particular, the tensor setting can be generalized in order to deal with tensors of arbitrary rank in coordinate-free manner (cf. [**1, 23, 28, 2**]).

As an important constituent of the tensor formalism, we define the derivative of a smooth function with respect to its tensor argument. In that case, the well-known Fréchet derivative of a tensor-valued function is represented by a fourth-rank tensors in a natural way (cf. [**2**]). Next, an important class of functions is that of defined on the space of symmetric second-rank tensors (cf. [**22, 30**]). We discuss the treatment of a gradient of such functions[3]. Some authors refer to the problem of *non uniqueness* of this derivative (see, for instance, [**11, 12, 16**]). Following the concept of the Fréchet derivative, we treat such gradient as a linear operator, defined on the subset of symmetric tensors. The derivative is therefore *unique* in our setting. However, this derivative may permit different types of representations through second- or fourth-rank tensors (cf. [**22, 30, 11, 12, 16**]). In this work we discuss two such representations. The first representation is the classical one (see [**22, 30**]). It is based on the extension of the domain of a function from the set of symmetric tensors to the set of all second-rank tensors. The second representation makes use of equivalence classes on the sets of second- and fourth-rank tensors. We emphasize that the use of equivalence classes allows us to deal with the non-uniqueness in a natural way.

For the practical realization of the tensor setting one needs appropriate data types and a collection of procedures that manipulate instances of the types. We note that the coordinate-free approach *rules out the necessity* of using coordinate systems, but the use of coordinates is *not prohibited.* In particular, a coordinate representation of the tensor formalism is elaborated in this study. The representation is natural and straight-forward.

---

[2] The use of coordinate-free mathematics as a guideline in structuring numerical software is referred to as a *coordinate-free numerics* (see [**5, 4**]), even if coordinates are used for the realization of the tensor setting.

[3] Such gradient is sometimes referenced as a "derivative with respect to the symmetric tensor".

Especial attention, however, is paid to the tedious computation of inverse of a fourth-rank tensor, and inverse of a linear transformation on the space of symmetric second-rank tensors.

A global implicit time stepping in the context of displacement based finite element method (FEM) requires a proper material subroutine [**32**]. Such subroutine provides the stresses and the consistent tangent operator as a function of the local cumulative strain history. In general, the numerical implementation of a material subroutine leads to a complicated system of differential and algebraic equations. In order to construct a practical numerical algorithm, different simplifying assumptions are usually made, thus reducing the flexibility of the numerical scheme. For instance, in the context of metal plasticity, small elastic strains are usually assumed, and special formes of the stored-energy function are implemented in combination with simplified hardening rules.

In [**27**], a material model of nonlinear kinematic hardening was proposed, which is based on the kinematic assumption of a double multiplicative split (cf. [**20, 8**]). As an example of possible application of our tensor setting we discuss the implementation of an implicit integration algorithm, which was proposed in [**27**]. Using modified Euler-Backward method (MEBM) (see [**9, 27**]) and the exponential method (EM), the time-stepping problem is reduced to a nonlinear system of algebraic equations. After this system is decoupled, the numerical solution is found by the combination of the Newton-Raphson method (for a system of tensor equations) and the Newton method (for a single scalar equation). To this end, we linearize the corresponding nonlinear system of tensor equations with respect to tensor-valued unknowns. Finally, the consistent tangent operator is evaluated by implicit differentiation of the nonlinear system of equations. In this work we analyze the problem in the general form, and finite elastic strains are allowed. A variety of stored-energy functions can be implemented as well.

2. Tensors and operations on tensors

Most of processes relevant to engineering applications take place in three-dimensional Euclidean space. All considerations of this paper are therefore restricted to tensors in $\mathbb{R}^3$. We treat $\mathbb{R}^3$ as a Hilbert space equipped with the standard scalar product $\mathbf{x} \cdot \mathbf{y}$. This Euclidean structure allows us to simplify the description of mechanical processes. Instead of abstract *tensor analysis on manifolds* (see, for example [**23, 19, 28**]), the *classical tensor analysis* can be used[4]. In order to use the classical tensor analysis we identify the tangent and cotangent spaces $T_x\mathcal{B}$, $T_x^*\mathcal{B}$ with $\mathbb{R}^3$ (cf., for example, [**28, 2**]). The identification of $T_x\mathcal{B}$ with $\mathbb{R}^3$ is trivial. Next, using the inner product on $\mathbb{R}^3$, any one-form $\alpha \in T_x^*\mathcal{B} = (\mathbb{R}^3)^*$ is uniquely identified with the element $\alpha^\sharp \in \mathbb{R}^3$ through the relation[5]

$$\alpha(\mathbf{x}) = \alpha^\sharp \cdot \mathbf{x}, \quad \text{for all } \mathbf{x} \in \mathbb{R}^3. \tag{3.1}$$

Therefore, we do not distinct covariant, contravariant and mixed tensors in this work.

---

[4] The tensor analysis on manifolds is introduced in the context of manifolds modeled on Banach spaces (see [**19**]). In that case the inner product $\mathbf{x} \cdot \mathbf{y}$ is, in general, *not defined* and, therefore, the distinction between tangent and cotangent spaces becomes relevant.

[5] In general, for Hilbert spaces, this identification is justified by the Riesz representation theorem.

2.1. Second-rank tensors. The space of linear transformations of $\mathbb{R}^3$ into itself is called the space of *second-rank tensors* and is denoted by $Lin = \mathscr{L}(\mathbb{R}^3)$. A second-rank tensor $\mathbf{A}$ is thus a linear operator $\mathbf{A} : \mathbb{R}^3 \to \mathbb{R}^3$. Note that *Lin* is endowed naturally with a vector space structure (that means that vector addition and scalar multiplication are properly defined (cf. [**6**])).

We denote by $\mathbf{Ax} = \mathbf{A} \cdot \mathbf{x}$ the result of $\mathbf{A}$ being applied to $\mathbf{x} \in \mathbb{R}^3$. The inner product on $\mathbb{R}^3$ enables the following definition. Denote by $\mathbf{xA} = \mathbf{x} \cdot \mathbf{A}$ such element of $\mathbb{R}^3$ that

$$(\mathbf{x} \cdot \mathbf{A}) \cdot \mathbf{y} = \mathbf{x} \cdot (\mathbf{A} \cdot \mathbf{y}), \quad \text{for all } \mathbf{y} \in \mathbb{R}^3. \tag{3.2}$$

The *identity tensor* $\mathbf{1} = \mathrm{id}_{\mathbb{R}^3}$ is defined by

$$\mathbf{1} \cdot \mathbf{x} = \mathbf{x}, \quad \text{for all } \mathbf{x} \in \mathbb{R}^3.$$

The *transposed* to $\mathbf{A}$ is a tensor $\mathbf{A}^{\mathrm{T}}$ such that

$$(\mathbf{Ax}) \cdot \mathbf{y} = \mathbf{x} \cdot (\mathbf{A}^{\mathrm{T}}\mathbf{y}), \quad \text{for all } \mathbf{x}, \mathbf{y} \in \mathbb{R}^3. \tag{3.3}$$

From (3.3) follows that

$$\mathbf{A}^{\mathrm{T}}\mathbf{x} = \mathbf{xA}, \quad \text{for all } \mathbf{x} \in \mathbb{R}^3, \text{ for all } \mathbf{A} \in Lin. \tag{3.4}$$

Proof. Note that for all $\mathbf{x}, \mathbf{y} \in \mathbb{R}^3$, $\mathbf{A} \in Lin$ we have $(\mathbf{A}^{\mathrm{T}}\mathbf{x}) \cdot \mathbf{y} \overset{(3.3)}{=} \mathbf{x} \cdot (\mathbf{Ay}) \overset{(3.2)}{=} (\mathbf{xA}) \cdot \mathbf{y}$. □

The subspaces of *symmetric* and *skew-symmetric* tensors are defined respectively by

$$Sym = \{\mathbf{A} \in Lin : \mathbf{A} = \mathbf{A}^{\mathrm{T}}\}, \quad Skew = \{\mathbf{A} \in Lin : \mathbf{A} = -\mathbf{A}^{\mathrm{T}}\}. \tag{3.5}$$

The *symmetric part* of a tensor is defined through $\mathrm{sym}(\mathbf{A}) = \frac{1}{2}(\mathbf{A} + \mathbf{A}^{\mathrm{T}})$.

The *composition* of two operators $\mathbf{A}$ and $\mathbf{B}$ is a tensor $\mathbf{AB} = \mathbf{A} \cdot \mathbf{B}$ defined by the rule

$$(\mathbf{AB})\mathbf{x} = \mathbf{A}(\mathbf{Bx}), \quad \text{for all } \mathbf{x} \in \mathbb{R}^3. \tag{3.6}$$

Suppose that for a second-rank tensor $\mathbf{A}$ there exists $\mathbf{B}$ such that

$$\mathbf{AB} = \mathbf{BA} = \mathbf{1}. \tag{3.7}$$

Then we say that $\mathbf{A}$ is *invertible*, the operator $\mathbf{B}$ is called the *inverse* of $\mathbf{A}$ and denoted by $\mathbf{A}^{-1}$.

If $\mathbf{A}$ is invertible, then $\mathbf{A}^{-1}$ is uniquely defined by (3.7). The set of invertible second-rank tensors forms a non-Abelian group $GL(\mathbb{R}^3)$.

Next, we define the *tensor exponential* by

$$\exp\Big(\mathbf{B}\Big) = \sum_{n=0}^{\infty} \frac{1}{n!}\mathbf{B}^n, \quad \text{for all } \mathbf{B} \in Lin. \tag{3.8}$$

The notion of *trace* is coordinate free. Indeed, there exists a unique linear isotropic functional $\mathrm{tr} : Lin \to \mathbb{R}$ such that $\mathrm{tr}(\mathbf{1}) = 3$. Thus, we identify the trace operation with tr. Moreover, the notion of *determinant* is coordinate free as well[6].

For any $\mathbf{x}, \mathbf{y} \in \mathbb{R}^3$ define the *dyadic product* $\mathbf{x} \otimes \mathbf{y} \in Lin$ by the rule

$$(\mathbf{x} \otimes \mathbf{y})\mathbf{z} = \mathbf{x}(\mathbf{y} \cdot \mathbf{z}), \quad \text{for all } \mathbf{z} \in \mathbb{R}^3. \tag{3.9}$$

---

[6] One elegant geometric definition of determinant is presented in [**6**].

One useful identity is

$$\operatorname{tr}(\mathbf{x} \otimes \mathbf{y}) = \mathbf{x} \cdot \mathbf{y}. \tag{3.10}$$

The space *Lin* can be treated as a real Hilbert space with a scalar product given by

$$\mathbf{A} : \mathbf{B} = \operatorname{tr}(\mathbf{A}\mathbf{B}^{\mathrm{T}}). \tag{3.11}$$

This scalar product gives rise to the norm on *Lin* by

$$\|\mathbf{A}\| = \sqrt{\mathbf{A} : \mathbf{A}}. \tag{3.12}$$

2.2. Fourth-rank tensors. The space of linear transformations of *Lin* into itself is called the space of *fourth-rank tensors* and is denoted by $LinLin = \mathscr{L}(Lin)$. A fourth-rank tensor $\mathbb{A}$ is thus a linear operator $\mathbb{A} : Lin \to Lin$. Note that *LinLin* is endowed naturally with a vector space structure.

We denote by $\mathbb{A}\mathbf{X} = \mathbb{A} : \mathbf{X}$ the result of $\mathbb{A}$ being applied to $\mathbf{X} \in Lin$. The inner product on *Lin* enables the following definition. By $\mathbf{X}\mathbb{A} = \mathbf{X} : \mathbb{A}$ denote such element of *Lin* that

$$(\mathbf{X} : \mathbb{A}) : \mathbf{Y} = \mathbf{X} : (\mathbb{A} : \mathbf{Y}), \quad \text{for all } \mathbf{Y} \in Lin. \tag{3.13}$$

The *fourth-rank identity tensor* $\mathbb{I} = \mathrm{id}_{Lin}$ is defined by

$$\mathbb{I} : \mathbf{X} = \mathbf{X}, \quad \text{for all } \mathbf{X} \in Lin.$$

The *transposed* to $\mathbb{A}$ is a tensor $\mathbb{A}^{\mathrm{T}}$ such that[7]

$$(\mathbb{A}\mathbf{X}) : \mathbf{Y} = \mathbf{X} : (\mathbb{A}^{\mathrm{T}}\mathbf{Y}), \quad \text{for all } \mathbf{X}, \mathbf{Y} \in Lin. \tag{3.14}$$

It follows immediately from (3.14) that

$$\mathbb{A}^{\mathrm{T}} : \mathbf{X} = \mathbf{X} : \mathbb{A}, \quad \text{for all } \mathbf{X} \in Lin, \quad \text{for all } \mathbb{A} \in LinLin. \tag{3.15}$$

Two specific operations are defined by

$$\mathbb{A}^{\mathrm{ti}}\, \mathbf{X} = \mathbb{A}(\mathbf{X}^{\mathrm{T}}), \quad \mathbb{A}^{\mathrm{to}}\, \mathbf{X} = (\mathbb{A}\mathbf{X})^{\mathrm{T}}, \quad \text{for all } \mathbf{X} \in Lin. \tag{3.16}$$

We interpret $(\cdot)^{\mathrm{ti}}$ and $(\cdot)^{\mathrm{to}}$ as "*transposition of input*" and "*transposition of output*", respectively[8].

The *composition* of two operators $\mathbb{A}$ and $\mathbb{B}$ is a fourth-rank tensor $\mathbb{A}\mathbb{B} = \mathbb{A} : \mathbb{B}$, defined by

$$(\mathbb{A}\mathbb{B})\mathbf{X} = \mathbb{A}(\mathbb{B}\mathbf{X}), \quad \text{for all } \mathbf{X} \in Lin. \tag{3.17}$$

Suppose that for a fourth-rank tensor $\mathbb{A}$ there exists $\mathbb{B}$ such that

$$\mathbb{A}\mathbb{B} = \mathbb{B}\mathbb{A} = \mathbb{I}. \tag{3.18}$$

Then we say that $\mathbb{A}$ is *invertible*, the tensor $\mathbb{B}$ is called the *inverse* of $\mathbb{A}$ and denoted by $\mathbb{A}^{-1}$. If $\mathbb{A}$ is invertible, then $\mathbb{A}^{-1}$ is uniquely defined by (3.18). The set of invertible fourth-rank tensors forms a non-Abelian group $GL(Lin)$.

Next, operators $\otimes : Lin \times Lin \to LinLin$ and $\odot : Lin \times Lin \to LinLin$ are defined through

$$(\mathbf{A} \otimes \mathbf{B}) : \mathbf{X} = \mathbf{A}(\mathbf{B} : \mathbf{X}), \quad \text{for all } \mathbf{A}, \mathbf{B}, \mathbf{X} \in Lin, \tag{3.19}$$

---

[7] This definition agrees with the general definition of *adjoint operator in Hilbert space* (see, for example, [**18**]).

[8] Somewhat different interpretation of $(\cdot)^{\mathrm{ti}}$ and $(\cdot)^{\mathrm{to}}$ was proposed in [**16**]. The properties $\mathbb{A}^{\mathrm{ti}} = \mathbb{A}$ and $\mathbb{A}^{\mathrm{to}} = \mathbb{A}$ are referenced to as *left subsymmetry* and *right subsymmetry*, respectively (cf. [**2**]).

$$(\mathbf{A} \odot \mathbf{B}) : \mathbf{X} = \mathbf{AXB}, \quad \text{for all } \mathbf{A}, \mathbf{B}, \mathbf{X} \in Lin. \tag{3.20}$$

The first operator $\otimes : Lin \times Lin \to LinLin$ is the classical *tensor product*. The second operator $\odot : Lin \times Lin \to LinLin$ (see the paper [**12**] by Itskov) is of practical assistance in analytical tensor computations. Operators $\otimes$ and $\odot$ are *bilinear* (linear in each of two arguments).

Warning 1. Some authors (see, for instance, [**11, 12, 16**]) use symbols $\otimes$ and $\times$ to denote operators $\odot$ and $\otimes$, respectively.

Let us consider a linear isomorphism $R : LinLin \to LinLin$ defined through the relation[9]

$$(\mathbf{a} \otimes \mathbf{b}) : \mathbb{A}^R : (\mathbf{c} \otimes \mathbf{d}) = (\mathbf{a} \otimes \mathbf{c}) : \mathbb{A} : (\mathbf{d} \otimes \mathbf{b}), \quad \text{for all } \mathbb{A} \in LinLin, \ \text{for all } \mathbf{a}, \mathbf{b}, \mathbf{c}, \mathbf{d} \in \mathbb{R}^3. \tag{3.21}$$

Its inverse $L = R^{-1}$ is defined by the rule

$$(\mathbf{a} \otimes \mathbf{b}) : \mathbb{A}^L : (\mathbf{c} \otimes \mathbf{d}) = (\mathbf{a} \otimes \mathbf{d}) : \mathbb{A} : (\mathbf{b} \otimes \mathbf{c}), \quad \text{for all } \mathbb{A} \in LinLin, \ \text{for all } \mathbf{a}, \mathbf{b}, \mathbf{c}, \mathbf{d} \in \mathbb{R}^3. \tag{3.22}$$

Operators $\otimes : Lin \times Lin \to LinLin$ and $\odot : Lin \times Lin \to LinLin$ are interrelated as follows.

Proposition 2.1 For all $\mathbf{A}, \mathbf{B} \in Lin$ we have

$$(\mathbf{A} \otimes \mathbf{B})^R = \mathbf{A} \odot \mathbf{B}. \tag{3.23}$$

Proof. Using (3.10) check that for all $\mathbf{a}, \mathbf{b}, \mathbf{c}, \mathbf{d} \in \mathbb{R}^3$

$$(\mathbf{a} \otimes \mathbf{b}) : (\mathbf{A} \otimes \mathbf{B})^R : (\mathbf{c} \otimes \mathbf{d}) = (\mathbf{aAc})(\mathbf{dBb}) = (\mathbf{a} \otimes \mathbf{b}) : (\mathbf{A} \odot \mathbf{B}) : (\mathbf{c} \otimes \mathbf{d}). \tag{3.24}$$

□

We abbreviate $(\mathbf{a} \otimes \mathbf{b}) \otimes (\mathbf{c} \otimes \mathbf{d})$ by $\mathbf{a} \otimes \mathbf{b} \otimes \mathbf{c} \otimes \mathbf{d}$.

Warning 2. In some works the notation $\mathbf{a} \otimes \mathbf{b} \otimes \mathbf{c} \otimes \mathbf{d}$ is used to abbreviate $(\mathbf{a} \otimes \mathbf{b}) \odot (\mathbf{c} \otimes \mathbf{d})$ (cf. [**11, 12, 16**]).

The *simple contraction* of a fourth-rank tensor with a second-rank tensors is defined by

$$(\mathbf{B} \cdot \mathbb{A}) : \mathbf{X} = \mathbf{B}(\mathbb{A} : \mathbf{X}), \quad \text{for all } \mathbf{B}, \mathbf{X} \in Lin, \text{for all } \mathbb{A} \in LinLin, \tag{3.25}$$

$$(\mathbb{A} \cdot \mathbf{C}) : \mathbf{X} = (\mathbb{A} : \mathbf{X})\mathbf{C}, \quad \text{for all } \mathbf{C}, \mathbf{X} \in Lin, \text{for all } \mathbb{A} \in LinLin, \tag{3.26}$$

$$(\mathbf{B} \cdot \mathbb{A}) \cdot \mathbf{C} = \mathbf{B} \cdot (\mathbb{A} \cdot \mathbf{C}) = \mathbf{B} \cdot \mathbb{A} \cdot \mathbf{C}, \quad \text{for all } \mathbf{B}, \mathbf{C} \in Lin, \text{for all } \mathbb{A} \in LinLin. \tag{3.27}$$

We note that (cf. [**11**])

$$\mathbf{A} \cdot (\mathbf{B} \odot \mathbf{C}) \cdot \mathbf{D} = (\mathbf{AB}) \odot (\mathbf{CD}), \quad \text{for all } \mathbf{A}, \mathbf{B}, \mathbf{C}, \mathbf{D} \in Lin. \tag{3.28}$$

Indeed, for all $\mathbf{A}, \mathbf{B}, \mathbf{C}, \mathbf{D}, \mathbf{X} \in Lin$, it follows from (3.20), (3.27) that

$$\Big[\mathbf{A} \cdot (\mathbf{B} \odot \mathbf{C}) \cdot \mathbf{D}\Big] : \mathbf{X} = \mathbf{ABXCD} = \Big[(\mathbf{AB}) \odot (\mathbf{CD})\Big] : \mathbf{X}. \tag{3.29}$$

The *deviatoric projection tensor* $\mathbb{P}$ is defined by the rule

$$\mathbb{P} : \mathbf{X} = \mathbf{X}^{\mathrm{D}}, \quad \mathbf{X}^{\mathrm{D}} = \mathbf{X} - \frac{1}{3}\mathrm{tr}(\mathbf{X})\mathbf{1}, \quad \text{for all } \mathbf{X} \in Lin. \tag{3.30}$$

Therefore, $\mathbb{P} = \mathbb{I} - \frac{1}{3}\mathbf{1} \otimes \mathbf{1}$.

---

[9] The operators R and L are sometimes referred to as "processes of basis rearrangement", but we do not use this terminology here, since there is no basis of *LinLin* in our setting.

To stress that the operator $sym : Lin \to Lin$ is linear, we denote it by $\mathbb{S}$. Thus,

$$\mathbb{S} : \mathbf{X} = sym(\mathbf{X}), \quad \text{for all } \mathbf{X} \in Lin. \tag{3.31}$$

In what follows we may abuse notation and let $\mathbf{0}$ denote the zero element in $\mathbb{R}^3$, *Lin*, and *LinLin*.

3. Differentiation

3.1. General definition: Fréchet derivative. Let X, Y be Banach spaces equipped with norms $\|\cdot\|_X$ and $\|\cdot\|_Y$, and U be an open subset of X. Consider a function $f : U \to Y$. The function f is called *Fréchet differentiable* at $x_0 \in U$ (see, for example [**23, 10, 2**]) if there exists a bounded linear operator $Df(x_0) : X \to Y$ such that

$$\lim_{\Delta x \to 0} \frac{\|f(x_0 + \Delta x) - f(x_0) - Df(x_0)(\Delta x)\|_Y}{\|\Delta x\|_X} = 0. \tag{3.32}$$

In this case the operator $Df(x_0)$ is uniquely determined by (3.32) and we call it the *Fréchet derivative* of f at x_0 (we abuse x_0 in $Df(x_0)(\Delta x)$ when convenient)[10]. This derivative can be understood as a measure of changes in the function due to small changes in the independent variable:

$$f(x_0 + \Delta x) - f(x_0) \underset{\Delta x \to 0}{\approx} Df(x_0)(\Delta x). \tag{3.33}$$

Here, the symbol $\approx$ denotes *asymptotic equivalence* of functions: $f \approx g \;\Leftrightarrow\; f - g = \mathrm{o}(g)$.

Since spaces $\mathbb{R}$, $\mathbb{R}^3$, *Sym*, *Lin*, and *LinLin* are finite dimensional, they are Banach. Thus, the notion of Fréchet derivative is applicable for any $X, Y \in \{\mathbb{R}, \mathbb{R}^3, Sym, Lin, LinLin\}$[11].

Remark: Some authors use a directional (Gâteaux) derivative in order to define a derivative with respect to a tensor argument. But, an additional assumption that this derivative is a *bounded linear operator* is usually made (see for instance [**30, 12, 15**]). Therefore, this directional derivative is effectively a Fréchet derivative.

3.2. Differentiation with respect to a tensor.

3.2.1. *Derivative of a real-valued function with respect to a tensor.* Consider a function $\psi : U \subset Lin \to \mathbb{R}$, where U is an open subset of *Lin*. The Fréchet derivative $D\psi$ (if exists) is an element of the dual space Lin^*. Using the scalar product in *Lin*, we define the derivative[12] $\frac{\partial \psi(\mathbf{A})}{\partial \mathbf{A}}\Big|_{\mathbf{A}=\mathbf{A}_0} \in Lin$ such that

$$\frac{\partial \psi(\mathbf{A})}{\partial \mathbf{A}}\Big|_{\mathbf{A}=\mathbf{A}_0} : \mathbf{X} = D\psi(\mathbf{A}_0)(\mathbf{X}), \quad \text{for all } \mathbf{X} \in Lin. \tag{3.34}$$

3.2.2. *Derivative of a tensor-valued function with respect to a tensor.* Consider a function $\mathbf{B} : U \subset Lin \to Lin$. By definition, we put (cf. [**3, 22, 30, 2**])

$$\frac{\partial \mathbf{B}(\mathbf{A})}{\partial \mathbf{A}}\Big|_{\mathbf{A}=\mathbf{A}_0} = D\mathbf{B}(\mathbf{A}_0) \in LinLin. \tag{3.35}$$

---

[10] This coordinate-free definition of the derivative was considered in the engineering literature (cf. [**26**], [**22**], [**2**]).

[11] Since we are dealing with finite dimensional spaces, the boundedness condition on $Df(x_0)$ is superfluous, and the Fréchet derivative can be associated with a Jacobi matrix. Nevertheless, we keep the presentation general in order to benefit from the coordinate-free setting. Moreover, definitions based on the explicit use of partial derivatives are forbidden in the coordinate-free setting.

[12] Such derivatives are routinely met in formulations of hyperelastic constitutive relations (cf. [**17**]).

3.2.3. *Some properties of differentiation with respect to a tensor.* After some algebraic computations we obtain the following useful identities[13] (cf. [**26, 3, 22, 30, 1, 11, 12**])

$$\frac{\partial\psi(\mathbf{A}(\mathbf{B}))}{\partial\mathbf{B}} = \frac{\partial\psi}{\partial\mathbf{A}} : \frac{\partial\mathbf{A}}{\partial\mathbf{B}}, \quad \frac{\partial\mathrm{tr}(\mathbf{A}^n)}{\partial\mathbf{A}} = n(\mathbf{A}^{\mathrm{T}})^{n-1}, \quad \frac{\partial\det(\mathbf{A})}{\partial\mathbf{A}} = \det(\mathbf{A})\ \mathbf{A}^{-\mathrm{T}}, \tag{3.36}$$

$$\frac{\partial\mathbf{A}}{\partial\mathbf{A}} = \mathbb{I}, \quad \frac{\partial\mathbf{A}(\mathbf{B}(\mathbf{C}))}{\partial\mathbf{C}} = \frac{\partial\mathbf{A}}{\partial\mathbf{B}} : \frac{\partial\mathbf{B}}{\partial\mathbf{C}}, \quad \frac{\partial\mathbf{A}}{\partial\mathbf{B}} = \left(\frac{\partial\mathbf{B}}{\partial\mathbf{A}}\right)^{-1}, \tag{3.37}$$

$$\frac{\partial(\mathbf{A}\mathbf{B})}{\partial\mathbf{C}} = \frac{\partial\mathbf{A}}{\partial\mathbf{C}}\cdot\mathbf{B} + \mathbf{A}\cdot\frac{\partial\mathbf{B}}{\partial\mathbf{C}}, \quad \frac{\partial(\mathbf{A}^n)}{\partial\mathbf{A}} = \sum_{k=0}^{n-1}\mathbf{A}^{n-1-k}\odot\mathbf{A}^k, \quad \frac{\partial\mathbf{A}^{-1}}{\partial\mathbf{A}} = -\mathbf{A}^{-1}\odot\mathbf{A}^{-1}, \tag{3.38}$$

$$\frac{\partial\mathbf{A}(\psi(\mathbf{B}))}{\partial\mathbf{B}} = \frac{\partial\mathbf{A}}{\partial\psi}\otimes\frac{\partial\psi}{\partial\mathbf{B}}, \quad \frac{\partial\big(\psi(\mathbf{B})\mathbf{A}(\mathbf{B})\big)}{\partial\mathbf{B}} = \mathbf{A}\otimes\frac{\partial\psi}{\partial\mathbf{B}} + \psi\frac{\partial\mathbf{A}}{\partial\mathbf{B}}, \tag{3.39}$$

$$\frac{\partial\mathbf{A}^{\mathrm{D}}}{\partial\mathbf{A}} = \mathbb{P}, \quad \frac{\partial\mathbf{A}^{\mathrm{T}}}{\partial\mathbf{A}} = \frac{\partial\mathbf{A}}{\partial\mathbf{A}^{\mathrm{T}}} = \mathbb{I}^{\mathrm{to}} = \mathbb{I}^{\mathrm{ti}}, \quad \frac{\partial\mathbf{A}^{\mathrm{T}}}{\partial\mathbf{B}} = \left(\frac{\partial\mathbf{A}}{\partial\mathbf{B}}\right)^{\mathrm{to}}, \quad \frac{\partial\mathbf{A}}{\partial\mathbf{B}^{\mathrm{T}}} = \left(\frac{\partial\mathbf{A}}{\partial\mathbf{B}}\right)^{\mathrm{ti}}. \tag{3.40}$$

The left-hand sides of these identities are defined and the identities hold whenever the corresponding right-hand sides are defined.

Now let us prove some of these rules.

Proof. $(3.36)_1$: Let $\Delta\mathbf{B}\to\mathbf{0}$ be a small change in $\mathbf{B}$. Then for corresponding changes in $\mathbf{A}$ and ψ we have:
$\Delta\mathbf{A}\approx\frac{\partial\mathbf{A}}{\partial\mathbf{B}}:\Delta\mathbf{B}$, $\Delta\psi\approx\frac{\partial\psi}{\partial\mathbf{A}}:\Delta\mathbf{A}$. Thus, $\Delta\psi\approx\left(\frac{\partial\psi}{\partial\mathbf{A}}:\frac{\partial\mathbf{A}}{\partial\mathbf{B}}\right):\Delta\mathbf{B}$.
$(3.37)_2$: Let $\Delta\mathbf{C}\to\mathbf{0}$. Then $\Delta\mathbf{B}\approx\frac{\partial\mathbf{B}}{\partial\mathbf{C}}:\Delta\mathbf{C}$, $\Delta\mathbf{A}\approx\frac{\partial\mathbf{A}}{\partial\mathbf{B}}:\Delta\mathbf{B}$. Therefore,
$\Delta\mathbf{A}\approx\left(\frac{\partial\mathbf{A}}{\partial\mathbf{B}}:\frac{\partial\mathbf{B}}{\partial\mathbf{C}}\right):\Delta\mathbf{C}$.
$(3.39)_1$: Let $\Delta\mathbf{B}\to\mathbf{0}$. Then $\Delta\psi\approx\frac{\partial\psi}{\partial\mathbf{B}}:\Delta\mathbf{B}$, $\Delta\mathbf{A}\approx\frac{\partial\mathbf{A}}{\partial\psi}\Delta\psi$. Thus,
$\Delta\mathbf{A}\approx\frac{\partial\mathbf{A}}{\partial\psi}\Big(\frac{\partial\psi}{\partial\mathbf{B}}:\Delta\mathbf{B}\Big)\overset{(3.19)}{=}\left(\frac{\partial\mathbf{A}}{\partial\psi}\otimes\frac{\partial\psi}{\partial\mathbf{B}}\right):\Delta\mathbf{B}$.
$(3.38)_1$: Let $\Delta\mathbf{C}\to\mathbf{0}$. Then $\Delta\mathbf{A}\approx\frac{\partial\mathbf{A}}{\partial\mathbf{C}}:\Delta\mathbf{C}$, $\Delta\mathbf{B}\approx\frac{\partial\mathbf{B}}{\partial\mathbf{C}}:\Delta\mathbf{C}$. Moreover,
$\Delta(\mathbf{A}\mathbf{B})=(\mathbf{A}+\Delta\mathbf{A})(\mathbf{B}+\Delta\mathbf{B})-\mathbf{A}\mathbf{B}\approx\Delta\mathbf{A}\ \mathbf{B}+\mathbf{A}\ \Delta\mathbf{B}$. Finally, we obtain
$\Delta(\mathbf{A}\mathbf{B})\approx\Big(\frac{\partial\mathbf{A}}{\partial\mathbf{C}}:\Delta\mathbf{C}\Big)\mathbf{B}+\mathbf{A}\Big(\frac{\partial\mathbf{B}}{\partial\mathbf{C}}:\Delta\mathbf{C}\Big)=\left(\frac{\partial\mathbf{A}}{\partial\mathbf{C}}\cdot\mathbf{B}+\mathbf{A}\cdot\frac{\partial\mathbf{B}}{\partial\mathbf{C}}\right):\Delta\mathbf{C}$.
$(3.39)_2$: Let $\Delta\mathbf{B}\to\mathbf{0}$. In a similar way as above, we have $\Delta(\psi\mathbf{A})=(\psi+\Delta\psi)(\mathbf{A}+\Delta\mathbf{A})-\psi\mathbf{A}\approx\Delta\psi\ \mathbf{A}+\psi\ \Delta\mathbf{A}\approx\Big(\frac{\partial\psi}{\partial\mathbf{B}}:\Delta\mathbf{B}\Big)\mathbf{A}+\psi\frac{\partial\mathbf{A}}{\partial\mathbf{B}}:\Delta\mathbf{B}=\Big(\mathbf{A}\otimes\frac{\partial\psi}{\partial\mathbf{B}}+\psi\frac{\partial\mathbf{A}}{\partial\mathbf{B}}\Big):\Delta\mathbf{B}$.
$(3.38)_3$: Obviously, $\mathbf{1}\odot\mathbf{1}=\mathbb{I}=\frac{\partial\mathbf{A}}{\partial\mathbf{A}}$. Using this identity, we obtain

$$\mathbf{A}^{-1}\odot\mathbf{A}^{-1}+\frac{\partial\mathbf{A}^{-1}}{\partial\mathbf{A}}\overset{(3.28)}{=}\mathbf{A}^{-1}\cdot\left(\frac{\partial\mathbf{A}}{\partial\mathbf{A}}\cdot\mathbf{A}^{-1}+\mathbf{A}\cdot\frac{\partial\mathbf{A}^{-1}}{\partial\mathbf{A}}\right)\overset{(3.38)_1}{=}\mathbf{A}^{-1}\cdot\frac{\partial(\mathbf{A}\mathbf{A}^{-1})}{\partial\mathbf{A}}=\mathbf{0}. \qquad \square$$

3.3. Differentiation with respect to a symmetric tensor. The title of this section can be misleading. In fact, we analyze in this section the differentiation of functions defined on the space of symmetric second-rank tensors.

---

[13] More general coordinate-free formulations of *chain rule* and *product rule* for mappings in Euclidean spaces can be found in [**26**].

3.3.1. *Derivative of a tensor-valued function with respect to a symmetric tensor.* Consider a function $\mathbf{B}|_{Sym} : V \subset Sym \to Lin$, where V is an open subset of Sym (the notation $\mathbf{B}|_{Sym}$ is used to stress that the function is defined on Sym, but not on Lin). Let $\mathbf{A}_0 \in V$. Then the Fréchet derivative $D\mathbf{B}|_{Sym}(\mathbf{A}_0)$ is a linear mapping from Sym to Lin.

Proposition 3.2 Let $\mathbf{B} : U \subset Lin \to Lin$. Suppose $\mathbf{B}$ is Fréchet differentiable at $\mathbf{A}_0 \in U \cap Sym$ and $\mathbf{B}|_{Sym} : U \cap Sym \to Lin$ is a restriction of $\mathbf{B}$ to Sym. Then

$$D\mathbf{B}|_{Sym}(\mathbf{A}_0) = (D\mathbf{B}(\mathbf{A}_0))|_{Sym}. \tag{3.41}$$

In other words, a Fréchet derivative of the restriction is a restriction of the Fréchet derivative. In order to compute the derivative with respect to a symmetric tensor, it is sufficient to compute the general derivative (if exists). To this end, identities (3.36) — (3.40) can be used.

The linear operator $D\mathbf{B}|_{Sym}(\mathbf{A}_0)$ permits different types of representations using fourth-rank tensors. In this paper we use equivalence classes on $LinLin$. Let us consider an *equivalence relation* $\sim$ on $LinLin$:

$$\text{For all } \mathbb{X}, \mathbb{Y} \in LinLin, \quad \mathbb{X} \sim \mathbb{Y} \quad \text{if and only if} \quad \mathbb{X} : \mathbf{Z} = \mathbb{Y} : \mathbf{Z}, \quad \text{for all } \mathbf{Z} \in Sym. \tag{3.42}$$

For any $\mathbb{X} \in LinLin$, the *equivalence class* of $\mathbb{X}$ is a subset $\pi(\mathbb{X}) = \{\mathbb{Y} : \mathbb{X} \sim \mathbb{Y}\}$. The set of all equivalence classes is endowed naturally with a vector space structure.

We define $\dfrac{\partial \mathbf{B}|_{Sym}}{\partial \mathbf{A}}$ as an equivalence class

$$\frac{\partial \mathbf{B}|_{Sym}}{\partial \mathbf{A}}\Big|_{\mathbf{A}=\mathbf{A}_0} = \{\mathbb{X} \in LinLin : \ \mathbb{X} : \mathbf{Z} = D\mathbf{B}|_{Sym}(\mathbf{A}_0)(\mathbf{Z}), \quad \text{for all } \mathbf{Z} \in Sym\}. \tag{3.43}$$

In this notation, identity (3.41) can be rewritten as

$$\frac{\partial \mathbf{B}|_{Sym}}{\partial \mathbf{A}}\Big|_{\mathbf{A}=\mathbf{A}_0} = \pi\Big(\frac{\partial \mathbf{B}}{\partial \mathbf{A}}\Big|_{\mathbf{A}=\mathbf{A}_0}\Big). \tag{3.44}$$

Next, it is convenient to introduce the following operations with equivalence classes

$$\mathbb{A} : \pi(\mathbb{B}) = \pi(\mathbb{A} : \mathbb{B}) \quad \text{for all } \mathbb{A}, \mathbb{B} \in LinLin, \tag{3.45}$$

$$\pi(\mathbb{A}) : \mathbb{B} = \mathbb{A} : \mathbb{B} \quad \text{for all } \mathbb{A}, \mathbb{B} \in LinLin \text{ such that } \mathbb{B} = \mathbb{S} : \mathbb{B}, \tag{3.46}$$

$$\pi(\mathbb{A}) : \pi(\mathbb{B}) = \pi(\mathbb{A} : \mathbb{B}) \quad \text{for all } \mathbb{A}, \mathbb{B} \in LinLin \text{ such that } \mathbb{B} : \mathbb{S} = \mathbb{S} : \mathbb{B} : \mathbb{S}, \tag{3.47}$$

$$\mathbf{A} \cdot \pi(\mathbb{B}) = \pi(\mathbf{A} \cdot \mathbb{B}), \qquad \pi(\mathbb{B}) \cdot \mathbf{A} = \pi(\mathbb{B} \cdot \mathbf{A}), \quad \text{for all } \mathbf{A} \in Lin, \ \mathbb{B} \in LinLin\ . \tag{3.48}$$

It can be easily shown that these definitions are well posed, in the sense that they do not depend on the specific choice of $\mathbb{A}$ and $\mathbb{B}$. When convenient, we abuse notation and let $\mathbb{A}$ denote $\pi(\mathbb{A})$.

Remark: A different representation of $D\mathbf{B}|_{Sym}(\mathbf{A}_0)$ have been implemented in [**22, 30**]. According to this representation, $\dfrac{\partial \mathbf{B}|_{Sym}}{\partial \mathbf{A}}$ is identified with the derivative of $\Big(\mathbf{B}|_{Sym} \circ \text{sym}\Big) : Lin \to Lin$. In other words, the domain of the function $\mathbf{B}|_{Sym}$ is extended by artificial symmetrization of the argument. This procedure yields a unique result. Moreover, the resulting fourth-rank tensor enjoys a minor symmetry: since $\Big(\mathbf{B}|_{Sym} \circ \ \text{sym}\Big) = \Big(\Big(\mathbf{B}|_{Sym} \circ \ \text{sym}\Big) \circ \ \text{sym}\Big)$, we arrive at

$$\frac{\partial\Big(\mathbf{B}|_{Sym} \circ \ \text{sym}\Big)}{\partial \mathbf{A}}\Big|_{\mathbf{A}=\mathbf{A}_0} = \frac{\partial\Big(\mathbf{B}|_{Sym} \circ \ \text{sym}\Big)}{\partial \mathbf{A}}\Big|_{\mathbf{A}=\mathbf{A}_0} : \mathbb{S}. \tag{3.49}$$

Proposition 3.2 implies that both representations are interconnected as follows

$$\frac{\partial \mathbf{B}|_{Sym}}{\partial \mathbf{A}}\Big|_{\mathbf{A}=\mathbf{A}_0} = \pi\left(\frac{\partial\Big(\mathbf{B}|_{Sym} \circ \ \mathrm{sym}\Big)}{\partial \mathbf{A}}\Big|_{\mathbf{A}=\mathbf{A}_0}\right). \tag{3.50}$$

In deciding between the two alternatives, the preference should be given to the most convenient one, depending on the specific application. The main advantage of using the equivalence class (3.43), rather than the derivative of $\Big(\mathbf{B}|_{Sym} \circ \ \mathrm{sym}\Big)$, lies in the fact that *any* representative element of the equivalence class can represent $\frac{\partial \mathbf{B}|_{Sym}}{\partial \mathbf{A}}$.

Warning 3. For a given function $\mathbf{B} : U \subset Lin \to Lin$, any mathematically consistent definition of $\frac{\partial \mathbf{B}|_{Sym}}{\partial \mathbf{A}}$ should be based on the representation of the Fréchet derivative $D\mathbf{B}|_{Sym}$, but not of $D\mathbf{B}$, since it may not exist.

3.3.2. *Derivative of a real-valued function with respect to a symmetric tensor.* Consider a function $\psi|_{Sym} : V \subset Sym \to \mathbb{R}$, where V is an open subset of Sym (the notation $\psi|_{Sym}$ is used to stress that the function is defined on Sym, but not on Lin). The Fréchet derivative $D\psi|_{Sym}(\mathbf{A}_0)$ is an element of Sym^*. Similarly to Section 3.3.1, different representations of $D\psi|_{Sym}$ by second-rank tensors are possible. These representations can be handled in much the same way as in Section 3.3.1. To this end, the following proposition will be needed.

Proposition 3.4 Consider a real-valued function $\psi : U \subset Lin \to \mathbb{R}$. Suppose ψ is Fréchet differentiable at $\mathbf{A}_0 \in U \cap Sym$ and $\psi|_{Sym} : U \cap Sym \to \mathbb{R}$ is the restriction of ψ to Sym. Then

$$D\psi|_{Sym}(\mathbf{A}_0) = (D\psi(\mathbf{A}_0))|_{Sym}. \tag{3.51}$$

The use of equivalence classes on Lin would naturally reflect the following fact. If $D\psi|_{Sym}$ is represented by some $\mathbf{X} \in Lin$, then the skew part of $\mathbf{X}$ remains indeterminate (cf. [**2**]). More precisely, for any $\mathbf{X} \in \frac{\partial \psi|_{Sym}}{\partial \mathbf{A}}\Big|_{\mathbf{A}=\mathbf{A}_0}$

$$\frac{\partial \psi|_{Sym}}{\partial \mathbf{A}}\Big|_{\mathbf{A}_0} = \mathbf{X} + Skew. \tag{3.52}$$

4. Numerical implementation of tensor setting

4.1. Coordinate representation. Now we discuss the coordinate representation of tensors and basic operations on tensor. Let $\mathbf{e}_\alpha$ be the basis of a curvilinear coordinate system. By $\mathbf{e}^\alpha$ denote the basis dual to $\mathbf{e}_\alpha$; that is, $\mathbf{e}^\alpha \cdot \mathbf{e}_\beta = \delta^\alpha_\beta$ (see, for example, [**23**]). We use the Einstein summation convention in this section. Let us note that $\{\mathbf{e}_\alpha\}$, $\{\mathbf{e}_\alpha \otimes \mathbf{e}_\beta\}$, and $\{\mathbf{e}_\alpha \otimes \mathbf{e}_\beta \otimes \mathbf{e}_\gamma \otimes \mathbf{e}_\delta\}$ form bases of $\mathbb{R}^3$, Lin, and $LinLin$, respectively. Therefore, vectors $\mathbf{a} \in \mathbb{R}^3$, second-rank tensors $\mathbf{A} \in Lin$, and fourth-rank tensors $\mathbb{A} \in LinLin$ can be represented as follows

$$\mathbf{a} = \mathbf{a}^\alpha \mathbf{e}_\alpha, \quad \mathbf{a}^\alpha = \mathbf{e}^\alpha \cdot \mathbf{a}, \tag{3.53}$$

$$\mathbf{A} = \mathbf{A}^{\alpha\beta} \mathbf{e}_\alpha \otimes \mathbf{e}_\alpha, \quad \mathbf{A}^{\alpha\beta} = \mathbf{e}^\alpha \mathbf{A} \mathbf{e}^\beta = \mathbf{A} : (\mathbf{e}^\alpha \otimes \mathbf{e}^\beta), \tag{3.54}$$

$$\mathbb{A} = \mathbb{A}^{\alpha\beta\gamma\delta} \mathbf{e}_\alpha \otimes \mathbf{e}_\beta \otimes \mathbf{e}_\gamma \otimes \mathbf{e}_\delta, \quad \mathbb{A}^{\alpha\beta\gamma\delta} = (\mathbf{e}^\alpha \otimes \mathbf{e}^\beta) : \mathbb{A} : (\mathbf{e}^\gamma \otimes \mathbf{e}^\delta). \tag{3.55}$$

Remark: We use notations $\mathbf{a}^\alpha, \mathbf{A}^{\alpha\beta}, \mathbb{A}^{\alpha\beta\gamma\delta}$ rather than $a^\alpha, A^{\alpha\beta}, A^{\alpha\beta\gamma\delta}$ for the following reason. Coordinates of tensors are uniquely determined by $(3.53)_2$, $(3.54)_2$, $(3.55)_2$. Thus, within the coordinate-free approach, the coordinates $\mathbf{a}^\alpha$, $\mathbf{A}^{\alpha\beta}$, $\mathbb{A}^{\alpha\beta\gamma\delta}$ are understood as functions of $\mathbf{a}$, $\mathbf{A}$, $\mathbb{A}$, respectively. For example, the function $(\cdot)^\alpha$ takes each $\mathbf{a}$ to $\mathbf{a}^\alpha$.

The coordinate representations of invariant relations follow from (3.53) — (3.55) in a straight-forward manner:

$$\mathbf{a}\cdot\mathbf{b} = \mathbf{a}^{\alpha}\mathbf{b}_{\alpha} = \mathbf{a}_{\alpha}\mathbf{b}^{\alpha}, \tag{3.56}$$

$$(\mathbf{A}\mathbf{x})^{\alpha} = \mathbf{A}^{\alpha\beta}\mathbf{x}_{\beta} = \mathbf{A}^{\alpha}{}_{\beta}\mathbf{x}^{\beta}, \tag{3.57}$$

$$(\mathbf{x}\mathbf{A})^{\alpha} \overset{(3.2)}{=} \mathbf{x}_{\beta}\mathbf{A}^{\beta\alpha} \overset{(3.2)}{=} \mathbf{x}^{\beta}\mathbf{A}_{\beta}{}^{\alpha}, \tag{3.58}$$

$$\mathbf{1}^{\alpha\beta} = \mathbf{e}^{\alpha}\cdot\mathbf{e}^{\beta}, \quad \mathbf{1}_{\alpha\beta} = \mathbf{e}_{\alpha}\cdot\mathbf{e}_{\beta}, \quad \mathbf{1}_{\alpha}{}^{\beta} = \mathbf{1}^{\beta}{}_{\alpha} = \delta^{\beta}_{\alpha}, \tag{3.59}$$

$$(\mathbf{A}^{\mathrm{T}})^{\alpha\beta} \overset{(3.3)}{=} \mathbf{A}^{\beta\alpha}, \quad (\mathbf{A}^{\mathrm{T}})^{\alpha}{}_{\beta} \overset{(3.3)}{=} \mathbf{A}_{\beta}{}^{\alpha}, \tag{3.60}$$

$$(\mathbf{A}\mathbf{B})^{\alpha\beta} \overset{(3.6)}{=} \mathbf{A}^{\alpha}{}_{\gamma}\mathbf{B}^{\gamma\beta} \overset{(3.6)}{=} \mathbf{A}^{\alpha\gamma}\mathbf{B}_{\gamma}{}^{\beta}, \tag{3.61}$$

$$\begin{gathered}(\mathbf{x}\otimes\mathbf{y})^{\alpha\beta} \overset{(3.9)}{=} \mathbf{x}^{\alpha}\mathbf{y}^{\beta}, \quad (\mathbf{x}\otimes\mathbf{y})_{\alpha\beta} \overset{(3.9)}{=} \mathbf{x}_{\alpha}\mathbf{y}_{\beta}, \\ (\mathbf{x}\otimes\mathbf{y})^{\alpha}{}_{\beta} \overset{(3.9)}{=} \mathbf{x}^{\alpha}\mathbf{y}_{\beta}, \quad (\mathbf{x}\otimes\mathbf{y})_{\alpha}{}^{\beta} \overset{(3.9)}{=} \mathbf{x}_{\alpha}\mathbf{y}^{\beta},\end{gathered} \tag{3.62}$$

$$\mathbf{A}:\mathbf{B} \overset{(3.10),(3.11)}{=} \mathbf{A}^{\alpha\beta}\mathbf{B}_{\alpha\beta} \overset{(3.10),(3.11)}{=} \mathbf{A}_{\alpha\beta}\mathbf{B}^{\alpha\beta} \overset{(3.10),(3.11)}{=} \mathbf{A}^{\alpha}{}_{\beta}\mathbf{B}_{\alpha}{}^{\beta} \overset{(3.10),(3.11)}{=} \mathbf{A}_{\alpha}{}^{\beta}\mathbf{B}^{\alpha}{}_{\beta}, \tag{3.63}$$

$$(\mathbb{A}:\mathbf{X})^{\alpha\beta} = \mathbb{A}^{\alpha\beta\gamma\delta}\mathbf{X}_{\gamma\delta} = \mathbb{A}^{\alpha\beta}{}_{\gamma\delta}\mathbf{X}^{\gamma\delta}, \tag{3.64}$$

$$(\mathbf{X}:\mathbb{A})^{\alpha\beta} \overset{(3.13)}{=} \mathbf{X}_{\gamma\delta}\mathbb{A}^{\gamma\delta\alpha\beta} \overset{(3.13)}{=} \mathbf{X}^{\gamma\delta}\mathbb{A}_{\gamma\delta}{}^{\alpha\beta}, \tag{3.65}$$

$$\mathbb{I}^{\alpha\beta\gamma\delta} = \mathbf{1}^{\alpha\gamma}\mathbf{1}^{\beta\delta}, \quad \mathbb{I}_{\alpha\beta\gamma\delta} = \mathbf{1}_{\alpha\gamma}\mathbf{1}_{\beta\delta}, \quad \mathbb{I}^{\alpha\beta}{}_{\gamma\delta} = \mathbb{I}_{\gamma\delta}{}^{\alpha\beta} = \delta^{\alpha}_{\gamma}\delta^{\beta}_{\delta}, \tag{3.66}$$

$$(\mathbb{A}^{\mathrm{T}})^{\alpha\beta\gamma\delta} \overset{(3.14)}{=} \mathbb{A}^{\gamma\delta\alpha\beta}, \quad (\mathbb{A}^{\mathrm{T}})_{\alpha\beta\gamma\delta} \overset{(3.14)}{=} \mathbb{A}_{\gamma\delta\alpha\beta}, \tag{3.67}$$

$$(\mathbb{A}^{\mathrm{ti}})^{\alpha\beta\gamma\delta} \overset{(3.16)_1}{=} \mathbb{A}^{\alpha\beta\delta\gamma}, \quad (\mathbb{A}^{\mathrm{ti}})_{\alpha\beta\gamma\delta} \overset{(3.16)_1}{=} \mathbb{A}_{\alpha\beta\delta\gamma}, \tag{3.68}$$

$$(\mathbb{A}^{\mathrm{to}})^{\alpha\beta\gamma\delta} \overset{(3.16)_2}{=} \mathbb{A}^{\beta\alpha\gamma\delta}, \quad (\mathbb{A}^{\mathrm{to}})_{\alpha\beta\gamma\delta} \overset{(3.16)_2}{=} \mathbb{A}_{\beta\alpha\gamma\delta}, \tag{3.69}$$

$$(\mathbb{A}:\mathbb{B})^{\alpha\beta\gamma\delta} \overset{(3.17)}{=} \mathbb{A}^{\alpha\beta\zeta\eta}\mathbb{B}_{\zeta\eta}{}^{\gamma\delta} \overset{(3.17)}{=} \mathbb{A}^{\alpha\beta}{}_{\zeta\eta}\mathbb{B}^{\zeta\eta\gamma\delta}, \tag{3.70}$$

$$(\mathbf{A}\otimes\mathbf{B})^{\alpha\beta\gamma\delta} \overset{(3.19)}{=} \mathbf{A}^{\alpha\beta}\mathbf{B}^{\gamma\delta}, \quad (\mathbf{A}\otimes\mathbf{B})^{\alpha\beta}{}_{\gamma\delta} \overset{(3.19)}{=} \mathbf{A}^{\alpha\beta}\mathbf{B}_{\gamma\delta}, \tag{3.71}$$

$$(\mathbf{A}\odot\mathbf{B})^{\alpha\beta\gamma\delta} \overset{(3.20)}{=} \mathbf{A}^{\alpha\gamma}\mathbf{B}^{\delta\beta}, \quad (\mathbf{A}\odot\mathbf{B})^{\alpha}{}_{\beta}{}^{\gamma}{}_{\delta} \overset{(3.20)}{=} \mathbf{A}^{\alpha\gamma}\mathbf{B}_{\delta\beta}, \tag{3.72}$$

$$(\mathbb{A}^{\mathrm{R}})^{\alpha\beta\gamma\delta} \overset{(3.21)}{=} \mathbb{A}^{\alpha\gamma\delta\beta}, \quad (\mathbb{A}^{\mathrm{R}})_{\alpha\beta\gamma\delta} \overset{(3.21)}{=} \mathbb{A}_{\alpha\gamma\delta\beta}, \quad (\mathbb{A}^{\mathrm{R}})^{\alpha}{}_{\beta}{}^{\gamma}{}_{\delta} \overset{(3.21)}{=} \mathbb{A}^{\alpha\gamma}{}_{\delta\beta}, \tag{3.73}$$

$$(\mathbf{B}\cdot\mathbb{A})^{\alpha\beta\gamma\delta} \overset{(3.25)}{=} \mathbf{B}^{\alpha}{}_{\zeta}\mathbb{A}^{\zeta\beta\gamma\delta}, \tag{3.74}$$

$$(\mathbb{A}\cdot\mathbf{C})^{\alpha\beta\gamma\delta} \overset{(3.26)}{=} \mathbb{A}^{\alpha\eta\gamma\delta}\mathbf{C}_{\eta}{}^{\beta}. \tag{3.75}$$

Warning 4. Some authors use alternative bases in *LinLin*. For instance, since $\{\mathbf{e}_{\alpha}\otimes\mathbf{e}_{\beta}\otimes\mathbf{e}_{\gamma}\otimes\mathbf{e}_{\delta}\}$ forms a basis of *LinLin*, so is $\{R(\mathbf{e}_{\alpha}\otimes\mathbf{e}_{\beta}\otimes\mathbf{e}_{\gamma}\otimes\mathbf{e}_{\delta})\}$. Such basis was used in [**11, 12, 16**]. Therefore, coordinate representations may differ from the current ones.

4.2. Computation of inverse of a second-rank tensor. The coordinate representations of inverse $\mathbf{A}^{-1}$ of a second-rank tensor $\mathbf{A}$ are given by the following matrix identities:

$$\begin{gathered}(\mathbf{A}^{-1})^{\alpha\beta} = (\mathbf{A}_{\alpha\beta})^{-1}, \quad (\mathbf{A}^{-1})_{\alpha\beta} = (\mathbf{A}^{\alpha\beta})^{-1}, \\ (\mathbf{A}^{-1})^{\alpha}{}_{\beta} = (\mathbf{A}^{\alpha}{}_{\beta})^{-1}, \quad (\mathbf{A}^{-1})_{\alpha}{}^{\beta} = (\mathbf{A}_{\alpha}{}^{\beta})^{-1},\end{gathered} \tag{3.76}$$

where $(\mathbf{A}_{\alpha\beta})^{-1}$, $(\mathbf{A}^{\alpha\beta})^{-1}$, $(\mathbf{A}^{\alpha}{}_{\beta})^{-1}$, $(\mathbf{A}_{\alpha}{}^{\beta})^{-1}$ are inverse matrices of $\mathbf{A}_{\alpha\beta}$, $\mathbf{A}^{\alpha\beta}$, $\mathbf{A}^{\alpha}{}_{\beta}$, $\mathbf{A}_{\alpha}{}^{\beta}$, respectively. Indeed, (3.76) follows from

$$\delta_{\alpha,\beta} = (\mathbf{A}^{-1})^{\alpha\gamma}\mathbf{A}_{\gamma\beta} = (\mathbf{A}^{-1})_{\alpha\gamma}\mathbf{A}^{\gamma\beta} = (\mathbf{A}^{-1})^{\alpha}{}_{\gamma}\mathbf{A}^{\gamma}{}_{\beta} = (\mathbf{A}^{-1})_{\alpha}{}^{\gamma}\mathbf{A}_{\gamma}{}^{\beta} \quad \text{(summing over } \gamma\text{)}. \tag{3.77}$$

4.3. Computation of inverse of a fourth-rank tensor. Given coordinates (covariant, contravariant, or mixed) of a fourth-rank tensor we need to compute the coordinates of its inverse (if exists). To this end, we use an isomorphism $\Pi_g : LinLin \to \mathbb{R}^{9\times 9}$ which preserves the multiplication

$$\Pi_g(\mathbb{A} : \mathbb{B}) = \Pi_g(\mathbb{A}) \cdot \Pi_g(\mathbb{B}), \quad \text{for all } \mathbb{A}, \mathbb{B} \in LinLin. \tag{3.78}$$

Here $(\cdot)$ stands for matrix multiplication in $\mathbb{R}^{9\times 9}$. It follows from (3.78) that

$$\mathbb{A}^{-1} = \Pi_g^{-1}\Big(\Big[\Pi_g(\mathbb{A})\Big]^{-1}\Big), \quad \text{for all } \mathbb{A} \in GL(Lin), \tag{3.79}$$

where $GL(Lin)$ is the group of invertible fourth-rank tensors, and $\Big[\Pi_g(\mathbb{A})\Big]^{-1} \in \mathbb{R}^{9\times 9}$ is the inverse matrix of $\Pi_g(\mathbb{A}) \in \mathbb{R}^{9\times 9}$.

In this paper, we construct the isomorphism Π_g as follows. Let $\Phi_g : Lin \to \mathbb{R}^9$ be a linear isomorphism (Φ_g is linear and invertible). Denote by $\overrightarrow{e_k}$ the standard basis of $\mathbb{R}^9$

$$\overrightarrow{e_1} = (1, 0, ..., 0), \quad \overrightarrow{e_2} = (0, 1, 0, ..., 0), \quad ... , \quad \overrightarrow{e_9} = (0, ..., 0, 1). \tag{3.80}$$

Then $\Phi_g^{-1}(\overrightarrow{e_k})$ is a basis of Lin, and we define Π_g through the relation

$$\Pi_g(\mathbb{A}) = \Big[\mathbb{A}; \Phi_g^{-1}(\overrightarrow{e_k})\Big], \quad \text{for all } \mathbb{A} \in GL(Lin). \tag{3.81}$$

In other words, $\Pi_g(\mathbb{A})$ is the matrix of the linear operator $\mathbb{A} : Lin \to Lin$ with respect to the basis $\Phi_g^{-1}(\overrightarrow{e_k})$ (for more details see [**6**]). Thus, the 9×9 matrix $\Pi_g(\mathbb{A})$ is uniquely determined by

$$\mathbb{A} : \Phi_g^{-1}(\overrightarrow{e_l}) = \sum_{k=1}^{9} \Big[\Pi_g(\mathbb{A})\Big]_{kl} \Phi_g^{-1}(\overrightarrow{e_k}), \qquad l = 1, ..., 9. \tag{3.82}$$

Note that (3.78) follows from (3.81). Another useful identity is

$$\Phi_g(\mathbb{A} : \mathbf{B}) = \Pi_g(\mathbb{A}) \cdot \Phi_g(\mathbf{B}), \quad \text{for all } \mathbb{A} \in LinLin, \ \text{for all } \mathbf{B} \in Lin. \tag{3.83}$$

To be definite, we define $\Phi_g : Lin \to \mathbb{R}^9$ by

$$\Phi_g(\mathbf{e}^\alpha \otimes \mathbf{e}^\beta) = e_{\bar{k}(\alpha,\beta)}, \quad \bar{k}(\alpha, \beta) = 3(\alpha - 1) + \beta, \quad \alpha, \beta = 1, 2, 3. \tag{3.84}$$

Note that there are unique functions $\bar{\alpha}(k), \bar{\beta}(k)$ such that

$$\Phi_g^{-1}(\overrightarrow{e_k}) = \mathbf{e}^{\bar{\alpha}(k)} \otimes \mathbf{e}^{\bar{\beta}(k)}, \quad k = 1, ..., 9. \tag{3.85}$$

We evaluate the components of $\Pi_g(\mathbb{A}) \in \mathbb{R}^{9\times 9}$ using (3.82), (3.85)

$$\Big[\Pi_g(\mathbb{A})\Big]_{kl} = \mathbb{A}_{\bar{\alpha}(k)\bar{\beta}(k)}{}^{\bar{\alpha}(l)\bar{\beta}(l)}, \quad k, l = 1, ..., 9. \tag{3.86}$$

It follows immediately from (3.86) that

$$\Big(\Pi_g^{-1}\big(M\big)\Big)_{\alpha\beta}{}^{\gamma\delta} = M_{\bar{k}(\alpha,\beta)\bar{k}(\gamma,\delta)}, \quad \text{for all } M \in \mathbb{R}^{9\times 9}, \quad \alpha, \beta, \gamma, \delta = 1, 2, 3. \tag{3.87}$$

Finally, the coordinates of $\mathbb{A}^{-1}$ are computed according to (3.79), (3.87) as

$$(\mathbb{A}^{-1})_{\alpha\beta}{}^{\gamma\delta} = [\Pi_g(\mathbb{A})]^{-1}_{\bar{k}(\alpha,\beta)\bar{k}(\gamma,\delta)}, \quad \alpha, \beta, \gamma, \delta = 1, 2, 3, \tag{3.88}$$

where $\Pi_g(\mathbb{A})$ is computed by (3.86).

4.4. Computation of inverse in $GL(Sym)$. By $GL(Sym)$ denote the group of invertible transformations of Sym into itself. Let us discuss the computation of inverse to $\mathcal{A} \in GL(Sym)$.

In some applications it is useful to represent elements of $\mathscr{L}(Sym)$ by $\mathbb{A} \in LinLin^{SS}$, where

$$LinLin^{SS} = \Big\{\mathbb{A} \in LinLin : \mathbb{A}^{\mathrm{ti}} = \mathbb{A}^{\mathrm{to}} = \mathbb{A}\Big\}. \tag{3.89}$$

Indeed, $\mathscr{L}(Sym)$ and $LinLin^{SS}$ are isomorphic (cf. Theorem 1. in [**3**] [14]). The isomorphism $\mathfrak{L} : \mathscr{L}(Sym) \to LinLin^{SS}$ takes each linear mapping $\mathcal{A} \in \mathscr{L}(Sym)$ to a fourth-rank tensor $\mathfrak{L}(\mathcal{A}) \in LinLin^{SS}$ by

$$\mathfrak{L}(\mathcal{A}) : \mathbf{X} = \mathcal{A}(\mathrm{sym}(\mathbf{X})), \quad \mathrm{sym}(\mathbf{X}) = \frac{1}{2}(\mathbf{X} + \mathbf{X}^{\mathrm{T}}), \quad \text{for all } \mathbf{X} \in Lin. \tag{3.90}$$

Its inverse $\mathfrak{L}^{-1} = \mathfrak{R} : LinLin^{SS} \to \mathscr{L}(Sym)$ takes each $\mathbb{A} \in LinLin^{SS}$ to $\mathfrak{R}(\mathbb{A}) \in \mathscr{L}(Sym)$ by

$$\Big(\mathfrak{R}(\mathbb{A})\Big)(\mathbf{X}) = \mathbb{A} : \mathbf{X}, \quad \text{for all } \mathbf{X} \in Sym. \tag{3.91}$$

It can be easily seen that the isomorphism $\mathfrak{L}$ preserves the multiplication, that is

$$\mathfrak{L}(\mathcal{A}\mathcal{B}) = \mathfrak{L}(\mathcal{A}) : \mathfrak{L}(\mathcal{B}), \quad \text{for all } \mathcal{A}, \mathcal{B} \in \mathscr{L}(Sym). \tag{3.92}$$

Here $\mathcal{A}\mathcal{B}$ stands for multiplication (composition) of operators $\mathcal{A}$ and $\mathcal{B}$.

Problem statement. Suppose that coordinates of $\mathbb{A} \in \mathfrak{L}(GL(Sym))$ are given. We need to compute the coordinates of $\mathfrak{L}\Big(\big(\mathfrak{R}(\mathbb{A})\big)^{-1}\Big)$.

To this end, in much the same way as in Section 4.3, we consider an isomorphism $\Pi_s : \mathscr{L}(Sym) \to \mathbb{R}^{6\times 6}$ such that

$$\Pi_s(\mathcal{A}\mathcal{B}) = \Pi_s(\mathcal{A}) \cdot \Pi_s(\mathcal{B}), \quad \text{for all } \mathcal{A}, \mathcal{B} \in \mathscr{L}(Sym). \tag{3.93}$$

It follows immediately from (3.93) that

$$\mathcal{A}^{-1} = \Pi_s^{-1}\Big(\Big[\Pi_s(\mathcal{A})\Big]^{-1}\Big), \quad \text{for all } \mathcal{A} \in GL(Sym), \tag{3.94}$$

where $\Big[\Pi_s(\mathcal{A})\Big]^{-1}$ is the inverse matrix of $\Pi_s(\mathcal{A}) \in GL(\mathbb{R}^6) \subset \mathbb{R}^{6\times 6}$. We abbreviate

$$\Pi = \Pi_s \mathfrak{R} : LinLin^{SS} \to \mathbb{R}^{6\times 6}, \quad \Pi^{-1} = \mathfrak{L}\Pi_s^{-1} : \mathbb{R}^{6\times 6} \to LinLin^{SS}. \tag{3.95}$$

In this notation we obtain

$$\mathfrak{L}\Big(\big(\mathfrak{R}(\mathbb{A})\big)^{-1}\Big) = \Pi^{-1}\Big(\Big[\Pi(\mathbb{A})\Big]^{-1}\Big) \quad \text{for all } \mathbb{A} \in \mathfrak{L}(GL(Sym)). \tag{3.96}$$

The situation can be summarized in a commutative diagram (see figure 3.1).

We construct the required isomorphism Π_s as follows. Let us consider a linear isomorphism $\Phi_s : Sym \to \mathbb{R}^6$. By $\overrightarrow{e_k}$ denote now the standard basis of $\mathbb{R}^6$

$$\overrightarrow{e_1} = (1,0,0,0,0,0), \quad \overrightarrow{e_2} = (0,1,0,0,0,0), \quad \ldots, \quad \overrightarrow{e_6} = (0,0,0,0,0,1). \tag{3.97}$$

Then $\Phi_s^{-1}(\overrightarrow{e_k})$ is a basis of Sym. The isomorphism Π_s is given by

$$\Pi_s(\mathcal{A}) = \Big[\mathcal{A}; \Phi_g^{-1}(\overrightarrow{e_k})\Big], \quad \text{for all } \mathcal{A} \in GL(Sym). \tag{3.98}$$

---

[14] The definition of $LinLin^{SS}$ used by Del Piero in [**3**] is as follows:
$LinLin^{SS} = \big\{\mathbb{A} \in LinLin : \mathbb{A} = \mathbb{S} : \mathbb{A} : \mathbb{S}\big\}$. We see that this definition is equivalent to (3.89).

$$\begin{tikzcd}
\mathfrak{L}\Big(GL(Sym)\Big) \arrow[r, "\mathfrak{R}"] \arrow[rr, bend left, "\Pi"] & GL(Sym) \arrow[r, "\Pi_s"] \arrow[d, "(\cdot)^{-1}"] & GL(\mathbb{R}^6) \arrow[d, "(\cdot)^{-1}"] \\
\mathfrak{L}\Big(GL(Sym)\Big) & GL(Sym) \arrow[l, "\mathfrak{L}"'] & GL(\mathbb{R}^6) \arrow[l, "\Pi_s^{-1}"'] \arrow[ll, bend left, "\Pi^{-1}"]
\end{tikzcd}$$

Figure 3.1. Commutative diagram: computation of inverse in $GL(Sym)$.

Thus, the 6×6 matrix $\Pi_s(\mathcal{A})$ is uniquely defined by

$$\mathcal{A}(\Phi_s^{-1}(\overrightarrow{e_l})) = \sum_{k=1}^{6} \Big[\Pi_s(\mathcal{A})\Big]_{kl} \Phi_s^{-1}(\overrightarrow{e_k}), \qquad l = 1, ..., 6. \tag{3.99}$$

Note that

$$\Phi_s(\mathcal{A}(\mathbf{B})) = \Pi_s(\mathcal{A}) \cdot \Phi_s(\mathbf{B}), \quad \text{for all } \mathcal{A} \in \mathscr{L}(Sym), \ \text{for all } \mathbf{B} \in Sym. \tag{3.100}$$

To be definite, we define $\Phi_s : Sym \to \mathbb{R}^6$ by

$$\Phi_s\Big(\sqrt{2 - \delta_{\alpha\beta}}\ \mathrm{sym}(\mathbf{e}^{\alpha} \otimes \mathbf{e}^{\beta})\Big) = e_{\tilde{k}(\alpha,\beta)}, \quad 1 \leq \alpha \leq \beta \leq 3, \tag{3.101}$$

$$\tilde{k}(1,1) = 1, \ \tilde{k}(1,2) = 2, \ \tilde{k}(1,3) = 3, \ \tilde{k}(2,2) = 4, \ \tilde{k}(2,3) = 5, \ \tilde{k}(3,3) = 6. \tag{3.102}$$

Note that there exist unique functions $\tilde{\alpha}(k) \leq \tilde{\beta}(k)$ such that

$$\Phi_s^{-1}(\overrightarrow{e_k}) = \sqrt{2 - \delta_{\tilde{\alpha}(k)\tilde{\beta}(k)}}\ \mathrm{sym}(\mathbf{e}^{\tilde{\alpha}(k)} \otimes \mathbf{e}^{\tilde{\beta}(k)}), \quad k = 1, ..., 6. \tag{3.103}$$

For $\mathbb{A} \in LinLin^{SS}$ we evaluate the components of matrix $\Pi(\mathbb{A}) \in \mathbb{R}^{6\times6}$ using (3.99), (3.103)

$$\Big[\Pi(\mathbb{A})\Big]_{kl} = \sqrt{2 - \delta_{\tilde{\alpha}(k)\tilde{\beta}(k)}}\ \sqrt{2 - \delta_{\tilde{\alpha}(l)\tilde{\beta}(l)}}\ \mathbb{A}_{\tilde{\alpha}(k)\tilde{\beta}(k)}{}^{\tilde{\alpha}(l)\tilde{\beta}(l)}, \quad k, l = 1, ..., 6. \tag{3.104}$$

We see that $\Pi(\mathbb{A})$ corresponds to a well-known Mandel-Voigt representation of $\mathbb{A} \in LinLin^{SS}$. It follows immediately from (3.104) that for $1 \leq \alpha \leq \beta \leq 3, \ 1 \leq \gamma \leq \delta \leq 3$

$$\Big(\Pi^{-1}\big(M\big)\Big)_{\alpha\beta}{}^{\gamma\delta} = \frac{1}{\sqrt{2 - \delta_{\alpha\beta}}} \frac{1}{\sqrt{2 - \delta_{\gamma\delta}}} M_{\tilde{k}(\alpha,\beta),\tilde{k}(\gamma,\delta)}, \quad \text{for all } M \in \mathbb{R}^{6\times6}. \tag{3.105}$$

The coordinates of $\Pi^{-1}\big(M\big)$ are computed from (3.105) using both minor symmetries

$$\Big(\Pi^{-1}\big(M\big)\Big)_{\alpha\beta}{}^{\gamma\delta} \overset{(3.68)}{=} \Big(\Pi^{-1}\big(M\big)\Big)_{\alpha\beta}{}^{\delta\gamma} \overset{(3.69)}{=} \Big(\Pi^{-1}\big(M\big)\Big)_{\beta\alpha}{}^{\gamma\delta}, \quad \text{for all } M \in \mathbb{R}^{6\times6}. \tag{3.106}$$

Finally, the coordinates of $\mathfrak{L}\Big(\big(\mathfrak{R}(\mathbb{A})\big)^{-1}\Big)$ are evaluated according to (3.96), (3.104), (3.105), and (3.106).

Remark: Another way of proving (3.88) and (3.105) is to generalize relations (3.76) for arbitrary linear transformations in a finite-dimensional space. On the other hand, we will show in Section 5 that operators Π_g, Φ_g, Π_s, Π, and Φ_s can be useful in connection with the analysis of a system of tensor equations.

4.5. Computation of tensor exponential and its derivative. We evaluate the tensor exponential using the truncated power series[15]

$$\exp\Big(\mathbf{B}\Big) \approx \sum_{n=0}^{N} \frac{1}{n!}\mathbf{B}^n. \tag{3.107}$$

The derivative of the exponential tensor function is then computed by (see [**13**])

$$\frac{\partial \exp(\mathbf{B})}{\partial \mathbf{B}} \overset{(3.38)_2}{\approx} \sum_{n=1}^{N} \frac{1}{n!} \sum_{k=0}^{n-1} \mathbf{B}^{n-1-k} \odot \mathbf{B}^k. \tag{3.108}$$

5. Numerical implementation of a viscoplastic material model

5.1. Material model. Let us consider a material model of visoplasticity in finite strain range, which was proposed in [**27**]. The model is essentially based on the double multiplicative decomposition[16]

$$\mathbf{F} = \hat{\mathbf{F}}_{\mathrm{e}}\mathbf{F}_{\mathrm{i}}, \quad \mathbf{F}_{\mathrm{i}} = \check{\mathbf{F}}_{\mathrm{ie}}\mathbf{F}_{\mathrm{ii}}. \tag{3.109}$$

The first decomposition is motivated by the idea of a local elastic unloading[17]. The second decomposition was proposed by Lion (see [**20, 8**]) in order to represent kinematic hardening effects. The tensor $\check{\mathbf{F}}_{\mathrm{ie}}$ is related to local elastic deformations induced by strong inhomogeneities of dislocations. Along with the well-known right Cauchy-Green tensor $\mathbf{C} = \mathbf{F}^{\mathrm{T}}\mathbf{F}$, we introduce two strain-like internal variables

$$\mathbf{C}_{\mathrm{i}} = \mathbf{F}_{\mathrm{i}}^{\mathrm{T}}\mathbf{F}_{\mathrm{i}}, \quad \mathbf{C}_{\mathrm{ii}} = \mathbf{F}_{\mathrm{ii}}^{\mathrm{T}}\mathbf{F}_{\mathrm{ii}}. \tag{3.110}$$

These variables are interpreted respectively as inelastic right Cauchy-Green tensor and inelastic right Cauchy-Green tensor of microstructure. We use material (or Lagrangian) description to formulate the material model[18].

For a given deformation history $\mathbf{C}(t)$, the material response in the time interval $t \in [0, T]$ is governed by the following system of ordinary differential and algebraic equations with respect to $\mathbf{C}_{\mathrm{i}}(t)$, $\mathbf{C}_{\mathrm{ii}}(t)$, $s(t)$, $s_d(t)$, $\lambda_{\mathrm{i}}(t)$

$$\dot{\mathbf{C}}_{\mathrm{i}} = 2\frac{\lambda_{\mathrm{i}}}{\mathfrak{F}}\Big(\mathbf{C}\tilde{\mathbf{T}} - \mathbf{C}_{\mathrm{i}}\tilde{\mathbf{X}}\Big)^{\mathrm{D}}\mathbf{C}_{\mathrm{i}}, \quad \mathbf{C}_{\mathrm{i}}|_{t=0} = \mathbf{C}_{\mathrm{i}}^0,\ \det \mathbf{C}_{\mathrm{i}}^0 = 1,\ \mathbf{C}_{\mathrm{i}}^0 \in Sym, \tag{3.111}$$

$$\dot{\mathbf{C}}_{\mathrm{ii}} = 2\lambda_{\mathrm{i}}\varkappa(\mathbf{C}_{\mathrm{i}}\tilde{\mathbf{X}}\Big)^{\mathrm{D}}\mathbf{C}_{\mathrm{ii}}, \quad \mathbf{C}_{\mathrm{ii}}|_{t=0} = \mathbf{C}_{\mathrm{ii}}^0,\ \det \mathbf{C}_{\mathrm{ii}}^0 = 1,\ \mathbf{C}_{\mathrm{ii}}^0 \in Sym, \tag{3.112}$$

$$\dot{s} = \sqrt{\frac{2}{3}}\lambda_{\mathrm{i}}, \quad \dot{s}_{\mathrm{d}} = \frac{\beta}{\gamma}\dot{s}R, \quad s|_{t=0} = s^0,\ s_{\mathrm{d}}|_{t=0} = s_{\mathrm{d}}^0, \tag{3.113}$$

$$\tilde{\mathbf{T}} = 2\rho_{\mathrm{R}}\frac{\partial\psi_{\mathrm{el}}(\mathbf{C}\mathbf{C}_{\mathrm{i}}{}^{-1})}{\partial\mathbf{C}}\Big|_{\mathbf{C}_{\mathrm{i}}=\mathrm{const}}, \quad \tilde{\mathbf{X}} = 2\rho_{\mathrm{R}}\frac{\partial\psi_{\mathrm{kin}}(\mathbf{C}_{\mathrm{i}}\mathbf{C}_{\mathrm{ii}}{}^{-1})}{\partial\mathbf{C}_{\mathrm{i}}}\Big|_{\mathbf{C}_{\mathrm{ii}}=\mathrm{const}}, \tag{3.114}$$

---

[15] In some applications this approach fails due to the roundoff errors, and more sophisticated techniques are required (see, for example, [**24, 13, 14, 21**]). In what follows we will suppose that $\|\mathbf{B}\| \leq 0.4$ (cf. [**27**]). Under that condition the roundoff errors are negligible and (3.107) with $N \approx 10$ yields exact results up to machine precision.

[16] For a critical analysis of multiplicative plasticity see, for instance, [**25, 2, 31**].

[17] On the other hand, decomposition $(3.109)_1$ can be derived from the concept of material isomorphism (see [**2**]).

[18] In [**27**], the material model was originally formulated in intermediate configurations. After that, the constitutive relations were transformed to the reference configuration in order to simplify the numerical treatment.

$$R = \gamma s_{\mathrm{e}}, \quad s_{\mathrm{e}} = s - s_{\mathrm{d}}, \tag{3.115}$$

$$\lambda_{\mathrm{i}} = \frac{1}{\eta}\Big\langle \frac{1}{k_0} f \Big\rangle^{m}, \quad f = \mathfrak{F} - \sqrt{\frac{2}{3}}\big[K + R\big], \quad \mathfrak{F} = \sqrt{\mathrm{tr}\Big[\big(\mathbf{C}\tilde{\mathbf{T}} - \mathbf{C}_{\mathrm{i}}\tilde{\mathbf{X}}\big)^{\mathrm{D}}\Big]^2}. \tag{3.116}$$

The material parameters $\rho_{\mathrm{R}} > 0$, $\varkappa \geq 0$, $\beta \geq 0$, $\gamma > 0$, $\eta \geq 0$, $m \geq 1$, $K > 0$, and the isotropic real-valued functions ψ_{el}, ψ_{kin} are assumed to be known; $k_0 > 0$ is used to obtain a dimensionless term in the bracket.

The functions $s(t)$, $s_d(t)$, $\lambda_{\mathrm{i}}(t)$ are interpreted respectively as inelastic arc length, dissipative part of inelastic arc length, and inelastic multiplier. The quantities $\mathbf{C}$, $\mathbf{C}_{\mathrm{i}}$, $\mathbf{C}_{\mathrm{ii}}$, s, and s_d uniquely define the 2nd Piola-Kirchhoff tensor $\tilde{\mathbf{T}}(t)$, the backstress tensor $\tilde{\mathbf{X}}(t)$, the isotropic hardening $R(t)$, the overstress $f(t)$, and the norm of the driving force $\mathfrak{F}(t)$.

The above definitions imply that $\mathbf{C}$ and $\mathbf{C}_{\mathrm{i}}$ are symmetric. Since functions ψ_{el} and ψ_{kin} are isotropic, *it makes no difference* whether the derivatives in (3.114) are interpreted as general derivatives or as derivatives with respect to a symmetric tensor. To prove this, we show that the general derivative in (3.114) yields symmetric tensors $\tilde{\mathbf{T}}$ and $\tilde{\mathbf{X}}$. Indeed, if we do not take the symmetry into account, potential relations (3.114) can be rewritten in the form (cf. [**27**])

$$\mathbf{C}\tilde{\mathbf{T}} = 2\rho_{\mathrm{R}} \sum_{k=1}^{3} \frac{\partial \psi_{\mathrm{el}}}{\partial J_k(\mathbf{C}{\mathbf{C}_{\mathrm{i}}}^{-1})} (\mathbf{C}{\mathbf{C}_{\mathrm{i}}}^{-1})^k, \quad \mathbf{C}_{\mathrm{i}}\tilde{\mathbf{X}} = 2\rho_{\mathrm{R}} \sum_{k=1}^{3} \frac{\partial \psi_{\mathrm{kin}}}{\partial J_k(\mathbf{C}_{\mathrm{i}}{\mathbf{C}_{\mathrm{ii}}}^{-1})} (\mathbf{C}_{\mathrm{i}}{\mathbf{C}_{\mathrm{ii}}}^{-1})^k, \tag{3.117}$$

where $\{J_k\}_{k=1,2,3}$ is a full system of invariants

$$J_1(\mathbf{A}) = \mathrm{tr}\ \mathbf{A}, \quad J_2(\mathbf{A}) = \frac{1}{2}\mathrm{tr}\ \mathbf{A}^2, \quad J_3(\mathbf{A}) = \frac{1}{3}\mathrm{tr}\ \mathbf{A}^3. \tag{3.118}$$

Multiplying both sides of $(3.117)_1$ with $\mathbf{C}^{-1}$, we conclude that $(3.114)_1$ yields a symmetric stress tensor $\tilde{\mathbf{T}}$ (if $\mathbf{C}$ and $\mathbf{C}_{\mathrm{i}}$ are symmetric). A similar result holds for $\tilde{\mathbf{X}}$.

Next, relations (3.117) imply that the right-hand sides in $(3.111)_1$, $(3.112)_1$ are symmetric. Moreover, taking into account the property $\mathrm{tr}(\mathbf{AB}) = \mathrm{tr}(\mathbf{BA})$ and combining the Jacobi formulae $(3.36)_3$ with the evolution equation (3.111), we have

$$\Big(\det \mathbf{C}_{\mathrm{i}}\Big)^{\cdot} = \frac{\partial \det(\mathbf{C}_{\mathrm{i}})}{\partial \mathbf{C}_{\mathrm{i}}} : \dot{\mathbf{C}}_{\mathrm{i}} = 2\frac{\lambda_{\mathrm{i}}}{\mathfrak{F}} \det(\mathbf{C}_{\mathrm{i}})\, \mathbf{C}_{\mathrm{i}}^{-1} : \Big(\mathbf{C}\tilde{\mathbf{T}} - \mathbf{C}_{\mathrm{i}}\tilde{\mathbf{X}}\Big)^{\mathrm{D}} \mathbf{C}_{\mathrm{i}} = 2\frac{\lambda_{\mathrm{i}}}{\mathfrak{F}} \mathrm{tr}\Big[\Big(\mathbf{C}\tilde{\mathbf{T}} - \mathbf{C}_{\mathrm{i}}\tilde{\mathbf{X}}\Big)^{\mathrm{D}}\Big] = 0. \tag{3.119}$$

In a similar way it follows from (3.112) that $\Big(\det \mathbf{C}_{\mathrm{ii}}\Big)^{\cdot} = 0$. Therefore, the exact solution of (3.111) – (3.116) has the following *geometric property*

$$\mathbf{C}_{\mathrm{i}}, \mathbf{C}_{\mathrm{ii}} \in M, \quad M = \Big\{\mathbf{B} \in Sym : \det \mathbf{B} = 1\Big\}. \tag{3.120}$$

Thus, we are dealing with a system of differential and algebraic equations on the manifold (for details see [**7**]).

In what follows, we will consider an example of ψ_{el}, ψ_{kin} given by (cf. [**8**])

$$\rho_{\mathrm{R}}\psi_{\mathrm{el}}(\mathbf{C}\mathbf{C}_{\mathrm{i}}^{-1}) = \frac{k}{2}\Big(\ln \sqrt{\det \mathbf{C}\mathbf{C}_{\mathrm{i}}^{-1}}\Big)^2 + \frac{\mu}{2}\Big(\mathrm{tr}\overline{\mathbf{C}\mathbf{C}_{\mathrm{i}}^{-1}} - 3\Big), \quad \rho_{\mathrm{R}}\psi_{\mathrm{kin}}(\mathbf{C}_{\mathrm{i}}\mathbf{C}_{\mathrm{ii}}^{-1}) = \frac{c}{4}\Big(\mathrm{tr}\overline{\mathbf{C}_{\mathrm{i}}\mathbf{C}_{\mathrm{ii}}^{-1}} - 3\Big), \tag{3.121}$$

where $k > 0$, $\mu > 0$, $c > 0$ are material constants. The overline $\overline{(\cdot)}$ denotes the unimodular part of a tensor

$$\overline{\mathbf{A}} = (\det \mathbf{A})^{-1/3}\mathbf{A}\ . \tag{3.122}$$

Taking (3.120) into account, we obtain in this special case

$$\tilde{\mathbf{T}} = k \ln \sqrt{\det(\mathbf{C})}\ \mathbf{C}^{-1} + \mu\ \mathbf{C}^{-1}(\overline{\mathbf{C}}\mathbf{C}_{\mathrm{i}}^{-1})^{\mathrm{D}}, \qquad \tilde{\mathbf{X}} = \frac{c}{2}\ \mathbf{C}_{\mathrm{i}}^{-1}(\mathbf{C}_{\mathrm{i}}\mathbf{C}_{\mathrm{ii}}^{-1})^{\mathrm{D}}. \tag{3.123}$$

5.2. Time discretization. In order to implement the material model in FEM, a proper integration algorithm is required (see, for example, [**32**]). This algorithm should provide the stresses and the consistent tangent operator as a function of the strain history. More precisely, suppose that the right Cauchy-Green tensor ${}^{n+1}\mathbf{C}$ at the time $t_{n+1} = t_n + \Delta t$ is known and assume that the internal variables $\mathbf{C}_{\mathrm{i}}, \mathbf{C}_{\mathrm{ii}}, s, s_{\mathrm{d}}$ at the time t_n are given by ${}^{n}\mathbf{C}_{\mathrm{i}}, {}^{n}\mathbf{C}_{\mathrm{ii}}, {}^{n}s, {}^{n}s_{\mathrm{d}}$, respectively. We need to compute the stress tensor (an element of *Sym*) ${}^{n+1}\tilde{\mathbf{T}} = {}^{n+1}\tilde{\mathbf{T}}({}^{n+1}\mathbf{C}, {}^{n}\mathbf{C}_{\mathrm{i}}, {}^{n}\mathbf{C}_{\mathrm{ii}}, {}^{n}s, {}^{n}s_{\mathrm{d}})$ and the consistent tangent operator (an equivalence class on *LinLin*[19]) $\dfrac{\partial^{n+1}\tilde{\mathbf{T}}}{\partial^{n+1}\mathbf{C}} = \dfrac{\partial^{n+1}\tilde{\mathbf{T}}({}^{n+1}\mathbf{C}, {}^{n}\mathbf{C}_{\mathrm{i}}, {}^{n}\mathbf{C}_{\mathrm{ii}}, {}^{n}s, {}^{n}s_{\mathrm{d}})}{\partial^{n+1}\mathbf{C}}$.

For what follows it is convenient to introduce the incremental inelastic parameter

$$\xi = \Delta t\ {}^{n+1}\lambda_{\mathrm{i}}. \tag{3.124}$$

We specialize the modified Euler-Backward method (MEBM) and the exponential method (EM) (for details see [**27**]) to discretize equations (3.111), (3.112). The scalar evolution equations $(3.113)_1$, $(3.113)_2$ are discretized by implicit Euler scheme. Discretization yields the following system of algebraic equations with respect to the internal variables at the time t_{n+1}

$${}^{n+1}\mathbf{C}_{\mathrm{i}} - \overline{\mathrm{sym}\Big(\mathbf{K}_{\mathrm{i}}({}^{n+1}\mathbf{C}, {}^{n+1}\mathbf{C}_{\mathrm{i}}, {}^{n+1}\mathbf{C}_{\mathrm{ii}}, \xi)\Big)} = \mathbf{0}, \tag{3.125}$$

$${}^{n+1}\mathbf{C}_{\mathrm{ii}} - \overline{\mathrm{sym}\Big(\mathbf{K}_{\mathrm{ii}}({}^{n+1}\mathbf{C}_{\mathrm{i}}, {}^{n+1}\mathbf{C}_{\mathrm{ii}}, \xi)\Big)} = \mathbf{0}, \tag{3.126}$$

$$\xi = \frac{\Delta t}{\eta}\Big\langle \frac{{}^{n+1}f}{k_0} \Big\rangle^m, \tag{3.127}$$

$${}^{n+1}s = {}^{n}s + \sqrt{\frac{2}{3}}\xi, \quad {}^{n+1}s_{\mathrm{d}} = {}^{n}s_{\mathrm{d}} + \frac{\beta}{\gamma}\sqrt{\frac{2}{3}}\xi\ {}^{n+1}R, \tag{3.128}$$

$${}^{n+1}R = \gamma({}^{n+1}s - {}^{n+1}s_{\mathrm{d}}), \quad {}^{n+1}f = {}^{n+1}\mathfrak{F} - \sqrt{\frac{2}{3}}(K + {}^{n+1}R), \tag{3.129}$$

$${}^{n+1}\mathfrak{F} = \sqrt{\mathrm{tr}\Big[\Big({}^{n+1}\mathbf{C}\ {}^{n+1}\tilde{\mathbf{T}} - {}^{n+1}\mathbf{C}_{\mathrm{i}}\ {}^{n+1}\tilde{\mathbf{X}}\Big)^{\mathrm{D}}\Big]^2}, \tag{3.130}$$

where the operators $\mathbf{K}_{\mathrm{k}}$ are defined for $\mathrm{k} \in \{\mathrm{i}, \mathrm{ii}\}$ by

$$\mathbf{K}_{\mathrm{k}} = \begin{cases} \Big[\mathbf{1} - \mathbf{B}_{\mathrm{k}}\Big]^{-1}\ {}^{n}\mathbf{C}_{\mathrm{k}} & \text{if MEBM is employed} \\ \exp\Big[\mathbf{B}_{\mathrm{k}}\Big]\ {}^{n}\mathbf{C}_{\mathrm{k}} & \text{if EM is employed} \end{cases}, \tag{3.131}$$

$$\mathbf{B}_{\mathrm{i}}({}^{n+1}\mathbf{C}, {}^{n+1}\mathbf{C}_{\mathrm{i}}, {}^{n+1}\mathbf{C}_{\mathrm{ii}}, \xi) = 2\frac{\xi}{{}^{n+1}\mathfrak{F}}\Big({}^{n+1}\mathbf{C}\ {}^{n+1}\tilde{\mathbf{T}} - {}^{n+1}\mathbf{C}_{\mathrm{i}}\ {}^{n+1}\tilde{\mathbf{X}}\Big)^{\mathrm{D}}, \tag{3.132}$$

$$\mathbf{B}_{\mathrm{ii}}({}^{n+1}\mathbf{C}_{\mathrm{i}}, {}^{n+1}\mathbf{C}_{\mathrm{ii}}, \xi) = 2\ \xi\ \varkappa\Big({}^{n+1}\mathbf{C}_{\mathrm{i}}\ {}^{n+1}\tilde{\mathbf{X}}\Big)^{\mathrm{D}}. \tag{3.133}$$

Here ${}^{n+1}\tilde{\mathbf{T}}$, ${}^{n+1}\tilde{\mathbf{X}}$ are functions of ${}^{n+1}\mathbf{C}, {}^{n+1}\mathbf{C}_{\mathrm{i}}, {}^{n+1}\mathbf{C}_{\mathrm{ii}}$, given by (3.114) (or by (3.123) if the special form of ψ_{el}, ψ_{kin} is used).

---

[19] Or any element of *LinLin* which can represent this equivalence class.

It follows from (3.125), (3.126) that

$$ {}^{n+1}\mathbf{C}_{\mathrm{i}}, {}^{n+1}\mathbf{C}_{\mathrm{i}} \in M. \tag{3.134} $$

Therefore, the numerical scheme *preserves the geometric property* (3.120).

5.3. Solution strategy and numerical implementation. In what follows we denote ${}^{n+1}\mathbf{C}$, ${}^{n+1}\mathbf{C}_{\mathrm{i}}$, ${}^{n+1}\mathbf{C}_{\mathrm{ii}}$ by $\mathbf{C}$, $\mathbf{C}_{\mathrm{i}}$, $\mathbf{C}_{\mathrm{ii}}$, respectively. To reduce the number of unknowns we exclude ${}^{n+1}s, {}^{n+1}s_{\mathrm{d}}$ from (3.128), $(3.129)_1$ (cf. [**9**], [**27**]) and obtain

$$ {}^{n+1}R = R(\xi) = \frac{{}^{\mathrm{t}}R + \sqrt{\frac{2}{3}}\gamma\xi}{1 + \sqrt{\frac{2}{3}}\beta\xi}, \quad {}^{\mathrm{t}}R = \gamma({}^{n}s - {}^{n}s_{\mathrm{d}}). \tag{3.135} $$

Next, substituting (3.130) and (3.135) in $(3.129)_2$, we represent ${}^{n+1}f$ as a function of $\mathbf{C}_{\mathrm{i}}, \mathbf{C}_{\mathrm{ii}}, \xi$. The problem is thus reduced to system (3.125), (3.126), (3.127) with respect to $\mathbf{C}_{\mathrm{i}}, \mathbf{C}_{\mathrm{ii}}, \xi$.

We decompose the problem (3.125), (3.126), (3.127) as follows (cf. [**27**]). The variables $\mathbf{C}_{\mathrm{i}}, \mathbf{C}_{\mathrm{ii}}$ are uniquely determined by system (3.125), (3.126) with a given ξ. Let us denote the corresponding solution by $\Big(\mathbf{C}_{\mathrm{i}}(\mathbf{C}, \xi), \mathbf{C}_{\mathrm{ii}}(\mathbf{C}, \xi)\Big)$. Substituting this solution in (3.130), we represent $\mathfrak{F}$ as a function of $\mathbf{C}$ and ξ

$$ \mathfrak{F}_1(\mathbf{C}, \xi) = \mathfrak{F}\Big(\mathbf{C}, \mathbf{C}_{\mathrm{i}}(\mathbf{C}, \xi), \mathbf{C}_{\mathrm{ii}}(\mathbf{C}, \xi)\Big). \tag{3.136} $$

If $\mathfrak{F}_1(\mathbf{C}, 0) - \sqrt{\frac{2}{3}}(K + {}^{t}R) \leq 0$, then we set $\xi = 0$, $\mathbf{C}_{\mathrm{i}} = {}^{n}\mathbf{C}_{\mathrm{i}}$, $\mathbf{C}_{\mathrm{ii}} = {}^{n}\mathbf{C}_{\mathrm{ii}}$ (no inelastic flow occurs). Otherwise, ξ is computed using equation (3.127). More precisely, substituting $(3.129)_2$ for ${}^{n+1}f$ in (3.127), we obtain two possible equations for finding ξ

$$ H(\mathbf{C}, \xi) = \frac{\eta\xi}{\Delta t} - \left(\frac{\mathfrak{F}_1(\mathbf{C}, \xi) - \sqrt{\frac{2}{3}}(K + R(\xi))}{k_0} \right)^{m} = 0, \tag{3.137} $$

$$ D(\mathbf{C}, \xi) = \left(\frac{\eta\xi}{\Delta t} \right)^{1/m} - \frac{\mathfrak{F}_1(\mathbf{C}, \xi) - \sqrt{\frac{2}{3}}(K + R(\xi))}{k_0} = 0. \tag{3.138} $$

An optimal choice between (3.137) and (3.138) was discussed in [**27**] (cf. Chapter 2). After ξ is found, the values of $\mathbf{C}_{\mathrm{i}}$, $\mathbf{C}_{\mathrm{ii}}$ are given by $\mathbf{C}_{\mathrm{i}}(\mathbf{C}, \xi)$, $\mathbf{C}_{\mathrm{ii}}(\mathbf{C}, \xi)$. Finally, we update s and s_{d} by (3.128), (3.135).

5.3.1. *Linearization of* (3.125), (3.126) *with respect to* $\mathbf{C}_i$, $\mathbf{C}_{ii}$. Let us discuss the application of the Newton-Raphson method to the computation of $\Big(\mathbf{C}_{\mathrm{i}}(\mathbf{C}, \xi), \mathbf{C}_{\mathrm{ii}}(\mathbf{C}, \xi)\Big)$ from (3.125), (3.126). We rewrite (3.125), (3.126) in the form

$$ \mathbf{M}^{\mathrm{i}}(\mathbf{C}, \mathbf{C}_{\mathrm{i}}, \mathbf{C}_{\mathrm{ii}}, \xi) = \mathbf{0}, \tag{3.139} $$

$$ \mathbf{M}^{\mathrm{ii}}(\mathbf{C}_{\mathrm{i}}, \mathbf{C}_{\mathrm{ii}}, \xi) = \mathbf{0}, \tag{3.140} $$

where

$$ \mathbf{M}^{\mathrm{k}}(\mathbf{C}, \mathbf{C}_{\mathrm{i}}, \mathbf{C}_{\mathrm{ii}}, \xi) = \mathbf{C}_{\mathrm{k}} - \overline{\mathrm{sym}\Big(\mathbf{K}_{\mathrm{k}}(\mathbf{C}, \mathbf{C}_{\mathrm{i}}, \mathbf{C}_{\mathrm{ii}}, \xi)\Big)}, \quad \mathrm{k} \in \{\mathrm{i}, \mathrm{ii}\}. \tag{3.141} $$

The Newton-Raphson iterations for fixed $(\mathbf{C}, \xi)$ are organized as follows. The initial approximation is given by the solution at the previous time step

$$ \mathbf{C}_{\mathrm{i}}^{0} = {}^{n}\mathbf{C}_{\mathrm{i}}, \quad \mathbf{C}_{\mathrm{ii}}^{0} = {}^{n}\mathbf{C}_{\mathrm{ii}}. \tag{3.142} $$

For $k \geq 1$ the linearized equations at $\mathbf{C}_{\mathrm{i}}^k$, $\mathbf{C}_{\mathrm{ii}}^k$ with respect to the increments $\Delta\mathbf{C}_{\mathrm{i}} = \mathbf{C}_{\mathrm{i}}^{k+1} - \mathbf{C}_{\mathrm{i}}^k$, $\Delta\mathbf{C}_{\mathrm{ii}} = \mathbf{C}_{\mathrm{ii}}^{k+1} - \mathbf{C}_{\mathrm{ii}}^k$ are expressed using the tensor formalism by

$$\frac{\partial \mathbf{M}^{\mathrm{i}}(\mathbf{C},\mathbf{C}_{\mathrm{i}}^k,\mathbf{C}_{\mathrm{ii}}^k,\xi)}{\partial \mathbf{C}_{\mathrm{i}}} : \Delta\mathbf{C}_{\mathrm{i}} + \frac{\partial \mathbf{M}^{\mathrm{i}}(\mathbf{C},\mathbf{C}_{\mathrm{i}}^k,\mathbf{C}_{\mathrm{ii}}^k,\xi)}{\partial \mathbf{C}_{\mathrm{ii}}} : \Delta\mathbf{C}_{\mathrm{ii}} = -\mathbf{M}^{\mathrm{i}}(\mathbf{C},\mathbf{C}_{\mathrm{i}}^k,\mathbf{C}_{\mathrm{ii}}^k,\xi), \tag{3.143}$$

$$\frac{\partial \mathbf{M}^{\mathrm{ii}}(\mathbf{C}_{\mathrm{i}}^k,\mathbf{C}_{\mathrm{ii}}^k,\xi)}{\partial \mathbf{C}_{\mathrm{i}}} : \Delta\mathbf{C}_{\mathrm{i}} + \frac{\partial \mathbf{M}^{\mathrm{ii}}(\mathbf{C}_{\mathrm{i}}^k,\mathbf{C}_{\mathrm{ii}}^k,\xi)}{\partial \mathbf{C}_{\mathrm{ii}}} : \Delta\mathbf{C}_{\mathrm{ii}} = -\mathbf{M}^{\mathrm{ii}}(\mathbf{C}_{\mathrm{i}}^k,\mathbf{C}_{\mathrm{ii}}^k,\xi), \tag{3.144}$$

$$\Delta\mathbf{C}_{\mathrm{i}}, \Delta\mathbf{C}_{\mathrm{ii}} \in Sym. \tag{3.145}$$

Note that the derivatives in (3.143), (3.144) are understood as general derivatives, without taking the symmetry of $\mathbf{C}_{\mathrm{i}}, \mathbf{C}_{\mathrm{ii}}$ into account. This approach can be justified by identity (3.44).

Remark: In the present investigation the additional constraint (3.145) is imposed to reduce the number of unknowns. Indeed, linear system (3.143) — (3.145) can be formulated with respect to twelve real unknowns instead of eighteen real unknowns for (3.143), (3.144).

The vector-matrix representation of system (3.143) — (3.145) is obtained as follows. First, we note that

$$\frac{\partial \mathbf{M}^{\mathrm{k}}}{\partial \mathbf{Z}} : \mathbb{S} \in LinLin^{SS}, \qquad \text{for all k} \in \{\mathrm{i}, \mathrm{ii}\}, \quad \text{for all } \mathbf{Z} \ \in \{\mathbf{C}, \mathbf{C}_{\mathrm{i}}, \mathbf{C}_{\mathrm{ii}}\}. \tag{3.146}$$

Next, we abbreviate $\Pi(\mathbf{M}^{\mathrm{k}}_{\mathbf{Z}}) = \Pi\Big(\dfrac{\partial \mathbf{M}^{\mathrm{k}}}{\partial \mathbf{Z}} : \mathbb{S}\Big)$, where Π is given by (3.95). According to (3.100), system (3.143) — (3.145) is equivalent to

$$\Pi(\mathbf{M}^{\mathrm{i}}_{\mathbf{C}_{\mathrm{i}}}) \cdot \Phi_s(\Delta\mathbf{C}_{\mathrm{i}}) + \Pi(\mathbf{M}^{\mathrm{i}}_{\mathbf{C}_{\mathrm{ii}}}) \cdot \Phi_s(\Delta\mathbf{C}_{\mathrm{ii}}) = -\Phi_s(\mathbf{M}^{\mathrm{i}}), \tag{3.147}$$

$$\Pi(\mathbf{M}^{\mathrm{ii}}_{\mathbf{C}_{\mathrm{i}}}) \cdot \Phi_s(\Delta\mathbf{C}_{\mathrm{i}}) + \Pi(\mathbf{M}^{\mathrm{ii}}_{\mathbf{C}_{\mathrm{ii}}}) \cdot \Phi_s(\Delta\mathbf{C}_{\mathrm{ii}}) = -\Phi_s(\mathbf{M}^{\mathrm{ii}}). \tag{3.148}$$

The increment $(\Delta\mathbf{C}_{\mathrm{i}}, \Delta\mathbf{C}_{\mathrm{ii}})$ is therefore computed by

$$\begin{pmatrix} \Phi_s(\Delta\mathbf{C}_{\mathrm{i}}) \\ \Phi_s(\Delta\mathbf{C}_{\mathrm{ii}}) \end{pmatrix} = - \begin{pmatrix} \Pi(\mathbf{M}^{\mathrm{i}}_{\mathbf{C}_{\mathrm{i}}}) & \Pi(\mathbf{M}^{\mathrm{i}}_{\mathbf{C}_{\mathrm{ii}}}) \\ \Pi(\mathbf{M}^{\mathrm{ii}}_{\mathbf{C}_{\mathrm{i}}}) & \Pi(\mathbf{M}^{\mathrm{ii}}_{\mathbf{C}_{\mathrm{ii}}}) \end{pmatrix}^{-1} \begin{pmatrix} \Phi_s(\mathbf{M}^{\mathrm{i}}) \\ \Phi_s(\mathbf{M}^{\mathrm{ii}}) \end{pmatrix}. \tag{3.149}$$

5.3.2. *Differentiation of* $\mathbf{M}^i, \mathbf{M}^{ii}$ *with respect to* $\mathbf{C}$*,* $\mathbf{C}_i$*, and* $\mathbf{C}_{ii}$*.* Now let us work out the coordinate-free expressions for the derivatives in (3.143), (3.144), which are understood as general derivatives. For $\mathrm{k} \in \{\mathrm{i}, \mathrm{ii}\}$ and $\mathbf{Z} \in \{\mathbf{C}, \mathbf{C}_{\mathrm{i}}, \mathbf{C}_{\mathrm{ii}}\}$ we have

$$\frac{\partial \mathbf{M}^{\mathrm{k}}(\mathbf{C}, \mathbf{C}_{\mathrm{i}}, \mathbf{C}_{\mathrm{ii}}, \xi)}{\partial \mathbf{Z}} \overset{(3.141)}{=} \left(\begin{cases} \mathbb{I} & \text{if } \mathbf{Z} = \mathbf{C}_{\mathrm{k}} \\ \mathbf{0} & \text{if } \mathbf{Z} \neq \mathbf{C}_{\mathrm{k}} \end{cases} \right) - \frac{\partial\, \overline{\mathrm{sym}(\mathbf{K}_{\mathrm{k}})}}{\partial \mathbf{Z}}, \tag{3.150}$$

$$\begin{aligned} \frac{\partial\, \overline{\mathrm{sym}(\mathbf{K}_{\mathrm{k}})}}{\partial \mathbf{Z}} \overset{(3.39)_2,(3.36)_1}{=} \mathrm{sym}(\mathbf{K}_{\mathrm{k}}) \otimes \Big(\frac{\partial (\det\, \mathrm{sym}(\mathbf{K}_{\mathrm{k}}))^{-\frac{1}{3}}}{\partial\, \mathrm{sym}(\mathbf{K}_{\mathrm{k}})} : \frac{\partial\, \mathrm{sym}(\mathbf{K}_{\mathrm{k}})}{\partial \mathbf{Z}} \Big) \\ + (\det\, \mathrm{sym}(\mathbf{K}_{\mathrm{k}}))^{-\frac{1}{3}}\, \frac{\partial\, \mathrm{sym}(\mathbf{K}_{\mathrm{k}})}{\partial \mathbf{Z}}, \end{aligned} \tag{3.151}$$

$$\frac{\partial\, \mathrm{sym}(\mathbf{K}_{\mathrm{k}})}{\partial \mathbf{Z}} \overset{(3.40)_3}{=} \frac{1}{2}\Big[\frac{\partial\, \mathbf{K}_{\mathrm{k}}}{\partial \mathbf{Z}} + \Big(\frac{\partial\, \mathbf{K}_{\mathrm{k}}}{\partial \mathbf{Z}} \Big)^{\mathrm{to}} \Big] = \mathbb{S} : \frac{\partial\, \mathbf{K}_{\mathrm{k}}}{\partial \mathbf{Z}}, \tag{3.152}$$

$$\frac{\partial\, \mathbf{K}_{\mathrm{k}}}{\partial \mathbf{Z}} \overset{(3.131),(3.38)_1}{=} \begin{cases} \dfrac{\partial \left[\mathbf{1} - \mathbf{B}_{\mathrm{k}}\right]^{-1}}{\partial \mathbf{Z}} \cdot {}^n\mathbf{C}_{\mathrm{k}} & \text{if MEBM is employed} \\ \dfrac{\partial\, \exp \left[\mathbf{B}_{\mathrm{k}}\right]}{\partial \mathbf{Z}} \cdot {}^n\mathbf{C}_{\mathrm{k}} & \text{if EM is employed} \end{cases}, \tag{3.153}$$

$$\frac{\partial\,\Big[\mathbf{1}-\mathbf{B}_{\mathrm{k}}\Big]^{-1}}{\partial\mathbf{Z}} \overset{(3.38)_3}{=} \left(\Big[\mathbf{1}-\mathbf{B}_{\mathrm{k}}\Big]^{-1}\odot\Big[\mathbf{1}-\mathbf{B}_{\mathrm{k}}\Big]^{-1}\right):\frac{\partial\,\mathbf{B}_{\mathrm{k}}}{\partial\mathbf{Z}}, \tag{3.154}$$

$$\frac{\partial\,\exp\Big[\mathbf{B}_{\mathrm{k}}\Big]}{\partial\mathbf{Z}} = \frac{\partial\,\exp\Big[\mathbf{B}_{\mathrm{k}}\Big]}{\partial\mathbf{B}_{\mathrm{k}}}:\frac{\partial\,\mathbf{B}_{\mathrm{k}}}{\partial\mathbf{Z}}, \tag{3.155}$$

$$\frac{\partial\,\mathbf{B}_{\mathrm{i}}}{\partial\mathbf{Z}} \overset{(3.132),(3.39)_2}{=} 2\Big(\mathbf{C}\tilde{\mathbf{T}}-\mathbf{C}_{\mathrm{i}}\tilde{\mathbf{X}}\Big)^{\mathrm{D}}\otimes\xi\frac{\partial(1/\mathfrak{F})}{\partial\mathbf{Z}}+2\frac{\xi}{\mathfrak{F}}\frac{\partial\,\Big(\mathbf{C}\tilde{\mathbf{T}}-\mathbf{C}_{\mathrm{i}}\tilde{\mathbf{X}}\Big)^{\mathrm{D}}}{\partial\mathbf{Z}}, \tag{3.156}$$

$$\frac{\partial\,\mathbf{B}_{\mathrm{ii}}}{\partial\mathbf{Z}} \overset{(3.133)}{=} 2\,\xi\,\varkappa\,\frac{\partial\,\Big(\mathbf{C}_{\mathrm{i}}\tilde{\mathbf{X}}\Big)^{\mathrm{D}}}{\partial\mathbf{Z}}, \tag{3.157}$$

where $\tilde{\mathbf{T}}=\tilde{\mathbf{T}}(\mathbf{C},\mathbf{C}_{\mathrm{i}})$, $\tilde{\mathbf{X}}=\tilde{\mathbf{X}}(\mathbf{C}_{\mathrm{i}},\mathbf{C}_{\mathrm{ii}})$, $\mathfrak{F}=\mathfrak{F}(\mathbf{C},\mathbf{C}_{\mathrm{i}},\mathbf{C}_{\mathrm{ii}})$. Next,

$$\frac{\partial(1/\mathfrak{F})}{\partial\mathbf{Z}}=-\frac{1}{\mathfrak{F}^2}\frac{\partial\mathfrak{F}}{\partial\mathbf{Z}},\quad \frac{\partial\mathfrak{F}}{\partial\mathbf{Z}} \overset{(3.36)_1}{=} \frac{\partial\mathfrak{F}}{\partial\Big(\mathbf{C}\tilde{\mathbf{T}}-\mathbf{C}_{\mathrm{i}}\tilde{\mathbf{X}}\Big)^{\mathrm{D}}}:\frac{\partial\,\Big(\mathbf{C}\tilde{\mathbf{T}}-\mathbf{C}_{\mathrm{i}}\tilde{\mathbf{X}}\Big)^{\mathrm{D}}}{\partial\mathbf{Z}}, \tag{3.158}$$

$$\frac{\partial\mathfrak{F}}{\partial\Big(\mathbf{C}\tilde{\mathbf{T}}-\mathbf{C}_{\mathrm{i}}\tilde{\mathbf{X}}\Big)^{\mathrm{D}}} \overset{(3.36)_2,(3.116)_3}{=} \frac{1}{\mathfrak{F}}\Big[\Big(\mathbf{C}\tilde{\mathbf{T}}-\mathbf{C}_{\mathrm{i}}\tilde{\mathbf{X}}\Big)^{\mathrm{D}}\Big]^{\mathrm{T}}, \tag{3.159}$$

$$\frac{\partial\,\Big(\mathbf{C}\tilde{\mathbf{T}}\Big)^{\mathrm{D}}}{\partial\mathbf{Z}} \overset{(3.40)_1}{=} \mathbb{P}:\frac{\partial\,\Big(\mathbf{C}\tilde{\mathbf{T}}\Big)}{\partial\mathbf{Z}},\quad \frac{\partial\,\Big(\mathbf{C}_{\mathrm{i}}\tilde{\mathbf{X}}\Big)^{\mathrm{D}}}{\partial\mathbf{Z}} \overset{(3.40)_1}{=} \mathbb{P}:\frac{\partial\,\Big(\mathbf{C}_{\mathrm{i}}\tilde{\mathbf{X}}\Big)}{\partial\mathbf{Z}}. \tag{3.160}$$

Combining (3.117) with $(3.36)_2$, $(3.38)_2$, and $(3.39)_2$, we obtain

$$\begin{aligned}\frac{\partial\,\Big(\mathbf{C}\tilde{\mathbf{T}}\Big)}{\partial\mathbf{Z}} = 2\rho_{\mathrm{R}}\sum_{k=1}^{3}\Bigg\{&\Big(\mathbf{C}\mathbf{C}_{\mathrm{i}}^{-1}\Big)^{k}\otimes\sum_{l=1}^{3}\frac{\partial^2\psi_{\mathrm{el}}}{\partial J_k\partial J_l}\Big(\mathbf{C}_{\mathrm{i}}^{-1}\mathbf{C}\Big)^{l-1}\\ &+\frac{\partial\psi_{\mathrm{el}}}{\partial J_k}\sum_{l=1}^{k}\Big(\mathbf{C}\mathbf{C}_{\mathrm{i}}^{-1}\Big)^{k-l}\odot\Big(\mathbf{C}\mathbf{C}_{\mathrm{i}}^{-1}\Big)^{l-1}\Bigg\}:\frac{\partial\,\Big(\mathbf{C}\mathbf{C}_{\mathrm{i}}^{-1}\Big)}{\partial\mathbf{Z}},\end{aligned} \tag{3.161}$$

$$\begin{aligned}\frac{\partial\,\Big(\mathbf{C}_{\mathrm{i}}\tilde{\mathbf{X}}\Big)}{\partial\mathbf{Z}} = 2\rho_{\mathrm{R}}\sum_{k=1}^{3}\Bigg\{&\Big(\mathbf{C}_{\mathrm{i}}\mathbf{C}_{\mathrm{ii}}^{-1}\Big)^{k}\otimes\sum_{l=1}^{3}\frac{\partial^2\psi_{\mathrm{kin}}}{\partial J_k\partial J_l}\Big(\mathbf{C}_{\mathrm{ii}}^{-1}\mathbf{C}_{\mathrm{i}}\Big)^{l-1}\\ &+\frac{\partial\psi_{\mathrm{kin}}}{\partial J_k}\sum_{l=1}^{k}\Big(\mathbf{C}_{\mathrm{i}}\mathbf{C}_{\mathrm{ii}}^{-1}\Big)^{k-l}\odot\Big(\mathbf{C}_{\mathrm{i}}\mathbf{C}_{\mathrm{ii}}^{-1}\Big)^{l-1}\Bigg\}:\frac{\partial\,\Big(\mathbf{C}_{\mathrm{i}}\mathbf{C}_{\mathrm{ii}}^{-1}\Big)}{\partial\mathbf{Z}}.\end{aligned} \tag{3.162}$$

It follows from $(3.38)_1$, $(3.38)_3$ that

$$\frac{\partial\,\Big(\mathbf{C}\mathbf{C}_{\mathrm{i}}^{-1}\Big)}{\partial\mathbf{Z}}=\begin{cases}\mathbf{1}\odot\mathbf{C}_{\mathrm{i}}^{-1} & \text{if } \mathbf{Z}=\mathbf{C}\\ -(\mathbf{C}\mathbf{C}_{\mathrm{i}}^{-1})\odot\mathbf{C}_{\mathrm{i}}^{-1} & \text{if } \mathbf{Z}=\mathbf{C}_{\mathrm{i}}\\ \mathbf{0} & \text{if } \mathbf{Z}=\mathbf{C}_{\mathrm{ii}}\end{cases}, \tag{3.163}$$

$$\frac{\partial\,\Big(\mathbf{C}_{\mathrm{i}}\mathbf{C}_{\mathrm{ii}}^{-1}\Big)}{\partial\mathbf{Z}}=\begin{cases}\mathbf{0} & \text{if } \mathbf{Z}=\mathbf{C}\\ \mathbf{1}\odot\mathbf{C}_{\mathrm{ii}}^{-1} & \text{if } \mathbf{Z}=\mathbf{C}_{\mathrm{i}}\\ -(\mathbf{C}_{\mathrm{i}}\mathbf{C}_{\mathrm{ii}}^{-1})\odot\mathbf{C}_{\mathrm{ii}}^{-1} & \text{if } \mathbf{Z}=\mathbf{C}_{\mathrm{ii}}\end{cases}. \tag{3.164}$$

If the special form (3.121) of ψ_{el}, ψ_{kin} is used, then the general expressions (3.160) — (3.164) can be replaced by the specific ones:

$$\frac{\partial\left(\mathbf{C}\tilde{\mathbf{T}}\right)^{\mathrm{D}}}{\partial\mathbf{Z}} \overset{(3.123)_1}{=} \mu\,\mathbb{P} : \frac{\partial\left(\overline{\mathbf{C}}\mathbf{C}_{\mathrm{i}}^{-1}\right)}{\partial\mathbf{Z}}, \quad \frac{\partial\left(\mathbf{C}_{\mathrm{i}}\tilde{\mathbf{X}}\right)^{\mathrm{D}}}{\partial\mathbf{Z}} \overset{(3.123)_2}{=} \frac{c}{2}\,\mathbb{P} : \frac{\partial\left(\mathbf{C}_{\mathrm{i}}\mathbf{C}_{\mathrm{ii}}^{-1}\right)}{\partial\mathbf{Z}}, \tag{3.165}$$

$$\frac{\partial\left(\overline{\mathbf{C}}\mathbf{C}_{\mathrm{i}}^{-1}\right)}{\partial\mathbf{Z}} = \begin{cases} \left(\mathbf{C}\otimes\dfrac{\partial J^{-2/3}}{\partial\mathbf{C}} + J^{-2/3}\mathbb{I}\right)\cdot\mathbf{C}_{\mathrm{i}}^{-1} & \text{if } \mathbf{Z}=\mathbf{C} \\ -(\overline{\mathbf{C}}\mathbf{C}_{\mathrm{i}}^{-1})\odot\mathbf{C}_{\mathrm{i}}^{-1} & \text{if } \mathbf{Z}=\mathbf{C}_{\mathrm{i}} \\ \mathbf{0} & \text{if } \mathbf{Z}=\mathbf{C}_{\mathrm{ii}} \end{cases}, \tag{3.166}$$

where $J=\det(\mathbf{F})=\sqrt{\det(\mathbf{C})}$ stands for the Jacobian, and

$$\frac{\partial J^{-2/3}}{\partial\mathbf{C}} \overset{(3.36)_3}{=} -\frac{1}{3}J^{-2/3}\mathbf{C}^{-1}. \tag{3.167}$$

5.3.3. *Linearization of* (3.137) *or* (3.138) *with respect to* ξ. Let us discuss the application of the Newton method to the computation of $\xi=\xi(\mathbf{C})$ from (3.137) or (3.138). We can assume that $\mathfrak{F}_1(\mathbf{C},0)-\sqrt{\frac{2}{3}}(K+{}^tR)>0$ (otherwise no inelastic flow occurs and $\xi=0$). After some computations we obtain

$$\frac{\partial H(\mathbf{C},\xi)}{\partial\xi} \overset{(3.137)}{=} \frac{\eta}{\Delta t} - m k_0^{-m}\Big(\mathfrak{F}_1(\mathbf{C},\xi) - \sqrt{\frac{2}{3}}(K+R(\xi))\Big)^{m-1}\left(\frac{\partial\mathfrak{F}_1(\mathbf{C},\xi)}{\partial\xi} - \sqrt{\frac{2}{3}}\frac{dR}{d\xi}\right), \tag{3.168}$$

$$\frac{\partial D(\mathbf{C},\xi)}{\partial\xi} \overset{(3.138)}{=} \frac{\eta}{m\Delta t}\left(\frac{\eta\xi}{\Delta t}\right)^{\frac{1-m}{m}} - k_0^{-1}\left(\frac{\partial\mathfrak{F}_1(\mathbf{C},\xi)}{\partial\xi} - \sqrt{\frac{2}{3}}\frac{dR}{d\xi}\right), \tag{3.169}$$

$$\frac{dR}{d\xi} \overset{(3.135)}{=} \sqrt{\frac{2}{3}}\frac{\gamma - {}^tR\beta}{\left(1+\sqrt{\frac{2}{3}}\beta\xi\right)^2}, \tag{3.170}$$

$$\frac{\partial\mathfrak{F}_1(\mathbf{C},\xi)}{\partial\xi} \overset{(3.136)}{=} \frac{\partial\mathfrak{F}(\mathbf{C},\mathbf{C}_{\mathrm{i}},\mathbf{C}_{\mathrm{ii}})}{\partial\mathbf{C}_{\mathrm{i}}} : \frac{\partial\mathbf{C}_{\mathrm{i}}(\mathbf{C},\xi)}{\partial\xi} + \frac{\partial\mathfrak{F}(\mathbf{C},\mathbf{C}_{\mathrm{i}},\mathbf{C}_{\mathrm{ii}})}{\partial\mathbf{C}_{\mathrm{ii}}} : \frac{\partial\mathbf{C}_{\mathrm{ii}}(\mathbf{C},\xi)}{\partial\xi}, \tag{3.171}$$

where tensors $\dfrac{\partial\mathfrak{F}(\mathbf{C},\mathbf{C}_{\mathrm{i}},\mathbf{C}_{\mathrm{ii}})}{\partial\mathbf{C}_{\mathrm{i}}}$ and $\dfrac{\partial\mathfrak{F}(\mathbf{C},\mathbf{C}_{\mathrm{i}},\mathbf{C}_{\mathrm{ii}})}{\partial\mathbf{C}_{\mathrm{ii}}}$ are given by $(3.158)_2$. Derivatives $\dfrac{\partial\mathbf{C}_{\mathrm{i}}(\mathbf{C},\xi)}{\partial\xi}$, $\dfrac{\partial\mathbf{C}_{\mathrm{ii}}(\mathbf{C},\xi)}{\partial\xi}$ can be computed by implicit differentiation of (3.139), (3.140). Indeed, using (3.100), we obtain

$$\begin{pmatrix} \Phi_s\Big(\dfrac{\partial\mathbf{C}_{\mathrm{i}}(\mathbf{C},\xi)}{\partial\xi}\Big) \\ \Phi_s\Big(\dfrac{\partial\mathbf{C}_{\mathrm{ii}}(\mathbf{C},\xi)}{\partial\xi}\Big) \end{pmatrix} = -\begin{pmatrix} \Pi(\mathbf{M}^{\mathrm{i}}_{\mathbf{C}_{\mathrm{i}}}) & \Pi(\mathbf{M}^{\mathrm{i}}_{\mathbf{C}_{\mathrm{ii}}}) \\ \Pi(\mathbf{M}^{\mathrm{ii}}_{\mathbf{C}_{\mathrm{i}}}) & \Pi(\mathbf{M}^{\mathrm{ii}}_{\mathbf{C}_{\mathrm{ii}}}) \end{pmatrix}^{-1} \begin{pmatrix} \Phi_s\Big(\frac{\partial\mathbf{M}^{\mathrm{i}}}{\partial\xi}\Big) \\ \Phi_s\Big(\frac{\partial\mathbf{M}^{\mathrm{ii}}}{\partial\xi}\Big) \end{pmatrix}. \tag{3.172}$$

Here $\dfrac{\partial\mathbf{M}^{\mathrm{i}}}{\partial\xi}=\dfrac{\partial\mathbf{M}^{\mathrm{i}}(\mathbf{C},\mathbf{C}_{\mathrm{i}},\mathbf{C}_{\mathrm{ii}},\xi)}{\partial\xi}$, $\dfrac{\partial\mathbf{M}^{\mathrm{ii}}}{\partial\xi}=\dfrac{\partial\mathbf{M}^{\mathrm{ii}}(\mathbf{C}_{\mathrm{i}},\mathbf{C}_{\mathrm{ii}},\xi)}{\partial\xi}$. Next, for $\mathrm{k}\in\{\mathrm{i},\mathrm{ii}\}$

$$\frac{\partial\mathbf{M}^{\mathrm{k}}}{\partial\xi} \overset{(3.36)_3}{=} \Big[\det\Big(\mathrm{sym}(\mathbf{K}_{\mathrm{k}})\Big)\Big]^{-\frac{1}{3}}\left(\frac{1}{3}\Big\{\Big[\mathrm{sym}(\mathbf{K}_{\mathrm{k}})\Big]^{-1} : \frac{\partial\mathrm{sym}(\mathbf{K}_{\mathrm{k}})}{\partial\xi}\Big\}\mathrm{sym}(\mathbf{K}_{\mathrm{k}}) - \frac{\partial\mathrm{sym}(\mathbf{K}_{\mathrm{k}})}{\partial\xi}\right), \tag{3.173}$$

$$\frac{\partial\,\mathrm{sym}(\mathbf{K}_{\mathrm{k}})}{\partial\xi} = \mathrm{sym}\Big(\frac{\partial\mathbf{K}_{\mathrm{k}}}{\partial\xi}\Big), \tag{3.174}$$

$$\frac{\partial \mathbf{K}_{\mathrm{k}}}{\partial \xi} \overset{(3.131)}{=} \begin{cases} \dfrac{\partial \left[\mathbf{1} - \mathbf{B}_{\mathrm{k}}\right]^{-1}}{\partial \xi} \cdot {}^{n}\mathbf{C}_{\mathrm{k}} & \text{if MEBM is employed} \\ \dfrac{\partial \ \exp\left[\mathbf{B}_{\mathrm{k}}\right]}{\partial \xi} \cdot {}^{n}\mathbf{C}_{\mathrm{k}} & \text{if EM is employed} \end{cases} . \tag{3.175}$$

It follows from (3.132), (3.133) that $\mathbf{B}_{\mathrm{k}}(\mathbf{C}, \mathbf{C}_{\mathrm{i}}, \mathbf{C}_{\mathrm{ii}}, \xi) = \xi\, \mathbf{D}_{\mathrm{k}}(\mathbf{C}, \mathbf{C}_{\mathrm{i}}, \mathbf{C}_{\mathrm{ii}})$, where $\mathbf{D}_{\mathrm{i}}(\mathbf{C}, \mathbf{C}_{\mathrm{i}}, \mathbf{C}_{\mathrm{ii}}) = \frac{2}{\mathfrak{F}}\Big(\mathbf{C}\tilde{\mathbf{T}} - \mathbf{C}_{\mathrm{i}}\tilde{\mathbf{X}}\Big)^{\mathrm{D}}$ and $\mathbf{D}_{\mathrm{ii}}(\mathbf{C}_{\mathrm{i}}, \mathbf{C}_{\mathrm{ii}}) = 2\, \varkappa\Big(\mathbf{C}_{\mathrm{i}}\ \tilde{\mathbf{X}}\Big)^{\mathrm{D}}$. Thus, we obtain

$$\frac{\partial \left[\mathbf{1} - \mathbf{B}_{\mathrm{k}}\right]^{-1}}{\partial \xi} = \mathbf{D}_{\mathrm{k}}\Big[\mathbf{1} - \mathbf{B}_{\mathrm{k}}\Big]^{-2}, \quad \frac{\partial \ \exp\left[\mathbf{B}_{\mathrm{k}}\right]}{\partial \xi} = \mathbf{D}_{\mathrm{k}}\ \exp\Big[\mathbf{B}_{\mathrm{k}}\Big]. \tag{3.176}$$

5.3.4. *Evaluation of the consistent tangent operator.* Let us denote the solution of (3.137) (or (3.138)) with a given $\mathbf{C}$ by $\xi = \xi(\mathbf{C})$. Using this notation we abbreviate

$$\mathbf{C}_{\mathrm{i}}(\mathbf{C}) = \mathbf{C}_{\mathrm{i}}(\mathbf{C}, \xi(\mathbf{C})). \tag{3.177}$$

Next we consider a function

$$\tilde{\mathbf{T}}_1(\mathbf{C}) = \tilde{\mathbf{T}}(\mathbf{C}, \mathbf{C}_{\mathrm{i}}(\mathbf{C})), \tag{3.178}$$

where $\tilde{\mathbf{T}}(\mathbf{C}, \mathbf{C}_{\mathrm{i}})$ is given by $(3.114)_1$. We interpret $\frac{\partial \tilde{\mathbf{T}}_1}{\partial \mathbf{C}}$ as an equivalence class on *LinLin* (cf. identity (3.43)). In general, the consistent tangent operator can be computed using

$$\frac{\partial \tilde{\mathbf{T}}_1}{\partial \mathbf{C}} \overset{(3.38)_1,(3.38)_3}{=} \frac{\partial\Big(\mathbf{C}^{-1}(\mathbf{C}\tilde{\mathbf{T}}_1)\Big)}{\partial \mathbf{C}} = -\mathbf{C}^{-1} \odot \tilde{\mathbf{T}} + \mathbf{C}^{-1} \cdot \Big[\frac{\partial(\mathbf{C}\tilde{\mathbf{T}})}{\partial \mathbf{C}}|_{\mathbf{C}_{\mathrm{i}}=\mathrm{const}} + \frac{\partial(\mathbf{C}\tilde{\mathbf{T}})}{\partial \mathbf{C}_{\mathrm{i}}}|_{\mathbf{C}=\mathrm{const}} : \frac{\partial \mathbf{C}_{\mathrm{i}}}{\partial \mathbf{C}}\Big]. \tag{3.179}$$

Here $\frac{\partial(\mathbf{C}\tilde{\mathbf{T}})}{\partial \mathbf{C}}|_{\mathbf{C}_{\mathrm{i}}=\mathrm{const}}$ and $\frac{\partial(\mathbf{C}\tilde{\mathbf{T}})}{\partial \mathbf{C}_{\mathrm{i}}}|_{\mathbf{C}=\mathrm{const}}$ are given by (3.161). For the special case when relations (3.123) are used, we obtain from $(3.38)_1$, $(3.38)_3$, and $(3.39)_2$

$$\frac{\partial \tilde{\mathbf{T}}_1}{\partial \mathbf{C}} = \frac{k}{2}\mathbf{C}^{-1} \otimes \mathbf{C}^{-1} - k \ln J\ \mathbf{C}^{-1} \odot \mathbf{C}^{-1} - \mu\ (\mathbf{C}^{-1} \odot \mathbf{C}^{-1}) \cdot (\overline{\mathbf{C}}\mathbf{C}_{\mathrm{i}}^{-1})^{\mathrm{D}} + \mu \mathbf{C}^{-1} \cdot \frac{\partial(\overline{\mathbf{C}}\mathbf{C}_{\mathrm{i}}^{-1})^{\mathrm{D}}}{\partial \mathbf{C}}, \tag{3.180}$$

$$\frac{\partial(\overline{\mathbf{C}}\mathbf{C}_{\mathrm{i}}^{-1})^{\mathrm{D}}}{\partial \mathbf{C}} \overset{(3.39)_2}{=} (\mathbf{C}\mathbf{C}_{\mathrm{i}}^{-1})^{\mathrm{D}} \otimes \frac{\partial J^{-2/3}}{\partial \mathbf{C}} + J^{-2/3}\mathbb{P} : \frac{\partial(\mathbf{C}\mathbf{C}_{\mathrm{i}}^{-1})}{\partial \mathbf{C}}, \tag{3.181}$$

$$\frac{\partial(\mathbf{C}\mathbf{C}_{\mathrm{i}}^{-1})}{\partial \mathbf{C}} = \frac{\partial(\mathbf{C}\mathbf{C}_{\mathrm{i}}^{-1})}{\partial \mathbf{C}}|_{\mathbf{C}_{\mathrm{i}}=\mathrm{const}} + \frac{\partial(\mathbf{C}\mathbf{C}_{\mathrm{i}}^{-1})}{\partial \mathbf{C}_{\mathrm{i}}}|_{\mathbf{C}=\mathrm{const}} : \frac{\partial \mathbf{C}_{\mathrm{i}}(\mathbf{C})}{\partial \mathbf{C}}. \tag{3.182}$$

Here, $\frac{\partial J^{-2/3}}{\partial \mathbf{C}}$ is computed by (3.167), and $\frac{\partial(\mathbf{C}\mathbf{C}_{\mathrm{i}}^{-1})}{\partial \mathbf{C}}|_{\mathbf{C}_{\mathrm{i}}=\mathrm{const}}$, $\frac{\partial(\mathbf{C}\mathbf{C}_{\mathrm{i}}^{-1})}{\partial \mathbf{C}_{\mathrm{i}}}|_{\mathbf{C}=\mathrm{const}}$ by (3.163). Thus, it remains to evaluate $\frac{\partial \mathbf{C}_{\mathrm{i}}(\mathbf{C})}{\partial \mathbf{C}}$. Recall that $\Big(\mathbf{C}_{\mathrm{i}}(\mathbf{C}, \xi), \mathbf{C}_{\mathrm{ii}}(\mathbf{C}, \xi)\Big)$ is a solution of (3.125), (3.126) with a given $(\mathbf{C}, \xi)$. Then

$$\frac{\partial \mathbf{C}_{\mathrm{i}}(\mathbf{C})}{\partial \mathbf{C}} \overset{(3.39)_1,(3.177)}{=} \frac{\partial \mathbf{C}_{\mathrm{i}}(\mathbf{C}, \xi)}{\partial \mathbf{C}} + \frac{\partial \mathbf{C}_{\mathrm{i}}(\mathbf{C}, \xi)}{\partial \xi} \otimes \frac{\partial \xi(\mathbf{C})}{\partial \mathbf{C}}, \tag{3.183}$$

where $\frac{\partial \mathbf{C}_{\mathrm{i}}(\mathbf{C}, \xi)}{\partial \xi}$ can be evaluated by (3.172). Next, note that the equivalence classes $\frac{\partial \mathbf{C}_{\mathrm{i}}(\mathbf{C}, \xi)}{\partial \mathbf{C}}$, $\frac{\partial \mathbf{C}_{\mathrm{ii}}(\mathbf{C}, \xi)}{\partial \mathbf{C}}$ can be computed by the implicit differentiation of (3.125), (3.126)

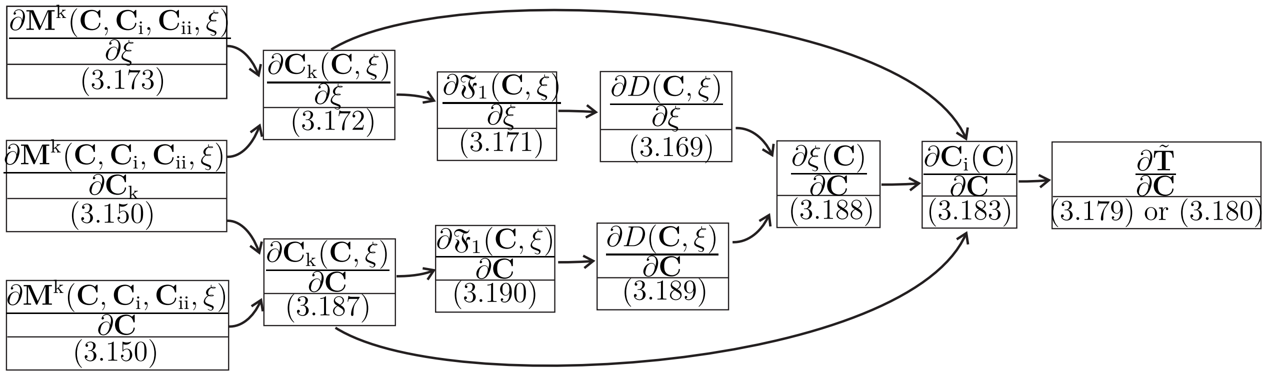

Figure 3.2. Evaluation of the consistent tangent operator.

with respect to $\mathbf{C}$. Indeed, using (3.100) we obtain the following relation between the small changes in $\mathbf{C}$, $\mathbf{C}_\mathrm{i}$, and $\mathbf{C}_\mathrm{ii}$

$$\begin{pmatrix}\Phi_s\big(\Delta\mathbf{C}_\mathrm{i}\big)\\ \Phi_s\big(\Delta\mathbf{C}_\mathrm{ii}\big)\end{pmatrix} \approx -\begin{pmatrix}\Pi(\mathbf{M}^\mathrm{i}_{\mathbf{C}_\mathrm{i}}) & \Pi(\mathbf{M}^\mathrm{i}_{\mathbf{C}_\mathrm{ii}})\\ \Pi(\mathbf{M}^\mathrm{ii}_{\mathbf{C}_\mathrm{i}}) & \Pi(\mathbf{M}^\mathrm{ii}_{\mathbf{C}_\mathrm{ii}})\end{pmatrix}^{-1}\begin{pmatrix}\Pi(\mathbf{M}^\mathrm{i}_{\mathbf{C}})\Phi_s\big(\Delta\mathbf{C}\big)\\ \Pi(\mathbf{M}^\mathrm{ii}_{\mathbf{C}})\Phi_s\big(\Delta\mathbf{C}\big)\end{pmatrix}, \quad \text{as } \Delta\mathbf{C}\to\mathbf{0}. \tag{3.184}$$

Denote

$$\begin{pmatrix}A_1 & A_2\\ A_3 & A_4\end{pmatrix} = -\begin{pmatrix}\Pi(\mathbf{M}^\mathrm{i}_{\mathbf{C}_\mathrm{i}}) & \Pi(\mathbf{M}^\mathrm{i}_{\mathbf{C}_\mathrm{ii}})\\ \Pi(\mathbf{M}^\mathrm{ii}_{\mathbf{C}_\mathrm{i}}) & \Pi(\mathbf{M}^\mathrm{ii}_{\mathbf{C}_\mathrm{ii}})\end{pmatrix}^{-1}, \tag{3.185}$$

where A_i are 6×6 matrices. With this notation we obtain for small $\Delta\mathbf{C}$

$$\Phi_s\big(\Delta\mathbf{C}_\mathrm{i}\big) \approx \big(A_1\Pi(\mathbf{M}^\mathrm{i}_{\mathbf{C}})+A_2\Pi(\mathbf{M}^\mathrm{ii}_{\mathbf{C}})\big)\Phi_s\big(\Delta\mathbf{C}\big),\ \Phi_s\big(\Delta\mathbf{C}_\mathrm{ii}\big) \approx \big(A_3\Pi(\mathbf{M}^\mathrm{i}_{\mathbf{C}})+A_4\Pi(\mathbf{M}^\mathrm{ii}_{\mathbf{C}})\big)\Phi_s\big(\Delta\mathbf{C}\big). \tag{3.186}$$

Without loss of generality it can be assumed that $\dfrac{\partial\mathbf{C}_\mathrm{i}(\mathbf{C},\xi)}{\partial\mathbf{C}}, \dfrac{\partial\mathbf{C}_\mathrm{ii}(\mathbf{C},\xi)}{\partial\mathbf{C}} \in LinLin^{SS}$. Thus,

$$\frac{\partial\mathbf{C}_\mathrm{i}(\mathbf{C},\xi)}{\partial\mathbf{C}} = \Pi^{-1}\Big(A_1\Pi(\mathbf{M}^\mathrm{i}_{\mathbf{C}}) + A_2\Pi(\mathbf{M}^\mathrm{ii}_{\mathbf{C}})\Big), \qquad \frac{\partial\mathbf{C}_\mathrm{ii}(\mathbf{C},\xi)}{\partial\mathbf{C}} = \Pi^{-1}\Big(A_3\Pi(\mathbf{M}^\mathrm{i}_{\mathbf{C}}) + A_4\Pi(\mathbf{M}^\mathrm{ii}_{\mathbf{C}})\Big), \tag{3.187}$$

where $\Pi^{-1}(\cdot)$ can be computed by (3.105), (3.106).

To evaluate $\dfrac{\partial\xi(\mathbf{C})}{\partial\mathbf{C}}$ we perform an implicit differentiation of (3.138):

$$\frac{\partial\xi(\mathbf{C})}{\partial\mathbf{C}} = -\Big(\frac{\partial D(\mathbf{C},\xi)}{\partial\xi}\Big)^{-1}\frac{\partial D(\mathbf{C},\xi)}{\partial\mathbf{C}}. \tag{3.188}$$

Here $\dfrac{\partial D(\mathbf{C},\xi)}{\partial\xi}$ can be computed by (3.169). The derivative $\dfrac{\partial D(\mathbf{C},\xi)}{\partial\mathbf{C}}$ may be evaluated as follows

$$\frac{\partial D(\mathbf{C},\xi)}{\partial\mathbf{C}} \overset{(3.138)}{=} -\frac{1}{k_0}\frac{\partial\mathfrak{F}_1(\mathbf{C},\xi)}{\partial\mathbf{C}}, \tag{3.189}$$

$$\frac{\partial\mathfrak{F}_1(\mathbf{C},\xi)}{\partial\mathbf{C}} \overset{(3.136)}{=} \frac{\partial\mathfrak{F}(\mathbf{C},\mathbf{C}_\mathrm{i},\mathbf{C}_\mathrm{ii})}{\partial\mathbf{C}} + \frac{\partial\mathfrak{F}(\mathbf{C},\mathbf{C}_\mathrm{i},\mathbf{C}_\mathrm{ii})}{\partial\mathbf{C}_\mathrm{i}} : \frac{\partial\mathbf{C}_\mathrm{i}(\mathbf{C},\xi)}{\partial\mathbf{C}} + \frac{\partial\mathfrak{F}(\mathbf{C},\mathbf{C}_\mathrm{i},\mathbf{C}_\mathrm{ii})}{\partial\mathbf{C}_\mathrm{ii}} : \frac{\partial\mathbf{C}_\mathrm{ii}(\mathbf{C},\xi)}{\partial\mathbf{C}}, \tag{3.190}$$

where $\dfrac{\partial\mathfrak{F}(\mathbf{C},\mathbf{C}_\mathrm{i},\mathbf{C}_\mathrm{ii})}{\partial\mathbf{C}}, \dfrac{\partial\mathfrak{F}(\mathbf{C},\mathbf{C}_\mathrm{i},\mathbf{C}_\mathrm{ii})}{\partial\mathbf{C}_\mathrm{i}}, \dfrac{\partial\mathfrak{F}(\mathbf{C},\mathbf{C}_\mathrm{i},\mathbf{C}_\mathrm{ii})}{\partial\mathbf{C}_\mathrm{ii}}$ are computed by $(3.158)_2$. Finally, the evaluation of the consistent tangent operator is summarized diagrammatically in figure 3.2.

6. Conclusion

We build a systematic approach to the coordinate-free tensor setting in $\mathbb{R}^3$. As a result, a simple tensor formalism based on the representation of tensors as linear transformations is constructed. The formalism allows one to formulate problems of continuum mechanics in a way independent of the choice of coordinate system. Moreover, this formalism allows to avoid tedious "index wrestling" in tensor computations and to avoid possible confusion of indexing conventions used in the engineering literature.

Two different representations of the derivative with respect to a symmetric tensor were considered. The first representation is based on the extension of the domain of the function, and the second one makes use of equivalence classes on *LinLin* (or *Lin*). It follows from (3.50) that both approaches are interchangeable. In deciding between the two approaches, the preference should be given to the most convenient one, depending on the specific application. We note that the first approach makes use of symmetrization of the argument. On the other hand, the second approach allows us to represent the derivative in a natural way without the artificial symmetrization.

The tensor formalism is applied to the analysis of a nonlinear system of differential and algebraic equations governing a visoplastic material response. In particular, the analytical linearization of a nonlinear system of tensor equations is discussed.

The application of the tensor formalism allows to broaden the range of mechanical phenomena covered by the numerical simulation. For instance, finite elastic strains can be included and a variety of stored-energy functions can be implemented, resulting in more flexible numerical algorithms. The coordinate-free results, obtained in Section 5.3, can be used in combination with any coordinate system by choosing appropriate implementations of the tensor setting (cf. Section 4).

Acknowledgements

This research was supported by German National Science Foundation (DFG) within the collaborative research center SFB 692 "High-strength aluminium based light weight materials for reliable components".

Bibliography

[1] J. Altenbach, H. Altenbach, Einführung in die Kontinuumsmechanik (Teubner Studienbücher, Stuttgart, 1994).

[2] A. Bertram, Elasticity and Plasticity of Large Deformations (Springer, 2005).

[3] G. Del Piero, Some properties of the set of fourth-order tensors, with application to elasticity, Journal of elasticity, **9**(3), 245–261 (1979).

[4] H. A. Friis, T. A. Johansen, M. Haveraaen, H. Munthe-Kaas, A. Drottning, Use of coordinate-free numerics in elastic wave simulation, Applied Numerical Mathematics, **39**, 151–171 (2001).

[5] P. W. Grant, M. Haveraaen, M. F. Webster, Coordinate free programming of computational fluid dynamics problems, Scientific Programming, **8**, 211–230 (2000).

[6] P. R. Halmos, Finite-dimensional vector spaces (Princeton University Press, 2001).

[7] E. Hairer, Geometric Integration of Ordinary Differential Equations on Manifolds, BIT Numerical Mathematics, **41**(5), 996–1007 (2001).

[8] D. Helm, Formgedächtnislegierungen, experimentelle Untersuchung, phänomenologische Modellierung und numerische Simulation der thermomechanischen Materialeigenschaften, (Universitätsbibliothek Kassel, 2001).

[9] D. Helm, Stress computation in finite thermoviscoplasticity. International Journal of Plasticity, **22**, 1699–1721 (2006).

[10] J. K. Hunter, B. Nachtergaele, Applied Analysis (World Scientific Publishing Company, 2001).

[11] M. Itskov, On the theory of fourth-order tensors and their applications in computational mechanics, Computer Methods in Applied Mechanics and Engineering, **189**, 419–438 (2000).

[12] M. Itskov, The derivative with respect to a tensor: some theoretical aspects and applications, ZAMM - Journal of Applied Mathematics and Mechanics, **82**(8), 535–544 (2002).

[13] M. Itskov, N. Aksel, A closed-form representation for the derivative of non-symmetric tensor power series, International Journal of Solids and Structures, **39**, 5963–5978 (2002).

[14] M. Itskov, Computation of the exponential and other isotropic tensor functions and their derivatives, Computer Methods in Applied Mechanics and Engineering, **192**, 3985–3999 (2003).

[15] M. Itskov, Tensor Algebra and Tensor Analysis for Engineers: With Applications to Continuum Mechanics (Springer, 2007).

[16] O. Kintzel, Y. Başar, Fourth-order tensors − tensor differentiation with applications to continuum mechanics. Part I: Classical tensor analysis, ZAMM - Journal of Applied Mathematics and Mechanics, **86**(4), 291–311 (2006).

[17] S. N. Korobeynikov, Objective tensor rates and applications in formulation of hyperelastic relations. Journal of Elasticity, **93**(2), 105–140 (2008).

[18] A. N. Kolmogorov, S. V. Fomin, Introductory Real Analysis (Dover Publications, 1975).

[19] S. Lang, Differential and Riemannian Manifolds (Springer, 1995).

[20] A. Lion, Constitutive modelling in finite thermoviscoplasticity: a physical approach based on nonlinear rheological elements, International Journal of Plasticity, **16**, 469–494 (2000).

[21] J. Lu, Exact expansions of arbitrary tensor functions **F** and their derivatives, International Journal of Solids and Structures, **41**, 337–349 (2004).

[22] A. I. Lurie, Nonlinear Theory of Elasticity (North-Holland, Amsterdam, 1990).

[23] J. E. Marsden, T. J. R. Hughes, Mathematical Foundations of Elasticity (Dover Publications, New York, 1994).

[24] C. Miehe, Exponential map algorithm for stress updates in anisotropic multiplicative elastoplasticity for single crystals, International Journal for Numerical Methods in Engineering, **39**, 3367–3390 (1996).

[25] P. Naghdi, A critical review of the state of finite plasticity, Journal of Applied Mathematics and Physics, **41**, 315–394 (1990).

[26] W. Noll, Lectures on the foundations of continuum mechanics and thermodynamics, Archive for Rational Mechanics and Analysis, **52**, 62–92 (1973).

[27] A. V. Shutov, R. Kreißig, Finite strain viscoplasticity with nonlinear kinematic hardening: Phenomenological modeling and time integration, Computer Methods in Applied Mechanics and Engineering, **197**, 2015–2029 (2008).

[28] H. Stumpf, U. Hoppe, The application of tensor algebra on manifolds to nonlinear continuum mechanics - invited survey article, ZAMM - Journal of Applied Mathematics and Mechanics, **77**(5), 327—339 (1997).

[29] B. Svendsen, A logarithmic-exponential backward-Euler-based split of the flow rule for anisotropic inelastic behaviour at small elastic strain, Internatopnal journal for numerical methods in engineering, **70**, 496—504 (2007).

[30] C. Truesdell, W. Noll, The Non-Linear Field Theories of Mechanics, 2nd ed. (Springer, 1992).

[31] H. Xiao, O. T. Bruhns, A. Meyers, Elastoplasticity beyond small deformations, Acta Mechanica, **182**, 31–111 (2006).

[32] O. C. Zienkiewicz, R. L. Taylor, The Finite Element Method, Volume 2: Solid Mechanics (Butterworth-Heinemann, 2000).

KAPITEL 4

Geometric integrators for multiplicative viscoplasticity: analysis of error accumulation

A. V. Shutov,[1] R. Kreißig.
Chemnitz University of Technology,
Str. d. Nationen 62, D-09111 Chemnitz, Germany

Abstract: *The inelastic incompressibility is a typical feature of metal plasticity/viscoplasticity. Over the last decade, there has been a great amount of research related to construction of numerical integration algorithms which exactly preserve this property. In this paper we examine, both numerically and mathematically, the excellent accuracy and convergence characteristics of such integrators. In order to simplify the considerations, we consider strain-driven processes without hardening effects.*

In terms of a classical model of multiplicative viscoplasticity, we illustrate the notion of exponential stability of the exact solution. We show that this property enables the construction of effective and stable numerical algorithms, if the incompressibility is exactly satisfied. On the other hand, if the incompressibility constraint is violated, spurious degrees of freedom are introduced. In general, this results in the loss of the exponential stability and a dramatic deterioration of convergence of numerical methods.

Keywords: viscoplasticity; finite strains; contractivity; exponential stability; inelastic incompressibility; integration algorithm; error accumulation.
AMS Subject Classification: 74C20; 65L20.

Nomenclature

$\mathbf{C}_{\rm i}$	inelastic right Cauchy-Green tensor (see (4.24))
$\tilde{\mathbf{T}}$	2nd Piola-Kirchhoff tensor (see (4.26))
$\mathbf{1}$	second-rank identity tensor
$\mathbf{A} \cdot \mathbf{B} = \mathbf{AB}$	product (composition) of two second-rank tensors
$\mathbf{A} : \mathbf{B}$	scalar product of two second-rank tensors
$\mathbf{A} \otimes \mathbf{B}$	tensor product of two second-rank tensors
$\Vert\mathbf{A}\Vert$	l_2 norm of a second-rank tensor (Frobenius norm)
$\Vert\mathbf{A}\Vert^*$	induced norm of a second-rank tensor (spectral norm) (see (4.1))

---

[1] Corresponding author. alexey.v.shutov@gmail.com
web: http://sites.google.com/site/materialmodeling

This chapter is reproduced from the paper: A. V. Shutov, R. Kreißig. Geometric integrators for multiplicative viscoplasticity: analysis of error accumulation. Computer Methods in Applied Mechanics and Engineering. 2010. 199, 700-711. Copyright Elsevier. Reproduced with permission.

$(\cdot)^{\mathrm{D}}$	deviatoric part of a tensor
$(\cdot)^{\mathrm{T}}$	transposition of a tensor
$(\cdot)^{-\mathrm{T}}$	inverse of transposed tensor
$\mathrm{tr}(\cdot)$	trace of a second-rank tensor
$\overline{(\cdot)}$	unimodular part of a tensor (see (4.2))
$\mathrm{sym}(\cdot)$	symmetric part of a tensor
$\langle x \rangle$	MacCauley bracket (see $(4.14)_3$)
ψ_{el}	specific free energy density
$\mathrm{Dist}(\cdot,\cdot)$	"distance" between two solutions (see (4.35))
K	yield stress
λ_{i}	proportionality factor (inelastic multiplier) (see $(4.27)_1$)
f	overstress (see $(4.27)_2$)
$\mathfrak{F}$	norm of the driving force (see $(4.27)_3$)
Sym	space of symmetric second-rank tensors
M	invariant manifold (cf. (4.4), (4.28))
ρ_{R}	mass density in the reference configuration
k	bulk modulus (see (4.30))
μ	shear modulus (see (4.30))

1. Introduction

The mechanical processing of materials may involve very large inelastic deformations. For instance, for equal channel angular extrusion of aluminium alloys, the introduced accumulated inelastic strain usually varies between 100 and 900 percent (depending on the number of extrusions [**34**]). Even larger deformations can be introduced by some incremental forming procedures like spin extrusion [**20**] (the accumulated inelastic strain ranges up to 1000 percent). Due to the highly nonlinear character of the underlying mechanical problem, a correct numerical simulation of such "long" processes is by no means a trivial task. It is desirable to have numerical algorithms which would be stable with respect to numerical errors, even if working with big time intervals and big time steps.

The assumption of *exact inelastic incompressibility* is widely implemented for construction of material models of metal plasticity and creep (see, for instance, [**11**]). Extensive studies were carried out concerning the construction of so-called geometrical numerical integrators which exactly preserve the incompressibility of the inelastic flow [**4, 10, 12, 19, 22, 26, 27, 30, 31**].[2]

In this paper, we assess those factors that result in more accurate computations, especially when integrating with big time steps and for long times. To this end, we analyze the structural properties of the inelastic flow governed by a classical material model of multiplicative viscoplasticity. The material model is based on the multiplicative decomposition of the deformation gradient into inelastic and elastic parts. For simplicity, no hardening behavior is considered in this paper. However, the proposed methodology can be generalized

---

[2] The incompressibility condition is given by a linear invariant in the case of infinitesimal strains inelasticity. Since the linear invariants are exactly conserved by most of integration procedures (cf. [**6**]), the problem of the conservation of incompressibility only appears when working with finite strains.

to cover more complicated material behavior as well.[3] Only strain-driven processes are considered in this paper. The analysis of a general initial-boundary value problem lies beyond the scope of the current work.

We pay especial attention to the *exponential stability* of the inelastic flow, which is the key notion of the current study. We say that the solution to a Cauchy problem is exponentially stable, if for small perturbations of initial data an exponential decay estimate holds (see Section 2.1). From mechanical standpoint, the exponential stability implies fading memory behavior.[4] Moreover, the exponential stability is deeply connected to *contractivity* (B-stability) of the system of equations, which can be used for stability analysis of numerical algorithms (see the monograph by Simo and Hughes [**29**]).

The main conclusions of this paper regarding the problem of finite strain viscoplasticity are as follows.

- The exact solution is *exponentially stable* for strain-driven processes with respect to small perturbations of initial data, if the incompressibility constraint is not violated.
- In the case of exponential stability, the numerical error is *uniformly bounded.* In particular, there is *no error accumulation* even within large time periods.
- If the incompressibility constraint is violated by some numerical algorithm, then, in general, the numerical error tends to *accumulate over time.*

There exists a rich mathematical literature dealing with existence, uniqueness, regularity, and asymptotic behavior of solutions for certain plasticity/viscoplasticity problems in the context of infinitesimal strains (see [**1, 7, 13**] and references therein). A class of material models of monotone type which includes the class of generalized standard materials was defined and analyzed by Alber in [**1**]. In the context of finite strain viscoplasticity, however, only few theoretical works exist. Some preliminary investigations have been made by Neff in [**23**].

In this paper, we analyze the well-known material model of multiplicative viscoplasticity. The stability is proved analogously to the classical Lyapunov approach, based on the use of Lyapunov-candidate-functions. More precisely, the hyperelastic potential is used to construct a suitable Lyapunov candidate (cf. [**29**]).

The paper is organized as follows. In Section 2, we define the notion of exponential stability and prove the main theorem, which states that the numerical error is uniformly bounded if the exact solution is exponentially stable. A simple one-dimensional example is presented. In the next section, a classical material model of multiplicative viscoplasticity is formulated in the reference configuration. The change of the reference configuration is likewise discussed. Section 4 contains the definition and analysis of the distance between two solutions in terms of energy (Lyapunov candidate). Next, the time-evolution of the distance is evaluated and the exponential stability of the exact solution is proved. Finally, the results

---

[3] By means of a series of numerical tests, it was shown for strain-controlled processes in [**27**] that the use of geometric integrators allows to eliminate the error accumulation even in the case of a complex material behaviour with nonlinear isotropic and kinematic hardening. In general, however, the construction of consistent integration procedures for the finite strain inelasticity is still an open problem (cf. [**33**]).

[4] As Truesdell and Noll [**32**] have formulated, "Deformations that occurred in the distant past should have less influence in determining the present stress than those that occurred in the recent past".

of numerical tests are presented in Section 5, which illustrate the excellent accuracy and convergence characteristics of geometric integrators.

We conclude this introduction with a few words regarding notation. Expression $a := b$ means a is defined to be another name for b. Throughout this article, bold-faced symbols denote first- and second-rank tensors in $\mathbb{R}^3$. A coordinate-free tensor setting is used in this paper (cf. [**14, 28**]). The scalar product of two second rank tensors is defined by $\mathbf{A} : \mathbf{B} = \mathrm{tr}(\mathbf{A}\mathbf{B}^{\mathrm{T}})$.[5] This scalar product gives rise to the norm by $\|\mathbf{A}\| := \sqrt{\mathbf{A} : \mathbf{A}}$. Moreover, we denote by $\| \cdot \|^*$ the induced norm of a tensor

$$\|\mathbf{A}\|^* := \max_{\|\mathbf{x}\|_2 = 1} \|\mathbf{A}\mathbf{x}\|_2, \quad \|\mathbf{x}\|_2 := \sqrt{\mathbf{x} \cdot \mathbf{x}}. \tag{4.1}$$

The overline $\overline{(\cdot)}$ stands for the unimodular part of a tensor

$$\overline{\mathbf{A}} := (\det \mathbf{A})^{-1/3} \mathbf{A}. \tag{4.2}$$

The deviatoric part of a tensor is defined as $\mathbf{A}^{\mathrm{D}} := \mathbf{A} - \frac{1}{3}\mathrm{tr}(\mathbf{A})\mathbf{1}$. The notation O stands for "Big-O" Landau symbol: $f(x) = O(g(x))$ as $x \ \rightarrow x_0$ if and only if there exists $C < \infty$ such that $\|f(x)\| \leq C\|g(x)\|$ as $x \ \rightarrow x_0$. The inequality $f(x) \leq O(g(x))$ is understood as follows: there exists $\acute{f}(x) = O(g(x))$ such that $f(x) \leq \acute{f}(x)$.

2. Differential equations on manifolds and exponential stability

2.1. General definitions. Let us consider the Cauchy problem (initial value problem) for a smooth function $y(t) \in \mathbb{R}^n$

$$\dot{y}(t) = f(y(t), d(t)), \quad y(t_0) = y_0. \tag{4.3}$$

Here, the initial value y_0 and the function $d(t)$ are supposed to be given.[6] Denote the exact solution to (4.3) by $\tilde{y}(t, y_0, t_0)$. In particular, we have

$$\tilde{y}(t_0, y_0, t_0) = y_0.$$

Suppose that all solutions lie on some manifold $M \subset \mathbb{R}^n$

$$\tilde{y}(t, y_0, t_0) \in M, \quad \text{for all } t \geq t_0, \ y_0 \in M. \tag{4.4}$$

Then we say that (4.3) is a *differential equation on the manifold* M (cf. [**5, 6**]).

Next, we say that the solution $y(t)$ to the problem (4.3) is *locally exponentially stable* on M, if there exist $\delta > 0, \ \gamma > 0, \ C_1 < \infty$, such that the following decay estimate holds

$$\|\tilde{y}(t, y_0^{(1)}, t_0) - \tilde{y}(t, y_0^{(2)}, t_0)\| \leq C_1 \ \mathrm{e}^{-\gamma(t \, - \, t_0)} \ \|y_0^{(1)} - y_0^{(2)}\|, \tag{4.5}$$

for all $t_0 \geq 0$, $y_0^{(1)}, y_0^{(2)} \in M$ such that $\|y_0^{(1)} - y(t_0)\| \leq \delta$, $\|y_0^{(2)} - y(t_0)\| \leq \delta$.

We note that a somewhat different interpretation of the exponential stability can be met in the literature as well (cf., for example, Section 2.5 of [**15**]).

Next, let us consider a numerical algorithm which solves (4.3) on the time interval $[0, T]$. Denote by ${}^n y$ the numerical solutions at time instances ${}^n t$, where $0 = {}^0 t < {}^1 t < {}^2 t <$

---

[5] Although the notion of trace of a second rank tensor is coordinate free (cf. [**28**]), we may use a Cartesian coordinate system in order to define it as follows: $\mathrm{tr}(\mathbf{A}) := A_{11} + A_{22} + A_{33}$.

[6] The system (4.3) is a system with input, and $d(t)$ is interpreted as a forcing function.

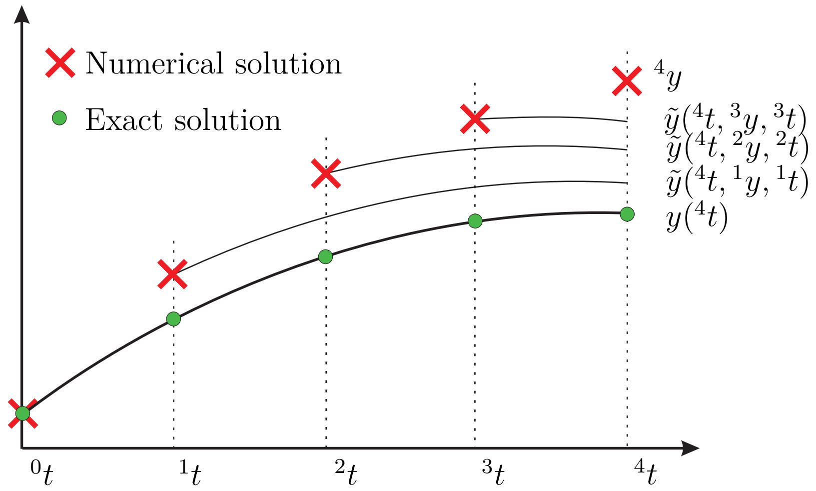

Figure 4.1. Analysis of error accumulation.

... $< {}^Nt = T$, and ${}^0y = y_0$. Suppose that the error on the step is bounded by the second power of the step size. More precisely

$$\|\tilde{y}(^{n+1}t, {}^ny, {}^nt) - {}^{n+1}y\| \leq C_2(^{n+1}t - {}^nt)^2, \tag{4.6}$$

where $C_2 < \infty$ (cf. Fig. 4.1). For simplicity, we will consider constant time-steps only: $\Delta t = {}^{n+1}t - {}^nt = const.$

2.2. Main theorem. With definitions from the previous subsection we formulate the following theorem.

Theorem 1.

Let $y(t) = \tilde{y}(t, y_0, 0)$ be the exact solution. Suppose that conditions (4.5) and (4.6) hold. Moreover, suppose that the numerical solution of problem (4.3) lies exactly on M. Then there exists a constant $C < \infty$ such that

$$\|{}^ny - y(^nt)\| \leq C\Delta t, \quad \text{as } \Delta t \to 0. \tag{4.7}$$

Here, the constant C does not depend on the size of the time interval $[0, T]$.

Proof. The proof is a modification of the standard error analysis (cf. [**2**]). In this paper we prove the theorem under the assumption that $\delta = \infty$. The proof can be easily generalized to cover arbitrary values of $\delta > 0$ by using mathematical induction and by assuming $\Delta t \leq \gamma\delta/(2\max(C_1, 1)\, C_2)$.

First, note that $\tilde{y}(^nt, {}^0y, {}^0t) = y(^nt)$. The triangle inequality yields (cf. Fig. 4.1)

$$\|{}^ny - y(^nt)\| \leq \|{}^ny - \tilde{y}(^nt, {}^{n-1}y, {}^{n-1}t)\| + \|\tilde{y}(^nt, {}^{n-1}y, {}^{n-1}t) - \tilde{y}(^nt, {}^{n-2}y, {}^{n-2}t)\| + \ldots$$
$$+ \|\tilde{y}(^nt, {}^1y, {}^1t) - \tilde{y}(^nt, {}^0y, {}^0t)\|. \tag{4.8}$$

Next, using (4.5) we obtain for all $k = 1, 2, \ldots, n-1$

$$\|\tilde{y}(^nt, {}^ky, {}^kt) - \tilde{y}(^nt, {}^{k-1}y, {}^{k-1}t)\| \leq C_1\, \mathrm{e}^{-\gamma(^nt\, -\, ^kt)}\, \|\tilde{y}(^kt, {}^ky, {}^kt) - \tilde{y}(^kt, {}^{k-1}y, {}^{k-1}t)\|. \tag{4.9}$$

Substituting (4.9) in (4.8), we arrive at

$$\|{}^n y - y({}^n t)\| \leq$$
$$\|{}^n y - \tilde{y}({}^n t, {}^{n-1}y, {}^{n-1}t)\| + C_1 \sum_{k=1}^{n-1} \mathrm{e}^{-\gamma({}^n t - {}^k t)} \ \|\tilde{y}({}^k t, {}^k y, {}^k t) - \tilde{y}({}^k t, {}^{k-1}y, {}^{k-1}t)\|. \quad (4.10)$$

Obviously, $\tilde{y}({}^k t, {}^k y, {}^k t) = {}^k y$. Without loss of generality, we can assume that $C_1 \geq 1$. Next, substituting error estimation (4.6) into (4.10), we obtain

$$\|{}^n y - y({}^n t)\| \leq C_1 \ C_2 \ (\Delta t)^2 \sum_{k=1}^{n} \mathrm{e}^{-\gamma({}^n t - {}^k t)}. \quad (4.11)$$

But, ${}^n t - {}^k t = (n-k)\Delta t$. Thus, taking into account the well-known expression for an infinite geometric series ($\sum_{i=0}^{\infty} r^i = 1/(1-r)$ for $|r| < 1$) and that $\dfrac{1}{1+O(\Delta t)} = 1 + O(\Delta t)$, we obtain for small Δt

$$\sum_{k=1}^{n} \mathrm{e}^{-\gamma({}^n t - {}^k t)} \leq \sum_{i=0}^{\infty} \mathrm{e}^{-i\gamma\Delta t} = \frac{1}{1-\mathrm{e}^{-\gamma\Delta t}} = \frac{1}{\gamma\Delta t + O((\Delta t)^2)}$$
$$= \frac{1}{\gamma\Delta t}\frac{1}{1+O(\Delta t)} = \frac{1}{\gamma\Delta t}(1+O(\Delta t)) \leq 2\frac{1}{\gamma\Delta t}. \quad (4.12)$$

Finally, it follows from (4.11) and (4.12) that

$$\|{}^n y - y({}^n t)\| \leq \frac{2C_1 \ C_2}{\gamma} \ \Delta t, \quad \text{as } \Delta t \to 0 \qquad \blacksquare$$

Remark 1. The proof is essentially based on the assumption that ${}^k y \in M$. In general, if the numerical solution ${}^k y$ leaves the manifold M, the decay estimation (4.5) is not valid.

Remark 2. The theorem states that the error is uniformly bounded in the case of exponential stability. Thus, there is no error accumulation in the sense that the constant C in (4.7) does not depend on the overall time T. Moreover, let $\epsilon > 0$ be some small value. By choosing $\Delta t \leq \gamma\epsilon/(2C_1C_2)$ the numerical error $\|{}^n y - y({}^n t)\|$ is guaranteed to be less than ϵ.

Remark 3. If the exponential stability is replaced by the assumption that the right-hand side of (4.3) is a smooth function of y, a weaker error estimation is valid (cf. [**2**])

$$\|{}^n y - y({}^n t)\| \leq C\mathrm{e}^{LT} T \ \Delta t, \quad \text{as } \Delta t \to 0, \quad (4.13)$$

where $L = \sup \|f_y\|$. The effect of the growing multiplier on the right hand side of (4.13) is referred to as an effect of error accumulation. In that case, in order to guarantee a sufficient accuracy, the upper bound for Δt must depend on T. That makes the practical solution of some problems extremely expensive for large values of T.

2.3. One-dimensional example. Let us consider a simple example which illustrates the notion of exponential stability. We examine the response of a one-dimensional viscoplastic device shown in Figure 4.2 (a).

The closed system of (constitutive) equations is as follows: The total strain is decomposed into the elastic part ε_{e}, and the inelastic part ε_{i}

$$\varepsilon = \varepsilon_{\mathrm{e}} + \varepsilon_{\mathrm{i}}.$$

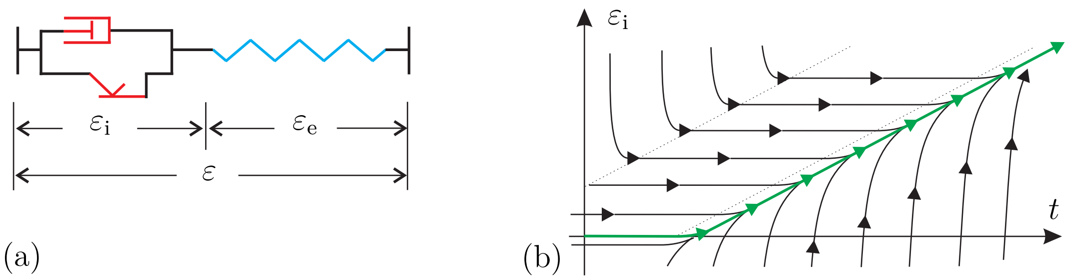

(a) (b)

Figure 4.2. Rheological model (a), and inelastic flow under monotonic loading (b).

The stress σ on the elastic spring is governed by the elasticity law

$$\sigma = E\varepsilon_{\mathrm{e}}, \quad E = const > 0.$$

The time derivative of the inelastic strain is given by

$$\dot{\varepsilon}_{\mathrm{i}} = \frac{1}{\eta}\langle f \rangle \frac{\sigma}{|\sigma|}, \quad f := |\sigma| - K, \quad \langle x \rangle := \max(x, 0), \tag{4.14}$$

where the material constants $K > 0$ and $\eta > 0$ are referred to as yield stress and viscosity, respectively.

In order to use the results of previous subsections, we rewrite the problem in the form

$$\dot{\varepsilon}_{\mathrm{i}} = \dot{\varepsilon}_{\mathrm{i}}(\varepsilon_{\mathrm{i}}, \varepsilon(t)) = \frac{1}{\eta}\langle E|\varepsilon(t) - \varepsilon_{\mathrm{i}}| - K \rangle \ \mathrm{sign}(\varepsilon(t) - \varepsilon_{\mathrm{i}}). \tag{4.15}$$

Let $\varepsilon_{\mathrm{i}}^{(1)}(t)$ and $\varepsilon_{\mathrm{i}}^{(2)}(t)$ be two solutions to (4.15). Following [**29**], we recall that $\sqrt{\frac{1}{2}E(\varepsilon_{\mathrm{i}}^{(1)} - \varepsilon_{\mathrm{i}}^{(2)})^2}$ defines an *energy norm* which is the natural norm for the problem under consideration.[7] Next, we consider a monotonic loading

$$\varepsilon(t) = \dot{\varepsilon} t, \quad \dot{\varepsilon} = const > 0.$$

Let us show that the exact solution satisfying the initial condition $\varepsilon_{\mathrm{i}} = 0$ is exponentially stable.[8] Without loss of generality, we can assume that $t_0 = 0$ in estimation (4.5). If $|\varepsilon_{\mathrm{i}}^{(k)}(0) - 0| \leq \delta$ for k $\in \{1, 2\}$, then there exists a time instance $t' = t'(\delta)$ such that the condition $f \geq f_0 > 0$ holds for both solutions $(\varepsilon_{\mathrm{i}}^{(1)}(t)$ and $\varepsilon_{\mathrm{i}}^{(2)}(t))$, if $t \geq t'$ (see Figure 4.2 (b)). Then, under that assumption, we obtain

$$\frac{\partial \dot{\varepsilon}_{\mathrm{i}}(\varepsilon_{\mathrm{i}}, \varepsilon(t))}{\partial \varepsilon_{\mathrm{i}}} = -\frac{E}{\eta}, \quad \dot{\varepsilon}_{\mathrm{i}}(\varepsilon_{\mathrm{i}}^{(1)}, \varepsilon(t)) - \dot{\varepsilon}_{\mathrm{i}}(\varepsilon_{\mathrm{i}}^{(2)}, \varepsilon(t)) = -\frac{E}{\eta}(\varepsilon_{\mathrm{i}}^{(1)} - \varepsilon_{\mathrm{i}}^{(2)}). \tag{4.16}$$

Therefore, we obtain from (4.16)

$$\frac{d}{dt}\left(\frac{1}{2}E(\varepsilon_{\mathrm{i}}^{(1)} - \varepsilon_{\mathrm{i}}^{(2)})^2\right) = E(\varepsilon_{\mathrm{i}}^{(1)} - \varepsilon_{\mathrm{i}}^{(2)})(\dot{\varepsilon}_{\mathrm{i}}^{(1)} - \dot{\varepsilon}_{\mathrm{i}}^{(2)}) = -\frac{E^2}{\eta}(\varepsilon_{\mathrm{i}}^{(1)} - \varepsilon_{\mathrm{i}}^{(2)})^2, \text{ for } t \geq t'. \tag{4.17}$$

Due to the contractivity (for details see [**29**]), $\frac{1}{2}E(\varepsilon_{\mathrm{i}}^{(1)}(t') - \varepsilon_{\mathrm{i}}^{(2)}(t'))^2 \leq \frac{1}{2}E(\varepsilon_{\mathrm{i}}^{(1)}(0) - \varepsilon_{\mathrm{i}}^{(2)}(0))^2$. Moreover, integrating (4.17) over $[t', t]$ and taking the contractivity into account,

---

[7] It is known (see [**29**]) that $\frac{1}{2}E(\varepsilon_{\mathrm{i}}^{(1)}(t) - \varepsilon_{\mathrm{i}}^{(2)}(t))^2$ is not increasing. This effect is referred to as *contractivity*. The contractivity can be easily proved by checking that $\frac{d}{dt}(\frac{1}{2}E(\varepsilon_{\mathrm{i}}^{(1)}(t) - \varepsilon_{\mathrm{i}}^{(2)}(t))^2) \leq 0$.

[8] For the current example, the geometric property $y \in M$ is trivial: we put $M = \mathbb{R}$.

we arrive at

$$\frac{1}{2}E(\varepsilon_{\mathrm{i}}^{(1)}(t)-\varepsilon_{\mathrm{i}}^{(2)}(t))^2 \leq \frac{1}{2}E(\varepsilon_{\mathrm{i}}^{(1)}(0)-\varepsilon_{\mathrm{i}}^{(2)}(0))^2 \mathrm{e}^{-\frac{2E}{\eta}(t-t')}.$$

Taking the square root of both sides we obtain the required exponential decay estimation (4.5) with $C_1 = \mathrm{e}^{\dfrac{Et'}{\eta}} < \infty$ and $\gamma = \dfrac{E}{\eta} > 0$.

We note that the equations for the Maxwell material are covered by equations (4.14) as a special case (as $K = 0$). Therefore, the corresponding inelastic flow of the Maxwell material is exponentially stable as well.

3. Material model of multiplicative viscoplasticity

In this section we discuss a classical material model of finite strain viscoplasticity. The main ingredients of this model are: multiplicative split of the deformation gradient, hyperelastic relations of Neo-Hooke type, classical Mises-Huber yield function in combination with the associative flow rule (J_2 flow theory), Perzyna-type viscoplasticity. The model is a special case among some relatively new models of viscoplasticity (cf. [**10, 27**]). The rheological motivation for the constitutive equations is presented in Fig. 4.2a.

3.1. Constitutive equations. Let us consider the multiplicative split of the deformation gradient $\mathbf{F}$

$$\mathbf{F} = \hat{\mathbf{F}}_{\mathrm{e}} \mathbf{F}_{\mathrm{i}}. \tag{4.18}$$

Here, $\hat{\mathbf{F}}_{\mathrm{e}}$ and $\mathbf{F}_{\mathrm{i}}$ stand for *elastic* and *inelastic* parts, respectively (see [**16, 17**]). The multiplicative split can be motivated by the idea of a local elastic unloading. A somewhat more consistent motivation can be derived from the concept of material isomorphism [**3**].

The elastic right Cauchy-Green tensor and inelastic Almansi tensor are defined respectively by

$$\hat{\mathbf{C}}_{\mathrm{e}} := \hat{\mathbf{F}}_{\mathrm{e}}^{\mathrm{T}} \hat{\mathbf{F}}_{\mathrm{e}}, \quad \hat{\mathbf{\Gamma}}_{\mathrm{i}} := \frac{1}{2}(\mathbf{1} - \mathbf{F}_{\mathrm{i}}^{-\mathrm{T}} \mathbf{F}_{\mathrm{i}}^{-1}). \tag{4.19}$$

Let $\mathbf{T}$ be the Cauchy stress tensor. The weighted Cauchy tensor (or Kirchhoff stress tensor) as well as the 2nd Piola-Kirchhoff tensors operating on $\hat{\mathcal{K}}$ and $\tilde{\mathcal{K}}$ are defined respectively through

$$\mathbf{S} := (\det\mathbf{F})\mathbf{T}, \quad \hat{\mathbf{S}} := \hat{\mathbf{F}}_{\mathrm{e}}^{-1} \mathbf{S} \hat{\mathbf{F}}_{\mathrm{e}}^{-\mathrm{T}}, \quad \tilde{\mathbf{T}} := \mathbf{F}^{-1} \mathbf{S} \mathbf{F}^{-\mathrm{T}}. \tag{4.20}$$

The hyperelastic potential relation for stresses and the classical Mises-Huber yield function (see, for example, [**29**]) are used in this paper [9]

$$\hat{\mathbf{S}} = 2\rho_{\mathrm{R}} \frac{\partial \psi_{\mathrm{el}}(\hat{\mathbf{C}}_{\mathrm{e}})}{\partial \hat{\mathbf{C}}_{\mathrm{e}}}, \quad f := \|(\hat{\mathbf{C}}_{\mathrm{e}} \hat{\mathbf{S}})^{\mathrm{D}}\| - \sqrt{\frac{2}{3}} K. \tag{4.21}$$

The mass density $\rho_{\mathrm{R}} > 0$, the isotropic real-valued function ψ_{el}, and the initial yield stress K are assumed to be known.

Next, a covariant Oldroyd derivative is introduced as follows

$$\overset{\triangle}{(\cdot)} := \frac{d}{dt}(\cdot) + \hat{\mathbf{L}}_{\mathrm{i}}^{\mathrm{T}}(\cdot) + (\cdot)\hat{\mathbf{L}}_{\mathrm{i}}, \quad \hat{\mathbf{L}}_{\mathrm{i}} := \dot{\mathbf{F}}_{\mathrm{i}} \mathbf{F}_{\mathrm{i}}^{-1}. \tag{4.22}$$

---

[9] The yield function f is formulated in terms of the Mandel stress tensor $\hat{\mathbf{C}}_{\mathrm{e}}\hat{\mathbf{S}}$ operating on $\hat{\mathcal{K}}$. A more common definition of the Mises-Huber yield function can be found in the literature as $f := \|\mathbf{S}^{\mathrm{D}}\| - \sqrt{\frac{2}{3}}K$, where $\mathbf{S}$ stands for the Kirchhoff stress tensor. Using (4.18) it can be shown that $(4.21)_2$ follows from this general definition.

Finally, the plastic flow is governed by the associative flow rule in combination with the Perzyna law (cf., for example, [**10, 11, 26, 27**])[10]

$$\overset{\triangle}{\hat{\mathbf{\Gamma}}}_{\mathrm{i}} = \lambda_{\mathrm{i}} \frac{(\hat{\mathbf{C}}_{\mathrm{e}}\hat{\mathbf{S}})^{\mathrm{D}}}{\|(\hat{\mathbf{C}}_{\mathrm{e}}\hat{\mathbf{S}})^{\mathrm{D}}\|}, \quad \lambda_{\mathrm{i}} = \frac{1}{\eta}\Big\langle \frac{1}{k_0} f \Big\rangle^{m}. \tag{4.23}$$

Here, $\eta \geq 0$ and $m \geq 1$ are known material parameters; $k_0 > 0$ is used to obtain a dimensionless term in the bracket; the yield function f is interpreted as overstress within the context of Perzyna-type viscoplasticity [**24, 25**].

In order to simplify the numerical treatment of the problem, we rewrite the constitutive equations in terms of tensor-valued variables which operate on the reference configuration $\tilde{\mathcal{K}}$. Along with the well-known right Cauchy-Green tensor $\mathbf{C} = \mathbf{F}^{\mathrm{T}}\mathbf{F}$, we introduce an internal variable (inelastic right Cauchy-Green tensor) as

$$\mathbf{C}_{\mathrm{i}} := \mathbf{F}_{\mathrm{i}}^{\mathrm{T}}\mathbf{F}_{\mathrm{i}}. \tag{4.24}$$

We rewrite the evolution equation $(4.23)_1$ (cf., for example, [**10, 26, 27**]) and supplement it with the initial condition as follows

$$\dot{\mathbf{C}}_{\mathrm{i}} = 2\frac{\lambda_{\mathrm{i}}}{\mathfrak{F}}\Big(\mathbf{C}\tilde{\mathbf{T}}\Big)^{\mathrm{D}}\mathbf{C}_{\mathrm{i}}, \quad \mathbf{C}_{\mathrm{i}}|_{t=0} = \mathbf{C}_{\mathrm{i}}^{0}, \ \det \mathbf{C}_{\mathrm{i}}^{0} = 1, \ \mathbf{C}_{\mathrm{i}}^{0} \in \mathit{Sym}. \tag{4.25}$$

Here, the 2nd Piola-Kirchhoff tensor $\tilde{\mathbf{T}}$, the norm of the driving force $\mathfrak{F}$, and the inelastic multiplier λ_{i} are functions of $(\mathbf{C}, \mathbf{C}_{\mathrm{i}})$, given by

$$\tilde{\mathbf{T}} = 2\rho_{\mathrm{R}} \frac{\partial \psi_{\mathrm{el}}(\mathbf{C}{\mathbf{C}_{\mathrm{i}}}^{-1})}{\partial \mathbf{C}}\Big|_{\mathbf{C}_{\mathrm{i}}=\mathrm{const}}, \tag{4.26}$$

$$\lambda_{\mathrm{i}} = \frac{1}{\eta}\Big\langle \frac{1}{k_0} f \Big\rangle^{m}, \quad f = \mathfrak{F} - \sqrt{\frac{2}{3}}K, \quad \mathfrak{F} := \sqrt{\mathrm{tr}\Big[\Big(\mathbf{C}\tilde{\mathbf{T}}\Big)^{\mathrm{D}}\Big]^{2}}. \tag{4.27}$$

Remark 4. The right Cauchy strain tensor $\mathbf{C}$ is symmetric. Since the function ψ_{el} is isotropic, it makes no difference whether the derivative in (4.26) is understood as a general derivative or as a derivative with respect to a symmetric tensor (cf. [**28**]).

Next, we remark that the right-hand side in $(4.25)_1$ is symmetric (cf. [**28**]). Moreover, taking into account the property $\mathrm{tr}(\mathbf{AB}) = \mathrm{tr}(\mathbf{BA})$ and combining the Jacobi formula $\dfrac{\partial \det(\mathbf{A})}{\partial \mathbf{A}} = \det(\mathbf{A})\ \mathbf{A}^{-\mathrm{T}}$ with the evolution equation $(4.25)_1$, we obtain

$$\frac{d}{dt}\Big(\det \mathbf{C}_{\mathrm{i}}\Big) = \frac{\partial \det(\mathbf{C}_{\mathrm{i}})}{\partial \mathbf{C}_{\mathrm{i}}} : \dot{\mathbf{C}}_{\mathrm{i}} = 2\frac{\lambda_{\mathrm{i}}}{\mathfrak{F}}\det(\mathbf{C}_{\mathrm{i}})\ \mathbf{C}_{\mathrm{i}}^{-1} : \Big(\mathbf{C}\tilde{\mathbf{T}}\Big)^{\mathrm{D}}\mathbf{C}_{\mathrm{i}} = 2\frac{\lambda_{\mathrm{i}}}{\mathfrak{F}}\mathrm{tr}\Big[\Big(\mathbf{C}\tilde{\mathbf{T}}\Big)^{\mathrm{D}}\Big] = 0.$$

Therefore, the exact solution of (4.25) – (4.27) has the following geometric property

$$\mathbf{C}_{\mathrm{i}} \in M, \quad M := \Big\{\mathbf{B} \in \mathit{Sym} \mid \det\mathbf{B} = 1\Big\}. \tag{4.28}$$

We note that the current material model is *thermodynamically consistent.* That means that the Clausius-Duhem inequality holds for arbitrary mechanical loadings

$$\delta_{\mathrm{i}} := \frac{1}{2\rho_{\mathrm{R}}}\tilde{\mathbf{T}} : \dot{\mathbf{C}} - \frac{d}{dt}\Big(\psi_{\mathrm{el}}(\mathbf{C}{\mathbf{C}_{\mathrm{i}}}^{-1})\Big) \geq 0.$$

---

[10] Moreover, the form of the evolution equation $(4.23)_1$ can be uniquely determined by the principle of maximum plastic dissipation, if the yield function f is given by $(4.21)_2$ (see [**29**]).

$$\begin{tikzcd}
\tilde{\mathcal{K}} \arrow[rr, bend left, "\mathbf{F}"] \arrow[dr, "\mathbf{F}_{\mathrm{i}}"] & & \mathcal{K} \\
& \hat{\mathcal{K}} \arrow[ur, "\hat{\mathbf{F}}_{\mathrm{e}}^{\mathrm{new}} = \hat{\mathbf{F}}_{\mathrm{e}}"] & \\
\tilde{K}^{\mathrm{new}} \arrow[uu, "\mathbf{F}_0^{-1}"] \arrow[ur, "\mathbf{F}_{\mathrm{i}}^{\mathrm{new}}"] \arrow[uurr, bend right, "\mathbf{F}^{\mathrm{new}}"'] & &
\end{tikzcd}$$

Figure 4.3. Commutative diagram: change of the reference configuration.

In particular, we have a reduced inequality for relaxation processes ($\mathbf{C} = \mathrm{const}$)

$$\frac{d}{dt}\Big(\psi_{\mathrm{el}}(\mathbf{C}\mathbf{C}_{\mathrm{i}}{}^{-1})\Big) \leq 0. \tag{4.29}$$

One mathematical interpretation of this inequality will be discussed in Section 4.1.

To be definite, we use the following expression for the free energy density ψ_{el} (generalized Neo-Hooke model [**11**])

$$\rho_{\mathrm{R}}\psi_{\mathrm{el}}(\mathbf{A}) := \frac{k}{2}\Big(\ln\sqrt{\det\mathbf{A}}\Big)^2 + \frac{\mu}{2}\Big(\mathrm{tr}\overline{\mathbf{A}} - 3\Big), \tag{4.30}$$

where $k > 0$, $\mu > 0$ are known material constants (bulk modulus and shear modulus, respectively).[11] Substituting (4.30) in (4.26) we obtain the 2nd Piola-Kirchhoff stress tensor in the form

$$\tilde{\mathbf{T}} = k\,\ln\sqrt{\det(\mathbf{C})}\ \mathbf{C}^{-1} + \mu\ \mathbf{C}^{-1}(\overline{\mathbf{C}}\mathbf{C}_{\mathrm{i}}^{-1})^{\mathrm{D}}. \tag{4.31}$$

In this paper we consider strain-driven processes. More precisely, we assume the deformation history $\mathbf{C}(t)$ to be given. In the following we analyze the exponential stability of the corresponding exact solution $\mathbf{C}_{\mathrm{i}}(t)$.

3.2. Change of the reference configuration. We note that the constitutive equations of the previous section were formulated with respect to a certain fixed reference configuration $\tilde{\mathcal{K}}$. In order to simplify the analysis of the material response, it may be useful to rewrite the constitutive equations with respect to some "new" local reference configuration $\tilde{\mathcal{K}}^{\mathrm{new}} = \mathbf{F}_0\tilde{\mathcal{K}}$ (see Fig. 4.3). We define "new" variables and corresponding constitutive equations with respect to these variables in such a way that the same mechanical response (Cauchy stresses) is predicted. In what follows, we suppose that the mapping $\mathbf{F}_0$ is isochoric, i.e. $\det(\mathbf{F}_0) = 1$.

The "new" deformation gradient, inelastic and elastic parts of the deformation gradient, the right Cauchy tensor, and the inelastic right Cauchy tensor are given by

$$\mathbf{F}^{\mathrm{new}} := \mathbf{F}\mathbf{F}_0^{-1}, \quad \mathbf{F}_{\mathrm{i}}^{\mathrm{new}} := \mathbf{F}_{\mathrm{i}}\mathbf{F}_0^{-1}, \quad \hat{\mathbf{F}}_{\mathrm{e}}^{\mathrm{new}} := \hat{\mathbf{F}}_{\mathrm{e}},$$

$$\mathbf{C}^{\mathrm{new}} := \mathbf{F}_0^{-\mathrm{T}}\mathbf{C}\mathbf{F}_0^{-1}, \quad \mathbf{C}_{\mathrm{i}}^{\mathrm{new}} := \mathbf{F}_0^{-\mathrm{T}}\mathbf{C}_{\mathrm{i}}\mathbf{F}_0^{-1}, \quad \mathbf{C}_{\mathrm{i}}^{0\ \mathrm{new}} := \mathbf{F}_0^{-\mathrm{T}}\mathbf{C}_{\mathrm{i}}^0\mathbf{F}_0^{-1}. \tag{4.32}$$

The situation is summarized in diagram 4.3.

---

[11] As it will be clear in the following, the concrete ansatz for the volumetric part of the strain-energy function does not influence the considerations of the current paper. It was noted in [**9**] that the volumetric part of the strain-energy function (4.30) is not convex in $\det\mathbf{A}$.

The 2nd Piola-Kirchhoff tensor $\tilde{\mathbf{T}}$, the norm of the driving force $\mathfrak{F}$, the inelastic multiplier λ_{i}, and the overstress f are transformed as follows

$$\tilde{\mathbf{T}}^{\mathrm{new}} := \mathbf{F}_0 \tilde{\mathbf{T}} \mathbf{F}_0^{\mathrm{T}}, \quad \mathfrak{F}^{\mathrm{new}} := \mathfrak{F}, \quad \lambda_{\mathrm{i}}^{\mathrm{new}} := \lambda_{\mathrm{i}} \quad f^{\mathrm{new}} := f.$$

Since ψ_{el} is isotropic, $\psi_{\mathrm{el}}(\mathbf{AB}) = \psi_{\mathrm{el}}(\mathbf{BA})$. Using that property, it can be checked that $\psi_{\mathrm{el}}(\mathbf{C}{\mathbf{C}_{\mathrm{i}}}^{-1})$ is invariant under the change of the reference configuration

$$\psi_{\mathrm{el}}(\mathbf{C}^{\mathrm{new}}(\mathbf{C}_{\mathrm{i}}^{\mathrm{new}})^{-1}) = \psi_{\mathrm{el}}(\mathbf{C}{\mathbf{C}_{\mathrm{i}}}^{-1}). \tag{4.33}$$

Let $\mathbf{C}_{\mathrm{i}}(t)$ be the solution of (4.25) — (4.27) for a given strain-controlled process $\{\mathbf{C}(t)\}_{t \in [0,T]}$ and given $\mathbf{C}_{\mathrm{i}}^0$. With the help of the relations (4.32), a one-to-one correspondence between the original and "new" quantities $\mathbf{C}(t)$, $\mathbf{C}_{\mathrm{i}}(t)$, and $\mathbf{C}_{\mathrm{i}}^0$ is defined. It can be easily seen that the closed system of equations which describes the evolution of $\mathbf{C}_{\mathrm{i}}^{\mathrm{new}}(t)$ is obtained from (4.25) — (4.27) by formal replacing of original quantities by their "new" counterparts.

We conclude that the mechanical response becomes invariant under the change of the reference configuration if the loading program $\mathbf{C}(t)$ and the initial value $\mathbf{C}_{\mathrm{i}}^0$ are transformed according to (4.32).

4. Analysis of exponential stability for multiplicative viscoplasticity

4.1. Measuring the distance between solutions in terms of energy. Suppose that $\mathbf{C}_{\mathrm{i}}^{(1)}(t)$ and $\mathbf{C}_{\mathrm{i}}^{(2)}(t)$ are two solutions to the problem (4.25) — (4.27) (with the same forcing function $\mathbf{C}(t)$). Next, suppose that there exists a constant $L < \infty$ such that

$$\|(\mathbf{C}_{\mathrm{i}}^{(k)})^{1/2}(t)\| < L, \quad \|(\mathbf{C}_{\mathrm{i}}^{(k)})^{-1/2}(t)\| < L \quad \text{for all } t > 0, \ k \in \{1, 2\}. \tag{4.34}$$

We introduce the following measure of distance between two solutions in terms of energy [12]

$$\mathrm{Dist}(\mathbf{C}_{\mathrm{i}}^{(1)}, \mathbf{C}_{\mathrm{i}}^{(2)}) := \sqrt{\rho_{\mathrm{R}} \psi_{\mathrm{el}}\Big(\mathbf{C}_{\mathrm{i}}^{(1)} (\mathbf{C}_{\mathrm{i}}^{(2)})^{-1}\Big)}. \tag{4.35}$$

This measure has the following properties:

(i) Invariance under the change of the reference configuration (cf. Section 3.2)

$$\mathrm{Dist}\Big((\mathbf{C}_{\mathrm{i}}^{(1)})^{\mathrm{new}}, (\mathbf{C}_{\mathrm{i}}^{(2)})^{\mathrm{new}}\Big) = \mathrm{Dist}\Big(\mathbf{C}_{\mathrm{i}}^{(1)}, \mathbf{C}_{\mathrm{i}}^{(2)}\Big). \tag{4.36}$$

(ii) For small $\mathbf{C}_{\mathrm{i}}^{(1)} - \mathbf{C}_{\mathrm{i}}^{(2)}$, there exist constants $C_3 > 0$ and $C_4 < \infty$ such that

$$C_3 \, \|\mathbf{C}_{\mathrm{i}}^{(1)} - \mathbf{C}_{\mathrm{i}}^{(2)}\| \leq \mathrm{Dist}(\mathbf{C}_{\mathrm{i}}^{(1)}, \mathbf{C}_{\mathrm{i}}^{(2)}) \leq C_4 \|\mathbf{C}_{\mathrm{i}}^{(1)} - \mathbf{C}_{\mathrm{i}}^{(2)}\|. \tag{4.37}$$

(iii) For all $\mathbf{C}_{\mathrm{i}}^{(1)}(t), \mathbf{C}_{\mathrm{i}}^{(2)}(t) \in M$ we have $\mathrm{Dist}(\mathbf{C}_{\mathrm{i}}^{(1)}, \mathbf{C}_{\mathrm{i}}^{(2)}) \geq 0$ and

$$\mathrm{Dist}(\mathbf{C}_{\mathrm{i}}^{(1)}, \mathbf{C}_{\mathrm{i}}^{(2)}) = 0, \text{ if and only if } \ \mathbf{C}_{\mathrm{i}}^{(1)} = \mathbf{C}_{\mathrm{i}}^{(2)}. \tag{4.38}$$

Proof.

(i): Identity (4.36) can be proved similarly to the invariance property (4.33).

(ii): First, it follows from (4.30) that for small $\mathbf{\Delta}$ we have (see Appendix A)

$$\rho_{\mathrm{R}} \psi_{\mathrm{el}}(\mathbf{1} + \mathbf{\Delta}) = \frac{k}{8} (\mathrm{tr} \mathbf{\Delta})^2 + \frac{\mu}{4} \mathrm{tr}\Big((\mathbf{\Delta}^{\mathrm{D}})^2\Big) + O(\Delta^3),$$

---

[12] The relation (4.35) can be seen as a generalization of the energy norm $\sqrt{\frac{1}{2} E(\varepsilon_{\mathrm{i}}^{(1)} - \varepsilon_{\mathrm{i}}^{(2)})^2}$ (cf. Section 2.3).

where $\Delta = \|\mathbf{\Delta}\|$. Note that $\mathrm{tr}\Big((\mathbf{\Delta}^{\mathrm{D}})^2\Big) = \|\mathbf{\Delta}^{\mathrm{D}}\|^2$ for $\mathbf{\Delta} \in Sym$. Thus, $\frac{k}{8}(\mathrm{tr}\mathbf{\Delta})^2 + \frac{\mu}{4}\mathrm{tr}\Big((\mathbf{\Delta}^{\mathrm{D}})^2\Big)$ is a norm on Sym. Since all norms on Sym are equivalent, there exist constants $C_3' > 0$ and $C_4' < \infty$ such that for small $\mathbf{\Delta} \in Sym$ we have

$$C_3'\|\mathbf{\Delta}\|^2 \leq \rho_{\mathrm{R}}\psi_{\mathrm{el}}(\mathbf{1} + \mathbf{\Delta}) \leq C_4'\|\mathbf{\Delta}\|^2. \tag{4.39}$$

Next, due to the property

$$\psi_{\mathrm{el}}(\mathbf{AB}) = \psi_{\mathrm{el}}(\mathbf{BA}), \tag{4.40}$$

we have

$$\mathrm{Dist}(\mathbf{C}_{\mathrm{i}}^{(1)}, \mathbf{C}_{\mathrm{i}}^{(2)}) = \sqrt{\rho_{\mathrm{R}}\psi_{\mathrm{el}}\Big((\mathbf{C}_{\mathrm{i}}^{(2)})^{-1/2}\ \mathbf{C}_{\mathrm{i}}^{(1)}\ (\mathbf{C}_{\mathrm{i}}^{(2)})^{-1/2}\Big)}. \tag{4.41}$$

Moreover, taking into account that $\|\mathbf{AB}\|_* \leq \|\mathbf{A}\|_*\ \|\mathbf{B}\|_*$, and that the norms $\|\cdot\|_*$ and $\|\cdot\|$ are equivalent, we arrive at

$$\|\mathbf{ABC}\| \leq \acute{C}\|\mathbf{A}\|\ \|\mathbf{B}\|\ \|\mathbf{C}\|, \tag{4.42}$$

with some constant $\acute{C} < \infty$. Thus,

$$\begin{aligned} \Big\|(\mathbf{C}_{\mathrm{i}}^{(2)})^{-1/2}\ \mathbf{C}_{\mathrm{i}}^{(1)}\ (\mathbf{C}_{\mathrm{i}}^{(2)})^{-1/2} - \mathbf{1}\Big\| &= \Big\|(\mathbf{C}_{\mathrm{i}}^{(2)})^{-1/2}\ \Big(\mathbf{C}_{\mathrm{i}}^{(1)} - \mathbf{C}_{\mathrm{i}}^{(2)}\Big)\ (\mathbf{C}_{\mathrm{i}}^{(2)})^{-1/2}\Big\| \\ &\overset{(4.42)}{\leq} \acute{C}\Big\|(\mathbf{C}_{\mathrm{i}}^{(2)})^{-1/2}\Big\|^2\ \Big\|\mathbf{C}_{\mathrm{i}}^{(1)} - \mathbf{C}_{\mathrm{i}}^{(2)}\Big\|, \end{aligned} \tag{4.43}$$

$$\begin{aligned} \Big\|\mathbf{C}_{\mathrm{i}}^{(1)} - \mathbf{C}_{\mathrm{i}}^{(2)}\Big\| &= \Big\|(\mathbf{C}_{\mathrm{i}}^{(2)})^{1/2}\Big((\mathbf{C}_{\mathrm{i}}^{(2)})^{-1/2}\ \mathbf{C}_{\mathrm{i}}^{(1)}\ (\mathbf{C}_{\mathrm{i}}^{(2)})^{-1/2} - \mathbf{1}\Big)(\mathbf{C}_{\mathrm{i}}^{(2)})^{1/2}\Big\| \\ &\overset{(4.42)}{\leq} \acute{C}\Big\|(\mathbf{C}_{\mathrm{i}}^{(2)})^{1/2}\Big\|^2\ \Big\|(\mathbf{C}_{\mathrm{i}}^{(2)})^{-1/2}\ \mathbf{C}_{\mathrm{i}}^{(1)}\ (\mathbf{C}_{\mathrm{i}}^{(2)})^{-1/2} - \mathbf{1}\Big\|. \end{aligned} \tag{4.44}$$

Furthermore, substituting $\mathbf{\Delta} = (\mathbf{C}_{\mathrm{i}}^{(2)})^{-1/2}\ \mathbf{C}_{\mathrm{i}}^{(1)}\ (\mathbf{C}_{\mathrm{i}}^{(2)})^{-1/2} - \mathbf{1}$ in (4.39), and combining it with (4.41), (4.43), and (4.44) we have

$$\tilde{C}_3\|(\mathbf{C}_{\mathrm{i}}^{(2)})^{1/2}\|^{-2}\ \|\mathbf{C}_{\mathrm{i}}^{(1)} - \mathbf{C}_{\mathrm{i}}^{(2)}\| \leq \mathrm{Dist}(\mathbf{C}_{\mathrm{i}}^{(1)}, \mathbf{C}_{\mathrm{i}}^{(2)}) \leq \tilde{C}_4\|(\mathbf{C}_{\mathrm{i}}^{(2)})^{-1/2}\|^2\ \|\mathbf{C}_{\mathrm{i}}^{(1)} - \mathbf{C}_{\mathrm{i}}^{(2)}\|. \tag{4.45}$$

Finally, combining (4.45) with (4.34) we obtain (4.37).

(iii): We note that $\psi_{\mathrm{el}}(\mathbf{A}) \geq 0$. Moreover, $\psi_{\mathrm{el}}(\mathbf{A}) = 0$ if and only if $\mathbf{A} = \mathbf{1}$ ■

In view of properties (i) — (iii), the function Dist is a natural measure of distance for the problem under consideration.[13]

Moreover, the dissipation inequality (4.29), which holds for all relaxation processes, can be interpreted as follows: During relaxation, the distance (measured in terms of energy) between any solution $\mathbf{C}_{\mathrm{i}}^{(2)}$ and a constant solution $\mathbf{C}_{\mathrm{i}}^{(1)} \equiv \mathbf{C} = const$ is not increasing.

4.2. Sufficient condition for exponential stability. Let us consider a loading program (strain-driven process) $\{\mathbf{C}(t)\}_{t\in[0,T]}$ on the time interval $[0, T]$. Let $\mathbf{C}_{\mathrm{i}}^{(1)}, \mathbf{C}_{\mathrm{i}}^{(2)} \in M$ be two solutions. In order to prove the exponential stability, it is sufficient to prove that there exists $t' \geq 0$ and $\gamma > 0$ such that for all $t \geq t'$ (cf. (4.17))

$$\frac{d}{dt}\Big(\mathrm{Dist}(\mathbf{C}_{\mathrm{i}}^{(1)}, \mathbf{C}_{\mathrm{i}}^{(2)})^2\Big) \leq -\gamma\ \mathrm{Dist}(\mathbf{C}_{\mathrm{i}}^{(1)}, \mathbf{C}_{\mathrm{i}}^{(2)})^2. \tag{4.46}$$

---

[13] The function Dist is not symmetric: $\mathrm{Dist}(\mathbf{A}, \mathbf{B}) \neq \mathrm{Dist}(\mathbf{B}, \mathbf{A})$. Symmetrized functions can be defined by $\mathrm{Dist}_1^{Sym}(\mathbf{A}, \mathbf{B}) := 1/2(\mathrm{Dist}(\mathbf{A}, \mathbf{B}) + \mathrm{Dist}(\mathbf{B}, \mathbf{A}))$, $\mathrm{Dist}_2^{Sym}(\mathbf{A}, \mathbf{B}) := \sqrt{\mathrm{Dist}(\mathbf{A}, \mathbf{B})\mathrm{Dist}(\mathbf{B}, \mathbf{A})}$. Nevertheless, none of these functions determine a metric on M, since the triangle inequality does not hold.

Indeed, in that case, using Gronwall's inequality we obtain from (4.46) the following decay estimation

$$\mathrm{Dist}(\mathbf{C}_{\mathrm{i}}^{(1)}(t), \mathbf{C}_{\mathrm{i}}^{(2)}(t))^2 \leq \mathrm{Dist}(\mathbf{C}_{\mathrm{i}}^{(1)}(t'), \mathbf{C}_{\mathrm{i}}^{(2)}(t'))^2 \ \mathrm{e}^{-\gamma(t-t')}. \tag{4.47}$$

Combining this result with (4.37), we obtain the required estimation of the type (4.5). Thus, the uniform error estimation of Theorem 1 follows immediately from (4.47).

4.3. Reduction of the stability analysis to a simplified problem with $\mathbf{C} = \mathbf{1}$. Let t^0 be an arbitrary time instance. In this section we discuss a procedure which helps to simplify the examination of the inequality (4.46) at the time t^0.

The first simplification of the problem is as follows. We note that the quantities $\mathrm{Dist}(\mathbf{C}_{\mathrm{i}}^{(1)}(t^0), \mathbf{C}_{\mathrm{i}}^{(2)}(t^0))^2$, and $\frac{d}{dt}\Big(\mathrm{Dist}(\mathbf{C}_{\mathrm{i}}^{(1)}(t^0), \mathbf{C}_{\mathrm{i}}^{(2)}(t^0))^2\Big)$ depend solely on $\overline{\mathbf{C}}(t^0)$, $\mathbf{C}_{\mathrm{i}}^{(1)}(t^0)$, and $\mathbf{C}_{\mathrm{i}}^{(2)}(t^0)$ but not on $\dot{\mathbf{C}}(t^0)$. Therefore, on the examination of (4.46) at $t = t^0$ we can replace the actual loading program $\{\mathbf{C}\}_{t \in [0,T]}$ with a constant loading (relaxation process): we take a constant $\overline{\mathbf{C}}(t^0)$ instead of loading $\mathbf{C}(t)$, where $\overline{(\cdot)}$ stands for a unimodular part of a tensor.

The second simplification is as follows. Let $\mathbf{F}_0$ be some "new" reference configuration and $\det(\mathbf{F}_0) = 1$. There is a one-to-one correspondence between the solutions $\mathbf{C}_{\mathrm{i}}^{(1)}(t)$, $\mathbf{C}_{\mathrm{i}}^{(2)}(t)$ of the problem with the forcing function $\mathbf{C}(t)$ and the solutions $(\mathbf{C}_{\mathrm{i}}^{(1)})^{\mathrm{new}}(t)$, $(\mathbf{C}_{\mathrm{i}}^{(2)})^{\mathrm{new}}(t)$ with the forcing function $\mathbf{C}^{\mathrm{new}}(t)$ (cf. Section 3.2)

$$\mathbf{C}^{\mathrm{new}}(t) = \mathbf{F}_0^{-\mathrm{T}} \mathbf{C} \mathbf{F}_0^{-1}, \quad (\mathbf{C}_{\mathrm{i}}^{(\mathrm{k})})^{\mathrm{new}}(t) = \mathbf{F}_0^{-\mathrm{T}} \mathbf{C}_{\mathrm{i}}^{(\mathrm{k})}(t) \mathbf{F}_0^{-1}, \quad \mathrm{k} \in \{1, 2\}.$$

It follows from (4.36) that

$$\mathrm{Dist}\Big((\mathbf{C}_{\mathrm{i}}^{(1)})^{\mathrm{new}}(t^0), (\mathbf{C}_{\mathrm{i}}^{(2)})^{\mathrm{new}}(t^0)\Big) = \mathrm{Dist}\Big(\mathbf{C}_{\mathrm{i}}^{(1)}(t^0), \mathbf{C}_{\mathrm{i}}^{(2)}(t^0)\Big),$$

$$\frac{d}{dt}\Big[\mathrm{Dist}\Big((\mathbf{C}_{\mathrm{i}}^{(1)})^{\mathrm{new}}(t), (\mathbf{C}_{\mathrm{i}}^{(2)})^{\mathrm{new}}(t)\Big)^2\Big]|_{t=t^0} = \frac{d}{dt}\Big[\mathrm{Dist}\Big(\mathbf{C}_{\mathrm{i}}^{(1)}(t), \mathbf{C}_{\mathrm{i}}^{(2)}(t)\Big)^2\Big]|_{t=t^0},$$

Therefore, estimation (4.46) is equivalent to

$$\frac{d}{dt}\Big[\mathrm{Dist}\Big((\mathbf{C}_{\mathrm{i}}^{(1)})^{\mathrm{new}}(t), (\mathbf{C}_{\mathrm{i}}^{(2)})^{\mathrm{new}}(t)\Big)^2\Big]|_{t=t^0} \leq -\gamma \ \mathrm{Dist}\Big((\mathbf{C}_{\mathrm{i}}^{(1)})^{\mathrm{new}}(t^0), (\mathbf{C}_{\mathrm{i}}^{(2)})^{\mathrm{new}}(t^0)\Big)^2.$$

Without loss of generality we assume $\det(\mathbf{C}(t^0)) = 1$. By choosing $\mathbf{F}_0 = \Big(\mathbf{C}(t^0)\Big)^{1/2}$ the problem can be reduced to the simplified problem with $\mathbf{C}(t^0) = \mathbf{1}$.[14]

4.4. Evaluation of $\frac{d}{dt}\Big(\mathbf{Dist}(\mathbf{C}_{\mathbf{i}}^{(1)}, \mathbf{C}_{\mathbf{i}}^{(2)})^2\Big)$. In this section we evaluate $\frac{d}{dt}\Big(\mathrm{Dist}(\mathbf{C}_{\mathrm{i}}^{(1)}, \mathbf{C}_{\mathrm{i}}^{(2)})^2\Big)$ at some fixed time instance t^0. Without loss of generality (cf. the previous section) it can be assumed that $\mathbf{C}(t^0) = \mathbf{1}$. In that reduced case, the evolution equation (4.25) takes the form

$$\dot{\mathbf{C}}_{\mathrm{i}} = \alpha(\|(\mathbf{C}_{\mathrm{i}}^{-1})^{\mathrm{D}}\|)(\mathbf{C}_{\mathrm{i}}^{-1})^{\mathrm{D}} \ \mathbf{C}_{\mathrm{i}}, \quad \alpha(x) := \frac{1}{\eta \mu x} \Big\langle \frac{\mu x - \sqrt{2/3} K}{k_0} \Big\rangle^m. \tag{4.48}$$

---

[14] Alternatively, the problem can be reduced to the case $\mathbf{C}_{\mathrm{i}}^{(1)}(t^0) = \mathbf{1}$ by choosing $\mathbf{F}_0 = \big(\mathbf{C}_{\mathrm{i}}^{(1)}(t^0)\big)^{1/2}$.

Next, using the product rule we obtain from $(4.48)_1$

$$\begin{aligned}\frac{d}{dt}\Big(\mathbf{C}_{\mathrm{i}}^{(1)}\mathbf{C}_{\mathrm{i}}^{(2)-1}\Big) &= \dot{\mathbf{C}}_{\mathrm{i}}^{(1)}\mathbf{C}_{\mathrm{i}}^{(2)-1} + \mathbf{C}_{\mathrm{i}}^{(1)}(\mathbf{C}_{\mathrm{i}}^{(2)-1})^{\cdot} \\ &= \mathbf{C}_{\mathrm{i}}^{(1)}\mathbf{C}_{\mathrm{i}}^{(1)-1}\dot{\mathbf{C}}_{\mathrm{i}}^{(1)}\mathbf{C}_{\mathrm{i}}^{(2)-1} + \mathbf{C}_{\mathrm{i}}^{(1)}(\mathbf{C}_{\mathrm{i}}^{(2)-1})^{\cdot}\mathbf{C}_{\mathrm{i}}^{(2)}\mathbf{C}_{\mathrm{i}}^{(2)-1} \\ &\overset{(4.48)_1}{=} \mathbf{C}_{\mathrm{i}}^{(1)}\Big[\alpha^{(1)}(\mathbf{C}_{\mathrm{i}}^{(1)-1})^{\mathrm{D}} - \alpha^{(2)}(\mathbf{C}_{\mathrm{i}}^{(2)-1})^{\mathrm{D}}\Big]\mathbf{C}_{\mathrm{i}}^{(2)-1}, \qquad (4.49)\end{aligned}$$

where $\alpha^{(k)} := \alpha(\|(\mathbf{C}_{\mathrm{i}}^{(k)-1})^{\mathrm{D}}\|)$ for $k \in \{1,2\}$.

Furthermore, we compute the derivative of $\psi_{\mathrm{el}}(\mathbf{A})$ using a coordinate-free tensor setting (see, for example, [**14, 28**])

$$\rho_{\mathrm{R}}\frac{\partial\psi_{\mathrm{el}}(\mathbf{A})}{\partial\mathbf{A}} = \frac{k}{2}\ln\sqrt{\det\mathbf{A}}\ \mathbf{A}^{-\mathrm{T}} + \frac{\mu}{2}\mathbf{A}^{-\mathrm{T}}\ (\overline{\mathbf{A}}^{\mathrm{T}})^{\mathrm{D}}. \qquad (4.50)$$

We abbreviate $\Delta := \|\mathbf{C}_{\mathrm{i}}^{(2)} - \mathbf{C}_{\mathrm{i}}^{(1)}\|$. Since $\mathbf{C}_{\mathrm{i}}^{(1)}, \mathbf{C}_{\mathrm{i}}^{(2)} \in M$, the following estimations hold (cf. Appendix B)

$$\mathrm{tr}\Big((\mathbf{C}_{\mathrm{i}}^{(2)-1} - \mathbf{C}_{\mathrm{i}}^{(1)-1})\mathbf{C}_{\mathrm{i}}^{(1)}\Big) = O(\Delta^2), \quad \mathrm{tr}\Big(\mathbf{C}_{\mathrm{i}}^{(1)}(\mathbf{C}_{\mathrm{i}}^{(1)-1} - \mathbf{C}_{\mathrm{i}}^{(2)-1})\Big) = O(\Delta^2), \text{as } \Delta \to 0. \qquad (4.51)$$

Thus, using $(4.51)_1$ we arrive at

$$\Big(\mathbf{C}_{\mathrm{i}}^{(2)-1}\mathbf{C}_{\mathrm{i}}^{(1)}\Big)^{\mathrm{D}} = \Big((\mathbf{C}_{\mathrm{i}}^{(2)-1} - \mathbf{C}_{\mathrm{i}}^{(1)-1})\mathbf{C}_{\mathrm{i}}^{(1)} + \mathbf{1}\Big)^{\mathrm{D}} = (\mathbf{C}_{\mathrm{i}}^{(2)-1} - \mathbf{C}_{\mathrm{i}}^{(1)-1})\mathbf{C}_{\mathrm{i}}^{(1)} + O(\Delta^2). \qquad (4.52)$$

Combining (4.50) with (4.52) we obtain

$$\begin{aligned}&\rho_{\mathrm{R}}\frac{\partial\psi_{\mathrm{el}}(\mathbf{C}_{\mathrm{i}}^{(1)}\mathbf{C}_{\mathrm{i}}^{(2)-1})}{\partial(\mathbf{C}_{\mathrm{i}}^{(1)}\mathbf{C}_{\mathrm{i}}^{(2)-1})} = \frac{\mu}{2}\Big(\mathbf{C}_{\mathrm{i}}^{(1)}\mathbf{C}_{\mathrm{i}}^{(2)-1}\Big)^{-\mathrm{T}}\ \Big[\overline{\Big(\mathbf{C}_{\mathrm{i}}^{(1)}\mathbf{C}_{\mathrm{i}}^{(2)-1}\Big)}^{\mathrm{T}}\Big]^{\mathrm{D}} \\ &= \frac{\mu}{2}\mathbf{C}_{\mathrm{i}}^{(1)-1}\mathbf{C}_{\mathrm{i}}^{(2)}(\mathbf{C}_{\mathrm{i}}^{(2)-1} - \mathbf{C}_{\mathrm{i}}^{(1)-1})\mathbf{C}_{\mathrm{i}}^{(1)} + O(\Delta^2) = \frac{\mu}{2}(\mathbf{C}_{\mathrm{i}}^{(2)-1} - \mathbf{C}_{\mathrm{i}}^{(1)-1})\mathbf{C}_{\mathrm{i}}^{(1)} + O(\Delta^2). \qquad (4.53)\end{aligned}$$

Next, denote by $\acute{\alpha}$ the derivative of $\alpha(x)$ at $x = \|(\mathbf{C}_{\mathrm{i}}^{(1)-1})^{\mathrm{D}}\|$. Therefore,

$$\begin{aligned}\alpha^{(1)} - \alpha^{(2)} &= \acute{\alpha}\ (\|(\mathbf{C}_{\mathrm{i}}^{(1)-1})^{\mathrm{D}}\| - \|(\mathbf{C}_{\mathrm{i}}^{(2)-1})^{\mathrm{D}}\|) + O(\Delta^2) \\ &= \frac{\acute{\alpha}}{\|(\mathbf{C}_{\mathrm{i}}^{(1)-1})^{\mathrm{D}}\|}(\mathbf{C}_{\mathrm{i}}^{(1)-1})^{\mathrm{D}} : (\mathbf{C}_{\mathrm{i}}^{(1)-1} - \mathbf{C}_{\mathrm{i}}^{(2)-1}) + O(\Delta^2). \qquad (4.54)\end{aligned}$$

It can be assumed that the overstress $f = \mu\|(\mathbf{C}_{\mathrm{i}}^{(1)-1})^{\mathrm{D}}\| - \sqrt{\frac{2}{3}}K$ is positive and bounded by $\sqrt{\frac{2}{3}}K$. Thus, we suppose $\sqrt{\frac{2}{3}}K/\mu < \|(\mathbf{C}_{\mathrm{i}}^{(1)-1})^{\mathrm{D}}\| \leq 2\sqrt{\frac{2}{3}}K/\mu$.

Using the property $\mathbf{A} : (\mathbf{BCD}) = (\mathbf{B}^{\mathrm{T}}\mathbf{A}\mathbf{D}^{\mathrm{T}}) : \mathbf{C}$ it follows from (4.49) and (4.53) that

$$\begin{aligned}&\frac{d}{dt}\Big(\mathrm{Dist}(\mathbf{C}_{\mathrm{i}}^{(1)}, \mathbf{C}_{\mathrm{i}}^{(2)})^2\Big) \overset{(4.35)}{=} \frac{d}{dt}\Big(\rho_{\mathrm{R}}\psi_{\mathrm{el}}(\mathbf{C}_{\mathrm{i}}^{(1)}\mathbf{C}_{\mathrm{i}}^{(2)-1})\Big) = \rho_{\mathrm{R}}\frac{\partial\psi_{\mathrm{el}}(\mathbf{C}_{\mathrm{i}}^{(1)}\mathbf{C}_{\mathrm{i}}^{(2)-1})}{\partial(\mathbf{C}_{\mathrm{i}}^{(1)}\mathbf{C}_{\mathrm{i}}^{(2)-1})} : \frac{d}{dt}\Big(\mathbf{C}_{\mathrm{i}}^{(1)}\mathbf{C}_{\mathrm{i}}^{(2)-1}\Big) \\ &\overset{(4.49),(4.53)}{=} -\frac{\mu}{2}\Big(\mathbf{C}_{\mathrm{i}}^{(1)}(\mathbf{C}_{\mathrm{i}}^{(1)-1} - \mathbf{C}_{\mathrm{i}}^{(2)-1})\Big) : \Big(\alpha^{(1)}(\mathbf{C}_{\mathrm{i}}^{(1)-1})^{\mathrm{D}} - \alpha^{(2)}(\mathbf{C}_{\mathrm{i}}^{(2)-1})^{\mathrm{D}}\Big) + O(\Delta^3) \\ &\overset{(4.51)_2}{=} -\frac{\mu}{2}\Big(\mathbf{C}_{\mathrm{i}}^{(1)}(\mathbf{C}_{\mathrm{i}}^{(1)-1} - \mathbf{C}_{\mathrm{i}}^{(2)-1})\Big) : \Big(\alpha^{(1)}\mathbf{C}_{\mathrm{i}}^{(1)-1} - \alpha^{(2)}\mathbf{C}_{\mathrm{i}}^{(2)-1}\Big) + O(\Delta^3) \\ &= -\frac{\mu}{2}\alpha^{(1)}\Big(\mathbf{C}_{\mathrm{i}}^{(1)}(\mathbf{C}_{\mathrm{i}}^{(1)-1} - \mathbf{C}_{\mathrm{i}}^{(2)-1})\Big) : \Big(\mathbf{C}_{\mathrm{i}}^{(1)-1} - \mathbf{C}_{\mathrm{i}}^{(2)-1}\Big) \\ &- \frac{\mu}{2}(\alpha^{(1)} - \alpha^{(2)})\Big(\mathbf{C}_{\mathrm{i}}^{(1)}(\mathbf{C}_{\mathrm{i}}^{(1)-1} - \mathbf{C}_{\mathrm{i}}^{(2)-1})\Big) : \mathbf{C}_{\mathrm{i}}^{(2)-1} + O(\Delta^3) \overset{(4.54)}{=} F_I + F_{II} + O(\Delta^3), \qquad (4.55)\end{aligned}$$

where F_I and F_{II} are given by

$$F_I := -\frac{\mu}{2}\alpha^{(1)}\mathrm{tr}\Big(\big(\mathbf{C}_\mathrm{i}^{(1)-1} - \mathbf{C}_\mathrm{i}^{(2)-1}\big)\mathbf{C}_\mathrm{i}^{(1)}\big(\mathbf{C}_\mathrm{i}^{(1)-1} - \mathbf{C}_\mathrm{i}^{(2)-1}\big)\Big), \tag{4.56}$$

$$F_{II} := -\frac{\mu}{2}\frac{\acute{\alpha}}{\|(\mathbf{C}_\mathrm{i}^{(1)-1})^\mathrm{D}\|}\Big((\mathbf{C}_\mathrm{i}^{(1)-1})^\mathrm{D} : (\mathbf{C}_\mathrm{i}^{(1)-1} - \mathbf{C}_\mathrm{i}^{(2)-1})\Big)\Big(\mathbf{1} : (\mathbf{C}_\mathrm{i}^{(1)-1} - \mathbf{C}_\mathrm{i}^{(2)-1})\Big).$$

Now, for any pair of real positive numbers (θ, Δ) let us define a subset of $M \times M$ by

$$S(\theta, \Delta) := \{(\mathbf{C}_\mathrm{i}^{(1)}, \mathbf{C}_\mathrm{i}^{(2)}) \in M \times M \mid \|(\mathbf{C}_\mathrm{i}^{(1)-1})^\mathrm{D}\| \leq \theta,\ \|\mathbf{C}_\mathrm{i}^{(1)} - \mathbf{C}_\mathrm{i}^{(2)}\| \leq \Delta\}. \tag{4.57}$$

By definition, put

$$\Phi(\mathbf{C}_\mathrm{i}^{(1)}, \mathbf{C}_\mathrm{i}^{(2)}) := -\frac{2\alpha^{(1)}F_{II}}{\acute{\alpha}F_I} = \frac{-2\Big(\frac{(\mathbf{C}_\mathrm{i}^{(1)-1})^\mathrm{D}}{\|(\mathbf{C}_\mathrm{i}^{(1)-1})^\mathrm{D}\|} : (\mathbf{C}_\mathrm{i}^{(1)-1} - \mathbf{C}_\mathrm{i}^{(2)-1})\Big)\Big(\mathbf{1} : (\mathbf{C}_\mathrm{i}^{(1)-1} - \mathbf{C}_\mathrm{i}^{(2)-1})\Big)}{\mathrm{tr}\Big(\big(\mathbf{C}_\mathrm{i}^{(1)-1} - \mathbf{C}_\mathrm{i}^{(2)-1}\big)\mathbf{C}_\mathrm{i}^{(1)}\big(\mathbf{C}_\mathrm{i}^{(1)-1} - \mathbf{C}_\mathrm{i}^{(2)-1}\big)\Big)}. \tag{4.58}$$

There exists a function $q(\theta) > 0$ such that

$$q(\theta) \geq \Phi(\mathbf{C}_\mathrm{i}^{(1)}, \mathbf{C}_\mathrm{i}^{(2)}) + O(\Delta) \quad \text{for all } (\mathbf{C}_\mathrm{i}^{(1)}, \mathbf{C}_\mathrm{i}^{(2)}) \in S(\theta, \Delta). \tag{4.59}$$

The numerical evaluation of the function $q(\theta)$ is discussed in the Appendix C. The function can be approximated by $q(\theta) \approx \theta^3/12$ for $0 \leq \theta \leq 0.2$ (see Appendix C). Moreover, suppose that (cf. Section 4.5)

$$\alpha^{(1)} \geq q\Big(2\sqrt{\frac{2}{3}}K/\mu\Big)\acute{\alpha}. \tag{4.60}$$

This condition will be discussed in the next section. Multiplying both sides of (4.60) by $F_I\dfrac{1}{\alpha^{(1)}} < 0$ and noting that $\dfrac{\acute{\alpha}}{\alpha^{(1)}}F_I O(\Delta) = O(\Delta^3)$ we get for all $(\mathbf{C}_\mathrm{i}^{(1)}, \mathbf{C}_\mathrm{i}^{(2)}) \in S(2\sqrt{\frac{2}{3}}K/\mu, \Delta)$

$$F_I \overset{(4.60)}{\leq} q\Big(2\sqrt{\frac{2}{3}}K/\mu\Big)\frac{\acute{\alpha}}{\alpha^{(1)}}F_I \overset{(4.59)}{\leq} \Big(\Phi(\mathbf{C}_\mathrm{i}^{(1)}, \mathbf{C}_\mathrm{i}^{(2)}) + O(\Delta)\Big)\frac{\acute{\alpha}}{\alpha^{(1)}}F_I \overset{(4.58)}{=} -2F_{II} + O(\Delta^3). \tag{4.61}$$

Multiplying both sides of (4.61) by 1/2 and adding $1/2F_I + F_{II}$, we have

$$F_I + F_{II} \leq (1/2)F_I + O(\Delta^3).$$

Combining this result with (4.55) we obtain

$$\frac{d}{dt}\Big(\mathrm{Dist}(\mathbf{C}_\mathrm{i}^{(1)}, \mathbf{C}_\mathrm{i}^{(2)})^2\Big) \leq (1/2)F_I + O(\Delta^3). \tag{4.62}$$

Next, if $f \geq f_0$ for some $f_0 > 0$, then there exists $C_5 > 0$ such that

$$F_I \overset{(4.56)}{=} -\frac{\mu}{2}\alpha^{(1)}\Big\|(\mathbf{C}_\mathrm{i}^{(1)-1} - \mathbf{C}_\mathrm{i}^{(2)-1})(\mathbf{C}_\mathrm{i}^{(1)})^{1/2}\Big\|^2 \leq -C_5\Delta^2.$$

Therefore, for small Δ, inequality (4.62) yields

$$\frac{d}{dt}\Big(\mathrm{Dist}(\mathbf{C}_\mathrm{i}^{(1)}, \mathbf{C}_\mathrm{i}^{(2)})^2\Big) \leq 1/4F_I. \tag{4.63}$$

Similarly to the proof of (4.37) we obtain with some $C_6 > 0$

$$
\begin{aligned}
F_I &\overset{(4.56)}{=} -\frac{\mu}{2}\alpha^{(1)}\Big\|(\mathbf{C}_{\mathrm{i}}^{(1)-1} - \mathbf{C}_{\mathrm{i}}^{(2)-1})(\mathbf{C}_{\mathrm{i}}^{(1)})^{1/2}\Big\|^2 \\
&\leq -\frac{\mu}{2}\alpha^{(1)}C_6\Big\|(\mathbf{C}_{\mathrm{i}}^{(1)})^{1/2}\Big\|^{-2}\ \Big\|(\mathbf{C}_{\mathrm{i}}^{(1)})^{1/2}(\mathbf{C}_{\mathrm{i}}^{(1)-1} - \mathbf{C}_{\mathrm{i}}^{(2)-1})(\mathbf{C}_{\mathrm{i}}^{(1)})^{1/2}\Big\|^2 \\
&= -\frac{\mu}{2}\alpha^{(1)}C_6\Big\|(\mathbf{C}_{\mathrm{i}}^{(1)})^{1/2}\Big\|^{-2}\ \Big\|(\mathbf{C}_{\mathrm{i}}^{(1)})^{1/2}\mathbf{C}_{\mathrm{i}}^{(2)-1}(\mathbf{C}_{\mathrm{i}}^{(1)})^{1/2} - \mathbf{1}\Big\|^2 \\
&\overset{(4.39)}{\leq} -\frac{\mu}{2}\alpha^{(1)}(C_6/C_4')\Big\|(\mathbf{C}_{\mathrm{i}}^{(1)})^{1/2}\Big\|^{-2}\rho_{\mathrm{R}}\psi_{\mathrm{el}}((\mathbf{C}_{\mathrm{i}}^{(1)})^{1/2}\mathbf{C}_{\mathrm{i}}^{(2)-1}(\mathbf{C}_{\mathrm{i}}^{(1)})^{1/2}) \\
&\overset{(4.40)}{=} -\frac{\mu}{2}\alpha^{(1)}(C_6/C_4')\Big\|(\mathbf{C}_{\mathrm{i}}^{(1)})^{1/2}\Big\|^{-2}\rho_{\mathrm{R}}\psi_{\mathrm{el}}(\mathbf{C}_{\mathrm{i}}^{(1)}\mathbf{C}_{\mathrm{i}}^{(2)-1}).
\end{aligned}
\tag{4.64}
$$

Finally, combining (4.63) with (4.64) we obtain the required estimation (4.46) if the following assumptions hold: $0 < f_0 \leq f \leq \sqrt{\frac{2}{3}}K$, $\alpha^{(1)} \geq q\Big(2\sqrt{\frac{2}{3}}K/\mu\Big)\acute{\alpha}$.

4.5. Analysis of the sufficient stability condition. In this subsection we analyze the condition (4.60) which was used previously to prove the inequality (4.46). For brevity, we write $\mathbf{C}_{\mathrm{i}}$ instead of $\mathbf{C}_{\mathrm{i}}^{(1)}$ in this subsection. The condition (4.60) can be rewritten as $\alpha(\|(\mathbf{C}_{\mathrm{i}}^{-1})^{\mathrm{D}}\|) \geq q\Big(2\sqrt{\frac{2}{3}}K/\mu\Big)\frac{d\alpha(x)}{dx}\ |_{x=\|(\mathbf{C}_{\mathrm{i}}^{-1})^{\mathrm{D}}\|}$ (see the sketch in Fig. 4.4).

Next, we suppose $\|(\mathbf{C}_{\mathrm{i}}^{-1})^{\mathrm{D}}\| > \sqrt{\frac{2}{3}}K/\mu$ to ensure that the overstress is larger than zero. Using $(4.48)_2$ it can be easily shown that (4.60) is equivalent to

$$
\|(\mathbf{C}_{\mathrm{i}}^{-1})^{\mathrm{D}}\| \geq x_{cr},
$$

where the critical value x_{cr} is given by

$$
x_{cr} := \Big(\sqrt{\frac{2}{3}}K + (m-1)\mu q(\theta) + \sqrt{(\sqrt{\frac{2}{3}}K + (m-1)\mu q(\theta))^2 + 4\mu q(\theta)\sqrt{\frac{2}{3}}K}\Big)/\big(2\mu\big),
$$

with $\theta = 2\sqrt{\frac{2}{3}}K/\mu$. For small values of $q(2\sqrt{\frac{2}{3}}K/\mu)$, a simplified estimation for x_{cr} is valid

$$
x_{cr} = \sqrt{\frac{2}{3}}K/\mu + mq(2\sqrt{\frac{2}{3}}K/\mu) + O\Big((q(2\sqrt{\frac{2}{3}}K/\mu))^2\Big).
$$

This result is visualized in Fig. 4.4 for $m = 1$.

We recall that the overstress is given by $f = \mu\|(\mathbf{C}_{\mathrm{i}}^{-1})^{\mathrm{D}}\| - \sqrt{\frac{2}{3}}K$. Therefore, in terms of the overstress, the condition (4.60) is equivalent to

$$
f \geq f_{cr},
\tag{4.65}
$$

where the critical overstress f_{cr} is estimated by

$$
f_{cr} = m\mu q(2\sqrt{\frac{2}{3}}K/\mu) + O\Big((q(2\sqrt{\frac{2}{3}}K/\mu))^2\Big).
\tag{4.66}
$$

The situation is summarized in Fig. 4.5.

Let us consider a concrete example in order to estimate the order of magnitude of $q(2\sqrt{\frac{2}{3}}K/\mu)$. For instance, we put for a typical aluminium alloy $K \approx 300$ MPa, $\mu \approx 25000$ MPa. Thus, $2\sqrt{\frac{2}{3}}K/\mu \approx 0.014$. Next, $q(0.014) \overset{(4.84)}{\approx} (0.014)^3/12 \approx 2.3 \cdot 10^{-7}$ (see Appendix C). Therefore, the critical overstress is given by $f_{cr} \overset{(4.66)}{\approx} m\ 0.0057$ MPa. For physically

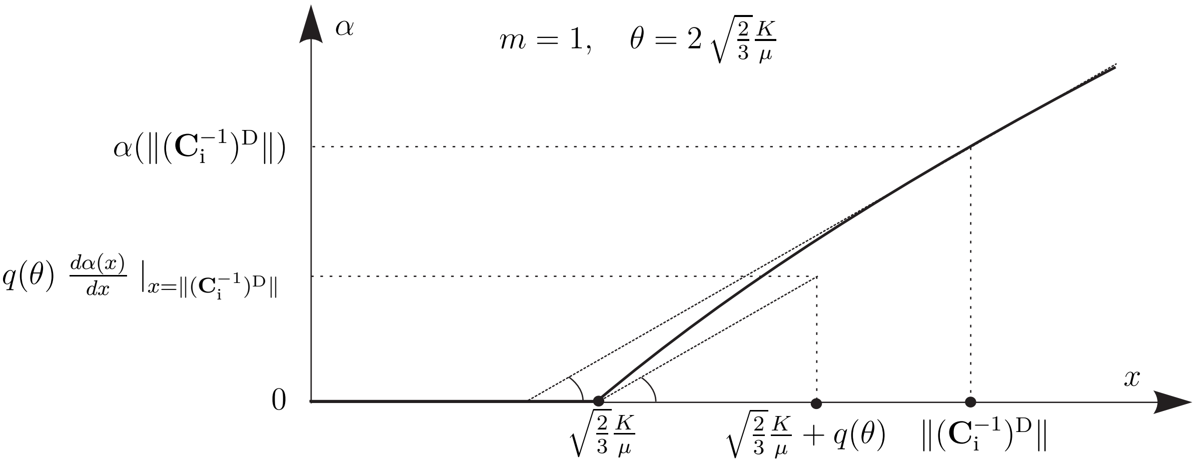

Figure 4.4. Sketch of condition (4.60) for $m = 1$.

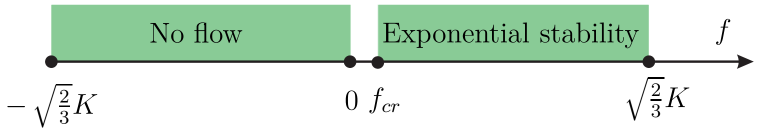

Figure 4.5. Domain of exponential stability.

reasonable values of m ($m \leq 100$) this critical value is negligible compared to the size of the elastic domain $\sqrt{\frac{2}{3}}K \approx 245$ MPa.

Remark 5. Since the overstress f is isolated from zero due to the sufficient stability condition (4.65), the current theory can not be applied to exactly quasistatic processes with $f \leq 0$. On the other hand, the theory is directly applicable to *nearly quasistatic* processes with the overstress f larger than f_{cr} but still negligible compared to the size of the elastic domain $\sqrt{\frac{2}{3}}K$.

5. Accuracy testing of implicit integrators

The numerical implementation of the material model (4.25) — (4.27) within a displacement-based Finite Element Method (FEM) with implicit time stepping is based on the implicit integration of the evolution equation (4.25) (see, for example, [**29**]). This procedure should provide the stresses as a function of the strain history.

More precisely, suppose that the right Cauchy-Green tensor ${}^{n+1}\mathbf{C}$ at the time $t_{n+1} = t_n + \Delta t$ is known and assume that the internal variable $\mathbf{C}_{\mathrm{i}}$ at the time t_n is given by ${}^{n}\mathbf{C}_{\mathrm{i}}$. We need to compute the internal variable $\mathbf{C}_{\mathrm{i}}$ at the time t_{n+1} in order to evaluate the stress tensor ${}^{n+1}\tilde{\mathbf{T}} = \tilde{\mathbf{T}}({}^{n+1}\mathbf{C}, {}^{n+1}\mathbf{C}_{\mathrm{i}})$.

Note that the norm of the driving force $\mathfrak{F}$ and the overstress f can be represented as functions of ${}^{n+1}\mathbf{C}$ and ${}^{n+1}\mathbf{C}_{\mathrm{i}}$:

$$\mathfrak{F}({}^{n+1}\mathbf{C}, {}^{n+1}\mathbf{C}_{\mathrm{i}}) = \sqrt{\mathrm{tr}\Big[\Big({}^{n+1}\mathbf{C}\ \tilde{\mathbf{T}}({}^{n+1}\mathbf{C}, {}^{n+1}\mathbf{C}_{\mathrm{i}})\Big)^{\mathrm{D}}\Big]^2}, \tag{4.67}$$

$$f({}^{n+1}\mathbf{C}, {}^{n+1}\mathbf{C}_{\mathrm{i}}) = \mathfrak{F}({}^{n+1}\mathbf{C}, {}^{n+1}\mathbf{C}_{\mathrm{i}}) - \sqrt{\frac{2}{3}}K.$$

For what follows it is useful to introduce the incremental inelastic parameter

$$\xi := \Delta t \ {}^{n+1}\lambda_{\mathrm{i}}.$$

Thus, according to the Perzyna rule, we have the following equation with respect to ${}^{n+1}\mathbf{C}$, ${}^{n+1}\mathbf{C}_{\mathrm{i}}$ and ξ

$$\xi = \frac{\Delta t}{\eta} \Big\langle \frac{f({}^{n+1}\mathbf{C}, {}^{n+1}\mathbf{C}_{\mathrm{i}})}{k_0} \Big\rangle^m. \tag{4.68}$$

The remaining equation for finding unknown ${}^{n+1}\mathbf{C}_{\mathrm{i}}$ and ξ is obtained through the time discretization of (4.25), which will be discussed in the next subsection.

5.1. Euler Backward Method and geometric implicit integrators. We introduce a nonlinear operator $\mathbf{B}({}^{n+1}\mathbf{C}, {}^{n+1}\mathbf{C}_{\mathrm{i}}, \xi)$ as (cf. the right-hand side of $(4.25)_1$)

$$\mathbf{B}({}^{n+1}\mathbf{C}, {}^{n+1}\mathbf{C}_{\mathrm{i}}, \xi) := 2 \frac{\xi}{\mathfrak{F}({}^{n+1}\mathbf{C}, {}^{n+1}\mathbf{C}_{\mathrm{i}})} \Big({}^{n+1}\mathbf{C} \ \tilde{\mathbf{T}}({}^{n+1}\mathbf{C}, {}^{n+1}\mathbf{C}_{\mathrm{i}}) \Big)^{\mathrm{D}},$$

where $\tilde{\mathbf{T}}({}^{n+1}\mathbf{C}, {}^{n+1}\mathbf{C}_{\mathrm{i}})$ and $\mathfrak{F}({}^{n+1}\mathbf{C}, {}^{n+1}\mathbf{C}_{\mathrm{i}})$ are given by (8.33) and (4.67), respectively.

Let us consider the classical Euler-Backward Method (EBM) (see, for example, [**4, 8, 29**]) being applied to the evolution problem (4.25)

$${}^{n+1}\mathbf{C}_{\mathrm{i}} = \Big[\mathbf{1} - \mathbf{B}({}^{n+1}\mathbf{C}, {}^{n+1}\mathbf{C}_{\mathrm{i}}, \xi)\Big]^{-1} \ {}^{n}\mathbf{C}_{\mathrm{i}}. \tag{4.69}$$

Since the symmetry of the internal variable ${}^{n+1}\mathbf{C}_{\mathrm{i}}$ is exactly preserved by the EBM[15], this equation is equivalent to

$${}^{n+1}\mathbf{C}_{\mathrm{i}} = \mathrm{sym}\Big(\Big[\mathbf{1} - \mathbf{B}({}^{n+1}\mathbf{C}, {}^{n+1}\mathbf{C}_{\mathrm{i}}, \xi)\Big]^{-1} \ {}^{n}\mathbf{C}_{\mathrm{i}}\Big). \tag{4.70}$$

The main disadvantage of the EBM is that *the incompressibility condition is violated.* In other words, in general, $\det({}^{n+1}\mathbf{C}_{\mathrm{i}}) \neq 1$. In order to avoid this problem, a modification of EBM was proposed by Helm in [**12**]. The Modified Euler-Backward Method (MEBM) (see [**12, 27**]) uses the following equation which is obtained by applying the projection operator $\overline{(\cdot)}$ to the right-hand side of (4.69)

$${}^{n+1}\mathbf{C}_{\mathrm{i}} = \overline{\Big[\mathbf{1} - \mathbf{B}({}^{n+1}\mathbf{C}, {}^{n+1}\mathbf{C}_{\mathrm{i}}, \xi)\Big]^{-1} \ {}^{n}\mathbf{C}_{\mathrm{i}}}. \tag{4.71}$$

Next, since the symmetry property is exactly preserved by MEBM (${}^{n+1}\mathbf{C}_{\mathrm{i}} \in \mathit{Sym}$), this method can be equivalently rewritten as

$${}^{n+1}\mathbf{C}_{\mathrm{i}} = \overline{\mathrm{sym}\Big(\Big[\mathbf{1} - \mathbf{B}({}^{n+1}\mathbf{C}, {}^{n+1}\mathbf{C}_{\mathrm{i}}, \xi)\Big]^{-1} \ {}^{n}\mathbf{C}_{\mathrm{i}}\Big)}. \tag{4.72}$$

Finally, the Exponential Method (EM) (see, for instance, [**4, 21, 22, 35**]) is based on the use of the tensor exponential $\exp(\cdot)$

$${}^{n+1}\mathbf{C}_{\mathrm{i}} = \exp\Big[\mathbf{B}({}^{n+1}\mathbf{C}, {}^{n+1}\mathbf{C}_{\mathrm{i}}, \xi)\Big] \ {}^{n}\mathbf{C}_{\mathrm{i}}, \tag{4.73}$$

where

$$\exp\Big[\mathbf{B}\Big] := \mathbf{1} + \mathbf{B} + \frac{1}{2!}\mathbf{B}^2 + \frac{1}{3!}\mathbf{B}^3 + \ldots \,. \tag{4.74}$$

---

[15] Moreover, it was shown in [**27**] that the *symmetry is exactly preserved* by the Euler-Backward Method and Exponential Method even in a more general case of a nonlinear kinematic hardening.

Since both the symmetry and unimodularity of the numerical solution are exactly preserved (${}^{n+1}\mathbf{C}_{\mathrm{i}} \in M$), the Exponential Method can be rewritten as follows (cf. [**27**]):

$$ {}^{n+1}\mathbf{C}_{\mathrm{i}} = \overline{\operatorname{sym}\Big(\exp \Big[\mathbf{B}({}^{n+1}\mathbf{C}, {}^{n+1}\mathbf{C}_{\mathrm{i}}, \xi) \Big] \; {}^{n}\mathbf{C}_{\mathrm{i}} \Big)}. \tag{4.75} $$

Combining (4.68) with one of the discretization methods (equations (4.70), (4.72) or (4.75)) a closed system of nonlinear algebraic equations for finding unknown ${}^{n+1}\mathbf{C}_{\mathrm{i}}$ and ξ is obtained. One possible solution strategy for the resulting system of equations was discussed in [**27**], and the application of a coordinate-free tensor formalism to the numerical solution was analyzed in [**28**]. We don't discuss the concrete solution strategies in this paper, since all robust procedures yield the same numerical result.

We recall that the geometric property of the exact flow ($\mathbf{C}_{\mathrm{i}} \in M$) is exactly satisfied by MEBM and EM. Therefore, we refer to these two methods as to *geometric integrators*.

For all the three methods, the error on the step is bounded by the second power of the step size (cf. estimation (4.6)), if the right-hand side is a smooth function. On the other hand, strong local nonlinearities due to the distinction into elastic and inelastic material behavior or due to the non-smoothness of the loading function $\mathbf{C}(t)$ may increase the error on the corresponding time step.

5.2. Testing results. The theoretical results obtained in this study are validated via a series of numerical tests. Let us simulate the material behavior under strain-controlled, nonproportional and non-monotonic loading in the time interval $t \in [0, 300]$. Suppose that the deformation gradient is defined by

$$ \mathbf{F}(t) = \overline{\mathbf{F}'(t)}, $$

where $\mathbf{F}'(t)$ is a piecewise linear function of time t such that $\mathbf{F}'(0) = \mathbf{F}_1$, $\mathbf{F}'(100) = \mathbf{F}_2$, $\mathbf{F}'(200) = \mathbf{F}_3$, and $\mathbf{F}'(300) = \mathbf{F}_4$ with

$$ \mathbf{F}_1 := \mathbf{1}, \ \mathbf{F}_2 := \begin{pmatrix} 2 & 0 & 0 \\ 0 & \dfrac{1}{\sqrt{2}} & 0 \\ 0 & 0 & \dfrac{1}{\sqrt{2}} \end{pmatrix}, \ \mathbf{F}_3 := \begin{pmatrix} 1 & 1 & 0 \\ 0 & 1 & 0 \\ 0 & 0 & 1 \end{pmatrix}, \ \mathbf{F}_4 := \begin{pmatrix} \dfrac{1}{\sqrt{2}} & 0 & 0 \\ 0 & 2 & 0 \\ 0 & 0 & \dfrac{1}{\sqrt{2}} \end{pmatrix}. $$

Thus, we put

$$ \mathbf{F}'(t) := \begin{cases} (1 - t/100)\mathbf{F}_1 + (t/100)\mathbf{F}_2 & \text{if } t \in [0, 100] \\ (2 - t/100)\mathbf{F}_2 + (t/100 - 1)\mathbf{F}_3 & \text{if } t \in (100, 200] \\ (3 - t/100)\mathbf{F}_3 + (t/100 - 2)\mathbf{F}_4 & \text{if } t \in (200, 300] \end{cases}. $$

The material parameters used in simulations are summarized in Table 4.1.

Table 4.1. Material parameters

k [MPa]	μ [MPa]	K [MPa]	m [-]	η [s]	k_0 [Mpa]
73500	28200	270	3.6	$2 \cdot 10^6$	1

Next, we suppose that the reference configuration is stress free at $t = 0$. Therefore, we put

$$ \mathbf{C}_{\mathrm{i}}|_{t=0} = \mathbf{1}. $$

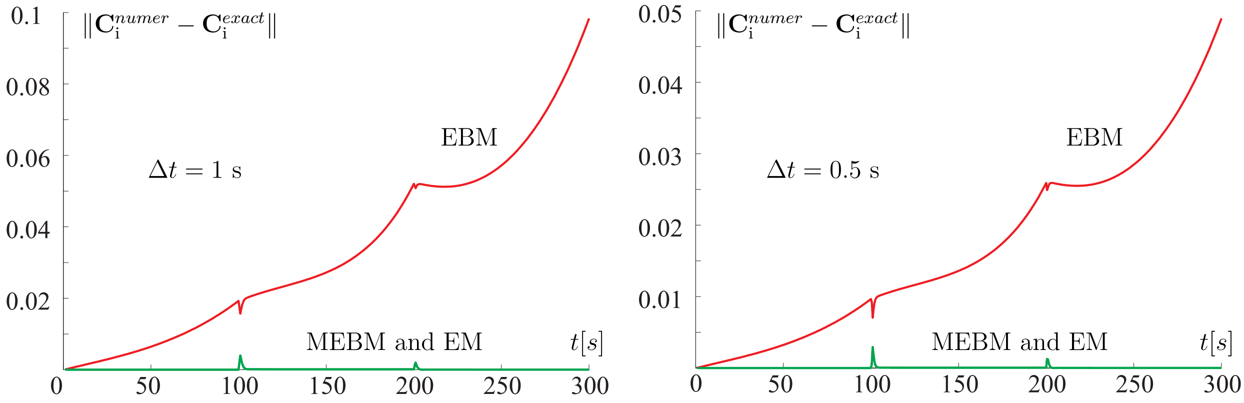

Figure 4.6. Accuracy analysis concerning Euler Backward Method (EBM), Modified Euler-Backward Method (MEBM), and Exponential Method (EM).

The numerical solution obtained with an extremely small time step ($\Delta t = 0.01$s) will be named the *exact solution* and denoted by $\mathbf{C}_{\mathrm{i}}^{exact}$. Next, the numerical solutions with $\Delta t = 1$s and $\Delta t = 0.5$s are denoted by $\mathbf{C}_{\mathrm{i}}^{numer}$. The error $\|\mathbf{C}_{\mathrm{i}}^{numer} - \mathbf{C}_{\mathrm{i}}^{exact}\|$ is plotted in Fig. 4.6.

For all three methods the error is proportional to Δt. Moreover, in accordance with Theorem 1 (cf. Section 2.2), the error is *uniformly* bounded for geometric integrators (MEBM and EM). More precisely, the error is bounded by $C\Delta t$ where the constant C *does not depend* on the size of the entire time interval. Next, since the incompressibility condition is violated by EBM, the geometric property (4.28) is lost and some *spurious degrees of freedom* are introduced. In that case, only a weaker error estimation is valid: $\|\mathbf{C}_{\mathrm{i}}^{numer} - \mathbf{C}_{\mathrm{i}}^{exact}\| \leq \widetilde{C}(T)\Delta t$, where $\widetilde{C}(T)$ depends on the size T of the entire time interval.

6. Discussion and conclusion

In the last decade, intensive research has been carried out concerning the development of so-called geometric integrators for the evolution equations of finite strain plasticity/viscoplasticity, which exactly preserve the inelastic incompressibility condition. The excellent accuracy and convergence properties of such algorithms were tested by numerical computations. Particularly, the long term accuracy of geometric integrators was analyzed in the paper [**27**], and the *absence of error accumulation* was numerically verified for strain-driven processes. In the current study, a rigorous mathematical formulation of this phenomenon is proposed. The main result of the current paper is as follows: The numerical error is *uniformly* bounded by $C\Delta t$ if the incompressibility condition is satisfied. In terms of a classical model of multiplicative viscoplasticity we prove that *all* first-order accurate geometric integrators are *equivalent* in that sense. This theoretical result corresponds with the numerical tests. Indeed, MEBM and EM are equivalent concerning the accuracy and convergence (cf. Fig. 4.6). The main results are summarized diagrammatically in Fig. 4.7.

The property of the exponential stability of the exact plastic flow was mathematically analyzed in this paper. Obviously, this property must be utilized during the development of new material models and corresponding algorithms in order to improve the accuracy and convergence of numerical computations.

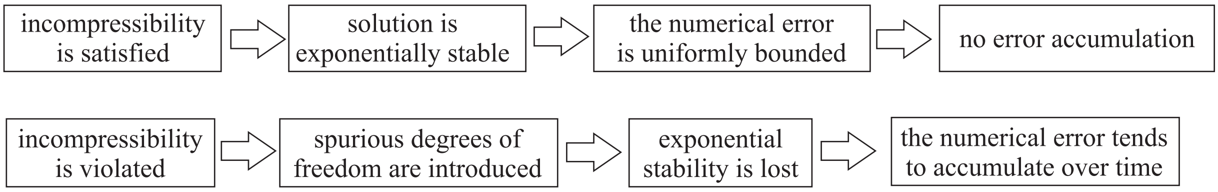

Figure 4.7. Summary of the main results.

Appendix A

Suppose $\Delta = \|\mathbf{\Delta}\| \to 0$. Let us show that

$$\rho_{\mathrm{R}}\psi_{\mathrm{el}}(\mathbf{1}+\mathbf{\Delta}) = \frac{k}{8}(\mathrm{tr}\mathbf{\Delta})^2 + \frac{\mu}{4}\mathrm{tr}\Big((\mathbf{\Delta}^{\mathrm{D}})^2\Big) + O(\Delta^3). \tag{4.76}$$

First, recall the Taylor expansion of $\det(\mathbf{1}+\mathbf{\Delta})$ up to second order

$$\det(\mathbf{1}+\mathbf{\Delta}) = 1 + \mathrm{tr}(\mathbf{\Delta}) + 1/2(\mathrm{tr}(\mathbf{\Delta}))^2 - 1/2\mathrm{tr}(\mathbf{\Delta}^2) + O(\Delta^3). \tag{4.77}$$

Therefore,

$$\sqrt{\det(\mathbf{1}+\mathbf{\Delta})} = 1 + 1/2\mathrm{tr}(\mathbf{\Delta}) + O(\Delta^2),$$

$$\frac{k}{2}\Big(\ln\sqrt{\det(\mathbf{1}+\mathbf{\Delta})}\Big)^2 = \frac{k}{8}(\mathrm{tr}\mathbf{\Delta})^2 + O(\Delta^3). \tag{4.78}$$

Next, note that for small ε we have

$$(1+\varepsilon)^{-1/3} = 1 - 1/3\varepsilon + 2/9\varepsilon^2 + O(\varepsilon^3).$$

Combining this with (4.77), we arrive at

$$\begin{aligned}\frac{\mu}{2}\Big(\mathrm{tr}(\overline{\mathbf{1}+\mathbf{\Delta}}) - 3\Big) &= \frac{\mu}{2}\Big((\det(\mathbf{1}+\mathbf{\Delta}))^{-1/3}\mathrm{tr}(\mathbf{1}+\mathbf{\Delta}) - 3\Big) \\ &= \frac{\mu}{2}\Big((1 - 1/3\mathrm{tr}\mathbf{\Delta} + 1/18(\mathrm{tr}\mathbf{\Delta})^2 + 1/6\mathrm{tr}(\mathbf{\Delta}^2) + O(\Delta^3))(3+\mathrm{tr}\mathbf{\Delta}) - 3\Big) \\ &= \frac{\mu}{4}\Big(\mathrm{tr}(\mathbf{\Delta}^2) - 1/3(\mathrm{tr}\mathbf{\Delta})^2\Big) + O(\Delta^3) = \frac{\mu}{4}\mathrm{tr}\Big((\mathbf{\Delta}^{\mathrm{D}})^2\Big) + O(\Delta^3).\end{aligned} \tag{4.79}$$

Finally, (4.76) follows from (4.30), using (4.78) and (4.79).

Appendix B

Let $\mathbf{A}, \mathbf{B} \in M$ and $\|\mathbf{A}-\mathbf{B}\| \to 0$. Let us prove, for instance, that

$$\mathbf{B}^{-1} : (\mathbf{A}-\mathbf{B}) = O(\|\mathbf{A}-\mathbf{B}\|^2). \tag{4.80}$$

Indeed, since $\det(\cdot)$ is a smooth function, we have

$$\det(\mathbf{A}) = \det(\mathbf{B}) + \frac{\partial\det(\mathbf{B})}{\partial\mathbf{B}} : (\mathbf{A}-\mathbf{B}) + O(\|\mathbf{A}-\mathbf{B}\|^2).$$

Next, using the Jacobi formula, we obtain

$$\det(\mathbf{A}) = \det(\mathbf{B}) + \det(\mathbf{B})\mathbf{B}^{-\mathrm{T}} : (\mathbf{A}-\mathbf{B}) + O(\|\mathbf{A}-\mathbf{B}\|^2).$$

Finally, taking into account that $\det(\mathbf{A}) = \det(\mathbf{B}) = 1$ and $\mathbf{B}^{-\mathrm{T}} = \mathbf{B}^{-1}$, we obtain (4.80).

Remark 6. Note that for the tangential space $T_{\mathbf{B}}M$ to the manifold M in Sym we have

$$T_{\mathbf{B}}M = \{\mathbf{X} \in Sym \mid \mathbf{B}^{-1} : \mathbf{X} = 0\}.$$

Thus, relation (4.80) implies that $\lim\limits_{\mathbf{A}\to\mathbf{B}} \Big((\mathbf{A}-\mathbf{B})/\|\mathbf{A}-\mathbf{B}\|\Big) \in T_{\mathbf{B}}M$ (if the limit exists).

Appendix C

We need to construct and evaluate a function $q(\theta)$ such that for small Δ

$$q(\theta) \geq \Phi(\mathbf{C}_{\mathrm{i}}^{(1)}, \mathbf{C}_{\mathrm{i}}^{(2)}) + O(\Delta) \quad \text{for all } (\mathbf{C}_{\mathrm{i}}^{(1)}, \mathbf{C}_{\mathrm{i}}^{(2)}) \in S(\theta, \Delta).$$

Let $(\mathbf{C}_{\mathrm{i}}^{(1)}, \mathbf{C}_{\mathrm{i}}^{(2)}) \in S(\theta, \Delta)$ (cf. (4.57)). It follows from (4.80), that

$$\Big(\mathbf{C}_{\mathrm{i}}^{(1)-1} - \mathbf{C}_{\mathrm{i}}^{(2)-1}\Big) : \mathbf{C}_{\mathrm{i}}^{(1)} = O(\Delta^2). \tag{4.81}$$

By $\mathbf{X}$ we denote the orthogonal projection of $\mathbf{C}_{\mathrm{i}}^{(1)-1} - \mathbf{C}_{\mathrm{i}}^{(2)-1}$ on the tangential space $T_{\mathbf{C}_{\mathrm{i}}^{(1)-1}}M$. Using (4.81), we obtain for $\mathbf{X}$

$$\mathbf{X} = \mathbf{C}_{\mathrm{i}}^{(1)-1} - \mathbf{C}_{\mathrm{i}}^{(2)-1} - \Big[\Big(\mathbf{C}_{\mathrm{i}}^{(1)-1} - \mathbf{C}_{\mathrm{i}}^{(2)-1}\Big) : \mathbf{C}_{\mathrm{i}}^{(1)} \frac{1}{\|\mathbf{C}_{\mathrm{i}}^{(1)}\|^2}\Big] \mathbf{C}_{\mathrm{i}}^{(1)} = \mathbf{C}_{\mathrm{i}}^{(1)-1} - \mathbf{C}_{\mathrm{i}}^{(2)-1} + O(\Delta^2). \tag{4.82}$$

Moreover, since $\operatorname{tr}\Big(\mathbf{X}\mathbf{C}_{\mathrm{i}}^{(1)}\mathbf{X}\Big) = \|\mathbf{X}(\mathbf{C}_{\mathrm{i}}^{(1)})^{1/2}\|^2$, we have

$$\frac{O(\Delta^3)}{\operatorname{tr}\Big(\mathbf{X}\mathbf{C}_{\mathrm{i}}^{(1)}\mathbf{X}\Big)} = O(\Delta). \tag{4.83}$$

Substituting (4.82) in (4.58) and taking (4.83) into account, we obtain

$$\Phi(\mathbf{C}_{\mathrm{i}}^{(1)}, \mathbf{C}_{\mathrm{i}}^{(2)}) = \frac{-2\Big(\frac{(\mathbf{C}_{\mathrm{i}}^{(1)-1})^{\mathrm{D}}}{\|(\mathbf{C}_{\mathrm{i}}^{(1)-1})^{\mathrm{D}}\|} : \mathbf{X}\Big)\Big(\mathbf{1} : \mathbf{X}\Big)}{\operatorname{tr}\Big(\mathbf{X}\mathbf{C}_{\mathrm{i}}^{(1)}\mathbf{X}\Big)} + O(\Delta).$$

Thus, we define $q(\theta)$ as

$$q(\theta) := \max_{\|(\mathbf{C}_{\mathrm{i}}^{(1)-1})^{\mathrm{D}}\| \leq \theta} \hat{q}(\mathbf{C}^{(1)}), \quad \hat{q}(\mathbf{C}^{(1)}) := \max_{\mathbf{X} \in T_{\mathbf{C}_{\mathrm{i}}^{(1)-1}}M} \frac{-2\Big(\frac{(\mathbf{C}_{\mathrm{i}}^{(1)-1})^{\mathrm{D}}}{\|(\mathbf{C}_{\mathrm{i}}^{(1)-1})^{\mathrm{D}}\|} : \mathbf{X}\Big)\Big(\mathbf{1} : \mathbf{X}\Big)}{\operatorname{tr}\Big(\mathbf{X}\mathbf{C}_{\mathrm{i}}^{(1)}\mathbf{X}\Big)}.$$

The function $\hat{q}(\mathbf{C}_{\mathrm{i}}^{(1)})$ can be evaluated as follows. First, for each $\mathbf{X}$ introduce $\mathbf{Y} = \mathbf{X}(\mathbf{C}_{\mathrm{i}}^{(1)})^{1/2}$. Next, define a vector space $T := \{\mathbf{Y} \in Sym \mid (\mathbf{C}_{\mathrm{i}}^{(1)})^{1/2} : \mathbf{Y} = 0\}$. Thus,

$$\mathbf{X} \in T_{\mathbf{C}_{\mathrm{i}}^{(1)-1}}M \quad \Longleftrightarrow \quad \mathbf{Y} \in T,$$

$$\operatorname{tr}\Big(\mathbf{X}\mathbf{C}_{\mathrm{i}}^{(1)}\mathbf{X}\Big) = \|\mathbf{Y}\|, \quad -2\frac{(\mathbf{C}_{\mathrm{i}}^{(1)-1})^{\mathrm{D}}}{\|(\mathbf{C}_{\mathrm{i}}^{(1)-1})^{\mathrm{D}}\|} : \mathbf{X} = \mathbf{B}_1 : \mathbf{Y}, \quad \mathbf{1} : \mathbf{X} = \mathbf{B}_2 : \mathbf{Y},$$

where

$$\mathbf{B}_1 := -2(\mathbf{C}_{\mathrm{i}}^{(1)})^{-1/2} \frac{(\mathbf{C}_{\mathrm{i}}^{(1)-1})^{\mathrm{D}}}{\|(\mathbf{C}_{\mathrm{i}}^{(1)-1})^{\mathrm{D}}\|}, \quad \mathbf{B}_2 := (\mathbf{C}_{\mathrm{i}}^{(1)})^{-1/2}.$$

Therefore,

$$\hat{q}(\mathbf{C}_{\mathrm{i}}^{(1)}) = \max_{\mathbf{Y} \in T, \|\mathbf{Y}\| = 1} \Big[\Big(\mathbf{B}_1 : \mathbf{Y}\Big)\Big(\mathbf{B}_2 : \mathbf{Y}\Big)\Big].$$

Next, we compute the orthogonal projections of $\mathbf{B}_1$ and $\mathbf{B}_2$ on T:

$$\mathbf{B}_{\mathrm{k}}^0 := \mathbf{B}_{\mathrm{k}} - \Big(\mathbf{B}_{\mathrm{k}} : (\mathbf{C}_{\mathrm{i}}^{(1)})^{1/2}\Big)(\mathbf{C}_{\mathrm{i}}^{(1)})^{1/2} \frac{1}{\|(\mathbf{C}_{\mathrm{i}}^{(1)})^{1/2}\|^2}, \quad \mathrm{k} \in \{1, 2\}.$$

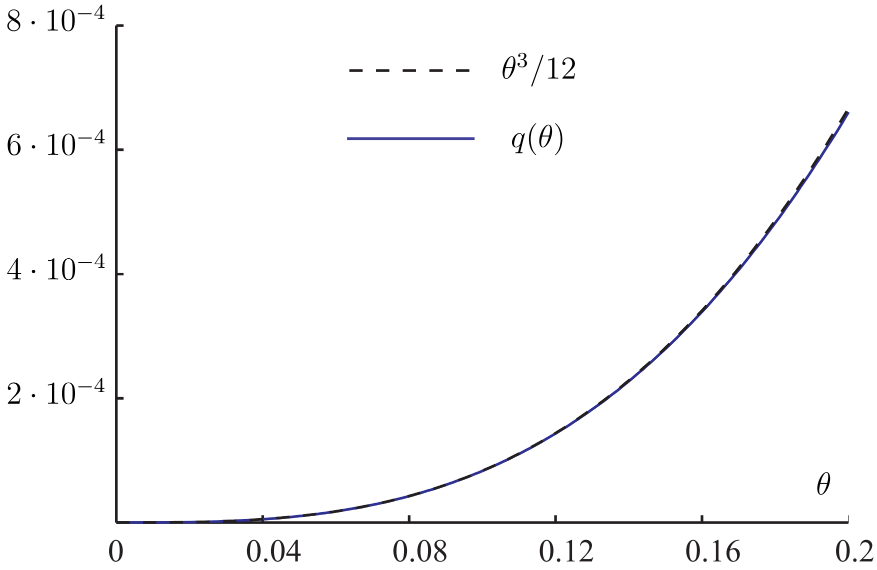

Figure 4.8. Function $q(\theta)$ and its approximation by $\theta^3/12$.

Thus,

$$\hat{q}(\mathbf{C}_{\mathrm{i}}^{(1)}) = \max_{\mathbf{Y} \in T, \|\mathbf{Y}\|=1} \Big[\mathbf{Y} : \mathrm{sym}\Big(\mathbf{B}_1^0 \otimes \mathbf{B}_2^0\Big) : \mathbf{Y} \Big] = \lambda_{\max}\Big(\mathrm{sym}\Big(\mathbf{B}_1^0 \otimes \mathbf{B}_2^0\Big)\Big),$$

where $\lambda_{\max}\Big(\mathrm{sym}\Big(\mathbf{B}_1^0 \otimes \mathbf{B}_2^0\Big)\Big)$ is the maximal eigenvalue of the symmetric operator $\mathrm{sym}\Big(\mathbf{B}_1^0 \otimes \mathbf{B}_2^0\Big) : Sym \rightarrow Sym$. Obviously, the same maximal eigenvalue has its restriction on $T^0 = \mathrm{Span}\{\mathbf{B}_1^0, \mathbf{B}_2^0\}$. It can be easily seen that

$$\mathrm{sym}\Big(\mathbf{B}_1^0 \otimes \mathbf{B}_2^0\Big)(\mathbf{B}_1^0) = 1/2(\mathbf{B}_1^0 : \mathbf{B}_2^0)\mathbf{B}_1^0 + 1/2(\mathbf{B}_1^0 : \mathbf{B}_1^0)\mathbf{B}_2^0,$$

$$\mathrm{sym}\Big(\mathbf{B}_1^0 \otimes \mathbf{B}_2^0\Big)(\mathbf{B}_2^0) = 1/2(\mathbf{B}_2^0 : \mathbf{B}_2^0)\mathbf{B}_1^0 + 1/2(\mathbf{B}_1^0 : \mathbf{B}_2^0)\mathbf{B}_2^0.$$

Therefore, the matrix of the restricted operator with respect to the basis $\{\mathbf{B}_1^0, \mathbf{B}_2^0\}$ has the following form

$$A := \frac{1}{2} \begin{pmatrix} \mathbf{B}_1^0 : \mathbf{B}_2^0 & \mathbf{B}_2^0 : \mathbf{B}_2^0 \\ \mathbf{B}_1^0 : \mathbf{B}_1^0 & \mathbf{B}_1^0 : \mathbf{B}_2^0 \end{pmatrix}.$$

Both eigenvalues of A are real, since A represents a symmetric tensor. Finally,

$$\hat{q}(\mathbf{C}_{\mathrm{i}}^{(1)}) = \lambda_{\max}\Big(\mathrm{sym}\Big(\mathbf{B}_1^0 \otimes \mathbf{B}_2^0\Big)\Big) = \lambda_{\max}(A).$$

Note that $\hat{q}(\mathbf{C}_{\mathrm{i}}^{(1)})$ is a continuous function of $\mathbf{C}_{\mathrm{i}}^{(1)}$. Therefore, the maximum $q(\theta) = \max_{\|(\mathbf{C}_{\mathrm{i}}^{(1)-1})^{\mathrm{D}}\| \leq \theta} \hat{q}(\mathbf{C}^{(1)})$ is well defined. We compute it by the brutal force method. Moreover, the following parametrization can be used to simplify the computations. For any tensor $\mathbf{C}_{\mathrm{i}}^{(1)}$ there exist a Cartesian coordinate system and real numbers $\lambda^1, \lambda^2 > 0$ such that the matrix of $\mathbf{C}_{\mathrm{i}}^{(1)}$ takes the diagonal form $\mathrm{diag}(\lambda^1, \lambda^2, 1/(\lambda^1 \lambda^1))$. The function $q(\theta)$ is plotted in Fig. 4.8 for $0 \leq \theta \leq 0.2$. The following simplified estimation approximates the function $q(\theta)$ with a high precision for $0 \leq \theta \leq 0.2$ (cf. Fig. 4.8)

$$q(\theta) \approx \theta^3/12. \tag{4.84}$$

Acknowledgement This research was supported by the German National Science Foundation (DFG) within the collaborative research center SFB 692 "High-strength aluminium based light weight materials for reliable components".

Bibliography

[1] H. D. Alber, Materials With Memory. Initial-Boundary Value Problems for Constitutive Equations with Internal Variables (Springer, 1997).

[2] N. S. Bahvalov, N. P. Jidkov, G. M. Kobelkov. Numerical methods. [in Russian] (Lab of base knowledge, 2001).

[3] A. Bertram, Elasticity and Plasticity of Large Deformations (Springer, 2005).

[4] W. Dettmer, S. Reese, On the theoretical and numerical modelling of Armstrong—Frederick kinematic hardening in the finite strain regime, Computer Methods in Applied Mechanics and Engineering, 193 (2004) 87—116.

[5] E. Hairer, Geometric Integration of Ordinary Differential Equations on Manifolds, BIT Numerical Mathematics, 41, 5 (2001) 996–1007.

[6] E. Hairer, C. Lubich, G. Wanner, Geometric Numerical Integration. Structure Preserving Algorithms for Ordinary Differential Equations (Springer, 2006).

[7] W. Han, B. D. Reddy, Plasticity. Mathematical Theory and Numerical Analysis. (Springer, 1999).

[8] S. Hartmann, G. Lührs, P. Haupt, An efficient stress algorithm with applications in viscoplasticity and plasticity, International Journal for Numerical Methods in Engineering, 40 (1997) 991–1013.

[9] S. Hartmann, P. Neff, Polyconvexity of generalized polynomial-type hyperelastic strain energy functions for near-incompressibility, International Journal of Solids and Structures, 40 (2003) 2767–2791.

[10] S. Hartmann, K. J. Quint, M. Arnold, On plastic incompressibility within time-adaptive finite elements combined with projection techniques, Computer Methods in Applied Mechanics and Engineering, 198 (2008) 178–173.

[11] P. Haupt, Continuum Mechanics and Theory of Materials, 2nd edition, Springer, 2002.

[12] D. Helm, Stress computation in finite thermoviscoplasticity. International Journal of Plasticity, 22 (2006) 1699–1721.

[13] I. R. Ionescu, M. Sofonea, Functional and Numerical Methods in Viscoplasticity, 1st edition, Oxford Mathematical Monographs (Oxford University Press, 1993.)

[14] M. Itskov, Tensor Algebra and Tensor Analysis for Engineers: With Applications to Continuum Mechanics (Springer, 2007).

[15] J. Kato, A. A. Martynyuk, A. A. Shestakov, Stability of Motion of Nonautonomous Systems (Method of Limiting Equations), Stability and Control: Theory Methods and Applications, Volume 3, (Gordon and Breach Publishers, 1996).

[16] E. Kröner, Allgemeine Kontinuumstheorie der Versetzungen und Eigenspannungen, Arch. Rational Mech. Anal., 4 (1959) 273-334.

[17] E. H. Lee, Elastic—plastic deformation at finite strains, J. Appl. Mech., 36 (1969) 1-6.

[18] A. Lion, Constitutive modelling in finite thermoviscoplasticity: a physical approach based on nonlinear rheological elements, International Journal of Plasticity, 16 (2000) 469–494.

[19] G. Lührs, S. Hartmann, P. Haupt, On the numerical treatment of finite deformations in elastoviscoplasticity, Computer Methods in Applied Mechanics and Engineering, 144 (1997) 1-–21.

[20] R. Michel, R. Kreißig, H. Ansorge, Thermomechanical finite element analysis (FEA) of spin extrusion, Forschung im Ingenieurwesen, 68 (2003) 19–24

[21] C. Miehe, E. Stein, A canonical model of multiplicative elasto-plasticity: formulation and aspects of the numerical implementation, European Journal of Mechanics A/Solids, 11 (1992) 25–43

[22] C. Miehe, Exponential map algorithm for stress updates in anisotropic multiplicative elastoplasticity for single crystals, International Journal for Numerical Methods in Engineering, 39 (1996) 3367–3390.

[23] P. Neff, Mathematische Analyse multiplikativer Viskoplastizität. Ph.D. Thesis TU Darmstadt. (Shaker Verlag, 2000).

[24] P. Perzyna. The constitutive equations for rate sensitive plastic materials, Quarterly of Applied Mathematics, 20 (1963) 321–331.

[25] P. Perzyna, Fundamental problems in visco-plasticity, G. Kuerti (Ed.), Advances in Applied Mechanics, vol. 9, Academic Press, New York, (1966) 243–377.

[26] S. Reese, D. Christ, Finite deformation pseudo-elasticity of shape memory alloys —- Constitutive modelling and finite element implementation, International Journal of Plasticity, 24 (2008) 455–482.

[27] A. V. Shutov, R. Kreißig, Finite strain viscoplasticity with nonlinear kinematic hardening: Phenomenological modeling and time integration, Computer Methods in Applied Mechanics and Engineering, **197**, 2015–2029 (2008).

[28] A. V. Shutov, R. Kreißig, Application of a coordinate-free tensor formalism to the numerical implementation of a material model, ZAMM, **88**, 11, 888-909 (2008).

[29] J. Simo, T. Hughes, Computational inelasticity, Springer, 1998.

[30] J. C. Simo, C. Miehe, Associative coupled thermoplasticity at finite strains: formulation, numerical analysis and implementation, Computer Methods in Applied Mechanics and Engineering, 98 (1992) 41—104.

[31] B. Svendsen, A logarithmic-–exponential backward-Euler-based split of the flow rule for anisotropic inelastic behaviour at small elastic strain, International Journal for Numerical Methods in Engineering, **70**, 496-504 (2007).

[32] C. Truesdell, W. Noll, The Non-Linear Field Theories of Mechanics, 2nd ed. (Springer, 1992).

[33] G. Vadillo, R. Zaera, J. Fernandez-Saez, Consistent integration of the constitutive equations of Gurson materials under adiabatic conditions, Computer Methods in Applied Mechanics and Engineering, **197**, 1280-1295 (2008).

[34] R. Z. Valiev, R. K. Islamgaliev, I. V. Alexandrov, Bulk nanostructured materials from severe plastic deformation, Progress in Materials Science, **45**, 103-189 (2000).

[35] G. Weber, L. Annand, Finite deformation constitutive equations and a time integration procedure for isotropic, hyperelastic-viscoelastic solids, Computer Methods in Applied Mechanics and Engineering, 79 (1990) 173-202.

KAPITEL 5

Regularized strategies for material parameter identification in the context of finite strain plasticity

A. V. Shutov,[1] R. Kreißig.
Chemnitz University of Technology, Str. d. Nationen 62, D-09111 Chemnitz, Germany

Abstract: *We analyze the problem of material parameter identification for a certain model of finite strain plasticity/viscoplasticity. The material model takes into account both nonlinear isotropic and kinematic hardening. The nonlinear kinematic hardening of Armstrong-Frederick type is modeled on the grounds of the double multiplicative split of the deformation gradient, which was proposed by Lion.*

From the mathematical viewpoint, the parameter identification problem is, in general, ill-conditioned, since the solution does not depend continuously on the input data. Numerical difficulties arise especially when the problem exhibits a strong correlation among the parameters. Thus, a challenge lies in developing regularized identification strategies which reduce the correlation between the parameters and the probability of getting trapped in a local minimum of the objective function. Moreover, a reliable parameter identification strategy should be robust with respect to small measurement errors.

We discuss a regularization technique which involves including additional equality constraints imposed on the material parameters. These constraints are based on mechanical considerations and may contain some additional information about the mechanical response of the material. The mechanical considerations allow us to reduce the number of independent parameters and in some cases to reduce the correlation among them. One general guideline for constructing such relations is discussed in the paper: First, some approximate analytical relations are derived in the simplified case of small strains. Next, basing on these simplified results, the relations are generalized to the finite strains.

The efficiency of the regularized approach for the estimation of hardening parameters using the experimental data for EN AW-7075 aluminium alloy processed by equal channel angular extrusion was demonstrated. Although the straight-forward approach results in a good correspondence between the experimental data and the model predictions, the problem of the material parameter identification is not a trivial one. In particular, the error functional exhibits numerous stationary points. It is shown that the use of the regularized strategies

---

[1] Corresponding author. alexey.v.shutov@gmail.com
web: http://sites.google.com/site/materialmodeling

This chapter is reproduced from the paper: A. V. Shutov, R. Kreißig. Regularized strategies for material parameter identification in the context of finite strain plasticity. Technische Mechanik. 2010. 30, 280-295.

allows to reduce the number of parameters being identified, and in some cases to avoid the problem of multiple stationary points.

1. Introduction

The most important requirements that are placed upon the phenomenological material models are as follows:

- accuracy of description of the real material response,
- stability and robustness of the corresponding numerical algorithms,
- possibility of reliable identification of material parameters.

These three requirements are not mutually exclusive but rather complimentary to each other. In this paper we analyze the material model of finite strain viscoplasticity [**15**]. This model takes both nonlinear isotropic and kinematic hardening into account in a thermodynamically consistent way. Moreover, as it was shown in [**13**], the case of isotropic softening can be covered as well. The accuracy and robustness of the local time integration algorithms were numerically tested in [**15**]. Some theoretical results concerning the accuracy, stability, and the error accumulation are presented in [**16**] for a simplified version of the material model.

In the current paper we deal with some aspects of the material parameter identification. The main difficulties associated to the parameter identification on the ground of minimization of a certain least-square functional are as follows:

- the majority of optimization procedures can not distinct between global and local minima,
- correlation among the parameters,
- several parameters must be identified simultaneously due to the coupling effects,[2]
- in general, there is no continuous dependence of the resulting solution on the input data (ill-posed problem).

The main aim of the current study is to reduce the number of material parameters being identified. As this takes place, the correlation among the remaining parameters must stay within the admissible range.[3]

Following the conventional approach, the parameter identification problem is reduced to the minimization of some least-squares functional (error functional)

$$\overrightarrow{p} = \arg\min_{\overrightarrow{p} \in P} \Phi(\overrightarrow{p}), \tag{5.1}$$

where $\overrightarrow{p} = (p_1, ..., p_n)$ stands for the vector of material parameters, the set $P \subseteq \mathbb{R}^n$ represents the set of admissible parameters. The error functional represents the discrepancy between the measurements data and corresponding model predictions [**10, 7**]

$$\Phi(\overrightarrow{p}) = \sum_i \Big(\text{Model prediction}_i(\overrightarrow{p}) - \text{Measured data}_i\Big)^2. \tag{5.2}$$

---

[2] In particular, since the isotropic and kinematic hardening effects are strongly coupled, the corresponding material parameters should be identified simultaneously.

[3] In this paper the correlation is estimated using the correlation matrix which contains the information about the first derivatives of the residuals with respect to the parameters [**1**].

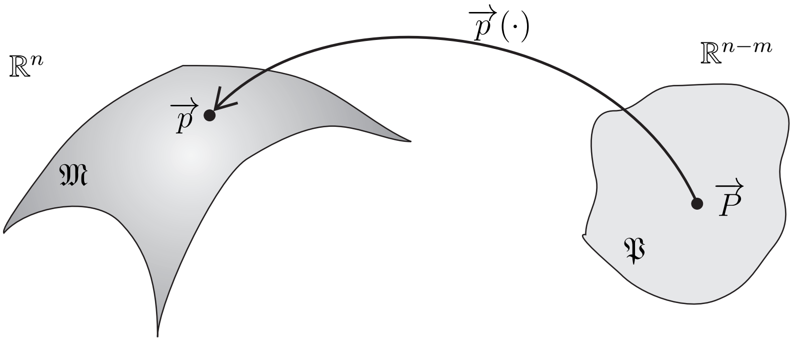

Figure 5.1. The mapping $\overrightarrow{p} : \overrightarrow{P} \in \mathfrak{P} \mapsto \overrightarrow{p}(\overrightarrow{P}) \in \mathfrak{M}$.

In order to reduce the number of material parameters, m additional equality constraints can be introduced $(m \leq n)$

$$\overrightarrow{g}(\overrightarrow{p}) = (g_1, ..., g_m)(\overrightarrow{p}) = 0. \tag{5.3}$$

We suppose that the set $\mathfrak{M} := \{\overrightarrow{p} \in P : \overrightarrow{g}(\overrightarrow{p}) = 0\}$ is a smooth $(n-m)$-dimensional manifold and there exists a smooth mapping $\overrightarrow{p} = \overrightarrow{p}(\overrightarrow{P})$, where $\overrightarrow{P} \in \mathbb{R}^{n-m}$ is a $(n-m)$-dimensional vector. More precisely, we suppose that the overall manifold $\mathfrak{M}$ can be covered by a single smooth homeomorphism[4]

$$\overrightarrow{p} : \overrightarrow{P} \in \mathfrak{P} \mapsto \overrightarrow{p}(\overrightarrow{P}) \in \mathfrak{M}, \tag{5.4}$$

where $\mathfrak{P}$ is an open subset of $\mathbb{R}^{n-m}$ (cf. figure 5.1).

Along with the standard minimization problem (5.1) we consider a restricted one

$$\overrightarrow{p} = \underset{\overrightarrow{p} \in P,\ s.t. \overrightarrow{g}(\overrightarrow{p})=0}{\arg\min} \Phi(\overrightarrow{p}) = \underset{\overrightarrow{p} \in \mathfrak{M},}{\arg\min} \Phi(\overrightarrow{p}). \tag{5.5}$$

Obviously, if we take the mapping $\overrightarrow{p} = \overrightarrow{p}(\overrightarrow{P})$ into account, the minimization problem (5.5) is equivalent to

$$\overrightarrow{P} = \underset{\overrightarrow{P} \in \mathfrak{P}}{\arg\min} \Phi(\overrightarrow{p}(\overrightarrow{P})). \tag{5.6}$$

Instead of identifying n parameters in (5.5), only $n-m$ parameters must be determined in (5.6). In that sense, the number of the parameters is reduced.

We note that constraints (5.3), independently of the error functional Φ, may contain a certain additional information concerning the mechanical response. For instance, that can be constraints on the saturation stresses, evolution of the size of the elastic domain, or the magnitude of the critical elongation (defined by the onset of the stress softening and localization of deformation). As it will be shown in the following, the introduction of additional constraints can essentially enhance the feasibility of the resulting set of material parameters. On the other hand, the constraints (5.3) must admit a smooth homeomorphism $\overrightarrow{p} = \overrightarrow{p}(\overrightarrow{P})$ in order to allow for the reduction of the material parameters number. Moreover, in order to solve practical problems, some robust and efficient procedures for computing $\overrightarrow{p}(\overrightarrow{P})$ are required.

---

[4] A smooth function f is called a smooth homeomorphism if its inverse f^{-1} exists and is smooth.

Apparently, any identification procedure with fixing some of the parameters can be considered as a trivial example of such approach.[5] Some experimentally motivated constraints were introduced in [**9**] in order to simplify the parameter identification for a material model of viscoelasticity. Particularly, 2N+1 constants describing a relaxation spectrum were calculated using three parameters only.

We note that the introduction of some additional equality constraints may have a regularizing effect even without computing the function $\overrightarrow{p}(\overrightarrow{P})$. Such constrained problem can be solved, for instance, using the method of Lagrange multipliers or its generalizations like the method of sequential quadratic programming [**17**]. However, in this paper we consider the equality constraints (5.3) in the context of simplifying the problem by reducing the number of parameters.

In order to avoid a possible ambiguity concerning the use of the terminology, we must remark that different approaches to the "regularization" of an inverse problem exist. In [**18**], for instance, a powerful regularization technique for ill-posed inverse problems was considered. This technique is based on the introduction of the so-called regularized operator such that the solution of the regularized problem becomes stable with respect to small changes of the input data (measurements).

In this work a relatively simple problem is analyzed. Here, only four hardening parameters are identified using experiments with homogeneous deformations. Nevertheless, the discussed methodology can be applied to the parameter identification basing on a series of experiments of different types, including experiments with inhomogeneous loadings [**10**].

2. Experimental data

Let us analyze the mechanical behavior of the EN AW-7075 aluminium alloy processed by equal channel angular pressing (ECAP) (a general overview concerning the ECAP is presented by Segal in [**12**]). The experimental setup and the measurements data for the material after four ECAP extrusions (route E) were reported previously in the paper [**13**]. In this section we briefly discuss the experimental results which are used for the phenomenological description of the material behavior. The reader, who is interested in details concerning the micromechanical characterization of the material is reffered to [**13**].

All experiments were conducted at room temperature. Firstly, a series of strain-controlled tension tests was performed with strain rate ranging from $10^{-4}s^{-1}$ to $10^{2}s^{-1}$. No clear rate-dependence of the material response could be identified in that range. Moreover, only quasi-static loadings are considered in the following.

We note that during ECAP a strong plastic anisotropy can be introduced. In order to analyze the initial anisotropy effects, a series of compression specimens was extracted from the ECAP-processed billet in three mutually orthogonal directions: the extrusion direction, the normal direction, and the transverse direction. No significant discrepancy was observed between the results of uniaxial compression tests for these three kinds of samples [**13**].

---

[5] For instance, the initial yield stress can be determined directly by evaluating the flow curve (graphical method).

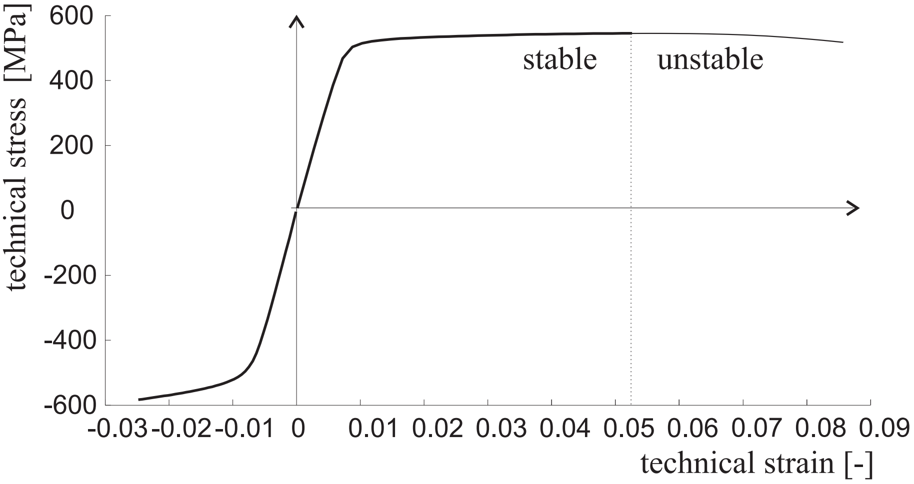

Figure 5.2. Experimental results: Monotonic tension and compression tests.

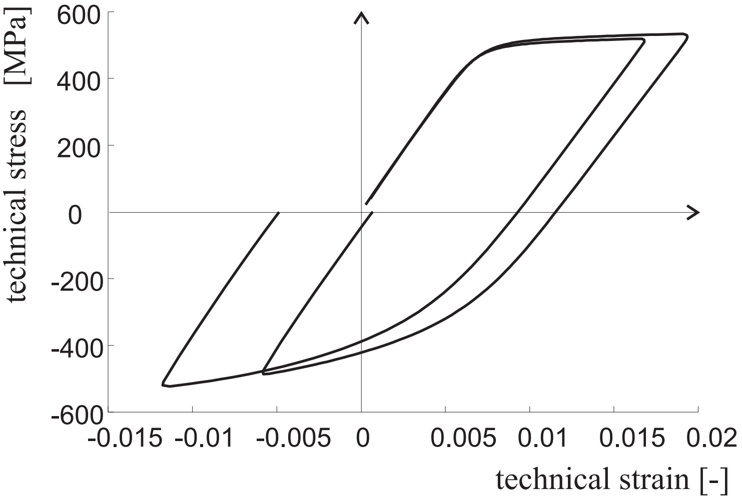

Figure 5.3. Experimental results: Tension-compression tests.

2.1. Monotonic tension and compression tests. In figure 5.2, the stress-strain curves corresponding to uniaxial monotonic tension and compression are presented (the specimens were extracted in the extrusion direction from the ECAP-processed billet).

We note that the flow stress under tension is approximately the same as under compression (cf. figure 5.2). In other words, no significant strength difference effect is observed. Next, the technical stress reaches a maximum at some critical strain level $\varepsilon_{cr} \approx 0.052$. Since the stress response beyond that level is unstable, the homogeneous deformation of the sample can not be guaranteed due to the eventual strain localization in a necked region. Therefore, we use the measurements data only up to that critical stain level.

Although the technical strains do not exceed 10 percent in this experiment, the difference between the stress response in tension and compression can be interpreted as a geometrically nonlinear effect.

2.2. Cyclic tension-compression tests. The quasistatic stress-strain response under uniaxial cyclic strain-controlled loading is presented in figure 5.3 for two different experiments. Note that during the tension phase the tensile yield strength increases, while the

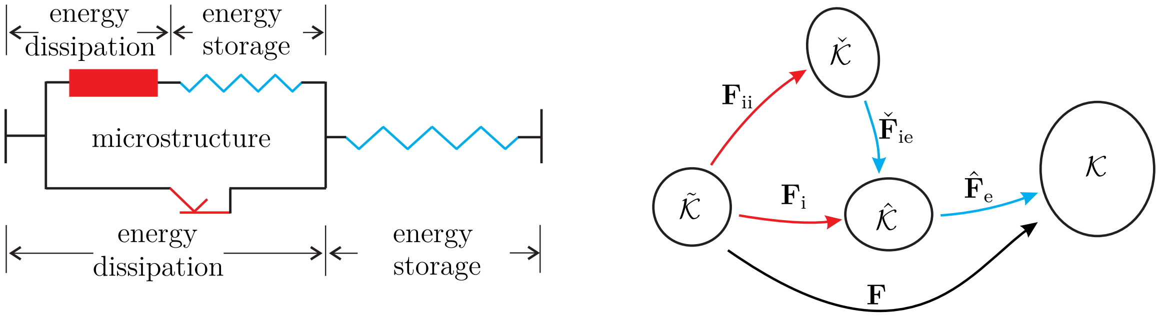

(a) (b)

Figure 5.4. Modeling of kinematic hardening: (a): Rheological model, (b) Commutative diagram showing corresponding configurations with transformations of material line elements.

yield strength of the material under compression grows smaller (Bauschinger effect). Moreover, the size of the elastic domain is substantially reduced (isotropic softening). Taking into account that the hardening behavior of the material is nonlinear, we conclude that the phenomenological description of the material response should be based on a material model of plasticity which takes a nonlinear kinematic hardening as well as a nonlinear isotropic softening into account.

3. Material model of finite strain viscoplasticity

3.1. Constitutive equations. In this subsection we discuss a material model of finite strain visoplasticity (see [**15**])[6]. The rheological motivation of the model is presented in figure 5.4a. This rheological interpretation motivates the double multiplicative decomposition (cf. the diagram in figure 5.4b)[7]

$$\mathbf{F} = \hat{\mathbf{F}}_{\mathrm{e}} \mathbf{F}_{\mathrm{i}}, \quad \mathbf{F}_{\mathrm{i}} = \check{\mathbf{F}}_{\mathrm{ie}} \mathbf{F}_{\mathrm{ii}}. \tag{5.7}$$

Firstly, the deformation gradient $\mathbf{F}$ is decomposed into the elastic and the inelastic parts. This decomposition is motivated by the idea of a local elastic unloading.[8] The second split was proposed by Lion (see [**8, 5**]) in order to represent the nonlinear kinematic hardening of Armstrong-Frederick type. The tensor $\check{\mathbf{F}}_{\mathrm{ie}}$ is related to local elastic deformations induced by strong inhomogeneities of dislocations. Along with the well-known right Cauchy-Green tensor $\mathbf{C} = \mathbf{F}^{\mathrm{T}}\mathbf{F}$, we introduce two tensor-valued internal variables

$$\mathbf{C}_{\mathrm{i}} = \mathbf{F}_{\mathrm{i}}^{\mathrm{T}} \mathbf{F}_{\mathrm{i}}, \quad \mathbf{C}_{\mathrm{ii}} = \mathbf{F}_{\mathrm{ii}}^{\mathrm{T}} \mathbf{F}_{\mathrm{ii}}. \tag{5.8}$$

These variables are interpreted respectively as inelastic right Cauchy-Green tensor and inelastic right Cauchy-Green tensor of microstructure. The material (or Lagrangian) description is used in this paper to formulate the material model.[9]

---

[6] A similar model of finite strain plasticity was proposed in [**19**].

[7] As it was formulated in [**11**]: The use of rheological models as a guideline in constructing constitutive equations allows for ensuring the thermodynamic consistency in a natural way.

[8] On the other hand, decomposition $(5.7)_1$ can be derived from the concept of material isomorphism (see [**2**]).

[9] In [**15**], the material model was originally formulated in intermediate configurations. Next, in order to simplify the numerical treatment of the evolution equations, the constitutive relations were transformed to the reference configuration.

For a given deformation history $\mathbf{C}(t)$, the material response in the time interval $t \in [0,T]$ is governed by the following system of ordinary differential and algebraic equations with respect to $\mathbf{C}_{\mathrm{i}}(t)$, $\mathbf{C}_{\mathrm{ii}}(t)$, $s(t)$, $s_d(t)$, $\lambda_{\mathrm{i}}(t)$

$$\dot{\mathbf{C}}_{\mathrm{i}} = 2\frac{\lambda_{\mathrm{i}}}{\mathfrak{F}}\Big(\mathbf{C}\tilde{\mathbf{T}} - \mathbf{C}_{\mathrm{i}}\tilde{\mathbf{X}}\Big)^{\mathrm{D}}\mathbf{C}_{\mathrm{i}}, \quad \mathbf{C}_{\mathrm{i}}|_{t=0} = \mathbf{C}_{\mathrm{i}}^{0},\ \det\mathbf{C}_{\mathrm{i}}^{0} = 1,\ \mathbf{C}_{\mathrm{i}}^{0} \in Sym, \tag{5.9}$$

$$\dot{\mathbf{C}}_{\mathrm{ii}} = 2\lambda_{\mathrm{i}}\varkappa\Big(\mathbf{C}_{\mathrm{i}}\tilde{\mathbf{X}}\Big)^{\mathrm{D}}\mathbf{C}_{\mathrm{ii}}, \quad \mathbf{C}_{\mathrm{ii}}|_{t=0} = \mathbf{C}_{\mathrm{ii}}^{0},\ \det\mathbf{C}_{\mathrm{ii}}^{0} = 1,\ \mathbf{C}_{\mathrm{ii}}^{0} \in Sym, \tag{5.10}$$

$$\dot{s} = \sqrt{\frac{2}{3}}\lambda_{\mathrm{i}}, \quad \dot{s}_{\mathrm{d}} = \frac{\beta}{\gamma}\dot{s}R, \quad s|_{t=0} = s^{0},\ s_{\mathrm{d}}|_{t=0} = s_{\mathrm{d}}^{0}, \tag{5.11}$$

$$\tilde{\mathbf{T}} = 2\rho_{\mathrm{R}}\frac{\partial\psi_{\mathrm{el}}(\mathbf{C}{\mathbf{C}_{\mathrm{i}}}^{-1})}{\partial\mathbf{C}}\Big|_{\mathbf{C}_{\mathrm{i}}=\mathrm{const}}, \quad \tilde{\mathbf{X}} = 2\rho_{\mathrm{R}}\frac{\partial\psi_{\mathrm{kin}}(\mathbf{C}_{\mathrm{i}}{\mathbf{C}_{\mathrm{ii}}}^{-1})}{\partial\mathbf{C}_{\mathrm{i}}}\Big|_{\mathbf{C}_{\mathrm{ii}}=\mathrm{const}}, \tag{5.12}$$

$$R = \gamma s_{\mathrm{e}}, \quad s_{\mathrm{e}} = s - s_{\mathrm{d}}, \tag{5.13}$$

$$\lambda_{\mathrm{i}} = \frac{1}{\eta}\Big\langle\frac{1}{k_0}f\Big\rangle^{m}, \quad f = \mathfrak{F} - \sqrt{\frac{2}{3}}\Big[K + R\Big], \quad \mathfrak{F} = \sqrt{\mathrm{tr}\Big[\Big(\mathbf{C}\tilde{\mathbf{T}} - \mathbf{C}_{\mathrm{i}}\tilde{\mathbf{X}}\Big)^{\mathrm{D}}\Big]^{2}}. \tag{5.14}$$

Here, $(\cdot)^{\mathrm{D}}$ stands for a deviatoric part of a second-rank tensor. The material parameters $\rho_{\mathrm{R}} > 0, \varkappa \geq 0, \beta \geq 0, \gamma \in \mathbb{R}, \eta \geq 0, m \geq 1, K > 0$, and the isotropic real-valued functions ψ_{el}, ψ_{kin} are assumed to be known. The constant $k_0 = 1$ MPa is used to obtain a dimensionless term in the bracket (not a material parameter).

The functions $s(t)$, $s_d(t)$, $\lambda_{\mathrm{i}}(t)$ are interpreted respectively as inelastic arc length, dissipative part of inelastic arc length, and inelastic multiplier. The quantities $\mathbf{C}$, $\mathbf{C}_{\mathrm{i}}$, $\mathbf{C}_{\mathrm{ii}}$, s, and s_d uniquely define the 2nd Piola-Kirchhoff tensor $\tilde{\mathbf{T}}(t)$, the backstress tensor $\tilde{\mathbf{X}}(t)$, the isotropic hardening $R(t)$, the overstress $f(t)$, and the norm of the driving force $\mathfrak{F}(t)$.

The above definitions imply that $\mathbf{C}$ and $\mathbf{C}_{\mathrm{i}}$ are symmetric. Since functions ψ_{el} and ψ_{kin} are isotropic, *it makes no difference* whether the derivatives in (10.6) are interpreted as general derivatives or as derivatives with respect to a symmetric tensor (see, for instance, the discussion in [**14**]).

In the following we will use a concrete ansatz for ψ_{el}, ψ_{kin} [**5**]

$$\rho_{\mathrm{R}}\psi_{\mathrm{el}}(\mathbf{C}\mathbf{C}_{\mathrm{i}}^{-1}) = \frac{k}{2}\Big(\ln\sqrt{\det\mathbf{C}\mathbf{C}_{\mathrm{i}}^{-1}}\Big)^{2} + \frac{\mu}{2}\Big(\mathrm{tr}\overline{\mathbf{C}\mathbf{C}_{\mathrm{i}}^{-1}} - 3\Big), \quad \rho_{\mathrm{R}}\psi_{\mathrm{kin}}(\mathbf{C}_{\mathrm{i}}\mathbf{C}_{\mathrm{ii}}^{-1}) = \frac{c}{4}\Big(\mathrm{tr}\overline{\mathbf{C}_{\mathrm{i}}\mathbf{C}_{\mathrm{ii}}^{-1}} - 3\Big), \tag{5.15}$$

where $k > 0$, $\mu > 0$, $c > 0$ are material constants. The overline $\overline{(\cdot)}$ denotes the unimodular part of a tensor

$$\overline{\mathbf{A}} = (\det\mathbf{A})^{-1/3}\mathbf{A}\ . \tag{5.16}$$

Taking the inelastic incompressibility into account ($\det(\mathbf{C}_{\mathrm{i}}) = \det(\mathbf{C}_{\mathrm{ii}}) = 1$), we obtain for stresses and backstresses

$$\tilde{\mathbf{T}} = k\ \ln\sqrt{\det(\mathbf{C})}\ \mathbf{C}^{-1} + \mu\ \mathbf{C}^{-1}(\overline{\mathbf{C}}\mathbf{C}_{\mathrm{i}}^{-1})^{\mathrm{D}}, \qquad \tilde{\mathbf{X}} = \frac{c}{2}\ \mathbf{C}_{\mathrm{i}}^{-1}(\mathbf{C}_{\mathrm{i}}\mathbf{C}_{\mathrm{ii}}^{-1})^{\mathrm{D}}. \tag{5.17}$$

As it was proved in [**15**], the material model is thermodynamically consistent for $\gamma \geq 0$ (isotropic hardening). The case $\gamma < 0$ (isotropic softening) was covered in [**13**] as well. The reader, who is interested in details concerning the numerical implementation of the material model is reffered to [**14**]. The time discretization of the evolution equations is based on so-called geometrical integrators. It was tested numerically in [**15**] for strain-controlled processes that the use of the geometrical integrators allows to avoid the error accumulation. The mathematical explanation of this fact can be found in [**16**].

3.2. Case of small strains. In this subsection we consider a simplified version of the constitutive equations under the assumption of small strains (rotations and displacements may remain finite). The consideration of the simplified case will provide clear insights into the construction of the regularized strategies for parameter identification. Firstly, we suppose

$$\mathbf{C} \to \mathbf{1}, \quad \mathbf{C}_{\mathrm{i}} \to \mathbf{1}, \quad \mathbf{C}_{\mathrm{ii}} \to \mathbf{1}. \tag{5.18}$$

Moreover, we assume in this subsection that there exists a constant $K_0 > 0$ such that for any time instance t we have the following estimation of the flow stress

$$K + R(t) \geq K_0 > 0. \tag{5.19}$$

For $\mathbf{E} := 1/2(\mathbf{C} - \mathbf{1})$, $\mathbf{E}_{\mathrm{i}} := 1/2(\mathbf{C}_{\mathrm{i}} - \mathbf{1})$, $\mathbf{E}_{\mathrm{ii}} := 1/2(\mathbf{C}_{\mathrm{ii}} - \mathbf{1})$, and $\Delta := \max(\|\mathbf{C} - \mathbf{1}\|, \|\mathbf{C}_{\mathrm{i}} - \mathbf{1}\|, \|\mathbf{C}_{\mathrm{ii}} - \mathbf{1}\|)$ we obtain from (5.18)

$$\det(\mathbf{C}) = 1 + 2\mathrm{tr}(\mathbf{E}) + O(\Delta^2), \quad \ln(\sqrt{\det(\mathbf{C})}) = \mathrm{tr}(\mathbf{E}) + O(\Delta^2), \tag{5.20}$$

$$\overline{\mathbf{C}} = \mathbf{1} + 2\mathbf{E}^{\mathrm{D}} + O(\Delta^2), \quad \mathbf{C}^{-1} = \mathbf{1} - 2\mathbf{E} + O(\Delta^2). \tag{5.21}$$

Here, O stands for "lage-O" Landau symbol. Equation $(5.21)_2$ follows immediately from the well-known Neumann series expansion. Moreover, we have

$$\mathbf{C}_{\mathrm{i}}^{-1} = \mathbf{1} - 2\mathbf{E}_{\mathrm{i}} + O(\Delta^2), \quad \mathbf{C}_{\mathrm{ii}}^{-1} = \mathbf{1} - 2\mathbf{E}_{\mathrm{ii}} + O(\Delta^2), \tag{5.22}$$

$$(\overline{\mathbf{C}}\mathbf{C}_{\mathrm{i}}^{-1})^{\mathrm{D}} = 2(\mathbf{E} - \mathbf{E}_{\mathrm{i}})^{\mathrm{D}} + O(\Delta^2), \quad (\mathbf{C}_{\mathrm{i}}\mathbf{C}_{\mathrm{ii}}^{-1})^{\mathrm{D}} = 2(\mathbf{E}_{\mathrm{i}} - \mathbf{E}_{\mathrm{ii}})^{\mathrm{D}} + O(\Delta^2), \tag{5.23}$$

$$\tilde{\mathbf{T}} = k\mathrm{tr}(\mathbf{E})\mathbf{1} + 2\mu(\mathbf{E} - \mathbf{E}_{\mathrm{i}})^{\mathrm{D}} + O(\Delta^2), \quad \tilde{\mathbf{X}} = c(\mathbf{E}_{\mathrm{i}} - \mathbf{E}_{\mathrm{ii}})^{\mathrm{D}} + O(\Delta^2). \tag{5.24}$$

Combining these results with the definition of the driving force $\mathfrak{F}$ (cf. equation $(5.14)_3$), we arrive at

$$\mathfrak{F} = \sqrt{\|(\tilde{\mathbf{T}} - \tilde{\mathbf{X}})^{\mathrm{D}}\|^2 + O(\Delta^3)}. \tag{5.25}$$

Next, it follows from (5.14) and (5.19) that $\lambda_{\mathrm{i}} = 0$ for $\mathfrak{F} < \sqrt{\frac{2}{3}}K_0$. On the other hand, it follows from (5.25) that $\mathfrak{F} \approx \|(\tilde{\mathbf{T}} - \tilde{\mathbf{X}})^{\mathrm{D}}\|$ for $\mathfrak{F} \geq \sqrt{2/3}K_0$, where "$\approx$" stands for asymptotic equivalence as $\Delta \to 0$. Thus, we have

$$\frac{\lambda_{\mathrm{i}}}{\mathfrak{F}} \approx \frac{1}{\eta}\left\langle \frac{\|(\tilde{\mathbf{T}} - \tilde{\mathbf{X}})^{\mathrm{D}}\| - \sqrt{2/3}\big[K + R\big]}{k_0} \right\rangle^m \frac{1}{\|(\tilde{\mathbf{T}} - \tilde{\mathbf{X}})^{\mathrm{D}}\|}. \tag{5.26}$$

Furthermore, we rewrite the evolution equations (5.9), (5.10) and put corresponding initial conditions

$$\dot{\mathbf{E}}_{\mathrm{i}} = \frac{\lambda_{\mathrm{i}}}{\mathfrak{F}}\Big(\big(\tilde{\mathbf{T}} - \tilde{\mathbf{X}}\big)^{\mathrm{D}} + O(\Delta^2)\Big), \quad \mathbf{E}_{\mathrm{i}}|_{t=0} = \mathbf{E}_{\mathrm{i}}^0, \ \mathrm{tr}(\mathbf{E}_{\mathrm{i}}^0) = O(\Delta^2), \ \mathbf{E}_{\mathrm{i}}^0 \in Sym, \tag{5.27}$$

$$\dot{\mathbf{E}}_{\mathrm{ii}} = \lambda_{\mathrm{i}}\varkappa\Big(\tilde{\mathbf{X}}^{\mathrm{D}} + O(\Delta^2)\Big), \quad \mathbf{E}_{\mathrm{ii}}|_{t=0} = \mathbf{E}_{\mathrm{ii}}^0, \ \mathrm{tr}(\mathbf{E}_{\mathrm{ii}}^0) = O(\Delta^2), \ \mathbf{E}_{\mathrm{ii}}^0 \in Sym. \tag{5.28}$$

To be definite, we put in the following $\mathbf{E}_{\mathrm{i}}^0 = \mathbf{E}_{\mathrm{ii}}^0 = \mathbf{0}$. Finally, the small-strain counterpart of the material model is obtained by neglecting the terms which are $O(\Delta^2)$ in (5.24), (5.27), and (5.28), and by using the approximation (5.26) for $\lambda_{\mathrm{i}}/\mathfrak{F}$. Note that this simplified model corresponds to the well-known classical material model of small strain viscoplasticity (cf.

[**3, 4**]), where the linearized strain tensor $\boldsymbol{\varepsilon}$ and the Cauchy stress tensor $\boldsymbol{\sigma}$ are formally replaced by the Green strain tensor $\mathbf{E}$ and the 2nd Piola-Kirchhoff tensor $\tilde{\mathbf{T}}$, respectively. [10]

3.3. Some analytical solutions. In this subsection we analyze some properties of the material model. As it will be clear from the discussion in following sections, the knowledge of this properties enables the development of regularized strategies of parameter identification.

Firstly, assuming the zero initial conditions for the isotropic hardening R, the accumulated inelastic arclength s and the dissipative part s_d ($s|_{t=0} = 0$, $s_d|_{t=0} = 0$) and integrating the evolution equation $(5.11)_2$ for s_d, the well-known Voce hardening rule is restored

$$R = R(s) = \frac{\gamma}{\beta}(1 - \mathrm{e}^{-\beta s}). \tag{5.29}$$

Note that this result is valid both for finite and for small strains.

Next, let us consider a Cartesian coordinate system $\{\mathbf{e}_1, \mathbf{e}_2, \mathbf{e}_3\}$ and assume a monotonic strain-controlled uniaxial loading along $\mathbf{e}_1$. Thus, in terms of the linearized strain tensor $\boldsymbol{\varepsilon}$ and the Cauchy stress tensor $\boldsymbol{\sigma}$ we have

$$\boldsymbol{\varepsilon} = \varepsilon \mathbf{e}_1 \otimes \mathbf{e}_1 - \hat{\varepsilon}(\mathbf{e}_2 \otimes \mathbf{e}_2 + \mathbf{e}_3 \otimes \mathbf{e}_3), \quad \boldsymbol{\sigma} = \sigma \mathbf{e}_1 \otimes \mathbf{e}_1, \tag{5.30}$$

where $\varepsilon = \varepsilon(t)$ is a given monotonic function; $\hat{\varepsilon}$ and σ are unknown. In this subsection we use notation $\mathbf{X}$ for the backstress tensor of the geometrically linear theory (Subsection 3.2). Substituting this relations into the evolution equations from Subsection 3.2, we obtain for the backstress $\mathbf{X}$

$$\mathbf{X} = x(s)\Big(\mathbf{e}_1 \otimes \mathbf{e}_1 - 1/2\ \mathbf{e}_2 \otimes \mathbf{e}_2 - 1/2\ \mathbf{e}_3 \otimes \mathbf{e}_3\Big), \quad x(s) = \sqrt{\frac{2}{3}}\frac{1}{\varkappa}(1 - \mathrm{e}^{-\sqrt{3/2}c\varkappa s}). \tag{5.31}$$

Moreover, for quasistatic processes we put (by ommiting the elastic deformation phase)

$$\|(\boldsymbol{\sigma} - \mathbf{X})^{\mathrm{D}}\| = \sqrt{2/3}\big[K + R\big]. \tag{5.32}$$

Combining this with (5.29), $(5.30)_2$, and (5.31) we obtain the axial component σ of the stress tensor under small strain condition:

$$\sigma(s) = K + \frac{\gamma}{\beta}(1 - \mathrm{e}^{-\beta s}) + \sqrt{\frac{3}{2}}\frac{1}{\varkappa}(1 - \mathrm{e}^{-\sqrt{3/2}c\varkappa s}). \tag{5.33}$$

4. Constraints on the material parameters

Suppose that parameters k, μ, K, η, and m are now known (cf. Section 5). We discuss some constraints which can be imposed on the hardening parameters α, β, $\varkappa$, c in order to simplify the parameter identification.[11]

First, we consider the case of small strains. If the saturation stress σ^{sat} under monotonic uniaxial tension is known, it may be reasonable to consider the constraint as follows

$$\tilde{g}_1(\gamma, \beta, \varkappa, c) = 0, \quad \tilde{g}_1(\gamma, \beta, \varkappa, c) := \lim_{s \to \infty} \sigma(s) - \sigma^{sat}, \tag{5.34}$$

---

[10] In general, such formal substitution can be justified as follows [**6**]: Any system of constitutive equations, which is valid under the geometrically linear conditions, can be generalized to small strains (finite rotations and displacements are allowed) by formally replacing ($\boldsymbol{\varepsilon}$, $\boldsymbol{\sigma}$, $\dot{\boldsymbol{\varepsilon}}$, $\dot{\boldsymbol{\sigma}}$) by ($\mathbf{E}$, $\tilde{\mathbf{T}}$, $\dot{\mathbf{E}}$, $\dot{\tilde{\mathbf{T}}}$).

[11] Obviously, along with the simplifying effect, the consideration of constraints allows for taking additional information on the material behavior into account.

where $\sigma(s)$ is the axial component of the Cauchy stress tensor given by the geometrically linear counterpart of the material model (we drop the dependence of $\sigma(s)$ on parameters to simplify the notation). Substituting the explicit expression (5.33) into (5.34), we arrive at

$$K + \frac{\gamma}{\beta} + \sqrt{\frac{3}{2}}\frac{1}{\varkappa} - \sigma^{sat} = 0. \tag{5.35}$$

This relation is equivalent to

$$\varkappa = \sqrt{\frac{3}{2}}\frac{1}{\sigma^{sat} - K - \gamma/\beta}. \tag{5.36}$$

Thus, the hardening parameter $\varkappa$ is represented as a function of the remaining hardening parameters γ, β, c. In general, in the case of finite strains, this relation is not applicable, since it is based on the assumption of small strains. But it can be seen as a simplified approximation for $\varkappa$ as long as the geometrically linear approach yields proper results [**13**].

Now let us discuss a generalization of this approach to the finite strain range. Suppose that a technical stress σ^{tech}_{*} is known at some point $\varepsilon = \varepsilon_*$, where ε stands for the technical strain.[12] Consider the constraint as follows

$$g_1(\gamma, \beta, \varkappa, c) = 0, \quad g_1(\gamma, \beta, \varkappa, c) := \sigma^{\text{tech}}|_{\varepsilon=\varepsilon_*} - \sigma^{\text{tech}}_{*}, \tag{5.37}$$

where $\sigma^{\text{tech}}|_{\varepsilon=\varepsilon_*}$ stands for the model prediction of the technical stress. The solution of equation $(5.37)_1$ with respect to $\varkappa$ is denoted by

$$\varkappa = \varkappa_1(\gamma, \beta, c). \tag{5.38}$$

The dependence of $\varkappa_1(\gamma, \beta, c)$ on σ^{tech}_{*} is omitted in order to simplify the notation. In this work the function $\varkappa_1(\gamma, \beta, c)$ is evaluated numerically using the Newton method.[13]

The next type of equality constraints is based on the knowledge of the critical strain ε_{cr} at which the maximal stress is reached (Cauchy stress and technical stress in geometrically linear and nonlinear cases, respectively). Thus, for small strains, we have

$$\tilde{g}_2(\gamma, \beta, \varkappa, c) = 0, \quad \tilde{g}_2(\gamma, \beta, \varkappa, c) := \frac{d\sigma(\varepsilon)}{d\varepsilon}|_{\varepsilon=\varepsilon_{cr}}, \tag{5.39}$$

where $\sigma(\varepsilon)$ is a model prediction. Note that such condition under small strain range can be reasonable only if $\gamma < 0$ (isotropic softening). If $\gamma > 0$ (isotropic hardening) then no peak stresses are predicted, and (5.39) makes no sense. By neglecting elastic strains, a somewhat more simple relation can be obtained

$$\check{g}_2(\gamma, \beta, \varkappa, c) = 0, \quad \check{g}_2(\gamma, \beta, \varkappa, c) := \frac{d\sigma(s)}{ds}|_{s=\varepsilon_{cr}}. \tag{5.40}$$

Substituting the explicit expression (5.33) into (5.40), and putting $s = \varepsilon_{cr}$, we arrive at

$$\gamma \mathrm{e}^{-\beta\varepsilon_{cr}} + \frac{3}{2}c\mathrm{e}^{-\sqrt{3/2}c\varkappa\varepsilon_{cr}} = 0. \tag{5.41}$$

Thus,

$$\varkappa = \sqrt{\frac{2}{3}}\frac{1}{c\varepsilon_{cr}} \ln\Big(-\frac{3c}{2\gamma} e^{\beta\varepsilon_{cr}} \Big). \tag{5.42}$$

---

[12] In the following we put $\varepsilon_* := \varepsilon_{cr}$, where ε_{cr} stands for the critical deformation (cf. Section 2.1).

[13] For certain finite-strain models it might be possible to obtain an explicit analytical expression for $\varkappa$, similar to the expression (5.36). In this paper, however, we use a more universal numerical approach.

Next, we generalize this approach to finite strains. Towards that end we replace the axial component of the Cauchy stress by the technical stress,

$$g_2(\gamma,\beta,\varkappa,c)=0, \quad g_2(\gamma,\beta,\varkappa,c):=\frac{d\sigma^{\text{tech}}(\varepsilon)}{d\varepsilon}|_{\varepsilon=\varepsilon_{cr}}. \tag{5.43}$$

Denote the solution of this equation with respect to $\varkappa$ by $\varkappa_2$

$$\varkappa=\varkappa_2(\gamma,\beta,c). \tag{5.44}$$

The dependence of $\varkappa_2(\gamma,\beta,c)$ on ε_{cr} is omitted to simplify the notation. In the following, the function $\varkappa_2$ is evaluated numerically.

Finally, let us discuss the third type of constraints. Suppose that at some point which is characterized by accumulated plastic strain $s=s_*$, the size of the elastic domain is known (cf. experimental data in Subsection 2.2): $S_*:=\sigma_{\text{tension}}-\sigma_{\text{compression}}>0$. In the case of small strains we can consider

$$g_3(\gamma,\beta)=0, \quad g_3(\gamma,\beta):=(K+R(s_*))-1/2S_*. \tag{5.45}$$

Substituting (5.29) for $R(s)$ we obtain

$$\gamma=\gamma_1(\beta), \quad \gamma_1(\beta):=\frac{\beta}{1-e^{-\beta s_*}}(1/2S_*-K). \tag{5.46}$$

Note that $\gamma<0$ for $S_*<2K$ (isotropic softening). This approach can be easily generalized to cover finite strains as well. However, in this paper we apply such relation for deformed states under relatively small strains only (cf. Section 5). Thus, the estimation (5.46) is supposed to yield good results in that case.

5. Parameter identification

The elasticity parameters can be identified using the measurements data in elastic range: $\mu=26300$ MPa, $k=68600$ MPa. The parameters of the Perzyna-law, for instance, can be obtained basing on the measurements of the overstress f for a series of loading rates. In this paper we neglect the viscous effects by putting $\eta=0$ s, $m=1$. Furthermore, the initial flow stress is identified by the qualitative analysis of the flow curve (graphical method): $K=485$ MPa. In the following we discuss some identification procedures for determining the hardening parameters.

5.1. Straight-forward approach. Four uniaxial experiments are considered in this section: one monotonic tension (cf. Section 2.1) for $\varepsilon\leq\varepsilon_{cr}=0.052$ ($n_1=35$ data points), one monotonic compression (cf. Section 2.1, $n_2=43$ data points), and two tension-compression experiments (cf. Section 2.2, $n_3=137, n_4=152$ data points). Let us denote the experimentally measured technical stresses by $\hat{\sigma}^{\text{tech}}_{k,i}$, where $k\in\{1,2,3,4\}$ stands for the number of the experiment and $i\in\{1,2,...,n_k\}$ for the corresponding measurement point.

Basing on these data, we consider an error functional as follows

$$\Phi(\gamma,\beta,\varkappa,c):=\sum_{k=1}^{4}\sum_{i=1}^{n_k}(\hat{\sigma}^{\text{tech}}_{k,i}-\sigma^{\text{tech}}_{k,i}(\gamma,\beta,\varkappa,c))^2, \tag{5.47}$$

where $\sigma^{\text{tech}}_{k,i}(\gamma,\beta,\varkappa,c)$ stands for the corresponding simulation results.

The error functional Φ is minimized using the Levenberg-Marquardt method (Newton method with damping). Two stationary points $\overrightarrow{p}_1$ and $\overrightarrow{p}_2$ were identified numerically.

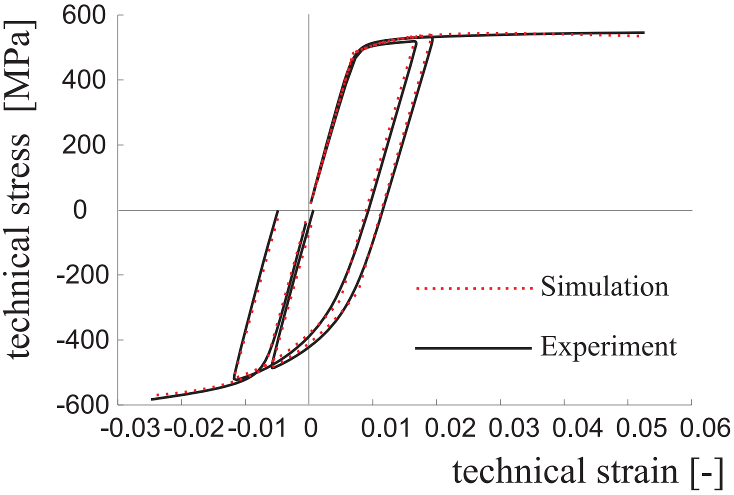

Figure 5.5. Simulation results for $\overrightarrow{p}_2$ (straight-forward approach).

The corresponding parameter sets are summarized in Table 5.6. Note that $\overrightarrow{p}_1$ and $\overrightarrow{p}_2$ are adjacent to each other. This illustrates the fact that even having a "very good" initial guess for the solution, the convergence to the global minimum can not be guaranteed.

Since $\Phi(\overrightarrow{p}_2)$ is smaller than $\Phi(\overrightarrow{p}_1)$ (see Table 5.6), we consider the set $\overrightarrow{p}_2$ to be the solution of the problem within the straight-forward approach. The corresponding simulation results are plotted in figure 5.5. The correlation matrix for $\overrightarrow{p}_2$ is presented in Table 5.1.

Table 5.1. Correlation matrix: straight-forward approach

	β	c	γ	$\varkappa$
β	1.0	0.58	-0.90	-0.16
c	0.58	1.0	-0.82	-0.27
γ	-0.90	-0.82	1.0	0.37
$\varkappa$	-0.16	-0.27	0.37	1.0

We see that the parameters β, γ and c are correlated. Nevertheless, the correlation remains in the admissible range. Thus, the parameter identification is possible. On the other hand, since the target function Φ possesses numerous stationary points (at least two), a series of optimization computations is required to find the global minimum of Φ. This circumstance makes the reliable parameter identification especially time consuming, if numerous parameters are to be identified simultaneously.

One important feature of the parameter sets $\overrightarrow{p}_1$ and $\overrightarrow{p}_2$, which has to be taken into account, is that smaller stresses are predicted by the model under tension and compression near the termination points. The second feature is that the technical stresses reach their maximum under tension at much smaller strains than in the experiment. In particular, this implies that the onset of unstable deformation (strain localization) occurs at smaller strains.[14]

---

[14] One possible way of dealing with this problems is to introduce additional terms like $\alpha_1(g_1)^2$ or $\alpha_2(g_2)^2$ into the formulation of the error functional (5.47), where coefficients α_i should be large enough in order

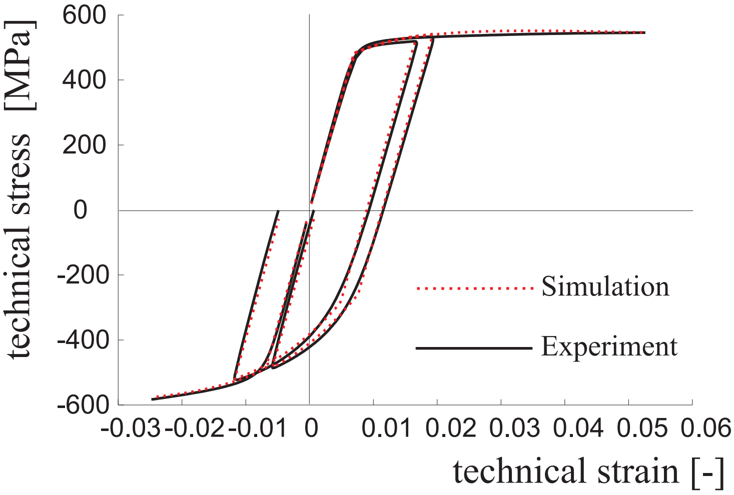

Figure 5.6. Simulation results for $\overrightarrow{p}_3$ (optimization under use of g_1).

5.2. Regularized strategies basing on g_1 and g_3. Now let us consider a constrained optimization problem basing on the equality constraint (5.37). We put in (5.37) $\varepsilon_* := \varepsilon_{cr} = 0.052$. Thus, we minimize $\Phi_{g_1}(\gamma, \beta, c) := \Phi(\gamma, \beta, \varkappa_1(\gamma, \beta, c), c)$. The functional was minimized with respect to γ, β, and c using a series of different initial approximations. The same parameter set $\overrightarrow{p}_3$ is obtained in all cases (no numerous stationary points identified). The correlation matrix is presented in Table 5.2. Note that the correlation between the parameters remains in the admissible range.

Table 5.2. Correlation matrix: use of g_1

	β	c	γ
β	1.0	0.80	-0.94
c	0.80	1.0	-0.92
γ	-0.94	-0.92	1.0

Although the identified minimum of the error functional $\Phi(\overrightarrow{p}_3)$ is somewhat larger than $\Phi(\overrightarrow{p}_2)$ (see Table 5.6), the stress response is better predicted near the termination points for tension and compression loadings (see figure 5.6).

The next strategy is based on the combination of equality constraints (5.37) and (5.45). Thus, we minimize now $\Phi_{g_1,g_3}(\beta, c) := \Phi_{g_1}(\gamma_1(\beta), \beta, c) = \Phi(\gamma_1(\beta), \beta, \varkappa_1(\gamma_1(\beta), \beta, c), c)$ with respect to β and c. In order to make use of (5.45), we put in this paper $S_* := 775$ MPa, $s_* := 0.019$. Similarly to the minimization of $\Phi_{g_1}(\gamma, \beta, c)$, only one stationary point $\overrightarrow{p}_4$ is identified. The correlation matrix is presented in Table 5.3. The simulation results basing on the set $\overrightarrow{p}_4$ are close to that of $\overrightarrow{p}_3$ (see figure 5.7).

Similar to the previous subsection, the common feature of parameter sets $\overrightarrow{p}_3$ and $\overrightarrow{p}_4$ is that the predicted critical strain is essentially smaller than the experimentally measured one.

---

to influence the optimization positively. On the other hand, the problem becomes ill-conditioned for large values of α_i. Thus, the optimal choice of the coefficients α_i is not a trivial task.

Table 5.3. Correlation matrix: use of g_1 and g_3

	β	c
β	1.0	0.78
c	0.78	1.0

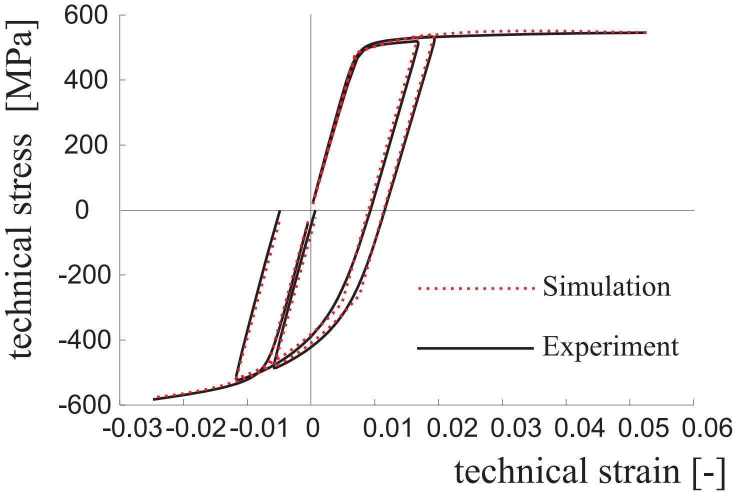

Figure 5.7. Simulation results for $\overrightarrow{p}_4$ (optimization under use of g_1 and g_3).

5.3. Regularized strategies basing on g_2 and g_3. On the grounds of the constraint (5.43) we consider now $\Phi_{g_2}(\gamma, \beta, c) := \Phi(\gamma, \beta, \varkappa_2(\gamma, \beta, c), c)$. The minimization of Φ_{g_2} yields the parameter vector $\overrightarrow{p}_5$. Note that $\Phi(\overrightarrow{p}_5)$ is larger than $\Phi(\overrightarrow{p}_2)$, $\Phi(\overrightarrow{p}_3)$, or $\Phi(\overrightarrow{p}_4)$. The corresponding simulation result is presented in figure 5.8. Apparently, the constraint (5.43) is *much more restrictive* than the constraints (5.37) and (5.45). The use of the constraint (5.43) can be justified if the correct prediction of the critical strain *has a primary importance.*[15] Note that the correlation between the parameters remains in the admissible range (Table 5.4).

Table 5.4. Correlation matrix: use of g_2

	β	c	γ
β	1.0	0.77	-0.94
c	0.77	1.0	-0.90
γ	-0.94	-0.90	1.0

Finally, if we impose the constraints (5.43) and (5.45) on the hardening parameters, we need to minimize $\Phi_{g_2,g_3}(\beta, c) := \Phi_{g_2}(\gamma_1(\beta), \beta, c) = \Phi(\gamma_1(\beta), \beta, \varkappa_2(\gamma_1(\beta), \beta, c), c)$. We denote the resulting parameter set by $\overrightarrow{p}_6$. As it follows from Table 5.5, the correlation between β and c remains within the admissible range. The corresponding simulation result is depicted

---

[15] Obviously, we are dealing with two conflicting requirements in this case : 1st: minimize $\Phi(\overrightarrow{p})$, 2nd: minimize $(g_2(\overrightarrow{p}))^2$. In general, such problems should be solved in the context of multi-criteria optimization. However, in this paper the constraints are used at the first place in order to simplify the problem. Therefore, the multi-criteria optimization is not addressed in this study.

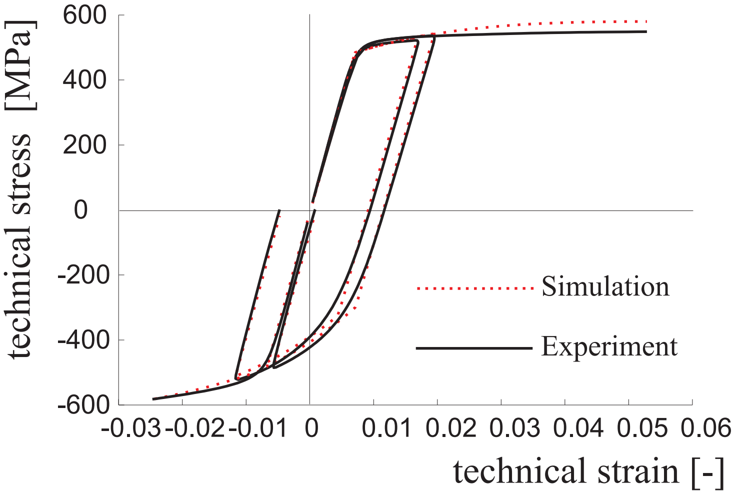

Figure 5.8. Simulation results for $\overrightarrow{p}_5$ (optimization under use of g_2).

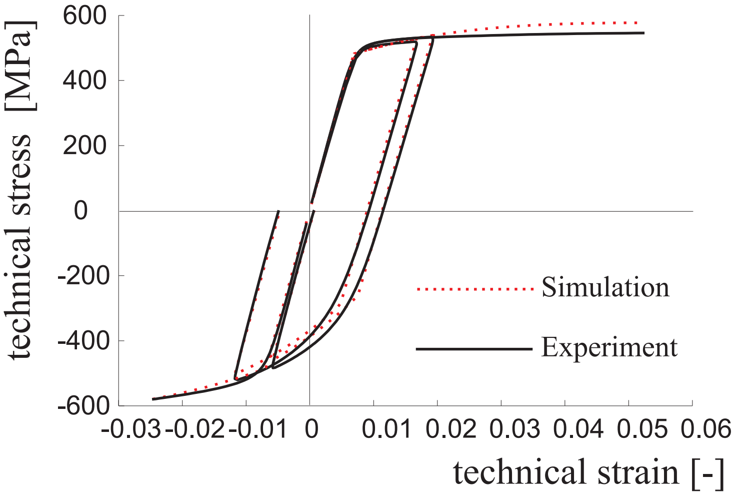

Figure 5.9. Simulation results for $\overrightarrow{p}_6$ (optimization under use of g_2 and g_3).

in figure 5.9. Note that the use of Φ_{g_2,g_3} yields similar results as the ones obtained by the minimization of Φ_{g_2}.

Table 5.5. Correlation matrix: use of g_2 and g_3

	β	c
β	1.0	0.88
c	0.88	1.0

Finally, the results of the parameter identification for different identification strategies are summarized in Table 5.6.

6. Conclusion and discussion

One approach to the parameter identification was numerically tested in this paper. The approach is based on the introduction of additional equality constraints during the formulation of minimization problem. The basic principles for choosing these constraints are as follows:

Table 5.6. Results of parameter identification

	constraints	γ [MPa]	β [-]	$\varkappa$[MPa^{-1}]	c [MPa]	$\Phi(\overrightarrow{p}_{\mathrm{i}})$[MPa^2]
$\overrightarrow{p}_1$		-12805	112.2	0.006377	16370	66421
$\overrightarrow{p}_2$		-14126	121.2	0.006317	17290	66012
$\overrightarrow{p}_3$	$g_1 = 0$	-12977	121.6	0.006226	15560	68527
$\overrightarrow{p}_4$	$g_1 = g_3 = 0$	-13111	122.4	0.006214	15660	68542
$\overrightarrow{p}_5$	$g_2 = 0$	-8921	103.7	0.005658	10890	98859
$\overrightarrow{p}_6$	$g_2 = g_3 = 0$	-12034	108.7	0.005080	12660	118280

- The constraints should admit a plausible mechanical interpretation.
- The mechanical quantities[16] used to formulate these constraints should be stable with respect to the measurement errors.
- The constraints should depend continuously on the input data.
- The constraints should admit the construction of a smooth homeomorphism $\overrightarrow{p} = \overrightarrow{p}(\overrightarrow{P})$ (cf. (5.4)).

In this paper we do not analyze mathematically the existence and smoothness of functions $\varkappa_1(\gamma, \beta, c)$ (cf. (5.37)) and $\varkappa_2(\gamma, \beta, c)$ (cf. (5.43)). Instead, we present, basing on a geometrically linear simplification of the model, some explicit analytical solutions (cf. equations (5.36) and (5.42)). These analytical solutions can be seen as an approximation for the case of moderate stains. Moreover, the numerical tests indicate that the Newton method allows to solve nonlinear equations (5.37) and (5.43) numerically, using results (5.36) and (5.42) as initial approximations. In particular, *no computational difficulties* were encountered in evaluating the functions $\varkappa_1$ and $\varkappa_2$. We note that the consideration of the geometrically linear simplification may serve as a guideline in formulating the constraints (and corresponding initial approximations) in the general case of finite strains. Obviously, the construction of reasonable constraints should be based both on the reliable *information* about the real mechanical behavior and the *understanding* of the material model.

As it was shown in the paper, the straight forward approach has three disadvantages: the presence of multiple stationary points, the incorrect prediction of the critical strain ε_{cr}, and underestimated stresses near the termination points under tension and compression (see figure 5.5). The introduction of additional constrains allows us to reduce the number of material parameters and to achieve a better prediction of the stress response near the termination points. The introduction of additional constraints does not lead to a bad correlation between the material parameters. Since the number of parameter is reduced, the eventual problem of multiple local minima can be dealt in a much simpler way. Moreover, for the example considered in this study, no numerous stationary points were observed for constrained minimization problems.

The requirement of correct prediction of the critical strain ε_{cr} appears to be restrictive for this current example such that $\Phi(\vec{p}_6)$ is almost two times larger than $\Phi(\vec{p}_2)$. On the other hand, the solution $\vec{p}_6$ is optimal in its class.

---

[16] Like the peak stress σ_* or the critical strain ε_{cr}.

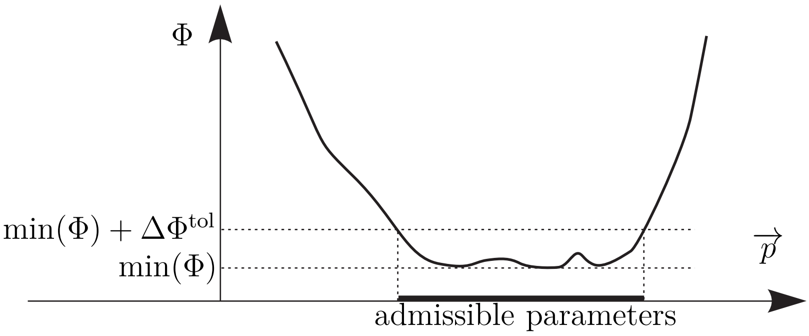

Figure 5.10. The set of admissible parameters in the context of the toleration condition (5.48).

In general, the problem of minimizing the error functional is ill-posed, since small changes of input data (experimental results) can lead to finite changes of the solution $\overrightarrow{p}$ (resulting parameter vector). In other words, the minimizing vector $\overrightarrow{p}$ is not a continuous function of the input data. On the other hand, the experimental data contain some measurement errors. Moreover, some small discrepancy between the real material behavior and the model prediction can be tolerated. Thus, there exists a toleration parameter $\Delta\Phi^{\text{tol}}$, such that all parameters $\overrightarrow{p}^*$ satisfying

$$\Phi(\overrightarrow{p}^*) \leq \min(\Phi) + \Delta\Phi^{\text{tol}}, \tag{5.48}$$

should be considered as admissible ones (see figure 5.10). A major *challenge* lies in developing identification strategies which fulfil two requirements as follows: (i) the parameters $\overrightarrow{p}^*$ must be admissible in the sense of (5.48), (ii) $\overrightarrow{p}^*$ must depend *continuously* on the input data.

We may put, for instance, $\Delta\Phi^{\text{tol}} := \min(\Phi)$. In that case, the results $\overrightarrow{p}_4$ and $\overrightarrow{p}_6$ can be seen as admissible (cf. Table 5.6). Moreover, the corresponding minimization problems (minimization of Φ_{g_1,g_3} and Φ_{g_2,g_3}) are advantageous over the straight-forward approach (minimization of Φ) since only one stationary point is observed. Furthermore, relations (5.36), (5.42) and (5.46) depend smoothly on the input data σ^{sat}, ε_{cr}, and S_*, and it was tested numerically that $\varkappa_1(\gamma, \beta, c)$ and $\varkappa_2(\gamma, \beta, c)$ depend continuously on σ_*^{tech} and ε_{cr}, respectively. Thus, we conclude that the minimization of Φ_{g_1,g_3} and Φ_{g_2,g_3} is a step towards meeting the major challenge mentioned above.

Acknowledgement

This research was supported by German Science Foundation (DFG) within the collaborative research center SFB 692 "High-strength aluminium based light weight materials for reliable components".

Bibliography

[1] J. V. Beck, K. J. Arnold, Parameter Estimation in Engineering and Science, Wiley, New York (1977).

[2] A. Bertram, Elasticity and Plasticity of Large Deformations, Springer (2005).

[3] J. L. Chaboche, G. Rousselier, On the Plastic and Viscoplastic Constitutive Equations, Part 1: Rules Developed with Internal Variable Concept, Journal of Pressure Vessel Technology, 105 (1983) 153 – 158.

[4] J. L. Chaboche, G. Rousselier, On the Plastic and Viscoplastic Constitutive Equations, Part 2: Application of Internal Variable Concept to the 316 Stainless Steel, Journal of Pressure Vessel Technology, 105 (1983) 159 – 164.

[5] D. Helm, Formgedächtnislegierungen, experimentelle Untersuchung, phänomenologische Modellierung und numerische Simulation der thermomechanischen Materialeigenschaften, Universitätsbibliothek Kassel, Kassel (2001).

[6] S. N. Korobeinikov, Nonlinear Deformation of Solids [in Russian], Izd. Sib. Otd. Ross. Akad. Nauk, Novosibirsk (2000).

[7] R. Kreißig, U. Benedix, U. Görke, M. Lindner, Identifikation and estimation of constitutive parameters for material laws in elastoplasticity, GAMM-Mitteilungen, 30(2) (2007) 458—480.

[8] A. Lion, Constitutive modelling in finite thermoviscoplasticity: a physical approach based on nonlinear rheological elements, International Journal of Plasticity, 16 (2000) 469—494.

[9] A. Lion, B. Yagimli, G. Baroud, U. Goerke, Constitutive modelling of PMMA-based bone cement: a functional model of viscoelasticity and its approximation for time domain investigations, Arch. Mech., 60(3) (2008) 221—242.

[10] R. Mahnken, E. Stein, A unified approach for parameter identification of inelastic material models in the frame of the finite element method, Computer Methods in Applied Mechanics and Engineering, 136 (1996) 225—258.

[11] IU. N. Rabotnov, Elements of hereditary solid mechanics [Rev. from the 1977 Russian ed.], Mir Publishers, Moscow (1980).

[12] V. M. Segal, Equal channel angular extrusion: from macromechanics to structure formation, Materials Science and Engineering, A271 (1999) 322 – 333.

[13] A. V. Shutov, K. Hockauf, T. Halle, R. Kreißig, L.W. Meyer, Experimentelle und phänomenologische Beschreibung des mechanischen Verhaltens der Aluminiumlegierung EN AW-7075 nach großer plastischer Vorverformung, Materialwissenschaft und Werkstofftechnik, 40(7) (2009) 551—558.

[14] A. V. Shutov, R. Kreißig, Application of a coordinate-free tensor formalism to the numerical implementation of a material model, Z. Angew. Math. Mech. (ZAMM), 88(11) (2008) 888—909.

[15] A. V. Shutov, R. Kreißig, Finite strain viscoplasticity with nonlinear kinematic hardening: Phenomenological modeling and time integration, Computer Methods in Applied Mechanics and Engineering, 197 (2008) 2015—2029.

[16] A. V. Shutov, R. Kreißig, Geometric integrators for multiplicative viscoplasticity: analysis of error accumulation, Computer Methods in Applied Mechanics and Engineering, 199 (2010) 700—711.

[17] J. Stoer, Foundations of recursive quadratic programming methods for solving nonlinear programs, in Computational Mathematical Programming NATO ASI Series (1985).

[18] A. N. Tikhonov, V. A. Arsenin, Solution of Ill-posed Problems, Winston & Sons, Washington (1977).

[19] I. N. Vladimirov, M. P. Pietryga, S. Reese, On the modelling of non-linear kinematic hardening at finite strains with application to springback — Comparison of time integration algorithms, International Journal for Numerical Methods in Engineering, 75 (2008) 1 – 28.

KAPITEL 6

Experimentelle Untersuchung und numerische Simulation des inkrementellen Umformverhaltens von Stahl 42CrMo4

Experimental investigation and numerical simulation of the incremental deformation of a 42CrMo4 steel

A. V. Shutov[1], C. Kuprin, J. Ihlemann, M. F.-X. Wagner, C. Silbermann.
Chemnitz University of Technology, Str. d. Nationen 62, D-09111 Chemnitz, Germany

Kurzfassung: *In dieser Arbeit werden die Verfestigungseigenschaften des Stahls 42CrMo4 untersucht. Die experimentelle Basis wird durch eine Reihe von Torsionsversuchen an dünnwandigen Rohrproben gebildet. Dabei werden Schubverzerrungen bis zu 160 % erreicht. Der Werkstoff weist bei einer Umkehr der Belastungsrichtung einen ausgeprägten Bauschinger-Effekt auf. Um diesen nichtlinearen Effekt adäquat zu erfassen, wird ein bereits existierendes Modell der Viskoplastizität von Shutov und Kreißig verallgemeinert. Die Verallgemeinerung besteht in der Einführung von zusätzlichen inneren Variablen sowie der Modifikation der entsprechenden Evolutionsgleichungen. Ein Teil der Experimente wird bei der Identifikation der Materialparameter verwendet. Die restlichen Experimente dienen der Validierung des erzielten Parametersatzes.*

Schlüsselworte: Viskoplastizität; inkrementelle Umformung; 42CrMo4; Bauschinger-Effekt; Modellvalidierung

Abstract: *In this work we analyze the strain hardening behaviour of a 42CrMo4 steel. The corresponding experimental data are obtained by a series of torsion tests on thin-walled tubes. In certain experiments the shear strains range up to 160 percent. When the strain path is reversed, the material exhibits a distinct Bauschinger effect. In order to describe this nonlinear effect, we generalize an existing model of finite strain viscoplasticity proposed by Shutov and Kreißig. The generalization consists of the introduction of additional internal variables and of a modification of corresponding evolution equations. A subset of the experimental data is used for the identification of the material parameters. The rest of the data serves the validation of the resulting set of material parameters.*

---

[1] Corresponding author. alexey.v.shutov@gmail.com
web: http://sites.google.com/site/materialmodeling

This chapter is reproduced from the paper: A. V. Shutov, C. Kuprin, J. Ihlemann, M. F.-X. Wagner, C. Silbermann. Experimentelle Untersuchung und numerische Simulation des inkrementellen Umformverhaltens von Stahl 42CrMo4. Materialwissenschaft und Werkstofftechnik. 2010. (41)9, 765-775. Copyright WILEY-VCH Verlag GmbH. Reproduced with permission.

Keywords: viscoplasticity; incremental deformation; 42CrMo4; Bauschinger effect; model validation

1. Einleitung

Inkrementelle Umformverfahren sind gekennzeichnet durch eine kleine plastische Umformzone, die sich in einem großen elastischen Bereich verschiebt. Die Verformung eines Volumenelements erfolgt dabei durch mehrere Be- und Entlastungszyklen [**1**]. Mit der wechselnden Verformungsrichtung sind häufig plastische Rückverformungsanteile verbunden, die nicht zu einer bleibenden Formänderung beitragen, sondern Walkarbeit leisten [**2**].

Aus diesen Merkmalen ergeben sich zahlreiche Vorteile für die Flexibilität des Fertigungsprozesses und die Eigenschaften des umgeformten Materials. So kann mit formspeicherarmen Werkzeugen bei kleinen Umformkräften gearbeitet und eine hohe Materialausnutzung erreicht werden. Der hohe hydrostatische Spannungsanteil begünstigt die Umformbarkeit des Materials. Der Umformpfad beeinflusst das Gefüge. Die großen lokalen Deformationen führen zu einer starken Kaltverfestigung. Festigkeit und Dauerfestigkeit des Bauteils werden erhöht. Dies ermöglicht Materialeinsparungen im Sinne des Leichtbaus.

Schwierigkeiten bei der Anwendung und Entwicklung inkrementeller Umformverfahren bereitet neben der oft komplizierten Werkzeugsteuerung die Abbildung der Prozesse in der FEM-Simulation. Es sind Konzepte der Datenverarbeitung notwendig (z.B. zur Speicherung der inneren Variablen bei Netzvergröberung), die eine hohe lokale Auflösung der Umformzone im Bauteil berücksichtigen und für jedes Volumenelement die Bereitstellung der Ergebnisse eines Umformschrittes für den nächsten gewährleisten. Außerdem muss ein Materialmodell verwendet werden, welches die wichtigsten Eigenschaften des Materials unter den komplexen Verformungsbedingungen abbildet. Große inelastische Verformungen mit wechselnden Verformungsrichtungen und die daraus resultierenden Veränderungen der Mikrostruktur gehen mit einem pfadabhängigen mechanischen Werkstoffverhalten einher. In diesem Artikel wird, basierend auf experimentellen Ergebnissen zum inkrementellen Materialverhalten, ein neues phänomenologisches Materialmodell der finiten Viskoplastizität präsentiert. Das Modell stellt eine Erweiterung eines Basismodells dar [**3**]. Das Basismodell und die entsprechende Methodik der Parameteridentifikation [**4**] wurden im Rahmen des SFB 692 für die Beschreibung des Verhaltens von Al-Legierungen entwickelt. Mit dem Modell werden die Abhängigkeit des Materialverhaltens von der Belastungsgeschwindigkeit sowie die nichtlineare kinematische und isotrope Verfestigung berücksichtigt.

Ein offenes Problem der phänomenologischen Materialmodellierung ist die Eignung des (durch eine Auswertung von Experimenten) erzielten Parametersatzes für weitere Belastungsfälle. Dieser Umstand macht eine nachfolgende Validierung des Materialmodells bzw. des Parametersatzes unumgänglich. Dabei soll eine solche Validierung auf dem Vergleich mit "neuen" Experimenten basieren, die nicht bei der eigentlichen Parameteridentifikation verwendet wurden. Mit zunehmender Anzahl der im Modell enthaltenen Materialparameter steigt die Anforderung an die Anzahl der erforderlichen Experimente und deren Informationsgehalt. In Torsionsversuchen, wie sie in der vorliegenden Arbeit zur Anwendung kommen, können komplizierte Verformungspfade mit großen Umformgraden ohne Reibungseinflüsse und ohne Dehnungslokalisierung realisiert werden. Sie eignen sich daher gut für die Parameteridentifikation. Die Versuche an dünnwandigen Hohlproben haben den weiteren Vorteil,

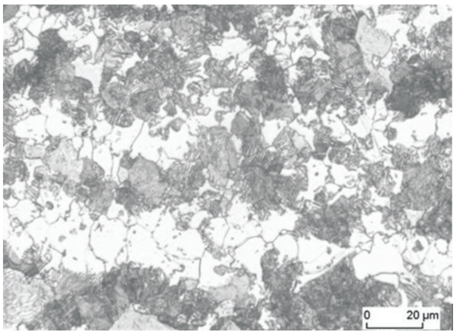

Figure 6.1. Optical micrograph of steel 42CrMo4 N.
Bild 6.1. Lichtmikroskopische Aufnahme eines Schliffes des Stahls 42CrMo4 N.

dass der Torsionsversuch, ähnlich wie bei der Auswertung von Versuchen mit homogenen Spannungs-Dehnungsfeldern, lokal simuliert werden kann (Lösung eines Anfangswertproblems für einen ausgewählten Materialpunkt statt Lösung eines Anfangsrandwertproblems), was die Auswertung von Experimenten selbst bei komplizierten Materialmodellen innerhalb akzeptabler Zeit ermöglicht.

2. Allgemeine Angaben zum Werkstoff

Für die Untersuchung des Fließverhaltens unter zyklisch inkrementeller Verformung wurde der legierte Vergütungsstahl 42CrMo4 verwendet. Die mittels Glimmentladungsspektroskopie bestimmte Zusammensetzung ist in Tabelle 6.1 angegeben.

Table 6.1. Chemical composition of steel 42CrMo4 N.
Tabelle 6.1. Chemische Zusammensetzung des Stahls 42CrMo4 N.

Element	C	Si	Mn	P	S	Cr	Mo
Elementgehalt in Gew. %	0,457	0,226	0,654	0,012	0,034	0,960	0,162

Das Material wurde im normalgeglühten Zustand untersucht (Bezeichnung im Folgenden: 42CrMo4 N). Bild 6.1 stellt das nach der Wärmebehandlung vorliegende Ferrit-Perlit-Gefüge mit einer Korngröße von etwa 15 μm dar. Es ist eine Zeiligkeit des Gefüges zu erkennen. Röntgenografische Untersuchungen ergaben keine Vorzugstextur der α-Phase. Bei der Simulation des Werkstoffs wird eine plastische Anfangsisotropie vorausgesetzt (siehe Abschnitt 5).

3. Experimentelle Untersuchungen und Ergebnisse

Torsionsversuche

Für die Untersuchung des Verfestigungsverhaltens und die Parameteranpassung des in Abschnitt 4 beschriebenen Materialmodells werden Fließkurven bis zu finiten Deformationen und unter wechselnder Beanspruchungsrichtung benötigt. Zur Erstellung solcher Kurven eignet sich der Torsionsversuch. Im Gegensatz zu Stauch- und Zugversuchen werden große Formänderungen ohne Reibungseinflüsse und ohne Änderung der Probengeometrie erreicht.

Die Verteilung von Schubspannung und der Schubverzerrungen im Querschnitt einer tordierten Probe ist im Allgemeinen inhomogen. Zur Beschreibung des Zusammenhangs zwischen dem angreifenden Drehmoment und den entstehenden Schubspannungen an Orten mit Abstand zur Längsachse dient die allgemeine Formel

$$M = 2\pi \int_{r_i}^{r_a} r \ \tau(r) \ r \ dr, \tag{6.1}$$

die gelöst werden kann, wenn die Schubspannungsverteilung $\tau(r)$ bekannt ist. Hierbei stehen r_a und r_i für den äußeren und den inneren Radius der betrachteten Probe.

Zur Gewinnung von Schubfließkurven aus Torsionsversuchen werden zumeist dünnwandige Hohlproben verwendet [**5**]. Dazu wird von einer linearen Verteilung der Spannung (erfüllt für linear elastisches Werkstoffverhalten) oder von einer konstanten Verteilung über den Radius (für idealplastisches Verhalten) ausgegangen. Mit abnehmender Wandstärke wird der Spannungsunterschied zwischen innerem und äußerem Radius minimiert und der Einfluss der gewählten Annahme zur Berechnung der Spannung nimmt ab. Außerdem kann für dünne Wandstärken von einem zweiachsigen, ebenen Spannungszustand ausgegangen werden. Unter Annahme einer linearen Verteilung berechnet sich die maximale Schubspannung τ_a am äußeren Radius zu

$$\tau_a = \frac{\pi}{128} \frac{M \ r_a}{(r_a^4 - r_i^4)}. \tag{6.2}$$

Gleichung (6.2) wird im vorliegenden Beitrag für die Berechnung der Schubspannung aus den experimentellen Daten verwendet.

Bei der Verdrehung einer stabförmigen Probe der Länge l geht eine Mantellinie in eine Schraubenlinie über, die um den Schiebewinkel $arctan(\gamma)$ bezüglich der ursprünglichen Linie geneigt ist. Wenn bei der Verdrehung Schraubenlinien gleichmäßiger Steigung entstehen, Querschnitte eben und Radien gerade bleiben, kann der lineare Zusammenhang zwischen Verdrehwinkel φ und Schubverzerrungen γ formuliert werden:

$$\gamma = \frac{\varphi \ r}{l}. \tag{6.3}$$

Die Schubverzerrung γ_a am äußeren Probenradius ergibt sich damit zu

$$\gamma_a = \frac{\varphi \ r_a}{l}. \tag{6.4}$$

Für die im Rahmen dieser Arbeit durchgeführten Torsionsversuche wurden dünnwandige Rohrproben mit den Radien $r_a = 6,25$ mm und $r_i = 5$ mm und der Messlänge l von 10 mm verwendet. Bild 6.2 zeigt die Geometrie der Proben, die während der Torsionsversuche in Spannzangen eingespannt werden.

Die Torsionsversuche wurden an einem Torsionsprüfstand durchgeführt, der die Einstellung unbegrenzter Verdrehwinkel erlaubt, Bild 6.3. Während der Verformung wurde das Drehmoment durch einen Drehmomentsensor (200 Nm/V) aufgezeichnet. Der Drehwinkel wurde an einem Einspannkopf der Probe abgenommen und über einen Zahnriemen auf einen Drehgeber übertragen (Auflösung $0,036^o$).

In Vorversuchen an dem Stahl 42CrMo4 N wurde zusätzlich durch Grauwertkorrelation eine dreidimensionale optische Deformationsanalyse des verformten Probenbereichs durchgeführt. Dafür wurde das System Aramis der Fa. GOM mbH verwendet. Es konnte die Homogenität der Verformung der Probenoberfläche innerhalb der Messlänge nachgewiesen

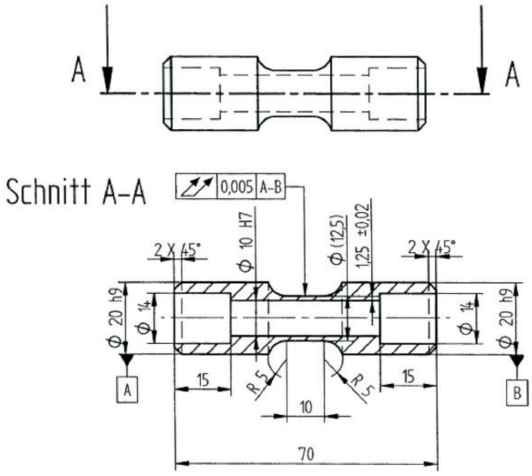

Figure 6.2. Geometry of the thin-walled tube sample.
Bild 6.2. Form der dünnwandigen Rohrproben.

Figure 6.3. Sample in the torsion testing device with rotation-angle sensor.
Bild 6.3. Probe im Torsionsprüfstand mit Drehgebern.

werden, Bild 6.4. Weiterhin wurde durch Auswertung der Differenzen von Längsverschiebungen und Verdrehungen einzelner Punkte $(\Delta z^*, \Delta\varphi^*)$ die Scherung γ^* direkt an der Probe ausgewertet. Einflüsse der elastischen Verformungen des gesamten Messaufbaus sowie im Bereich der Radien am Übergang von Messlänge zu den Einspannköpfen beeinflussen diese Auswertung nicht. Der Vergleich der mit optischer Deformationsanalyse und mit Gleichung (6.4) ausgewerteten Scherung ergibt einen steifigkeitsbedingten Faktor f, mit dem die aus den Drehgeber-Daten ermittelten Scherungen im Folgenden korrigiert wurden:

$$\gamma_a^k = f\ \gamma_a = \frac{\left(\dfrac{\varphi\ r_a}{l}\right)}{\left(\dfrac{\Delta\varphi^*\ r_a^*}{\Delta z^*}\right)}\ \gamma_a = 0,86\ \gamma_a. \tag{6.5}$$

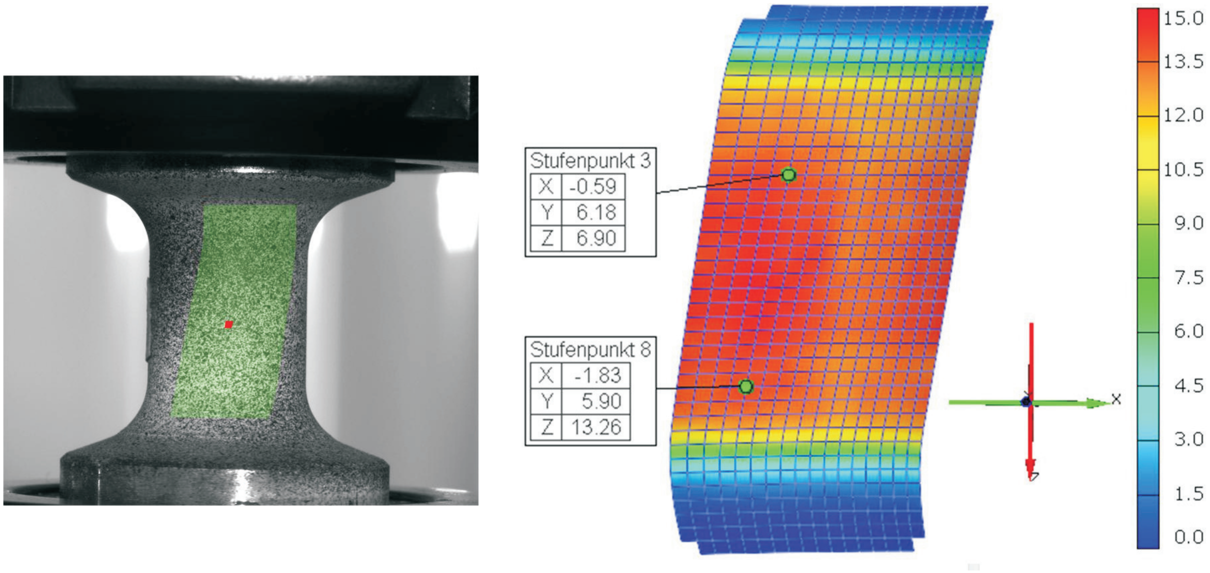

Figure 6.4. Application of optical deformation analysis in a torsion test in order to check the homogeneity of the deformation field: Camera image with tracked domain (left) and distribution of von Mises equivalent strain with marker points (right).

Bild 6.4. Anwendung der optischen Deformationsanalyse bei einem Torsionsversuch zur Überprüfung der Homogenität des Verformungsbereichs: Links ein Kamerabild mit dem markierten Auswertebereich, rechts die Darstellung der Vergleichsdehnung nach von Mises mit eingezeichneten Markierungspunkten für die Bestimmung der Differenzen von Verschiebung und Verdrehung.

Alle Versuche wurden mit einer Schergeschwindigkeit $\dot{\gamma}$ von $0,07$ s^{-1} durchgeführt. Diese Schergeschwindigkeit ist nicht als quasistatisch anzusehen. Um den Einfluss der Schergeschwindigkeit zu untersuchen, wurde eine Versuchsreihe mit unterschiedlichen Belastungsgeschwindigkeiten durchgeführt. In der Tabelle 7.1 sind die Messergebnisse für die Schubspannung nach 20% plastischer Schubverzerrung zusammengefasst. Der erkennbare Einfluss der Verformungsgeschwindigkeit wird bei der numerischen Simulation (Abschnitte 4 und 5) berücksichtigt.

Table 6.2. Shear stress τ_{20} after 20 % shear strain at different shear strain rates $\dot{\gamma}$.

Tabelle 6.2. Schubspannung τ_{20} nach 20% plastischer Schubverzerrung bei unterschiedlichen Schergeschwindigkeiten $\dot{\gamma}$.

$\dot{\gamma}$ $[s^{-1}]$	0,001	0,002	0,07
τ_{20} [MPa]	468	488	509

Die Torsionsversuche fanden bei Raumtemperatur statt. Durch die plastische Verformung entsteht Wärme, die bei der gewählten mittleren Umformgeschwindigkeit teils in der Probe verbleibt und mit zunehmender Verformung zu einem Temperaturanstieg führt. Die

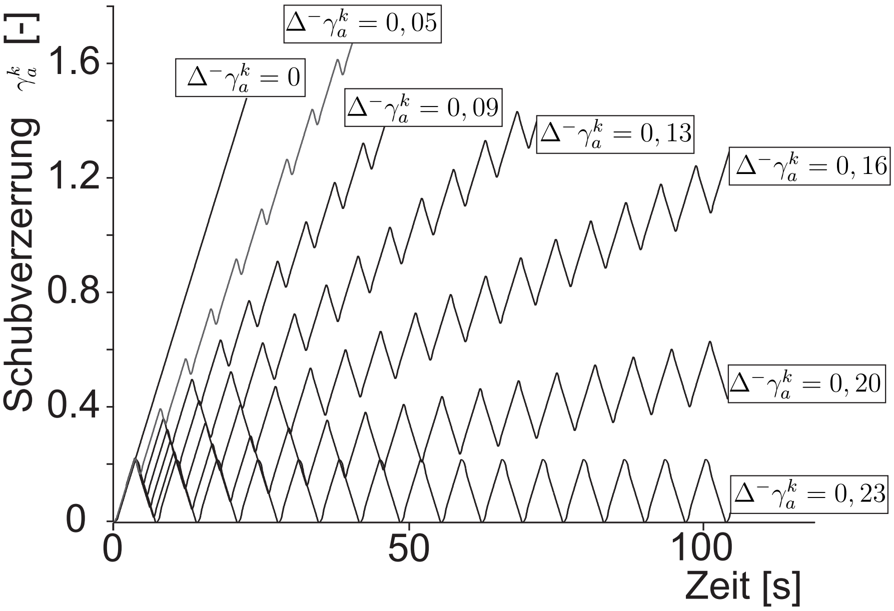

Figure 6.5. Schematic representation of the loading paths: monotonic torsion and cyclic torsion with a forward shear strain step size $\Delta^+\gamma_a^k = 0,23$ and different back shear strain step size $\Delta^-\gamma_a^k$.

Bild 6.5. Schematische Darstellung der Verformungspfade: einsinnige Torsion und zyklische Torsion mit $\Delta^+\gamma_a^k = 0,23$ und unterschiedlichen Rückverformungsschrittweiten $\Delta^-\gamma_a^k$.

Temperaturerhöhung der Proben infolge der entstehenden Umformwärme in den durchgeführten Versuchen betrug 20-25 K. Vorversuche ergaben, dass eine Temperaturerhöhung um 25 K zur Verringerung der Schubfließspannung um weniger als 2 MPa führten. Deshalb wird der Einfluss der Temperatur auf die Fließspannung in dieser Arbeit vernachlässigt.

Das Fließverhalten unter Torsionsbeanspruchung wurde sowohl bei einsinniger als auch bei zyklischer Verformung untersucht. Alle Versuche mit zyklischer Beanspruchung wurden mit einer positiven Schubverzerrungsschrittweite $\Delta^+\gamma_a^k$ durchgeführt. Die negative Schubverzerrungsschrittweite $\Delta^-\gamma_a^k$ wurde variiert von 0,05 bis 0,2 für zyklisch inkrementelle Verformungspfade bzw. bis 0,23 (zyklisch geschlossener Verformungspfad). Damit sollte ein typisches Merkmal inkrementeller Umformverfahren abgebildet werden: das Erreichen einer resultierenden Formänderung in mehreren Schritten mit hohen Anteilen an Walkarbeit [**2**]. Die verschiedenen Verformungspfade sind schematisch in Bild 6.5 dargestellt.

Werkstoffverhalten

Der Werkstoff weist bei der Erstbelastung eine ausgeprägte Schergrenze bei τ_a =260 MPa (untere Schergrenze) auf. Als Ursachen für die Spannungsüberhöhung am ersten Fließbeginn werden interstitiell gelöste Fremdatome (Cottrell-Wolken) im Eisen angesehen, die sich bei der Wärmebehandlung energetisch günstig zu den Spannungsfeldern von Versetzungen anordnen. Beim Beginn der plastischen Verformung müssen diese Anordnungen zunächst mit einem zusätzlichen Spannungsbetrag überwunden werden [**6**]. Die Schubfließkurven (Schubspannungen als Funktion der Schubverzerrungen) sind in Bild 6.6 dargestellt.

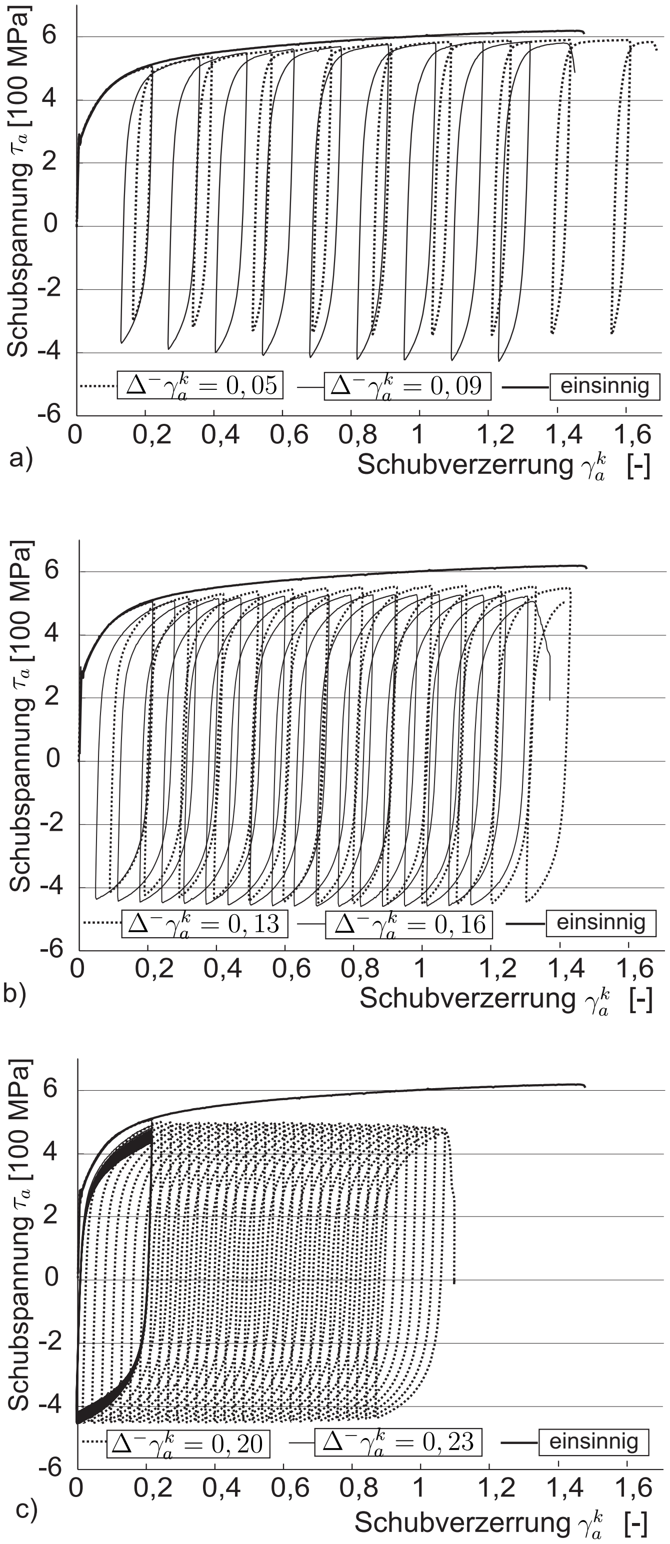

Figure 6.6. Flow curves for a monotonic as well as cyclic torsional loading with a forward shear strain step size $\Delta^{+}\gamma_a^k = 0,23$ and different back shear strain step size $\Delta^{-}\gamma_a^k$.

Bild 6.6. Schubfließkurven bei einsinniger und zyklischer Torsion mit $\Delta^{+}\gamma_a^k = 0,23$ und unterschiedlichen Rückverformungsschrittweiten $\Delta^{-}\gamma_a^k$.

Die einsinnige Fließkurve zeigt nach der Schergrenze eine starke Zunahme der Fließspannung. Die Zunahme schwächt sich mit zunehmender Verformung ab und lässt die Kurve einer Sättigung zustreben. Aus der Literatur zu den mikrostrukturellen Untersuchungen ist bekannt, dass die Verformungsverfestigung zunehmend durch dynamische Erholungsvorgänge überlagert wird. Die Neubildung von Versetzungen und gegenseitige Auslöschung oder Anordnung zu energetisch günstigen Strukturen gleichen sich aus. Von zahlreichen Autoren wird die Bildung von Versetzungszellen bis hin zu Subkorngrenzen beobachtet [**7, 8**].

Bei den zyklischen Kurven ist der erste Belastungshalbzyklus durch die deutliche Schergrenze gekennzeichnet und entspricht der einsinnigen Fließkurve. Bei der ersten Belastungsumkehr erfolgt zunächst die elastische Entlastung, die allmählich in eine elastisch-plastische Verformung übergeht. Anschließend tritt eine starke Verformungsverfestigung ein, bis der nächste Umkehrpunkt erreicht ist. Mit Beginn der ersten Rückverformung stellt sich eine Form der Hystereseschleifen ein, die im Laufe der weiteren Verformung erhalten bleibt. Die Übergänge vom elastischen zum plastischen Werkstoffverhalten verlaufen stetig. Der Werkstoff weist einen stark ausgeprägten Bauschinger-Effekt auf, der den früheren Fließbeginn nach einer Richtungsumkehr im Vergleich zur Weiterbelastung beschreibt. Als Ursachen für den Bauschinger-Effekt werden Rückspannungen angesehen, die bei der plastischen Verformung durch Wechselwirkung von Versetzungen mit Hindernissen entstehen und bei der Richtungsumkehr das Einsetzen plastischen Fließens unterstützen [**9, 10**]. Für den untersuchten Stahl wurde nach einer Richtungsumkehr das Einsetzen des plastischen Fließens schon vor der vollständigen Entlastung beobachtet, diese Ergebnisse sind in [**11**] dargestellt. Da in diesem Falle eine vollständige rein elastische Entlastung nicht realisierbar ist, dürfen die inelastischen Verzerrungen nicht als die nach der Entlastung verbleibenden Verzerrungen definiert werden (siehe Abschnitt 4).

Der Verlauf der maximalen Spannungen je Verformungszyklus wird von der Rückverformungsschrittweite bestimmt. Bei der Belastung mit einem zyklisch geschlossenen Pfad (Bild 6.6c) sinkt die maximale Spannung je Verformungszyklus mit zunehmender Verformung ab. Bei zyklisch geschlossenen Verformungspfaden wird eine Abnahme der Spannungsmaxima bei konstanter Dehnungsschrittweite als zyklische Entfestigung bezeichnet, eine Zunahme als zyklische Verfestigung [**12**]. Diese Begriffe sollen hier auch auf Fließkurven von zyklisch inkrementellen Verformungspfaden mit $\Delta^{+}\gamma_a^k$ ungleich $\Delta^{-}\gamma_a^k$ angewendet werden. Bei großen Rückverformungsanteilen wird somit eine zyklische Entfestigung beobachtet (Bild 6.6c). Mit kleiner werdenden Rückverformungsanteilen kommt es zu zyklischer Verfestigung (Bild 6.6a). Dabei bleiben die Spannungsbeträge aller zyklischen Fließkurven stets unter denen der einsinnigen Fließkurve [**13**].

4. Das Materialmodell der finiten Viskoplastizität

In diesem Abschnitt wird das bereits bestehende Materialmodell der finiten Viskoplastizität [**3**] verallgemeinert. Als Ausgangspunkt bei der Modellkonzipierung dient das im Bild 6.7a dargestellte rheologische Modell des modifizierten Schwedoff-Körpers (m.Schw). Wir postulieren, dass dieser aus zwei modifizierten Maxwell-Körpern (m.M), einem St.-Venant'schen Körper (St.-V) und einem Hooke'schen Körper (H), gemäß Strukturformel

$$\text{m.Schw} = (\text{m.M}|\ \text{m.M}|\ \text{St.-V}) \text{ - H} \tag{6.6}$$

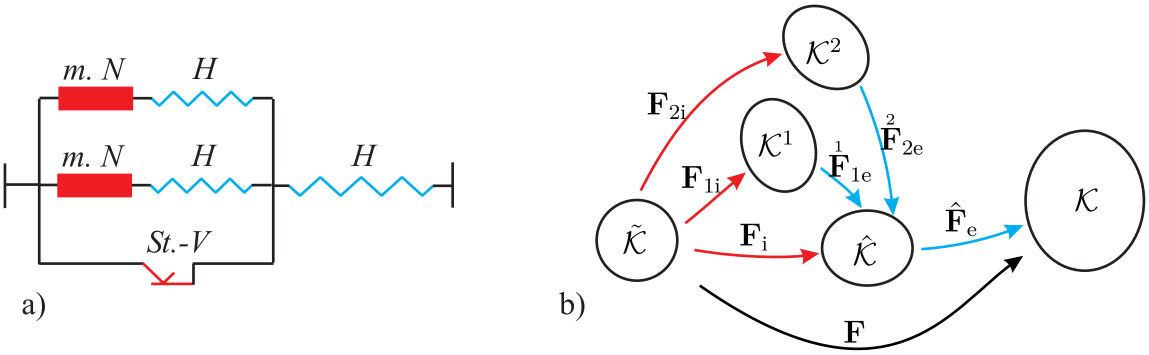

Figure 6.7. a) Rheological model, b) commutative diagram describing the kinematics.

Bild 6.7. a) Rheologisches Modell, b) kommutatives Diagramm zur Beschreibung der Kinematik.

aufgebaut ist. Der horizontale Strich bedeutet eine "Schaltung in Reihe" und der vertikale Strich "Parallelschaltung" [**14**]. Für den modifizierten Maxwell-Körper postulieren wir m.M = m.N - H, wobei m.N. für den modifizierten Newton-Körper steht.

Die (konstitutiven) Gleichungen zur Beschreibung des Verhaltens des modifizierten Newton-Körpers resultieren aus den Gleichungen des gewöhnlichen Newton-Körpers indem man formal die physikalische Zeit t durch den inelastischen Umformgrad s ersetzt. Der inelastische Umformgrad spiegelt dabei die akkumulierte Verzerrung des St.-Venant'schen Körpers wieder, und stellt somit eine monoton wachsende Größe dar. Ein phänomenologisches Modell der finiten Viskoplastizität basierend auf dem Schwedoff-Modell mit einem modifizierten Maxwell-Körper wurde bereits in [**3**] konstruiert.

Das rheologische Modell in Bild 6.7a dient als Gedankenmodell, das die Konzipierung des Stoffgesetzes erleichtert. Dabei sollen die Eigenschaften des rheologischen Modells von dem entwickelten Stoffgesetz qualitativ wiedergegeben werden. Zu diesem Zweck werden die Kräfte und Längenänderungen (relative Verschiebungen) formal durch die Spannungen und Verzerrungen ersetzt. Die Einführung der modifizierten Maxwell-Elemente kann wie folgt interpretiert werden: Die Verformung eines solchen Elements wird in Verbindung mit inelastischen Fließvorgängen gebracht, die auf die Bewegung von Versetzungen zurückzuführen sind. Dies stellt einen dissipativen Vorgang dar, bei dem mechanische Energie in Wärme umgewandelt wird. Die Bewegung von Versetzungen wird von der Dichte und Anordnung der im Werkstoff vorhandenen Versetzungen beeinflusst. Die Wechselwirkungen der lokalen Spannungsfelder von mobilen Versetzungen und Hindernissen können eine Energiespeicherung bewirken und zu einer Richtungsabhängigkeit der Fließspannung führen [**9**]. Die Kräfte, die in den modifizierten Maxwell-Elementen herrschen, dienen somit als ein Modell für die Rückspannungen, die bei monotoner Belastung das plastische Fließen erschweren und bei der Richtungsumkehr das plastische Fließen unterstützen (vgl. Abschnitt 3).

Die Gesamtdeformation wird mit dem Deformationsgradienten $\mathbf{F}$ beschrieben [**15**]. Der Operator $\mathbf{F}$ wird in einen konservativen Anteil $\hat{\mathbf{F}}_\mathrm{e}$ und einen dissipativen Anteil $\mathbf{F}_\mathrm{i}$ zerlegt (siehe Bild 6.7b). Da bei dem untersuchten Werkstoff im Allgemeinen keine rein elastische Entlastung möglich ist (vgl. Abschnitt 3), darf diese Zerlegung nicht durch eine solche Entlastung motiviert werden. Stattdessen kann das rheologische Modell auf Bild 6.7a zur Erklärung dieser Zerlegung herangezogen werden. Laut dem rheologischen Modell setzt sich die Gesamtdeformation aus der Verformung des (m.M| m.M| St.-V)-Körpers (wird mit $\mathbf{F}_\mathrm{i}$ erfasst) und der Deformation des Hooke-Körpers (wird mit $\hat{\mathbf{F}}_\mathrm{e}$ beschrieben) zusammen. Entsprechend der Definition des Deformationsgradienten $\mathbf{F}$ geht das Linienelement $d\mathbf{X}$ infolge der Gesamtdeformation in das Element $\mathbf{F}\ d\mathbf{X}$ auf der Momentankonfiguration über. Im Rahmen einer Modellvorstellung geht aber das Element $d\mathbf{X}$ infolge der Verformung des (m.M| m.M| St.-V)-Körpers in ein fiktives Element $\mathbf{F}_\mathrm{i}\ d\mathbf{X}$ über. Die nachgeschaltete Deformation des Hooke-Körpers transformiert dieses Element zu $\hat{\mathbf{F}}_\mathrm{e}(\mathbf{F}_\mathrm{i} d\mathbf{X}) = \hat{\mathbf{F}}_\mathrm{e}\mathbf{F}_\mathrm{i} d\mathbf{X}$, das mit $\mathbf{F}d\mathbf{X}$ übereinstimmen soll. Da $d\mathbf{X}$ ein beliebiges Linienelement ist, erhält man somit $\mathbf{F} = \hat{\mathbf{F}}_\mathrm{e}\mathbf{F}_\mathrm{i}$.

Der Körper (m.M| m.M| St.-V) beinhaltet zwei parallel geschaltete modifizierte Maxwell-Körper. Ihre Gesamtverformung wird mit $\mathbf{F}_\mathrm{i}$ erfasst und setzt sich aus der Deformation des modifizierten Newton-Elements und der nachgeschalteten Deformation des Hooke-Körpers zusammen (siehe Bild 6.7a). Laut der Modellvorstellung idealer Körper ist die Verformung eines modifizierten Maxwell-Körpers (wird mit $\mathbf{F}_{1\mathrm{i}}$ oder $\mathbf{F}_{2\mathrm{i}}$ erfasst) mit rein dissipativen Vorgängen verbunden. Auf der anderen Seite ist die Verformung eines Hooke-Körpers (wird mit $\overset{1}{\mathbf{F}}_{1\mathrm{e}}$ oder $\overset{2}{\mathbf{F}}_{2\mathrm{e}}$ erfasst) stets rein konservativ. Auf eine ähnliche Weise wie bei der Gesamtdeformation wird der Anteil $\mathbf{F}_\mathrm{i}$ in $\overset{1}{\mathbf{F}}_{1\mathrm{e}}$ und $\mathbf{F}_{1\mathrm{i}}$ bzw. in $\overset{2}{\mathbf{F}}_{2\mathrm{e}}$ und $\mathbf{F}_{2\mathrm{i}}$ multiplikativ aufgeteilt, siehe Bild 6.7b. Diese Zerlegung von $\mathbf{F}_\mathrm{i}$ in konservative und dissipative Anteile sowie die oben erwähnte Motivation wurde ursprünglich von Lion in [**16**] vorgeschlagen. Die Kinematik des Materialmodells wird somit insgesamt durch drei multiplikative Zerlegungen charakterisiert:

$$\mathbf{F} = \hat{\mathbf{F}}_\mathrm{e}\mathbf{F}_\mathrm{i}, \quad \mathbf{F}_\mathrm{i} = \overset{1}{\mathbf{F}}_{1\mathrm{e}}\mathbf{F}_{1\mathrm{i}}, \quad \mathbf{F}_\mathrm{i} = \overset{2}{\mathbf{F}}_{2\mathrm{e}}\mathbf{F}_{2\mathrm{i}}. \tag{6.7}$$

Laut dem Prinzip der Materiellen Objektivität (siehe z.B. [**15**]) wird die mechanische Belastung mit dem rechten Cauchy-Green-Tensor $\mathbf{C} := \mathbf{F}^\mathrm{T}\mathbf{F}$ erfasst. Zur Charakterisierung des momentanen Zustandes des Materials werden die inneren Variablen $\mathbf{C}_\mathrm{i}, \mathbf{C}_{1\mathrm{i}}, \mathbf{C}_{2\mathrm{i}}$ eingeführt:

$$\mathbf{C}_\mathrm{i} := \mathbf{F}_\mathrm{i}^\mathrm{T}\mathbf{F}_\mathrm{i}, \quad \mathbf{C}_{1\mathrm{i}} := \mathbf{F}_{1\mathrm{i}}^\mathrm{T}\mathbf{F}_{1\mathrm{i}}, \quad \mathbf{C}_{2\mathrm{i}} := \mathbf{F}_{2\mathrm{i}}^\mathrm{T}\mathbf{F}_{2\mathrm{i}}. \tag{6.8}$$

Diese Größen sind symmetrisch und positiv definit.

In der vorliegenden Arbeit ist die Möglichkeit vorgesehen, auf eine einheitliche Weise sowohl eine isotrope Verfestigung als auch eine isotrope Entfestigung zu simulieren. Um die Sättigung von diesen unterschiedlichen Prozessen zu erfassen, werden zwei skalarwertige innere Variablen s_{d1} und s_{d2} vom Verzerrungstyp eingeführt, die als dissipative Anteile des inelastischen Umformgrads s aufgefasst werden (vgl. (6.9)).

Es wird von der materiellen (Lagrange'schen) Vorgehensweise zur Formulierung von konstitutiven Gleichungen Gebrauch gemacht. Im Rahmen dieser Vorgehensweise wird folgender Ansatz für die spezifische Helmholtz'sche freie Energie verwendet:

$$\begin{aligned}\psi &= \psi(\mathbf{C}, \mathbf{C}_\mathrm{i}, \mathbf{C}_{1\mathrm{i}}, \mathbf{C}_{2\mathrm{i}}, s, s_\mathrm{d1}, s_\mathrm{d2}) \\ &= \psi_\mathrm{el}(\mathbf{C}{\mathbf{C}_\mathrm{i}}^{-1}) + \psi_\mathrm{kin1}(\mathbf{C}_\mathrm{i}{\mathbf{C}_{1\mathrm{i}}}^{-1}) + \psi_\mathrm{kin2}(\mathbf{C}_\mathrm{i}{\mathbf{C}_{2\mathrm{i}}}^{-1}) + \psi_\mathrm{iso1}(s - s_\mathrm{d1}) + \psi_\mathrm{iso2}(s - s_\mathrm{d2}),\end{aligned} \tag{6.9}$$

wobei mit $\psi_\mathrm{el}(\mathbf{C}{\mathbf{C}_\mathrm{i}}^{-1})$, $\psi_\mathrm{kin1}(\mathbf{C}_\mathrm{i}{\mathbf{C}_{1\mathrm{i}}}^{-1}) + \psi_\mathrm{kin2}(\mathbf{C}_\mathrm{i}{\mathbf{C}_{2\mathrm{i}}}^{-1})$ und $\psi_\mathrm{iso1}(s - s_\mathrm{d1}) + \psi_\mathrm{iso2}(s - s_\mathrm{d2})$ die Energiespeicherung infolge elastischer Deformation, kinematischer Verfestigung und isotroper Verfestigung erfasst wird. In diesem Artikel werden folgende konkrete Ansätze eingeführt (vgl. [**3, 17**]):

$$\begin{aligned}
\rho_{\mathrm{R}}\psi_{\mathrm{el}}(\mathbf{A}) &= \frac{k}{2}\Big(\ln\sqrt{\det\mathbf{A}}\Big)^2 + \frac{\mu}{2}\Big(\mathrm{tr}\overline{\mathbf{A}} - 3\Big),\\
\rho_{\mathrm{R}}\psi_{\mathrm{kin1}}(\mathbf{A}) &= \frac{c_1}{4}\Big(\mathrm{tr}\overline{\mathbf{A}} - 3\Big), \quad \rho_{\mathrm{R}}\psi_{\mathrm{kin2}}(\mathbf{A}) = \frac{c_2}{4}\Big(\mathrm{tr}\overline{\mathbf{A}} - 3\Big),\\
\rho_{\mathrm{R}}\psi_{\mathrm{iso1}}(s_{\mathrm{e}}) &= \frac{\gamma_1}{2}\,(s_{\mathrm{e}})^2, \qquad \rho_{\mathrm{R}}\psi_{\mathrm{iso2}}(s_{\mathrm{e}}) = \frac{\gamma_2}{2}\,(s_{\mathrm{e}})^2, \quad \overline{\mathbf{A}} = (\det\mathbf{A})^{-1/3}\mathbf{A},
\end{aligned} \tag{6.10}$$

wobei $\mathbf{A}$ einen beliebigen Tensor 2. Stufe und s_{e} eine beliebige skalare Größe kennzeichnen; $\overline{\mathbf{A}} = (\det\mathbf{A})^{-1/3}\mathbf{A}$ und k, μ, c_1, c_2, γ_1, γ_2 sind Materialparameter; tr bezeichnet die Spur eines Tensors. Die oben eingeführten Funktionen ψ_{el}, ψ_{kin1} und ψ_{kin2} sind isotrop. Anhand von diesen Funktionen werden die Potentialbeziehungen für den 2. Piola-Kirchhoff-Spannungstensor $\tilde{\mathbf{T}}$, die Rückspannungstensoren $\tilde{\mathbf{X}}_1$ und $\tilde{\mathbf{X}}_2$ sowie die Anteile der isotropen Verfestigung/Entfestigung formuliert (vgl. [**3**]):

$$\begin{aligned}
\tilde{\mathbf{T}} &= 2\rho_{\mathrm{R}}\frac{\partial\psi_{\mathrm{el}}(\mathbf{C}\mathbf{C}_{\mathrm{i}}{}^{-1})}{\partial\mathbf{C}}\Big|_{\mathbf{C}_{\mathrm{i}}=\mathrm{const}},\\
\tilde{\mathbf{X}}_1 &= 2\rho_{\mathrm{R}}\frac{\partial\psi_{\mathrm{kin1}}(\mathbf{C}_{\mathrm{i}}\mathbf{C}_{1\mathrm{i}}{}^{-1})}{\partial\mathbf{C}_{\mathrm{i}}}\Big|_{\mathbf{C}_{1\mathrm{i}}=\mathrm{const}},\\
\tilde{\mathbf{X}}_2 &= 2\rho_{\mathrm{R}}\frac{\partial\psi_{\mathrm{kin2}}(\mathbf{C}_{\mathrm{i}}\mathbf{C}_{2\mathrm{i}}{}^{-1})}{\partial\mathbf{C}_{\mathrm{i}}}\Big|_{\mathbf{C}_{2\mathrm{i}}=\mathrm{const}},\\
R_1 = \rho_{\mathrm{R}}\frac{\partial\psi_{\mathrm{iso1}}(s - s_{d1})}{\partial s}\Big|_{s_{d1}=\mathrm{const}}&, \quad R_2 = \rho_{\mathrm{R}}\frac{\partial\psi_{\mathrm{iso2}}(s - s_{d2})}{\partial s}\Big|_{s_{d2}=\mathrm{const}}.
\end{aligned} \tag{6.11}$$

Der gesamte Rückspannungstensor $\tilde{\mathbf{X}}$ sowie die gesamte isotrope Verfestigung/Entfestigung R werden wie folgt definiert: $\tilde{\mathbf{X}} = \tilde{\mathbf{X}}_1 + \tilde{\mathbf{X}}_2$, $R = R_1 + R_2$. Die Überspannung f wird anhand folgender Beziehungen bestimmt:

$$f = \mathfrak{F} - \sqrt{\frac{2}{3}}\Big(K + R\Big), \quad \mathfrak{F} = \sqrt{\mathrm{tr}\Big[\Big(\mathbf{C}\tilde{\mathbf{T}} - \mathbf{C}_{\mathrm{i}}\tilde{\mathbf{X}}\Big)^{\mathrm{D}}\Big]^2}, \tag{6.12}$$

wobei K einen Materialparameter (Anfangsfließspannung) darstellt, $(\cdot)^{\mathrm{D}}$ ist der deviatorische Anteil eines Tensors, die Größe $\mathfrak{F}$ kann als die Norm der treibenden Kraft für das inelastische Fließen interpretiert werden. Der inelastische Multiplikator λ_{i} wird entsprechend der Perzyna-Regel berechnet:

$$\lambda_{\mathrm{i}} = \frac{1}{\eta}\Big\langle\frac{1}{k_0}f\Big\rangle^m, \quad \langle x\rangle := \max(x, 0). \tag{6.13}$$

Hierbei sind η und m Materialparameter; k_0 dient der Entdimensionierung des Ausdrucks in den eckigen Klammern (kein Materialparameter). Der Multiplikator λ_{i} gibt die Geschwindigkeit des inelastischen Fließens an. Nach der Perzyna-Regel verhält sich ein Werkstoff ideal elastisch, solange $f \leq 0$ gilt. Bei $f > 0$ dagegen tritt viskoplastisches Fließen ein. Das Fließen wird mit folgenden gewöhnlichen Differentialgleichungen erfasst:

$$\begin{aligned}
\dot{\mathbf{C}}_{\mathrm{i}} &= 2\frac{\lambda_{\mathrm{i}}}{\mathfrak{F}}\Big(\mathbf{C}\tilde{\mathbf{T}} - \mathbf{C}_{\mathrm{i}}\tilde{\mathbf{X}}\Big)^{\mathrm{D}}\mathbf{C}_{\mathrm{i}},\\
\dot{\mathbf{C}}_{1\mathrm{i}} &= 2\ \lambda_{\mathrm{i}}\ (\varkappa_1 F_1)^{q_1-1}\ \varkappa_1\ \Big(\mathbf{C}_{\mathrm{i}}\tilde{\mathbf{X}}_1\Big)^{\mathrm{D}}\mathbf{C}_{1\mathrm{i}}, \ \text{mit}\ F_1 := \sqrt{\mathrm{tr}\Big[\Big(\mathbf{C}_{\mathrm{i}}\tilde{\mathbf{X}}_1\Big)^{\mathrm{D}}\Big]^2},\\
\dot{\mathbf{C}}_{2\mathrm{i}} &= 2\ \lambda_{\mathrm{i}}\ (\varkappa_2 F_2)^{q_2-1}\ \varkappa_2\ \Big(\mathbf{C}_{\mathrm{i}}\tilde{\mathbf{X}}_2\Big)^{\mathrm{D}}\mathbf{C}_{2\mathrm{i}}, \ \text{mit}\quad F_2 := \sqrt{\mathrm{tr}\Big[\Big(\mathbf{C}_{\mathrm{i}}\tilde{\mathbf{X}}_2\Big)^{\mathrm{D}}\Big]^2},
\end{aligned} \tag{6.14}$$

$$\dot{s} = \sqrt{\frac{2}{3}}\lambda_{\mathrm{i}}, \quad \dot{s}_{d1} = \frac{\beta_1}{\gamma_1}\dot{s}R_1, \quad \dot{s}_{d2} = \frac{\beta_2}{\gamma_2}\dot{s}R_2,$$

wobei $\varkappa_1$, $\varkappa_2$, q_1, q_2, β_1, β_2 Materialparameter sind; $\dot{(\cdot)}$ steht für die Ableitung nach der Zeit t (materielle Zeitableitung). Es lässt sich zeigen, dass $\mathrm{tr}\Big[\Big(\mathbf{C}_{\mathrm{i}}\tilde{\mathbf{X}}_1\Big)^{\mathrm{D}}\Big]^2 \geq 0$ und $\mathrm{tr}\Big[\Big(\mathbf{C}_{\mathrm{i}}\tilde{\mathbf{X}}_2\Big)^{\mathrm{D}}\Big]^2 \geq 0$ gilt. Somit sind die Größen F_1 und F_2 wohl bestimmt. Die Entwicklungsgleichungen (6.14) stellen eine Verallgemeinerung der konstitutiven Gleichungen aus [**3**] dar, die durch Einführung eines zusätzlichen modifizierten Maxwell-Elements und der Multiplikatoren $(\varkappa_1 F_1)^{q_1-1}$, $(\varkappa_2 F_2)^{q_2-1}$ erreicht wurde. Nach der Integration der Entwicklungsgleichungen für s_{d1} und s_{d2} bekommt man die isotrope Verfestigung als eine Funktion des inelastischen Umformgrades: $R = R(s)$.

Da eine *Anfangsisotropie* vorausgesetzt wird (vgl. Abschnitt 2), werden folgende Anfangsbedingungen (zum Zeitpunkt $t = 0$) festgelegt:

$$\mathbf{C}_{\mathrm{i}}|_{t=0} = \mathbf{C}_{1\mathrm{i}}|_{t=0} = \mathbf{C}_{2\mathrm{i}}|_{t=0} = \mathbf{1}, \quad s|_{t=0} = s_{d1}|_{t=0} = s_{d2}|_{t=0} = 0. \tag{6.15}$$

Im Allgemeinen besteht die Möglichkeit, eine eventuelle *Anfangsanisotropie* durch entsprechende Wahl von Anfangsbedingungen für $\mathbf{C}_{1\mathrm{i}}$ und $\mathbf{C}_{2\mathrm{i}}$ zu erfassen.

Für $\eta \to 0$ sind die Gleichungen der geschwindigkeitsunabhängigen Plastizität als Grenzfall von (6.7)-(6.14) enthalten. Die Entwicklungsgleichungen (6.14) beschreiben inkompressibles Fließen:

$$\det(\mathbf{C}_{\mathrm{i}}) = \det(\mathbf{C}_{1\mathrm{i}}) = \det(\mathbf{C}_{2\mathrm{i}}) = 1. \tag{6.16}$$

Das in diesem Abschnitt dargestellte System konstitutiver Gleichungen wurde unter Einbeziehung so genannter geometrischer Integratoren umgesetzt. Solche Algorithmen besitzen die charakteristische Eigenschaft, dass die Inkompressibilitätsbedingung (6.16) auch für die numerische Lösung identisch erfüllt ist. In [**3**] wurde gezeigt, dass bei der Verwendung von geometrischen Integratoren der numerische Fehler mit zunehmender Zeit nicht akkumuliert wird. Die mathematische Erklärung von diesem günstigen Verhalten wurde in [**18**] ausgearbeitet. Die Tatsache, dass sich der numerische Fehler nicht akkumuliert, ist besonders wichtig für die Simulation von "langen" Umformprozessen mit großem akkumulierten Umformgrad. Da die Ergebnisse der Parameteridentifikation besonders stark von den Berechnungsfehlern beeinflusst werden können, spielt die Berechnungsgenauigkeit eine große Rolle.

5. Identifikation der im Modell enthaltenen Parameter

Identifikation der Elastizitätsparameter

Aus der Auswertung der Messdaten für den elastischen Bereich wird zunächst der Schubmodul identifiziert: $\mu = 52000$ MPa. Für die Poisson-Zahl erhält man $\nu = 0,33$. Die elastische Konstante k (Kompressionsmodul - vgl. (6.10)) ergibt sich mittels der Umrechnungsformel

$$k = \frac{2(1+\nu)}{3(1-2\nu)}\mu \tag{6.17}$$

zu $k = 135600$ MPa.

Identifikation der Parameter für die Geschwindigkeitsabhängigkeit

Die Parameter η und m der Perzyna-Regel (6.13) werden basierend auf Messdaten für die Schubspannung τ bei unterschiedlichen Schergeschwindigkeiten $\dot{\gamma}$ bestimmt (vgl. Tabelle

7.1). Es wird ein einsinniger Torsionsversuch betrachtet. Da der Rückspannungstensor $\tilde{\mathbf{X}}$ sowie die isotrope Verfestigung R lediglich von der Bahnkurve von $\mathbf{C}_\mathrm{i}$ abhängen (aber nicht von der Geschwindigkeit, mit der sich $\mathbf{C}_\mathrm{i}$ entlang dieser Bahnkurve bewegt), sind $\tilde{\mathbf{X}}$ und R für jede vorgegebene Schubverzerrung nahezu geschwindigkeitsunabhängig. Für den Fall kleiner Verformungen bei Vernachlässigung elastischer Deformationen bekommt man aus (6.13) folgenden analytischen Zusammenhang zwischen der Schubspannung τ_{20} und der Schergeschwindigkeit $\dot{\gamma}$:

$$\frac{1}{\sqrt{2}}\dot{\gamma} = \frac{1}{\eta}\Big\langle \frac{\sqrt{2}\tau_{20} - \sqrt{2}\alpha}{k_0} \Big\rangle^m, \tag{6.18}$$

wobei α eine unbekannte Konstante ist. Sie entspricht dem Wert der Schubspannung bei unendlich kleiner Schergeschwindigkeit, sodass man für die Überspannung den Zusammenhang $f = \sqrt{2}\tau_{20} - \sqrt{2}\alpha$ erhält. Die Entdimensionierungskonstante k_0 wird gleich 1MPa festgelegt. Im numerischen Experiment wurde festgestellt, dass der Wert der Überspannung bei der Simulation eines einsinnigen Torsionsversuchs mit konstanter Schergeschwindigkeit selbst bei finiten Schubverzerrungen nahezu konstant bleibt. Somit wird der Zusammenhang (6.18) im Falle finiter Deformationen als eine Näherungsformel verwendet.

Unter Berücksichtigung der Messwerte (vgl. Tabelle 7.1) erhält man aus (6.18) drei nichtlineare Gleichungen zur Bestimmung von η, m und α. Da dieses nichtlineare Gleichungssystem im Allgemeinen nicht lösbar ist, werden die gesuchten Materialparameter mit der Methode der kleinsten Quadrate numerisch bestimmt, und es ergibt sich: $\eta = 500000$ s, $m = 2,26$.

Bestimmung der Anfangsfließspannung

Durch die grafische Auswertung der Fließkurve des einsinnigen Versuchs, der mit einer Schergeschwindigkeit $\dot{\gamma}$ von $0,07s^{-1}$ durchgeführt wurde (Bild 6.6), lässt sich die dynamische Schubfließspannung bestimmen: $\tau_\mathrm{dynam} = 255,6$ MPa. Die Geschwindigkeitsabhängigkeit des Materialverhaltens wird bei der Ermittlung der Anfangsfließspannung K wie folgt berücksichtigt. Im Rahmen der Viskoplastizität vom Überspannungstyp resultiert die Schubfließkurve aus der Kurve eines quasistatischen Versuchs durch eine Vergrößerung von Schubspannungen um $f/\sqrt{2}$, wobei f die aktuelle Überspannung kennzeichnet. Aus dem bekannten Wert der Schergeschwindigkeit $\dot{\gamma}$ und bekannten Materialparametern η und m errechnet sich unter Zuhilfenahme der Gleichung (6.13) die aktuelle Überspannung zu $f = 87,9$ MPa. Für die Schubfließspannung des quasistatischen Versuchs bekommt man dann $\tau_\mathrm{quasistat} = \tau_\mathrm{dynam} - f/\sqrt{2} = 193,4$ MPa. Die Anfangsfließspannung K ergibt sich schließlich mittels der Umrechnungsformel $K = \sqrt{3}\,\tau_\mathrm{quasistat}$ zu $K = 335$ MPa.

Identifikation der Verfestigungsparameter

Da der Anfangszustand als isotrop angenähert wird, kann der Torsionsversuch (vgl. Abschnitt 3) lokal simuliert werden. Es wird dabei angenommen, dass der Deformationsgradient $\mathbf{F}$ in Bezug auf ein kartesisches Koordinatensystem $\{\mathbf{e}_1, \mathbf{e}_2, \mathbf{e}_3\}$ folgende Gestalt annimmt:

$$\mathbf{F} = \alpha_1 \mathbf{e}_1 \otimes \mathbf{e}_1 + \gamma\alpha_1 \mathbf{e}_1 \otimes \mathbf{e}_2 + \mathbf{e}_2 \otimes \mathbf{e}_2 + \alpha_2 \mathbf{e}_3 \otimes \mathbf{e}_3, \tag{6.19}$$

wobei α_1 und α_2 unbekannt sind; γ ist die vorgegebene Schubverzerrung (die Werte von γ entsprechen den im Experiment aus den vorgegebenen Werten des Verdrehwinkels φ ermittelten Werten γ_k^a). Die Unbekannten α_1 und α_2 werden zu jedem Zeitpunkt aus der Bedingung

$$T_{11} = 0, \quad T_{33} = 0 \tag{6.20}$$

identifiziert, wobei **T** den Cauchy'schen Spannungstensor kennzeichnet (wahre Spannungen). Das System (6.20) wird für jeden Zeitschritt numerisch mit der Newton-Raphson-Methode gelöst.

Bei der Identifikation der Verfestigungsparameter ist eine Fehlerquadratsumme so zu minimieren, dass numerisch ermittelte Spannungswerte den Messwerten möglichst weit angenähert werden. In der vorliegenden Arbeit ergeben sich die Fehlerquadrate aus der Differenz der gemessenen Schubspannungen und den berechneten Schubspannungen auf der Basis des Materialmodells:

$$\Phi(\overrightarrow{p}) = \sum_{k=1}^{3} \sum_{i=1}^{n_k} \left(\tau_{k,i}^{gemessen} - \tau_{k,i}(\overrightarrow{p}) \right)^2 . \tag{6.21}$$

Hierbei steht k für die Referenznummer des Experiments, n_k für die Anzahl der Messwerte im Experiment k, $\overrightarrow{p}$ für den Parametersatz, $\tau_{k,i}^{gemessen}$ für den i-ten Messwert und $\tau_{k,i}(\overrightarrow{p})$ für die entsprechende Modelvorhersage. Zum Aufbau des Fehlerfunktionals (6.21) werden insgesamt die drei zyklischen Versuche mit $\Delta^{-}\gamma_a^k = 0,09$, mit $\Delta^{-}\gamma_a^k = 0,13$ und mit $\Delta^{-}\gamma_a^k = 0,20$ herangezogen. Da beim Aufbau des Fehlerfunktionals bei allen drei Experimenten nahezu die gleiche Anzahl von Messpunkten verwendet wurde und keine Wichtung der Experimente erfolgte, werden die Experimente näherungsweise gleichberechtigt berücksichtigt. Die zyklischen Versuche mit $\Delta^{-}\gamma_a^k = 0,05$, $\Delta^{-}\gamma_a^k = 0,16$ und $\Delta^{-}\gamma_a^k = 0,23$ sowie der einsinnige Versuch werden zur Validierung des erzielten Parametersatzes verwendet.

Zur Minimierung des Fehlerfunktionals wird der Levenberg-Marquardt-Algorithmus verwendet, wobei die Berechnung der benötigten Ableitungen der Residuen nach den Parametern numerisch erfolgt. Die identifizierten Parameter sind der Tabelle 6.3 zu entnehmen.

Table 6.3. The set of identified material parameters.
Tabelle 6.3. Identifizierter Materialparametersatz.

c_1 [MPa]	c_2 [MPa]	γ_1 [MPa]	γ_2 [MPa]	$\varkappa_1$ [1/MPa]	$\varkappa_2$ [1/MPa]
1343	15900	-130,3	237,7	0,003959	0,004524

q_1 [-]	q_2 [-]	β_1 [-]	β_2 [-]
1,173	0,7300	0,1723	0,7233

Die Ergebnisse der numerischen Simulation mit dem identifizierten Parametersatz sind in Bild 6.8 dargestellt. Der Effekt, dass die Schubspannungen bei zyklisch inkrementeller Belastung kleiner bleiben als bei einsinniger Belastung, wird vom Materialmodell erfasst. Das simulierte Materialverhalten ist in ähnlicher Weise wie im Experiment durch einen stetigen Übergang vom elastischen zum plastischen Fließverhalten gekennzeichnet.

Obwohl die Messdaten für die zyklischen Versuche mit $\Delta^{-}\gamma_a^k = 0,05$, $\Delta^{-}\gamma_a^k = 0,16$ und $\Delta^{-}\gamma_a^k = 0,23$ sowie für den einsinnigen Versuch bei der Parameteridentifikation nicht berücksichtigt wurden, ist deren numerische Simulation mit akzeptabler Genauigkeit möglich. Sowohl im Experiment als auch bei der Simulation nehmen die Spannungsmaxima für $\Delta^{-}\gamma_a^k = 0,20$ und $\Delta^{-}\gamma_a^k = 0,23$ im Laufe der Verformung ab.

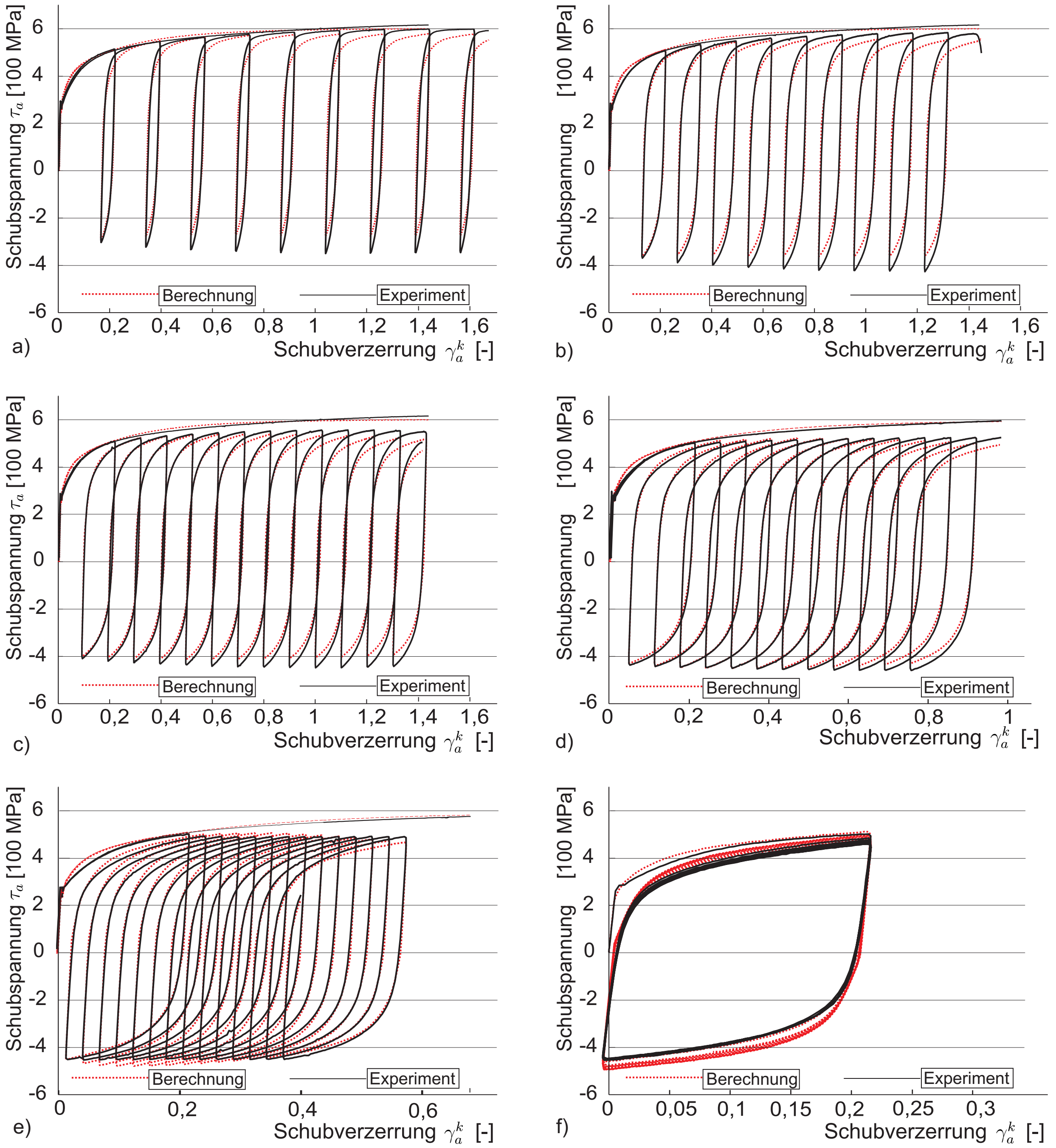

Figure 6.8. Measurements and simulation results with different back shear strain step size at the same forward shear strain step size.
Bild 6.8. Messdaten und Berechnungsergebnisse für unterschiedliche Rückverformungsschrittweiten bei gleicher positiver Schubverzerrungsschrittweite.

6. Diskussion und Schlussfolgerungen

Für den Stahl 42CrMo4 N wurde für einen Werkstoffzustand und unter weitgehend konstanten Versuchsbedingungen der Einfluss von Rückverformungsanteilen im Belastungspfad und der akkumulierten Schubverzerrung auf die Fließspannung untersucht. In Abhängigkeit von der negativen Schubverzerrungsschrittweite $\Delta^{-}\gamma_a^k$ konnte an den experimentellen Fließkurven zyklische Ver- oder Entfestigung beobachtet werden. Der in diesem Artikel eingeführte Ansatz lässt eine Kombination aus isotroper Ver- und Entfestigung zu, wobei lediglich der akkumulierte Umformgrad s die Größe der isotropen Verfestigung (bzw. Entfestigung) bestimmt: $R = R(s)$. Der untersuchte Stahl weist einen stark ausgeprägten Bauschinger-Effekt auf. Dieser Effekt wird im Allgemeinen mit der Bildung von Rückspannungen im plastisch verformten Material begründet, die bei der Umkehr der Belastungsrichtung die Bewegung der Versetzungen unterstützten. In diesem Artikel werden die Rückspannungen auf Basis einer mehrfachen multiplikativen Zerlegung des Deformationsgradienten $\mathbf{F}$ erfasst.

Das Fließverhalten metallischer Werkstoffe wird von der Wechselwirkung entstehender Versetzungen mit Hindernissen bestimmt. Für die Ver- und Entfestigung metallischer Werkstoffe mit unterschiedlichem Gleitcharakter wird je nach Belastungsbedingungen die Ausbildung unterschiedlicher Versetzungsstrukturen angegeben [**12**]. Die zyklische Entfestigung eines plastisch vorverformten, unlegierten Stahls wird mit Erholungsvorgängen durch Bildung von Versetzungsstrukturen geringer Energie bzw. gegenseitiger Auslöschung begründet. Dies Äußert sich in der Verringerung der Versetzungsdichte in den vorher gebildeten Versetzungszellen, der Abnahme der Breite der Versetzungszellwände und der Bildung gleichmäßiger Zellen [**19**]. Erholungsvorgänge werden durch die zyklische Verformung begünstigt [**19**].

Die in diesem Beitrag verwendeten zyklisch inkrementellen Belastungen liegen zwischen einsinniger und zyklischer Verformung mit geschlossenem Verformungspfad. Die einsinnige Verformung führt zur Bildung von Versetzungszellen mit breiten Zellwänden und hoher Versetzungsdichte im Zellinneren. Mit zunehmendem Anteil an Rückverformung bzw. Walkarbeit im Verformungspfad entstehen Versetzungszellen mit schmalen Zellwänden und versetzungsarmem Innerem [**13**]. Anhand der experimentellen Schubfließkurven wurde mit zunehmender Rückverformungsschrittweite der zyklischen Verformungspfade der Übergang von zyklischer Verfestigung zu zyklischer Entfestigung beobachtet. Bei Rückverformungsschrittweiten kleiner als 0,2 trat zyklische Verfestigung auf, die Rückverformungsschrittweite $\Delta^{-}\gamma_a^k = 0,20$ ergab nahezu gleich bleibende Spannungsmaxima während der geschlossene Verformungspfad mit $\Delta^{-}\gamma_a^k = 0,23$ zu zyklischer Entfestigung führte. Eine adäquate Erfassung dieses Verhaltens bei der numerischen Simulation stellt ein besonders kompliziertes Problem dar. Dabei kann der für Metallplastizität übliche Ansatz $R = R(s)$ als zu restriktiv erscheinen. Bei der Simulation der Materialantwort werden die Spannungsmaxima für kleine Rückverformungsschritte unterschätzt (siehe Bild 6.8a,b), für große dagegen leicht überschätzt (siehe Bild 6.8e,f). Obwohl die Torsionsversuche unter komplexen Verformungsbedingungen durchgeführt wurden, werden alle Messergebnisse anhand des Materialmodells mit guter Näherung abgebildet. Das in diesem Artikel präsentierte Materialmodell und die entsprechende Methodik der Parameteridentifikation lassen sich auf andere Klassen der metallischen Werkstoffe (z.B. Aluminiumlegierungen) direkt übertragen.

Danksagung

Die Autoren danken der DFG für die Förderung im Rahmen des Sonderforschungsbereiches SFB 692.

Literaturverzeichnis

[1] P. Groche, D. Fritsche, E. A. Tekkaya, J. M. Allwood, G. Hirt, R. Neugebauer, Incremental Bulk Metal Forming. Annals of the CIRP 2007, 56, 635-656.

[2] F. Hahn, Untersuchung des zyklisch plastischen Werkstoffverhaltens unter umformnahen Bedingungen. Ph.D. Thesis, TU Chemnitz, Germany, 2003.

[3] A. V. Shutov, R. Kreißig, Finite strain viscoplasticity with nonlinear kinematic hardening: Phenomenological modeling and time integration. Comput. Methods Appl. Mech. Engrg. 2008, 197, 2015-2029.

[4] A. Shutov, K. Hockauf, T. Halle, R. Kreißig, L.W. Meyer, Experimentelle und phänomenologische Beschreibung des mechanischen Verhaltens der Aluminiumlegierung EN AW-7075 nach großer plastischer Vorverformung. Materialwissenschaft und Werkstofftechnik 2009, 40, 7, 551-558.

[5] M.W, Brown, Torsional stresses in tubular specimens. Journal of strain analysis 1978, 13, 23-28.

[6] P. Haasen, Physikalische Metallkunde. 3. Auflage, Springer-Verlag Berlin Heidelberg New York, 1994.

[7] B. Gardey, S. Bouvier, V. Richard, B. Bacroix, Texture and dislocation structures observation in a dual-phase steel under strain-path changes at large deformation. Materials Science and Engineering 2005 A 400-401, 136-141.

[8] N. Hansen, X. Huang, Microstructure and flow stress of polycrystals and single crystals. Acta mater. 1998, 46, 1827-1836.

[9] B. Peeters, M. Seefeldt, C. Teodosiu, S.R. Kalidindi, P. Van Houtte, E. Aernoudt, Work-hardening/softening behaviour of b.c.c. polycrystals during changing strain paths: I. an integrated model based on substructure and texture evolution, and its prediction of the stress-strain behaviour of an IF steel during two-stage strain paths. Acta mater. 2001, 49, 1607-1619.

[10] H. Mughrabi, The effect of geometrically necessary dislocations on the flow stress of deformed crystals containing a heterogeneous dislocation distribution. Materials Science and Engineering 2001, A319-321, 139-143.

[11] L.W. Meyer, C. Kuprin, A. Shutov, Experimental yield point determination in metals after large plastic strains. Proceedings of 3rd Forming Technology Forum, Institute of Virtual Manufacturing, ETH Zurich Switzerland 2009, S. 71-76.

[12] H.-J. Christ, Wechselverformung von Metallen. Springer-Verlag Berlin Heidelberg New York, 1991.

[13] L. W. Meyer, C. Kuprin, G. Fritsche, F. Hahn, Evolution of microstrains at cyclic incremental deformation of steel 42CrMo4. Materials Science Forum 2006, 524-525, 925-930.

[14] M. Reiner, Rheologie, Fachbuchverlag und Carl Hanser Verlag, Leipzig und München, 1968.

[15] P. Haupt, Continuum Mechanics and Theory of Materials, 2nd edition, 2001.

[16] A. Lion, Constitutive modelling in finite thermoviscoplasticity: a physical approach based on nonlinear rheological elements. Int. J. Plast. 2000, 16, 469 - 494.

[17] D. Helm, Formgedächtnislegierungen, experimentelle Untersuchung, phänomenologische Modellierung und numerische Simulation der thermomechanischen Materialeigenschaften. Ph.D. Thesis, Universität Kassel, Germany, 2001.

[18] A. V. Shutov, R. Kreißig, Geometric integrators for multiplicative viscoplasticity: analysis of error accumulation. Comput. Methods Appl. Mech. Engrg. 2010, 199, 700-711.

[19] H.-F. Chai, C. Laird, Mechanisms of cyclic softening and cyclic creep in low carbon steel, Materials Science and Engineering 1987, 93, 159-174.

KAPITEL 7

On the simulation of plastic forming under consideration of thermal effects

Zur Simulation plastischer Umformvorgänge unter Berücksichtigung thermischer Effekte

A. V. Shutov[1], J. Ihlemann.
Chemnitz University of Technology, Str. d. Nationen 62, D-09111 Chemnitz, Germany

Abstract: *A new model of finite strain thermo-viscoplasticity is constructed. The model takes a combined nonlinear isotropic-kinematic hardening into account in a thermodynamically consistent manner. The yield stress and some of the hardening parameters are temperature dependent. The equation of the heat conduction is obtained directly using the energy balance. In particular, the thermoelastic effect and the mechanical dissipation are obtained in a natural way. Unlike the classical Taylor-Quinney rule, which yields in the case of a strong kinematic hardening inconsistent simulation results, the developed model enables physically reasonable computations. In order to capture the energy storage associated with the inelastic deformation more precisely, an additional component of the free energy - the so-called detached free energy - is introduced. Using this constitutive assumption, a better fitting of the model prediction concerning the real temperature evolution can be achieved.*
Keywords: thermo-plasticity; viscoplasticity; large strains; kinematic hardening; detached free energy

Kurzfassung: *Ein neues Modell der Thermoviskoplastizität bei finiten Deformationen wurde konstruiert. Mit dem Modell wird eine kombinierte nichtlineare isotrop-kinematische Verfestigung auf eine thermodynamisch konsistente Weise berücksichtigt. Die Fließspannung und einige der Verfestigungsparameter sind temperaturabhängig. Die Wärmeleitungsgleichung wurde direkt aus der Energiebilanz abgeleitet. Dabei wurden der thermoelastische Effekt und die mechanische Dissipation auf einem natürlichen Wege erhalten. Im Gegensatz zum klassischen Taylor-Quinney-Ansatz, der bei großer kinematischer Verfestigung auf inkonsistente Simulationsergebnisse führt, werden mit dem entwickelten Materialmodell physikalisch sinnvolle Berechnungen ermöglicht. Mit dem Ziel, die Energiespeicherung infolge inelastischer Vorgänge noch genauer zu erfassen, wurde eine zusätzliche Komponente der freien Energie eingeführt - die sogenannte abgetrennte freie Energie. Mit dieser konstitutiven Annahme*

---

[1] Corresponding author. alexey.v.shutov@gmail.com
web: http://sites.google.com/site/materialmodeling

This chapter is reproduced from the paper: A. V. Shutov, J. Ihlemann. On the simulation of plastic forming under consideration of thermal effects. Materialwissenschaft und Werkstofftecnhik. 2011. (42)7, 632-638. Copyright WILEY-VCH Verlag GmbH. Reproduced with permission.

kann eine bessere Anpassung der Modelvorhersage bezüglich der tatsächlichen Temperaturentwicklung erreicht werden.

Schlüsselworte: Thermoplastizität; Viskoplstizität; große Deformationen; kinematische Verfestigung; abgetrennte freie Energie

1. Introduction

In this paper we consider a phenomenological modelling of thermoplastic behaviour of metallic materials in the large strain context. Such type of material modelling is required, for instance, for the simulation of metal forming processes accompanied by non-uniform temperature distribution. For the general introduction to the material modelling at large strains see, for example, [**1**]. One of the most popular approaches to thermoplasticity is presented in the paper by Simo and Miehe [**2**]. The current study, although, is essentially based on the work of Lion [**3**]. Following Lion, we implement a multiplicative split of the deformation gradient into thermal and mechanical parts as well as a double multiplicative split of the mechanical part in order to take a nonlinear kinematic hardening into account. Some other models with nonlinear kinematic hardening, which are based on the double multiplicative decomposition, can be found in [**4, 5, 6, 7, 8**]. Alternative approaches to the finite strain thermoplasticity with nonlinear kinematic hardening can be found in [**1, 9**].

The classical method used to derive the differential equation for the temperature evolution is based on the empirical Taylor-Quinney rule [**10**]. Within this approach, it is assumed that a certain constant ratio of the plastic work is dissipated as heat. Although this approach is simple and easy to implement, it is, in general, *not thermodynamically admissible* [**11**]. In this work we implement a consistent approach which results in a natural way form the consideration of the energy balance [**11, 12, 13, 14**]. The 1st law of thermodynamics provides the connection between the heat production due to the internal dissipation and the energy storage at the microstructural level (e.g. energy storage due to lattice defects like dislocations, disclinations, grain boundaries etc.). The experimental data on the heating of samples in a series of experiments can be evaluated to draw additional information concerning the energy storage mechanisms associated to inelastic deformations. Such information can not be derived from the stress response of the material observed at constant temperature [**15**].

In this paper we present a straight-forward generalization of the material model presented in [**7**]. Note that the material parameters of the resulting thermo-mechanical model (like the yield stress, viscosity etc.) should be considered as functions of the temperature. Thus, the model of thermo-viscoplasticity contains more material parameters than its thermostatic counterpart, which complicates the parameter identification. In order to make a reliable parameter identification possible, we assume that some parameters are temperature independent. On the other hand, the material modelling considered in the current study is open for further developments. In particular, the distortional hardening can be taken into account similar as it was done in [**16**].

A coordinate-free tensor formalism is used in this work [**17, 18**]. The paper is organized as follows. First, a new material model of finite strain viscoplasticity is formulated, which takes thermal effects into account. Next, the numerical implementation of this model is

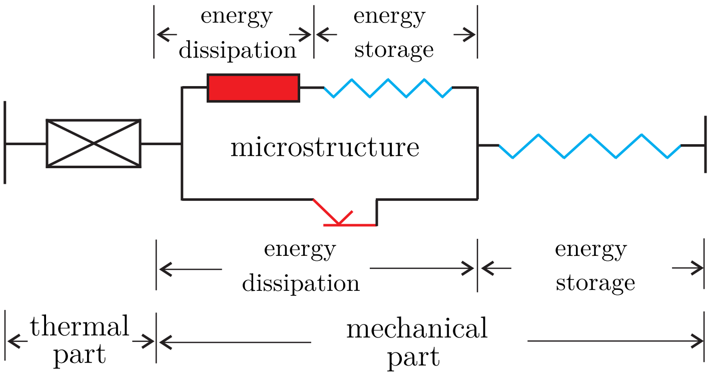

Figure 7.1. Rheological analogy: The basic model consists of an idealized element of thermal expansion and the modified Schwedoff-body (cf. [**3**]).
Bild 7.1. Rheologische Analogie: Das zugrunde gelegte Modell besteht aus einem idealisierten thermischen Element und dem modifizierten Schwedoff-Körper (vgl. [**3**]).

discussed. Finally, the model is validated basing on the simulation results for homogeneous experiments. Both isothermal and non-isothermal conditions are considered.

2. Material model of finite strain thermo-viscoplasticity

2.1. Description of kinematics. The rheological motivation for the material model is presented in Figure 7.1. Following Lion [**3**], it is based on the modified Schwedoff-body connected in series with an idealized element of thermal expansion.

Let $\mathbf{F}$ be the deformation gradient. We decompose it into a mechanical part $\mathbf{F}_{\mathrm{M}}$ and a thermal part $\mathbf{F}_{\theta}$ (cf. for example [**19, 3**])

$$\mathbf{F} = \mathbf{F}_{\mathrm{M}}\mathbf{F}_{\theta}, \quad \mathbf{F}_{\theta} = (\varphi(\theta))^{1/3}\mathbf{1}.$$

Thus, the thermal expansion is assumed to be isotropic, and one obtains the ratio for the thermal volume change in the form: $\det(\mathbf{F}_{\theta}) = \varphi(\theta)$. Let ρ_{R} and $\rho_{\theta} = \rho_{\mathrm{R}}/\varphi(\theta)$ represent the mass density w.r.t. the reference configuration and the thermomechanical intermediate configuration, respectively. To be definite, we put $\varphi(\theta) = 1 + \alpha\ (\theta - \theta_0)$, where θ and θ_0 are the current and the reference temperatures, respectively. The material parameter α stands for the coefficient of the thermal expansion such that $\varphi' = \frac{d\varphi(\theta)}{d\theta} = \alpha = const \geq 0$. Next, we consider the well-known decomposition of the mechanical part into an inelastic part $\mathbf{F}_{\mathrm{i}}$ and an elastic part $\hat{\mathbf{F}}_{\mathrm{e}}$

$$\mathbf{F}_{\mathrm{M}} = \hat{\mathbf{F}}_{\mathrm{e}}\mathbf{F}_{\mathrm{i}}.$$

Following Lion [**3**], in order to capture a nonlinear kinematic hardening we decompose the inelastic part into a dissipative part $\mathbf{F}_{\mathrm{ii}}$ and a conservative part $\check{\mathbf{F}}_{\mathrm{ie}}$

$$\mathbf{F}_{\mathrm{i}} = \check{\mathbf{F}}_{\mathrm{ie}}\mathbf{F}_{\mathrm{ii}}.$$

The multiplicative decompositions are summarized using the commutative diagram in Figure 7.2.

In what follows we will need the tensors of the right Cauchy-Green type:

$$\mathbf{C} := \mathbf{F}^{\mathrm{T}}\mathbf{F}, \ \overset{\theta}{\mathbf{C}}_{\mathrm{M}} := \mathbf{F}_{\mathrm{M}}^{\mathrm{T}}\mathbf{F}_{\mathrm{M}}, \ \hat{\mathbf{C}}_{\mathrm{e}} := \hat{\mathbf{F}}_{\mathrm{e}}^{\mathrm{T}}\hat{\mathbf{F}}_{\mathrm{e}}, \ \check{\mathbf{C}}_{\mathrm{ie}} := \check{\mathbf{F}}_{\mathrm{ie}}^{\mathrm{T}}\check{\mathbf{F}}_{\mathrm{ie}}.$$

$$\begin{tikzcd}
 & & \check{\mathcal{K}} \arrow[d, "\check{\mathbf{F}}_{\mathrm{ie}}"] & \\
\tilde{\mathcal{K}} \arrow[r, "\mathbf{F}_\theta"] \arrow[rrr, bend right=40, "\mathbf{F}"'] & \mathcal{K}^\theta \arrow[ur, "\mathbf{F}_{\mathrm{ii}}"] \arrow[r, "\mathbf{F}_{\mathrm{i}}"] \arrow[rr, bend right, "\mathbf{F}_{\mathrm{M}}"'] & \hat{\mathcal{K}} \arrow[r, "\hat{\mathbf{F}}_{\mathrm{e}}"] & \mathcal{K}
\end{tikzcd}$$

Figure 7.2. Summary of the multiplicative decompositions of the deformation gradient with the help of a commutative diagram (cf. [**3**]).
Bild 7.2 Zusammenfassung von multiplikativen Zerlegungen des Deformationsgradienten in Form eines kommutativen Diagramms (vgl. [**3**]).

Basing on these definitions, we introduce strain-like tensors $\mathbf{E}$, $\hat{\mathbf{\Gamma}}_{\mathrm{e}}$, $\check{\mathbf{\Gamma}}_{\mathrm{ie}}$ of Green type which capture the total deformation, the elastic deformation and the elastic deformation of the microstructure, respectively:

$$\mathbf{E} := \frac{1}{2}(\mathbf{C} - \mathbf{1}),\ \hat{\mathbf{\Gamma}}_{\mathrm{e}} := \frac{1}{2}(\hat{\mathbf{C}}_{\mathrm{e}} - \mathbf{1}),\ \check{\mathbf{\Gamma}}_{\mathrm{ie}} := \frac{1}{2}(\check{\mathbf{C}}_{\mathrm{ie}} - \mathbf{1}).$$

In order to capture the rate of the plastic flow as well as the rate of the flow on the microstructural level we define the inelastic strain rate tensors $\hat{\mathbf{D}}_{\mathrm{i}}$ and $\hat{\mathbf{D}}_{\mathrm{ii}}$:

$$\hat{\mathbf{D}}_{\mathrm{i}} := \mathrm{sym}(\mathbf{L}_{\mathrm{i}}),\ \mathbf{L}_{\mathrm{i}} := \dot{\mathbf{F}}_{\mathrm{i}}\mathbf{F}_{\mathrm{i}}^{-1},\ \hat{\mathbf{D}}_{\mathrm{ii}} := \mathrm{sym}(\mathbf{L}_{\mathrm{ii}}),\ \mathbf{L}_{\mathrm{ii}} := \dot{\mathbf{F}}_{\mathrm{ii}}\mathbf{F}_{\mathrm{ii}}^{-1},$$

where the dot stands for the material time derivative.[2] Let us denote the inelastic arc-length (Odqvist parameter) by s. Its dissipative part is denoted by s_{d}, such that $s_{\mathrm{e}} = s - s_{\mathrm{d}}$ controls the energy storage due to the isotropic hardening (see Subsection 2.3).

2.2. Description of stresses. Let $\mathbf{T}$ be the Cauchy stress tensor. The Kirchhoff stress $\mathbf{S}$ and a weighted stress $\mathbf{S}_{\mathrm{M}}$ are then defined through

$$\mathbf{S} := \det(\mathbf{F})\mathbf{T},\ \mathbf{S}_{\mathrm{M}} := \det(\mathbf{F}_{\mathrm{M}})\mathbf{T}.$$

The elastic contravariant pull-back of the weighted tensor to the stress free intermediate configuration is given by

$$\hat{\mathbf{S}}_{\mathrm{M}} := (\hat{\mathbf{F}}_{\mathrm{e}}^{-\mathrm{T}})^{*}\mathbf{S}_{\mathrm{M}},\ \text{where } (\mathbf{M}^{-\mathrm{T}})^{*}(\cdot) = \mathbf{M}^{-1}(\cdot)\mathbf{M}^{-\mathrm{T}} \text{ for all } \mathbf{M}.$$

Let $\tilde{\mathbf{T}}$ be the second Piola-Kirchhoff stress tensor. The Kirchhoff stress tensor on the thermomechanical intermediate configuration is defined through

$$\overset{\theta}{\mathbf{T}}_{\mathrm{M}} := (\hat{\mathbf{F}}_{\mathrm{i}}^{-\mathrm{T}})^{*}\hat{\mathbf{S}}_{\mathrm{M}}.$$

Let $\check{\mathbf{X}}$ be the backstress tensor which is conjugate to the strain measure $\mathbf{F}_{\mathrm{i}}^{-\mathrm{T}}\mathbf{E}\mathbf{F}_{\mathrm{i}}^{-1}$. The contravariant push-forward to the stress free configuration yields

$$\hat{\mathbf{X}} := (\check{\mathbf{F}}_{\mathrm{ie}}^{-\mathrm{T}})_{*}\check{\mathbf{X}},\ \text{where } (\mathbf{M}^{-\mathrm{T}})_{*}(\cdot) = \mathbf{M}(\cdot)\mathbf{M}^{\mathrm{T}} \text{ for all } \mathbf{M}.$$

---

[2] In this paper we prefer to use the symmetrised tensors $\hat{\mathbf{D}}_{\mathrm{i}}$ and $\hat{\mathbf{D}}_{\mathrm{ii}}$ rather than the inelastic deformation rates $\mathbf{L}_{\mathrm{i}}$ and $\mathbf{L}_{\mathrm{ii}}$. Thus, the inelastic spins do not enter the formulation of the flow rule, which makes the constitutive equations less complicated. Note that the same approach was adopted in the thermostatic case [**7**].

A detailed motivation for these transformations can be found in [**7**]: the relations can be derived from the concept of dual variables proposed by Haupt and Tsakmakis. By $\hat{\mathbf{\Sigma}}$ and $\check{\mathbf{\Xi}}$ we denote the driving forces for the inelastic flow and the flow on the microstructural level, respectively (cf. [**7**]):

$$\hat{\mathbf{\Sigma}} := \hat{\mathbf{C}}_{\mathrm{e}}\hat{\mathbf{S}}_{\mathrm{M}} - \hat{\mathbf{X}}, \ \check{\mathbf{\Xi}} := \check{\mathbf{C}}_{\mathrm{ie}}\check{\mathbf{X}}.$$

2.3. Free energy and potential relations for stresses. We assume an additive decomposition of the free energy density ψ in the form

$$\psi = \psi_{\mathrm{el}}(\hat{\mathbf{\Gamma}}_{\mathrm{e}}) + \psi_{\mathrm{kin}}(\check{\mathbf{\Gamma}}_{\mathrm{ie}}) + \psi_{\mathrm{iso}}(s_{\mathrm{e}}) + \psi_{\mathrm{deta}} + \psi_{\theta}(\theta). \tag{7.1}$$

Here, $\psi_{\mathrm{el}}(\hat{\mathbf{\Gamma}}_{\mathrm{e}})$ is an isotropic function which captures the energy storage due to macroscopic elastic deformations. The inelastic part $\psi_{\mathrm{kin}}(\check{\mathbf{\Gamma}}_{\mathrm{ie}}) + \psi_{\mathrm{iso}}(s_{\mathrm{e}}) + \psi_{\mathrm{deta}}$ represents the energy of crystal lattice defects. More precisely, isotropic function $\psi_{\mathrm{kin}}(\check{\mathbf{\Gamma}}_{\mathrm{ie}})$ corresponds to the energy storage associated with the kinematic hardening; $\psi_{\mathrm{iso}}(s_{\mathrm{e}})$ captures the energy storage associated with the isotropic hardening; and ψ_{deta} stands for the remaining part of the energy storage on the microstructural level, which is not directly connected to any hardening effects ("detached" energy). Finally, $\psi_{\theta}(\theta)$ represents the heat capacity of the material. To be definite, we use the following concrete assumptions for the free energy (cf. [**4, 6, 7**])

$$\rho_{\mathrm{R}}\psi_{\mathrm{el}}(\hat{\mathbf{\Gamma}}_{\mathrm{e}}) = \frac{k}{2}\Big(\ln\sqrt{\det\hat{\mathbf{C}}_{\mathrm{e}}}\Big)^2 + \frac{\mu}{2}\Big(\mathrm{tr}\overline{\hat{\mathbf{C}}_{\mathrm{e}}} - 3\Big),$$

$$\rho_{\mathrm{R}}\psi_{\mathrm{kin}}(\check{\mathbf{\Gamma}}_{\mathrm{ie}}) = \frac{c}{4}\Big(\mathrm{tr}\overline{\check{\mathbf{C}}_{\mathrm{ie}}} - 3\Big),$$

$$\rho_{\mathrm{R}}\psi_{\mathrm{iso}}(s_{\mathrm{e}}) = \frac{\gamma}{2}\ (s_{\mathrm{e}})^2,$$

$$\rho_{\mathrm{R}}\psi_{\theta}(\theta) = -c_{\theta 0}(\theta\ln(\theta/\theta_0) - (\theta - \theta_0)),$$

where $k > 0$, $\mu > 0$, $c > 0$, $\gamma \geq 0$, and $c_{\theta 0} > 0$ are material parameters. The evolution of the detached free energy ψ_{deta} will be discussed in Section 2.5. Now we formally postulate the following potential relations for stresses, backstresses, isotropic hardening R, and entropy ζ (cf. [**3, 7**]):

$$\hat{\mathbf{S}}_{\mathrm{M}} = \rho_{\theta}\frac{\partial\psi_{\mathrm{el}}(\hat{\mathbf{\Gamma}}_{\mathrm{e}})}{\partial\hat{\mathbf{\Gamma}}_{\mathrm{e}}}, \tag{7.2}$$

$$\check{\mathbf{X}} = \rho_{\theta}\frac{\partial\psi_{\mathrm{kin}}(\check{\mathbf{\Gamma}}_{\mathrm{ie}})}{\partial\check{\mathbf{\Gamma}}_{\mathrm{ie}}}, \tag{7.3}$$

$$R = \rho_{\theta}\frac{\partial\psi_{\mathrm{iso}}(s_{\mathrm{e}})}{\partial s_{\mathrm{e}}}, \tag{7.4}$$

$$\zeta = \frac{\varphi'}{3\rho_{\mathrm{R}}}\overset{\theta}{\mathbf{T}}_{\mathrm{M}} : \overset{\theta}{\mathbf{C}}_{\mathrm{M}} - \frac{\partial\psi_{\theta}(\theta)}{\partial\theta}. \tag{7.5}$$

The relations (7.2)-(7.5) in combination with the evolution equations from the next subsection are sufficient for the thermodynamic consistency of the material model. Note that the detached energy ψ_{deta} has no impact on the stresses or entropy, but its evolution has to be taken into account in order to build a proper energy balance and the equation of heat conduction.

2.4. Clausius-Duhem inequality. Let us consider the Clausius-Duhem inequality in the material representation (see, for example, [**1**])

$$\frac{1}{\rho_{\mathrm{R}}}\tilde{\mathbf{T}} : \dot{\mathbf{E}} - \dot{\psi} - \dot{\theta}\zeta - \frac{1}{\rho_{\mathrm{R}}\theta}\mathbf{q}_{\mathrm{R}} \cdot \mathbf{g}_{\mathrm{R}} \geq 0, \tag{7.6}$$

where $\mathbf{g}_{\mathrm{R}}$ is the material temperature gradient, $\mathbf{q}_{\mathrm{R}}$ is the Piola-Kirchhoff heat flux vector, and $\mathbf{q}_{\mathrm{R}} \cdot \mathbf{g}_{\mathrm{R}}$ stands for their scalar product. Following the standard procedure (cf. [**20**]), we assume that the inequalities $\frac{1}{\rho_{\mathrm{R}}}\tilde{\mathbf{T}} : \dot{\mathbf{E}} - \dot{\psi} - \dot{\theta}\zeta \geq 0$ and $\frac{1}{\rho_{\mathrm{R}}\theta}\mathbf{q}_{\mathrm{R}} \cdot \mathbf{g}_{\mathrm{R}} \leq 0$ must hold as well. The second inequality can be satisfied identically, for instance, if Fourier's law of heat conduction is adopted. In order to validate the first inequality we note that the stress power can be decomposed into a thermal part and a mechanical part, as follows (see [**3**], eq. (2.3)):

$$\frac{1}{\rho_{\mathrm{R}}}\tilde{\mathbf{T}} : \dot{\mathbf{E}} = \frac{1}{\rho_{\theta}}\Big(\frac{\varphi'}{3\varphi}\dot{\theta}\overset{\theta}{\mathbf{T}}_{\mathrm{M}} : \overset{\theta}{\mathbf{C}}_{\mathrm{M}} + \overset{\theta}{\mathbf{T}}_{\mathrm{M}} : \frac{1}{2}\overset{\dot{\theta}}{\mathbf{C}}_{\mathrm{M}}\Big).$$

After some computations (similar computations can be found, for instance, in [**3, 7**]), we obtain the first inequality in the form as follows:

$$\rho_{\theta}\delta_{\mathrm{i}} = \hat{\mathbf{\Sigma}} : \hat{\mathbf{D}}_{\mathrm{i}} - R\ \dot{s} +\ \check{\mathbf{\Xi}} : \check{\mathbf{D}}_{\mathrm{ii}} +\ R\ \dot{s}_{\mathrm{d}} - \rho_{\theta}\dot{\psi}_{\mathrm{deta}} \geq 0. \tag{7.7}$$

Note that the reduced inequality takes the from which is similar to the thermostatic case [**7**].[3]

2.5. Flow rule. Let the yield function (overstress) be defined by

$$f := \|\hat{\mathbf{\Sigma}}^{\mathrm{D}}\| - \sqrt{\frac{2}{3}}\Big[K(\theta) + R\Big],$$

where $K(\theta) \geq 0$ is the temperature dependent yield stress, $\mathbf{A}^{\mathrm{D}} := \mathbf{A} - \frac{1}{3}\mathrm{tr}(\mathbf{A})\mathbf{1}$, $\|\mathbf{A}\| := \sqrt{\mathbf{A} : \mathbf{A}}$. We postulate the evolution equations such that the reduced Clausius-Duhem inequality (7.7) is identically satisfied

$$\hat{\mathbf{D}}_{\mathrm{i}} = \lambda_{\mathrm{i}}\frac{\hat{\mathbf{\Sigma}}^{\mathrm{D}}}{\|\hat{\mathbf{\Sigma}}^{\mathrm{D}}\|},\ \check{\mathbf{D}}_{\mathrm{ii}} = \lambda_{\mathrm{i}}\ \varkappa(\theta)\ \check{\mathbf{\Xi}}^{\mathrm{D}},\ \dot{s} = \sqrt{\frac{2}{3}}\lambda_{\mathrm{i}},\ \dot{s}_{\mathrm{d}} := \frac{\beta(\theta)}{\gamma}\dot{s}R, \tag{7.8}$$

where $\varkappa(\theta) \geq 0$, $\beta(\theta) \geq 0$ are temperature dependent material functions controlling the saturation of the kinematic and isotropic hardening, respectively. The inelastic multiplier λ_{i} is determined using the Perzyna rule of viscoplasticity

$$\lambda_{\mathrm{i}} = \frac{1}{\eta(\theta)}\Big\langle\frac{1}{k_0}f\Big\rangle^{m(\theta)},\ \langle x\rangle := \max(x, 0).$$

Here, $\eta(\theta) \geq 0$ stands for the viscosity; $m(\theta) \geq 1$ is the Perzyna exponent; $k_0 > 0$ is used to obtain a dimensionless term (not a material parameter). Suppose that the evolution of the detached energy is connected to the inelastic dissipation process:

$$\rho_{\theta}\dot{\psi}_{\mathrm{deta}} = \Phi_{\mathrm{i}}\Big(\hat{\mathbf{\Sigma}} : \hat{\mathbf{D}}_{\mathrm{i}} - R\ \dot{s}\Big) + \Phi_{\mathrm{kin}}\ \check{\mathbf{\Xi}} : \check{\mathbf{D}}_{\mathrm{ii}} + \Phi_{\mathrm{iso}}\ R\ \dot{s}_{\mathrm{d}},$$

---

[3] The detached free energy ψ_{deta} does not affect the stress response in a thermostatic case. Therefore, we may put $\psi_{\mathrm{deta}} = 0$ in (7.7), thus restoring the dissipation inequality from [**7**].

where $0 \leq \Phi_{\mathrm{i}}, \Phi_{\mathrm{kin}}, \Phi_{\mathrm{iso}} \leq 1$ are material parameters. Using this assumption we simplify the Clausius-Duhem inequality as follows:[4]

$$\rho_\theta \delta_{\mathrm{i}} = (1-\Phi_{\mathrm{i}})\Big(\hat{\mathbf{\Sigma}} : \hat{\mathbf{D}}_{\mathrm{i}} - R\ \dot{s}\Big) + (1-\Phi_{\mathrm{kin}})\check{\mathbf{\Xi}} : \check{\mathbf{D}}_{\mathrm{ii}} + (1-\Phi_{\mathrm{iso}})R\ \dot{s}_{\mathrm{d}} \geq 0. \tag{7.9}$$

It can be easily shown (cf. [**7**]) that each of the terms from the left-hand side is non-negative. Thus, the proposed material model is thermodynamically consistent. According to (7.8), the inelastic flow and the flow on the microstructural level are incompressible: $\det(\mathbf{F}_{\mathrm{i}}) = \det(\mathbf{F}_{\mathrm{ii}}) = 1$.

2.6. Equation of heat conduction. In order to derive the equation of heat conduction, we consider the local energy balance in the material representation (see [**1**]):

$$\theta\dot{\zeta} = \frac{1}{\rho_{\mathrm{R}}}\tilde{\mathbf{T}} : \dot{\mathbf{E}} - \dot{\psi} - \frac{1}{\rho_{\mathrm{R}}}\mathrm{Div}\mathbf{q}_{\mathrm{R}} + r - \zeta\dot{\theta},$$

where $\mathrm{Div}\mathbf{q}_{\mathrm{R}}$ is the material divergence of the heat flux; r stands for the local heat supply per unit mass. After some transformations we obtain the energy balance in the form $\theta\dot{\zeta} = \delta_{\mathrm{i}} - \frac{1}{\rho_{\mathrm{R}}}\mathrm{Div}\mathbf{q}_{\mathrm{R}} + r$, where the internal mechanical dissipation δ_{i} is defined by (7.7) or (7.9). Next, noting that $\overset{\theta}{\mathbf{T}}_{\mathrm{M}} : \overset{\theta}{\dot{\mathbf{C}}}_{\mathrm{M}} = 3\varphi^{-1}\ k\ \ln\Big(\sqrt{\det \overset{\theta}{\mathbf{C}}_{\mathrm{M}}}\Big)$ and differentiating (7.5) we obtain the time derivative of the entropy

$$\dot{\zeta} = \frac{\varphi' k}{2\rho_{\mathrm{R}}\varphi}\mathbf{C}^{-1} : \dot{\mathbf{C}} + \left(\frac{(\varphi')^2 k}{\rho_{\mathrm{R}}\varphi^2}\Big[\ln\varphi - \frac{1}{2}\ln(\det\mathbf{C}) - 1\Big] + \frac{c_{\theta 0}}{\rho_{\mathrm{R}}\theta}\right)\dot{\theta}.$$

Substituting this result into the energy balance we obtain the differential equation for the temperature evolution (equation of heat conduction)

$$c_\theta\dot{\theta} = -\frac{\varphi'\ k\ \theta}{2\rho_{\mathrm{R}}\varphi}\mathbf{C}^{-1} : \dot{\mathbf{C}} + \delta_{\mathrm{i}} - \frac{1}{\rho_{\mathrm{R}}}\mathrm{Div}\mathbf{q}_{\mathrm{R}} + r, \tag{7.10}$$

with

$$c_\theta = \frac{(\varphi')^2\ k\ \theta}{\rho_{\mathrm{R}}\varphi^2}\Big[\ln\varphi - \frac{1}{2}\ln(\det\mathbf{C}) - 1\Big] + \frac{c_{\theta 0}}{\rho_{\mathrm{R}}}.$$

The term $-\frac{\varphi'\ k\ \theta}{2\rho_{\mathrm{R}}\varphi}\mathbf{C}^{-1} : \dot{\mathbf{C}}$ in (7.10) is responsible for the thermoelastic effect, δ_{i} captures the heating due to the inelastic energy dissipation, and $-\frac{1}{\rho_{\mathrm{R}}}\mathrm{Div}\mathbf{q}_{\mathrm{R}} + r$ describes the heat conduction.

2.7. Dependence of the material functions on the temperature. For simplicity, suppose that the initial yield stress is a linear function of the temperature

$$K(\theta) = K_0 - K_1(\theta - \theta_0),\ K_0 > 0,\ K_1 > 0.$$

Moreover, the temperature dependent parameters of the Perzyna rule are assumed to be linear functions: $\eta(\theta) = \eta_0 + \eta_1(\theta - \theta_0)$, $m(\theta) = m_0 + m_1(\theta - \theta_0)$. Note that the saturated

---

[4] Note that a similar expression for the inelsatic dissipation was implemented in [**15**] for a simplified material model (without kinematic hardening) in order to achieve a better agreement with experimental results. In the current study, in contrast to [**15**], the correction factors $(1-\Phi_{\mathrm{i}})$, $(1-\Phi_{\mathrm{kin}})$, and $(1-\Phi_{\mathrm{iso}})$ are obtained due to the introduction of the detached energy ψ_{deta}.

value of the isotropic hardening at constant temperature equals $R_{\max} = \gamma/\beta$. Assuming that $R_{\max}$ is a linear function of the temperature, we obtain the following ansatz for β:

$$\beta(\theta) = \Big(\frac{1}{\beta_0} - \frac{1}{\beta_1}(\theta - \theta_0)\Big)^{-1}, \ \beta_0 > 0, \ \beta_1 > 0.$$

Note that the saturated value of the backstress is proportional to $1/\varkappa$ (at least for small strains). Moreover, we suppose that the relation between the saturated isotropic and kinematic hardening is temperature independent. Thus, we obtain for $\varkappa$

$$\varkappa(\theta) = \beta(\theta)\frac{\varkappa_0}{\beta_0}, \ \varkappa_0 \geq 0.$$

The material parameters K_0, β_0, and $\varkappa_0$ can be identified using a single experiment with a non-monotonic quasi-static loading at a reference temperature. The remaining parameters K_1 and β_1 can be determined from a series of quasi-static experiments at different constant temperatures. Finally, a series of experiments with different loading rates at different temperatures is required to determine the parameters of the Perzyna law.

2.8. Numerical implementation. Note that the flow rule (7.8) and the expression for the mechanical dissipation (7.7) are formulated with respect to some fictitious intermediate configurations. In order to simplify the numerical treatment of (7.8) and (7.10), these constitutive equations should be transformed to the reference configuration (cf. [**3**]). Toward that end, the pull-back transformations from the paper [**7**] can be implemented, thus leading to ordinary differential equations describing the evolution of the internal variables. The implemented numerical schemes preserve the incompressibility of the inelastic flow exactly.[5]

3. Simulation results and validation of the model

In this section we neglect the viscosity effects by putting $\eta(\theta) = 0$, $m(\theta) = 1$. The remaining material parameters are summarized in Table 7.1. An initial plastic isotropy is assumed.

Table 7.1. Material parameters used to validate the material model.
Tabelle 7.1. Materialparameter, die zur Validierung des Materialmodells herangezogen wurden.

k [MPa]	μ [MPa]	c [MPa]	γ [MPa]	K_0 [MPa]	K_1 [MPa/K]
73500	28200	677	294	58.5	0.13

β_0 [-]	β_1 [K]	$\varkappa_0$ [1/MPa]	α [1/K]	ρ_{R} [kg/mm^3]	$c_{\theta 0}$ [MPa/K]
3.6	1090	0.0325	$2.3 \cdot 10^{-5}$	$2.7 \cdot 10^{-6}$	2.43

---

[5] Using the example of a classical material model of multiplicative viscoplasticity, it was shown in [**21**] that the exact preservation of the inelastic incompressibility condition allows to avoid the accumulation of the numerical error. Thus, somewhat larger time steps can be used for the simulation of "long" processes.

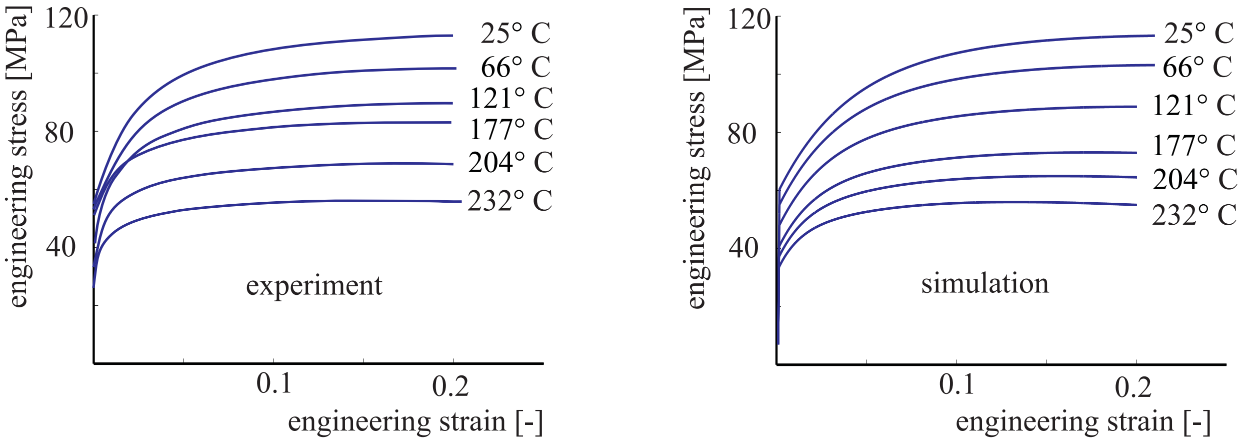

Figure 7.3. Experimental data concerning AA3003-H111 alloy according to Abedrabbo et al. [**22**] (left) and simulation results (right) for tension tests.
Bild 7.3. Messdaten für Al-Legierung AA3003-H111 nach Abedrabbo et al. [**22**] (links) und Simulationsergebnisse (rechts) von Zugversuchen.

3.1. Uniaxial tension at constant temperature. Let us consider a series of uniaxial tension tests performed at different temperatures. For simplicity, in this subsection we put $\alpha = 0$ [1/K] in order to neglect the thermal expansion of the sample. Since, for each test, the temperature is explicitly prescribed, the equation of heat conduction is not needed for the simulation. Instead, the known prescribed values of the temperature are used. In order to model the uniaxial tension, we suppose that the deformation gradient is described by $\mathbf{F} = (1+\varepsilon)\mathbf{e}_1 \otimes \mathbf{e}_1 + \alpha_{12}(\mathbf{e}_2 \otimes \mathbf{e}_2 + \mathbf{e}_3 \otimes \mathbf{e}_3)$, where ε is the prescribed engineering strain, $\alpha_{12} - 1$ is the unknown transverse strain. The parameter α_{12} is determined numerically using the condition that the stresses in the transverse direction are zero. Note that the ratio of the current cross-sectional area to the original one is given by $(\alpha_{12})^2$. Therefore, for a given Cauchy stress tensor $\mathbf{T}$, the engineering stress is computed according to $\sigma = (\alpha_{12})^2 \mathbf{T}_{11}$.

The experimental data for aluminum alloy AA3003-H111 [**22**] are presented along with the simulation results in Figure 7.3. As one can see, the temperature dependence of the hardening behaviour can be described by the model in a satisfactory manner. Moreover, for elevated temperatures a certain reduction of the critical strain is observed experimentally. This effect is reproduced by the material model. The stress maxima are captured well for all temperature levels except $\theta = 177°\mathrm{C}$. The discrepancy for $\theta = 177°\mathrm{C}$ is probably due to the scatter of the measurement results.

3.2. Incremental torsion with heat transfer. In this subsection we simulate an incremental loading of a thin-walled tube sample. Suppose that the initial temperature of the sample coincides with the surrounding temperature θ_0=293.15 K. The temperature evolution is obtained with the help of the heat conduction equation. In order to formulate this equation we suppose that the local heat flow is proportional to the temperature difference. Thus, we substitute in (7.10)

$$-\frac{1}{\rho_{\mathrm{R}}}\mathrm{Div}\mathbf{q}_{\mathrm{R}} + r = -w\ (\theta - \theta_0),\ \ w > 0.$$

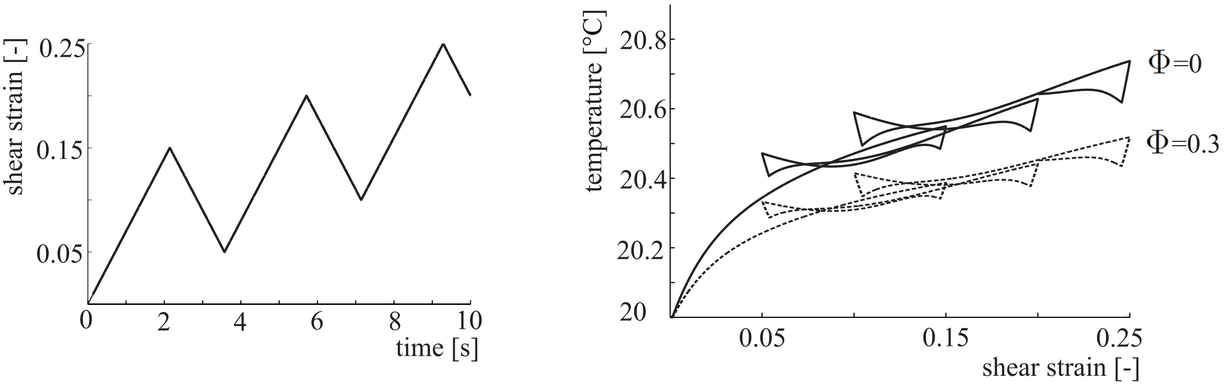

Figure 7.4. Prescribed loading program and temperature evolution for different values of material parameter Φ (cf. equation (7.11)).
Bild 7.4. Das vorgegebene Belastungsprogramm und der Temperaturverlauf in Abhängigkeit des Materialparameters Φ (vgl. Gleichung (7.11)).

In this subsection we use $w = 2500[(\text{MPa mm}^3)/(\text{K kg s})]$. For simplicity, we assume that the material parameters $\Phi_{\text{i}}, \Phi_{\text{kin}}, \Phi_{\text{iso}}$ are equal:

$$\Phi_{\text{i}} = \Phi_{\text{kin}} = \Phi_{\text{iso}} = \Phi. \tag{7.11}$$

Suppose that the deformation gradient is given by $\mathbf{F} = \alpha_1 \mathbf{e}_1 \otimes \mathbf{e}_1 + \gamma \alpha_1 \mathbf{e}_1 \otimes \mathbf{e}_2 + \mathbf{e}_2 \otimes \mathbf{e}_2 + \alpha_2 \mathbf{e}_3 \otimes \mathbf{e}_3$, where the shear strain γ is a known function of the time (see Figure 7.4 left). The quantities $\alpha_1 - 1$ and $\alpha_2 - 1$ stand for unknown strains in the hoop and radial directions, respectively (cf., for example, [**16**]). These parameters are identified numerically using the condition that the stresses in the hoop and radial directions are zero.

The simulated temperature evolution is presented in Figure 7.4 (right) for two different values of Φ. Note that the thermoelastic effect is negligible in the case of torsion. Therefore, the simulated temperature evolution represents the balance of two competing processes (cf. (7.10)): internal heating due to inelastic dissipation and the natural cooling of the sample. The overall temperature level is sensitive with respect to the parameter Φ. Therefore, this parameter can be determined experimentally, if the temperature evolution is measured.

4. Discussion and conclusion

A new phenomenological model of large strain thermo-viscoplasticity is constructed. The model is a generalization of the model presented in [**7**], which was formulated in a thermostatic case. Nonlinear isotropic and kinematic hardening effects are taken into account. Unlike the classical Taylor-Quinney rule, the proposed model is based directly on the 1st law of thermodynamics, and it is thermodynamically consistent.

A refined assumption for the energy storage is presented in the current study (cf. equation (7.1)). Note that the detached free energy component ψ_{deta}, under thermostatic conditions, has no impact on the hardening behaviour of the material. This energy component thus can not be identified basing on the thermostatic experimental observations of the stress-strain response. On the other hand, the energy storage due to lattice defects can be described more accurately, if the detached energy is taken into account. In order to identify the detached energy component, some calorimetry measurements or measurements of temperature evolution (cf. Subsection 3.2) are needed. Note that such processes like ductile damage evolution, grain refinement due to severe plastic deformation etc. are strongly dependent on the accumulated energy of crystal lattice defects, which can be set equal to $\psi_{\mathrm{kin}}(\check{\mathbf{\Gamma}}_{\mathrm{ie}}) + \psi_{\mathrm{iso}}(s_{\mathrm{e}}) + \psi_{\mathrm{deta}}$. Therefore, the proposed approach is promising and has potential for development of advanced material models.

Acknowledgement
This research was supported by German Science Foundation (DFG) within the collaborative research center SFB 692 "High-strength aluminium based light weight materials for reliable components".

Bibliography

[1] P. Haupt, Continuum Mechanics and Theory of Materials, 2nd edition, Springer, 2002.

[2] J.C. Simo, C. Miehe, Associative coupled thermoplasticity at finite strains: formulation, numerical analysis and implementation. Comput. Meth. Appl. Mech. Eng. 1992, 98, 41-104.

[3] A. Lion, Constitutive modelling in finite thermoviscoplasticity: a physical approach based on nonlinear rheological elements, Int. J. Plast. 2000, 16, 469-494.

[4] D. Helm. Formgedächtnislegierungen, experimentelle Untersuchung, phänomenologische Modellierung und numerische Simulation der thermomechanischen Materialeigenschaften, PhD Thesis, Univetsity of Kassel, Germany, 2001.

[5] Ch. Tsakmakis and A. Willuweit, A comparative study of kinematic hardening rules at finite deformations, Int. J. Non-Linear Mech., 2004, 39(2), 539-554.

[6] W. Dettmer, S. Reese, On the theoretical and numerical modelling of Armstrong-Frederick kinematic hardening in the finite strain regime, Comput. Methods Appl. Mech. Eng. 2004, 193, 87-116.

[7] A.V. Shutov, R. Kreißig, Finite strain viscoplasticity with nonlinear kinematic hardening: Phenomenological modeling and time integration, Comput. Methods Appl. Mech. Eng., 2008, 197, 2015-2029.

[8] I.N. Vladimirov, M. P. Pietryga, S. Reese, Anisotropic finite elastoplasticity with nonlinear kinematic and isotropic hardening and application to sheet metal forming, Int. J. Plast., 2010, 26, 659-687.

[9] M. Canadija, J. Brinc, A dissipation model for cyclic non-associative thermoplasticity at finite strains, Mechanics Research Communications, 2010, Volume 37, Issue 6, 510-514.

[10] G. Taylor, M. Quinney, The latent energy remaining in a metal after cold working. Proceedings of the Royal Society of London A, 1934, 143, 307.

[11] P. Hakansson, M. Wallin, M. Ristinmaa, Comparison of isotropic hardening and kinematic hardening in thermoplasticity. Int. J. Plasticity, 2005, 21, 1435-1460.

[12] A. Ibrahimbegovic, L. Chorfi, Covariant principal axis formulation of associated coupled thermoplasticity at finite strains and its numerical implementation. Int. J. Solids Struct., 2002, 39, 499-528.

[13] M. Canadija, J. Brnic, Associative coupled thermoplasticity at finite strain with temperature-dependent material parameters. Int. J. Plasticity, 2004, 20, 1851-1874.

[14] M. Canadija, J. Mosler, On the thermomechanical coupling in finite strain plasticity theory with nonlinear kinematic hardening by means of incremental energy minimization, International Journal of Solids and Structures, 2011, 48, 1120-1129.

[15] D. Helm, Stress computation in finite thermoviscoplasticity. International Journal of Plasticity, 2006, 22, 1699-1721.

[16] A.V. Shutov, S. Panhans, and R. Kreißig, A phenomenological model of finite strain viscoplasticity with distortional hardening, ZAMM, 2011, 91(8), 653 - 680.

[17] A.V. Shutov, R. Kreißig, Application of a coordinate-free tensor formalism to the numerical implementation of a material model, ZAMM, 2008, 88(11), 888 - 909.

[18] M. Itskov, Tensor Algebra and Tensor Analysis for Engineers: With Applications to Continuum Mechanics (Springer), 2007.

[19] S.C.H. Lu, K.D. Pister. Decomposition of deformation and representation of the free energy function for isotropic thermoelastic solids. Int. J. Solids Struc., 1975, 11, 927-934.

[20] C. Truesdell, W. Noll. The non-linear field theories. Handbuch der Physik, vol. III/3. Springer-Verlag, Berlin, 1965.

[21] Shutov, A. V.; Kreißig, R.: Geometric integrators for multiplicative viscoplasticity: analysis of error accumulation. Computer Methods in Applied Mechanics and Engineering, 2010, 199, 700-711.

[22] N. Abedrabbo, F. Pourboghrat, J. Carsley, Forming of aluminum alloys at elevated temperatures - Part 1: Material characterization, International Journal of Plasticity, 2006, 22, 314-341.

KAPITEL 8

A phenomenological model of finite strain viscoplasticity with distortional hardening

A. V. Shutov[1], S. Panhans, R. Kreißig.
Chemnitz University of Technology, Str. d. Nationen 62, D-09111 Chemnitz, Germany

Abstract: *In this paper we suggest a thermodynamically consistent approach to the simulation of a rate dependent material response at finite strains. The nonlinear mechanical phenomena which are covered by the proposed material model include distortional, kinematic, and isotropic hardening.*

Firstly, we present a new two-dimensional rheological model of distortional hardening, which predicts the yield curve in the stress space to be a limacon of Pascal. Such effects like the distortion of the yield surface in the stress space and its orientation depending on the loading path are captured by the rheological model in a vivid way. Next, the rheological model serves as a guideline for the construction of the constitutive equations. In particular, the kinematic assumptions, the ansatz for the free energy, and the form of the yield function are motivated by the rheological model. Further, two types of flow rules are considered in this study: a normality rule and a radial rule, both thermodynamically consistent. Moreover, we formulate explicitly the constraints on the material parameters, which guarantee the convexity of the yield surface. Furthermore, implicit time-stepping methods are considered which exactly preserve the incompressibility of the inelastic flow. Finally, the basic features of the predicted material response are illustrated by a series of numerical simulations. In particular, the simulation results are compared to the real experimental data.

Keywords: viscoplasticity; finite strains; distortional hardening; kinematic hardening; limaçon of Pascal
MSC2000: 74C20; 74S05

---

[1] Corresponding author. alexey.v.shutov@gmail.com
web: http://sites.google.com/site/materialmodeling

This chapter is reproduced from the paper: A. V. Shutov, S. Panhans, R. Kreißig. A phenomenological model of finite strain viscoplasticity with distortional hardening. Zeitschrift für Angewandte Mathematik und Mechanik (ZAMM). 2011. (91)8, 653-680. Copyright WILEY-VCH Verlag GmbH. Reproduced with permission.

Nomenclature

$\mathrm{sym}(\mathbf{A})$	symmetric part of a tensor,
$\mathbf{A} : \mathbf{B}$	scalar product of two second rank tensors (see (8.2)),
$\mathbf{A}^{\mathrm{T}}$	transposition of a second-rank tensor,
$\mathbf{A}^{\mathrm{D}}$	deviatoric part of a second-rank tensor,
$\overline{\mathbf{A}}$	projection on the group of unimodular tensors (see (8.1)),
$\tilde{\mathbf{X}}_{\mathrm{k}}, \hat{\mathbf{X}}_{\mathrm{k}}, \overset{\mathrm{k}}{\mathbf{X}}_{\mathrm{k}}$	back stresses operating on $\tilde{\mathcal{K}}$, $\hat{\mathcal{K}}$, and $\mathcal{K}^{\mathrm{k}}$,
$\tilde{\mathbf{X}}_{\mathrm{d}}, \hat{\mathbf{X}}_{\mathrm{d}}, \overset{\mathrm{d}}{\mathbf{X}}_{\mathrm{d}}$	distortional back stresses operating on $\tilde{\mathcal{K}}$, $\hat{\mathcal{K}}$, and $\mathcal{K}^{\mathrm{d}}$,
$\mathbf{M}^{*}(\cdot), \mathbf{M}_{*}(\cdot)$	pull back and push-forward operations (see (8.11)),
$\mathbf{C}_{\mathrm{i}}, \mathbf{C}_{\mathrm{ki}}, \mathbf{C}_{\mathrm{di}}$	internal variables of Cauchy-Green type (see (8.14)),
$\mathfrak{O}_{\mathrm{i}}, \mathfrak{O}_{\mathrm{ki}}, \mathfrak{O}_{\mathrm{di}}$	covariant Oldroyd derivatives (see (8.20)),
$\mathbf{S}, \hat{\mathbf{S}}$	Kirchhoff tensor and Kirchhoff tensor on $\hat{K}$, respectively (see (8.24)),
$\mathbf{T}, \tilde{\mathbf{T}}$	Cauchy stress tensor and the 2nd Piola-Kirchhoff stress tensor, respectively,
f	yield function (overstress) (see (8.45)),
$\langle\cdot\rangle$	MacCauley bracket (see (8.48)),
$\check{\lambda}_{\mathrm{i}}$, λ_{i}	inelastic multipliers (see (8.48), (8.60)),
$\mathfrak{F}$	the norm of the effective stresses (see (8.78), (8.83)),
α_{d}, $\tilde{\alpha}_{\mathrm{d}}$	multiplier (see (8.68), (8.88)),
g	correction factor for the normality flow rule (cf. (8.60), (8.95)),
ε, γ	axial and shear strains (see Section 5.1),
σ, τ	axial and shear stresses (see Section 5.1).

1. Introduction

The modeling of the mechanical response of metallic materials under non-monotonic and non-proportional loading conditions is of great importance for many engineering applications. In addition to isotropic expansion and kinematic translation of the yield surface, a distortion and (or) rotation of the yield locus is observed, both under monotonic and cyclic loading. According to experimental investigations, already very small inelastic deformations of metallic materials may lead to a significant change of the yield surface compared to the initial state (see, for instance [**2, 9, 47**]). Therefore, the adequate simulation of the highly nonlinear phenomena mentioned above is an extremely challenging task, especially when working with finite strains. The main requirements which are imposed on the phenomenological material models include the stability, robustness and efficiency of the corresponding numerical algorithms. Moreover, since the material parameters, in general, can not be measured directly, a complicated and time-consuming parameter identification and validation is required. Therefore, all material parameters used in the model must be well defined

In the classical phenomenological model of Chaboche and Rousselier [**6, 7**], which was formulated in geometrically linear case, the original von Mises yield condition is extended by the consideration of the isotropic and kinematic hardening. Hence, the yield surface is given by a hypersphere in the deviatoric space (5-dimensional vector space of traceless second rank tensors).[2] But the application domain of this model is often limited to (nearly) proportional loadings, since the distortion of the yield surface must be taken into account

---

[2] Alternatively, the yield surface can be represented by a hypersphere in Ilyushin's space [**24**].

in order to capture the material response under nonproportional loading conditions. The possible extensions of the classical model to cover the distortional hardening are manifold: Streilein [**48**], Kowalsky et al. [**27**], Steck et al. [**47**] modified the Chaboche-Rousselier-model by including some 4th and 6th rank tensors. A quadratic yield condition containing a 4th rank tensor as an internal variable with appropriate evolution equations allows the modeling of varying axis-relations and rotations of the hyperellipsoid. But the measured yield locus curves may differ essentially from the elliptic form. For a more precise reproduction of the experimental data, a more general cubic yield condition can be considered.[3] For instance, in the paper [**14**] by Grewolls and Kreißig some evolution equations are formulated in order to capture the evolution of tensor-valued internal variables of higher order. These equations are obtained by a formal extension of Danilov's approach [**8**]. Kurtyka and Zyczkowski [**29, 30**] suggested a geometric approach in order to simulate a complex distortion of the yield surface.

Among the variety of different extensions of the classical Chaboche-Rousselier-model we mention an elegant approach suggested by François [**11**]. The model of François is based on the introduction of so-called "distorted stresses", which are given by a 2nd rank backstress-like tensor $\mathbf{X}$. Within this approach egg-shaped yield surface can be modeled. Moreover, the egg-axis is oriented along the tensor $\mathbf{X}$ and the distortion is proportional to $\|\mathbf{X}\|$. The orientation of the yield surface follows the loading path such that the change of the loading direction leads to a reorientation of the yield surface. As it will be clear in the following, the material model introduced in the current study exhibits similar properties. One important advantage of this approach is its simplicity, since scalar-valued or 2nd rank-valued internal variables are used only. Let us mention that the idea of using the backstress-like tensors in order to capture the distortion and orientation of the yield surface was suggested even earlier (see, for instance, [**1, 2**]). In particular, the distorted yield surface can be obtained as an equidistant surface for two hyperspheres.

Next, within the approach proposed by Panhans [**34, 35**] the distortional hardening was captured with the help of a tensor-valued internal variable of the 2nd rank. The form of the yield surface is given by the so-called limaçon of Pascal.[4] Within the approach of Panhans *it can be easily guaranteed* that the elastic domain is simply connected and convex.

Unfortunately, in the case of finite strains there exists only few phenomenological models of metal plasticity designed to capture the distortion of the yield locus. In the paper [**4**] a finite strain viscoplasticity model was proposed by Böhlke et al. The model is based on the multiplicative split of the deformation gradient and on some additive split of the effective elasticity tensor, motivated by the crystallite orientation distribution. The crystallographic texture is captured with the help of a micro-mechanically defined 4th rank texture tensor. The evolution of this tensor is described by a rigid-viscoplastic Taylor type model. Considering the basic ideas of Mandel and Dafalias, Bucher et al. [**5**] introduced a new substructure intermediate configuration in order to distinguish between the kinematics of the continuum and the kinematics of the underlying substructure. The proposed model can capture nonlinear kinematic and distortional hardening effects. Another phenomenological model for texture development and anisotropic hardening in metals was proposed by Wang et al. [**51**]. The model captures hardening stagnation and the cross-hardening effect. A quadratic yield

---

[3] The 6th rank tensors can be used to implemented a cubic yield condition.

[4] This fourth order curve is also referred to as a Pascal's snail.

function of Hill's type was used by Vladimirov et al. [**50**] in order to capture the *initial* distorted form of the yield locus. The corresponding 4th rank anisotropy tensor is described with the help of some constant structure tensors.

A relatively new concept of representative directions [**12**] has much potential being combined with the classical phenomenological models of plasticity/viscoplasticity. For instance, in the paper [**13**] by Freund et al. this concept was combined with the model of finite strain viscoplasticity with kinematic hardening proposed in [**42**].

A new phenomenological model is proposed in the current study. The main ingredients of the current model are as follows: (i) a simple rheological interpretation/motivation; (ii) a multiplicative decomposition of the deformation gradient into an inelastic part and an elastic part; (iii) multiplicative decompositions of the inelastic part into some energy storage parts and some dissipative parts; (iv) an additive decomposition of the free energy function, elastic isotropy; (v) the yield locus is given by the limaçon of Pascal. For simplicity, the temperature field is assumed to be constant in time and space.

The paper is organized as follows. First, in Section 2 we present a new two-dimensional rheological model of distortional hardening, which is based on a modification of the idealized Schwedoff-body. We show that this model implies a yield surface in the form of a limaçon of Pascal. Next, in Section 3 we present a new phenomenological material model, which takes the distortional hardening into account. The thermodynamical consistency of the model is proved. Moreover, in order to simplify the numerical treatment of the evolution equations, we transform the constitutive equation to the reference configuration. Further, in Section 4 an implicit time-stepping scheme, which is based on the Modified Euler-Backward Method [**22, 42, 43, 44**], is developed. Furthermore, in Section 5 we present some simulation results concerning the torsion-tension tests on tubular thin-walled specimens. The simulation results are compared to the experimental data for the structural steel S355 J2G3. Finally, we discuss the main results of the paper in Section 6. Some assertions which are used in this study are proved in Appendix such that the mathematical details do not obscure the main points of the paper.

We conclude this introduction with a few words regarding notation. The elements of $\mathbb{R}^2$ are denoted by $\overrightarrow{A}$, $\overrightarrow{B}$, ... A coordinate-free tensor formalism is used in this contribution [**25, 43**]. Bold-faced symbols denote 1st- and 2nd-rank tensors in $\mathbb{R}^3$. Superimposed dot denotes the the material time derivative: $(\cdot)^{\cdot} = \frac{d}{dt}(\cdot)$. The overline $\overline{(\cdot)}$ denotes the unimodular part of a tensor

$$\overline{\mathbf{A}} := (\det \mathbf{A})^{-1/3}\mathbf{A} \ . \tag{8.1}$$

The symbol ": " stands the scalar product of two second-rank tensors

$$\mathbf{A} : \mathbf{B} \ := \mathrm{tr}(\mathbf{A} \cdot \mathbf{B}^{\mathrm{T}}). \tag{8.2}$$

This scalar product gives rise to the Frobenius norm as follows

$$\|\mathbf{A}\| := \sqrt{\mathbf{A} : \mathbf{A}}. \tag{8.3}$$

The identity tensor is denoted by **1**. The notation $\mathbf{A}^{\mathrm{D}}$ stands for a deviatoric part of a tensor $\mathbf{A}^{\mathrm{D}} := \mathbf{A} - \frac{1}{3}\mathrm{tr}(\mathbf{A})\mathbf{1}$. Finally, we denote by $\dfrac{\partial\psi(\mathbf{A})}{\partial\mathbf{A}}$ the Fréchet derivative of a real-valued

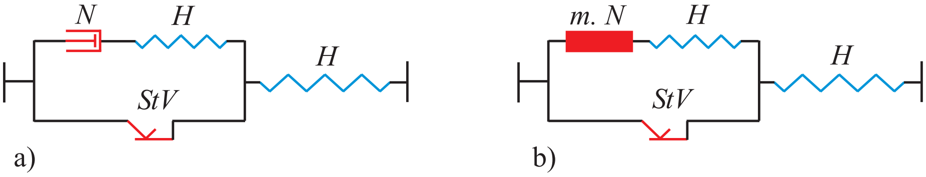

Figure 8.1. Model for a Schwedoff-body: a) the classical model which is build up of a Newton-body (N), two Hooke-bodies (H) and a St. Venant body (StV), b) the model with a modified Newton-body ($m.N$) which can be used to motivate rate-independent plasticity.

function ψ with respect to its tensor-valued argument $\mathbf{A}$:

$$\psi(\mathbf{A}+\Delta\mathbf{A})-\psi(\mathbf{A}) \underset{\Delta\mathbf{A}\to\mathbf{0}}{\approx} \frac{\partial\psi(\mathbf{A})}{\partial\mathbf{A}} : \Delta\mathbf{A}. \tag{8.4}$$

2. A rheological model of distortional hardening

The rheological models are widely used to provide an insight into some aspects of material modeling [**40**]. Especially large body of information is provided if these models are filled with a physical content (cf. [**37**]). We note that there exists a number of two-dimensional models, describing a complicated behavior of materials and structures (see, for example, [**38, 39, 40, 23, 46**]). In this section we present a *new* two-dimensional rheological model which *takes a distortional hardening into account*. As a starting point we consider the one-dimensional model of Schwedoff (1890) (Fig. 8.1a). The classical Schwedoff-body ($Schw$) is built up of a Maxwell-body (M), a St. Venant element (StV), and a Hooke-body (H), according to the structural formula $Schw = (M|StV) - H$ (see [**40**]). Here, the horizontal dash ($-$) indicates "coupling in series" and the vertical dash ($|$) indicates "coupling in parallel". The Maxwell-element, in turn, is build up of a Newton-body (N) and an another Hook-body (H): $M = N - H$.

The Schwedoff model can be modified by changing the constitutive equations of the Newton-body, if the physical time t is formally replaced by the accumulated inelastic arc-length s. More precisely, Newton's law of viscous flow which reads $\frac{d}{dt}\varepsilon = \frac{1}{\eta}\sigma$ is replaced now by the relation $\frac{d}{ds}\varepsilon = \varkappa\ \sigma$. Here, ε may be seen as the elongation of the element, σ as the force which causes this elongation, and $\eta > 0$, $\varkappa > 0$ are some material parameters.[5] The resulting variant of the Newton-body will be referred to as *modified Newton-body* ($m.N$). The corresponding modification of the Schwedoff-body (see Fig. 8.1b) was considered in [**32, 10, 42**] as a starting point for constitutive modeling of nonlinear kinematic hardening at finite strains. In the following we present some rheological models which contain the elements of the Newton type. Those elements should be interpreted as modified Newton elements, which we do not stress explicitly in order to shorten the presentation.

Let us generalize the classical Schwedoff model to two dimensions. Consider a mechanical system which consists of a tank with a flat bottom filled with a viscous fluid, a heavy

---

[5] Such modification is possible whenever the inelastic arc-length s is available. The arc-length s will be introduced formally in Section 3. The use of this parameter instead of the time t enables the construction of rate-independent constitutive equations.

Figure 8.2. Two-dimensional rheological models: a) Schwedoff model $(M|StV) - H$, b) Schwedoff model with a modified St. Venant element $(M|m.StV) - H$. The vertical plate of the $(m.StV)$-element acts like a keel preventing the sideways drift.

solid made of a circular plate rigidly connected to a rod (StV), two elastic springs (H) connected to the rod,[6] and a sphere (N) floating on the surface of the fluid (Fig. 8.2a). The circular plate rests upon the bottom of the tank and there is solid friction between them. Similar to the classical one-dimensional approach (cf. [**40**]), we suppose that as long as the force acting on the plate is smaller than the friction $\sqrt{2/3}K > 0$,[7] the plate remains at rest. When the force reaches the friction $\sqrt{2/3}K$, the plate starts to move in the direction of the force. Moreover, we suppose that the fluid resistance opposed to the motion of the solid is negligible, and the force acting on the plate can not exceed the friction $\sqrt{2/3}K$. Next, following Newton's law of viscous flow we assume that the fluid resistance to the motion of the sphere (N) is proportional to the velocity of the sphere with respect to the bottom of the tank. Thus, analogously to the one-dimensional approach, the body built up of the sphere connected in series to the elastic spring is referred to as a Maxwell element. In the following the corresponding spring will be referred to as a Maxwell spring. Obviously, the model can be easily extended by introducing a series of additional Maxwell elements. We note that the Schwedoff model depicted in Fig. 8.2a can serve as a motivation for the constitutive equations describing the viscoplastic material behavior with kinematic hardening [**32, 10, 42**].

In order to capture the effects similar to the distortional hardening we introduce a new model as follows.[8] Let us consider a solid made of two circular plates rigidly connected by a flat plate $(m.StV)$ as it is shown in Fig. 8.2b. The plate acts like a keel preventing the sideways drift. Thus, the solid *can slide along the keel direction only.* The external force which acts on the solid will be denoted by $\overrightarrow{F}$ as shown in (Fig. 8.2b). We postulate that the fluid and the frictional contact do not resist the turn of the solid,[9] and that the plate is always oriented along $\overrightarrow{F}$, as it is shown in Fig. 8.2b.[10] Next, it is natural to assume

---

[6] We postulate that the spring force is proportional to the length of the spring. Thus, the Hook-bodies possess a zero length in unloaded state.

[7] For simplicity, we do not distinct the static and kinetic friction in this work. Moreover, we suppose that the friction is constant. The meaning of the multiplier $\sqrt{2/3}$ will be clear from what follows (cf. (8.45)).

[8] The animated versions of the rheological model are available at http://www.youtube.com/watch?v=RHtSSVZph2g and http://www.youtube.com/watch?v=qYoN8g6yldI

[9] Thus, zero energy dissipation is associated with the rotation of the solid.

[10] Intuitively one may explain the last assumption by thinking of the elastic spring as being connected at the intersection of the circular plate with the keel-plate. The balance of rotational momentum requires

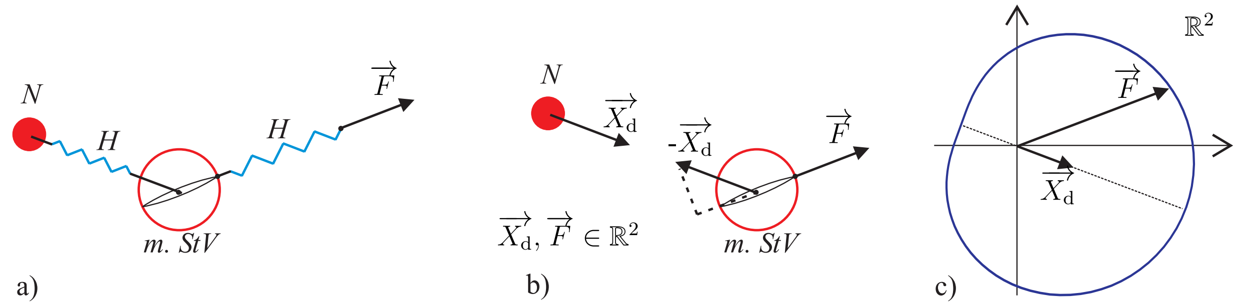

Figure 8.3. a) Modified Schwedoff model seen from above, b) The $(m.StV)$-element exerts a force $\overrightarrow{X}_{\mathrm{d}}$ on the (N)-body. The (N)-body acts on the $(m.StV)$-element with $-\overrightarrow{X}_{\mathrm{d}}$. The resulting force $\overrightarrow{F} - \overrightarrow{X}_{\mathrm{d}}$ is projected on $\overrightarrow{F}/\|\overrightarrow{F}\|$ (the arrows are meant to visualize the elements of $\mathbb{R}^2$), c) The critical states in terms of force $\overrightarrow{F}$ (here $\|\overrightarrow{X}_{\mathrm{d}}\| = (1/2)\sqrt{2/3}K$).

that as long as the force of the two elastic springs acting on the solid *being projected to the keel-direction* is smaller than the friction $\sqrt{2/3}K > 0$, the element remains at rest. When the *projection* of the force reaches the friction $\sqrt{2/3}K$, the element starts to move in the keel direction. A simplified two-dimensional diagram of the modified Schwedoff model is presented in Fig. 8.3a.

The force which acts on the (N)-body will be interpreted later as a distortional force and denoted by $\overrightarrow{X}_{\mathrm{d}}$. Thus, according to Newton's third law, the (N)-body acts on the solid with the force $-\overrightarrow{X}_{\mathrm{d}}$ (see Fig. 8.3b). Let $\overrightarrow{X}_{\mathrm{d}}, \overrightarrow{F} \in \mathbb{R}^2$. For a given $\overrightarrow{X}_{\mathrm{d}}$ the admissible values of the force $\overrightarrow{F}$ are defined by the inequality as follows

$$\left\| \left[(\overrightarrow{F} - \overrightarrow{X}_{\mathrm{d}}) \cdot \frac{\overrightarrow{F}}{\|\overrightarrow{F}\|} \right] \frac{\overrightarrow{F}}{\|\overrightarrow{F}\|} \right\| \leq \sqrt{2/3}K, \tag{8.5}$$

where $\overrightarrow{x} \cdot \overrightarrow{y} = x_1 y_1 + x_2 y_2$, $\|\overrightarrow{x}\| = \sqrt{\overrightarrow{x} \cdot \overrightarrow{x}}$ for all $\overrightarrow{x}, \overrightarrow{y} \in \mathbb{R}^2$. In what follows we suppose that $\|\overrightarrow{X}_{\mathrm{d}}\| < \sqrt{2/3}K$. Under that condition the inequality (8.5) is equivalent to (cf. Appendix A)

$$\left\|\overrightarrow{F}\right\| - \frac{\overrightarrow{X}_{\mathrm{d}} \cdot \overrightarrow{F}}{\|\overrightarrow{F}\|} \leq \sqrt{2/3}K, \tag{8.6}$$

and the critical states are described by (see Appendix A)

$$\left\|\overrightarrow{F}\right\| - \frac{\overrightarrow{X}_{\mathrm{d}} \cdot \overrightarrow{F}}{\|\overrightarrow{F}\|} = \sqrt{2/3}K. \tag{8.7}$$

Equation (8.7) describes the well-known limaçon of Pascal (cf. Fig. 8.3c). This curve is a smooth closed curve for $\|\overrightarrow{X}_{\mathrm{d}}\| < \sqrt{2/3}K$. The curve is convex whenever $\|\overrightarrow{X}_{\mathrm{d}}\| \leq (1/2)\sqrt{2/3}K$. For $\overrightarrow{X}_{\mathrm{d}} \neq 0$ the curve is oriented along $\overrightarrow{X}_{\mathrm{d}}$. For $\overrightarrow{X}_{\mathrm{d}} = 0$ the curve is a circle of radius $\sqrt{2/3}K$ that has a center at the origin.

---

that the keel direction is aligned exactly along $\overrightarrow{F}$. The Maxwell spring which is connected to the center of the circular plate does not influence the orientation (see Fig. 8.2b and Fig. 8.3a).

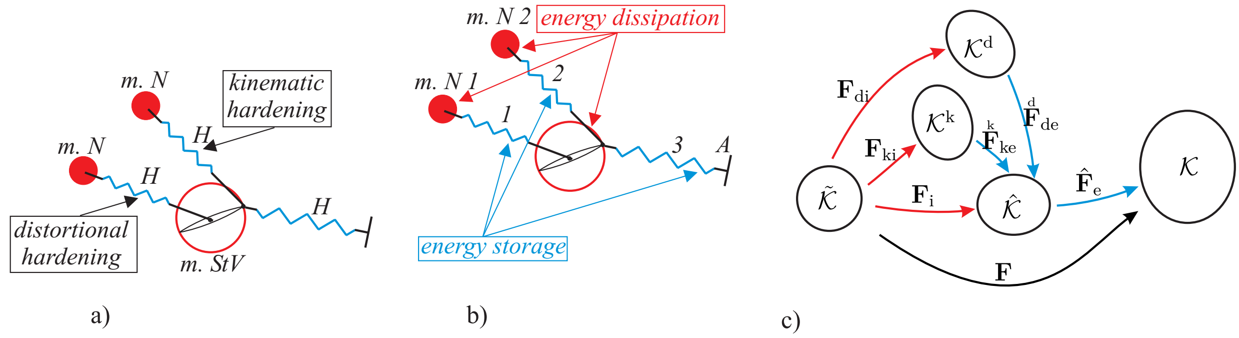

Figure 8.4. a) A rheological modeling for kinematic and distortional hardening, b) Energy storage and dissipation c) A commutative diagram showing corresponding configurations with transformations of material line elements.

Remark 1. We note that the limaçon of Pascal was used previously by Panhans [**34, 35**] in order to capture the effects of distortional hardening. In this paper, however, this form is obtained in a natural way using the rheological representation. Moreover, the rheological model takes into account such effects like the distortion of the yield surface and its orientation depending on the loading path.

Remark 2. In the paper [**11**] by François the classical von Mises yield condition was modified by the introduction of so-called "distorted stresses", thus obtaining "egg-shaped" yield surfaces. Moreover, a tensor which plays a similar role as $\overrightarrow{X}_{\mathrm{d}}$ was introduced. The approach proposed by François allows for the introduction of different kinds of yield surfaces (at least at small strains), but no rheological model was provided in [**11**].

3. Material model of finite strain viscoplasticity

In this section we consider a system of constitutive equations which is motivated by the rheological model presented in Fig. 8.4a. This model results from the model depicted in Fig. 8.3a by the introduction of an additional Maxwell element. The corresponding elastic spring is attached to the circular plate at the same point as the elastic spring loaded by the external force. Therefore, the admissible loadings are described now by (8.6) where the force $\overrightarrow{F}$ is formally replaced by $\overrightarrow{F} - \overrightarrow{X}_{\mathrm{k}}$, where $-\overrightarrow{X}_{\mathrm{k}}$ stands for the force acting on the plate due to the deformation of the additional elastic spring. As a result, the set of admissible external loadings is shifted. In that way the nonlinear kinematic hardening as well as the distortional hardening can be taken into account. Moreover, the material model presented in this section takes the nonlinear isotropic hardening into account (although it is not captured by the rheological model). The model of finite strain viscoplasticity with nonlinear kinematic hardening, which was presented in [**42**], is covered by the current model as a special case.

3.1. Description of kinematics. Let $\mathcal{K}$ be the current local configuration occupied by the solid (we omit the dependence of $\mathcal{K}$ on the time t in order to simplify the notation). Suppose $\tilde{\mathcal{K}}$ is the reference configuration, which is used to uniquely designate the material points (see, for example, [**20**]). Let us consider the classical multiplicative decomposition of the deformation gradient $\mathbf{F}$ into *elastic part* $\hat{\mathbf{F}}_{\mathrm{e}}$ and *inelastic part* $\mathbf{F}_{\mathrm{i}}$ ([**28, 31**])

$$\mathbf{F} = \hat{\mathbf{F}}_{\mathrm{e}}\mathbf{F}_{\mathrm{i}}. \tag{8.8}$$

The mechanical justification of (8.8) uses the idea of the local elastic unloading.[11] The multiplicative split (8.8) leads to the *stress-free intermediate configuration* $\hat{\mathcal{K}}$ (see Fig. 8.4c). The next multiplicative decomposition is introduced in order to simulate a nonlinear kinematic hardening of Armstrong-Frederick type (cf. [**32, 49, 10, 17, 42**]). Following Lion [**32**], we use the rheological model in Fig. 8.4a in order to motivate the multiplicative decomposition of $\mathbf{F}_{\mathrm{i}}$ into *energy storage part* $\overset{\mathrm{k}}{\mathbf{F}}_{\mathrm{ke}}$ and *dissipative part* $\mathbf{F}_{\mathrm{ki}}$

$$\mathbf{F}_{\mathrm{i}} = \overset{\mathrm{k}}{\mathbf{F}}_{\mathrm{ke}} \mathbf{F}_{\mathrm{ki}}. \tag{8.9}$$

Moreover, in this work we introduce an additional decomposition of $\mathbf{F}_{\mathrm{i}}$ into some conservative part $\overset{\mathrm{d}}{\mathbf{F}}_{\mathrm{de}}$ and some dissipative part $\mathbf{F}_{\mathrm{di}}$, which will be used to capture the distortional hardening

$$\mathbf{F}_{\mathrm{i}} = \overset{\mathrm{d}}{\mathbf{F}}_{\mathrm{de}} \mathbf{F}_{\mathrm{di}}. \tag{8.10}$$

The mappings $\overset{\mathrm{k}}{\mathbf{F}}_{\mathrm{ke}}$ and $\overset{\mathrm{d}}{\mathbf{F}}_{\mathrm{de}}$ describe the energy storage connected to the kinematic and distortional hardening, respectively. Decompositions (8.9) and (8.10) implement the *intermediate configuration of kinematic hardening* $\mathcal{K}^{\mathrm{k}}$ and the *intermediate configuration of distortional hardening* $\mathcal{K}^{\mathrm{d}}$, respectively (see Fig. 8.4c). The commutative diagram in Fig. 8.4c summarizes the multiplicative decompositions.

Remark 3. In this contribution we use a phenomenological approach to the simulation of the material response. Therefore, no physical justification of assumptions (8.9) and (8.10) is necessary. On the other hand, since the rheological model in Fig. 8.4a represents some mechanical effects (at least qualitatively), our goal is to construct the system of constitutive equations which captures the same effects in a similar way. In particular, the conservative parts $\overset{\mathrm{d}}{\mathbf{F}}_{\mathrm{de}}$ and $\overset{\mathrm{k}}{\mathbf{F}}_{\mathrm{ke}}$ can be associated with the deformation of the elastic springs 1 and 2, respectively (see Fig. 8.4b). The dissipative parts $\mathbf{F}_{\mathrm{di}}$ and $\mathbf{F}_{\mathrm{ki}}$, in turn, are associated to the movement of the modified Newton-bodies ($m.N1$) and ($m.N2$), respectively; where the deformation gradient $\mathbf{F}$ is connected to the displacement of point A (see Fig. 8.4b).

Suppose $\mathbf{M} \in \left\{\mathbf{F}, \mathbf{F}_{\mathrm{i}}, \mathbf{F}_{\mathrm{ki}}, \mathbf{F}_{\mathrm{di}}, \hat{\mathbf{F}}_{\mathrm{e}}, \overset{\mathrm{k}}{\mathbf{F}}_{\mathrm{ke}}, \overset{\mathrm{d}}{\mathbf{F}}_{\mathrm{de}}\right\}$. In order to describe the change of configurations we consider the well-known *covariant pull-back* $\mathbf{M}^{*}(\cdot)$ and *covariant push-forward* $\mathbf{M}_{*}(\cdot)$

$$\mathbf{M}^{*}(\cdot) := \mathbf{M}^{\mathrm{T}}(\cdot)\mathbf{M}, \quad \mathbf{M}_{*}(\cdot) := \mathbf{M}^{-\mathrm{T}}(\cdot)\mathbf{M}^{-1}. \tag{8.11}$$

Moreover, *contravariant pull-back* and *push-forward* operations are given respectively by

$$(\mathbf{M}^{-\mathrm{T}})^{*}(\cdot) = \mathbf{M}^{-1}(\cdot)\mathbf{M}^{-\mathrm{T}}, \quad (\mathbf{M}^{-\mathrm{T}})_{*}(\cdot) = \mathbf{M}(\cdot)\mathbf{M}^{\mathrm{T}}. \tag{8.12}$$

Thus, the right Cauchy-Green tensor is a covariant pull-back of identity tensor $\mathbf{1}$

$$\mathbf{C} := \mathbf{F}^{*}\mathbf{1} = \mathbf{F}^{\mathrm{T}}\mathbf{F}. \tag{8.13}$$

In the same way, we define the inelastic right Cauchy-Green tensor $\mathbf{C}_{\mathrm{i}}$ and inelastic right Cauchy-Green tensors $\mathbf{C}_{\mathrm{ki}}$, $\mathbf{C}_{\mathrm{di}}$ of microstructure, which operate on $\tilde{\mathcal{K}}$:

$$\mathbf{C}_{\mathrm{i}} := \mathbf{F}_{\mathrm{i}}^{*}\mathbf{1} = \mathbf{F}_{\mathrm{i}}^{\mathrm{T}}\mathbf{F}_{\mathrm{i}}, \quad \mathbf{C}_{\mathrm{ki}} := \mathbf{F}_{\mathrm{ki}}^{*}\mathbf{1} = \mathbf{F}_{\mathrm{ki}}^{\mathrm{T}}\mathbf{F}_{\mathrm{ki}}, \quad \mathbf{C}_{\mathrm{di}} := \mathbf{F}_{\mathrm{di}}^{*}\mathbf{1} = \mathbf{F}_{\mathrm{di}}^{\mathrm{T}}\mathbf{F}_{\mathrm{di}}. \tag{8.14}$$

---

[11] On the other hand, a pure elastic unloading is impossible in some cases. Therefore, a somewhat more consistent motivation for such decomposition was proposed by Bertram in [**3**] using the concept of material isomorphism.

Next, the elastic right Cauchy-Green tensor $\hat{\mathbf{C}}_{\mathrm{e}}$ and the elastic right Cauchy-Green tensors $\overset{\mathrm{k}}{\mathbf{C}}_{\mathrm{ke}}$, $\overset{\mathrm{d}}{\mathbf{C}}_{\mathrm{de}}$ of microstructure are defined through

$$\hat{\mathbf{C}}_{\mathrm{e}} := \hat{\mathbf{F}}^*_{\mathrm{e}}\mathbf{1} = \hat{\mathbf{F}}^{\mathrm{T}}_{\mathrm{e}}\hat{\mathbf{F}}_{\mathrm{e}}, \quad \overset{\mathrm{k}}{\mathbf{C}}_{\mathrm{ke}} := \overset{\mathrm{k}}{\mathbf{F}}{}^*_{\mathrm{ke}}\mathbf{1} = \overset{\mathrm{k}}{\mathbf{F}}{}^{\mathrm{T}}_{\mathrm{ke}}\overset{\mathrm{k}}{\mathbf{F}}_{\mathrm{ke}}, \quad \overset{\mathrm{d}}{\mathbf{C}}_{\mathrm{de}} := \overset{\mathrm{d}}{\mathbf{F}}{}^*_{\mathrm{de}}\mathbf{1} = \overset{\mathrm{d}}{\mathbf{F}}{}^{\mathrm{T}}_{\mathrm{de}}\overset{\mathrm{d}}{\mathbf{F}}_{\mathrm{de}}. \tag{8.15}$$

The accents set by $\hat{\mathbf{C}}_{\mathrm{e}}$, $\overset{\mathrm{k}}{\mathbf{C}}_{\mathrm{ke}}$, and $\overset{\mathrm{d}}{\mathbf{C}}_{\mathrm{de}}$ indicate that the corresponding mappings operate on $\hat{\mathcal{K}}$, $\mathcal{K}^{\mathrm{k}}$, and $\mathcal{K}^{\mathrm{d}}$, respectively.

Furthermore, we consider the well-known Green strain tensor $\mathbf{E} := \frac{1}{2}(\mathbf{C} - \mathbf{1})$. In the following we will need the covariant push-forwards of $\mathbf{E}$

$$\hat{\mathbf{\Gamma}} := (\mathbf{F}_{\mathrm{i}})_*\mathbf{E} = \mathbf{F}_{\mathrm{i}}^{-\mathrm{T}}\mathbf{E}\mathbf{F}_{\mathrm{i}}^{-1}, \quad \mathbf{\Gamma} := \mathbf{F}_*\mathbf{E} = \mathbf{F}^{-\mathrm{T}}\mathbf{E}\mathbf{F}^{-1}.$$

One advantage of the intermediate configuration $\hat{\mathcal{K}}$ is that the multiplicative decomposition (8.8) implements the additive split of $\hat{\mathbf{\Gamma}}$ into the inelastic Almansi tensor $\hat{\mathbf{\Gamma}}_{\mathrm{i}}$ and the elastic Green tensor $\hat{\mathbf{\Gamma}}_{\mathrm{e}}$, which operate on $\hat{\mathcal{K}}$:

$$\hat{\mathbf{\Gamma}} \overset{(8.8)}{=} \hat{\mathbf{\Gamma}}_{\mathrm{i}} + \hat{\mathbf{\Gamma}}_{\mathrm{e}}, \quad \hat{\mathbf{\Gamma}}_{\mathrm{i}} := \frac{1}{2}(\mathbf{1} - \mathbf{F}_{\mathrm{i}}^{-\mathrm{T}}\mathbf{F}_{\mathrm{i}}^{-1}), \quad \hat{\mathbf{\Gamma}}_{\mathrm{e}} := \frac{1}{2}(\hat{\mathbf{F}}^{\mathrm{T}}_{\mathrm{e}}\hat{\mathbf{F}}_{\mathrm{e}} - \mathbf{1}) = \frac{1}{2}(\hat{\mathbf{C}}_{\mathrm{e}} - \mathbf{1}). \tag{8.16}$$

Further, we introduce covariant pull-backs of $\hat{\mathbf{\Gamma}}_{\mathrm{i}}$ to $\mathcal{K}^{\mathrm{k}}$ and $\mathcal{K}^{\mathrm{d}}$

$$\overset{\mathrm{k}}{\mathbf{\Gamma}}_{\mathrm{i}} := \overset{\mathrm{k}}{\mathbf{F}}{}^*_{\mathrm{ke}}\hat{\mathbf{\Gamma}}_{\mathrm{i}} = \overset{\mathrm{k}}{\mathbf{F}}{}^{\mathrm{T}}_{\mathrm{ke}}\hat{\mathbf{\Gamma}}_{\mathrm{i}}\overset{\mathrm{k}}{\mathbf{F}}_{\mathrm{ke}}, \quad \overset{\mathrm{d}}{\mathbf{\Gamma}}_{\mathrm{i}} := \overset{\mathrm{d}}{\mathbf{F}}{}^*_{\mathrm{de}}\hat{\mathbf{\Gamma}}_{\mathrm{i}} = \overset{\mathrm{d}}{\mathbf{F}}{}^{\mathrm{T}}_{\mathrm{de}}\hat{\mathbf{\Gamma}}_{\mathrm{i}}\overset{\mathrm{d}}{\mathbf{F}}_{\mathrm{de}}.$$

Similar to (8.16), multiplicative decompositions (8.9) and (8.10) imply the additive decompositions of $\overset{\mathrm{k}}{\mathbf{\Gamma}}_{\mathrm{i}}$ and $\overset{\mathrm{d}}{\mathbf{\Gamma}}_{\mathrm{i}}$ as follows

$$\overset{\mathrm{k}}{\mathbf{\Gamma}}_{\mathrm{i}} \overset{(8.9)}{=} \overset{\mathrm{k}}{\mathbf{\Gamma}}_{\mathrm{ki}} + \overset{\mathrm{k}}{\mathbf{\Gamma}}_{\mathrm{ke}}, \quad \overset{\mathrm{d}}{\mathbf{\Gamma}}_{\mathrm{i}} \overset{(8.10)}{=} \overset{\mathrm{d}}{\mathbf{\Gamma}}_{\mathrm{di}} + \overset{\mathrm{d}}{\mathbf{\Gamma}}_{\mathrm{de}}, \tag{8.17}$$

where

$$\overset{\mathrm{k}}{\mathbf{\Gamma}}_{\mathrm{ki}} := \frac{1}{2}(\mathbf{1} - \mathbf{F}_{\mathrm{ki}}^{-\mathrm{T}}\mathbf{F}_{\mathrm{ki}}^{-1}), \quad \overset{\mathrm{k}}{\mathbf{\Gamma}}_{\mathrm{ke}} := \frac{1}{2}(\overset{\mathrm{k}}{\mathbf{F}}{}^{\mathrm{T}}_{\mathrm{ke}}\overset{\mathrm{k}}{\mathbf{F}}_{\mathrm{ke}} - \mathbf{1}) = \frac{1}{2}(\overset{\mathrm{k}}{\mathbf{C}}_{\mathrm{ke}} - \mathbf{1}), \tag{8.18}$$

$$\overset{\mathrm{d}}{\mathbf{\Gamma}}_{\mathrm{di}} := \frac{1}{2}(\mathbf{1} - \mathbf{F}_{\mathrm{di}}^{-\mathrm{T}}\mathbf{F}_{\mathrm{di}}^{-1}), \quad \overset{\mathrm{d}}{\mathbf{\Gamma}}_{\mathrm{de}} := \frac{1}{2}(\overset{\mathrm{d}}{\mathbf{F}}{}^{\mathrm{T}}_{\mathrm{de}}\overset{\mathrm{d}}{\mathbf{F}}_{\mathrm{de}} - \mathbf{1}) = \frac{1}{2}(\overset{\mathrm{d}}{\mathbf{C}}_{\mathrm{de}} - \mathbf{1}). \tag{8.19}$$

We conclude this subsection introducing the inelastic pull-back of $\hat{\mathbf{\Gamma}}_{\mathrm{i}}$ to $\tilde{\mathcal{K}}$

$$\tilde{\mathbf{\Gamma}}_{\mathrm{i}} := \mathbf{F}^*_{\mathrm{i}}\hat{\mathbf{\Gamma}}_{\mathrm{i}} = \frac{1}{2}(\mathbf{C}_{\mathrm{i}} - \mathbf{1}).$$

3.2. The concept of dual variables. In this study we implement the formalism of dual variables developed by Haupt and Tsakmakis [**18**]. Following this concept, we introduce the covariant Oldroyd rates $\mathfrak{O}_{\mathrm{i}}$, $\mathfrak{O}_{\mathrm{ki}}$, and $\mathfrak{O}_{\mathrm{di}}$ with respect to fictitious intermediate configurations $\hat{\mathcal{K}}$, $\mathcal{K}^{\mathrm{k}}$, and $\mathcal{K}^{\mathrm{d}}$, respectively:

$$\mathfrak{O}_{\mathrm{i}}(\cdot) := \mathbf{F}_{\mathrm{i}*}\Big(\frac{d}{dt}\big(\mathbf{F}^*_{\mathrm{i}}(\cdot)\big)\Big), \quad \mathfrak{O}_{\mathrm{ki}}(\cdot) := \mathbf{F}_{\mathrm{ki}*}\Big(\frac{d}{dt}\big(\mathbf{F}^*_{\mathrm{ki}}(\cdot)\big)\Big), \quad \mathfrak{O}_{\mathrm{di}}(\cdot) := \mathbf{F}_{\mathrm{di}*}\Big(\frac{d}{dt}\big(\mathbf{F}^*_{\mathrm{di}}(\cdot)\big)\Big), \tag{8.20}$$

where $\frac{d}{dt}(\cdot)$ stands for material time derivative. An alternative representation of covariant Oldroyd rates can be derived form (8.20) as follows

$$\mathfrak{O}_{\mathrm{i}}(\cdot) = \frac{d}{dt}(\cdot) + \hat{\mathbf{L}}^{\mathrm{T}}_{\mathrm{i}}(\cdot) + (\cdot)\hat{\mathbf{L}}_{\mathrm{i}}, \quad \mathfrak{O}_{\mathrm{ki}}(\cdot) = \frac{d}{dt}(\cdot) + \overset{\mathrm{k}}{\mathbf{L}}{}^{\mathrm{T}}_{\mathrm{ki}}(\cdot) + (\cdot)\overset{\mathrm{k}}{\mathbf{L}}{}^{\mathrm{T}}_{\mathrm{ki}}, \quad \mathfrak{O}_{\mathrm{di}}(\cdot) = \frac{d}{dt}(\cdot) + \overset{\mathrm{d}}{\mathbf{L}}{}^{\mathrm{T}}_{\mathrm{di}}(\cdot) + (\cdot)\overset{\mathrm{d}}{\mathbf{L}}{}^{\mathrm{T}}_{\mathrm{di}}, \tag{8.21}$$

$$\hat{\mathbf{L}}_{\mathrm{i}} := \dot{\mathbf{F}}_{\mathrm{i}}\mathbf{F}_{\mathrm{i}}^{-1}, \quad \overset{\mathrm{k}}{\mathbf{L}}_{\mathrm{ki}} := \dot{\mathbf{F}}_{\mathrm{ki}}\mathbf{F}_{\mathrm{ki}}^{-1}, \quad \overset{\mathrm{d}}{\mathbf{L}}_{\mathrm{di}} := \dot{\mathbf{F}}_{\mathrm{di}}\mathbf{F}_{\mathrm{di}}^{-1}.$$

Using (8.20) it can be shown that $\mathfrak{D}_{\mathrm{i}}(\hat{\boldsymbol{\Gamma}}_{\mathrm{i}})$, $\mathfrak{D}_{\mathrm{ki}}(\overset{\mathrm{k}}{\boldsymbol{\Gamma}}_{\mathrm{ki}})$, and $\mathfrak{D}_{\mathrm{di}}(\overset{\mathrm{d}}{\boldsymbol{\Gamma}}_{\mathrm{di}})$ are symmetric parts of $\hat{\mathbf{L}}_{\mathrm{i}}$, $\overset{\mathrm{k}}{\mathbf{L}}_{\mathrm{ki}}$, and $\overset{\mathrm{d}}{\mathbf{L}}_{\mathrm{di}}$, respectively:

$$\mathfrak{D}_{\mathrm{i}}(\hat{\boldsymbol{\Gamma}}_{\mathrm{i}}) = \mathrm{sym}(\hat{\mathbf{L}}_{\mathrm{i}}), \quad \mathfrak{D}_{\mathrm{ki}}(\overset{\mathrm{k}}{\boldsymbol{\Gamma}}_{\mathrm{ki}}) = \mathrm{sym}(\overset{\mathrm{k}}{\mathbf{L}}_{\mathrm{ki}}), \quad \mathfrak{D}_{\mathrm{di}}(\overset{\mathrm{d}}{\boldsymbol{\Gamma}}_{\mathrm{di}}) = \mathrm{sym}(\overset{\mathrm{d}}{\mathbf{L}}_{\mathrm{di}}). \tag{8.22}$$

Here, the symmetric part of a tensor is given by $\mathrm{sym}(\cdot) := \frac{1}{2}\Big((\cdot) + (\cdot)^{\mathrm{T}}\Big)$.

Let us denote by $\mathbf{T}$ the Cauchy stress tensor. The weighted Cauchy tensor (or Kirchhoff stress tensor) is then defined by

$$\mathbf{S} := (\det\mathbf{F})\mathbf{T}. \tag{8.23}$$

Next, we define the 2nd Piola-Kirchhoff tensors operating on $\hat{\mathcal{K}}$ and $\tilde{\mathcal{K}}$ using a contravariant pull-back of $\mathbf{S}$

$$\hat{\mathbf{S}} := \Big(\hat{\mathbf{F}}_{\mathrm{e}}^{-\mathrm{T}}\Big)^{*}\mathbf{S}, \quad \tilde{\mathbf{T}} := \Big(\mathbf{F}^{-\mathrm{T}}\Big)^{*}\mathbf{S} = \Big(\mathbf{F}_{\mathrm{i}}^{-\mathrm{T}}\Big)^{*}\hat{\mathbf{S}}. \tag{8.24}$$

The introduced stress and strain tensors form conjugate pairs as follows: $(\mathbf{S}, \boldsymbol{\Gamma})$, $(\hat{\mathbf{S}}, \hat{\boldsymbol{\Gamma}})$, $(\tilde{\mathbf{T}}, \mathbf{E})$, such that the work and the stress power are invariant under the change of configuration:[12]

$$\mathbf{S} : \boldsymbol{\Gamma} = \hat{\mathbf{S}} : \hat{\boldsymbol{\Gamma}} = \tilde{\mathbf{T}} : \mathbf{E}, \quad \hat{\mathbf{S}} : \mathfrak{D}_{\mathrm{i}}(\hat{\boldsymbol{\Gamma}}) = \tilde{\mathbf{T}} : \dot{\mathbf{E}}. \tag{8.25}$$

Here, ": " stands for the scalar product of two second-rank tensors.

Besides, we denote by $\overset{\mathrm{k}}{\mathbf{X}}_{\mathrm{k}}$ and $\overset{\mathrm{d}}{\mathbf{X}}_{\mathrm{d}}$ the *back stress tensor* and the *distortional back stress tensor*, respectively.[13] The tensor $\overset{\mathrm{k}}{\mathbf{X}}_{\mathrm{k}}$ operates on $\mathcal{K}^{\mathrm{k}}$ and can be interpreted as a generalized force, associated with the strain measure $\overset{\mathrm{k}}{\boldsymbol{\Gamma}}_{\mathrm{i}}$ and the strain rate $\mathfrak{D}_{\mathrm{ki}}(\overset{\mathrm{k}}{\boldsymbol{\Gamma}}_{\mathrm{i}})$. Similarly, $\overset{\mathrm{d}}{\mathbf{X}}_{\mathrm{d}}$ operates on $\mathcal{K}^{\mathrm{d}}$ and can be seen as a generalized force, associated with $\overset{\mathrm{d}}{\boldsymbol{\Gamma}}_{\mathrm{i}}$ and $\mathfrak{D}_{\mathrm{di}}(\overset{\mathrm{d}}{\boldsymbol{\Gamma}}_{\mathrm{i}})$. Following the concept of dual variables, we define transformation rules for the tensors $\overset{\mathrm{k}}{\mathbf{X}}_{\mathrm{k}}$ and $\overset{\mathrm{d}}{\mathbf{X}}_{\mathrm{d}}$, such that the inner product of dual stress and strain tensors as well as the specific stress power remain invariant under the change of configurations:

$$\tilde{\mathbf{X}}_{\mathrm{k}} := \Big(\mathbf{F}_{\mathrm{ki}}^{-\mathrm{T}}\Big)^{*}\overset{\mathrm{k}}{\mathbf{X}}_{\mathrm{k}} = \mathbf{F}_{\mathrm{ki}}^{-1}\overset{\mathrm{k}}{\mathbf{X}}_{\mathrm{k}}\mathbf{F}_{\mathrm{ki}}^{-\mathrm{T}}, \quad \hat{\mathbf{X}}_{\mathrm{k}} := \Big(\overset{\mathrm{k}}{\mathbf{F}}{}_{\mathrm{ke}}^{-\mathrm{T}}\Big)_{*}\overset{\mathrm{k}}{\mathbf{X}}_{\mathrm{k}} = \overset{\mathrm{k}}{\mathbf{F}}_{\mathrm{ke}}\overset{\mathrm{k}}{\mathbf{X}}_{\mathrm{k}}\overset{\mathrm{k}}{\mathbf{F}}{}_{\mathrm{ke}}^{\mathrm{T}}, \tag{8.26}$$

$$\tilde{\mathbf{X}}_{\mathrm{d}} := \Big(\mathbf{F}_{\mathrm{di}}^{-\mathrm{T}}\Big)^{*}\overset{\mathrm{d}}{\mathbf{X}}_{\mathrm{d}} = \mathbf{F}_{\mathrm{di}}^{-1}\overset{\mathrm{d}}{\mathbf{X}}_{\mathrm{d}}\mathbf{F}_{\mathrm{di}}^{-\mathrm{T}}, \quad \hat{\mathbf{X}}_{\mathrm{d}} := \Big(\overset{\mathrm{d}}{\mathbf{F}}{}_{\mathrm{de}}^{-\mathrm{T}}\Big)_{*}\overset{\mathrm{d}}{\mathbf{X}}_{\mathrm{d}} = \overset{\mathrm{d}}{\mathbf{F}}_{\mathrm{de}}\overset{\mathrm{d}}{\mathbf{X}}_{\mathrm{d}}\overset{\mathrm{d}}{\mathbf{F}}{}_{\mathrm{de}}^{\mathrm{T}}. \tag{8.27}$$

The invariance relations take then the form as follows:

$$\overset{\mathrm{k}}{\mathbf{X}}_{\mathrm{k}} : \overset{\mathrm{k}}{\boldsymbol{\Gamma}}_{\mathrm{i}} = \hat{\mathbf{X}}_{\mathrm{k}} : \hat{\boldsymbol{\Gamma}}_{\mathrm{i}} = \tilde{\mathbf{X}}_{\mathrm{k}} : \tilde{\boldsymbol{\Gamma}}_{\mathrm{i}}, \quad \overset{\mathrm{k}}{\mathbf{X}}_{\mathrm{k}} : \mathfrak{D}_{\mathrm{ki}}(\overset{\mathrm{k}}{\boldsymbol{\Gamma}}_{\mathrm{i}}) = \hat{\mathbf{X}}_{\mathrm{k}} : \mathfrak{D}_{\mathrm{i}}(\hat{\boldsymbol{\Gamma}}_{\mathrm{i}}) = \tilde{\mathbf{X}}_{\mathrm{k}} : \dot{\tilde{\boldsymbol{\Gamma}}}_{\mathrm{i}}, \tag{8.28}$$

$$\overset{\mathrm{d}}{\mathbf{X}}_{\mathrm{d}} : \overset{\mathrm{d}}{\boldsymbol{\Gamma}}_{\mathrm{i}} = \hat{\mathbf{X}}_{\mathrm{d}} : \hat{\boldsymbol{\Gamma}}_{\mathrm{i}} = \tilde{\mathbf{X}}_{\mathrm{d}} : \tilde{\boldsymbol{\Gamma}}_{\mathrm{i}}, \quad \overset{\mathrm{d}}{\mathbf{X}}_{\mathrm{d}} : \mathfrak{D}_{\mathrm{di}}(\overset{\mathrm{d}}{\boldsymbol{\Gamma}}_{\mathrm{i}}) = \hat{\mathbf{X}}_{\mathrm{d}} : \mathfrak{D}_{\mathrm{i}}(\hat{\boldsymbol{\Gamma}}_{\mathrm{i}}) = \tilde{\mathbf{X}}_{\mathrm{d}} : \dot{\tilde{\boldsymbol{\Gamma}}}_{\mathrm{i}}. \tag{8.29}$$

The physical importance of invariance relations (8.25), (8.28), and (8.29) will be apparent in the following.

---

[12] Some general definitions of conjugacy for objective stresses and strains as well as some rules for the construction of conjugate pairs are presented in [**26**].

[13] In [**11**], the tensor which plays a similar role as $\mathbf{X}_{\mathrm{d}}$ is termed a back stress tensor.

3.3. Free energy and potential relations for stresses. Since a thermodynamically consistent approach to the modeling of the material behavior is pursued in this work, a proper ansatz for the free energy function is needed. The rheological model (see Fig. 8.4a) motivates the additive split $\psi = \psi_{\mathrm{el}} + \psi_{\mathrm{kin}} + \psi_{\mathrm{dis}}$ of the stored energy into elastic part ψ_{el} (cf. elastic spring 3 in Fig. 8.4b), a part associated with the kinematic hardening ψ_{kin} (cf. elastic spring 2 in Fig. 8.4b) and the distortional part ψ_{dis} (cf. elastic spring 1 in Fig. 8.4b).

Moreover, in order to capture the energy storage due to the isotropic hardening we introduce two real-valued internal variables of strain type: s and s_{d}. In some cases the variable s can be associated with the inelastic arc length (Odqvist parameter), and s_{d} is interpreted as a dissipative part of s, such that

$$s_{\mathrm{e}} := s - s_{\mathrm{d}} \tag{8.30}$$

controls the energy storage associated with the isotropic hardening. Thus, we suppose that the free energy is given as a sum of isotropic functions (cf. [**32, 49, 21, 10, 42**])

$$\psi = \psi(\hat{\mathbf{C}}_{\mathrm{e}}, \overset{\mathrm{k}}{\mathbf{C}}_{\mathrm{ke}}, \overset{\mathrm{d}}{\mathbf{C}}_{\mathrm{de}}, s_{\mathrm{e}}) = \psi_{\mathrm{el}}(\hat{\mathbf{C}}_{\mathrm{e}}) + \psi_{\mathrm{kin}}(\overset{\mathrm{k}}{\mathbf{C}}_{\mathrm{ke}}) + \psi_{\mathrm{dis}}(\overset{\mathrm{d}}{\mathbf{C}}_{\mathrm{de}}) + \psi_{\mathrm{iso}}(s_{\mathrm{e}}), \tag{8.31}$$

where the tensors $\hat{\mathbf{C}}_{\mathrm{e}}$, $\overset{\mathrm{k}}{\mathbf{C}}_{\mathrm{ke}}$, and $\overset{\mathrm{d}}{\mathbf{C}}_{\mathrm{de}}$ are defined by (8.15). Here, $\psi_{\mathrm{el}}(\hat{\mathbf{C}}_{\mathrm{e}})$ corresponds to the energy, stored due to macroscopic elastic deformations. The "inelastic" part $\psi_{\mathrm{kin}}(\overset{\mathrm{k}}{\mathbf{C}}_{\mathrm{ke}}) + \psi_{\mathrm{dis}}(\overset{\mathrm{d}}{\mathbf{C}}_{\mathrm{de}}) + \psi_{\mathrm{iso}}(s_{\mathrm{e}})$ represents the energy, stored at the microstructural level during the viscoplastic flow due to the heterogeneity of the dislocation field. The following special form of the free energy can be used (cf. [**21, 42**])[14]

$$\rho_{\mathrm{R}} \psi_{\mathrm{el}}(\hat{\mathbf{C}}_{\mathrm{e}}) = \frac{k}{2}\Big(\ln \sqrt{\det \hat{\mathbf{C}}_{\mathrm{e}}}\Big)^2 + \frac{\mu}{2}\Big(\mathrm{tr}\overline{\hat{\mathbf{C}}_{\mathrm{e}}} - 3\Big), \tag{8.32}$$

$$\rho_{\mathrm{R}} \psi_{\mathrm{kin}}(\overset{\mathrm{k}}{\mathbf{C}}_{\mathrm{ke}}) = \frac{c_{\mathrm{k}}}{4}\Big(\mathrm{tr}\overline{\overset{\mathrm{k}}{\mathbf{C}}_{\mathrm{ke}}} - 3\Big), \quad \rho_{\mathrm{R}} \psi_{\mathrm{dis}}(\overset{\mathrm{d}}{\mathbf{C}}_{\mathrm{de}}) = \frac{c_{\mathrm{d}}}{4}\Big(\mathrm{tr}\overline{\overset{\mathrm{d}}{\mathbf{C}}_{\mathrm{de}}} - 3\Big), \quad \rho_{\mathrm{R}} \psi_{\mathrm{iso}}(s_{\mathrm{e}}) = \frac{\gamma}{2}\,(s_{\mathrm{e}})^2. \tag{8.33}$$

Here, $k > 0$, $\mu > 0$, $c_{\mathrm{k}} > 0$, $c_{\mathrm{d}} > 0$, $\gamma \in \mathbb{R}$ are material constants; $\rho_{\mathrm{R}} > 0$ stands for the mass density in the reference configuration. The overline $\overline{(\cdot)}$ denotes the unimodular part of a tensor.

We recall that $\hat{\mathbf{C}}_{\mathrm{e}} = 2\hat{\mathbf{\Gamma}}_{\mathrm{e}} + \mathbf{1}$, $\overset{\mathrm{k}}{\mathbf{C}}_{\mathrm{ke}} = 2\overset{\mathrm{k}}{\mathbf{\Gamma}}_{\mathrm{ke}} + \mathbf{1}$, and $\overset{\mathrm{d}}{\mathbf{C}}_{\mathrm{de}} = 2\overset{\mathrm{d}}{\mathbf{\Gamma}}_{\mathrm{de}} + \mathbf{1}$. Using these identities we introduce formally the following relations for stresses $\hat{\mathbf{S}}$, $\overset{\mathrm{k}}{\mathbf{X}}_{\mathrm{k}}$, $\overset{\mathrm{d}}{\mathbf{X}}_{\mathrm{d}}$ and for isotropic hardening R

$$\hat{\mathbf{S}} = \rho_{\mathrm{R}} \frac{\partial \psi_{\mathrm{el}}(2\hat{\mathbf{\Gamma}}_{\mathrm{e}} + \mathbf{1})}{\partial \hat{\mathbf{\Gamma}}_{\mathrm{e}}}, \quad \overset{\mathrm{k}}{\mathbf{X}}_{\mathrm{k}} = \rho_{\mathrm{R}} \frac{\partial \psi_{\mathrm{kin}}(2\overset{\mathrm{k}}{\mathbf{\Gamma}}_{\mathrm{ke}} + \mathbf{1})}{\partial \overset{\mathrm{k}}{\mathbf{\Gamma}}_{\mathrm{ke}}}, \quad \overset{\mathrm{d}}{\mathbf{X}}_{\mathrm{d}} = \rho_{\mathrm{R}} \frac{\partial \psi_{\mathrm{dis}}(2\overset{\mathrm{d}}{\mathbf{\Gamma}}_{\mathrm{de}} + \mathbf{1})}{\partial \overset{\mathrm{d}}{\mathbf{\Gamma}}_{\mathrm{de}}}, \quad R = \rho_{\mathrm{R}} \frac{\partial \psi_{\mathrm{iso}}(s_{\mathrm{e}})}{\partial s_{\mathrm{e}}}. \tag{8.34}$$

As it will be shown in Sections 3.4 and 3.5, relations (8.34) in combination with evolution equations from Section 3.5 lead to a thermodynamically consistent material model.

Basing on $(8.26)_2$, $(8.27)_2$, (8.33), and (8.34) it can be easily shown that $\mathrm{tr}(\hat{\mathbf{X}}_{\mathrm{k}}) = \mathrm{tr}(\hat{\mathbf{X}}_{\mathrm{d}}) = 0$.

---

[14] Obviously, some other assumptions for the volumetric part in (8.32) can be implemented as well. It was noted in [**16**] that $\big(\ln \sqrt{\det \hat{\mathbf{C}}_{\mathrm{e}}}\big)^2$ is not convex in $\det \hat{\mathbf{C}}_{\mathrm{e}}$, and non-physical behavior can be observed for very large elastic bulk strains.

3.4. Specification of the Clausius-Duhem inequality. Let us consider the Clausius-Duhem inequality which states that the internal dissipation δ_{i} is always nonnegative. Thus, an additional constraint is imposed on the system of constitutive equations. Since isothermal processes are considered in this paper, the inequality takes the form as follows (see [**20**])

$$\delta_{\mathrm{i}} := \frac{1}{\rho_{\mathrm{R}}} \tilde{\mathbf{T}} : \dot{\mathbf{E}} - \dot{\psi} \geq 0. \tag{8.35}$$

In this subsection we elaborate on the Clausius-Duhem inequality by taking the specific constitutive relations from previous subsections into account. First, we note that $\hat{\mathbf{S}}$, $\overset{\mathrm{k}}{\mathbf{X}}_{\mathrm{k}}$, and $\overset{\mathrm{d}}{\mathbf{X}}_{\mathrm{d}}$ are isotropic functions of $\hat{\boldsymbol{\Gamma}}_{\mathrm{e}}$, $\overset{\mathrm{k}}{\boldsymbol{\Gamma}}_{\mathrm{ke}}$, and $\overset{\mathrm{d}}{\boldsymbol{\Gamma}}_{\mathrm{de}}$ respectively. In particular, since $\hat{\mathbf{S}}$ and $\hat{\boldsymbol{\Gamma}}_{\mathrm{e}}$ commute ($\hat{\mathbf{S}}\hat{\boldsymbol{\Gamma}}_{\mathrm{e}} = \hat{\boldsymbol{\Gamma}}_{\mathrm{e}}\hat{\mathbf{S}}$), we deduce that $\hat{\boldsymbol{\Gamma}}_{\mathrm{e}}\hat{\mathbf{S}} \in Sym$ and

$$\hat{\mathbf{S}} : \Big(\hat{\mathbf{L}}_{\mathrm{i}}^{\mathrm{T}}\hat{\boldsymbol{\Gamma}}_{\mathrm{e}} + \hat{\boldsymbol{\Gamma}}_{\mathrm{e}}\hat{\mathbf{L}}_{\mathrm{i}}\Big) \overset{(8.2)}{=} 2\Big(\hat{\boldsymbol{\Gamma}}_{\mathrm{e}}\hat{\mathbf{S}}\Big) : \hat{\mathbf{L}}_{\mathrm{i}} \overset{\hat{\boldsymbol{\Gamma}}_{\mathrm{e}}\hat{\mathbf{S}} \in Sym}{=} 2\Big(\hat{\boldsymbol{\Gamma}}_{\mathrm{e}}\hat{\mathbf{S}}\Big) : \mathrm{sym}(\hat{\mathbf{L}}_{\mathrm{i}}) \overset{(8.22)_1}{=} 2\Big(\hat{\boldsymbol{\Gamma}}_{\mathrm{e}}\hat{\mathbf{S}}\Big) : \mathfrak{O}_{\mathrm{i}}(\hat{\boldsymbol{\Gamma}}_{\mathrm{i}}). \tag{8.36}$$

Furthermore, noting that $\mathbf{1} + 2\hat{\boldsymbol{\Gamma}}_{\mathrm{e}} = \hat{\mathbf{C}}_{\mathrm{e}}$, we obtain

$$\begin{aligned} &\hat{\mathbf{S}} : \mathfrak{O}_{\mathrm{i}}(\hat{\boldsymbol{\Gamma}}) \overset{(8.16)_1}{=} \hat{\mathbf{S}} : \mathfrak{O}_{\mathrm{i}}(\hat{\boldsymbol{\Gamma}}_{\mathrm{e}}) + \hat{\mathbf{S}} : \mathfrak{O}_{\mathrm{i}}(\hat{\boldsymbol{\Gamma}}_{\mathrm{i}}) \overset{(8.21)_1}{=} \\ &\quad \hat{\mathbf{S}} : \frac{d}{dt}(\hat{\boldsymbol{\Gamma}}_{\mathrm{e}}) + \hat{\mathbf{S}} : \Big(\hat{\mathbf{L}}_{\mathrm{i}}^{\mathrm{T}}\hat{\boldsymbol{\Gamma}}_{\mathrm{e}} + \hat{\boldsymbol{\Gamma}}_{\mathrm{e}}\hat{\mathbf{L}}_{\mathrm{i}}\Big) + \hat{\mathbf{S}} : \mathfrak{O}_{\mathrm{i}}(\hat{\boldsymbol{\Gamma}}_{\mathrm{i}}) \overset{(8.36)}{=} \hat{\mathbf{S}} : \frac{d}{dt}(\hat{\boldsymbol{\Gamma}}_{\mathrm{e}}) + \Big(\hat{\mathbf{C}}_{\mathrm{e}}\hat{\mathbf{S}}\Big) : \mathfrak{O}_{\mathrm{i}}(\hat{\boldsymbol{\Gamma}}_{\mathrm{i}}). \end{aligned} \tag{8.37}$$

Similarly, since $\overset{\mathrm{k}}{\mathbf{X}}_{\mathrm{k}}\overset{\mathrm{k}}{\boldsymbol{\Gamma}}_{\mathrm{ke}} = \overset{\mathrm{k}}{\boldsymbol{\Gamma}}_{\mathrm{ke}}\overset{\mathrm{k}}{\mathbf{X}}_{\mathrm{k}}$ and $\overset{\mathrm{d}}{\mathbf{X}}_{\mathrm{d}}\overset{\mathrm{d}}{\boldsymbol{\Gamma}}_{\mathrm{de}} = \overset{\mathrm{d}}{\boldsymbol{\Gamma}}_{\mathrm{de}}\overset{\mathrm{d}}{\mathbf{X}}_{\mathrm{d}}$, we obtain from (8.17), $(8.21)_2$, $(8.21)_3$, $(8.22)_2$, and $(8.22)_3$

$$\overset{\mathrm{k}}{\mathbf{X}}_{\mathrm{k}} : \mathfrak{O}_{\mathrm{ki}}(\overset{\mathrm{k}}{\boldsymbol{\Gamma}}_{\mathrm{i}}) = \overset{\mathrm{k}}{\mathbf{X}}_{\mathrm{k}} : \frac{d}{dt}(\overset{\mathrm{k}}{\boldsymbol{\Gamma}}_{\mathrm{ke}}) + \Big(\overset{\mathrm{k}}{\mathbf{C}}_{\mathrm{ke}}\overset{\mathrm{k}}{\mathbf{X}}_{\mathrm{k}}\Big) : \mathfrak{O}_{\mathrm{ki}}(\overset{\mathrm{k}}{\boldsymbol{\Gamma}}_{\mathrm{ki}}), \tag{8.38}$$

$$\overset{\mathrm{d}}{\mathbf{X}}_{\mathrm{d}} : \mathfrak{O}_{\mathrm{di}}(\overset{\mathrm{d}}{\boldsymbol{\Gamma}}_{\mathrm{i}}) = \overset{\mathrm{d}}{\mathbf{X}}_{\mathrm{d}} : \frac{d}{dt}(\overset{\mathrm{d}}{\boldsymbol{\Gamma}}_{\mathrm{de}}) + \Big(\overset{\mathrm{d}}{\mathbf{C}}_{\mathrm{de}}\overset{\mathrm{d}}{\mathbf{X}}_{\mathrm{d}}\Big) : \mathfrak{O}_{\mathrm{di}}(\overset{\mathrm{d}}{\boldsymbol{\Gamma}}_{\mathrm{di}}). \tag{8.39}$$

Therefore, we obtain for the stress power

$$\begin{aligned} &\tilde{\mathbf{T}} : \dot{\mathbf{E}} \overset{(8.25)_2}{=} \hat{\mathbf{S}} : \mathfrak{O}_{\mathrm{i}}(\hat{\boldsymbol{\Gamma}}) \overset{(8.28)_2,(8.29)_2}{=} \\ &\quad \hat{\mathbf{S}} : \mathfrak{O}_{\mathrm{i}}(\hat{\boldsymbol{\Gamma}}) - \hat{\mathbf{X}}_{\mathrm{k}} : \mathfrak{O}_{\mathrm{i}}(\hat{\boldsymbol{\Gamma}}_{\mathrm{i}}) + \overset{\mathrm{k}}{\mathbf{X}}_{\mathrm{k}} : \mathfrak{O}_{\mathrm{ki}}(\overset{\mathrm{k}}{\boldsymbol{\Gamma}}_{\mathrm{i}}) - \hat{\mathbf{X}}_{\mathrm{d}} : \mathfrak{O}_{\mathrm{i}}(\hat{\boldsymbol{\Gamma}}_{\mathrm{i}}) + \overset{\mathrm{d}}{\mathbf{X}}_{\mathrm{d}} : \mathfrak{O}_{\mathrm{di}}(\overset{\mathrm{d}}{\boldsymbol{\Gamma}}_{\mathrm{i}}) \overset{(8.37)-(8.39)}{=} \\ &\quad \hat{\mathbf{S}} : \frac{d}{dt}(\hat{\boldsymbol{\Gamma}}_{\mathrm{e}}) + \Big(\hat{\mathbf{C}}_{\mathrm{e}}\hat{\mathbf{S}} - \hat{\mathbf{X}}_{\mathrm{k}} - \hat{\mathbf{X}}_{\mathrm{d}}\Big) : \mathfrak{O}_{\mathrm{i}}(\hat{\boldsymbol{\Gamma}}_{\mathrm{i}}) + \overset{\mathrm{k}}{\mathbf{X}}_{\mathrm{k}} : \frac{d}{dt}(\overset{\mathrm{k}}{\boldsymbol{\Gamma}}_{\mathrm{ke}}) + \Big(\overset{\mathrm{k}}{\mathbf{C}}_{\mathrm{ke}}\overset{\mathrm{k}}{\mathbf{X}}_{\mathrm{k}}\Big) : \mathfrak{O}_{\mathrm{ki}}(\overset{\mathrm{k}}{\boldsymbol{\Gamma}}_{\mathrm{ki}}) + \\ &\qquad + \overset{\mathrm{d}}{\mathbf{X}}_{\mathrm{d}} : \frac{d}{dt}(\overset{\mathrm{d}}{\boldsymbol{\Gamma}}_{\mathrm{de}}) + \Big(\overset{\mathrm{d}}{\mathbf{C}}_{\mathrm{de}}\overset{\mathrm{d}}{\mathbf{X}}_{\mathrm{d}}\Big) : \mathfrak{O}_{\mathrm{di}}(\overset{\mathrm{d}}{\boldsymbol{\Gamma}}_{\mathrm{di}}). \end{aligned} \tag{8.40}$$

Hence, the internal dissipation takes the form

$$\begin{aligned} \delta_{\mathrm{i}} &= \frac{1}{\rho_{\mathrm{R}}}\tilde{\mathbf{T}} : \dot{\mathbf{E}} - \dot{\psi} \overset{(8.40)}{=} \Big(\frac{1}{\rho_{\mathrm{R}}}\hat{\mathbf{S}} - \frac{\partial \psi_{\mathrm{el}}}{\partial \hat{\boldsymbol{\Gamma}}_{\mathrm{e}}}\Big) : \frac{d}{dt}(\hat{\boldsymbol{\Gamma}}_{\mathrm{e}}) + \Big(\frac{1}{\rho_{\mathrm{R}}}\overset{\mathrm{k}}{\mathbf{X}}_{\mathrm{k}} - \frac{\partial \psi_{\mathrm{kin}}}{\partial \overset{\mathrm{k}}{\boldsymbol{\Gamma}}_{\mathrm{ke}}}\Big) : \frac{d}{dt}(\overset{\mathrm{k}}{\boldsymbol{\Gamma}}_{\mathrm{ke}}) + \\ &+ \Big(\frac{1}{\rho_{\mathrm{R}}}\overset{\mathrm{d}}{\mathbf{X}}_{\mathrm{d}} - \frac{\partial \psi_{\mathrm{dis}}}{\partial \overset{\mathrm{d}}{\boldsymbol{\Gamma}}_{\mathrm{de}}}\Big) : \frac{d}{dt}(\overset{\mathrm{d}}{\boldsymbol{\Gamma}}_{\mathrm{de}}) + \frac{1}{\rho_{\mathrm{R}}}\Big(\hat{\mathbf{C}}_{\mathrm{e}}\hat{\mathbf{S}} - \hat{\mathbf{X}}_{\mathrm{k}} - \hat{\mathbf{X}}_{\mathrm{d}}\Big) : \mathfrak{O}_{\mathrm{i}}(\hat{\boldsymbol{\Gamma}}_{\mathrm{i}}) + \frac{1}{\rho_{\mathrm{R}}}\Big(\overset{\mathrm{k}}{\mathbf{C}}_{\mathrm{ke}}\overset{\mathrm{k}}{\mathbf{X}}_{\mathrm{k}}\Big) : \mathfrak{O}_{\mathrm{ki}}(\overset{\mathrm{k}}{\boldsymbol{\Gamma}}_{\mathrm{ki}}) + \\ &\qquad + \frac{1}{\rho_{\mathrm{R}}}\Big(\overset{\mathrm{d}}{\mathbf{C}}_{\mathrm{de}}\overset{\mathrm{d}}{\mathbf{X}}_{\mathrm{d}}\Big) : \mathfrak{O}_{\mathrm{di}}(\overset{\mathrm{d}}{\boldsymbol{\Gamma}}_{\mathrm{di}}) - \frac{\partial \psi_{\mathrm{iso}}}{\partial s_{\mathrm{e}}}\ \dot{s}_{\mathrm{e}}. \end{aligned} \tag{8.41}$$

We abbreviate

$$\hat{\boldsymbol{\Sigma}} := \hat{\mathbf{C}}_{\mathrm{e}}\hat{\mathbf{S}} - \hat{\mathbf{X}}_{\mathrm{k}}, \quad \overset{\mathrm{k}}{\boldsymbol{\Xi}}_{\mathrm{k}} := \overset{\mathrm{k}}{\mathbf{C}}_{\mathrm{ke}}\overset{\mathrm{k}}{\mathbf{X}}_{\mathrm{k}}, \quad \overset{\mathrm{d}}{\boldsymbol{\Xi}}_{\mathrm{d}} := \overset{\mathrm{d}}{\mathbf{C}}_{\mathrm{de}}\overset{\mathrm{d}}{\mathbf{X}}_{\mathrm{d}}. \tag{8.42}$$

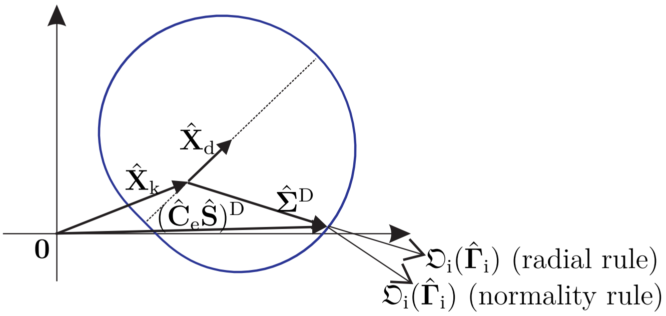

Figure 8.5. Schematic representation of the yield surface: the critical values of $(\hat{\mathbf{C}}_{\mathrm{e}}\hat{\mathbf{S}})^{\mathrm{D}}$ for given $\hat{\mathbf{X}}_{\mathrm{k}}$ and $\hat{\mathbf{X}}_{\mathrm{d}}$.

Finally, taking into account potential relations (8.34), we simplify (8.41) to obtain the Clausius-Duhem inequality in the form

$$\rho_{\mathrm{R}}\delta_{\mathrm{i}} = \Big((\hat{\boldsymbol{\Sigma}} - \hat{\mathbf{X}}_{\mathrm{d}}) : \mathfrak{D}_{\mathrm{i}}(\hat{\boldsymbol{\Gamma}}_{\mathrm{i}}) - R\ \dot{s}_{\mathrm{e}}\Big) + \overset{\mathrm{k}}{\boldsymbol{\Xi}}_{\mathrm{k}} : \mathfrak{D}_{\mathrm{ki}}(\overset{\mathrm{k}}{\boldsymbol{\Gamma}}_{\mathrm{ki}}) + \overset{\mathrm{d}}{\boldsymbol{\Xi}}_{\mathrm{d}} : \mathfrak{D}_{\mathrm{di}}(\overset{\mathrm{d}}{\boldsymbol{\Gamma}}_{\mathrm{di}}) \geq 0. \tag{8.43}$$

Remark 4. Some terms from the left-hand side of (8.43) can obtain a simple interpretation using the rheological model in Fig. 8.4b. In particular, the quantity $(\hat{\boldsymbol{\Sigma}} - \hat{\mathbf{X}}_{\mathrm{d}}) : \mathfrak{D}_{\mathrm{i}}(\hat{\boldsymbol{\Gamma}}_{\mathrm{i}})$ corresponds to the energy dissipation due to the friction of the $(St - V)$-element. The terms $\overset{\mathrm{k}}{\boldsymbol{\Xi}}_{\mathrm{k}} : \mathfrak{D}_{\mathrm{ki}}(\overset{\mathrm{k}}{\boldsymbol{\Gamma}}_{\mathrm{ki}})$ and $\overset{\mathrm{d}}{\boldsymbol{\Xi}}_{\mathrm{d}} : \mathfrak{D}_{\mathrm{di}}(\overset{\mathrm{d}}{\boldsymbol{\Gamma}}_{\mathrm{di}})$ correspond to the energy dissipation due to the friction of the modified Newton-bodies $(m.N2)$ and $(m.N1)$, respectively.

3.5. Yield function and evolution equations. In what follows suppose that[15]

$$\|\hat{\mathbf{X}}_{\mathrm{d}}\| < \sqrt{\frac{2}{3}}\Big[K + R\Big]. \tag{8.44}$$

We assume the yield function in the form

$$f = f(\hat{\boldsymbol{\Sigma}}, \hat{\mathbf{X}}_{\mathrm{d}}, R) := \|\hat{\boldsymbol{\Sigma}}^{\mathrm{D}}\| - \hat{\mathbf{X}}_{\mathrm{d}} : \frac{\hat{\boldsymbol{\Sigma}}^{\mathrm{D}}}{\|\hat{\boldsymbol{\Sigma}}^{\mathrm{D}}\|} - \sqrt{\frac{2}{3}}\Big[K + R\Big], \quad \text{for all } \hat{\boldsymbol{\Sigma}}^{\mathrm{D}} \neq \mathbf{0}, \tag{8.45}$$

where $K > 0$ stands for the initial flow stress. In view of (8.44), $f < 0$ as $\hat{\boldsymbol{\Sigma}}^{\mathrm{D}} \to \mathbf{0}$. To be definite, we put $f := -K$ for $\hat{\boldsymbol{\Sigma}}^{\mathrm{D}} = \mathbf{0}$. The influence of $\hat{\mathbf{X}}_{\mathrm{k}}$ and $\hat{\mathbf{X}}_{\mathrm{d}}$ on the form of the yield locus is sketched in Fig. 8.5.

Remark 5. The yield function (8.45) results from the constraint (8.6) if $\overrightarrow{F}$ and $\overrightarrow{X_{\mathrm{d}}}$ are formally replaced by $\hat{\boldsymbol{\Sigma}}^{\mathrm{D}}$ and $\hat{\mathbf{X}}_{\mathrm{d}}$, respectively. Note that a similar yield function was considered in [**34, 35**] in the case of small strains. On the other hand, as it is shown in Appendix A, relation (8.5) would lead to the similar results as (8.6) (at least in the case of the rate-independent plasticity).

Remark 6. The assumption (8.45) implies that the onset of inelastic yielding is independent of the hydrostatic stress $\mathrm{tr}\hat{\boldsymbol{\Sigma}}$.

Note that in the case $\hat{\mathbf{X}}_{\mathrm{k}} = \hat{\mathbf{X}}_{\mathrm{d}} = \mathbf{0}$, $R = 0$, the classical Mises-Huber yield function is restored, which reads $f_{MH} = \|(\hat{\mathbf{C}}_{\mathrm{e}}\hat{\mathbf{S}})^{\mathrm{D}}\| - \sqrt{2/3}K$ (see, for example, [**41**]).

In the following subsections some evolution equations will be formulated such that inequality (8.43) is identically satisfied (cf. (8.59), (8.65), (8.67), (8.70)). In other words, a

---

[15] A constraint is discussed in Subsection 3.5.5, which should be imposed on material parameters in order to guarantee the satisfaction of (8.44).

thermodynamically consistent material model will be formulated. Moreover, the corresponding inelastic flows will be incompressible (cf. (8.62), (8.63), (8.66), (8.69))

$$\mathrm{tr}\Big(\mathfrak{D}_{\mathrm{i}}(\hat{\mathbf{\Gamma}}_{\mathrm{i}})\Big) = \mathrm{tr}\Big(\mathfrak{D}_{\mathrm{ki}}(\overset{\mathrm{k}}{\mathbf{\Gamma}}_{\mathrm{ki}})\Big) = \mathrm{tr}\Big(\mathfrak{D}_{\mathrm{di}}(\overset{\mathrm{d}}{\mathbf{\Gamma}}_{\mathrm{di}})\Big) = 0, \quad (\mathrm{det}\mathbf{F}_{\mathrm{i}})^{\cdot} = (\mathrm{det}\mathbf{F}_{\mathrm{ki}})^{\cdot} = (\mathrm{det}\mathbf{F}_{\mathrm{di}})^{\cdot} = 0. \tag{8.46}$$

Therefore, under proper initial conditions we arrive at

$$\mathrm{det}\mathbf{F}_{\mathrm{i}} = \mathrm{det}\mathbf{F}_{\mathrm{ki}} = \mathrm{det}\mathbf{F}_{\mathrm{di}} = \mathrm{det}\overset{\mathrm{k}}{\mathbf{F}}_{\mathrm{ke}} = \mathrm{det}\overset{\mathrm{d}}{\mathbf{F}}_{\mathrm{de}} = 1. \tag{8.47}$$

3.5.1. *Perzyna rule and evolution equations for s, s_d.* We introduce the inelastic multiplier $\check{\lambda}_{\mathrm{i}}$ according to the well-known Perzyna rule [**36**]

$$\check{\lambda}_{\mathrm{i}} := \frac{1}{\eta}\Big\langle \frac{1}{k_0} f \Big\rangle^{m}, \quad \langle x \rangle := \max(x, 0). \tag{8.48}$$

Here, $\eta > 0$ and $m \geq 1$, are material parameters, $k_0 > 0$ is used to obtain a dimensionless term in the bracket. In the context of (8.48), the yield function f represents an overstress. According to (8.48), the inelastic flow takes place if the overstress f is positive. A case of rate-independent plasticity is covered as $\eta \to 0$.[16] Next, we consider an evolution equation for s combined with an initial condition

$$\dot{s} = \sqrt{\frac{2}{3}}\check{\lambda}_{\mathrm{i}}, \quad s|_{t=0} = s^0. \tag{8.49}$$

Note that $\dot{s} \geq 0$. It follows from (8.30), $(8.33)_3$, and $(8.34)_4$ that $R = \gamma s_{\mathrm{e}} = \gamma(s - s_{\mathrm{d}})$. In order to obtain the isotropic hardening R as a function of s we consider the evolution equation for s_{d} as follows

$$\dot{s}_{\mathrm{d}} = \frac{\beta}{\gamma}\dot{s}R, \quad \gamma \in \mathbb{R}, \ \beta \geq 0; \quad s_{\mathrm{d}}|_{t=0} = s^0_{\mathrm{d}}. \tag{8.50}$$

In particular, the Voce hardening rule can be restored by integrating $(8.50)_1$ if zero initial conditions for s and s_{d} are assumed, and if s is interpreted as the inelastic arc length:

$$R(s) = \frac{\gamma}{\beta}(1 - \exp(-\beta s)) \text{ for } \beta > 0, \quad R(s) = \gamma s \text{ for } \beta = 0. \tag{8.51}$$

Note that for $\gamma > 0$ the isotropic hardening is predicted: $R \geq 0$. On the other hand, for $\gamma < 0$, we obtain $R \leq 0$ (isotropic softening). Moreover, it is natural to impose the following constraint on the material parameters

$$K + \gamma/\beta \geq 0. \tag{8.52}$$

Using (8.50) it can be shown (see Appendix B) that

$$R(1 - \dot{s}_{\mathrm{e}}/\dot{s}) \geq 0, \text{ for } \gamma > 0; \quad R(1 - \dot{s}_{\mathrm{e}}/\dot{s}) \geq \gamma/\beta, \ \text{ for } \gamma < 0, |\gamma(s^0 - s^0_{\mathrm{d}})| \leq -\gamma/\beta. \tag{8.53}$$

These results will be used in the following in order to prove the thermodynamic consistency of the model.

---

[16] To the best of our knowledge, a rigorous mathematical proof of this statement is still missing (cf. [**19**]).

3.5.2. *Normality rule for* $\mathfrak{D}_i(\hat{\mathbf{\Gamma}}_i)$. It follows immediately from (8.45) that

$$\frac{\partial f(\hat{\mathbf{\Sigma}}, \hat{\mathbf{X}}_{\mathrm{d}}, R)}{\partial \hat{\mathbf{\Sigma}}} = \frac{\hat{\mathbf{\Sigma}}^{\mathrm{D}}}{\|\hat{\mathbf{\Sigma}}^{\mathrm{D}}\|} - \frac{\hat{\mathbf{X}}_{\mathrm{d}}}{\|\hat{\mathbf{\Sigma}}^{\mathrm{D}}\|} + \frac{\hat{\mathbf{X}}_{\mathrm{d}} : \hat{\mathbf{\Sigma}}^{\mathrm{D}}}{\|\hat{\mathbf{\Sigma}}^{\mathrm{D}}\|^3} \hat{\mathbf{\Sigma}}^{\mathrm{D}}. \tag{8.54}$$

Following the normality rule (cf. Fig. 8.5), we consider the constitutive equation as follows

$$\mathfrak{D}_{\mathrm{i}}(\hat{\mathbf{\Gamma}}_{\mathrm{i}}) = \check{\lambda}_{\mathrm{i}} \frac{\partial f(\hat{\mathbf{\Sigma}}, \hat{\mathbf{X}}_{\mathrm{d}}, R)}{\partial \hat{\mathbf{\Sigma}}} = \check{\lambda}_{\mathrm{i}} \bigg(\frac{\hat{\mathbf{\Sigma}}^{\mathrm{D}}}{\|\hat{\mathbf{\Sigma}}^{\mathrm{D}}\|} - \frac{\hat{\mathbf{X}}_{\mathrm{d}}}{\|\hat{\mathbf{\Sigma}}^{\mathrm{D}}\|} + \frac{\hat{\mathbf{X}}_{\mathrm{d}} : \hat{\mathbf{\Sigma}}^{\mathrm{D}}}{\|\hat{\mathbf{\Sigma}}^{\mathrm{D}}\|^3} \hat{\mathbf{\Sigma}}^{\mathrm{D}} \bigg). \tag{8.55}$$

Let us show that the parenthetical term in (8.43) is non-negative. Indeed, for $\dot{s} > 0$ we arrive at

$$(\hat{\mathbf{\Sigma}} - \hat{\mathbf{X}}_{\mathrm{d}}) : \mathfrak{D}_{\mathrm{i}}(\hat{\mathbf{\Gamma}}_{\mathrm{i}}) - R\, \dot{s}_{\mathrm{e}} = \check{\lambda}_{\mathrm{i}} \bigg(\|\hat{\mathbf{\Sigma}}^{\mathrm{D}}\| - \hat{\mathbf{X}}_{\mathrm{d}} : \frac{\hat{\mathbf{\Sigma}}^{\mathrm{D}}}{\|\hat{\mathbf{\Sigma}}^{\mathrm{D}}\|} + \frac{\|\hat{\mathbf{X}}_{\mathrm{d}}\|^2}{\|\hat{\mathbf{\Sigma}}^{\mathrm{D}}\|} - \frac{(\hat{\mathbf{X}}_{\mathrm{d}} : \hat{\mathbf{\Sigma}}^{\mathrm{D}})^2}{\|\hat{\mathbf{\Sigma}}^{\mathrm{D}}\|^3} - \sqrt{\frac{2}{3}} \frac{\dot{s}_{\mathrm{e}}}{\dot{s}} R \bigg). \tag{8.56}$$

Next, since $\dot{s} > 0$, we conclude that $f > 0$. Combining this with (8.45) we obtain

$$\|\hat{\mathbf{\Sigma}}^{\mathrm{D}}\| > \hat{\mathbf{X}}_{\mathrm{d}} : \frac{\hat{\mathbf{\Sigma}}^{\mathrm{D}}}{\|\hat{\mathbf{\Sigma}}^{\mathrm{D}}\|} + \sqrt{\frac{2}{3}} \big[K + R \big]. \tag{8.57}$$

Moreover, using the Cauchy–Schwarz inequality we arrive at

$$(\hat{\mathbf{X}}_{\mathrm{d}} : \hat{\mathbf{\Sigma}}^{\mathrm{D}})^2 \leq \|\hat{\mathbf{X}}_{\mathrm{d}}\|^2 \, \|\hat{\mathbf{\Sigma}}^{\mathrm{D}}\|^2, \quad \frac{\|\hat{\mathbf{X}}_{\mathrm{d}}\|^2}{\|\hat{\mathbf{\Sigma}}^{\mathrm{D}}\|} - \frac{(\hat{\mathbf{X}}_{\mathrm{d}} : \hat{\mathbf{\Sigma}}^{\mathrm{D}})^2}{\|\hat{\mathbf{\Sigma}}^{\mathrm{D}}\|^3} \geq 0. \tag{8.58}$$

Substituting (8.57) and $(8.58)_2$ in (8.56) we thus obtain

$$(\hat{\mathbf{\Sigma}} - \hat{\mathbf{X}}_{\mathrm{d}}) : \mathfrak{D}_{\mathrm{i}}(\hat{\mathbf{\Gamma}}_{\mathrm{i}}) - R\, \dot{s}_{\mathrm{e}} \geq \sqrt{\frac{2}{3}} \check{\lambda}_{\mathrm{i}} \Big(K + R(1 - \dot{s}_{\mathrm{e}}/\dot{s}) \Big) \overset{(8.52),(8.53)}{\geq} 0. \tag{8.59}$$

The case $\dot{s} = 0$ is trivial.

For what follows it is useful to introduce a multiplier λ_{i} and a correction factor g as follows

$$\lambda_{\mathrm{i}} := \|\mathfrak{D}_{\mathrm{i}}(\hat{\mathbf{\Gamma}}_{\mathrm{i}})\| = g\, \check{\lambda}_{\mathrm{i}}, \quad g := \bigg\| \frac{\hat{\mathbf{\Sigma}}^{\mathrm{D}}}{\|\hat{\mathbf{\Sigma}}^{\mathrm{D}}\|} - \frac{\hat{\mathbf{X}}_{\mathrm{d}}}{\|\hat{\mathbf{\Sigma}}^{\mathrm{D}}\|} + \frac{\hat{\mathbf{X}}_{\mathrm{d}} : \hat{\mathbf{\Sigma}}^{\mathrm{D}}}{\|\hat{\mathbf{\Sigma}}^{\mathrm{D}}\|^3} \hat{\mathbf{\Sigma}}^{\mathrm{D}} \bigg\|. \tag{8.60}$$

Using (8.3) and taking $(8.58)_2$ into account one gets from (8.60)

$$g^2 = 1 + \frac{\|\hat{\mathbf{X}}_{\mathrm{d}}\|^2}{\|\hat{\mathbf{\Sigma}}^{\mathrm{D}}\|^2} - \frac{(\hat{\mathbf{X}}_{\mathrm{d}} : \hat{\mathbf{\Sigma}}^{\mathrm{D}})^2}{\|\hat{\mathbf{\Sigma}}^{\mathrm{D}}\|^4}, \quad g \geq 1. \tag{8.61}$$

Recall that $\mathrm{tr}(\hat{\mathbf{X}}_{\mathrm{d}}) = 0$. Therefore, the normality rule (8.55) implies an incompressible flow:

$$\mathrm{tr}(\mathfrak{D}_{\mathrm{i}}(\hat{\mathbf{\Gamma}}_{\mathrm{i}})) = 0. \tag{8.62}$$

3.5.3. *Radial flow rule for* $\mathfrak{D}_i(\hat{\mathbf{\Gamma}}_i)$. Alternatively to (8.55) let us consider now the radial flow rule as follows (cf. Fig. 8.5)

$$\mathfrak{D}_{\mathrm{i}}(\hat{\mathbf{\Gamma}}_{\mathrm{i}}) = \check{\lambda}_{\mathrm{i}} \frac{\hat{\mathbf{\Sigma}}^{\mathrm{D}}}{\|\hat{\mathbf{\Sigma}}^{\mathrm{D}}\|}. \tag{8.63}$$

Moreover, for $\lambda_{\mathrm{i}} = \|\mathfrak{D}_{\mathrm{i}}(\hat{\mathbf{\Gamma}}_{\mathrm{i}})\|$ we have now $\lambda_{\mathrm{i}} = g\check{\lambda}_{\mathrm{i}}$ with $g = 1$.

Remark 7. Due to (8.49) and (8.63), we have $\dot{s} = \sqrt{\frac{2}{3}} \|\mathfrak{D}_{\mathrm{i}}(\hat{\mathbf{\Gamma}}_{\mathrm{i}})\|$. Therefore, the variable s represents now the accumulated inelastic arc length (Odqvist parameter).

Remark 8. The radial flow rule (8.63) is consistent with the rheological model presented in Fig. 8.4a, since the flow direction coincides with the keel direction.

Similar to the previous subsection we show that the parenthetical term in (8.43) is non-negative. Indeed, for $\dot{s} > 0$ we arrive at

$$(\hat{\mathbf{\Sigma}} - \hat{\mathbf{X}}_{\mathrm{d}}) : \mathfrak{D}_{\mathrm{i}}(\hat{\mathbf{\Gamma}}_{\mathrm{i}}) - R\ \dot{s}_{\mathrm{e}} = \check{\lambda}_{\mathrm{i}}\Big(\|\hat{\mathbf{\Sigma}}^{\mathrm{D}}\| - \hat{\mathbf{X}}_{\mathrm{d}} : \frac{\hat{\mathbf{\Sigma}}^{\mathrm{D}}}{\|\hat{\mathbf{\Sigma}}^{\mathrm{D}}\|} - \sqrt{\frac{2}{3}}\frac{\dot{s}_{\mathrm{e}}}{\dot{s}}R\Big). \tag{8.64}$$

Furthermore, since $\dot{s} > 0$, we conclude that (8.57) holds. Substituting (8.57) in (8.64) we obtain

$$(\hat{\mathbf{\Sigma}} - \hat{\mathbf{X}}_{\mathrm{d}}) : \mathfrak{D}_{\mathrm{i}}(\hat{\mathbf{\Gamma}}_{\mathrm{i}}) - R\ \dot{s}_{\mathrm{e}} \geq \sqrt{\frac{2}{3}}\check{\lambda}_{\mathrm{i}}\Big(K + R\ (1 - \dot{s}_{\mathrm{e}}/\dot{s})\Big) \overset{(8.52),(8.53)}{\geq} 0. \tag{8.65}$$

3.5.4. *Evolution equation for* $\overset{k}{\mathbf{\Gamma}}_{ki}$. We postulate the constitutive equation for $\mathfrak{D}_{\mathrm{ki}}(\overset{\mathrm{k}}{\mathbf{\Gamma}}_{\mathrm{ki}})$ as follows

$$\mathfrak{D}_{\mathrm{ki}}(\overset{\mathrm{k}}{\mathbf{\Gamma}}_{\mathrm{ki}}) = \lambda_{\mathrm{i}}\ \varkappa_{\mathrm{k}}\ \overset{\mathrm{k}}{\mathbf{\Xi}}{}^{\mathrm{D}}_{\mathrm{k}}. \tag{8.66}$$

Here, $\varkappa_{\mathrm{k}} \geq 0$ is a material parameter. For the corresponding term in the Clausius-Duhem inequality (8.43) we have

$$\overset{\mathrm{k}}{\mathbf{\Xi}}_{\mathrm{k}} : \mathfrak{D}_{\mathrm{ki}}(\overset{\mathrm{k}}{\mathbf{\Gamma}}_{\mathrm{ki}}) \geq 0. \tag{8.67}$$

Similar constitutive equations were considered in [**32, 10, 42**] in order to capture the saturation of the kinematic hardening. Note that relation (8.66) can be (partially) motivated by the rheological model in Fig. 8.4a.

3.5.5. *Evolution equation for* $\overset{d}{\mathbf{\Gamma}}_{di}$. The constitutive equation for $\mathfrak{D}_{\mathrm{di}}(\overset{\mathrm{d}}{\mathbf{\Gamma}}_{\mathrm{di}})$ is given by a slight modification of the equation for $\mathfrak{D}_{\mathrm{ki}}(\overset{\mathrm{k}}{\mathbf{\Gamma}}_{\mathrm{ki}})$. First, we introduce a scalar-valued function $\alpha_{\mathrm{d}}(\overset{\mathrm{d}}{\mathbf{C}}_{\mathrm{de}})$

$$\alpha_{\mathrm{d}}(\overset{\mathrm{d}}{\mathbf{C}}_{\mathrm{de}}) := \frac{\|\overset{\mathrm{d}}{\mathbf{C}}{}^{\mathrm{D}}_{\mathrm{de}}\| \cdot \|(\overset{\mathrm{d}}{\mathbf{C}}_{\mathrm{de}}\overset{\mathrm{d}}{\mathbf{C}}{}^{\mathrm{D}}_{\mathrm{de}})^{\mathrm{D}}\|}{\overset{\mathrm{d}}{\mathbf{C}}{}^{\mathrm{D}}_{\mathrm{de}} : (\overset{\mathrm{d}}{\mathbf{C}}_{\mathrm{de}}\overset{\mathrm{d}}{\mathbf{C}}{}^{\mathrm{D}}_{\mathrm{de}})^{\mathrm{D}}}, \quad \text{for } \overset{\mathrm{d}}{\mathbf{C}}_{\mathrm{de}} \neq \mathbf{1}; \quad \alpha_{\mathrm{d}}(\mathbf{1}) := 1. \tag{8.68}$$

The function α_{d} is isotropic. Moreover, the function is smooth and $\alpha_{\mathrm{d}}(\overset{\mathrm{d}}{\mathbf{C}}_{\mathrm{de}}) \geq 1$ if $\overset{\mathrm{d}}{\mathbf{C}}_{\mathrm{de}}$ is positive definite, $\overset{\mathrm{d}}{\mathbf{C}}_{\mathrm{de}} = \overset{\mathrm{d}}{\mathbf{C}}{}^{\mathrm{T}}_{\mathrm{de}}$, and $\det(\overset{\mathrm{d}}{\mathbf{C}}_{\mathrm{de}}) = 1$ (see Appendix C).

We consider the evolution equation for $\overset{\mathrm{d}}{\mathbf{\Gamma}}_{\mathrm{di}}$ as follows

$$\mathfrak{D}_{\mathrm{di}}(\overset{\mathrm{d}}{\mathbf{\Gamma}}_{\mathrm{di}}) = \lambda_{\mathrm{i}}\ \alpha_{\mathrm{d}}(\overset{\mathrm{d}}{\mathbf{C}}_{\mathrm{de}})\ \varkappa_{\mathrm{d}}\ \overset{\mathrm{d}}{\mathbf{\Xi}}{}^{\mathrm{D}}_{\mathrm{d}}. \tag{8.69}$$

Here $\varkappa_{\mathrm{d}} \geq 0$ is a material parameter. Since $\alpha_{\mathrm{d}}(\overset{\mathrm{d}}{\mathbf{C}}_{\mathrm{de}}) \geq 1$ and $\varkappa_{\mathrm{d}} \geq 0$, we obtain for the corresponding term in the Clausius-Duhem inequality (8.43)

$$\overset{\mathrm{d}}{\mathbf{\Xi}}_{\mathrm{d}} : \mathfrak{D}_{\mathrm{di}}(\overset{\mathrm{d}}{\mathbf{\Gamma}}_{\mathrm{di}}) \geq 0. \tag{8.70}$$

Similar to the previous subsection, equation (8.69) implies an incompressible flow.

The motivation for the introduction of the multiplier $\alpha_{\mathrm{d}}(\overset{\mathrm{d}}{\mathbf{C}}_{\mathrm{de}})$ is as follows. The convexity of the yield surface $\{f(\hat{\mathbf{\Sigma}}) = 0\}$ (cf. (8.45)) can be guaranteed if and only if

$$\|\hat{\mathbf{X}}_{\mathrm{d}}\| \leq \frac{1}{2}\sqrt{\frac{2}{3}}\big[K + R\big]. \tag{8.71}$$

Moreover, even if the convexity condition (8.71) is dropped for some reason, the assumption (8.44) still has to be satisfied. Therefore, it is desirable to provide a possibility to control the upper bound of $\|\hat{\mathbf{X}}_{\mathrm{d}}\|$. Such bound is given by the following assertion.

Assertion. Suppose $\|\hat{\mathbf{X}}_\mathrm{d}\||_{t=0} \leq 1/\varkappa_\mathrm{d}$ and relation (8.69) is used to determine $\mathfrak{D}_\mathrm{di}(\overset{\mathrm{d}}{\mathbf{\Gamma}}_\mathrm{di})$; then $\|\hat{\mathbf{X}}_\mathrm{d}\| \leq 1/\varkappa_\mathrm{d}$ at any instance of time. For the proof see Appendix D.

In other words, the multiplier $\alpha_\mathrm{d}(\overset{\mathrm{d}}{\mathbf{C}}_\mathrm{de})$ in (8.69) ensures that the norm of the distortional back stress is bounded by $1/\varkappa_\mathrm{d}$. Thus, by choosing the material parameters such that $1/\varkappa_\mathrm{d} \leq \frac{1}{2}\sqrt{\frac{2}{3}}\big[K + R\big]$, *the convexity of the yield surface is a priori satisfied.* The inequality (8.44) holds identically when $1/\varkappa_\mathrm{d} < \sqrt{\frac{2}{3}}\big[K + R\big]$.

3.6. Transformation to the reference configuration. A closed system of constitutive equations was formulated in previous sections. On the other hand, a direct numerical treatment of evolution equations which were formulated with respect to fictitious configurations $\hat{\mathcal{K}}$, $\mathcal{K}^\mathrm{k}$, and $\mathcal{K}^\mathrm{d}$ is not a trivial task. In order to overcome this problem, we rewrite the constitutive relations in terms of internal variables $\mathbf{C}_\mathrm{i}$, $\mathbf{C}_\mathrm{ki}$, $\mathbf{C}_\mathrm{di}$, s, and s_d, such that the rate of the internal variables will be given by the material time derivative.

3.6.1. *Representation of the free energy.* Let (J_1, J_2, J_3) be a system of invariants of a second-rank tensor, defined by

$$J_1(\mathbf{A}) := \mathrm{tr}\ \mathbf{A}, \quad J_2(\mathbf{A}) := \frac{1}{2}\mathrm{tr}\ \mathbf{A}^2, \quad J_3(\mathbf{A}) := \frac{1}{3}\mathrm{tr}\ \mathbf{A}^3. \tag{8.72}$$

Using multiplicative decompositions (8.8) — (8.10) and the property $\mathrm{tr}(\mathbf{AB}) = \mathrm{tr}(\mathbf{BA})$, it is easily proved that

$$J_n(\hat{\mathbf{C}}_\mathrm{e}) = J_n(\mathbf{C}\mathbf{C}_\mathrm{i}{}^{-1}), \quad J_n(\overset{\mathrm{k}}{\mathbf{C}}_\mathrm{ke}) = J_n(\mathbf{C}_\mathrm{i}\mathbf{C}_\mathrm{ki}{}^{-1}), \quad J_n(\overset{\mathrm{d}}{\mathbf{C}}_\mathrm{de}) = J_n(\mathbf{C}_\mathrm{i}\mathbf{C}_\mathrm{di}{}^{-1}), \quad n \in \{1, 2, 3\}. \tag{8.73}$$

Since $\psi_\mathrm{el}(\hat{\mathbf{C}}_\mathrm{e})$, $\psi_\mathrm{kin}(\overset{\mathrm{k}}{\mathbf{C}}_\mathrm{ke})$, and $\psi_\mathrm{dis}(\overset{\mathrm{d}}{\mathbf{C}}_\mathrm{de})$ are isotropic functions it follows from (8.31) and (8.73) that

$$\psi = \psi(\mathbf{C}, \mathbf{C}_\mathrm{i}, \mathbf{C}_\mathrm{ki}, \mathbf{C}_\mathrm{di}, s, s_\mathrm{d}) = \psi_\mathrm{el}(\mathbf{C}\mathbf{C}_\mathrm{i}{}^{-1}) + \psi_\mathrm{kin}(\mathbf{C}_\mathrm{i}\mathbf{C}_\mathrm{ki}{}^{-1}) + \psi_\mathrm{dis}(\mathbf{C}_\mathrm{i}\mathbf{C}_\mathrm{di}{}^{-1}) + \psi_\mathrm{iso}(s - s_\mathrm{d}).$$

3.6.2. *Transformation of the potential relations for stresses.* Let us rewrite the potential relations $(8.34)_1$ — $(8.34)_3$ in terms of tensors which operate on the reference configuration $\tilde{\mathcal{K}}$. Recall that for a scalar-valued function $\psi(\mathbf{A})$ we have (cf. equation (9.60) in [**20**])

$$\mathbf{A}^\mathrm{T}\frac{\partial\psi(\mathbf{ABA}^\mathrm{T})}{\partial(\mathbf{ABA}^\mathrm{T})}\mathbf{A} = \frac{\partial\psi(\mathbf{ABA}^\mathrm{T})}{\partial\mathbf{B}}\Big|_{\mathbf{A}=\mathrm{const}}. \tag{8.74}$$

Next, in order to apply this relation, we note that (cf. $(8.24)_2$, $(8.26)_1$, $(8.27)_1$, (8.34))

$$\frac{\tilde{\mathbf{T}}}{2\rho_\mathrm{R}} = \mathbf{F}_\mathrm{i}^{-1}\frac{\partial\psi_\mathrm{el}(\hat{\mathbf{C}}_\mathrm{e})}{\partial\hat{\mathbf{C}}_\mathrm{e}}\mathbf{F}_\mathrm{i}^{-\mathrm{T}}, \quad \frac{\tilde{\mathbf{X}}_\mathrm{k}}{2\rho_\mathrm{R}} = \mathbf{F}_\mathrm{ki}^{-1}\frac{\partial\psi_\mathrm{kin}(\overset{\mathrm{k}}{\mathbf{C}}_\mathrm{ke})}{\partial\overset{\mathrm{k}}{\mathbf{C}}_\mathrm{ke}}\mathbf{F}_\mathrm{ki}^{-\mathrm{T}}, \quad \frac{\tilde{\mathbf{X}}_\mathrm{d}}{2\rho_\mathrm{R}} = \mathbf{F}_\mathrm{di}^{-1}\frac{\partial\psi_\mathrm{dis}(\overset{\mathrm{d}}{\mathbf{C}}_\mathrm{de})}{\partial\overset{\mathrm{d}}{\mathbf{C}}_\mathrm{de}}\mathbf{F}_\mathrm{di}^{-\mathrm{T}}.$$

Moreover, it follows from (8.15) that

$$\hat{\mathbf{C}}_\mathrm{e} = \mathbf{F}_\mathrm{i}^{-\mathrm{T}}\mathbf{C}\mathbf{F}_\mathrm{i}^{-1}, \quad \overset{\mathrm{k}}{\mathbf{C}}_\mathrm{ke} = \mathbf{F}_\mathrm{ki}^{-\mathrm{T}}\mathbf{C}_\mathrm{i}\mathbf{F}_\mathrm{ki}^{-1}, \quad \overset{\mathrm{d}}{\mathbf{C}}_\mathrm{de} = \mathbf{F}_\mathrm{di}^{-\mathrm{T}}\mathbf{C}_\mathrm{i}\mathbf{F}_\mathrm{di}^{-1}.$$

Substituting $(\mathbf{F}_\mathrm{i}^{-\mathrm{T}}, \mathbf{C}, \hat{\mathbf{C}}_\mathrm{e})$, $(\mathbf{F}_\mathrm{ki}^{-\mathrm{T}}, \mathbf{C}_\mathrm{i}, \overset{\mathrm{k}}{\mathbf{C}}_\mathrm{ke})$, and $(\mathbf{F}_\mathrm{di}^{-\mathrm{T}}, \mathbf{C}_\mathrm{i}, \overset{\mathrm{d}}{\mathbf{C}}_\mathrm{de})$ for $(\mathbf{A}, \mathbf{B}, \mathbf{ABA}^\mathrm{T})$ in (8.74), we obtain

$$\frac{\tilde{\mathbf{T}}}{2\rho_\mathrm{R}} = \frac{\partial\psi_\mathrm{el}(\mathbf{C}\mathbf{C}_\mathrm{i}{}^{-1})}{\partial\mathbf{C}}\Big|_{\mathbf{C}_\mathrm{i}=\mathrm{const}}, \quad \frac{\tilde{\mathbf{X}}_\mathrm{k}}{2\rho_\mathrm{R}} = \frac{\partial\psi_\mathrm{kin}(\mathbf{C}_\mathrm{i}\mathbf{C}_\mathrm{ki}{}^{-1})}{\partial\mathbf{C}_\mathrm{i}}\Big|_{\mathbf{C}_\mathrm{ki}=\mathrm{const}}, \quad \frac{\tilde{\mathbf{X}}_\mathrm{d}}{2\rho_\mathrm{R}} = \frac{\partial\psi_\mathrm{dis}(\mathbf{C}_\mathrm{i}\mathbf{C}_\mathrm{di}{}^{-1})}{\partial\mathbf{C}_\mathrm{i}}\Big|_{\mathbf{C}_\mathrm{di}=\mathrm{const}}. \tag{8.75}$$

Next, let us show that $\mathbf{C}\tilde{\mathbf{T}}$, $\mathbf{C}_{\mathrm{i}}\tilde{\mathbf{X}}_{\mathrm{k}}$, and $\mathbf{C}_{\mathrm{i}}\tilde{\mathbf{X}}_{\mathrm{d}}$ are isotropic functions of $\mathbf{C}\mathbf{C}_{\mathrm{i}}{}^{-1}$, $\mathbf{C}_{\mathrm{i}}\mathbf{C}_{\mathrm{ki}}{}^{-1}$, and $\mathbf{C}_{\mathrm{i}}\mathbf{C}_{\mathrm{di}}{}^{-1}$, respectively. Indeed, we have

$$\frac{\partial\psi(\mathbf{A}\mathbf{B}^{-1})}{\partial\mathbf{A}}\Big|_{\mathbf{B}=\mathrm{const}} = \frac{\partial\psi(\mathbf{A}\mathbf{B}^{-1})}{\partial(\mathbf{A}\mathbf{B}^{-1})}\mathbf{B}^{-\mathrm{T}}; \quad \frac{\partial J_n(\mathbf{A})}{\partial\mathbf{A}} = (\mathbf{A}^{\mathrm{T}})^{n-1}, \quad n = 1, 2, 3. \tag{8.76}$$

Therefore, using (8.75) and (8.76), we arrive at

$$\frac{\mathbf{C}\tilde{\mathbf{T}}}{2\rho_{\mathrm{R}}} = \sum_{n=1}^{3}\frac{\partial\psi_{\mathrm{el}}}{\partial J_n}(\mathbf{C}\mathbf{C}_{\mathrm{i}}{}^{-1})^n, \ \frac{\mathbf{C}_{\mathrm{i}}\tilde{\mathbf{X}}_{\mathrm{k}}}{2\rho_{\mathrm{R}}} = \sum_{n=1}^{3}\frac{\partial\psi_{\mathrm{kin}}}{\partial J_n}(\mathbf{C}_{\mathrm{i}}\mathbf{C}_{\mathrm{ki}}{}^{-1})^n, \ \frac{\mathbf{C}_{\mathrm{i}}\tilde{\mathbf{X}}_{\mathrm{d}}}{2\rho_{\mathrm{R}}} = \sum_{n=1}^{3}\frac{\partial\psi_{\mathrm{dis}}}{\partial J_n}(\mathbf{C}_{\mathrm{i}}\mathbf{C}_{\mathrm{di}}{}^{-1})^n.$$

If the special form (8.32), (8.33) of the free energy is used, then, taking into account incompressibility relations (8.47), we obtain

$$\tilde{\mathbf{T}} = k\ln\sqrt{\det(\mathbf{C})}\,\mathbf{C}^{-1} + \mu\,\mathbf{C}^{-1}(\overline{\mathbf{C}}\mathbf{C}_{\mathrm{i}}^{-1})^{\mathrm{D}}, \quad \tilde{\mathbf{X}}_{\mathrm{k}} = \frac{c_{\mathrm{k}}}{2}\,\mathbf{C}_{\mathrm{i}}^{-1}(\mathbf{C}_{\mathrm{i}}\mathbf{C}_{\mathrm{ki}}^{-1})^{\mathrm{D}}, \quad \tilde{\mathbf{X}}_{\mathrm{d}} = \frac{c_{\mathrm{d}}}{2}\,\mathbf{C}_{\mathrm{i}}^{-1}(\mathbf{C}_{\mathrm{i}}\mathbf{C}_{\mathrm{di}}^{-1})^{\mathrm{D}}. \tag{8.77}$$

3.6.3. *Representation of the yield function.* First, let us introduce a scalar-valued function $\mathfrak{F}$ as

$$\mathfrak{F} := \|\hat{\mathbf{\Sigma}}^{\mathrm{D}}\|. \tag{8.78}$$

Next, we note that

$$\mathrm{tr}\hat{\mathbf{\Sigma}} \overset{(8.42)_1}{=} \mathrm{tr}(\hat{\mathbf{C}}_{\mathrm{e}}\hat{\mathbf{S}} - \hat{\mathbf{X}}_{\mathrm{k}}) = \mathrm{tr}(\mathbf{C}\tilde{\mathbf{T}} - \mathbf{C}_{\mathrm{i}}\tilde{\mathbf{X}}_{\mathrm{k}}). \tag{8.79}$$

Moreover, since $\hat{\mathbf{\Sigma}}^{\mathrm{D}} \in Sym$, we have

$$\mathfrak{F}^2 = \|\hat{\mathbf{\Sigma}}^{\mathrm{D}}\|^2 = \hat{\mathbf{\Sigma}}^{\mathrm{D}} : \hat{\mathbf{\Sigma}}^{\mathrm{D}} = \Big[\Big(\mathbf{F}_{\mathrm{i}}^{-\mathrm{T}}\Big)^{*}\hat{\mathbf{\Sigma}}^{\mathrm{D}}\Big] : \Big[\Big(\mathbf{F}_{\mathrm{i}}\Big)^{*}\hat{\mathbf{\Sigma}}^{\mathrm{D}}\Big] = \mathrm{tr}\Big\{\Big[\Big(\mathbf{F}_{\mathrm{i}}^{-\mathrm{T}}\Big)^{*}\hat{\mathbf{\Sigma}}^{\mathrm{D}}\Big]\Big[\Big(\mathbf{F}_{\mathrm{i}}\Big)^{*}\hat{\mathbf{\Sigma}}^{\mathrm{D}}\Big]\Big\}. \tag{8.80}$$

In order to implement this relation, we compute the inelastic contravariant and covariant pull-backs of $\hat{\mathbf{\Sigma}}^{\mathrm{D}}$

$$\Big(\mathbf{F}_{\mathrm{i}}^{-\mathrm{T}}\Big)^{*}\hat{\mathbf{\Sigma}}^{\mathrm{D}} = \mathbf{C}_{\mathrm{i}}^{-1}\mathbf{C}\tilde{\mathbf{T}} - \tilde{\mathbf{X}}_{\mathrm{k}} - 1/3\ \mathrm{tr}\hat{\mathbf{\Sigma}}\ \mathbf{C}_{\mathrm{i}}^{-1} \overset{(8.79)}{=} \mathbf{C}_{\mathrm{i}}^{-1}\Big(\mathbf{C}\tilde{\mathbf{T}} - \mathbf{C}_{\mathrm{i}}\tilde{\mathbf{X}}_{\mathrm{k}}\Big)^{\mathrm{D}}, \tag{8.81}$$

$$\Big(\mathbf{F}_{\mathrm{i}}\Big)^{*}\hat{\mathbf{\Sigma}}^{\mathrm{D}} = \mathbf{C}\tilde{\mathbf{T}}\mathbf{C}_{\mathrm{i}} - \mathbf{C}_{\mathrm{i}}\tilde{\mathbf{X}}_{\mathrm{k}}\mathbf{C}_{\mathrm{i}} - 1/3\ \mathrm{tr}\hat{\mathbf{\Sigma}}\ \mathbf{C}_{\mathrm{i}} \overset{(8.79)}{=} \Big(\mathbf{C}\tilde{\mathbf{T}} - \mathbf{C}_{\mathrm{i}}\tilde{\mathbf{X}}_{\mathrm{k}}\Big)^{\mathrm{D}}\mathbf{C}_{\mathrm{i}}. \tag{8.82}$$

Substituting (8.81) and (8.82) in (8.80) we obtain $\mathfrak{F}$ as follows:

$$\mathfrak{F} = \|\hat{\mathbf{\Sigma}}^{\mathrm{D}}\| = \sqrt{\mathrm{tr}\Big[\Big(\mathbf{C}\tilde{\mathbf{T}} - \mathbf{C}_{\mathrm{i}}\tilde{\mathbf{X}}_{\mathrm{k}}\Big)^{\mathrm{D}}\Big]^2}. \tag{8.83}$$

Furthermore,

$$\hat{\mathbf{\Sigma}}^{\mathrm{D}} : \hat{\mathbf{X}}_{\mathrm{d}} = \Big[\Big(\mathbf{F}_{\mathrm{i}}\Big)^{*}\hat{\mathbf{\Sigma}}^{\mathrm{D}}\Big] : \Big[\Big(\mathbf{F}_{\mathrm{i}}^{-\mathrm{T}}\Big)^{*}\hat{\mathbf{X}}_{\mathrm{d}}\Big]; \quad \Big(\mathbf{F}_{\mathrm{i}}^{-\mathrm{T}}\Big)^{*}\hat{\mathbf{X}}_{\mathrm{d}} = \mathbf{F}_{\mathrm{i}}^{-1}\hat{\mathbf{X}}_{\mathrm{d}}\mathbf{F}_{\mathrm{i}}^{-\mathrm{T}} \overset{(8.27)}{=} \tilde{\mathbf{X}}_{\mathrm{d}}. \tag{8.84}$$

Therefore, combining (8.82) and (8.84) we arrive at

$$\hat{\mathbf{\Sigma}}^{\mathrm{D}} : \hat{\mathbf{X}}_{\mathrm{d}} = \mathrm{tr}\Big[\Big(\mathbf{C}\tilde{\mathbf{T}} - \mathbf{C}_{\mathrm{i}}\tilde{\mathbf{X}}_{\mathrm{k}}\Big)^{\mathrm{D}}\mathbf{C}_{\mathrm{i}}\tilde{\mathbf{X}}_{\mathrm{d}}\Big]. \tag{8.85}$$

Finally, we obtain the representation of the yield function f as follows (cf. (8.45))

$$f = \mathfrak{F} - \frac{1}{\mathfrak{F}}\mathrm{tr}\Big[\Big(\mathbf{C}\tilde{\mathbf{T}} - \mathbf{C}_{\mathrm{i}}\tilde{\mathbf{X}}_{\mathrm{k}}\Big)^{\mathrm{D}}\mathbf{C}_{\mathrm{i}}\tilde{\mathbf{X}}_{\mathrm{d}}\Big] - \sqrt{\frac{2}{3}}\Big[K + R\Big]. \tag{8.86}$$

3.6.4. *Transformation of the evolution equations.* Firstly, we note that for $\overset{\mathrm{d}}{\mathbf{C}}_{\mathrm{de}} \neq \mathbf{1}$

$$\alpha_{\mathrm{d}}(\overset{\mathrm{d}}{\mathbf{C}}_{\mathrm{de}}) \overset{(8.68)}{=} \frac{\sqrt{\mathrm{tr}\Big[\Big(\overset{\mathrm{d}}{\mathbf{C}}{}^{\mathrm{D}}_{\mathrm{de}}\Big)^2\Big]} \cdot \sqrt{\mathrm{tr}\Big[\Big((\overset{\mathrm{d}}{\mathbf{C}}_{\mathrm{de}}\overset{\mathrm{d}}{\mathbf{C}}{}^{\mathrm{D}}_{\mathrm{de}})^{\mathrm{D}}\Big)^2\Big]}}{\mathrm{tr}\Big[\Big(\overset{\mathrm{d}}{\mathbf{C}}{}^{\mathrm{D}}_{\mathrm{de}}\Big)^2 \overset{\mathrm{d}}{\mathbf{C}}_{\mathrm{de}}\Big]}. \tag{8.87}$$

Similarly to $(8.73)_3$, $\overset{\mathrm{d}}{\mathbf{C}}_{\mathrm{de}}$ can be replaced by $\mathbf{C}_{\mathrm{i}}\mathbf{C}_{\mathrm{di}}{}^{-1}$ in (8.87)

$$\alpha_{\mathrm{d}}(\overset{\mathrm{d}}{\mathbf{C}}_{\mathrm{de}}) = \tilde{\alpha}_{\mathrm{d}}(\mathbf{C}_{\mathrm{i}}, \mathbf{C}_{\mathrm{di}}) = \frac{\sqrt{\mathrm{tr}\Big[\Big((\mathbf{C}_{\mathrm{i}}\mathbf{C}_{\mathrm{di}}{}^{-1})^{\mathrm{D}}\Big)^2\Big]} \cdot \sqrt{\mathrm{tr}\Big[\Big((\mathbf{C}_{\mathrm{i}}\mathbf{C}_{\mathrm{di}}{}^{-1}(\mathbf{C}_{\mathrm{i}}\mathbf{C}_{\mathrm{di}}{}^{-1})^{\mathrm{D}})^{\mathrm{D}}\Big)^2\Big]}}{\mathrm{tr}\Big[\Big((\mathbf{C}_{\mathrm{i}}\mathbf{C}_{\mathrm{di}}{}^{-1})^{\mathrm{D}}\Big)^2 \mathbf{C}_{\mathrm{i}}\mathbf{C}_{\mathrm{di}}{}^{-1}\Big]}. \tag{8.88}$$

Next, in the same way as it was done for (8.79) we show that

$$\mathrm{tr}\ \overset{\mathrm{k}}{\mathbf{\Xi}}_{\mathrm{k}} \overset{(8.42)_2}{=} \mathrm{tr}\ (\overset{\mathrm{k}}{\mathbf{C}}_{\mathrm{ke}}\overset{\mathrm{k}}{\mathbf{X}}_{\mathrm{k}}) = \mathrm{tr}(\mathbf{C}_{\mathrm{i}}\tilde{\mathbf{X}}_{\mathrm{k}}), \quad \mathrm{tr}\ \overset{\mathrm{d}}{\mathbf{\Xi}}_{\mathrm{d}} \overset{(8.42)_3}{=} \mathrm{tr}\ (\overset{\mathrm{d}}{\mathbf{C}}_{\mathrm{de}}\overset{\mathrm{d}}{\mathbf{X}}_{\mathrm{d}}) = \mathrm{tr}(\mathbf{C}_{\mathrm{i}}\tilde{\mathbf{X}}_{\mathrm{d}}). \tag{8.89}$$

Further, using these results we compute the covariant pull-backs $\Big(\mathbf{F}_{\mathrm{ki}}\Big)^{*}\overset{\mathrm{k}}{\mathbf{\Xi}}{}^{\mathrm{D}}_{\mathrm{k}}$ and $\Big(\mathbf{F}_{\mathrm{di}}\Big)^{*}\overset{\mathrm{d}}{\mathbf{\Xi}}{}^{\mathrm{D}}_{\mathrm{d}}$:

$$\Big(\mathbf{F}_{\mathrm{ki}}\Big)^{*}\overset{\mathrm{k}}{\mathbf{\Xi}}{}^{\mathrm{D}}_{\mathrm{k}} = \Big(\mathbf{C}_{\mathrm{i}}\tilde{\mathbf{X}}_{\mathrm{k}}\Big)^{\mathrm{D}}\mathbf{C}_{\mathrm{ki}}, \quad \Big(\mathbf{F}_{\mathrm{di}}\Big)^{*}\overset{\mathrm{d}}{\mathbf{\Xi}}{}^{\mathrm{D}}_{\mathrm{d}} = \Big(\mathbf{C}_{\mathrm{i}}\tilde{\mathbf{X}}_{\mathrm{d}}\Big)^{\mathrm{D}}\mathbf{C}_{\mathrm{di}}. \tag{8.90}$$

Now let us rewrite the normality flow rule (8.55). If we take relations (8.82), (8.83), and (8.85) into account, the application of a covariant Pull-back $\mathbf{F}_{\mathrm{i}}{}^{*}$ to both sides of (8.55) yields

$$\dot{\mathbf{C}}_{\mathrm{i}} = 2\mathbf{F}_{\mathrm{i}}{}^{*}\Big(\mathfrak{D}_{\mathrm{i}}(\hat{\mathbf{\Gamma}}_{\mathrm{i}})\Big) = 2\check{\lambda}_{\mathrm{i}}\Bigg\{\Bigg(\frac{1}{\mathfrak{F}} + \frac{\mathrm{tr}\Big[\Big(\mathbf{C}\tilde{\mathbf{T}} - \mathbf{C}_{\mathrm{i}}\tilde{\mathbf{X}}_{\mathrm{k}}\Big)^{\mathrm{D}}\mathbf{C}_{\mathrm{i}}\tilde{\mathbf{X}}_{\mathrm{d}}\Big]}{\mathfrak{F}^3}\Bigg)\Big(\mathbf{C}\tilde{\mathbf{T}} - \mathbf{C}_{\mathrm{i}}\tilde{\mathbf{X}}_{\mathrm{k}}\Big)^{\mathrm{D}} - \frac{1}{\mathfrak{F}}\mathbf{C}_{\mathrm{i}}\tilde{\mathbf{X}}_{\mathrm{d}}\Bigg\}\mathbf{C}_{\mathrm{i}}. \tag{8.91}$$

In the similar way, we obtain for the radial flow rule (8.63)

$$\dot{\mathbf{C}}_{\mathrm{i}} = 2\mathbf{F}_{\mathrm{i}}{}^{*}\Big(\mathfrak{D}_{\mathrm{i}}(\hat{\mathbf{\Gamma}}_{\mathrm{i}})\Big) = 2\frac{\check{\lambda}_{\mathrm{i}}}{\mathfrak{F}}\Big(\mathbf{C}\tilde{\mathbf{T}} - \mathbf{C}_{\mathrm{i}}\tilde{\mathbf{X}}_{\mathrm{k}}\Big)^{\mathrm{D}}\mathbf{C}_{\mathrm{i}}. \tag{8.92}$$

Recall that for both flow rules we have $\lambda_{\mathrm{i}} = \|\mathfrak{D}_{\mathrm{i}}(\hat{\mathbf{\Gamma}}_{\mathrm{i}})\|$. Therefore,

$$\lambda_{\mathrm{i}} = \frac{1}{2}\sqrt{\mathrm{tr}\Big[\dot{\mathbf{C}}_{\mathrm{i}}\mathbf{C}_{\mathrm{i}}^{-1}\Big]^2}. \tag{8.93}$$

Moreover, the factor g must be evaluated. For the normality flow rule (8.55) we get $\lambda_{\mathrm{i}} = g\check{\lambda}_{\mathrm{i}}$, where the factor g is defined by $(8.60)_2$. Note that, analogously to (8.83), we have

$$\|\hat{\mathbf{X}}_{\mathrm{d}}\|^2 = \mathrm{tr}\Big[\mathbf{C}_{\mathrm{i}}\tilde{\mathbf{X}}_{\mathrm{d}}\Big]^2. \tag{8.94}$$

Substituting (8.85) and (8.94) into $(8.61)_1$ and taking the square root of both sides we obtain

$$g = g(\mathbf{C}, \mathbf{C}_{\mathrm{i}}, \mathbf{C}_{\mathrm{ki}}, \mathbf{C}_{\mathrm{di}}) = \sqrt{1 + \frac{1}{\mathfrak{F}^2}\mathrm{tr}\Big[\Big(\mathbf{C}_{\mathrm{i}}\tilde{\mathbf{X}}_{\mathrm{d}}\Big)^2\Big] - \frac{1}{\mathfrak{F}^4}\Big\{\mathrm{tr}\Big[\Big(\mathbf{C}\tilde{\mathbf{T}} - \mathbf{C}_{\mathrm{i}}\tilde{\mathbf{X}}_{\mathrm{k}}\Big)^{\mathrm{D}}\mathbf{C}_{\mathrm{i}}\tilde{\mathbf{X}}_{\mathrm{d}}\Big]\Big\}^2}. \tag{8.95}$$

Recall that for the radial flow rule we put $g = 1$.

Finally, applying the covariant Pull-backs $\mathbf{F}_{\mathrm{ki}}{}^{*}(\cdot)$ and $\mathbf{F}_{\mathrm{di}}{}^{*}(\cdot)$ to both sides of (8.66) and (8.69), respectively, we obtain

$$\dot{\mathbf{C}}_{\mathrm{ki}} = 2\ \lambda_{\mathrm{i}}\ \varkappa_{\mathrm{k}}\ \Big(\mathbf{C}_{\mathrm{i}}\tilde{\mathbf{X}}_{\mathrm{k}}\Big)^{\mathrm{D}}\mathbf{C}_{\mathrm{ki}}, \quad \dot{\mathbf{C}}_{\mathrm{di}} = 2\ \lambda_{\mathrm{i}}\ \tilde{\alpha}_{\mathrm{d}}(\mathbf{C}_{\mathrm{i}}, \mathbf{C}_{\mathrm{di}})\ \varkappa_{\mathrm{d}}\ \Big(\mathbf{C}_{\mathrm{i}}\tilde{\mathbf{X}}_{\mathrm{d}}\Big)^{\mathrm{D}}\mathbf{C}_{\mathrm{di}}. \tag{8.96}$$

The material model is summarized in table 8.1.

Table 8.1. Summary of the material model

Normality flow rule: $\dot{\mathbf{C}}_{\mathrm{i}} = 2\check{\lambda}_{\mathrm{i}}\Big\{\Big(\frac{1}{\mathfrak{F}} + \frac{1}{\mathfrak{F}^3}\mathrm{tr}\Big[\big(\mathbf{C}\tilde{\mathbf{T}} - \mathbf{C}_{\mathrm{i}}\tilde{\mathbf{X}}_{\mathrm{k}}\big)^{\mathrm{D}}\mathbf{C}_{\mathrm{i}}\tilde{\mathbf{X}}_{\mathrm{d}}\Big]\Big)\big(\mathbf{C}\tilde{\mathbf{T}} - \mathbf{C}_{\mathrm{i}}\tilde{\mathbf{X}}_{\mathrm{k}}\big)^{\mathrm{D}} - \frac{1}{\mathfrak{F}}\mathbf{C}_{\mathrm{i}}\tilde{\mathbf{X}}_{\mathrm{d}}\Big\}\mathbf{C}_{\mathrm{i}},$ $g = \sqrt{1 + \frac{1}{\mathfrak{F}^2}\mathrm{tr}\Big[\big(\mathbf{C}_{\mathrm{i}}\tilde{\mathbf{X}}_{\mathrm{d}}\big)^2\Big] - \frac{1}{\mathfrak{F}^4}\Big\{\mathrm{tr}\Big[\big(\mathbf{C}\tilde{\mathbf{T}} - \mathbf{C}_{\mathrm{i}}\tilde{\mathbf{X}}_{\mathrm{k}}\big)^{\mathrm{D}}\mathbf{C}_{\mathrm{i}}\tilde{\mathbf{X}}_{\mathrm{d}}\Big]\Big\}^2},$
Radial flow rule: $\dot{\mathbf{C}}_{\mathrm{i}} = 2\frac{\check{\lambda}_{\mathrm{i}}}{\mathfrak{F}}\big(\mathbf{C}\tilde{\mathbf{T}} - \mathbf{C}_{\mathrm{i}}\tilde{\mathbf{X}}_{\mathrm{k}}\big)^{\mathrm{D}}\mathbf{C}_{\mathrm{i}}, \quad g = 1,$
$\dot{\mathbf{C}}_{\mathrm{ki}} = 2\ \lambda_{\mathrm{i}}\ \varkappa_{\mathrm{k}}\ \big(\mathbf{C}_{\mathrm{i}}\tilde{\mathbf{X}}_{\mathrm{k}}\big)^{\mathrm{D}}\mathbf{C}_{\mathrm{ki}}, \quad \dot{\mathbf{C}}_{\mathrm{di}} = 2\ \lambda_{\mathrm{i}}\ \tilde{\alpha}_{\mathrm{d}}(\mathbf{C}_{\mathrm{i}}, \mathbf{C}_{\mathrm{di}})\ \varkappa_{\mathrm{d}}\ \big(\mathbf{C}_{\mathrm{i}}\tilde{\mathbf{X}}_{\mathrm{d}}\big)^{\mathrm{D}}\mathbf{C}_{\mathrm{di}},$ $\check{\lambda}_{\mathrm{i}} := \frac{1}{\eta}\Big\langle\frac{1}{k_0}f\Big\rangle^m, \quad \lambda_{\mathrm{i}} = g\check{\lambda}_{\mathrm{i}}, \quad \dot{s} = \sqrt{\frac{2}{3}}\check{\lambda}_{\mathrm{i}}, \quad \dot{s}_{\mathrm{d}} = \frac{\beta}{\gamma}\dot{s}R,$ $\tilde{\mathbf{T}} = 2\rho_{\mathrm{R}}\frac{\partial\psi_{\mathrm{el}}(\mathbf{C}{\mathbf{C}_{\mathrm{i}}}^{-1})}{\partial\mathbf{C}}\Big\|_{\mathbf{C}_{\mathrm{i}}=\mathrm{const}},$ $\tilde{\mathbf{X}}_{\mathrm{k}} = 2\rho_{\mathrm{R}}\frac{\partial\psi_{\mathrm{kin}}(\mathbf{C}_{\mathrm{i}}{\mathbf{C}_{\mathrm{ki}}}^{-1})}{\partial\mathbf{C}_{\mathrm{i}}}\Big\|_{\mathbf{C}_{\mathrm{ki}}=\mathrm{const}},$ $\tilde{\mathbf{X}}_{\mathrm{d}} = 2\rho_{\mathrm{R}}\frac{\partial\psi_{\mathrm{dis}}(\mathbf{C}_{\mathrm{i}}{\mathbf{C}_{\mathrm{di}}}^{-1})}{\partial\mathbf{C}_{\mathrm{i}}}\Big\|_{\mathbf{C}_{\mathrm{di}}=\mathrm{const}},$ $R = \gamma(s - s_{\mathrm{d}}), \quad \mathfrak{F} = \sqrt{\mathrm{tr}\Big[\big(\mathbf{C}\tilde{\mathbf{T}} - \mathbf{C}_{\mathrm{i}}\tilde{\mathbf{X}}_{\mathrm{k}}\big)^{\mathrm{D}}\Big]^2},$ $f = \mathfrak{F} - \frac{1}{\mathfrak{F}}\mathrm{tr}\Big[\big(\mathbf{C}\tilde{\mathbf{T}} - \mathbf{C}_{\mathrm{i}}\tilde{\mathbf{X}}_{\mathrm{k}}\big)^{\mathrm{D}}\mathbf{C}_{\mathrm{i}}\tilde{\mathbf{X}}_{\mathrm{d}}\Big] - \sqrt{\frac{2}{3}}\Big[K + R\Big].$

4. Numerical implementation

Let us consider a manifold $\mathbb{M} := \Big\{\mathbf{B} \in Sym : \det\mathbf{B} = 1\Big\}$ which consists of symmetric unimodular tensors. According to (8.47), the exact solution of the problem has under proper initial conditions the geometric property as follows: $\mathbf{C}_{\mathrm{i}}, \mathbf{C}_{\mathrm{ki}}, \mathbf{C}_{\mathrm{di}} \in \mathbb{M}$. In that sense, we are dealing with a *system of differential equations on the manifold* (cf. the paper [**15**]). Accordingly, the numerical schemes, which preserve this property are named geometric integrators. In [**44**] a mathematical proof considering a classical model of multiplicative viscoplasticity was provided for the absence of error accumulation if geometric integrators are used. Therefore, it is our goal to construct a corresponding numerical algorithm, such that the incompressibility and symmetry will be exactly satisfied.

4.1. System of algebraic equations. First, suppose that the deformation gradient ${}^{n+1}\mathbf{F}$ at the time $t_{n+1} = t_n + \Delta t$ is known. Further, assume that the set of internal variables at the time t_n is given by ${}^{n}\mathbf{C}_{\mathrm{i}}$, ${}^{n}\mathbf{C}_{\mathrm{ki}}$, ${}^{n}\mathbf{C}_{\mathrm{di}}$, ${}^{n}s$, ${}^{n}s_{\mathrm{d}}$. In this subsection we construct a system of algebraic equations for finding the internal variables at the time t_{n+1}. In order to discretize the evolution equations for $\mathbf{C}_{\mathrm{i}}$, $\mathbf{C}_{\mathrm{ki}}$, and $\mathbf{C}_{\mathrm{di}}$, we adopt the Modified Euler-Backward Method (MEBM) proposed by Helm (see, for example, [**22, 42**]).[17] Let us consider the Cauchy problem for a system of nonlinear ordinary differential equations

$$\dot{\mathbf{A}}(t) = \mathbf{f}(\mathbf{A}(t), t)\mathbf{A}(t), \quad \mathbf{A}(0) = \mathbf{A}^0, \quad \det(\mathbf{A}^0) = 1.$$

---

[17] Alternatively, the well-known exponential mapping can be used to obtain a geometric numerical scheme.

Suppose that the tensor-valued function $\mathbf{f}$ is sufficiently smooth, $\mathrm{tr}(\mathbf{f}(\mathbf{B},t)) = 0$, and (cf. [**42**])

$$\Big(\mathbf{f}(\mathbf{B},t)\Big)^{k}\mathbf{B} \in Sym \quad \text{for all } \mathbf{B} \in Sym,\ k = 1,2,3,\dots\,. \tag{8.97}$$

By ${}^{n}\mathbf{A}$ and ${}^{n+1}\mathbf{A}$ we denote the numerical solutions at t_n and t_{n+1}, respectively. The MEBM is given by

$${}^{n+1}\mathbf{A} = \overline{\Big[\mathbf{1} - \Delta t\ \mathbf{f}({}^{n+1}\mathbf{A}, t_{n+1})\Big]^{-1}\ {}^{n}\mathbf{A}}, \quad \Delta t := t_{n+1} - t_n > 0. \tag{8.98}$$

It was shown in [**42**] that MEBM preserves the symmetry of the solution if the right-hand side satisfies (8.97).[18] In that case, MEBM can be rewritten as

$${}^{n+1}\mathbf{A} = \overline{\mathrm{sym}\Big\{\Big[\mathbf{1} - \Delta t\ \mathbf{f}({}^{n+1}\mathbf{A}, t_{n+1})\Big]^{-1}\ {}^{n}\mathbf{A}\Big\}}. \tag{8.99}$$

We stress that the right-hand sides of (8.91), (8.92), and (8.96) satisfy requirements (8.97) (see Appendix E). Therefore, MEBM in the form (8.99) can be used to discretize these evolution equations.

The evolution equations for s and s_d are discretized by implicit Euler scheme. It is convenient to introduce the incremental inelastic parameter

$$\xi := \Delta t\ {}^{n+1}\check{\lambda}_\mathrm{i}. \tag{8.100}$$

After the discretization we obtain the following system of algebraic equations

$${}^{n+1}\mathbf{C}_\mathrm{i} = \overline{\mathrm{sym}\Big(\mathbf{K}_\mathrm{i}({}^{n+1}\mathbf{C}, {}^{n+1}\mathbf{C}_\mathrm{i}, {}^{n+1}\mathbf{C}_\mathrm{ki}, {}^{n+1}\mathbf{C}_\mathrm{di}, \xi)\Big)}, \tag{8.101}$$

$${}^{n+1}\mathbf{C}_\mathrm{ki} = \overline{\mathrm{sym}\Big(\mathbf{K}_\mathrm{ki}({}^{n+1}\mathbf{C}_\mathrm{i}, {}^{n+1}\mathbf{C}_\mathrm{ki}, \xi)\Big)}, \tag{8.102}$$

$${}^{n+1}\mathbf{C}_\mathrm{di} = \overline{\mathrm{sym}\Big(\mathbf{K}_\mathrm{di}({}^{n+1}\mathbf{C}_\mathrm{i}, {}^{n+1}\mathbf{C}_\mathrm{di}, \xi)\Big)}, \tag{8.103}$$

$$\xi = \frac{\Delta t}{\eta}\Big\langle \frac{{}^{n+1}f}{k_0} \Big\rangle^{m}, \tag{8.104}$$

$${}^{n+1}s = {}^{n}s + \sqrt{\frac{2}{3}}\xi, \quad {}^{n+1}s_\mathrm{d} = {}^{n}s_\mathrm{d} + \frac{\beta}{\gamma}\sqrt{\frac{2}{3}}\xi\ {}^{n+1}R, \tag{8.105}$$

$${}^{n+1}R = \gamma({}^{n+1}s - {}^{n+1}s_\mathrm{d}), \tag{8.106}$$

$${}^{n+1}f = {}^{n+1}\mathfrak{F} - \frac{1}{{}^{n+1}\mathfrak{F}}\mathrm{tr}\Big[\Big({}^{n+1}\mathbf{C}\ {}^{n+1}\tilde{\mathbf{T}} - {}^{n+1}\mathbf{C}_\mathrm{i}\ {}^{n+1}\tilde{\mathbf{X}}_\mathrm{k}\Big)^{\mathrm{D}}\, {}^{n+1}\mathbf{C}_\mathrm{i}\ {}^{n+1}\tilde{\mathbf{X}}_\mathrm{d}\Big] - \sqrt{\frac{2}{3}}\Big[K + R\Big], \tag{8.107}$$

$${}^{n+1}\mathfrak{F} = \sqrt{\mathrm{tr}\Big[\Big({}^{n+1}\mathbf{C}\ {}^{n+1}\tilde{\mathbf{T}} - {}^{n+1}\mathbf{C}_\mathrm{i}\ {}^{n+1}\tilde{\mathbf{X}}\Big)^{\mathrm{D}}\Big]^{2}}, \tag{8.108}$$

where the operators $\mathbf{K}_\mathrm{k}$ (for $\mathrm{k} \in \{\mathrm{i}, \mathrm{ki}, \mathrm{di}\}$) are defined by

$$\mathbf{K}_\mathrm{k} := \Big[\mathbf{1} - \mathbf{B}_\mathrm{k}\Big]^{-1}\ {}^{n}\mathbf{C}_\mathrm{k},\ \ \mathrm{k} \in \{\mathrm{i}, \mathrm{ki}, \mathrm{di}\},$$

---

[18] Moreover, the classical Euler Backward Method and the Exponential Method [**33**] preserve the symmetry as well, if (8.97) holds (see [**42**]).

$$\mathbf{B}_{\mathrm{i}} := 2\xi \frac{1}{{}^{n+1}\mathfrak{F}} \Bigg\{ \Bigg(1 + \frac{\mathrm{tr}\Big[\Big({}^{n+1}\mathbf{C}\ {}^{n+1}\tilde{\mathbf{T}} - {}^{n+1}\mathbf{C}_{\mathrm{i}}\ {}^{n+1}\tilde{\mathbf{X}}_{\mathrm{k}} \Big)^{\mathrm{D}}\, {}^{n+1}\mathbf{C}_{\mathrm{i}}\ {}^{n+1}\tilde{\mathbf{X}}_{\mathrm{d}} \Big]}{{}^{n+1}\mathfrak{F}^2} \Bigg)$$

$$\times \Big({}^{n+1}\mathbf{C}\ {}^{n+1}\tilde{\mathbf{T}} - {}^{n+1}\mathbf{C}_{\mathrm{i}}\ {}^{n+1}\tilde{\mathbf{X}}_{\mathrm{k}} \Big)^{\mathrm{D}} - {}^{n+1}\mathbf{C}_{\mathrm{i}}\ {}^{n+1}\tilde{\mathbf{X}}_{\mathrm{d}} \Bigg\}, \quad \text{if normality flow rule is implemented,} \tag{8.109}$$

$$\mathbf{B}_{\mathrm{i}} := 2\xi \frac{1}{{}^{n+1}\mathfrak{F}} \Big({}^{n+1}\mathbf{C}\ {}^{n+1}\tilde{\mathbf{T}} - {}^{n+1}\mathbf{C}_{\mathrm{i}}\ {}^{n+1}\tilde{\mathbf{X}}_{\mathrm{k}} \Big)^{\mathrm{D}}, \quad \text{if radial flow rule is implemented,} \tag{8.110}$$

$$\mathbf{B}_{\mathrm{ki}} := 2\ {}^{n+1}g\ \xi\ \varkappa_{\mathrm{k}} \Big({}^{n+1}\mathbf{C}_{\mathrm{i}}\ {}^{n+1}\tilde{\mathbf{X}}_{\mathrm{k}} \Big)^{\mathrm{D}}, \quad \mathbf{B}_{\mathrm{di}} := 2\ {}^{n+1}g\ \xi\ \varkappa_{\mathrm{d}}\ \tilde{\alpha}_{\mathrm{d}}({}^{n+1}\mathbf{C}_{\mathrm{i}}, {}^{n+1}\mathbf{C}_{\mathrm{di}})\ \Big({}^{n+1}\mathbf{C}_{\mathrm{i}}\ {}^{n+1}\tilde{\mathbf{X}}_{\mathrm{d}} \Big)^{\mathrm{D}}. \tag{8.111}$$

Here ${}^{n+1}\tilde{\mathbf{T}}$, ${}^{n+1}\tilde{\mathbf{X}}_{\mathrm{k}}$, ${}^{n+1}\tilde{\mathbf{X}}_{\mathrm{d}}$ are functions of ${}^{n+1}\mathbf{C}, {}^{n+1}\mathbf{C}_{\mathrm{i}}$, ${}^{n+1}\mathbf{C}_{\mathrm{ki}}$, ${}^{n+1}\mathbf{C}_{\mathrm{di}}$ given by (8.75) (or by (8.77) if the special form of ψ_{el}, ψ_{kin} and ψ_{dis} is used); ${}^{n+1}g$ is computed using (8.95) for the normality flow rule, and ${}^{n+1}g = 1$ for the radial rule.

4.2. Solution strategy. In this subsection we discuss a strategy which is used to solve the system of algebraic equations formulated above. First, we exclude ${}^{n+1}s, {}^{n+1}s_{\mathrm{d}}$ from (8.105) and (8.106) (cf. [**22**]) to represent ${}^{n+1}R$ as a function of ξ

$${}^{n+1}R = R(\xi) := \frac{{}^{\mathrm{t}}R + \sqrt{\frac{2}{3}}\gamma\xi}{1 + \sqrt{\frac{2}{3}}\beta\xi}, \quad {}^{\mathrm{t}}R := \gamma({}^{n}s - {}^{n}s_{\mathrm{d}}). \tag{8.112}$$

Next, substituting (8.108) and (8.112) in (8.107), we represent ${}^{n+1}f$ in the form $\check{f}({}^{n+1}\mathbf{C}_{\mathrm{i}}, {}^{n+1}\mathbf{C}_{\mathrm{ki}}, {}^{n+1}\mathbf{C}_{\mathrm{di}}, \xi)$, which does not depend on ${}^{n+1}s$ and ${}^{n+1}s_{\mathrm{d}}$. Thus, the problem is reduced to system (8.101) — (8.104) with respect to unknown ${}^{n+1}\mathbf{C}_{\mathrm{i}}$, ${}^{n+1}\mathbf{C}_{\mathrm{ki}}$, ${}^{n+1}\mathbf{C}_{\mathrm{di}}$, and ξ.

The variables ${}^{n+1}\mathbf{C}_{\mathrm{i}}$, ${}^{n+1}\mathbf{C}_{\mathrm{ki}}$, and ${}^{n+1}\mathbf{C}_{\mathrm{di}}$ are uniquely determined by the system (8.101) — (8.103) with a given ξ (at least for small ξ). Let us denote the corresponding solution by $\big(\mathbf{C}_{\mathrm{i}}(\xi), \mathbf{C}_{\mathrm{ki}}(\xi), \mathbf{C}_{\mathrm{di}}(\xi)\big)$. Substituting this solution in (8.107) and (8.108), we obtain a function $\tilde{f}(\xi) := \check{f}(\mathbf{C}_{\mathrm{i}}(\xi), \mathbf{C}_{\mathrm{ki}}(\xi), \mathbf{C}_{\mathrm{di}}(\xi), \xi)$.

If $\tilde{f}(0) \leq 0$, then we suppose that no inelastic flow occurs and put $\xi = 0$, ${}^{n+1}\mathbf{C}_{\mathrm{i}} = {}^{n}\mathbf{C}_{\mathrm{i}}$, ${}^{n+1}\mathbf{C}_{\mathrm{ki}} = {}^{n}\mathbf{C}_{\mathrm{ki}}$, and ${}^{n+1}\mathbf{C}_{\mathrm{di}} = {}^{n}\mathbf{C}_{\mathrm{di}}$. Otherwise, ξ is computed using equation (8.104). Substituting $\tilde{f}(\xi)$ for ${}^{n+1}f$ in (8.104), we obtain after some trivial transformations two alternative forms of the incremental Perzyna rule:[19]

$$H(\xi) = 0, \quad H(\xi) := \frac{\eta\xi}{\Delta t} - \left(\frac{\tilde{f}(\xi)}{k_0}\right)^m, \tag{8.113}$$

$$D(\xi) = 0, \quad D(\xi) := \left(\frac{\eta\xi}{\Delta t}\right)^{1/m} - \frac{\tilde{f}(\xi)}{k_0} = 0. \tag{8.114}$$

After the solution ξ is found, the values of ${}^{n+1}\mathbf{C}_{\mathrm{i}}$, ${}^{n+1}\mathbf{C}_{\mathrm{ki}}$, and ${}^{n+1}\mathbf{C}_{\mathrm{di}}$ are given by $\mathbf{C}_{\mathrm{i}}(\xi)$, $\mathbf{C}_{\mathrm{ki}}(\xi)$, and $\mathbf{C}_{\mathrm{di}}(\xi)$, respectively. Finally, we update s and s_{d} using relations (8.105).

The fixed point iteration is used to solve (8.101) — (8.103) and compute $\mathbf{C}_{\mathrm{i}}(\xi)$, $\mathbf{C}_{\mathrm{ki}}(\xi)$, $\mathbf{C}_{\mathrm{di}}(\xi)$.[20] Moreover, as it was noticed in [**42**], the straightforward application of Newton's method to the solution of $(8.113)_1$ or $(8.114)_1$ is not trivial. Indeed, for $\eta = 0$, $m > 1$, computational difficulties occur while solving $(8.113)_1$, since the first derivative of $H(\xi)$ is

---

[19] Note that for $\eta = 0$ an incremental procedure of rate-independent plasticity is restored.

[20] Alternatively, the Newton-Raphson method can be applied to solve (8.101) — (8.103).

zero at the root, and the convergence of the Newton method fails to be quadratic. On the other hand, for $\eta > 0$, the initial approximation $\xi^{(0)} = 0$ can not be used to compute the solution of $(8.114)_1$, since the function $D(\xi)$ is not differentiable at zero. To overcome these difficulties, only one Newton iteration is performed using $(8.113)_1$ with initial approximation $\xi^{(0)} = 0$, and the subsequent iterations are performed using $(8.114)_1$.

5. Numerical results and comparison with experimental data

5.1. Tension/compression and torsion of tubular thin-walled specimens. A non-proportional loading can be realized experimentally using thin-walled tube specimens under tension/compression and torsion. In this subsection we discuss a simplified idealization of such tests performed in order to identify the yield surface. Let l and l_0 denote the current length and the initial length of the specimen, respectively. Thus, the axial strain is given by $\varepsilon = l/l_0 - 1$. Next, by r_0 and ϕ we denote the initial radius of the cross-section[21] and the angle of twist, respectively. Therefore, the shear strain can be captured by $\gamma = \phi r_0/l_0$. Within the approach used in this contribution we simulate the mechanical response of the material at a single point. Let us consider at that point a local Cartesian coordinate system such that its basis vectors $\mathbf{e}_1$, $\mathbf{e}_2$, and $\mathbf{e}_3$ are oriented along the hoop, axial, and radial directions, respectively. Further, we suppose that the deformation gradient is given by the relation

$$\mathbf{F} = \alpha_1 \mathbf{e}_1 \otimes \mathbf{e}_1 + \gamma \alpha_1 \mathbf{e}_1 \otimes \mathbf{e}_2 + (1+\varepsilon)\mathbf{e}_2 \otimes \mathbf{e}_2 + \alpha_2 \mathbf{e}_3 \otimes \mathbf{e}_3, \tag{8.115}$$

where α_1 and α_2 are unknown.[22] At each time step with given ε and γ the unknowns α_1 and α_2 are found by solving the system of equations

$$\mathbf{T}_{11}(\alpha_1, \alpha_2) = 0, \quad \mathbf{T}_{33}(\alpha_1, \alpha_2) = 0, \tag{8.116}$$

which states that the hoop and radial stresses are equal to zero. Here, $\mathbf{T}$ stands for the Cauchy stress tensor. Moreover, we suppose that the stresses and strains are uniformly distributed over the cross section. Therefore, the applied axial force F and the applied torque M can be computed through

$$F = A_0 \ \alpha_1 \ \alpha_2 \ \mathbf{T}_{22}, \quad M = A_0 \ r_0 \ \alpha_1 \ (\alpha_2)^2 \ \mathbf{T}_{12}, \tag{8.117}$$

where A_0 stands for the initial cross section. For what follows it is convenient to introduce the axial stress $\sigma = F/A_0$ and the shear stress $\tau = M/(A_0 r_0)$.

Suppose that the initial state is isotropic and stress-free. Therefore we may put the following initial conditions

$$\mathbf{C}_{\mathrm{i}}|_{t=0} = \mathbf{C}_{\mathrm{ki}}|_{t=0} = \mathbf{C}_{\mathrm{di}}|_{t=0} = \mathbf{1}, \quad s|_{t=0} = s_{\mathrm{d}}|_{t=0} = 0. \tag{8.118}$$

5.2. Simulation results.

---

[21] Since thin-walled tubular specimens are considered here, we do not distinct outer and inner radius.

[22] The quantities $\alpha_1 - 1$ and $\alpha_2 - 1$ can be interpreted as strains in the hoop and radial directions, respectively.

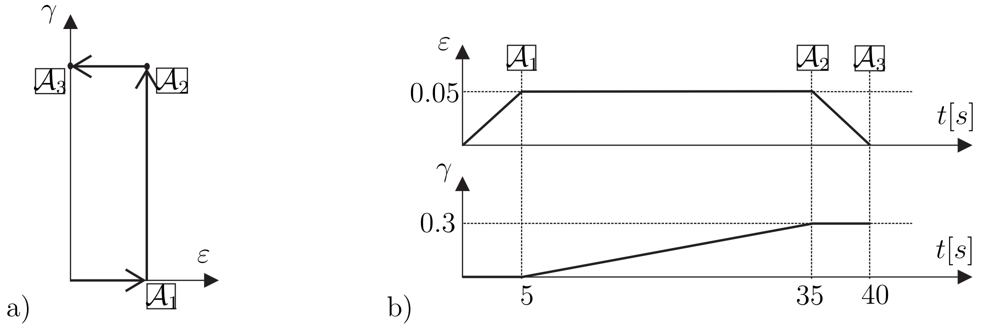

Figure 8.6. a) Route $\mathcal{A}$ in (ε, γ)-space, b) $\varepsilon(t)$ and $\gamma(t)$ for route $\mathcal{A}$.

5.2.1. *Comparison of radial and normal flow rules.* In order to test the influence of the flow rule on the overall material response we consider a loading path in the (ε, γ)-space as depicted in Fig. 8.6a (route $\mathcal{A}$). First, the axial strain ε is increased up to 0.05 with a constant strain rate $\dot{\varepsilon} = 0.01/\mathrm{s}$. The achieved state will be denoted by $\mathcal{A}_1$. Next, as ε remains constant the shear strain γ is increased to 0.3 with $\dot{\gamma} = 0.01/\mathrm{s}$, thus achieving the state $\mathcal{A}_2$. Finally, the axial strain ε is reduced to zero thus leading to the state $\mathcal{A}_3$, see Fig. 8.6b. The set of material parameters used for simulation is summarized in Table 8.2.

Table 8.2. Material parameters used to simulate route $\mathcal{A}$

k [MPa]	μ [MPa]	c_k [MPa]	c_d [MPa]	γ [MPa]
73529	28195	4000	7500	-750

K [MPa]	m [-]	η [s]	k_0 [MPa]	$\varkappa_\mathrm{k}$ [MPa^{-1}]	$\varkappa_\mathrm{d}$ [MPa^{-1}]	β [-]
270	3.6	$2 \cdot 10^6$	1	0.028	0.01113	5

The simulated stress response is demonstrated in Fig. 8.7a,b. The relaxation of the axial stress σ (see Fig. 8.7a) and of the shear stress τ (see Fig. 8.7b) in the case of the radial flow rule takes place faster than for the normality rule.

We recall that the yield surface is oriented along the distortional back stress tensor $\hat{\mathbf{X}}_\mathrm{d}$ (see Fig. 8.5). The evolution of the misorientation angle θ between the deviatoric part of the effective stress tensor $\hat{\mathbf{\Sigma}}^\mathrm{D}$ and $\hat{\mathbf{X}}_\mathrm{d}$ is presented in Fig. 8.7c, where θ is defined by

$$\theta := \arccos\left(\frac{\hat{\mathbf{\Sigma}}^\mathrm{D} : \hat{\mathbf{X}}_\mathrm{d}}{\|\hat{\mathbf{\Sigma}}^\mathrm{D}\| \cdot \|\hat{\mathbf{X}}_\mathrm{d}\|}\right). \tag{8.119}$$

The orientation time for both flow rules is approximately the same, but the maximum value of the misorientation angle θ is larger for the radial flow rule. The stress response depends on the choice of the flow rule shortly after the abrupt change of the loading direction. This corresponds to finite values of the misorientation angle θ. On the other hand, both flow rules yield similar results for small θ.

Note that for the states $\mathcal{A}_1$ and $\mathcal{A}_2$ the yield surface is oriented along the current effective stresses (see Fig. 8.7c). The form of the yield surfaces and the path in the $(\sigma, \sqrt{3}\tau)$-space are depicted in Fig. 8.7d for the normality flow rule. Due to the choice of material parameters we have $1/\varkappa_\mathrm{d} \leq \frac{1}{2}\sqrt{\frac{2}{3}}\big[K + R\big]$. Therefore, the yield surface remains convex.

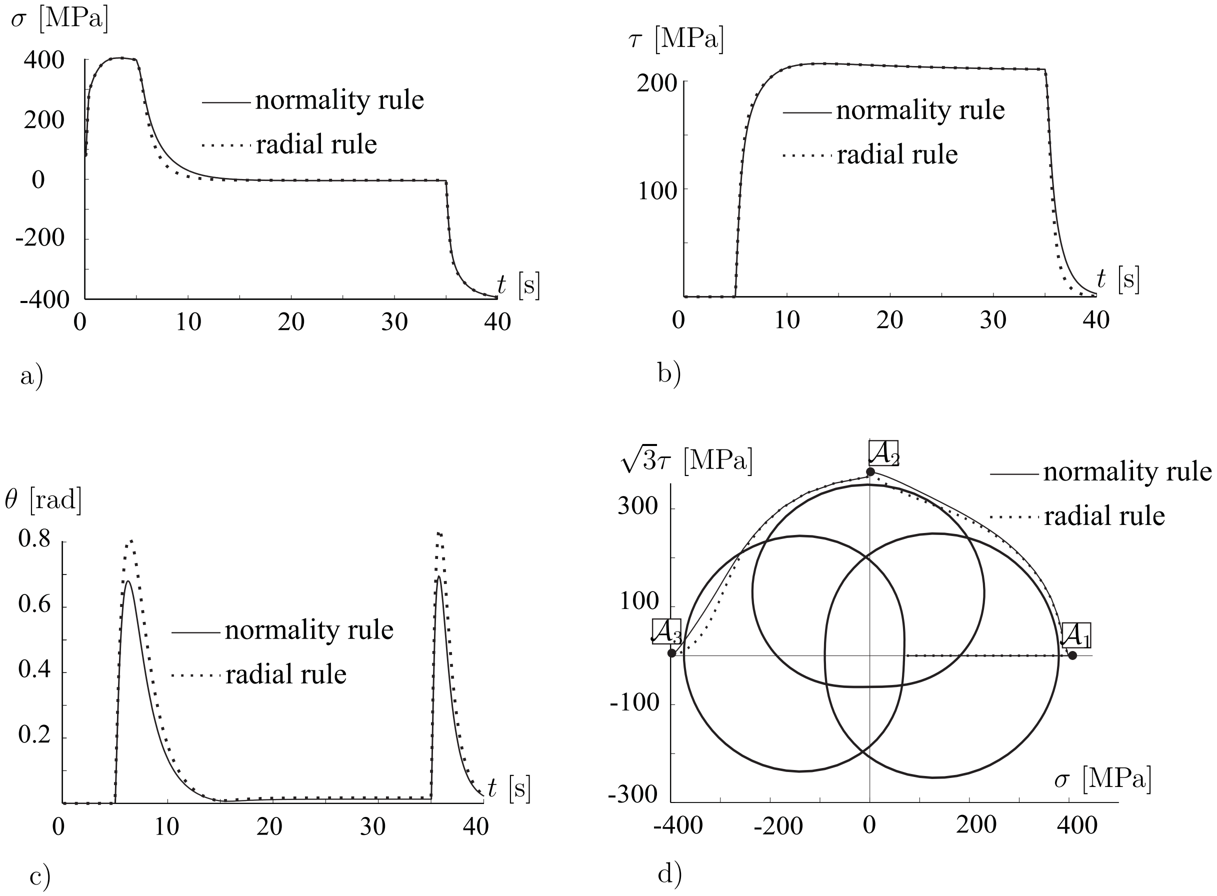

a) b) c) d)

Figure 8.7. Simulation results for the route $\mathcal{A}$: a) axial stress σ, b) shear stress τ, c) misorientation angle θ between $\hat{\mathbf{\Sigma}}^{\mathrm{D}}$ and $\hat{\mathbf{X}}_{\mathrm{d}}$, d) material response and the yield surfaces in (σ, $\sqrt{3}\tau$)-space.

5.2.2. *Comparison with experimental data.* In this subsection we demonstrate the possibility of capturing some effects, like the distortion and the orientation of the yield surface, observed in real experiments. Toward that end we compare the simulation results with the experimental data reported in [**9**] for the structural steel S355 J2G3[23] obtained with the help of the so-called multi-point-technique. The loading path in the $(\varepsilon, \gamma/\sqrt{3})$-space as depicted in Fig. 8.8a (route $\mathcal{B}$), which corresponds to a cyclic nonproportional loading. Since the experiments were performed at quasistatic strain rate, the rate dependence of the material response is neglected ($\eta = 0$ s, $m = 1$). The material parameters used for the simulation are summarized in Table 8.3. Normality flow rule is implemented in this subsection. A saturated process is observed in the simulation after 2 cycles, such that for each subsequent cycle almost the same mechanical response is predicted. The corresponding cyclic path in the (σ, $\sqrt{3}\tau$)-space as well as the yield surfaces are depicted in Fig. 8.8b. The experimental data for the yield surface are depicted in Fig. 8.8b as well.[24]

Although the inelastic deformations observed in the experiment are very small, the measured yield surfaces deviate significantly from the yield surface of the initial state [**9**].

---

[23] According to the German DIN standard 17100, this steel is also referred to as RSt52-3.

[24] See the experiment series S05-MPT in [**9**].

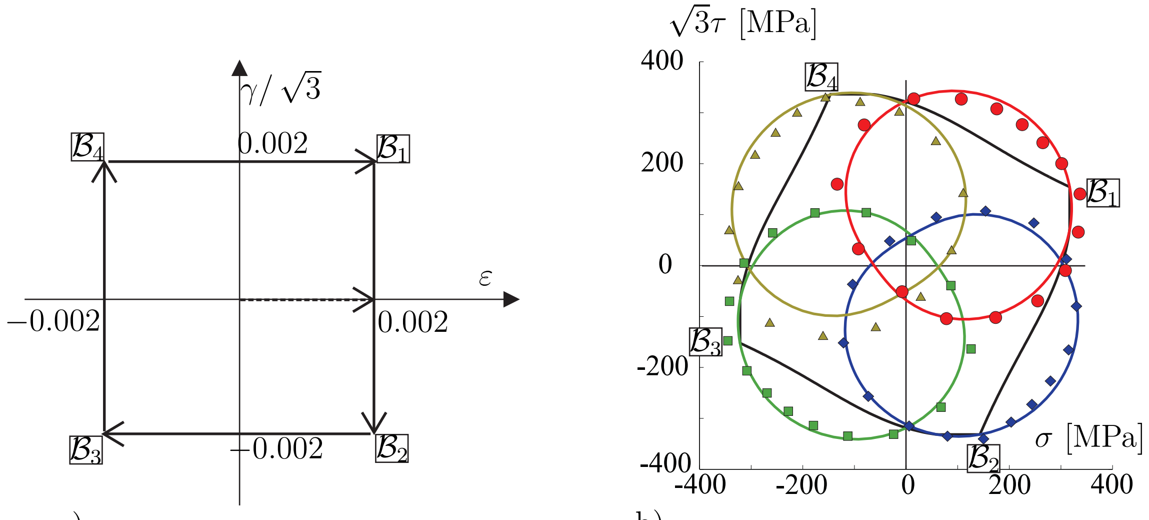

a) b)

Figure 8.8. Numerical simulation of the route $\mathcal{B}$: a) loading path in $(\varepsilon, \gamma/\sqrt{3})$-space, b) simulated cyclic path and yield surfaces in $(\sigma, \sqrt{3}\tau)$-space as well as the corresponding measurement results from [**9**].

Moreover, the yield surface exhibits a higher curvature in the loading direction and a flattening on the opposite side. These effect are reproduced by the proposed material model.

Note that the orientation of the yield surface follows the current state in the stress space with a certain time lag. Moreover, due to the symmetry of the loading path, each simulated yield surface can be obtained by the clockwise rotation at 90 degrees of the previous one.[25] The same holds for the experimental data with exception of the state $\mathcal{B}_4$. Next we note that the measurement results for the states $\mathcal{B}_1$, $\mathcal{B}_2$, and $\mathcal{B}_3$ are approximated by the model. On the other hand, a small discrepancy is observed between the experimental and simulated data for the state $\mathcal{B}_4$ concerning the points opposite to the loading direction. This discrepancy may be explained by the scatter of measurements of the yield surface opposite to the current loading direction [**9**].

Table 8.3. Material parameters used to simulate route $\mathcal{B}$

k [MPa]	μ [MPa]	c_k [MPa]	c_d [MPa]	γ [MPa]
164170	75770	37880	66620	0

K [MPa]	m [-]	η [s]	k_0 [MPa]	$\varkappa_\mathrm{k}$ [MPa^{-1}]	$\varkappa_\mathrm{d}$ [MPa^{-1}]	β [-]
210	1	0	1	0.002765	0.009720	1

6. Conclusion

For a series of metal forming applications it is important to characterize the introduced plastic anisotropy of the material. In this paper a *new* thermodynamically consistent approach to the phenomenological modeling of the hardening behavior at finite strains was suggested. The proposed model takes the isotropic widening and kinematic translation of

---

[25] Since saturated cyclic process is considered, the state $\mathcal{B}_4$ is previous to $\mathcal{B}_1$.

the yield surface as well as the increased curvature in the loading direction and the flattening on the opposite side (directional distortion) into account. The construction of the model is essentially based on the two-dimensional rheological model presented it this study. Such effects like the distortion of the yield surface and its orientation along the loading path are captured by the rheological model in a vivid way. In particular, the degree of distortion is proportional to $\|\overrightarrow{X_\mathrm{d}}\|$ and the orientation of the yield surface is given by $\overrightarrow{X_\mathrm{d}}/\|\overrightarrow{X_\mathrm{d}}\|$. An important advantage of the model based on this approach is that the distortional hardening is characterized by two material parameters only. Both parameters can be interpreted clearly: $\varkappa_\mathrm{d}$ is responsible for the maximum degree of distortion (see Section 3.5.5) and $c_\mathrm{d}\varkappa_\mathrm{d}$ controls the saturation time. Moreover, the orientation of the yield surface follows the loading path with a certain time lag (cf. Section 5), and this lag depends on the saturation time. The convexity of the yield surface holds a priori for a special choice of material parameters.

The normality flow rule and the radial flow rule are considered in this study. The choice of a certain rule for a specific application should be made depending on the real experimental data.

As it was shown in the paper, the proposed approach can be combined with the Perzyna-type of viscoplasticity, thus leading to a model of overstress type.

Another advantage of the model presented in this paper is that the well-established numerical techniques which were developed for models with kinematic hardening (see, for example [**42, 43**]) can be implemented. In particular, it was shown (cf. Subsection 4.1) that the Euler-Backward Method as well as the Exponential Method exactly preserve the symmetry of the internal variables $\mathbf{C}_\mathrm{i}$, $\mathbf{C}_\mathrm{ki}$, and $\mathbf{C}_\mathrm{di}$. Naturally, the preference should be given to so-called geometric integrators which exactly preserve the incompressibility of the inelastic flow (see [**17, 44**] for references).

The applicability of the material model for different metallic materials should be assessed based on the experimental results. If necessary, the model can be generalized in a variety of ways for a more precise description of the hardening behavior. For instance, additional Maxwell elements for distortional and kinematic hardening can be introduced and the evolution equations (8.66), (8.69) can be modified by considering nonlinear multipliers (cf. [**45**]). Moreover, the initial plastic anisotropy can be taken into account by appropriate calibration of the initial conditions for $\mathbf{C}_\mathrm{ki}$ and $\mathbf{C}_\mathrm{di}$. But it is still a challenging task to provide an efficient thermodynamically admissible approach which would allow us to cover the whole manifold of the experimental results. In particular, the "egg-shaped" yield surfaces typical for some metallic materials can not be idealized using the limaçon of Pascal. But, similar to the case of small strains [**11**], the use of second-rank backstress-like tensors, which was advocated in the current study, seems promising.

Acknowledgements

This research was supported by German Science Foundation grants KR 1419/11-1 and SFB 692. The help of Sten Urban with the animated version of the rheological model is acknowledged. The authors are grateful to Dr. M.G. Petrov for fruitful discussions.

Appendix A

Let $K > 0$. Suppose that $\overrightarrow{F}, \overrightarrow{X_{\mathrm{d}}} \in \mathbb{R}^2$. We define two functions $f_1(\overrightarrow{F})$ and $f_2(\overrightarrow{F})$ for all $\overrightarrow{F} \neq 0$ through

$$f_1(\overrightarrow{F}) := \Big\| \Big[(\overrightarrow{F} - \overrightarrow{X_{\mathrm{d}}}) \cdot \frac{\overrightarrow{F}}{\|\overrightarrow{F}\|} \Big] \frac{\overrightarrow{F}}{\|\overrightarrow{F}\|} \Big\| - \sqrt{\frac{2}{3}} K, \quad f_2(\overrightarrow{F}) := \Big\| \overrightarrow{F} \Big\| - \frac{\overrightarrow{X_{\mathrm{d}}} \cdot \overrightarrow{F}}{\|\overrightarrow{F}\|} - \sqrt{\frac{2}{3}} K. \tag{8.120}$$

Assertion 1. Suppose that

$$\|\overrightarrow{X_{\mathrm{d}}}\| < \sqrt{2/3} K. \tag{8.121}$$

Then $f_1(\overrightarrow{F}) = 0$ if and only if $f_2(\overrightarrow{F}) = 0$.

Proof. The proof for the case $\|\overrightarrow{X_{\mathrm{d}}}\| \leq \|\overrightarrow{F}\|$ is obvious. Indeed, using the Cauchy–Schwarz inequality we arrive at

$$\overrightarrow{X_{\mathrm{d}}} \cdot \overrightarrow{F} \leq \|\overrightarrow{F}\|^2, \quad 1 - \frac{\overrightarrow{X_{\mathrm{d}}} \cdot \overrightarrow{F}}{\|\overrightarrow{F}\|^2} \geq 0. \tag{8.122}$$

Therefore,

$$\Big\| \Big[(\overrightarrow{F} - \overrightarrow{X_{\mathrm{d}}}) \cdot \frac{\overrightarrow{F}}{\|\overrightarrow{F}\|} \Big] \frac{\overrightarrow{F}}{\|\overrightarrow{F}\|} \Big\| = \Big\| \Big(1 - \frac{\overrightarrow{X_{\mathrm{d}}} \cdot \overrightarrow{F}}{\|\overrightarrow{F}\|^2} \Big) \overrightarrow{F} \Big\| \overset{(8.122)_2}{=} \Big(1 - \frac{\overrightarrow{X_{\mathrm{d}}} \cdot \overrightarrow{F}}{\|\overrightarrow{F}\|^2} \Big) \|\overrightarrow{F}\| = \|\overrightarrow{F}\| - \frac{\overrightarrow{X_{\mathrm{d}}} \cdot \overrightarrow{F}}{\|\overrightarrow{F}\|}. \tag{8.123}$$

Thus, $f_1(\overrightarrow{F}) = f_2(\overrightarrow{F})$. It remains now to prove the assertion for $\|\overrightarrow{F}\| < \|\overrightarrow{X_{\mathrm{d}}}\|$. Let $f_1(\overrightarrow{F}) = 0$ and let us suppose for the moment that $\overrightarrow{X_{\mathrm{d}}} \cdot \overrightarrow{F} > 0$. In that case we have

$$\begin{aligned} \sqrt{\frac{2}{3}} K \overset{f_1(\overrightarrow{F})=0}{=} & \Big\| \Big[(\overrightarrow{F} - \overrightarrow{X_{\mathrm{d}}}) \cdot \frac{\overrightarrow{F}}{\|\overrightarrow{F}\|} \Big] \frac{\overrightarrow{F}}{\|\overrightarrow{F}\|} \Big\| = \Big| 1 - \frac{\overrightarrow{X_{\mathrm{d}}} \cdot \overrightarrow{F}}{\|\overrightarrow{F}\|^2} \Big| \|\overrightarrow{F}\| \overset{\overrightarrow{X_{\mathrm{d}}} \cdot \overrightarrow{F} > 0}{\leq} \max \Big(1, \frac{\overrightarrow{X_{\mathrm{d}}} \cdot \overrightarrow{F}}{\|\overrightarrow{F}\|^2} \Big) \|\overrightarrow{F}\| \\ & = \max \Big(\|\overrightarrow{F}\|, \frac{\overrightarrow{X_{\mathrm{d}}} \cdot \overrightarrow{F}}{\|\overrightarrow{F}\|} \Big) \leq \max \Big(\|\overrightarrow{F}\|, \|\overrightarrow{X_{\mathrm{d}}}\| \Big) \overset{\|\overrightarrow{F}\| < \|\overrightarrow{X_{\mathrm{d}}}\|}{=} \|\overrightarrow{X_{\mathrm{d}}}\|. \end{aligned} \tag{8.124}$$

But this result contradicts the assumption (8.121). Thus, $f_1(\overrightarrow{F}) = 0$ implies immediately $\overrightarrow{X_{\mathrm{d}}} \cdot \overrightarrow{F} \leq 0$. In that case we have

$$\begin{aligned} \sqrt{\frac{2}{3}} K \overset{f_1(\overrightarrow{F})=0}{=} & \Big\| \Big[(\overrightarrow{F} - \overrightarrow{X_{\mathrm{d}}}) \cdot \frac{\overrightarrow{F}}{\|\overrightarrow{F}\|} \Big] \frac{\overrightarrow{F}}{\|\overrightarrow{F}\|} \Big\| = \Big| 1 - \frac{\overrightarrow{X_{\mathrm{d}}} \cdot \overrightarrow{F}}{\|\overrightarrow{F}\|^2} \Big| \|\overrightarrow{F}\| \\ & \overset{\overrightarrow{X_{\mathrm{d}}} \cdot \overrightarrow{F} \leq 0}{=} \Big(1 - \frac{\overrightarrow{X_{\mathrm{d}}} \cdot \overrightarrow{F}}{\|\overrightarrow{F}\|^2} \Big) \|\overrightarrow{F}\| = \|\overrightarrow{F}\| - \frac{\overrightarrow{X_{\mathrm{d}}} \cdot \overrightarrow{F}}{\|\overrightarrow{F}\|} = f_2(\overrightarrow{F}) + \sqrt{\frac{2}{3}} K. \end{aligned} \tag{8.125}$$

Substituting $\sqrt{\frac{2}{3}} K$ from both sides of the equality we obtain $f_2(\overrightarrow{F}) = 0$. Thus, the implication $(f_1 = 0) \Rightarrow (f_2 = 0)$ is proved.

Now consider $f_2(\overrightarrow{F}) = 0$ and suppose for the moment that $\overrightarrow{X_{\mathrm{d}}} \cdot \overrightarrow{F} > 0$. Under these assumptions we have a contradiction

$$\|\overrightarrow{X_{\mathrm{d}}}\| \overset{(8.121)}{<} \sqrt{\frac{2}{3}} K \overset{f_2(\overrightarrow{F})=0}{=} \|\overrightarrow{F}\| - \frac{\overrightarrow{X_{\mathrm{d}}} \cdot \overrightarrow{F}}{\|\overrightarrow{F}\|} \overset{\overrightarrow{X_{\mathrm{d}}} \cdot \overrightarrow{F} > 0}{\leq} \|\overrightarrow{F}\| \overset{\|\overrightarrow{F}\| < \|\overrightarrow{X_{\mathrm{d}}}\|}{<} \|\overrightarrow{X_{\mathrm{d}}}\|. \tag{8.126}$$

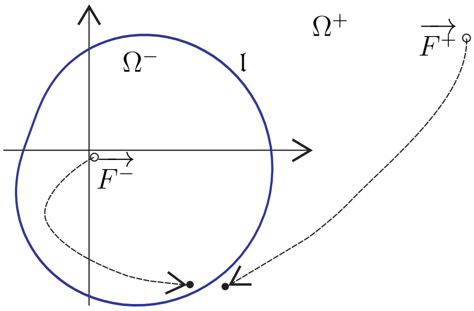

Figure 8.9. The limaçon of Pascal and the subdivision of $\mathbb{R}^2/\{0\}$.

Thus, $f_2(\overrightarrow{F}) = 0$ implies immediately $\overrightarrow{X_\mathrm{d}} \cdot \overrightarrow{F} \leq 0$. In that case (cf. (8.125)), we have $f_1(\overrightarrow{F}) = f_2(\overrightarrow{F}) = 0$. This completes the proof of the assertion.

Assertion 2. Suppose (8.121) holds; then $f_1(\overrightarrow{F}) \leq 0$ if and only if $f_2(\overrightarrow{F}) \leq 0$.

Proof. First, using Assertion 1 we conclude that a smooth closed curve can be defined through

$$\mathrm{I} := \{\overrightarrow{F} \in \mathbb{R}^2/\{0\} : f_1(\overrightarrow{F}) = 0\} = \{\overrightarrow{F} \in \mathbb{R}^2/\{0\} : f_2(\overrightarrow{F}) = 0\}, \tag{8.127}$$

whenever assumption (8.121) holds (see Fig. 8.9). Moreover, the curve I is a limaçon of Pascal.

Furthermore, it follows form (8.120) and (8.121) that $f_1(\overrightarrow{F}) < 0$ and $f_2(\overrightarrow{F}) < 0$ as $\|\overrightarrow{F}\| \to 0$. Thus, there is $\overrightarrow{F^-} \neq 0$ such that $f_1(\overrightarrow{F^-}) < 0$ and $f_2(\overrightarrow{F^-}) < 0$. Next, since $f_1(\overrightarrow{F}) > 0$ and $f_2(\overrightarrow{F}) > 0$ as $\|\overrightarrow{F}\| \to \infty$, there is $\overrightarrow{F^+}$ such that $f_1(\overrightarrow{F^+}) > 0$ and $f_2(\overrightarrow{F^+}) > 0$ (see Fig. 8.9). According to Fig. 8.9, the plane $\mathbb{R}^2/\{0\}$ is decomposed into three parts: Ω^-, Ω^+, and I. Here, the domains Ω^- and Ω^+ consist of points which can be reached along a path in $\mathbb{R}^2/\{0\}$ starting respectively from $\overrightarrow{F^-}$ and $\overrightarrow{F^+}$ without crossing I. Since the functions f_i are continuous in $\mathbb{R}^2/\{0\}$ and $f_\mathrm{i}(\overrightarrow{F})$ remain nonzero along the paths, we obtain

$$f_\mathrm{i}(\overrightarrow{F}) < 0, \text{ for all } \overrightarrow{F} \in \Omega^-, \mathrm{i} \in \{1,2\}; \quad f_\mathrm{i}(\overrightarrow{F}) > 0, \text{ for all } \overrightarrow{F} \in \Omega^+, \mathrm{i} \in \{1,2\}. \tag{8.128}$$

This conclusion completes the proof .

Remark 9. Assertion 1 and Assertion 2 can be easily generalized to any finite-dimensional Hilbert space. For instance, the space of symmetric second rank tensors $\mathbf{X}$ such that $\mathrm{tr}(\mathbf{X}) = 0$ can be covered as well, by reducing the considerations to a 2-dimensional subspace.

Appendix B

First, let us consider the case $\gamma > 0$. Using (8.30) and $(8.50)_1$ and recalling that $\beta > 0$ we arrive at

$$R(1 - \dot{s}_\mathrm{e}/\dot{s}) = R\dot{s}_\mathrm{d}/\dot{s} = R^2\beta/\gamma \geq 0. \tag{8.129}$$

Next, let $\gamma < 0$. Using (8.30) and $(8.50)_1$ we obtain

$$\dot{R} = \gamma(\dot{s} - \dot{s}_\mathrm{d}) = \gamma\Big(\dot{s} - (\beta/\gamma)\dot{s}R\Big) = \beta\dot{s}(\gamma/\beta - R). \tag{8.130}$$

Furthermore, due to the condition $|\gamma(s^0 - s^0_\mathrm{d})| \leq -\gamma/\beta$, we have

$$\gamma/\beta \leq R|_{t=0} \leq -\gamma/\beta. \tag{8.131}$$

Let us show that under that initial condition the solution of the differential equation (8.130) will remain in the closed interval $[\gamma/\beta, -\gamma/\beta]$. It follows from (8.130) that $\dot{R} \geq 0$ for $R < \gamma/\beta$. Thus, $R \geq \gamma/\beta$. It remains to show that $R \leq -\gamma/\beta$. Since $\gamma/\beta - R \leq 0$, we obtain from (8.130) $\dot{R} \leq 0$. Therefore, $R \leq R|_{t=0} \leq -\gamma/\beta$. Thus, $R \in [\gamma/\beta, -\gamma/\beta]$, $R^2 \leq (\gamma/\beta)^2$ and

$$R(1 - \dot{s}_{\mathrm{e}}/\dot{s}) = R\dot{s}_{\mathrm{d}}/\dot{s} = R^2\beta/\gamma \geq (\gamma/\beta)^2\beta/\gamma = \gamma/\beta. \tag{8.132}$$

Appendix C

Suppose that $\overset{\mathrm{d}}{\mathbf{C}}_{\mathrm{de}}$ is positive definite, $\overset{\mathrm{d}}{\mathbf{C}}_{\mathrm{de}} = \overset{\mathrm{d}}{\mathbf{C}}{}^{\mathrm{T}}_{\mathrm{de}}$, and $\det(\overset{\mathrm{d}}{\mathbf{C}}_{\mathrm{de}}) = 1$. Obviously,

$$\overset{\mathrm{d}}{\mathbf{C}}{}^{\mathrm{D}}_{\mathrm{de}} : (\overset{\mathrm{d}}{\mathbf{C}}_{\mathrm{de}}\overset{\mathrm{d}}{\mathbf{C}}{}^{\mathrm{D}}_{\mathrm{de}})^{\mathrm{D}} = \overset{\mathrm{d}}{\mathbf{C}}{}^{\mathrm{D}}_{\mathrm{de}} : (\overset{\mathrm{d}}{\mathbf{C}}_{\mathrm{de}}\overset{\mathrm{d}}{\mathbf{C}}{}^{\mathrm{D}}_{\mathrm{de}}) = \mathrm{tr}(\overset{\mathrm{d}}{\mathbf{C}}{}^{\mathrm{D}}_{\mathrm{de}}\overset{\mathrm{d}}{\mathbf{C}}_{\mathrm{de}}\overset{\mathrm{d}}{\mathbf{C}}{}^{\mathrm{D}}_{\mathrm{de}}) = \|\overset{\mathrm{d}}{\mathbf{C}}{}^{\mathrm{D}}_{\mathrm{de}}\overset{\mathrm{d}}{\mathbf{C}}{}^{1/2}_{\mathrm{de}}\|^2 \geq 0. \tag{8.133}$$

Moreover, since $\det(\overset{\mathrm{d}}{\mathbf{C}}_{\mathrm{de}}) = 1$, it follows from (8.133) that

$$\overset{\mathrm{d}}{\mathbf{C}}{}^{\mathrm{D}}_{\mathrm{de}} : (\overset{\mathrm{d}}{\mathbf{C}}_{\mathrm{de}}\overset{\mathrm{d}}{\mathbf{C}}{}^{\mathrm{D}}_{\mathrm{de}})^{\mathrm{D}} = 0 \quad \text{if and only if} \quad \overset{\mathrm{d}}{\mathbf{C}}_{\mathrm{de}} = \mathbf{1}. \tag{8.134}$$

On the other hand, using the Cauchy-Schwarz inequality we arrive at

$$\overset{\mathrm{d}}{\mathbf{C}}{}^{\mathrm{D}}_{\mathrm{de}} : (\overset{\mathrm{d}}{\mathbf{C}}_{\mathrm{de}}\overset{\mathrm{d}}{\mathbf{C}}{}^{\mathrm{D}}_{\mathrm{de}})^{\mathrm{D}} \leq \|\overset{\mathrm{d}}{\mathbf{C}}{}^{\mathrm{D}}_{\mathrm{de}}\| \cdot \|(\overset{\mathrm{d}}{\mathbf{C}}_{\mathrm{de}}\overset{\mathrm{d}}{\mathbf{C}}{}^{\mathrm{D}}_{\mathrm{de}})^{\mathrm{D}}\|. \tag{8.135}$$

But it follows from (8.133) and (8.134) that $\overset{\mathrm{d}}{\mathbf{C}}{}^{\mathrm{D}}_{\mathrm{de}} : (\overset{\mathrm{d}}{\mathbf{C}}_{\mathrm{de}}\overset{\mathrm{d}}{\mathbf{C}}{}^{\mathrm{D}}_{\mathrm{de}})^{\mathrm{D}} > 0$ for $\overset{\mathrm{d}}{\mathbf{C}}_{\mathrm{de}} \neq \mathbf{1}$. Dividing both sides of (8.135) by $\overset{\mathrm{d}}{\mathbf{C}}{}^{\mathrm{D}}_{\mathrm{de}} : (\overset{\mathrm{d}}{\mathbf{C}}_{\mathrm{de}}\overset{\mathrm{d}}{\mathbf{C}}{}^{\mathrm{D}}_{\mathrm{de}})^{\mathrm{D}}$ we obtain

$$\alpha_{\mathrm{d}}(\overset{\mathrm{d}}{\mathbf{C}}_{\mathrm{de}}) = \frac{\|\overset{\mathrm{d}}{\mathbf{C}}{}^{\mathrm{D}}_{\mathrm{de}}\| \cdot \|(\overset{\mathrm{d}}{\mathbf{C}}_{\mathrm{de}}\overset{\mathrm{d}}{\mathbf{C}}{}^{\mathrm{D}}_{\mathrm{de}})^{\mathrm{D}}\|}{\overset{\mathrm{d}}{\mathbf{C}}{}^{\mathrm{D}}_{\mathrm{de}} : (\overset{\mathrm{d}}{\mathbf{C}}_{\mathrm{de}}\overset{\mathrm{d}}{\mathbf{C}}{}^{\mathrm{D}}_{\mathrm{de}})^{\mathrm{D}}} \geq 1, \quad \text{for } \overset{\mathrm{d}}{\mathbf{C}}_{\mathrm{de}} \neq \mathbf{1}. \tag{8.136}$$

Remark 10. A geometric interpretation of the function α_{d} is as follows. Let Θ be the angle between $\overset{\mathrm{d}}{\mathbf{C}}{}^{\mathrm{D}}_{\mathrm{de}}$ and $(\overset{\mathrm{d}}{\mathbf{C}}_{\mathrm{de}}\overset{\mathrm{d}}{\mathbf{C}}{}^{\mathrm{D}}_{\mathrm{de}})^{\mathrm{D}}$ such that $-\pi < \Theta \leq \pi$. Thus, $\alpha_{\mathrm{d}} = 1/\cos(\Theta)$. Moreover, it follows from (8.133) that $-\pi/2 \leq \Theta \leq \pi/2$. Furthermore, in the case of small strains we may put $\overset{\mathrm{d}}{\mathbf{C}}_{\mathrm{de}} \to \mathbf{1}$. Therefore, $\overset{\mathrm{d}}{\mathbf{C}}{}^{\mathrm{D}}_{\mathrm{de}} \approx (\overset{\mathrm{d}}{\mathbf{C}}_{\mathrm{de}}\overset{\mathrm{d}}{\mathbf{C}}{}^{\mathrm{D}}_{\mathrm{de}})^{\mathrm{D}}$, $\Theta \to 0$ and $\alpha_{\mathrm{d}} \to 1$. This corresponds to the fact that the multiplier α_{d} is not needed in the geometrically linear case.

Appendix D

The proof of the assertion from Section 3.5.5 is based on the analysis of the evolution equation $(8.96)_2$ which governs the saturation of the distortional hardening. First, we recall that $\left(\mathbf{F}_{\mathrm{i}}^{-\mathrm{T}}\right)^{*}\hat{\mathbf{X}}_{\mathrm{d}} = \tilde{\mathbf{X}}_{\mathrm{d}}$ and $(\mathbf{F}_{\mathrm{i}})^{*}\hat{\mathbf{X}}_{\mathrm{d}} = \mathbf{C}_{\mathrm{i}}\tilde{\mathbf{X}}_{\mathrm{d}}\mathbf{C}_{\mathrm{i}}$. Therefore,

$$\|\hat{\mathbf{X}}_{\mathrm{d}}\|^2 = \hat{\mathbf{X}}_{\mathrm{d}} : \hat{\mathbf{X}}_{\mathrm{d}} = \Big[\left(\mathbf{F}_{\mathrm{i}}^{-\mathrm{T}}\right)^{*}\hat{\mathbf{X}}_{\mathrm{d}}\Big] : \Big[(\mathbf{F}_{\mathrm{i}})^{*}\hat{\mathbf{X}}_{\mathrm{d}}\Big] = \mathrm{tr}\Big[\left(\mathbf{C}_{\mathrm{i}}\tilde{\mathbf{X}}_{\mathrm{d}}\right)^2\Big] \overset{(8.77)_3}{=} \frac{c_{\mathrm{d}}^2}{4}\mathrm{tr}\Big[\left((\mathbf{C}_{\mathrm{i}}\mathbf{C}_{\mathrm{di}}^{-1})^{\mathrm{D}}\right)^2\Big]. \tag{8.137}$$

Suppose that at some time instance t_0 we have $\|\hat{\mathbf{X}}_{\mathrm{d}}\| > 1/\varkappa_{\mathrm{d}}$ and $\lambda_{\mathrm{i}} > 0$. In order to prove the assertion it is sufficient to show that $\frac{d}{dt}\|\hat{\mathbf{X}}_{\mathrm{d}}\|^2|_{t=t_0} \leq 0$. Toward that end we differentiate (8.137) with respect to t

$$\frac{d}{dt}\|\hat{\mathbf{X}}_{\mathrm{d}}\|^2 = \frac{c_{\mathrm{d}}^2}{2}\mathrm{tr}\Big[(\mathbf{C}_{\mathrm{i}}\mathbf{C}_{\mathrm{di}}^{-1})^{\mathrm{D}}\,(\mathbf{C}_{\mathrm{i}}\mathbf{C}_{\mathrm{di}}^{-1})^{\cdot}\Big] = \frac{c_{\mathrm{d}}^2}{2}\mathrm{tr}\Big[(\mathbf{C}_{\mathrm{i}}\mathbf{C}_{\mathrm{di}}^{-1})^{\mathrm{D}}\,(\dot{\mathbf{C}}_{\mathrm{i}}\mathbf{C}_{\mathrm{di}}^{-1}+\mathbf{C}_{\mathrm{i}}(\mathbf{C}_{\mathrm{di}}^{-1})^{\cdot})\Big] = \frac{c_{\mathrm{d}}^2}{2}(F_I - F_{II}), \tag{8.138}$$

where

$$F_I := \mathrm{tr}\Big[(\mathbf{C}_{\mathrm{i}}\mathbf{C}_{\mathrm{di}}^{-1})^{\mathrm{D}}\dot{\mathbf{C}}_{\mathrm{i}}\mathbf{C}_{\mathrm{di}}^{-1}\Big], \quad F_{II} := -\mathrm{tr}\Big[(\mathbf{C}_{\mathrm{i}}\mathbf{C}_{\mathrm{di}}^{-1})^{\mathrm{D}}\mathbf{C}_{\mathrm{i}}(\mathbf{C}_{\mathrm{di}}^{-1})^{\cdot}\Big]. \tag{8.139}$$

$$\begin{tikzcd}
\tilde{\mathcal{K}} \arrow[dr, "\mathbf{F}_{\mathrm{di}}"] \arrow[drr, bend left, "\mathbf{F}_{\mathrm{i}}"] & & \\
& \mathcal{K}^d \arrow[r, "\overset{\mathrm{d}}{\mathbf{F}}{}^{\mathrm{new}}_{\mathrm{de}} = \overset{\mathrm{d}}{\mathbf{F}}_{\mathrm{de}}"] & \hat{\mathcal{K}} \\
\tilde{\mathcal{K}}^{\mathrm{new}} \arrow[uu, "\mathbf{F}_0^{-1}"] \arrow[ur, "\mathbf{F}^{\mathrm{new}}_{\mathrm{di}}"] \arrow[urr, bend right, "\mathbf{F}^{\mathrm{new}}_{\mathrm{i}}"'] & &
\end{tikzcd}$$

Figure 8.10. Commutative diagram: change of the reference configuration $\tilde{\mathcal{K}}$.

Next, in order to simplify the evaluation of F_I and F_{II}, the following consideration can be made.[26] We recall that the constitutive equations were formulated with respect to a certain fixed reference configuration $\tilde{\mathcal{K}}$. Now it is useful to rewrite the constitutive relations with respect to some "new" local reference configuration $\tilde{\mathcal{K}}^{\mathrm{new}} = \mathbf{F}_0\tilde{\mathcal{K}}$ (see Fig. 8.10). Here, the mapping $\mathbf{F}_0$ is supposed to be isochoric, i.e. $\det(\mathbf{F}_0) = 1$. The intermediate configurations $\mathcal{K}^d$ and $\hat{\mathcal{K}}$ remain unchanged under that transformation. We define "new" variables and corresponding constitutive equations in such a way that the same distortional backstress $\hat{\mathbf{X}}_{\mathrm{d}}$ is predicted. Toward that end, we postulate the transformation rules for $\mathbf{F}_{\mathrm{i}}$, $\mathbf{F}_{\mathrm{di}}$, $\overset{\mathrm{d}}{\mathbf{F}}_{\mathrm{de}}$, $\mathbf{C}_{\mathrm{i}}$, and $\mathbf{C}_{\mathrm{di}}$

$$\mathbf{F}^{\mathrm{new}}_{\mathrm{i}} := \mathbf{F}_{\mathrm{i}}\mathbf{F}_0^{-1}, \quad \mathbf{F}^{\mathrm{new}}_{\mathrm{di}} := \mathbf{F}_{\mathrm{di}}\mathbf{F}_0^{-1}, \quad \overset{\mathrm{d}}{\mathbf{F}}{}^{\mathrm{new}}_{\mathrm{de}} := \overset{\mathrm{d}}{\mathbf{F}}_{\mathrm{de}},$$
$$\mathbf{C}^{\mathrm{new}}_{\mathrm{i}} := \mathbf{F}_0^{-\mathrm{T}}\mathbf{C}_{\mathrm{i}}\mathbf{F}_0^{-1}, \quad \mathbf{C}^{\mathrm{new}}_{\mathrm{di}} := \mathbf{F}_0^{-\mathrm{T}}\mathbf{C}_{\mathrm{di}}\mathbf{F}_0^{-1}. \tag{8.140}$$

The situation is summarized in diagram 8.10. Further, it follows from (8.93) and (8.140) that

$$\lambda_{\mathrm{i}} = \frac{1}{2}\sqrt{\mathrm{tr}\Big[\dot{\mathbf{C}}_{\mathrm{i}}\mathbf{C}_{\mathrm{i}}^{-1}\Big]^2} = \frac{1}{2}\sqrt{\mathrm{tr}\Big[\dot{\mathbf{C}}^{\mathrm{new}}_{\mathrm{i}}(\mathbf{C}^{\mathrm{new}}_{\mathrm{i}})^{-1}\Big]^2}; \quad \psi_{\mathrm{dis}}(\mathbf{C}_{\mathrm{i}}{\mathbf{C}_{\mathrm{di}}}^{-1}) = \psi_{\mathrm{dis}}(\mathbf{C}^{\mathrm{new}}_{\mathrm{i}}(\mathbf{C}^{\mathrm{new}}_{\mathrm{di}})^{-1}). \tag{8.141}$$

Let $\mathbf{C}_{\mathrm{di}}(t)$ be the solution of $(8.96)_2$ for a given $\{\mathbf{C}_{\mathrm{i}}(t)\}_{t\in[0,T]}$ (and some initial condition). The relations (8.140) provide a one-to-one correspondence between the original and "new" quantities $\mathbf{C}_{\mathrm{i}}(t)$, $\mathbf{C}_{\mathrm{di}}(t)$. It can be easily seen that the equation which describes the evolution of $\mathbf{C}^{\mathrm{new}}_{\mathrm{di}}(t)$ is now obtained from $(8.96)_2$ by replacement of original quantities by their "new" counterparts. Since $\overset{\mathrm{d}}{\mathbf{F}}{}^{\mathrm{new}}_{\mathrm{de}} = \overset{\mathrm{d}}{\mathbf{F}}_{\mathrm{de}}$, we conclude that $\hat{\mathbf{X}}_{\mathrm{d}}$ and $\frac{d}{dt}\|\hat{\mathbf{X}}_{\mathrm{d}}\|^2$ remain unchanged if $\mathbf{C}_{\mathrm{i}}(t)$ (and the initial value for $\mathbf{C}_{\mathrm{di}}$) are transformed according to (8.140). On the other hand, by choosing $\mathbf{F}_0 = \Big(\mathbf{C}_{\mathrm{i}}(t^0)\Big)^{1/2}$ the situation is reduced to $\mathbf{C}^{\mathrm{new}}_{\mathrm{i}}|_{t=t_0} = \mathbf{1}$. Therefore, without loss of generality we may assume $\mathbf{C}_{\mathrm{i}}|_{t=t_0} = \mathbf{1}$. In that case, the incompressibility condition $\mathrm{tr}\Big(\mathfrak{D}_{\mathrm{i}}(\hat{\mathbf{\Gamma}}_{\mathrm{i}})\Big) = 0$ takes the form $\mathrm{tr}(\dot{\mathbf{C}}_{\mathrm{i}})|_{t=t_0} = 0$. Substituting these results into $(8.139)_1$ we obtain for $t = t_0$

$$F_I|_{t=t_0} = \mathrm{tr}\Big[(\mathbf{C}_{\mathrm{di}}^{-1})^{\mathrm{D}}\dot{\mathbf{C}}_{\mathrm{i}}\mathbf{C}_{\mathrm{di}}^{-1}\Big] = \mathrm{tr}\Big[\mathbf{C}_{\mathrm{di}}^{-1}(\mathbf{C}_{\mathrm{di}}^{-1})^{\mathrm{D}}\dot{\mathbf{C}}_{\mathrm{i}}\Big] \overset{\mathrm{tr}(\dot{\mathbf{C}}_{\mathrm{i}})=0}{=} (\mathbf{C}_{\mathrm{di}}^{-1}(\mathbf{C}_{\mathrm{di}}^{-1})^{\mathrm{D}})^{\mathrm{D}} : \dot{\mathbf{C}}_{\mathrm{i}}. \tag{8.142}$$

Using the Cauchy-Schwarz inequality and taking $\lambda_{\mathrm{i}}|_{t=t_0} = \frac{1}{2}\|\dot{\mathbf{C}}_{\mathrm{i}}\|$ into account, we obtain

$$F_I|_{t=t_0} \leq \|(\mathbf{C}_{\mathrm{di}}^{-1}(\mathbf{C}_{\mathrm{di}}^{-1})^{\mathrm{D}})^{\mathrm{D}}\| \; \|\dot{\mathbf{C}}_{\mathrm{i}}\| = 2\lambda_{\mathrm{i}}\|(\mathbf{C}_{\mathrm{di}}^{-1}(\mathbf{C}_{\mathrm{di}}^{-1})^{\mathrm{D}})^{\mathrm{D}}\|. \tag{8.143}$$

---

[26] The similar approach was used in the paper [**44**] in order to simplify the analysis of the exponential stability of the inelastic flow.

On the other hand, since $\frac{d}{dt}(\mathbf{C}_{\mathrm{di}}\mathbf{C}_{\mathrm{di}}^{-1}) = 0$, we deduce from $(8.96)_2$:
$(\mathbf{C}_{\mathrm{di}}^{-1})^{\cdot} = -2\ \lambda_{\mathrm{i}}\ \tilde{\alpha}_{\mathrm{d}}(\mathbf{C}_{\mathrm{i}}, \mathbf{C}_{\mathrm{di}})\ \mathbf{C}_{\mathrm{di}}^{-1}\ \varkappa_{\mathrm{d}}\ \Big(\mathbf{C}_{\mathrm{i}}\tilde{\mathbf{X}}_{\mathrm{d}}\Big)^{\mathrm{D}}$. Substituting this into $(8.139)_2$ and taking into account that $\Big(\mathbf{C}_{\mathrm{i}}\tilde{\mathbf{X}}_{\mathrm{d}}\Big)^{\mathrm{D}} = \frac{c_{\mathrm{d}}}{2}\ (\mathbf{C}_{\mathrm{di}}^{-1})^{\mathrm{D}}$, we arrive at

$$F_{II}|_{t=t_0} = -\mathrm{tr}\Big[(\mathbf{C}_{\mathrm{di}}^{-1})^{\mathrm{D}}(\mathbf{C}_{\mathrm{di}}^{-1})^{\cdot}\Big] = 2\lambda_{\mathrm{i}}\ \tilde{\alpha}_{\mathrm{d}}(\mathbf{1}, \mathbf{C}_{\mathrm{di}})\ \frac{c_{\mathrm{d}}\varkappa_{\mathrm{d}}}{2}\ \mathrm{tr}\Big[(\mathbf{C}_{\mathrm{di}}^{-1})^{\mathrm{D}}\mathbf{C}_{\mathrm{di}}^{-1}(\mathbf{C}_{\mathrm{di}}^{-1})^{\mathrm{D}}\Big]. \tag{8.144}$$

Combining $\|\hat{\mathbf{X}}_{\mathrm{d}}|_{t=t_0}\| > 1/\varkappa_{\mathrm{d}}$ with (8.137) we obtain $(c_{\mathrm{d}}\varkappa_{\mathrm{d}})/2 > 1/\|(\mathbf{C}_{\mathrm{di}}^{-1})^{\mathrm{D}}\|$. Substituting this into (8.144) we obtain

$$F_{II}|_{t=t_0} \geq 2\lambda_{\mathrm{i}}\ (\tilde{\alpha}_{\mathrm{d}}(\mathbf{1}, \mathbf{C}_{\mathrm{di}})/\|(\mathbf{C}_{\mathrm{di}}^{-1})^{\mathrm{D}}\|)\ \mathrm{tr}\Big[(\mathbf{C}_{\mathrm{di}}^{-1})^{\mathrm{D}}\mathbf{C}_{\mathrm{di}}^{-1}(\mathbf{C}_{\mathrm{di}}^{-1})^{\mathrm{D}}\Big]. \tag{8.145}$$

Recall (8.88): $\tilde{\alpha}_{\mathrm{d}}(\mathbf{1}, \mathbf{C}_{\mathrm{di}}) = \Big(\|(\mathbf{C}_{\mathrm{di}}^{-1})^{\mathrm{D}}\|\ \|(\mathbf{C}_{\mathrm{di}}^{-1}(\mathbf{C}_{\mathrm{di}}^{-1})^{\mathrm{D}})^{\mathrm{D}}\|\Big)/\Big(\mathrm{tr}\Big[(\mathbf{C}_{\mathrm{di}}^{-1})^{\mathrm{D}}\mathbf{C}_{\mathrm{di}}^{-1}(\mathbf{C}_{\mathrm{di}}^{-1})^{\mathrm{D}}\Big]\Big)$. Therefore,

$$F_{II}|_{t=t_0} \geq 2\lambda_{\mathrm{i}}\ \|(\mathbf{C}_{\mathrm{di}}^{-1}(\mathbf{C}_{\mathrm{di}}^{-1})^{\mathrm{D}})^{\mathrm{D}}\|. \tag{8.146}$$

Combining this with (8.138) and (8.143) we conclude that $\frac{d}{dt}\|\hat{\mathbf{X}}_{\mathrm{d}}\|^2|_{t=t_0} \leq 0$. The assertion is proved.

Appendix E

Let us analyze, for instance, the right-hand side of equation (8.91). We have

$$\mathbf{f} = 2\check{\lambda}_{\mathrm{i}}\left\{\Big(\frac{1}{\mathfrak{F}} + \frac{\mathrm{tr}\Big[\Big(\mathbf{C}\tilde{\mathbf{T}} - \mathbf{C}_{\mathrm{i}}\tilde{\mathbf{X}}_{\mathrm{k}}\Big)^{\mathrm{D}}\mathbf{C}_{\mathrm{i}}\tilde{\mathbf{X}}_{\mathrm{d}}\Big]}{\mathfrak{F}^3}\Big)\Big(\mathbf{C}\tilde{\mathbf{T}} - \mathbf{C}_{\mathrm{i}}\tilde{\mathbf{X}}_{\mathrm{k}}\Big)^{\mathrm{D}} - \frac{1}{\mathfrak{F}}\mathbf{C}_{\mathrm{i}}\tilde{\mathbf{X}}_{\mathrm{d}}\right\}, \quad \mathbf{A} = \mathbf{C}_{\mathrm{i}}. \tag{8.147}$$

Due to the Hamilton-Cayley theorem, it is sufficient to check (8.97) for $k = 1, 2$. Moreover, since $\mathbf{C}\tilde{\mathbf{T}}$, $\mathbf{C}_{\mathrm{i}}\tilde{\mathbf{X}}_{\mathrm{k}}$, and $\mathbf{C}_{\mathrm{i}}\tilde{\mathbf{X}}_{\mathrm{d}}$ are isotropic functions of $\mathbf{C}\mathbf{C}_{\mathrm{i}}{}^{-1}$, $\mathbf{C}_{\mathrm{i}}\mathbf{C}_{\mathrm{ki}}{}^{-1}$, and $\mathbf{C}_{\mathrm{i}}\mathbf{C}_{\mathrm{di}}{}^{-1}$, respectively, we obtain with some suitable $d_n, h_n \in \mathbb{R}$

$$\mathbf{f} = d_1\mathbf{1} + d_2\mathbf{C}\mathbf{C}_{\mathrm{i}}^{-1} + d_3(\mathbf{C}\mathbf{C}_{\mathrm{i}}^{-1})^2 + d_4\mathbf{C}_{\mathrm{i}}\mathbf{C}_{\mathrm{ki}}^{-1} + d_5(\mathbf{C}_{\mathrm{i}}\mathbf{C}_{\mathrm{ki}}^{-1})^2 + d_6\mathbf{C}_{\mathrm{i}}\mathbf{C}_{\mathrm{di}}^{-1} + d_7(\mathbf{C}_{\mathrm{i}}\mathbf{C}_{\mathrm{di}}^{-1})^2,$$

$$\begin{aligned}\mathbf{f}^2 = h_1\mathbf{1} + h_2\mathbf{C}\mathbf{C}_{\mathrm{i}}^{-1} + h_3(\mathbf{C}\mathbf{C}_{\mathrm{i}}^{-1})^2 + h_4\mathbf{C}_{\mathrm{i}}\mathbf{C}_{\mathrm{ki}}^{-1} + h_5(\mathbf{C}_{\mathrm{i}}\mathbf{C}_{\mathrm{ki}}^{-1})^2 + h_6\mathbf{C}_{\mathrm{i}}\mathbf{C}_{\mathrm{di}}^{-1} + h_7(\mathbf{C}_{\mathrm{i}}\mathbf{C}_{\mathrm{di}}^{-1})^2 \\ + h_8\Big(\mathbf{C}\mathbf{C}_{\mathrm{i}}^{-1}\mathbf{C}_{\mathrm{i}}\mathbf{C}_{\mathrm{ki}}^{-1} + \mathbf{C}_{\mathrm{i}}\mathbf{C}_{\mathrm{ki}}^{-1}\mathbf{C}\mathbf{C}_{\mathrm{i}}^{-1}\Big) + h_9\Big(\mathbf{C}\mathbf{C}_{\mathrm{i}}^{-1}(\mathbf{C}_{\mathrm{i}}\mathbf{C}_{\mathrm{ki}}^{-1})^2 + (\mathbf{C}_{\mathrm{i}}\mathbf{C}_{\mathrm{ki}}^{-1})^2\mathbf{C}\mathbf{C}_{\mathrm{i}}^{-1}\Big) \\ +h_{10}\Big((\mathbf{C}\mathbf{C}_{\mathrm{i}}^{-1})^2\mathbf{C}_{\mathrm{i}}\mathbf{C}_{\mathrm{ki}}^{-1}+\mathbf{C}_{\mathrm{i}}\mathbf{C}_{\mathrm{ki}}^{-1}(\mathbf{C}\mathbf{C}_{\mathrm{i}}^{-1})^2\Big)+h_{11}\Big((\mathbf{C}\mathbf{C}_{\mathrm{i}}^{-1})^2(\mathbf{C}_{\mathrm{i}}\mathbf{C}_{\mathrm{ki}}^{-1})^2+(\mathbf{C}_{\mathrm{i}}\mathbf{C}_{\mathrm{ki}}^{-1})^2(\mathbf{C}\mathbf{C}_{\mathrm{i}}^{-1})^2\Big)+....\end{aligned}$$

Using these identities it can be easily checked that $\mathbf{f}\mathbf{C}_{\mathrm{i}}, \mathbf{f}^2\mathbf{C}_{\mathrm{i}} \in Sym$.

Bibliography

[1] B. D. Annin, Modern models of plastic bodies (In Russian), Novosibirsk, (Novosibirsk State University, 1975).

[2] B. D. Annin, Experimental investigation of plastic properties under complex loadings (In Russian). Mechanika tverdogo tela, 347—351 (1978).

[3] A. Bertram, Elasticity and Plasticity of Large Deformations (Springer, 2005).

[4] T. Böhlke, G. Risy, A. Bertram, A micro-mechanically based quadratic yield condition for textured polycrystals, ZAMM, **88**5, 379–387 (2008).

[5] A. Bucher, U. J. Görke, R. Kreißig, A material model for finite elasto-plastic deformations considering a substructure, International Journal of Plasticity, **20**, 619–642 (2004).

[6] J. L. Chaboche, G. Rousselier, On the plastic and viscoplastic constitutive equations, part 1: Rules developed with internal variable concept, Journal of Pressure Vessel Technology, **105**, 153 — 158 (1983).

[7] J. L. Chaboche, G. Rousselier, On the plastic and viscoplastic constitutive equations, part 2: Application of internal variable concept to the 316 stainless steel. Journal of Pressure Vessel Technology, **105**, 159 — 164 (1983).

[8] V. Danilov, On the formulation of the law of distortional hardening (In Russian). Mechanika tverdogo tela **6**, 146—150 (1971).

[9] S. Dannemeyer, Zur Veränderung der Fließfläche von Baustahl bei mehrachsiger plastischer Wechselbeanspruchung, Braunschweig (Carolo-Wilhelmina University, 1999).

[10] W. Dettmer, S. Reese, On the theoretical and numerical modelling of Armstrong—Frederick kinematic hardening in the finite strain regime, Computer Methods in Applied Mechanics and Engineering, **193**, 87—116 (2004).

[11] M. François, A plasticity model with yield surface distortion for non proportional loading, International Journal of Plasticity, **17**, 703–717 (2001).

[12] M. Freund, J. Ihlemann, Generalization of one-dimensionalmaterial models for the finite element method, ZAMM, **90**5, 399-417 (2010).

[13] M. Freund, H. Lorenz, D. Juhre, J. Ihlemann, M. Klüppel, Finite element implementation of a microstructure-based model for filled elastomers, accepted to International Journal of Plasticity.

[14] G. Grewolls, R. Kreißig, Anisotropic hardening —- numerical application of a cubic yield theory and consideration of variable r-values for sheet metal, European Journal of Mechanics A/Solids, **20**, 585–599 (2001).

[15] E. Hairer, Geometric Integration of Ordinary Differential Equations on Manifolds, BIT Numerical Mathematics, **41**(5), 996–1007 (2001).

[16] S. Hartmann, P. Neff, Polyconvexity of generalized polynomial-type hyperelastic strain energy functions for near-incompressibility. International Journal of Solids and Structures, **40**11, 2767—2791 (2003).

[17] S. Hartmann, K.J. Quint, M. Arnold, On plastic incompressibility within time-adaptive finite elements combined with projection techniques, Computer Methods in Applied Mechanics and Engineering, **198**, 173–178 (2008).

[18] P. Haupt, Ch. Tsakmakis, On the application of dual variables in continuum mechanics, Continuum Mechanics and Thermodynamics 1 (1989) 165–196.

[19] P. Haupt, M. Kamlah, Ch. Tsakmakis, On the thermodynamics of rate-independent plasticity as an asymptotic limit of viscoplasticity for slow processes. In Besdo, D. and Stein, E., editors, Finite Inelastic Deformations - Theory and Applications (1992) 107–116.

[20] P. Haupt, Continuum Mechanics and Theory of Materials, 2nd edition, Springer, 2002.

[21] D. Helm, Formgedächtnislegierungen, experimentelle Untersuchung, phänomenologische Modellierung und numerische Simulation der thermomechanischen Materialeigenschaften, (Universitätsbibliothek Kassel, 2001).

[22] D. Helm, Stress computation in finite thermoviscoplasticity. International Journal of Plasticity, **22**, 1699–1721 (2006).

[23] H. Hencky, Zur Theorie plastischer Deformationen und der hierdurch im Material hervorgerufenen Nachspannungen, ZAMM, **4** 4, 323 – 334 (1924).

[24] A. A. Ilyushin, On the Relation between Stresses and Small Strains in the Mechanics of Continua (In Russian), Prikl. Mat. Mech. **18**, 641–666 (1954).

[25] M. Itskov, Tensor Algebra and Tensor Analysis for Engineers: With Applications to Continuum Mechanics (Springer, 2007).

[26] S. N. Korobeynikov, Objective tensor rates and applications in formulation of hyperelastic relations, Journal of Elasticity, **93** 2, 105–140 (2008).

[27] U. Kowalsky, H. Ahrens, D. Dinkler, Distorted yield surfaces – modelling by higher order anisotropic hardening tensors, Comput. Mater. Sci. **16**, 81—88 (1999).

[28] E. Kröner, Allgemeine Kontinuumstheorie der Versetzungen und Eigenspannungen, Archive for Rational Mechanics and Analysis, **4** (1960) 237–334.

[29] T. Kurtyka, M. Zyczkowski, A geometric description of distortional plastic hardening of deviatoric materials, Arch. Mech., **37**, 383 – 395 (1985).

[30] T. Kurtyka, M. Zyczkowski, Evolution equations for distortional plastic hardening, International Journal of Plasticity, **12**, 191 – 213 (1996).

[31] E. H. Lee, Elastic-plastic deformation at finite strains, Journal of Applied Mechanics, 91 (1969) 1–6.

[32] A. Lion, Constitutive modelling in finite thermoviscoplasticity: a physical approach based on nonlinear rheological elements, International Journal of Plasticity, **16**, 469–494 (2000).

[33] C. Miehe, Exponential map algorithm for stress updates in anisotropic multiplicative elastoplasticity for single crystals, International Journal for Numerical Methods in Engineering, **39**, 3367–3390 (1996).

[34] S. Panhans, Ein viskoplastisches Materialmodell mit nichtquadratischer Fließfunktion. Dissertation, (TU Chemnitz, 2006).

[35] S. Panhans, R. Kreißig, A viscoplastic material model of overstress type with a non-quadratic yield function, European Journal of Mechanics A/Solids, **25**, 283–298 (2006).

[36] P. Perzyna, The constitutive equations for rate sensitive plastic materials, Quarterly of Applied Mathematics, 20 (1963) 321–331.

[37] M. G. Petrov, Rheological properties of materials from the point of view of physical kinetics, Journal of Applied Mechanics and Technical Physics, **39** 1 (1998) 104–112.

[38] W. Prager, Probleme der Plastizitätstheorie. Basel-Stuttgart, (Birkhäuser Verlag, 1955).

[39] L. Prandtl, Ein Gedankenmodell zur kinetischen Theorie der festen Körper, ZAMM, **8** 2, 85 – 106 (1928).

[40] M. Reiner, Deformation, Strain and Flow. An Elementary Introduction to Rheology. London, 2nd edition, (H.K.Lewis, 1960).

[41] J. Simo, T. Hughes, Computational inelasticity, Springer, 1998.

[42] A. V. Shutov, R. Kreißig, Finite strain viscoplasticity with nonlinear kinematic hardening: Phenomenological modeling and time integration, Computer Methods in Applied Mechanics and Engineering, **197**, 2015–2029 (2008).

[43] A. V. Shutov, R. Kreißig, Application of a coordinate-free tensor formalism to the numerical implementation of a material model, ZAMM, **88** 11, 888–909 (2008).

[44] A. V. Shutov, R. Kreißig, Geometric integrators for multiplicative viscoplasticity: analysis of error accumulation, Computer Methods in Applied Mechanics and Engineering, **199** 11, 700–711 (2010).

[45] A. V. Shutov, C. Kuprin, J. Ihlemann, M. F.-X. Wagner, C. Silbermann, Experimentelle Untersuchung und numerische Simulation des inkrementellen Umformverhaltens von Stahl 42CrMo4, Materialwissenschaft und Werkstofftechnik, **41** 9, 765–775 (2010).

[46] Z. Sobotka, Various kinds of two-dimensional rheological models, Journal of Macromolecular Science, Part B, **5** 2, 393–414 (1971).

[47] E. Steck, R. Ritter, U. Peil, A. Ziegenbein (Eds.), Deutsche Forschungsgemeinschaft, Plasticity of Materials: Experiments, Models, Computation. (Wiley-VCH Verlag GmbH, 2001).

[48] T. Streilein, Erfassung formativer Verfestigung in viskoplastischen Stoffmodellen (Consideration of distortional hardening in viscoplastic material models). PhD thesis, Bericht Nr. 97/83 (TU Braunschweig, 1997).

[49] Ch. Tsakmakis, A. Willuweit, A comparative study of kinematic hardening rules at finite deformations, International Journal of Non-Linear Mechanics, **39** 2, 539–554 (2004).

[50] I. N. Vladimirov, M. P. Pietryga, S. Reese, Anisotropic finite elastoplasticity with nonlinear kinematic and isotropic hardening and application to sheet metal forming, International Journal of Plasticity, **26**, 659–687 (2010).

[51] J. Wang, V. Levkovitch, F. Reusch, B. Svendsen, J. Huetink, M. Riel, On the modeling of hardening in metals during non-proportional loading, International Journal of Plasticity, **24**, 1039–1070 (2008).

KAPITEL 9

A viscoplasticity model with an enhanced control of the yield surface distortion

A. V. Shutov[1], J. Ihlemann
Chemnitz University of Technology, Str. d. Nationen 62, D-09111 Chemnitz, Germany

Abstract: *A new model of metal viscoplasticity, which takes combined isotropic, kinematic, and distortional hardening into account, is presented. The basic modeling assumptions are illustrated using a new two-dimensional rheological analogy. This demonstrative rheological model is used as a guideline for the construction of constitutive relations. The nonlinear kinematic hardening is captured using the well-known Armstrong-Frederick approach. The distortion of the yield surface is described with the help of a so-called distortional backstress. A distinctive feature of the model is that any smooth convex saturated form of the yield surface which is symmetric with respect to the loading direction can be captured. In particular, an arbitrary sharpening of the saturated yield locus in the loading direction combined with a flattening on the opposite side can be covered. Moreover, the yield locus evolves smoothly and its convexity is guaranteed at each hardening stage. A strict proof of the thermodynamic consistency is provided. Finally, the predictive capabilities of the material model are illustrated using the experimental data for a very high work hardening annealed aluminum alloy 1100 Al.*

Keywords: viscoplasticity; yield function; kinematic hardening; distortional hardening; rheology
MSC2000: 74C10; 74S05

Nomenclature

α	distortion parameter, cf. (9.13), (9.26)
$\mathbf{X}_{\mathrm{k}}$, $\mathbf{X}_{\mathrm{d}}$	backstress and distortional backstress, respectively
R	isotropic hardening, cf. $(9.18)_4$
$\boldsymbol{\sigma}_{\mathrm{eff}}$	effective stress, cf. $(9.20)_1$
$\boldsymbol{R}_{\mathrm{eff}}$	effective radial direction, cf. $(9.32)_2$
$\boldsymbol{\varepsilon}_{\mathrm{i}}$, $\boldsymbol{\varepsilon}_{\mathrm{e}}$	inelastic and elastic strains, respectively, cf. $(9.14)_1$
$\boldsymbol{\varepsilon}_{\mathrm{ki}}$, $\boldsymbol{\varepsilon}_{\mathrm{di}}$	dissipative parts of $\boldsymbol{\varepsilon}_{\mathrm{i}}$, cf. $(9.14)_2$, $(9.14)_3$

---

[1] Corresponding author. alexey.v.shutov@gmail.com
web: http://sites.google.com/site/materialmodeling

This chapter is reproduced from the paper: A. V. Shutov, J. Ihlemann. A viscoplasticity model with an enhanced control of the yield surface distortion. International Journal of Plasticity. 2012. (39), 152-167. Copyright Elsevier. Reproduced with permission.

$\boldsymbol{\varepsilon}_{\mathrm{ke}}$, $\boldsymbol{\varepsilon}_{\mathrm{de}}$	conservative parts of $\boldsymbol{\varepsilon}_{\mathrm{i}}$, cf. $(9.14)_2$, $(9.14)_3$
λ_{i}	inelastic multiplier, cf. $(9.24)_2$
p	accumulated inelastic arc-length (Odqvist parameter), cf. $(9.24)_3$
s, s_{d}	internal variables of isotropic hardening, cf. $(9.14)_4$, (9.28)
θ	angle between $\boldsymbol{\sigma}^{\mathrm{D}}_{\mathrm{eff}}$ and $\mathbf{X}_{\mathrm{d}}$, cf. $(9.20)_2$
f	overstress, cf. (9.10), (9.21)
$\bar{f}$	non-dimensional overstress, cf. (9.6)
$\mathrm{El}(\bar{K}(\cdot,\alpha))$	non-dimensional elastic domain, cf. (9.2) and Fig. 9.3b
$\bar{K}(\theta,\alpha)$	non-dimensional yield stress function, cf. (9.5)
$\bar{K}^{\mathrm{sat}}(\theta)$	non-dimensional saturated yield stress function
$\mathcal{D}(\vec{y}, A)$	distance between $\vec{y} \in \mathbb{R}^2$ and $A \subset \mathbb{R}^2$, cf. (9.3)

1. Introduction

Numerical simulation of complex metal forming operations is a powerful tool to reduce the development costs and to optimize the mechanical properties of a workpiece. For many polycrystalline metals, the initial yield surface can be approximated with sufficient accuracy by the conventional Huber-Mises yield condition which implies initial plastic isotropy. On the other hand, already very small plastic deformations may lead to a significant change of the yield surface compared to the initial state [**1, 60, 13, 48, 30, 31**]. It is well known that the residual stresses, springback, damage evolution, and failure are highly dependent on the accumulated plastic anisotropy of the material. In this work we concentrate on the *phenomenological* modeling of the plastic anisotropy with especial emphasis on the distortional hardening. A conventional approach to metal plasticity is used in the current study: we suppose that a unique yield surface exists and that the material behavior is purely elastic for stresses within the yield surface.[2]

The state of the art phenomenological plasticity is a result of accumulated efforts made by generations of researchers. Unfortunately, little academic credit was given to the paper written by Prager (1935) [**45**]. Already in 1935, Prager combined the isotropic hardening of Odqvist type, the distortional hardening for the prediction of cross hardening effect, and the kinematic hardening for the Bauschinger effect. Interestingly, the idea of modeling the Bauschinger effect by the kinematic translation of the Huber-Mises yield surface in the stress space was taken by Prager from a conference talk given by A. Reuß a year before - in 1934!

Within the classical phenomenological model of Chaboche and Rousselier (1983) [**6, 7**], the isotropic expansion and kinematic translation of the yield surface are considered, such that the yield surface is represented by a hypersphere in the deviatoric stress space.[3] Thus, the change of the form of the yield surface is neglected. Such models can be used to simulate the stress response under proportional loading. However, in general, the distortion of the yield surface has to be considered under nonproportional loading with abrupt change of the

---

[2] Alternatively, different unconventional concepts with numerous types of "yield" surfaces exist. The so-called "subloading surface models" (see [**21**] and references therein) allow to capture the plastic flow for stresses within the "yield" surface. Such approach allows to obtain a smooth transition from the elastic into the elasto-plastic range. Moreover, some models with a smooth stress response can be constructed using the concept of "bounding surface" (see, for instance, [**8**]).

[3] Such yield surface can be represented by a hypersphere in Ilyushin's space, as well (see Ilyshin (1954) [**28**]).

loading path. Such loading conditions are typical not only for multi-stage forming processes, but even for some single-stamping forming operations. In order to control the rotation of a hyperellipsoid which represents the yield surface withing a Hill-type theory[4], Baltov and Sawczuk (1964) [**3**] introduced a polynomial representation of the corresponding 4th rank Hill-type anisotropy tensor in terms of the strain tensor. According to Betten (1976) [**5**], 4th and 6th rank hardening tensors are postulated as functions of the plastic strain. Dafalias (1979) [**9**] considered a general representation of the 4th rank tensor as a polynomial function of the plastic strain. In the paper by Helling and Miller (1987) [**23**], the 4th rank Hill-type anisotropy tensor is assumed to be a function of two backstress-like tensors. In contrast to the above mentioned approaches, the approach of Helling allows to take the dependence on the strain path into account. For the same purpose, Rees (1984) [**46**], Streilein (1997) [**54**], Kowalsky et al. (1999) [**32**], Steck et al. (2001) [**48**], Dafalias et al. (2002) [**10**], Feigenbaum and Dafalias (2007) [**16**], Noman et al. (2010) [**36**], Dafalias and Feigenbaum (2011) [**11**], Pietryga et al. (2012) [**43**] and others modified the Chaboche-Rousselier model introducing ordinary differential equations which describe the evolution of tensor-valued internal variables of higher order (typically 4th and 6th rank tensors). An alternative integral approach was presented by Danilov (1971) [**12**]. In the paper by Grewolls and Kreißig (2001) [**20**], evolution equations for higher order tensors were formulated in integral form using the Danilov's approach. Both differential and integral approaches mentioned above allow to take the dependence of the hardening on the strain path. Kurtyka and Zyczkowski (1985) [**33**], Kurtyka and Zyczkowski (1996) [**34**] proposed a geometric approach in order to simulate a complex distortion of the yield surface.

As it was shown by Plesek et al. (2010) [**44**], the rigorous mathematical proof of convexity of the yield surface may become rather difficult, if evolving 4th rank tensors are utilized. Due to technical mathematical difficulties, some authors prefer to test the convexity of the yield surface by plotting its two-dimensional projection at different loading stages (see, for instance, Pietryga et al. (2012) [**43**]).

Probably, the most simple generalizations of the Chaboche-Rousselier model are based on the use of second-rank backstress-like tensors. Let $\mathbf{X}_{\mathrm{d}}$ be such tensor (director). Within this approach, the yield surface is oriented along $\mathbf{X}_{\mathrm{d}}/\|\mathbf{X}_{\mathrm{d}}\|$, and the degree of distortion is proportional to $\|\mathbf{X}_{\mathrm{d}}\|$. In particular, if Armstrong-Frederick type of hardening is used to describe the evolution of $\mathbf{X}_{\mathrm{d}}$, the distortion evolves in time smoothly. Moreover, the yield surface follows the loading path such that the change of the loading direction leads to a reorientation of the yield surface with a certain time lag. A short overview concerning different approaches based on the use of backstress-like tensors is presented by Wegener and Schlegel (1996) [**60**]. In particular, within the model of Ortiz and Popov (1983) [**37**], the size of the elastic domain along a radial line emanating from the origin of the yield surface depends on the angle θ between the effective deviatoric stress and the backstress direction. More precisely, the critical norm of the effective deviatoric stress is given by a Fourier cosine series of θ. Thus, theoretically, an arbitrary yield surface which is symmetric with respect to the backstress direction can be approximated. On the other hand, the need to ensure the convexity of the yield surface imposes constraints on the Fourier coefficients.

---

[4] The original approach of Hill [**27**] can be used to describe a certain *initial* plastic anisotropy, but not its evolution.

These constraints complicate the practical use of this approach, especially if the smooth evolution of the yield surface is intended. Another special case was considered by François (2001) [**18**]. Within this approach, certain egg-shaped yield surfaces can be modeled. The thermodynamic consistency was numerically tested by François. In the paper by Feigenbaum and Dafalias (2008) [**17**], an existing material model was simplified in a thermodynamically consistent manner such that second-rank backstress-like tensors are used only. Some other models utilizing directional backstresses were presented by Panhans (2006) [**39**] and Panhans and Kreißig (2006) [**40**]. Within the approach of Panhans and Kreißig, the form of the yield surface is given by the so-called limaçon of Pascal, and it can be easily guaranteed that the elastic domain is simply connected and convex. Later, in the paper by Shutov et al. (2011) [**52**] (cf. chapter 8 of this monograph), a two-dimensional rheological model of distortional hardening was suggested, which implies the yield surface to be the the limaçon of Pascal. This rheological model was used to construct thermodynamically consistent constitutive equations of finite strain plasticity/viscoplasticity.

A relatively new concept of representative directions (see, for example, Freund et al. (2012) [**19**]) allows to generalize a uniaxial material model to cover an arbitrary triaxial loading. In order to compute the stress response, a numerical integration on the sphere S^2 is required. This concept, if combined with a uniaxial phenomenological model of plasticity/viscoplasticity, can produce a new phenomenological model with some realistic distortional hardening effects. An interesting simplified approach to the description of plastic anisotropy was proposed by Barlat et al. (2011) [**4**]. Interestingly, this approach does not include the concept of kinematic hardening explicitly, but some distortional effects can be captured. The simplified approach to distortional hardening, which was developed by Aretz (2008) [**2**], does not include kinematic hardening as well. Further, we note that some models of crystal/polycrystal plasticity allow the description of the yield surface distortion in a natural way (cf. Rousselier et al. (2010) [**47**]). For instance, in the paper by Fang et al. (2011) [**15**], the impact of microstructural hardening parameters on the form of the yield locus was analyzed in the finite strain context. It was shown that for reduced latent hardening the yield surface exhibits a larger curvature in the loading direction.

A new phenomenological model of metal plasticity is proposed in the current study. The main features of the current model are as follows:

(i) a *two-dimensional rheological motivation* of constitutive equations, which provides insight into main modeling assumptions;
(ii) nonlinear isotropic hardening of Voce type and nonlinear kinematic hardening of Armstrong-Frederick type;
(iii) *arbitrary* smooth convex yield surface for saturated distortional hardening, which is symmetric with respect to a backstress-like tensor $\mathbf{X}_\mathrm{d}$;
(iv) degree of yield surface distortion is proportional to $\|\mathbf{X}_\mathrm{d}\|$; *the convexity of the yield surface is guaranteed* at each hardening stage;
(v) normality flow rule; pressure-insensitive plasticity;
(vi) explicit formulation of the free energy density and *thermodynamic consistency*;
(vii) overstress type of viscoplasticity according to Perzyna rule.

In this paper, the temperature field is assumed to be constant in time and space.[5] The model is formulated for infinitesimal strains such that the extreme simplicity of the current approach is not obscured by the geometric nonlinearities. At the same time, the elegant technique of Lion (2000) [**35**], which is based on the consideration of rheological analogies, can be used to generalize the constitutive equations to finite strains [**24, 56, 14, 25, 49, 26, 59**]. As it was shown by Shutov et al. (2011) [**52**], a similar technique can be implemented for two-dimensional rheological models, as well. Alternatively to the approach of Lion, the method of rheological models proposed by Palmow (1984) [**38**] can be used to construct finite-strain constitutive relations. This method is based on the additive decomposition of the strain rate tensor (see, for example, Svistkov and Lauke (2009) [**55**]).

We conclude the introduction with a few remarks regarding notation. The elements of $\mathbb{R}^2$ are denoted by $\vec{x} = (x_1, x_2)$, $\vec{y} = (y_1, y_2)$. The notations $\vec{x} \cdot \vec{y} := x_1 y_1 + x_2 y_2$ and $\|\vec{x}\| := \sqrt{\vec{x} \cdot \vec{x}}$ stand for the scalar product and the corresponding norm, respectively. A coordinate-free tensor setting in $\mathbb{R}^3$ is implemented (cf. [**29, 50**]). Bold-faced symbols denote 1st- and 2nd-rank tensors in $\mathbb{R}^3$. Superimposed dot denotes the material time derivative: $\dot{x} = \frac{d}{dt} x$. The symbol " : " stands for the scalar product of two second-rank tensors

$$\mathbf{A} : \mathbf{B} \ := \mathrm{tr}(\mathbf{A} \cdot \mathbf{B}^{\mathrm{T}}).$$

This scalar product gives rise to the Frobenius norm as follows

$$\|\mathbf{A}\| := \sqrt{\mathbf{A} : \mathbf{A}}.$$

The identity tensor is denoted by $\mathbf{1}$. The notation $\mathbf{A}^{\mathrm{D}}$ stands for the deviatoric part of a tensor

$$\mathbf{A}^{\mathrm{D}} := \mathbf{A} - \frac{1}{3} \mathrm{tr}(\mathbf{A}) \mathbf{1}.$$

2. Rheological analogy

2.1. Two-dimensional rheological model. Rheological models are useful for insight into the aspects of material modeling. Especially large body of information is provided by rheological models if they are filled with a physical content (Petrov, 1998 [**42**]). Obviously, the conventional 1-dimensional rheological models are not suitable for the description of the yield surface distortion. Therefore, all considerations of this section are carried out in two-dimensional space $\mathbb{R}^2$. In the paper by Shutov et al. (2011) [**52**] (chapter 8 of this thesis), a two-dimensional rheological model was suggested, which implies that the yield surface is given by the limaçon of Pascal. *A new extended rheological model* of distortional hardening will be presented in this section.

In analogy to Shutov et al. (2011) [**52**], we consider a mechanical system which consists of a tank filled with a viscous fluid, a heavy solid which rests on the flat bottom (modified St.-Venant element $m.StV$), three elastic springs (Hooke-bodies H_{ext}, H_{kin}, and H_{dis}) connected to the modified St.-Venant element, and two spheres (modified Newton elements $m.N_{\text{kin}}$ and

---

[5] The model is formulated in a thermodynamically admissible manner. Therefore, its generalization to thermoplasticity is straight-forward. The equation of heat conduction can be derived directly from the energy balance, and an additional type of free energy (so-called "detached" free energy) can be introduced for better prediction of temperature evolution, cf. Shutov and Ihlemann (2011) [**53**] (chapter 7 of this thesis).

$m.N_{\text{dis}}$) floating on the surface of the fluid (Fig. 9.1).[6] The mechanical properties of these idealized bodies are postulated as follows:

- (H): For the Hooke-bodies (see Fig. 9.2a), the spring force $\vec{\sigma}_H$ is proportional to the length of the body, and the force is oriented along the spring axis: $\vec{\sigma}_H = c\ \vec{\varepsilon}_H$. Here, $\vec{\varepsilon}_H = \overrightarrow{AB} \in \mathbb{R}^2$, and $c \geq 0$ is the stiffness of the spring. In particular, the Hooke-body possesses a zero length in unloaded state.
- ($m.N$): The two-dimensional Newton element is represented by a sphere which is floating on the surface. Following Newton's law of viscous flow, we assume that the fluid resistance $\vec{\sigma}_N$ to the motion of the sphere is proportional to its velocity $\frac{d}{dt}\vec{\varepsilon}_N$. Thus, $\frac{d}{dt}\vec{\varepsilon}_N = \varkappa\ \vec{\sigma}_N$, where $\varkappa \geq 0$ is a viscosity parameter. Next, in order to obtain the constitutive relations of the modified Newton-element, the physical time t is formally replaced by the accumulated inelastic arc-length (Odqvist parameter) p. Thus, we postulate for ($m.N$)-element (see Fig. 9.2b):

  $$\frac{d}{dp}\vec{\varepsilon}_N = \varkappa\ \vec{\sigma}_N. \tag{9.1}$$

  Such modification is possible whenever the inelastic arc-length p is available. The arc-length p will be introduced formally in the following. The use of this parameter instead of the time t allows us to construct rate-independent constitutive relations (see, for example, [**22**]).
- ($m.StV$): The heavy solid rests upon the bottom of the tank and there is a friction between them. By $\vec{\sigma}$, $-\vec{x}_{\text{k}}$, and $-\vec{x}_{\text{d}}$ denote now the forces imposed on the ($m.StV$)-element by the Hooke-bodies H_{ext}, H_{kin}, and H_{dis}, respectively (see Fig. 9.2c). The force $\vec{\sigma}$ will be understood as an external load; $\vec{x}_{\text{k}}$ and $\vec{x}_{\text{d}}$ will be responsible for the effects similar to kinematic and distortional hardening, respectively. The resulting (effective) force is thus given by $\vec{\sigma}_{\text{eff}} = \vec{\sigma} - \vec{x}_{\text{k}} - \vec{x}_{\text{d}}$. Let the axis of the ($m.StV$)-element be always oriented along the resulting (effective) force $\vec{\sigma}_{\text{eff}}$. We suppose that the fluid resistance opposed the rotation of the solid is negligible. The ($m.StV$)-element remains at rest as long as $\|\vec{\sigma}_{\text{eff}}\| \leq \sqrt{2/3}K$, where $\sqrt{2/3}K > 0$ is a *nonconstant* friction. The function K is computed as follows. For $\vec{x}_{\text{d}} = \vec{0}$, we put $K = K_0$, where K_0 is a given basic friction. Further, suppose that $\vec{x}_{\text{d}} \neq \vec{0}$. Let θ be the angle between the axis and $\vec{x}_{\text{d}}$: $\theta = \arccos\left(\frac{\vec{\sigma}_{\text{eff}}\ \cdot\ \vec{x}_{\text{d}}}{\|\vec{\sigma}_{\text{eff}}\|\ \|\vec{x}_{\text{d}}\|}\right)$. Moreover, let $\alpha = \|\vec{x}_{\text{d}}\|/x_d^{\max}$ be a distortion parameter, which is a unique function of $\|\vec{x}_{\text{d}}\|$. Here, $x_d^{\max} > 0$ is the upper bound for $\|\vec{x}_{\text{d}}\|$, therefore we have $\alpha \in [0,1]$. Finally, we consider the friction to be a function of θ and α: $K = \bar{K}(\theta,\alpha)\ K_0$. In particular, for a fixed $\vec{x}_{\text{d}} \neq \vec{0}$, the friction K depends solely on the angle θ. A simple ansatz for $\bar{K}(\theta,\alpha)$ will be presented in the next subsection.

Remark 1. The choice of notations in this section is dictated by the need to keep the structure of the rheological model similar to the structure of small strain plasticity. For that reason, the forces imposed on the ($m.StV$)-element by the Hooke-bodies are denoted by $-\vec{x}_{\text{k}}$, $-\vec{x}_{\text{d}}$ rather than $\vec{x}_{\text{k}}$, $\vec{x}_{\text{d}}$.

---

[6] An animated version of the rheological model with only one modified Newton element is available at http://youtu.be/QEPc3pixbC0

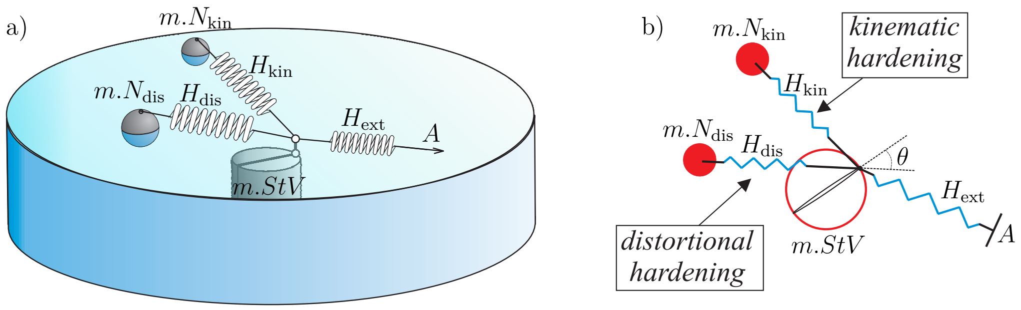

Figure 9.1. a) Two-dimensional rheological model is built up of a modified St.-Venant element ($m.StV$), Hooke-bodies H_{ext}, H_{kin}, H_{dis}, and modified Newton elements $m.N_{\mathrm{kin}}$ and $m.N_{\mathrm{dis}}$; b) Rheological model seen from above. The angle between the ($m.StV$)-axis and H_{dis} is denoted by θ.

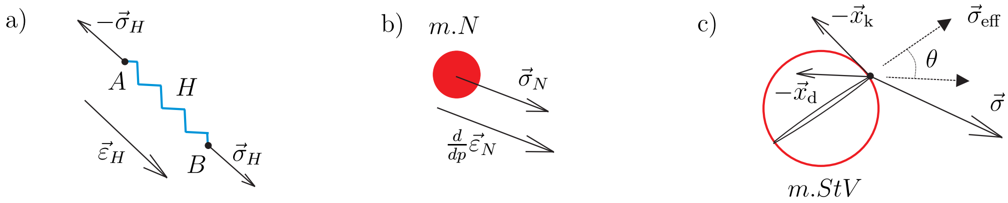

Figure 9.2. Behavior of idealized two-dimensional bodies: a) Hooke-body H. Its elongation is given by $\vec\varepsilon_H = \overrightarrow{AB} \in \mathbb{R}^2$; b) Modified Newton-body $m.N$. Inelastic arc-length p is used instead of the physical time t to formulate the constitutive equations; c) Modified St.-Venant element $m.StV$. The friction depends on the angle θ.

2.2. Direction-dependent friction and definition of overstress. Let $\vec e_1 = (1,0) \in \mathbb{R}^2$. In this subsection we construct the non-dimensional function $\bar K(\theta,\alpha)$ which plays a central role in the current study. In terms of the rheological model introduced above, this function is understood as a friction force, but in the following sections it will be treated as a non-dimensional yield stress. It is useful to interpret such functions geometrically in terms of a parametric family of closed subsets in $\mathbb{R}^2$: For each $\alpha \in [0,1]$ the corresponding subset $\mathrm{El}(\bar K(\cdot,\alpha))$ consists of $\vec y \in \mathbb{R}^2$ such that $\|\vec y\| \le \bar K(\theta,\alpha)$, where $\theta \in [0,\pi]$ is the angle between $\vec y$ and $\vec e_1$ (cf. Fig. 9.3b). More precisely, we put

$$\mathrm{El}(\bar K(\cdot,\alpha)) := \Big\{\vec y \in \mathbb{R}^2/\{\vec 0\} \;:\; \|\vec y\| \le \bar K(\theta,\alpha),\ \text{where } \theta = (\widehat{\vec y,\vec e_1})\Big\} \cup \{\vec 0\}, \tag{9.2}$$

$$(\widehat{\vec y,\vec e_1}) := \arccos\left(\frac{\vec y\cdot\vec e_1}{\|\vec y\|\,\|\vec e_1\|}\right).$$

First, for $\alpha = 0$, we postulate that $\bar K(\theta,0) = 1$, which implies that $\mathrm{El}(\bar K(\cdot,0))$ is a closed unit disc in $\mathbb{R}^2$ (see Fig. 9.3a). Further, suppose that a smooth function $\bar K^{\mathrm{sat}}(\theta)$ is given such that $\mathrm{El}^{\mathrm{sat}} := \mathrm{El}(\bar K^{\mathrm{sat}}(\cdot))$ is convex and $\bar K^{\mathrm{sat}}(0) = 1$ (see Fig. 9.3c). We need to find a smooth function $\bar K(\theta,\alpha)$ such that $\mathrm{El}(\bar K(\cdot,\alpha))$ will be convex for all α and

$$\bar K(0,\alpha) = 1 \text{ for } \alpha \in [0,1], \quad \bar K(\theta,1) = \bar K^{\mathrm{sat}}(\theta) \text{ for } \theta \in [0,\pi].$$

Remark 2. As it will be shown in the following, the given function $\bar K^{\mathrm{sat}}(\theta)$ corresponds to the form of a saturated distortional hardening with the maximum distortion (Fig. 9.3c).

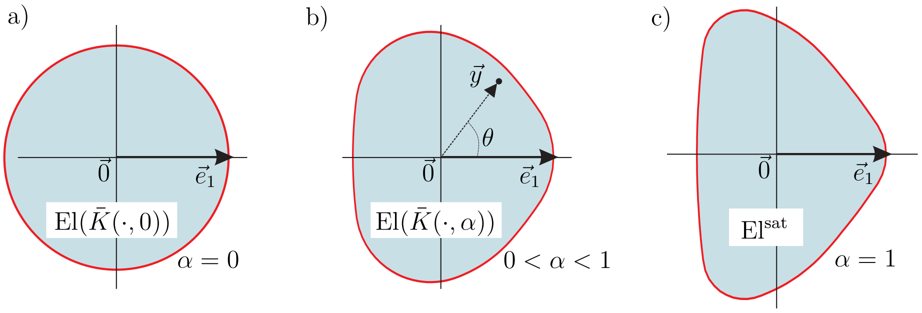

Figure 9.3. a) A closed unit disc which is used to represent the undistorted yield surface; b) Geometric interpretation of $\bar{K}(\theta, \alpha)$ for a fixed α. For each α a closed set $\mathrm{El}(\bar{K}(\cdot, \alpha)) \subset \mathbb{R}^2$ is defined; c) A convex set $\mathrm{El}^{\mathrm{sat}}$ corresponds to the given function $\bar{K}^{\mathrm{sat}}(\theta)$. The boundary of $\mathrm{El}^{\mathrm{sat}}$ can be associated with a saturated form of the yield surface.

Remark 3. The parameter α should be understood as a distortion parameter, such that $\alpha = 0$ and $\alpha = 1$ correspond to zero and maximum distortion, respectively.

In other words, an interpolation rule is needed between the intact initial unit disc (corresponds to $\alpha = 0$) and the maximum distorted set $\mathrm{El}^{\mathrm{sat}}$ (corresponds to $\alpha = 1$).

Remark 4. Unfortunately, the linear interpolation rule $\bar{K}(\theta, \alpha) = (1 - \alpha) + \alpha \bar{K}^{\mathrm{sat}}(\theta)$ is not suitable, since, in general, the convexity of $\mathrm{El}(\bar{K}(\cdot, \alpha))$ is violated for some $\alpha \in (0, 1)$.

The interpolation rule which is implemented in the current study is constructed as follows. First, for any $\vec{y} \in \mathbb{R}^2$, $A \subset \mathbb{R}^2$ we define the distance in a natural way

$$\mathcal{D}(\vec{y}, A) := \inf_{\vec{z} \in A} \|\vec{y} - \vec{z}\|. \tag{9.3}$$

Here, $\inf_{\vec{z} \in A}$ stands for infimum over all $\vec{z} \in A$. A simple graphical interpretation of the distance is shown in Fig. 9.4a. In particular, one obtains $\mathcal{D}(\vec{y}, A) \leq \|\vec{y} - \vec{z}\|$ for all $\vec{z} \in A$. Next, we define the product of $\alpha \in \mathbb{R}$ and $A \subset \mathbb{R}^2$ as $\alpha A := \{\alpha \vec{y} \ : \ \vec{y} \in A\}$. In other words, the set αA results from A by scaling. Finally, the set $\mathrm{El}(\bar{K}(\cdot, \alpha))$ is obtained from the set $\alpha \mathrm{El}^{\mathrm{sat}}$ by adding additional points whose distance from $\alpha \mathrm{El}^{\mathrm{sat}}$ does not exceed $1 - \alpha$ (see Fig. 9.4b)

$$\mathrm{El}(\bar{K}(\cdot, \alpha)) := \Big\{ \vec{y} \in \mathbb{R}^2 : \mathcal{D}(\vec{y}, \alpha \mathrm{El}^{\mathrm{sat}}) \leq 1 - \alpha \Big\}. \tag{9.4}$$

Since $\mathrm{El}^{\mathrm{sat}}$ is convex, so is $\mathrm{El}(\bar{K}(\cdot, \alpha))$.

Formally, since $\mathrm{El}^{\mathrm{sat}}$ is convex, for each $\theta \in [0, \pi]$, and $\alpha \in [0, 1]$ there is a unique $\vec{y}(\theta, \alpha)$ such that $\vec{y} = \|\vec{y}\|(\cos(\theta), \sin(\theta))$ and $\mathcal{D}(\vec{y}, \alpha \mathrm{El}^{\mathrm{sat}}) = 1 - \alpha$ (see Fig. 9.4b). Thus, in accordance with (9.4), we put

$$\bar{K}(\theta, \alpha) := \|\vec{y}(\theta, \alpha)\|. \tag{9.5}$$

In what follows, each set $\mathrm{El}(\bar{K}(\cdot, \alpha))$ will be used to reflect the elastic region in the stress space. Since a viscoplasticity model of overstress type is to be constructed, a proper definition of the overstress will be needed. For given $\vec{y} \in \mathbb{R}^2$ and $\alpha \in [0, 1]$ we define a non-dimensional overstress as a distance from elastic domain:

$$\bar{f}(\vec{y}, \alpha) := \mathcal{D}\Big(\vec{y}, \mathrm{El}(\bar{K}(\cdot, \alpha))\Big) = \Big\langle \mathcal{D}\Big(\vec{y}, \alpha \mathrm{El}^{\mathrm{sat}}\Big) - (1 - \alpha) \Big\rangle, \tag{9.6}$$

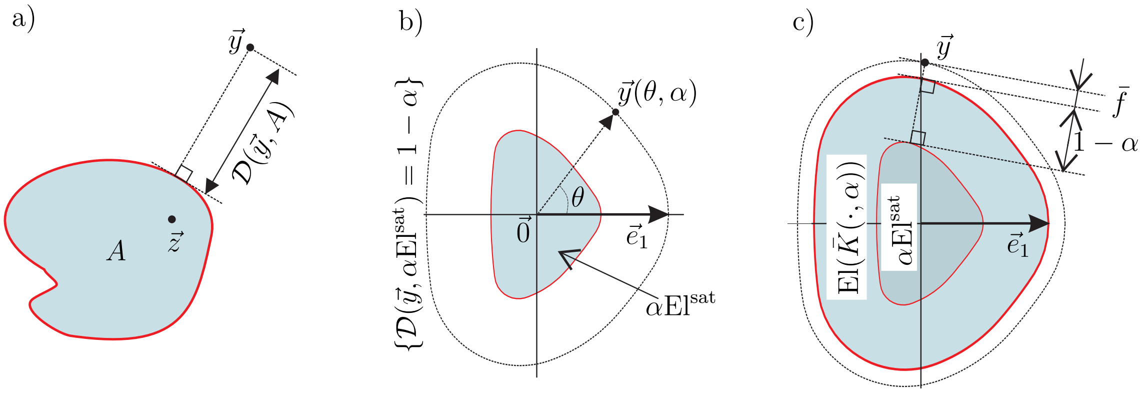

Figure 9.4. a) Definition of the distance $\mathcal{D}(\vec{y}, A)$ according to (9.3); b) Definition of $\vec{y}(\theta, \alpha)$ for $\theta \in [0, \pi]$, $\alpha \in [0, 1]$; c) A line of constant overstress $\bar{f}$ for a fixed $\alpha \in [0, 1]$.

where $\langle x \rangle := \max(x, 0)$. The definition is summarized in Fig. 9.4c. Thus, for the numerical computation of the overstress it is sufficient to evaluate $\mathcal{D}\big(\vec{y}, \alpha \mathrm{El}^{\mathrm{sat}}\big)$. Such computation can be performed explicitly if the boundary of $\mathrm{El}^{\mathrm{sat}}$ is represented by a set of circular arcs. A concrete algorithm is presented in Appendix A. Note that such requirement is not restrictive, since *any smooth convex curve* can be approximated by circular arcs with sufficient accuracy. In most cases, 4 or 5 arcs are sufficient for practical purposes.

Remark 5. The definition (9.6) of the overstress $\bar{f}$ will be advantageous in connection with a normality flow rule. In particular, the derivative of the overstress with respect to $\vec{y}$ possesses a unit norm for $\bar{f} > 0$, i.e., $\|\frac{\partial \bar{f}(\vec{y}, \alpha)}{\partial \vec{y}}\| = 1$. Moreover, the set $\{\vec{y} \ : \ \bar{f}(\vec{y}) \leq \bar{f}_0\}$ is convex for all $\bar{f}_0 \geq 0$.

Remark 6. Using the interpolation rule proposed above, the function $\bar{K}(\theta, \alpha)$ is uniquely defined by the material function $\bar{K}^{\mathrm{sat}}(\theta)$. Here, the function $\bar{K}^{\mathrm{sat}}(\theta)$ describes the saturated form of the convex symmetric yield surface. In some cases this form can be identified experimentally (cf. Remark 9). Figure 9.5 demonstrates that the function $\bar{K}^{\mathrm{sat}}(\theta)$ is not uniquely determined even if the form of the saturated yield surface is known. This is due to the fact the the position of the origin $\vec{0}$ relative to $\mathrm{El}^{\mathrm{sat}}$ is not unique. The function $\bar{K}^{\mathrm{sat}}(\theta)$ is uniquely determined by specifying $\bar{K}^{\mathrm{sat}}(\pi) > 0$, which is a material parameter "hidden" in the material function $\bar{K}^{\mathrm{sat}}(\theta)$. This parameter should be chosen in such a way that a better description of the experimental data is achieved.

2.3. Some constitutive equations in two-dimensions. Consider a system of (constitutive) equations as follows. The total displacement of the point A in Fig. 9.1 with respect to the bottom will be denoted by $\vec{\varepsilon}$. This displacement is a sum of the elastic elongation of the (H_{ext})-body and the inelastic displacement of the $(m.StV)$-body, denoted by $\vec{\varepsilon}_{\mathrm{e}}$ and $\vec{\varepsilon}_{\mathrm{i}}$, respectively:

$$\vec{\varepsilon} = \vec{\varepsilon}_{\mathrm{e}} + \vec{\varepsilon}_{\mathrm{i}}. \tag{9.7}$$

The displacement of the $(m.StV)$-body, in turn, is composed of the elastic (H_{kin})-elongation and the inelastic $(m.N_{\mathrm{kin}})$-displacement. Analogous decomposition holds for H_{dis} and $m.N_{\mathrm{dis}}$, as well:

$$\vec{\varepsilon}_{\mathrm{i}} = \vec{\varepsilon}_{\mathrm{ke}} + \vec{\varepsilon}_{\mathrm{ki}}, \quad \vec{\varepsilon}_{\mathrm{i}} = \vec{\varepsilon}_{\mathrm{de}} + \vec{\varepsilon}_{\mathrm{di}}. \tag{9.8}$$

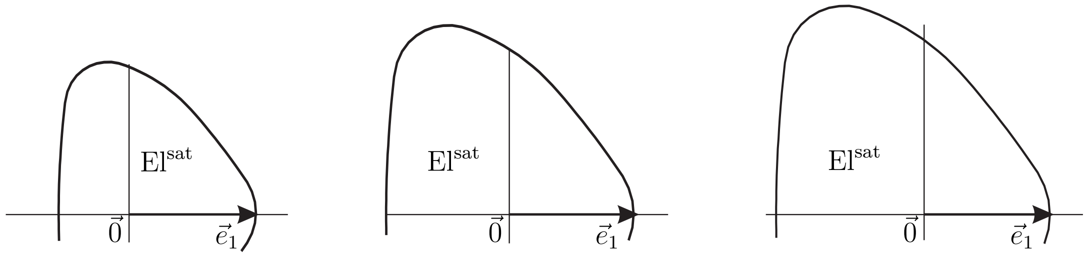

$\bar{K}^{\mathrm{sat}}(\pi) < 1 = \bar{K}^{\mathrm{sat}}(0)$ $\quad$ $\bar{K}^{\mathrm{sat}}(\pi) = 1 = \bar{K}^{\mathrm{sat}}(0)$ $\quad$ $\bar{K}^{\mathrm{sat}}(\pi) > 1 = \bar{K}^{\mathrm{sat}}(0)$

Figure 9.5. The material function $\bar{K}^{\mathrm{sat}}(\theta)$ is not uniquely determined by the form of the saturated yield surface. The function is unique if $\bar{K}^{\mathrm{sat}}(\pi) > 0$ is additionally specified.

The overall potential energy of the system is the sum of potential energies stored in the Hooke-bodies H_{ext}, H_{kin}, and H_{dis}

$$\psi = \psi_{\mathrm{el}}(\vec{\varepsilon}_{\mathrm{e}}) + \psi_{\mathrm{kin}}(\vec{\varepsilon}_{\mathrm{ke}}) + \psi_{\mathrm{dis}}(\vec{\varepsilon}_{\mathrm{de}}) = \mu \ \|\vec{\varepsilon}_{\mathrm{e}}\|^2 + \frac{c_{\mathrm{k}}}{2} \ \|\vec{\varepsilon}_{\mathrm{ke}}\|^2 + \frac{c_{\mathrm{d}}}{2} \ \|\vec{\varepsilon}_{\mathrm{de}}\|^2.$$

Here, $\mu \geq 0$, $c_{\mathrm{k}}/2 \geq 0$, $c_{\mathrm{d}}/2 \geq 0$ are the stiffnesses of H_{ext}, H_{kin}, and H_{dis}, respectively. For the forces $\vec{\sigma}$, $\vec{x}_{\mathrm{k}}$, and $\vec{x}_{\mathrm{d}}$ we arrive at

$$\vec{\sigma} = \frac{\partial \psi_{\mathrm{el}}(\vec{\varepsilon}_{\mathrm{e}})}{\partial \vec{\varepsilon}_{\mathrm{e}}}, \quad \vec{x}_{\mathrm{k}} = \frac{\partial \psi_{\mathrm{kin}}(\vec{\varepsilon}_{\mathrm{ke}})}{\partial \vec{\varepsilon}_{\mathrm{ke}}}, \quad \vec{x}_{\mathrm{d}} = \frac{\partial \psi_{\mathrm{dis}}(\vec{\varepsilon}_{\mathrm{de}})}{\partial \vec{\varepsilon}_{\mathrm{de}}}. \tag{9.9}$$

The overstress f is defined as a function of $\|\vec{\sigma}_{\mathrm{eff}}\| = \|\vec{\sigma} - \vec{x}_{\mathrm{k}} - \vec{x}_{\mathrm{d}}\|$, $\theta = \arccos\Big(\frac{\vec{\sigma}_{\mathrm{eff}} \ \cdot \ \vec{x}_{\mathrm{d}}}{\|\vec{\sigma}_{\mathrm{eff}}\| \ \|\vec{x}_{\mathrm{d}}\|}\Big)$, and the distortion parameter $\alpha = \|\vec{x}_{\mathrm{d}}\|/x_d^{\max}$ by

$$f(\vec{\sigma}, \vec{x}_{\mathrm{k}}, \vec{x}_{\mathrm{d}}) = \tilde{f}(\|\vec{\sigma}_{\mathrm{eff}}\|, \theta, \alpha) := \sqrt{\frac{2}{3}} K_0 \ \bar{f}(\vec{y}, \alpha), \tag{9.10}$$

$$\vec{y} := \frac{\|\vec{\sigma}_{\mathrm{eff}}\|}{\sqrt{2/3} K_0} (\cos(\theta), \sin(\theta)). \tag{9.11}$$

Recall that $\bar{f}(\vec{y}, \alpha)$ is defined through (9.6). Due to the fact that $\|\frac{\partial \bar{f}(\vec{y},\alpha)}{\partial \vec{y}}\| = 1$ for positive overstress, we have a useful property:

$$\Big\|\frac{\partial f(\vec{\sigma}, \vec{x}_{\mathrm{k}}, \vec{x}_{\mathrm{d}})}{\partial \vec{\sigma}}\Big\| = 1, \ \text{for } f > 0.$$

We postulate the normality flow rule (normality to the hypersurface of constant overstress) in combination with the Perzyna-type of viscoplasticity (Perzyna, 1963 [**41**])

$$\dot{\vec{\varepsilon}}_{\mathrm{i}} = \lambda_{\mathrm{i}} \frac{\partial f(\vec{\sigma}, \vec{x}_{\mathrm{k}}, \vec{x}_{\mathrm{d}})}{\partial \vec{\sigma}}, \ \text{for } f > 0, \quad \dot{\vec{\varepsilon}}_{\mathrm{i}} = \vec{0} \text{ for } f = 0; \quad \lambda_{\mathrm{i}} = \frac{1}{\eta} \Big(\frac{1}{k_0} f\Big)^m.$$

Here, $\eta > 0$ and $m \geq 1$ are parameters of the Perzyna rule; $k_0 > 0$ is used to obtain a dimensionless term in the parentheses.

Note that the forces $\vec{x}_{\mathrm{k}}$ and $\vec{x}_{\mathrm{d}}$ act on the modified Newton-elements $m.N_{\mathrm{kin}}$ and $m.N_{\mathrm{dis}}$, respectively. Thus, we obtain in accordance with (9.1)

$$\frac{d \ \vec{\varepsilon}_{\mathrm{ki}}}{dp} = \varkappa_{\mathrm{k}} \ \vec{x}_{\mathrm{k}}, \quad \frac{d \ \vec{\varepsilon}_{\mathrm{di}}}{dp} = \varkappa_{\mathrm{d}} \ \vec{x}_{\mathrm{d}}.$$

Here, $\varkappa_{\mathrm{k}} \geq 0$, $\varkappa_{\mathrm{d}} \geq 0$ are modified viscosity parameters describing $m.N_{\mathrm{kin}}$ and $m.N_{\mathrm{dis}}$, respectively. Let the evolution of the inelastic arc-length p be given by $\dot{p} = \lambda_{\mathrm{i}} = \|\dot{\vec{\varepsilon}}_{\mathrm{i}}\|$. Thus, we obtain

$$\dot{\vec{\varepsilon}}_{\mathrm{ki}} = \lambda_{\mathrm{i}} \, \varkappa_{\mathrm{k}} \, \vec{x}_{\mathrm{k}}, \quad \dot{\vec{\varepsilon}}_{\mathrm{di}} = \lambda_{\mathrm{i}} \, \varkappa_{\mathrm{d}} \, \vec{x}_{\mathrm{d}}. \tag{9.12}$$

It follows from $(9.9)_3$ and $(9.12)_2$ that for proper initial conditions we have $\|\vec{x}_{\mathrm{d}}\| \leq 1/\varkappa_{\mathrm{d}}$. By putting $x_d^{\max} = 1/\varkappa_{\mathrm{d}}$ we specify the definition of the distortion parameter α (cf. Section 2.1)

$$\alpha := \varkappa_{\mathrm{d}} \, \|\vec{x}_{\mathrm{d}}\|. \tag{9.13}$$

Equations (9.12) in combination with $(9.9)_2$ and $(9.9)_3$ describe the evolution of the "backstresses" in the hardening/recovery format. The saturation of $\vec{x}_{\mathrm{d}}$ implies the saturation of the "distortional hardening", which takes place much faster than the saturation of the "kinematic hardening". Thus, "slow" and "fast" saturation should be assumed for $\vec{x}_{\mathrm{k}}$ and $\vec{x}_{\mathrm{d}}$, respectively. Note that the dependence on the strain path is captured in a vivid way, such that the system exhibits a fading memory: only the most recent part of the $\vec{\varepsilon}$-path influences the current "stress" state $\vec{\sigma}$.

3. Material model of viscoplasticity

3.1. Closed system of constitutive equations. Let us formulate a system of constitutive equations of viscoplasticity. First, we suppose that the volumetric response is elastic. More precisely, the hydrostatic stress component $\mathrm{tr}\boldsymbol{\sigma}$ is assumed to be a linear function of $\mathrm{tr}\boldsymbol{\varepsilon}$. Next, suppose that the deviatoric stress component $\boldsymbol{\sigma}^{\mathrm{D}}$ depends solely on the history of the strain deviator $\boldsymbol{\varepsilon}^{\mathrm{D}}$. In order to describe this dependence, we generalize the two-dimensional constitutive equations presented in the previous section to five dimensions.[7] During the generalization we have to make sure that the resulting model inherits the properties of the two-dimensional rheological model. Toward that end, the displacements and forces are formally replaced by deviatoric strains and stresses, respectively; the scalar product in $\mathbb{R}^2$ is replaced by the scalar product of two second-rank tensors.[8] In order to take the isotropic hardening into account, the constant parameter K_0 is now formally replaced by $K_0 + R$, where R is a hardening variable. In order to describe the evolution of R, we introduce a scalar strain-like internal variable s (which is similar to the inelastic arc-length p), its dissipative part s_{d}, and its conservative part s_{e}.

For the strain tensor $\boldsymbol{\varepsilon}$ consider its inelastic part $\boldsymbol{\varepsilon}_{\mathrm{i}}$ and elastic part $\boldsymbol{\varepsilon}_{\mathrm{e}}$. Let $\boldsymbol{\varepsilon}_{\mathrm{ki}}$ and $\boldsymbol{\varepsilon}_{\mathrm{ke}}$ be the dissipative and conservative parts of $\boldsymbol{\varepsilon}_{\mathrm{i}}$, which are connected to the nonlinear kinematic hardening. Analogously, $\boldsymbol{\varepsilon}_{\mathrm{di}}$ and $\boldsymbol{\varepsilon}_{\mathrm{de}}$ are parts of $\boldsymbol{\varepsilon}_{\mathrm{i}}$ associated to the distortional hardening. More precisely, we postulate

$$\boldsymbol{\varepsilon} = \boldsymbol{\varepsilon}_{\mathrm{e}} + \boldsymbol{\varepsilon}_{\mathrm{i}}, \quad \boldsymbol{\varepsilon}_{\mathrm{i}} = \boldsymbol{\varepsilon}_{\mathrm{ke}} + \boldsymbol{\varepsilon}_{\mathrm{ki}}, \quad \boldsymbol{\varepsilon}_{\mathrm{i}} = \boldsymbol{\varepsilon}_{\mathrm{de}} + \boldsymbol{\varepsilon}_{\mathrm{di}}, \quad s = s_{\mathrm{e}} + s_{\mathrm{d}}. \tag{9.14}$$

Note that the first decomposition is related to (9.7). Moreover, $(9.14)_2$ and $(9.14)_3$ can be motivated by (9.8). The evolution of the state of the material is captured by the inelastic flow $\dot{\boldsymbol{\varepsilon}}_{\mathrm{i}}$ and the inelastic flow $(\dot{\boldsymbol{\varepsilon}}_{\mathrm{ki}}, \dot{\boldsymbol{\varepsilon}}_{\mathrm{di}}, \dot{s}_{\mathrm{d}})$ which takes place on the microstructural level.

---

[7] Mathematically, $\boldsymbol{\sigma}^{\mathrm{D}}$ and $\boldsymbol{\varepsilon}^{\mathrm{D}}$ are elements of a 5-dimensional vector space of trace-free (deviatoric) symmetric second rank tensors.

[8] Using a similar approach, a two-dimensional rheological model was already generalized to cover *finite strain* vsicoplasticity [**52**].

The specific free energy per unit mass is given by

$$\psi = \psi_{\mathrm{el}}(\boldsymbol{\varepsilon}_{\mathrm{e}}) + \psi_{\mathrm{kin}}(\boldsymbol{\varepsilon}_{\mathrm{ke}}) + \psi_{\mathrm{dis}}(\boldsymbol{\varepsilon}_{\mathrm{de}}) + \psi_{\mathrm{iso}}(s_{\mathrm{e}}), \tag{9.15}$$

$$\rho\psi_{\mathrm{el}}(\boldsymbol{\varepsilon}_{\mathrm{e}}) = \frac{k}{2}(\mathrm{tr}\ \boldsymbol{\varepsilon}_{\mathrm{e}})^2 + \mu\ \|\boldsymbol{\varepsilon}^{\mathrm{D}}_{\mathrm{e}}\|^2, \quad \rho\psi_{\mathrm{kin}}(\boldsymbol{\varepsilon}_{\mathrm{ke}}) = \frac{c_{\mathrm{k}}}{2}\ \|\boldsymbol{\varepsilon}^{\mathrm{D}}_{\mathrm{ke}}\|^2, \tag{9.16}$$

$$\rho\psi_{\mathrm{dis}}(\boldsymbol{\varepsilon}_{\mathrm{de}}) = \frac{c_{\mathrm{d}}}{2}\ \|\boldsymbol{\varepsilon}^{\mathrm{D}}_{\mathrm{de}}\|^2, \quad \rho\psi_{\mathrm{iso}}(s_{\mathrm{e}}) = \frac{\gamma}{2}(s_{\mathrm{e}})^2. \tag{9.17}$$

Here, $k, \mu, c_{\mathrm{k}}, c_{\mathrm{d}}, \gamma \geq 0$ are material parameters; $\rho > 0$ stands for the mass density. The quantity $\psi_{\mathrm{el}}(\boldsymbol{\varepsilon}_{\mathrm{e}})$ stands for the energy stored due to macroscopic elastic deformations. The remaining part $\psi_{\mathrm{kin}} + \psi_{\mathrm{dis}} + \psi_{\mathrm{iso}}$ is used to capture the energy associated with the defects of the crystal structure.[9] Next, we postulate the following relations for stresses, backstresses, and isotropic hardening

$$\boldsymbol{\sigma} = \rho\frac{\partial\psi_{\mathrm{el}}(\boldsymbol{\varepsilon}_{\mathrm{e}})}{\partial\boldsymbol{\varepsilon}_{\mathrm{e}}}, \ \boldsymbol{X}_{\mathrm{k}} = \rho\frac{\partial\psi_{\mathrm{kin}}(\boldsymbol{\varepsilon}_{\mathrm{ke}})}{\partial\boldsymbol{\varepsilon}_{\mathrm{ke}}}, \ \boldsymbol{X}_{\mathrm{d}} = \rho\frac{\partial\psi_{\mathrm{dis}}(\boldsymbol{\varepsilon}_{\mathrm{de}})}{\partial\boldsymbol{\varepsilon}_{\mathrm{de}}}, \ R = \rho\frac{\partial\psi_{\mathrm{iso}}(s_{\mathrm{e}})}{\partial s_{\mathrm{e}}}. \tag{9.18}$$

Substituting (9.16) and (9.17) into (9.18) we arrive at

$$\boldsymbol{\sigma} = k\ \mathrm{tr}(\boldsymbol{\varepsilon}_{\mathrm{e}})\mathbf{1} + 2\mu\boldsymbol{\varepsilon}^{\mathrm{D}}_{\mathrm{e}}, \ \boldsymbol{X}_{\mathrm{k}} = c_{\mathrm{k}}\boldsymbol{\varepsilon}^{\mathrm{D}}_{\mathrm{ke}}, \ \boldsymbol{X}_{\mathrm{d}} = c_{\mathrm{d}}\boldsymbol{\varepsilon}^{\mathrm{D}}_{\mathrm{de}}, \ R = \gamma s_{\mathrm{e}}. \tag{9.19}$$

On the one hand, these relations can be motivated by the rheological model from Section 2. On the other hand, as it will be shown in the following, relations (9.18) will be sufficient for the thermodynamic consistency of the material model. It follows immediately from (9.19) that $\mathrm{tr}\boldsymbol{X}_{\mathrm{k}} = \mathrm{tr}\boldsymbol{X}_{\mathrm{d}} = 0$.

Suppose that the degree of distortion α depends solely on $\|\boldsymbol{X}_{\mathrm{d}}\|$. A concrete dependence will be specified in the following (cf. (9.26)). The effective stress tensor and the angle θ are defined now through

$$\boldsymbol{\sigma}_{\mathrm{eff}} := \boldsymbol{\sigma} - \boldsymbol{X}_{\mathrm{k}} - \boldsymbol{X}_{\mathrm{d}}, \quad \theta := \arccos\Big(\frac{\boldsymbol{\sigma}^{\mathrm{D}}_{\mathrm{eff}}\ :\ \boldsymbol{X}_{\mathrm{d}}}{\|\boldsymbol{\sigma}^{\mathrm{D}}_{\mathrm{eff}}\|\ \|\boldsymbol{X}_{\mathrm{d}}\|}\Big). \tag{9.20}$$

Note that for $\|\boldsymbol{X}_{\mathrm{d}}\| = 0$ the angle θ is arbitrary. To be definite, we put $\theta = 0$ in that case. Further, analogously to (9.10) and (9.11), we define $\vec{y} \in \mathbb{R}^2$ and the corresponding overstress f (see Fig. 9.6a)

$$f(\boldsymbol{\sigma}, \boldsymbol{X}_{\mathrm{k}}, \boldsymbol{X}_{\mathrm{d}}, R) = \tilde{f}(\|\boldsymbol{\sigma}^{\mathrm{D}}_{\mathrm{eff}}\|, \theta, \alpha, R) := \sqrt{\frac{2}{3}}(K_0 + R)\ \bar{f}(\vec{y}, \alpha), \tag{9.21}$$

$$\vec{y} := \frac{\|\boldsymbol{\sigma}^{\mathrm{D}}_{\mathrm{eff}}\|}{\sqrt{2/3}(K_0 + R)}(\cos(\theta), \sin(\theta)). \tag{9.22}$$

Here, $K_0 > 0$ is a fixed material parameter (initial yield stress), and the function $\bar{f}(\vec{y}, \alpha)$ is defined through (9.6).

---

[9] Note that $\psi_{\mathrm{kin}} + \psi_{\mathrm{dis}} + \psi_{\mathrm{iso}}$ does not necessarily reflect the entire "defect energy". It is natural to assume that a part of the "defect energy" is not connected to any hardening mechanism (Shutov and Ihlemann, 2011 [**53**]). Alternatively, Henann and Anand (2009) [**26**] prefer to neglect the free energy storage ψ_{iso} which is associated with the isotropic hardening. Interestingly, Feigenbaum and Dafalias (2008) [**17**] suggest that the defect energy is released while the distortion of the yield surface takes place. Thus, again, a somewhat smaller energy storage will be predicted than by assumption (9.15). The choice between many alternatives is important for the prediction of the inelastic dissipation and should be based on relevant experimental observations.

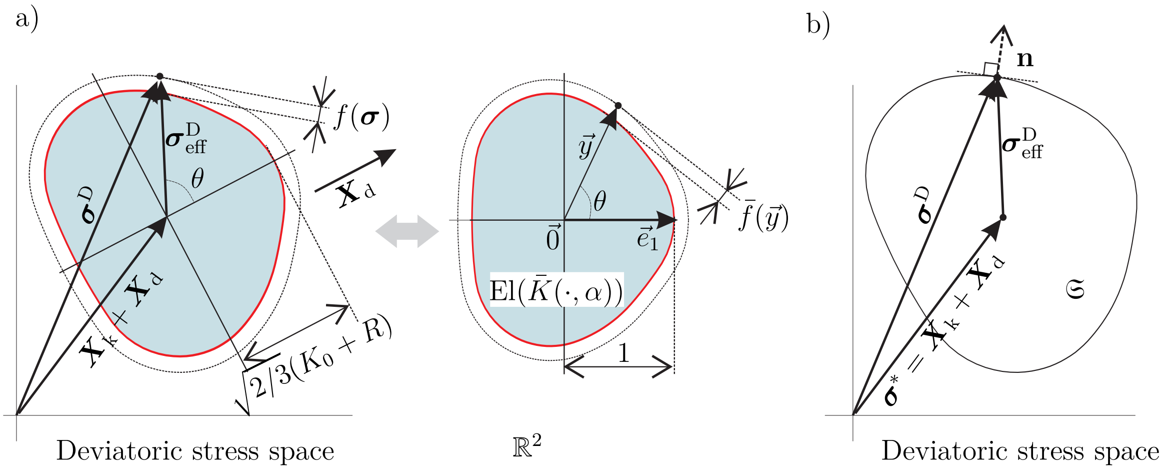

Figure 9.6. a) Sketch of the yield surface in the deviatoric stress space and definition of the overstress $f(\boldsymbol{\sigma})$ (cf. (9.20), (9.21)). The elastic domain in the stress space is associated with $\mathrm{El}(\bar{K}(\cdot, \alpha)) \subset \mathbb{R}^2$; b) Sketch of the proof of the inequality (9.27).

The elastic domain corresponds to stress states with zero overstress f. For a given stress tensor $\boldsymbol{\sigma}$, a non-dimensional vector $\vec{y} \in \mathbb{R}^2$ must be evaluated according to (9.22). Observe that the angle between $\vec{y}$ and $\vec{e}_1$ coincides with the angle between $\boldsymbol{\sigma}^{\rm D}_{\rm eff}$ and $\boldsymbol{X}_{\rm d}$ (see Fig. 9.6a). According to (9.21), the stress state $\boldsymbol{\sigma}$ lies within the elastic domain if and only if $\vec{y} \in \mathrm{El}(\bar{K}(\cdot, \alpha))$. The origin of the elastic domain corresponds to $\{\vec{y} = \vec{0}\}$ or, equivalently, $\{\boldsymbol{\sigma}^{\rm D}_{\rm eff} = \mathbf{0}\} = \{\boldsymbol{\sigma}^{\rm D} = \boldsymbol{X}_{\rm k} + \boldsymbol{X}_{\rm d}\}$. Next, observe that the direction of the elastic domain coincides with the direction of $\boldsymbol{X}_{\rm d}$, and the size of the elastic domain in that direction equals $\sqrt{\frac{2}{3}}(K_0 + R)$ (see Fig. 9.6a).

Remark 7. The relations (9.21) and (9.22) imply that the resistance to plastic deformation depends on the actual direction of the loading relative to the recent loading path. This dependence on the loading direction can be associated with the activation/deactivation of crystallographic slip planes as well as mobilization/demobilization of oriented dislocation structures. It is well known that the gliding of dislocations is obstructed by the cell walls under monotonic loading ($\theta = 0$), but after a strain path change ($\theta \neq 0$), the loading may drive the dislocations toward the cell interior (Viatkina et al., 2007 [**58**]). In the monograph by Viatkina (2005) [**57**], the mechanism of "directional remobilisation" under the strain path change is explained as a remobilisation of dislocation locks and dipoles which were formed during the previous loading, in contrast to the statistical remobilisation which is independent of the strain path change.

The normality flow rule in combination with the Perzyna rule is used

$$\dot{\boldsymbol{\varepsilon}}_{\rm i} = \lambda_{\rm i} \frac{\partial f(\boldsymbol{\sigma}, \boldsymbol{X}_{\rm k}, \boldsymbol{X}_{\rm d}, R)}{\partial \boldsymbol{\sigma}} \text{ for } f > 0, \ \dot{\boldsymbol{\varepsilon}}_{\rm i} = \mathbf{0} \text{ for } f = 0; \quad \lambda_{\rm i} = \frac{1}{\eta}\Big(\frac{1}{k_0} f\Big)^{m}. \tag{9.23}$$

Here, $\lambda_{\rm i} \geq 0$ is an inelastic multiplier which controls the rate of the inelastic flow. Indeed, since $\|\frac{\partial \bar{f}(\vec{y}, \alpha)}{\partial \vec{y}}\| = 1$ for $\bar{f} > 0$, we obtain (cf. (9.44))

$$\Big\|\frac{\partial f(\boldsymbol{\sigma}, \boldsymbol{X}_{\rm k}, \boldsymbol{X}_{\rm d}, R)}{\partial \boldsymbol{\sigma}}\Big\| = 1 \text{ for } f > 0, \quad \|\dot{\boldsymbol{\varepsilon}}_{\rm i}\| = \lambda_{\rm i}, \quad \dot{p} = \lambda_{\rm i}. \tag{9.24}$$

We emphasize that k_0 is not a material parameter, and we put $k_0 = 1$ MPa. A concrete algorithm for the evaluation of the derivative $\frac{\partial f(\boldsymbol{\sigma})}{\partial \boldsymbol{\sigma}}$ is presented in Appendix B. Note that the normality rule (9.23) implies an incompressible flow: $\mathrm{tr}\dot{\boldsymbol{\varepsilon}}_{\mathrm{i}} = 0$. In order to take the saturation of the kinematic and distortional hardening into account, we postulate for the inelastic flows on the microstructural level (cf. (9.12))

$$\dot{\boldsymbol{\varepsilon}}_{\mathrm{ki}} = \lambda_{\mathrm{i}}\, \varkappa_{\mathrm{k}}\, \boldsymbol{X}_{\mathrm{k}}, \quad \dot{\boldsymbol{\varepsilon}}_{\mathrm{di}} = \lambda_{\mathrm{i}}\, \varkappa_{\mathrm{d}}\, \boldsymbol{X}_{\mathrm{d}}. \tag{9.25}$$

Here, $\varkappa_{\mathrm{k}}, \varkappa_{\mathrm{d}} \geq 0$ are material parameters. Recall that $\mathrm{tr}\boldsymbol{X}_{\mathrm{k}} = \mathrm{tr}\boldsymbol{X}_{\mathrm{d}} = 0$. Thus, the inelastic flow on the microstructural level is incompressible as well: $\mathrm{tr}\dot{\boldsymbol{\varepsilon}}_{\mathrm{ki}} = \mathrm{tr}\dot{\boldsymbol{\varepsilon}}_{\mathrm{di}} = 0$. It can be easily shown that for $\|\boldsymbol{X}_{\mathrm{d}}\||_{t=0} \leq 1/\varkappa_{\mathrm{d}}$ we have $\|\boldsymbol{X}_{\mathrm{d}}\| \leq 1/\varkappa_{\mathrm{d}}$. Thus, analogously to (9.13), we define the distortion parameter $\alpha \in [0,1]$ by

$$\alpha := \varkappa_{\mathrm{d}}\, \|\boldsymbol{X}_{\mathrm{d}}\|. \tag{9.26}$$

For a given deviatoric stress $\boldsymbol{\sigma}^{\mathrm{D}}$ consider a convex set $\mathfrak{S} = \{\boldsymbol{\sigma}^* : \ \mathrm{tr}\boldsymbol{\sigma}^* = 0, \ \ f(\boldsymbol{\sigma}^*) \leq f(\boldsymbol{\sigma}^{\mathrm{D}})\}$. The gradient $\frac{\partial f(\boldsymbol{\sigma}, \boldsymbol{X}_{\mathrm{k}}, \boldsymbol{X}_{\mathrm{d}}, R)}{\partial \boldsymbol{\sigma}}$ coincides with the unit outward normal $\mathbf{n}$ to the boundary of $\mathfrak{S}$ at $\boldsymbol{\sigma}^{\mathrm{D}}$. Moreover, the stress state $\boldsymbol{\sigma}^* = \boldsymbol{X}_{\mathrm{k}} + \boldsymbol{X}_{\mathrm{d}}$ lies within $\mathfrak{S}$ (cf. Fig. 9.6b). Due to the convexity of $\mathfrak{S}$ we have

$$\boldsymbol{\sigma}^{\mathrm{D}}_{\mathrm{eff}} : \dot{\boldsymbol{\varepsilon}}_{\mathrm{i}} \overset{(9.23)}{=} \lambda_{\mathrm{i}}(\boldsymbol{\sigma}^{\mathrm{D}} - \boldsymbol{\sigma}^*) : \mathbf{n} \geq 0. \tag{9.27}$$

Having this inequality in mind we formulate the evolution equations for the internal variable s and its dissipative part s_{d}:

$$\dot{s} = \frac{\boldsymbol{\sigma}_{\mathrm{eff}} : \dot{\boldsymbol{\varepsilon}}_{\mathrm{i}}}{K_0 + R} \overset{\mathrm{tr}\dot{\boldsymbol{\varepsilon}}_{\mathrm{i}}=0}{=} \frac{\boldsymbol{\sigma}^{\mathrm{D}}_{\mathrm{eff}} : \dot{\boldsymbol{\varepsilon}}_{\mathrm{i}}}{K_0 + R}, \qquad \dot{s}_{\mathrm{d}} = \frac{\beta}{\gamma} \dot{s} R, \tag{9.28}$$

where $\beta \geq 0$ is a material parameter controlling the saturation of the isotropic hardening. It follows from (9.27) that $\dot{s} \geq 0$. Thus, similar to the inelastic arc-length, the variable s increases monotonically. Note that in the case of proportional monotonic loading we have $\theta \approx 0$. Thus, $\boldsymbol{\sigma}^{\mathrm{D}}_{\mathrm{eff}} : \dot{\boldsymbol{\varepsilon}}_{\mathrm{i}} \approx \|\boldsymbol{\sigma}^{\mathrm{D}}_{\mathrm{eff}}\|\, \|\dot{\boldsymbol{\varepsilon}}_{\mathrm{i}}\| = \|\boldsymbol{\sigma}^{\mathrm{D}}_{\mathrm{eff}}\|\, \lambda_{\mathrm{i}}$. Moreover, for slow loading we obtain $f \ll (K_0 + R)$. Therefore, $\|\boldsymbol{\sigma}^{\mathrm{D}}_{\mathrm{eff}}\| \approx \sqrt{2/3}\,(K_0 + R)$. Thus, under quasistatic proportional loading, the parameter s evolves similar to the inelastic arc-length: $\dot{s} \approx \sqrt{2/3}\, \|\dot{\boldsymbol{\varepsilon}}_{\mathrm{i}}\| = \sqrt{2/3}\lambda_{\mathrm{i}}$. Under general loading conditions, although, the evolution of s depends not only on the rate of the plastic flow, but also on its direction.

Finally, the system of constitutive equations is closed by initial conditions imposed on the strain-like internal variables

$$\boldsymbol{\varepsilon}_{\mathrm{i}}|_{t=0} = \boldsymbol{\varepsilon}^0_{\mathrm{i}}, \ \boldsymbol{\varepsilon}_{\mathrm{ki}}|_{t=0} = \boldsymbol{\varepsilon}^0_{\mathrm{ki}}, \ \boldsymbol{\varepsilon}_{\mathrm{di}}|_{t=0} = \boldsymbol{\varepsilon}^0_{\mathrm{di}}, \ s|_{t=0} = s^0, \ s_{\mathrm{d}}|_{t=0} = s^0_{\mathrm{d}}.$$

We suppose $\mathrm{tr}\boldsymbol{\varepsilon}^0_{\mathrm{i}} = \mathrm{tr}\boldsymbol{\varepsilon}^0_{\mathrm{ki}} = \mathrm{tr}\boldsymbol{\varepsilon}^0_{\mathrm{di}} = 0$. If the undeformed state is assumed to be stress free at $t = 0$, then $\boldsymbol{\varepsilon}^0_{\mathrm{i}} = \mathbf{0}$. The quantities $\boldsymbol{\varepsilon}^0_{\mathrm{ki}}$ and $\boldsymbol{\varepsilon}^0_{\mathrm{di}}$ can be used to capture the initial plastic anisotropy of the material.[10] In particular, the yield condition at $t = 0$ does not have to coincide with the Huber-Mises criterium.

---

[10] This is equivalent to the introduction of initial backstresses.

3.2. Proof of thermodynamic consistency. Let us consider the Clausius-Duhem inequality in the form (see, for example, [**22**])

$$\delta_{\mathrm{i}} := \frac{1}{\rho}\boldsymbol{\sigma} : \dot{\boldsymbol{\varepsilon}} - \dot{\psi} \geq 0. \tag{9.29}$$

Taking the kinematic relations (9.14) into account, we rewrite the stress power as follows

$$\boldsymbol{\sigma} : \dot{\boldsymbol{\varepsilon}} = \boldsymbol{\sigma} : (\dot{\boldsymbol{\varepsilon}}_{\mathrm{e}} + \dot{\boldsymbol{\varepsilon}}_{\mathrm{i}}) - \boldsymbol{X}_{\mathrm{k}} : \dot{\boldsymbol{\varepsilon}}_{\mathrm{i}} + \boldsymbol{X}_{\mathrm{k}} : (\dot{\boldsymbol{\varepsilon}}_{\mathrm{ki}} + \dot{\boldsymbol{\varepsilon}}_{\mathrm{ke}}) - \boldsymbol{X}_{\mathrm{d}} : \dot{\boldsymbol{\varepsilon}}_{\mathrm{i}} + \boldsymbol{X}_{\mathrm{d}} : (\dot{\boldsymbol{\varepsilon}}_{\mathrm{di}} + \dot{\boldsymbol{\varepsilon}}_{\mathrm{de}}). \tag{9.30}$$

Moreover, differentiating (9.15), we obtain the time derivative of the free energy

$$\dot{\psi} = \frac{\partial\psi_{\mathrm{el}}(\boldsymbol{\varepsilon}_{\mathrm{e}})}{\partial\boldsymbol{\varepsilon}_{\mathrm{e}}} : \dot{\boldsymbol{\varepsilon}}_{\mathrm{e}} + \frac{\partial\psi_{\mathrm{kin}}(\boldsymbol{\varepsilon}_{\mathrm{ke}})}{\partial\boldsymbol{\varepsilon}_{\mathrm{ke}}} : \dot{\boldsymbol{\varepsilon}}_{\mathrm{ke}} + \frac{\partial\psi_{\mathrm{dis}}(\boldsymbol{\varepsilon}_{\mathrm{de}})}{\partial\boldsymbol{\varepsilon}_{\mathrm{de}}} : \dot{\boldsymbol{\varepsilon}}_{\mathrm{de}} + \frac{\partial\psi_{\mathrm{iso}}(s_{\mathrm{e}})}{\partial s_{\mathrm{e}}}\dot{s}_{\mathrm{e}}. \tag{9.31}$$

Substituting (9.30) and (9.31) into (9.29) and taking the potential relations (9.18) into account, we obtain the Clausius-Duhem inequality in the following form

$$\rho\,\delta_{\mathrm{i}} = \Big(\boldsymbol{\sigma}_{\mathrm{eff}} : \dot{\boldsymbol{\varepsilon}}_{\mathrm{i}} - R\,\dot{s}\Big) + \boldsymbol{X}_{\mathrm{k}} : \dot{\boldsymbol{\varepsilon}}_{\mathrm{ki}} + \boldsymbol{X}_{\mathrm{d}} : \dot{\boldsymbol{\varepsilon}}_{\mathrm{di}} + R\dot{s}_{\mathrm{d}} \geq 0.$$

It follows immediately from (9.25) and $(9.28)_2$ that $\boldsymbol{X}_{\mathrm{k}} : \dot{\boldsymbol{\varepsilon}}_{\mathrm{ki}} \geq 0$, $\boldsymbol{X}_{\mathrm{d}} : \dot{\boldsymbol{\varepsilon}}_{\mathrm{di}} \geq 0$, and $R\dot{s}_{\mathrm{d}} \geq 0$. In order to prove the thermodynamic consistency of the material model it remains to show that $\boldsymbol{\sigma}_{\mathrm{eff}} : \dot{\boldsymbol{\varepsilon}}_{\mathrm{i}} - R\,\dot{s} \geq 0$. Indeed,

$$\boldsymbol{\sigma}_{\mathrm{eff}} : \dot{\boldsymbol{\varepsilon}}_{\mathrm{i}} - R\,\dot{s} \overset{(9.28)_1}{=} \boldsymbol{\sigma}^{\mathrm{D}}_{\mathrm{eff}} : \dot{\boldsymbol{\varepsilon}}_{\mathrm{i}}\ (1 - R/(K_0 + R)) = \boldsymbol{\sigma}^{\mathrm{D}}_{\mathrm{eff}} : \dot{\boldsymbol{\varepsilon}}_{\mathrm{i}}\ (K_0/(K_0 + R)) \overset{(9.27)}{\geq} 0.$$

The thermodynamic consistency of the material model is thus proved.

Remark 8. Note that the proof of the thermodynamic consistency is essentially based on the inequality $\boldsymbol{\sigma}^{\mathrm{D}}_{\mathrm{eff}} : \dot{\boldsymbol{\varepsilon}}_{\mathrm{i}} \geq 0$. *Any flow rule* which governs $\dot{\boldsymbol{\varepsilon}}_{\mathrm{i}}$ and complies with this inequality would yield a thermodynamically consistent material model, as well. For instance, the radial flow rule can be considered as a simplified alternative to the normality rule $(9.23)_1$

$$\dot{\boldsymbol{\varepsilon}}_{\mathrm{i}} = \lambda_{\mathrm{i}}\boldsymbol{R}_{\mathrm{eff}}, \quad \boldsymbol{R}_{\mathrm{eff}} := \frac{\boldsymbol{\sigma}^{\mathrm{D}}_{\mathrm{eff}}}{\|\boldsymbol{\sigma}^{\mathrm{D}}_{\mathrm{eff}}\|}. \tag{9.32}$$

3.3. Identification of material parameters. The material model contains 11 material parameters and a material function $\bar{K}^{\mathrm{sat}}(\theta)$. Let us discuss the identification of these quantities. First, the elasticity parameters k and μ can be determined basing on the experimental data for elastic deformations. Next, the initial yield stress K_0 can be calibrated using the graphical method from a quasistatic uniaxial tension test. The viscosity parameters η and m of the Perzyna law are typically identified using a series of tests under monotonic loading with different loading rates. Further, the material function $\bar{K}^{\mathrm{sat}}(\theta)$ is uniquely determined for the fixed $\bar{K}^{\mathrm{sat}}(\pi)$ if the form of the saturated yield surface is known (for details see Remark 6). For simplicity, one may assume $\bar{K}^{\mathrm{sat}}(\pi) = 1$. In that case, the parameters of isotropic hardening (γ and β) can be identified using the information about how the size of the elastic domain evolves under monotonic loading. Finally, it remains to identify two parameters of kinematic hardening (c_{k} and $\varkappa_{\mathrm{k}}$) and two distortional parameters (c_{d} and $\varkappa_{\mathrm{d}}$). This can be done by minimization of a least-squares functional which represents the discrepancy between measurements data and corresponding model predictions. Experimental measurements related to non-proportional loading are necessary in order to obtain a reliable identification procedure. Some regularization techniques can be used to reduce the correlation among the parameters and to reduce the probability of getting trapped in local minima (Shutov and Kreißig, 2010 [**51**]).

The success of the identification procedure depends on the quality of initial approximation chosen for the unknown parameters c_{k}, c_{d}, $\varkappa_{\mathrm{k}}$, and $\varkappa_{\mathrm{d}}$. The order of magnitude of these parameters can be estimated basing on the following considerations: The upper bounds for $\|\boldsymbol{X}_{\mathrm{k}}\|$ and $\|\boldsymbol{X}_{\mathrm{d}}\|$ are given by $\varkappa_{\mathrm{k}}^{-1}$ and $\varkappa_{\mathrm{d}}^{-1}$, respectively. At the same time, the increment of the inelastic arc-length which corresponds to the saturation of kinematic and distortional hardening under proportional loading is proportional to $(c_{\mathrm{k}}\varkappa_{\mathrm{k}})^{-1}$ and $(c_{\mathrm{d}}\varkappa_{\mathrm{d}})^{-1}$, respectively.

4. Numerical computations

In this study, for simplicity, the evolution equations (9.23), (9.25), and (9.28) are integrated numerically using the explicit Euler forward algorithm. If rate-independent material response is to be simulated, a viscous regularization with fictitious small viscosity $\eta > 0$ can be used.[11]

In this section we illustrate the predictive capabilities of the material model. Toward that end, we consider experimental data of Khan et al. (2010) [**30**] obtained for a very high work hardening aluminum alloy - annealed 1100 Al. The yield points were identified experimentally under combined tension-torsion of thin-walled tubular specimens using a small proof strain. In order to simulate the deformation of a thin-walled tubular specimen we compute the stress response at a single material point.[12] Consider a Cartesian coordinate system such that its basis vectors $\mathbf{e}_1$, $\mathbf{e}_2$, and $\mathbf{e}_3$ are oriented along the local axial, hoop, and radial directions, respectively. The strain tensor is then given by

$$\boldsymbol{\varepsilon} = \varepsilon_{11}\mathbf{e}_1 \otimes \mathbf{e}_1 + \varepsilon_{12}(\mathbf{e}_1 \otimes \mathbf{e}_2 + \mathbf{e}_2 \otimes \mathbf{e}_1) + \varepsilon_{22}\mathbf{e}_2 \otimes \mathbf{e}_2 + \varepsilon_{33}\mathbf{e}_3 \otimes \mathbf{e}_3. \tag{9.33}$$

Here, ε_{11} and ε_{12} stand for the prescribed axial and shear strain, respectively. For the uniaxial prestrain we put in this section $\dot{\varepsilon}_{11} = 0.01/\mathrm{s}$, $\varepsilon_{12} = 0$. Thus, a total loading time of 2s will be required to achieve 2% axial strain. This loading process is discretized using 800 equal time steps. The unknown strains ε_{22} and ε_{33} are determined numerically at each time step using the condition that the radial and hoop stresses are zero. The stress state can be idealized approximately as a special case of the plane stress:

$$\boldsymbol{\sigma} = \sigma_{11}\mathbf{e}_1 \otimes \mathbf{e}_1 + \sigma_{12}(\mathbf{e}_1 \otimes \mathbf{e}_2 + \mathbf{e}_2 \otimes \mathbf{e}_1). \tag{9.34}$$

Here, σ_{11} and σ_{12} are associated to the axial and torsional loading, respectively. The measurement results are represented in the $(\sigma_{11}, \sqrt{3}\sigma_{12})$-space in Fig. 9.7a. The initial yield surface can be approximated with sufficient accuracy using the conventional Huber-Mises yield condition. Therefore, an initial plastic isotropy will be assumed during the material modeling. The yield points which were determined after 2% axial prestrain are depicted in Fig. 9.7a, as well. The material parameters used to simulate the material response are

---

[11] Note that such viscous regularization allows to smoothen the sharp transition between elastic and plastic regions.

[12] In the current study we benefit from the fact that the stress-strain state in a thin-walled tubular specimens can be characterized by the consideration of a single material point. Under such assumption, no FEM simulations are needed.

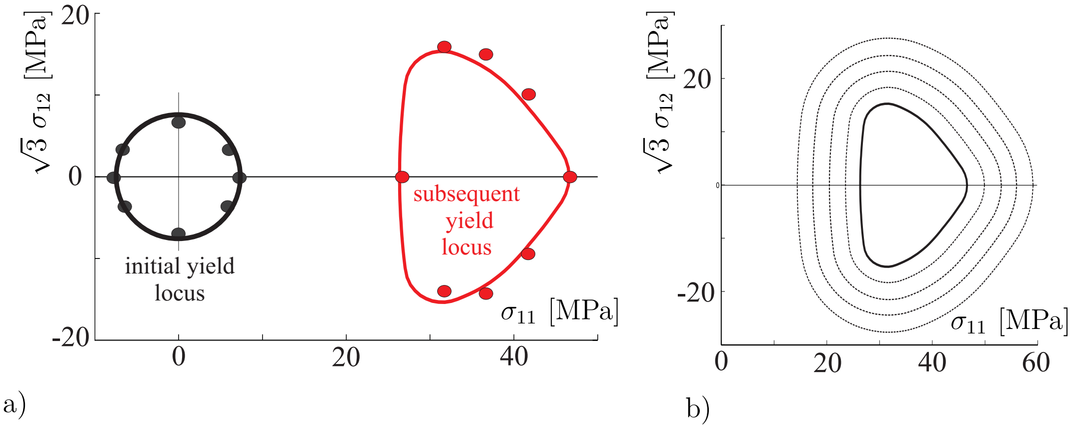

Figure 9.7. a) Experimental data for annealed 1100 aluminum alloy (Khan et al., 2010 [**30**]) and corresponding simulation results, b) Lines of constant overstress f corresponding to plastic anisotropy induced by 2% prestrain in the axial direction.

Table 9.1. Material parameters used for numerical computations: a small fictitious viscosity is used.

k [MPa]	μ [MPa]	c_{k} [MPa]	c_{d} [MPa]	γ [MPa]
69000	26000	1010	5000	245

K_0 [MPa]	m [-]	η [s]	$\varkappa_{\mathrm{k}}$ [MPa^{-1}]	$\varkappa_{\mathrm{d}}$ [MPa^{-1}]	β [-]
7.4	1	150	0.02	0.1	35

summarized in Table 9.1.[13] Moreover, due to the initial isotropy we consider the initial conditions as follows:

$$\boldsymbol{\varepsilon}_{\mathrm{i}}^0 = \boldsymbol{\varepsilon}_{\mathrm{di}}^0 = \boldsymbol{\varepsilon}_{\mathrm{ki}}^0 = \mathbf{0}, \quad s^0 = s_{\mathrm{d}}^0 = 0.$$

The smooth function $\bar{K}^{\mathrm{sat}}(\theta)$ which is needed to compute the overstress $\bar{f}(\vec{y})$ corresponds to the saturated form shown in Fig. 9.3c. Due to the axial prestrain, the distortion parameter α ranges from 0 up to 0.999993, which corresponds to the (almost) saturated distortional hardening. As it is shown in Fig. 9.7a, the yield locus undergoes the isotropic expansion, kinematic translation and distortion. The surfaces of constant overstress are depicted in Fig. 9.7b. In accordance with the modeling assumptions, these surfaces are slightly less distorted than the corresponding yield surface.

Remark 9. Note that the form of the yield surface in the $(\sigma_{11}, \sqrt{3}\sigma_{12})$-space coincides with the boundary of $\mathrm{El}(\bar{K}(\cdot, \alpha))$. This is due to the well-known fact that the scalar product of two symmetric tensors $\boldsymbol{\sigma}_I^{\mathrm{D}}$ and $\boldsymbol{\sigma}_{II}^{\mathrm{D}}$ (where $\boldsymbol{\sigma}_I$ and $\boldsymbol{\sigma}_{II}$ comply with (9.34)) corresponds to the product of two vectors $\vec{\sigma}_I, \vec{\sigma}_{II} \in \mathbb{R}^2$, defined by $\vec{\sigma}_I := (\sigma_{11}^I, \sqrt{3}\sigma_{12}^I)$, $\vec{\sigma}_{II} := (\sigma_{11}^{II}, \sqrt{3}\sigma_{12}^{II})$.

---

[13] It is not the aim of the current study to identify the material parameters corresponding to the 1100 aluminum alloy. Instead, we explain the material model by the qualitative description of some real experimental data. Observe that fitting only one distorted yield surface, as it is shown in 9.7a, is a rather trivial task.

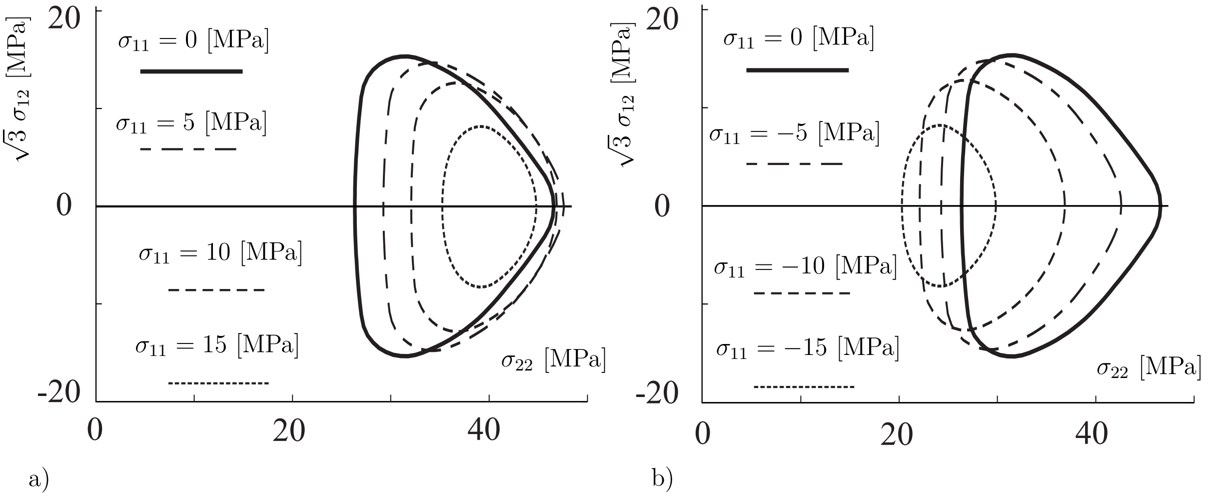

Figure 9.8. Influence of the axial stress σ_{11} on the form of the yield surface after 2% prestrain in the hoop direction: a) Positive axial stresses; b) Negative axial stresses.

More precisely

$$\boldsymbol{\sigma}^{\mathrm{D}}_{I} : \boldsymbol{\sigma}^{\mathrm{D}}_{II} = \frac{2}{3}(\sigma^{I}_{11}\sigma^{II}_{11} + 3\sigma^{I}_{12}\sigma^{II}_{12}) = \frac{2}{3}\vec{\sigma}_{I} \cdot \vec{\sigma}_{II}.$$

Therefore, in the context of (9.34), the angle between two deviatoric stress-states coincides with the angle between two corresponding vectors in the $(\sigma_{11},\ \sqrt{3}\sigma_{12})$-space:

$$\arccos\Big(\frac{\boldsymbol{\sigma}^{\mathrm{D}}_{I} : \boldsymbol{\sigma}^{\mathrm{D}}_{II}}{\|\boldsymbol{\sigma}^{\mathrm{D}}_{I}\|\ \|\boldsymbol{\sigma}^{\mathrm{D}}_{II}\|}\Big) = \arccos\Big(\frac{\vec{\sigma}_{I} \cdot \vec{\sigma}_{II}}{\|\vec{\sigma}_{I}\|\ \|\vec{\sigma}_{II}\|}\Big).$$

Thus, if the form of the saturated yield surface is determined experimentally in the $(\sigma_{11},\ \sqrt{3}\sigma_{12})$-space, it can be used to identify the smooth function $\bar{K}^{\mathrm{sat}}(\theta)$.

If, additionally, the specimen can be loaded by an internal pressure, the hoop stress σ_{22} must be considered, as well:

$$\boldsymbol{\sigma} = \sigma_{11}\mathbf{e}_1 \otimes \mathbf{e}_1 + \sigma_{22}\mathbf{e}_2 \otimes \mathbf{e}_2 + \sigma_{12}(\mathbf{e}_1 \otimes \mathbf{e}_2 + \mathbf{e}_2 \otimes \mathbf{e}_1),\ \ \sigma_{22} \geq 0.$$

We simulate the evolution of the yield surface in the process as follows. Starting from the same isotropic initial state, a 2% prestrain is prescribed in the hoop direction. Thus, a similar plastic anisotropy is introduced, as in the previous case. The form of the yield surface for a fixed axial stress σ_{11} is then represented in the $(\sigma_{22},\ \sqrt{3}\sigma_{12})$-space. As it can be seen in Fig. 9.8, the form and the size of the yield loci for $\sigma_{11} = 5$ MPa, $\sigma_{11} = 10$ MPa, and $\sigma_{11} = 15$ MPa are the same as for $\sigma_{11} = -5$ MPa, $\sigma_{11} = -10$ MPa, and $\sigma_{11} = -15$ MPa, respectively. Similar to the conventional Huber-Mises yield condition, the material yields at larger σ_{22} stresses for positive σ_{11} than for negative σ_{11}.

5. Conclusion

A new material model of metal viscoplasticity with an extremely simple structure is presented in the current study. The main modeling assumptions are visualized with the help of a new two-dimensional rheological model. Only second-rank backstress-like tensors are used to capture the path dependent evolution of the plastic anisotropy. Thus, mathematically, the model is not much more complicated than the classical model of Chaboche and Rousselier (1983) [**6, 7**]. At the same time, the proposed technique possess considerable generality and flexibility. No specific form of the saturated yield locus is considered, since *any* smooth convex yield locus can be captured.

An important ingredient of the material modeling is the interpolation between the initial intact yield surface and the saturated one. The interpolation rule proposed in the current study *ensures the convexity* of the yield surface at any stage of hardening. It is shown that this interpolation rule allows to obtain a thermodynamically consistent material model.

The model contains 6 hardening parameters with 2 parameters per hardening type. These parameters posses a clear mechanical interpretation and can be identified experimentally.

According to the modeling assumptions, the form of the saturated yield surface is the same for all directions of monotonic preloading. But, for some materials, there are experimental indications that the yield surface may exhibit a higher curvature under combined tension-torsion than under pure tension (see, for instance, Khan et al. (2010) [**30, 31**]). Moreover, a complex form of the yield surface can be observed after complete unloading. Such effects are still to be incorporated into material modeling in future work.

Acknowledgement
This research was supported by German Research Foundation (DFG) within SFB 692.

Appendix A

Let us discuss the numerical computation of $\mathcal{D}\Big(\vec{y}, \alpha \mathrm{El}^{\mathrm{sat}}\Big)$. Suppose that the upper half of the boundary of $\mathrm{El}^{\mathrm{sat}}$ is given by N circular arcs connecting $\vec{y}^{\ i-1}$ and $\vec{y}^{\ i}$ for $i \in \{1, ..., N\}$ as shown in Fig. 9.9a. The outward normal and the tangent at $\vec{y}^{\ i}$ will be denoted by $\vec{n}^{\ i}$ and $\vec{t}^{\ i}$, respectively. The orientation of the tangent is chosen in such way that the pair $\{\vec{n}^{\ i}, \vec{t}^{\ i}\}$ forms a right-handed corner. In particular, we have

$$\vec{y}^{\ 0} = (1, 0), \quad \vec{t}^{\ 0} = (0, 1), \quad \vec{t}^{\ N} = (0, -1).$$

For each arc connecting $\vec{y}^{\ i-1}$ and $\vec{y}^{\ i}$ consider its center $\vec{y_c}^{\ i}$ and its radius r^i. In order to make sure that the boundary of $\mathrm{El}^{\mathrm{sat}}$ is smooth, we require

$$\frac{\vec{y}^{\ 0} - \vec{y_c}^{\ 1}}{r^1} = \vec{n}^{\ 0}, \quad \frac{\vec{y}^{\ N} - \vec{y_c}^{\ N}}{r^N} = \vec{n}^{\ N};$$

$$\frac{\vec{y}^{\ i} - \vec{y_c}^{\ i}}{r^i} = \frac{\vec{y}^{\ i} - \vec{y_c}^{\ i+1}}{r^{i+1}} = \vec{n}^{\ i} \text{ for all } i \in \{1, ..., N-1\}.$$

Let $\alpha \in [0, 1]$ and $\vec{y} = \|\vec{y}\|(\cos(\theta), \sin(\theta))$ be given such that $\theta \in [0, \pi]$. The algorithm used to compute the distance $\mathcal{D}\Big(\vec{y}, \alpha \mathrm{El}^{\mathrm{sat}}\Big)$ is as follows.

- Check the inclusion: If $\|\vec{y}\| \leq \alpha \bar{K}^{\mathrm{sat}}(\theta)$ then $\mathcal{D}\Big(\vec{y}, \alpha \mathrm{El}^{\mathrm{sat}}\Big) = 0$.
- Otherwise, find the corresponding arc: Find $i \in \{1, ..., N\}$ such that (cf. Fig. 9.9b)

$$(\vec{y} - \alpha \vec{y}^{\ i-1}) \cdot \vec{t}^{\ i-1} \geq 0, \quad (\vec{y} - \alpha \vec{y}^{\ i}) \cdot (-\vec{t}^{\ i}) \geq 0, \tag{9.35}$$

$$(\vec{y} - \alpha \vec{y}^{\ i-1}) \cdot \mathbf{Q}(\vec{y}^{\ i} - \vec{y}^{\ i-1}) \geq 0, \quad \mathbf{Q}(\vec{y}) := (y_2, -y_1). \tag{9.36}$$

Here, $\mathbf{Q}(\cdot)$ is the 90° clockwise rotation.

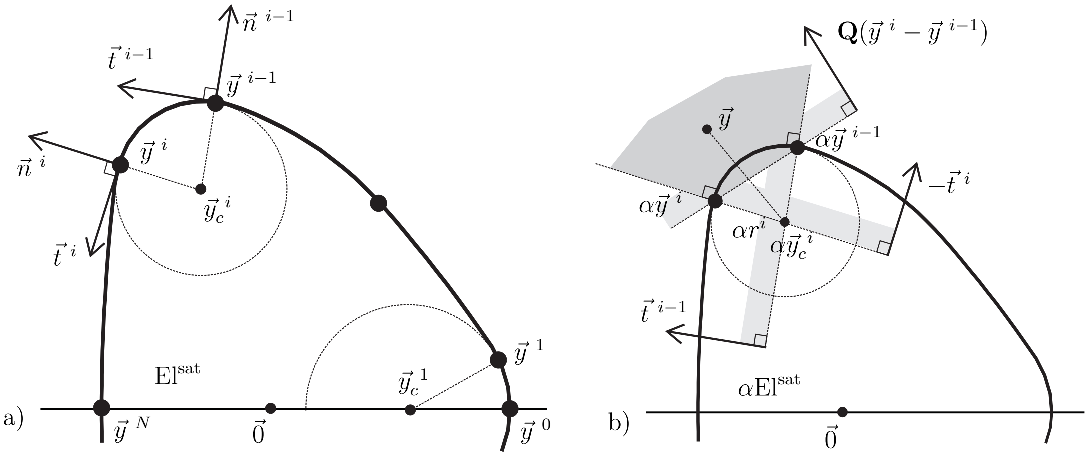

Figure 9.9. a) A smooth boundary of $\mathrm{El}^{\mathrm{sat}}$ is represented by a sequence of circular arcs. Each circle is characterized by its center $\vec{y}_c^{\,i}$ and radius r^i; b) For a given $\vec{y}$, the inequalities (9.35), (9.36) are satisfied within the shaded region. For the suitable i, the distance to $\alpha\mathrm{El}^{\mathrm{sat}}$ is computed as $\mathcal{D}\Big(\vec{y}, \alpha\mathrm{El}^{\mathrm{sat}}\Big) = \|\vec{y}-\alpha\vec{y}_c^{\,i}\| - \alpha r^i$.

- The distance is then given by

$$\mathcal{D}\Big(\vec{y}, \alpha\mathrm{El}^{\mathrm{sat}}\Big) = \|\vec{y}-\alpha\vec{y}_c^{\,i}\| - \alpha r^i.$$

Moreover, the outward unit normal is given by

$$\vec{n} = \frac{\partial \bar{f}\Big(\vec{y}, \alpha\Big)}{\partial \vec{y}} = \frac{\partial \mathcal{D}\Big(\vec{y}, \alpha\mathrm{El}^{\mathrm{sat}}\Big)}{\partial \vec{y}} = \frac{\vec{y}-\alpha\vec{y}_c^{\,i}}{\|\vec{y}-\alpha\vec{y}_c^{\,i}\|}. \tag{9.37}$$

Appendix B

Let us discuss the computation of the derivative $\frac{\partial f(\boldsymbol{\sigma})}{\partial \boldsymbol{\sigma}}$, which enters the formulation of the normality rule (9.23). Suppose $f > 0$. Thus, $\boldsymbol{\sigma}^{\mathrm{D}}_{\mathrm{eff}} \neq \mathbf{0}$ and the radial direction $\boldsymbol{R}_{\mathrm{eff}} := \boldsymbol{\sigma}^{\mathrm{D}}_{\mathrm{eff}}/\|\boldsymbol{\sigma}^{\mathrm{D}}_{\mathrm{eff}}\|$ is well defined. Recall that the hardening variables $\boldsymbol{X}_{\mathrm{k}}$, $\boldsymbol{X}_{\mathrm{d}}$, and R are to be held constant during differentiation. Having this in mind, we arrive at

$$\frac{\partial \|\boldsymbol{\sigma}^{\mathrm{D}}_{\mathrm{eff}}\|}{\partial \boldsymbol{\sigma}} = \frac{\boldsymbol{\sigma}^{\mathrm{D}}_{\mathrm{eff}}}{\|\boldsymbol{\sigma}^{\mathrm{D}}_{\mathrm{eff}}\|} = \boldsymbol{R}_{\mathrm{eff}}. \tag{9.38}$$

Next, taking into account that $\frac{d \ \arccos(\Phi)}{d\Phi} = -(\sin(\arccos(\Phi)))^{-1}$, we obtain for $\theta \neq 0$

$$\frac{\partial \theta}{\partial \boldsymbol{\sigma}} = \frac{\partial \ \arccos\Big(\frac{\boldsymbol{\sigma}^{\mathrm{D}}_{\mathrm{eff}} \,:\, \boldsymbol{X}_{\mathrm{d}}}{\|\boldsymbol{\sigma}^{\mathrm{D}}_{\mathrm{eff}}\| \ \|\boldsymbol{X}_{\mathrm{d}}\|}\Big)}{\partial \boldsymbol{\sigma}} = -\frac{1}{\sin\theta} \frac{\partial \Big(\frac{\boldsymbol{\sigma}^{\mathrm{D}}_{\mathrm{eff}} \,:\, \boldsymbol{X}_{\mathrm{d}}}{\|\boldsymbol{\sigma}^{\mathrm{D}}_{\mathrm{eff}}\| \ \|\boldsymbol{X}_{\mathrm{d}}\|}\Big)}{\partial \boldsymbol{\sigma}}. \tag{9.39}$$

Moreover, since $\theta \in [0, \pi]$ is the angle between $\boldsymbol{X}_{\mathrm{d}}$ and $\boldsymbol{R}_{\mathrm{eff}}$, we have

$$\sin\theta = \frac{\|\boldsymbol{X}_{\mathrm{d}} - (\boldsymbol{X}_{\mathrm{d}} : \boldsymbol{R}_{\mathrm{eff}})\boldsymbol{R}_{\mathrm{eff}}\|}{\|\boldsymbol{X}_{\mathrm{d}}\|}.$$

Substituting this result into (9.39) and taking into account that $\frac{\partial(\boldsymbol{\sigma}^{\mathrm{D}}_{\mathrm{eff}} : \boldsymbol{X}_{\mathrm{d}})}{\partial \boldsymbol{\sigma}} = \boldsymbol{X}_{\mathrm{d}}$ we obtain for $\theta \neq 0$

$$\frac{\partial \theta}{\partial \boldsymbol{\sigma}} = -\frac{1}{\|\boldsymbol{\sigma}^{\mathrm{D}}_{\mathrm{eff}}\|} \frac{\boldsymbol{X}_{\mathrm{d}} - (\boldsymbol{X}_{\mathrm{d}} : \boldsymbol{R}_{\mathrm{eff}})\boldsymbol{R}_{\mathrm{eff}}}{\|\boldsymbol{X}_{\mathrm{d}} - (\boldsymbol{X}_{\mathrm{d}} : \boldsymbol{R}_{\mathrm{eff}})\boldsymbol{R}_{\mathrm{eff}}\|}. \tag{9.40}$$

Further, differentiating (9.21) we arrive at

$$\frac{\partial f(\boldsymbol{\sigma}, \boldsymbol{X}_{\mathrm{k}}, \boldsymbol{X}_{\mathrm{d}}, R)}{\partial \boldsymbol{\sigma}} = \sqrt{\frac{2}{3}}(K_0 + R) \frac{\partial \bar{f}\Big(\vec{y}(\|\boldsymbol{\sigma}^{\mathrm{D}}_{\mathrm{eff}}\|, \theta), \alpha\Big)}{\partial \boldsymbol{\sigma}}, \tag{9.41}$$

where

$$\vec{y}(\|\boldsymbol{\sigma}^{\mathrm{D}}_{\mathrm{eff}}\|, \theta) = \frac{\sqrt{3/2}\ \|\boldsymbol{\sigma}^{\mathrm{D}}_{\mathrm{eff}}\|}{K_0 + R}(\cos(\theta), \sin(\theta)). \tag{9.42}$$

It follows from (9.42) that

$$\frac{\partial \vec{y}}{\partial \|\boldsymbol{\sigma}^{\mathrm{D}}_{\mathrm{eff}}\|} = \frac{\sqrt{3/2}}{K_0 + R}(\cos(\theta), \sin(\theta)), \ \frac{\partial \vec{y}}{\partial \theta} = \frac{\sqrt{3/2}\ \|\boldsymbol{\sigma}^{\mathrm{D}}_{\mathrm{eff}}\|}{K_0 + R}(-\sin(\theta), \cos(\theta)). \tag{9.43}$$

Next, note that the degree of distortion α is to be held constant as well, since it is a unique function of $\boldsymbol{X}_{\mathrm{d}}$. Thus, using the chain rule we obtain from (9.41)

$$\frac{\partial f(\boldsymbol{\sigma}, \boldsymbol{X}_{\mathrm{k}}, \boldsymbol{X}_{\mathrm{d}}, R)}{\partial \boldsymbol{\sigma}} = \sqrt{\frac{2}{3}}(K_0 + R)\left[\left(\frac{\partial \bar{f}\big(\vec{y}, \alpha\big)}{\partial \vec{y}} \cdot \frac{\partial \vec{y}}{\partial \|\boldsymbol{\sigma}^{\mathrm{D}}_{\mathrm{eff}}\|}\right)\frac{\partial \|\boldsymbol{\sigma}^{\mathrm{D}}_{\mathrm{eff}}\|}{\partial \boldsymbol{\sigma}} + \left(\frac{\partial \bar{f}\big(\vec{y}, \alpha\big)}{\partial \vec{y}} \cdot \frac{\partial \vec{y}}{\partial \theta}\right)\frac{\partial \theta}{\partial \boldsymbol{\sigma}}\right].$$

Substituting (9.38), (9.40), and (9.43) into this result we obtain for $\theta \neq 0$

$$\begin{aligned}\frac{\partial f(\boldsymbol{\sigma}, \boldsymbol{X}_{\mathrm{k}}, \boldsymbol{X}_{\mathrm{d}}, R)}{\partial \boldsymbol{\sigma}} = {} & \Big(\frac{\partial \bar{f}\big(\vec{y}, \alpha\big)}{\partial \vec{y}} \cdot (\cos(\theta), \sin(\theta))\Big)\boldsymbol{R}_{\mathrm{eff}} \\ & + \Big(\frac{\partial \bar{f}\big(\vec{y}, \alpha\big)}{\partial \vec{y}} \cdot (\sin(\theta), -\cos(\theta))\Big)\frac{\boldsymbol{X}_{\mathrm{d}} - (\boldsymbol{X}_{\mathrm{d}} : \boldsymbol{R}_{\mathrm{eff}})\boldsymbol{R}_{\mathrm{eff}}}{\|\boldsymbol{X}_{\mathrm{d}} - (\boldsymbol{X}_{\mathrm{d}} : \boldsymbol{R}_{\mathrm{eff}})\boldsymbol{R}_{\mathrm{eff}}\|}. \end{aligned} \tag{9.44}$$

Here, the gradient of the non-dimensional overstress is computed by (9.37). Finally, the normality vector tends to the radial direction as $\theta \to 0$. Therefore

$$\frac{\partial f(\boldsymbol{\sigma}, \boldsymbol{X}_{\mathrm{k}}, \boldsymbol{X}_{\mathrm{d}}, R)}{\partial \boldsymbol{\sigma}} = \boldsymbol{R}_{\mathrm{eff}} \quad \text{for } \theta = 0.$$

Bibliography

[1] Annin, B.D., 1978. Experimental investigation of plastic properties under complex loadings (In Russian). Mechanika tverdogo tela, 347–351.

[2] Aretz, H., 2008. A simple isotropic-distortional hardening model and its application in elastic—plastic analysis of localized necking in orthotropic sheet metals. International Journal of Plasticity, **24**, 1457–1480.

[3] Baltov, A., Sawczuk, A., 1964. A rule of anisotropic hardening. Acta Mechanika, **1**(2), 81–92.

[4] Barlat, F., Gracio, J.J., Lee, M.G., Rauch, E.F., Vincze, G. 2011. An alternative to kinematic hardening in classical plasticity. International Journal of Plasticity, **27**, 1309–1327.

[5] Betten, J., 1976. Plastische Anisotropie und Bauschinger-Effekt; allgemeine Formulierung und Vergleich mit experementell ermittelten Fließortkurven. Acta Mechanika, **25**, 79–94.

[6] Chaboche, J.L., Rousselier, G., 1983a. On the plastic and viscoplastic constitutive equations, part 1: Rules developed with internal variable concept. Journal of Pressure Vessel Technology, **105**, 153–158.

[7] Chaboche, J.L., Rousselier, G., 1983b. On the plastic and viscoplastic constitutive equations, part 2: Application of internal variable concept to the 316 stainless steel. Journal of Pressure Vessel Technology, **105**, 159–164.

[8] Dafalias, Y.F., Popov, E.P., 1975. A model of nonlinearly hardening materials for complex loading. Acta Mechanica, **21**, 173–192.

[9] Dafalias, Y.F., 1979. Anisotropic hardening of initially orthotropic materials. ZAMM, **59**, 437–446.

[10] Dafalias, Y.F., Schick, D., Tsakmakis, C. 2002. A simple model for describing yield surface evolution. Lecture note in applied and computational mechanics, K. Hutter and H. Baaser, eds., Springer, Berlin, 169–201.

[11] Dafalias, Y.F., Feigenbaum, H.P. 2011. Directional distortional hardening in plasticity within thermodynamics. In: Recent Advances in Mechanics, 61–78.

[12] Danilov, V., 1971. On the formulation of the law of distortional hardening (In Russian). Mechanika tverdogo tela **6**, 146–150.

[13] Dannemeyer, S., 1999. Zur Veränderung der Fließfläche von Baustahl bei mehrachsiger plastischer Wechselbeanspruchung. Braunschweig (Carolo-Wilhelmina University).

[14] Dettmer, W., Reese, S., 2004. On the theoretical and numerical modelling of Armstrong-Frederick kinematic hardening in the finite strain regime, Comput. Methods Appl. Mech. Eng., **193**, 87–116.

[15] Fang, L., Qiang, F., Cen, C., Naigang, L., 2011. An elasto-plastic damage constitutive theory and its prediction of evolution of subsequent yield surfaces and elastic constants. International Journal of Plasticity, **27**, 1355–1383.

[16] Feigenbaum, H.P., Dafalias, Y.F., 2007. Directional distortional hardening in metal plasticity within thermodynamics. International Journal of Solids and Structures, **44**, 7526–7542.

[17] Feigenbaum, H.P., Dafalias, Y.F., 2008. Simple model for directional distortional hardening in metal plasticity within thermodynamics. Journal of Engineering Mechanics, **134** 9, 730–738.

[18] François, M., 2001. A plasticity model with yield surface distortion for non proportional loading. International Journal of Plasticity, **17**, 703–717.

[19] Freund, M., Shutov, A.V., Ihlemann, J., 2012. Simulation of distortional hardening by generalizing a uniaxial model of finite strain viscoplasticity. International Journal of Plasticity, **36**, 113–129.

[20] Grewolls, G., Kreißig, R., 2001. Anisotropic hardening —- numerical application of a cubic yield theory and consideration of variable r-values for sheet metal. European Journal of Mechanics A/Solids, **20**, 585–599.

[21] Hashiguchi, K., 1989. Subloading surface model in unconventional plasticity. Int. J. Solids Structures, **25**,8, 917–945.

[22] Haupt, P., 2002. Continuum Mechanics and Theory of Materials, 2nd edition, Springer.

[23] Helling, D.E., Miller, A.K., 1987. The incorporation of yield surface distortion into a unified constitutive model, Part 1: equation development. Acta Mechanika **69**, 9–23.

[24] Helm, D., 2001. Formgedächtnislegierungen, experimentelle Untersuchung, phänomenologische Modellierung und numerische Simulation der thermomechanischen Materialeigenschaften (Universitätsbibliothek Kassel).

[25] Helm, D., 2007. Thermomechanics of martensitic phase transitions in shape memory alloys I. Constitutive theories for small and large deformations, Journal of Mechanics of Materials and Structures **2**,1, 87–112. 281–297.

[26] Henann, D.L., Anand, L., 2009. A large deformation theory for rate–dependent elastic—plastic materials with combined isotropic and kinematic hardening. International Journal of Plasticity 25, 1833–1878.

[27] Hill, R., 1948. A theory of the yielding and plastic flow of anisotropic metals. Proceedings Royal Society (London), Series A **193**, 281–297.

[28] Ilyushin, A.A., 1954. On the relation between stresses and small strains in the mechanics of continua (In Russian). Prikl. Mat. Mech. **18**, 641–666.

[29] Itskov, M., 2007. Tensor Algebra and Tensor Analysis for Engineers: With Applications to Continuum Mechanics (Springer).

[30] Khan, A.S., Pandey, A., Stoughton, T., 2010a. Evolution of subsequent yield surfaces and elastic constants with finite plastic deformation. Part II: A very high work hardening aluminum alloy (annealed 1100 Al). International Journal of Plasticity 26, 1421–1431.

[31] Khan, A.S., Pandey, A., Stoughton, T., 2010b. Evolution of subsequent yield surfaces and elastic constants with finite plastic deformation. Part III: Yield surface in tension—tension stress space (Al 6061–T 6511 and annealed 1100 Al). International Journal of Plasticity 26, 1432–1441.

[32] Kowalsky, U., Ahrens, H., Dinkler, D., 1999. Distorted yield surfaces – modelling by higher order anisotropic hardening tensors. Comput. Mater. Sci. **16**, 81–88.

[33] Kurtyka, T., Zyczkowski, M., 1985. A geometric description of distortional plastic hardening of deviatoric materials. Arch. Mech., **37**, 383–395.

[34] Kurtyka, T., Zyczkowski, M., 1996. Evolution equations for distortional plastic hardening. International Journal of Plasticity, **12**, 191–213.

[35] Lion, A., 2000. Constitutive modelling in finite thermoviscoplasticity: a physical approach based on nonlinear rheological elements. International Journal of Plasticity, **16**, 469–494.

[36] Noman, M., Clausmeyer, T., Barthel, C., Svendsen, B., Huétink, J., Riel, M., 2010. Experimental characterization and modeling of the hardening behavior of the sheet steel LH800. Materials Science and Engineering A **527**, 2515–2526.

[37] Ortiz, M., Popov, E.P., 1983. Distortional hardening rules for metal plasticity. J. Engng Mech., 109, 1042–1058.

[38] Palmow, W.A., 1984. Rheologische Modelle für Materialien bei endlichen Deformationen. Technische Mechanik, 4, 20–31.

[39] Panhans, S., 2006. Ein viskoplastisches Materialmodell mit nichtquadratischer Fließfunktion. PhD thesis, (TU Chemnitz).

[40] Panhans, S., Kreißig, R., 2006. A viscoplastic material model of overstress type with a non-quadratic yield function. European Journal of Mechanics A/Solids, **25**, 283–298.

[41] Perzyna, P., 1963. The constitutive equations for rate sensitive plastic materials. Quarterly of Applied Mathematics, **20** 321–331.

[42] Petrov, M.G., 1998. Rheological properties of materials from the point of view of physical kinetics. Journal of Applied Mechanics and Technical Physics, **39** 1, 104–112.

[43] Pietryga, M.P., Vladimirov, I.N., Reese, S., 2012. A finite deformation model for evolving flow anisotropy with distortional hardening including experimental validation. Mechanics of Materials, **44**, 163–173.

[44] Plesek, J., Feigenbaum, H.P., Dafalias, Y.F., 2010. Convexity of yield surface with directional distortional hardening rules. Journal of Engineering Mechanics, **136** 4, 477–484.

[45] Prager, W., 1935. Der Einfluß der Verformung auf die Fließbedingung zähplastischer Körper. ZAMM, **15** 1/2, 76–80.

[46] Rees, D.W.A., 1984. An examination of yield surface distortion and translation. Acta Mechanica, **52** 15–40.

[47] Rousselier, G., Barlat, F., Yoon, J.W., 2010. A novel approach for anisotropic hardening modeling. Part II: Anisotropic hardening in proportional and non-proportional loadings, application to initially isotropic material. International Journal of Plasticity, **26** 1029–1049.

[48] Steck, E., Ritter, R., Peil, U., Ziegenbein A., 2001. Deutsche Forschungsgemeinschaft, Plasticity of Materials: Experiments, Models, Computation. (Wiley-VCH Verlag GmbH).

[49] Shutov, A.V., Kreißig, R., 2008a. Finite strain viscoplasticity with nonlinear kinematic hardening: Phenomenological modeling and time integration. Computer Methods in Applied Mechanics and Engineering, **197**, 2015–2029.

[50] Shutov, A.V., Kreißig, R., 2008b. Application of a coordinate-free tensor formalism to the numerical implementation of a material model. ZAMM, **88** 11, 888–909.

[51] Shutov, A.V., Kreißig, R., 2010. Regularized strategies for material parameter identification in the context of finite strain plasticity. Technische Mechanik, **30** 1-3, 280–295.

[52] Shutov, A.V., Panhans, S., Kreißig, R., 2011. A phenomenological model of finite strain viscoplasticity with distortional hardening. ZAMM, **91** 8, 653–680.

[53] Shutov, A.V., Ihlemann, J., 2011. On the simulation of plastic forming under consideration of thermal effects. Materialwissenschaft und Werkstofftechnik, **42** 7, 632–638.

[54] Streilein, T., 1997. Erfassung formativer Verfestigung in viskoplastischen Stoffmodellen. PhD thesis, Bericht Nr. 97/83 (TU Braunschweig).

[55] Svistkov, A. L., Lauke, B., 2009. Differential constitutive equations of incompressible media with finite deformations, Journal of Applied Mechanics and Technical Physics, **50**, 3, 493–503.

[56] Tsakmakis, Ch., Willuweit, A., 2004. A comparative study of kinematic hardening rules at finite deformations, Int. J. Non-Linear Mech., **39**(2), 539–554.

[57] Viatkina, E.M., 2005. Micromechanical modelling of strain path dependency in FCC metals. Technische Universiteit Eindhoven, Eindhoven.

[58] Viatkina, E.M., Brekelmans, W.A.M., Geers, M.G.D., 2007. Modelling the evolution of dislocation structures upon stress reversal. International Journal of Solids and Structures, 44, 6030–6054.

[59] Vladimirov, I.N., Pietryga, M.P., Reese, S., 2010. Anisotropic finite elastoplasticity with nonlinear kinematic and isotropic hardening and application to sheet metal forming. International Journal of Plasticity, **26**, 659–687.

[60] Wegener, K., Schlegel, M., 1996. Suitability of yield functions for the approximation of subsequent yild surfaces. International Journal of Plasticity, **12**, 1151–1177.

KAPITEL 10

On the simulation of multi-stage forming processes: invariance under change of the reference configuration

Zur Simulation der mehrstufigen Umformung: Invarianz beim Wechsel der Referenzkonfiguration

A. V. Shutov[1], S. Pfeiffer, J. Ihlemann.
Chemnitz University of Technology, Str. d. Nationen 62, D-09111 Chemnitz, Germany

Abstract: *The need to change the reference configuration can naturally appear during the numerical simulation of multi-stage metal forming processes. In the current work, a refined approach to the consideration of previously induced plastic anisotropy is discussed, which is based on such configuration change. The model of finite strain viscoplasticity proposed by Shutov and Kreißig is considered in this study as a practical tool, suitable to capture the evolution of mechanical properties of material during inelastic deformation. The initial plastic anisotropy can be considered within this model by a special choice of initial conditions imposed on the relevant internal variables. A simple transformation law which is based on the isochoric change of the reference configuration is obtained in the current study. This transformation allows us to obtain relevant initial conditions with respect to a new reference configuration. Thus, the initial conditions are formulated using the simulation results from the foregoing loading. The advocated approach is exemplified by the numerical simulation of equal channel angular pressing of cylindrical billets. The plastic anisotropy accumulated during a single ECAP pass is estimated using a series of virtual tension tests. These test were performed on samples cut from processed billet with their gage lengths in different directions. Finally, the impact of the plastic anisotropy on the rotation of the workpiece within the output channel during ECAP is numerically estimated.*

Keywords: viscoplasticity; finite strains; change of reference configuration; kinematic hardening; ECAP

Kurzfassung: *Bei der numerischen Simulation der mehrstufigen Metallumformung kann ein Wechsel der Referenzkonfiguration auf eine natürliche Weise auftreten. In der aktuellen Studie wird ein verfeinerter Ansatz zur Beschreibung der zuvor induzierten plastischen Anisotropie diskutiert, basierend auf diesem Wechsel der Referenzkonfiguration. Ein Modell der*

---

[1] Corresponding author. alexey.v.shutov@gmail.com
web: http://sites.google.com/site/materialmodeling

This chapter is reproduced from the paper: A. V. Shutov, S. Pfeiffer, J. Ihlemann. On the simulation of multi-stage forming processes: invariance under change of the reference configuration. Materialwissenschaft und Werkstofftecnhik. 2012. (43)7, 617-625. Copyright WILEY-VCH Verlag GmbH. Reproduced with permission.

Viskoplastizität bei finiten Verzerrungen nach Shutov und Kreißig wird dabei als ein praktisches Werkzeug angesehen. Mit diesem Modell lässt sich die Evolution von mechanischen Eigenschaften des Materials im Laufe der inelastischen Deformation erfassen. Die plastische Anfangsanisotropie kann im Rahmen des Modells durch eine gezielte Auswahl der Anfangsbedingungen für relevante innere Variablen erfasst werden. In dieser Studie wurde, basierend auf dem Wechsel der Referenzkonfiguration, eine einfache Transformationsregel hergeleitet. Dieser Formalismus ermöglicht die Bestimmung relevanter Anfangsbedingungen bezogen auf die neue Referenzkonfiguration. Die Anfangsbedingungen werden somit unter Nutzung der Simulationsergebnisse der vorhergehenden Belastung formuliert. Der vorgeschlagene Zugang wurde anhand einer numerischen Simulation des Gleichkanal-Winkelpress-Vorgangs mit zylindrischem Halbzeug veranschaulicht. Die im Laufe eines ECAP-Durchgangs akkumulierte plastische Anisotropie wurde durch eine Serie von virtuellen Zugversuchen abgeschätzt. Dabei wurden die Versuche an Proben durchgeführt, die in unterschiedlichen Richtungen dem umgeformten Halbzeug entnommen wurden. Zum Schluss ist der Einfluss der plastischen Anisotropie auf die Halbzeugverdrehung innerhalb des Ausgangskanals beim ECAPieren numerisch abgeschätzt worden.

Schlüsselworte: Viskoplastizität; finite Deformationen; Wechsel der Referenzkonfiguration; kinematische Verfestigung; ECAP

1. Introduction

It is well known that the plastic properties of metals subjected to inelastic deformations can differ significantly compared to those of the initial state. The yield surface may exhibit isotropic expansion, kinematic translation and a certain distortion already for small levels of inelastic prestrain [**32, 3, 8, 24, 15, 16**]. As it was shown in [**17**], the anisotropy induced by plastic forming operations must be taken into account during the simulation of the subsequent crash response of the entire structure. This effect was also discussed in [**33**]. Moreover, dealing with multi-stage metal forming, the plastic anisotropy induced within the previous stages should be considered for a proper description of the material response.

A phenomenological approach to finite strain metal plasticity is considered in this work such that the current state of the material is described by a set of internal variables. For simplicity, constant temperature distribution is assumed; the considerations are restricted to "simple materials" [**19**]. A viscoplasticity model [**25**] with a combined nonlinear isotropic-kinematic hardening is analyzed.[2] But, the advocated approach can be applied to some models with distortional hardening, like the model presented in [**29**], or to models with a refined description of the kinematic hardening [**28**]. More precisely, this approach can be utilized for material models of finite strain plasticity such that, in the Total Lagrangian formulation, the corresponding constitutive equations remain *invariant under the isochoric change of the reference configuration.* Such invariance allows us to restart the numerical computation from a certain point using a new reference configuration. Corresponding definitions and a concrete example is given in Section 3 of this paper. A formalism of the isochoric configuration change is discussed, and a relevant transformation of the initial conditions is presented.

---

[2] This model is based on the double multiplicative decomposition of the deformation gradient proposed by Lion [**18**]. Some other models which utilize this constitutive assumption are presented in [**12, 21, 9, 10, 31**].

Concerning a certain deformation process, it is convenient to utilize the corresponding initial configuration as the reference. Thus, the need to change the reference configuration appears in a natural way in the context of a multi-stage forming.[3] The formalism of the configuration change, which is discussed in the current publication, utilizes the fact that the reference configuration is, in general, a *fictitious* configuration, set at will, and used to designate material points in a unique manner [**11**]. The goal of the current study is twofold:

- To show that the constitutive equations [**25**] are invariant under the isochoric change of the reference configuration.
- To analyze the principal applicability of this model to the simulation of multi-stage forming processes basing on the isochoric configuration change.

Suppose that the actual state of the material is described by a set of tensor-valued internal variables which operate on the reference configuration. In that case, in order to retain the correct description of the accumulated anisotropy, the internal variables must be transformed in a proper way during the configuration change. In terms of the model with kinematic hardening, this is equivalent to the introduction of initial back stresses induced by previous deformations.

The invariance of the constitutive equations under isochoric reference change should not be confused with the symmetry properties, which can be formulated in terms of the configuration change, as well [**19**]. Since viscoplastic *solids* are considered in this paper, the corresponding symmetry group is a subgroup of the orthogonal group.[4]

In order to exemplify the use of configuration change, numerical simulations of the equal channel angular pressing (ECAP) are considered. ECAP is an innovative technique which allows to develop an ultrafine-grained microstructure by severe plastic deformations, without net change in the billet's shape [**22, 23**].

There is a large number of numerical studies dealing with the influence of process parameters on the material flow during ECAP (see, for instance, references in [**30**]). One problem which is faced during the ECAP of cylindrical billets is the uncontrolled rotation of the billet within the output channel. The mechanisms responsible for this rotation are still not fully understood. In this paper we estimate the influence of the previously induced plastic anisotropy on the rotation. The role of material heterogeneity lies beyond the scope of this publication.

A coordinate-free tensor formalism is used in this work [**14, 26**]. Moreover, a classical tensor analysis is utilized. Thus, we do not distinct covariant, contravariant, and mixed tensors. The deviatoric part of a second rank tensor is denoted by $\mathbf{A}^{\mathrm{D}} := \mathbf{A} - \frac{1}{3}\mathrm{tr}(\mathbf{A})\mathbf{1}$. The overline denotes the unimodular part of a tensor: $\overline{\mathbf{A}} := (\det \mathbf{A})^{-1/3}\mathbf{A}$. We write $\mathbf{A} = \mathbf{A}^{\mathrm{T}} > 0$ if and only if the tensor $\mathbf{A}$ is symmetric and positive definite.

---

[3] The change of the reference configuration should not be confused with the implementation of the Updated Lagrangian formulation in this context.

[4] Moreover, if the symmetry group of the material coincides with the entire special linear group $SL(3)$, the material is considered to be a (thermo-) viscoelastic fluid [**19, 7**], which is an extremely restrictive assumption.

$$\begin{tikzcd}
 & \check{\mathcal{K}} \arrow[dr, "\check{\mathbf{F}}_{\mathrm{ie}}"] & \tilde{\mathcal{K}}^{\mathrm{new}} \arrow[l, "\mathbf{F}_{\mathrm{ii}}^{\mathrm{new}}"'] \arrow[d, "\mathbf{F}_{\mathrm{i}}^{\mathrm{new}}"] \arrow[dr, "\mathbf{F}^{\mathrm{new}}"] & \\
\tilde{\mathcal{K}} \arrow[ur, "\mathbf{F}_{\mathrm{ii}}"] \arrow[rr, "\mathbf{F}_{\mathrm{i}}"] \arrow[urr, bend left, "\mathbf{F}_0"] \arrow[rrr, bend right, "\mathbf{F}"'] & & \hat{\mathcal{K}} \arrow[r, "\hat{\mathbf{F}}_{\mathrm{e}}"] & \mathcal{K}
\end{tikzcd}$$

Figure 10.1. Commutative diagram showing configurations with transformations of material line elements. The transformations are depicted by arrows.
Bild 10.1. Kommutatives Diagramm mit Konfigurationen und Transformationen von materiellen Linienelementen. Die Transformationen sind mit Pfeilen gekennzeichnet.

2. Material model of finite strain viscoplasticity

Let us consider a material model of finite strain viscoplasticity which was proposed in [**25**]. The kinematics of the model is essentially based on the double multiplicative split of the deformation gradient (see Fig. 10.1)

$$\mathbf{F} = \hat{\mathbf{F}}_{\mathrm{e}} \mathbf{F}_{\mathrm{i}}, \quad \mathbf{F}_{\mathrm{i}} = \check{\mathbf{F}}_{\mathrm{ie}} \mathbf{F}_{\mathrm{ii}}. \tag{10.1}$$

The first decomposition in (10.1) is a classical one [**11**], and it is usually motivated by the idea of a local elastic unloading. The deformation gradient $\mathbf{F}$ is thus a product of the inelastic deformation gradient $\mathbf{F}_{\mathrm{i}}$ and the elastic deformation gradient $\hat{\mathbf{F}}_{\mathrm{e}}$. This constitutive assumption gives rise to the stress free configuration $\hat{K}$. The second decomposition was proposed by Lion [**18**] in order to represent nonlinear kinematic hardening of Armstrong-Frederick type. According to this assumption, the inelastic part $\mathbf{F}_{\mathrm{i}}$ is decomposed into a conservative part $\check{\mathbf{F}}_{\mathrm{ie}}$ and a dissipative part $\mathbf{F}_{\mathrm{ii}}$. This decomposition implies the configuration of kinematic hardening $\check{K}$.

In the current study we use material (or Lagrangian) description to formulate the material model.[5] Along with the well-known right Cauchy-Green tensor $\mathbf{C} := \mathbf{F}^{\mathrm{T}} \mathbf{F}$, we introduce two internal variables of Cauchy-Green type

$$\mathbf{C}_{\mathrm{i}} := \mathbf{F}_{\mathrm{i}}^{\mathrm{T}} \mathbf{F}_{\mathrm{i}}, \quad \mathbf{C}_{\mathrm{ii}} := \mathbf{F}_{\mathrm{ii}}^{\mathrm{T}} \mathbf{F}_{\mathrm{ii}}. \tag{10.2}$$

These variables are referred to as inelastic right Cauchy-Green tensor and inelastic right Cauchy-Green tensor of microstructure.[6] Observe that for a given $\mathbf{C}_{\mathrm{i}}$, the inelastic deformation $\mathbf{F}_{\mathrm{i}}$ is uniquely determined up to a rigid rotation. The same holds for $\mathbf{F}_{\mathrm{ii}}$ and $\mathbf{C}_{\mathrm{ii}}$. The product $\mathbf{C}_{\mathrm{i}} \mathbf{C}_{\mathrm{ii}}^{-1}$ is used to describe back stresses, accumulated in the material due to the plastic deformation. Next, in order to capture the nonlinear isotropic hardening of Voce

---

[5] In [**25**], the material model was originally formulated with respect to intermediate configurations. After that the constitutive equations were transformed to the reference configuration in order to simplify the numerical treatment.

[6] This terminology is motivated by the consideration of rheological models [**18, 25**].

type, the accumulated inelastic arc-length s is considered. Its dissipative part will be denoted by s_d.

For a given local deformation history $\mathbf{C}(t)$, the material response in the time interval $t \in [0, T]$ is governed by the following system of ordinary differential and algebraic equations with respect to the internal variables $\mathbf{C}_\mathrm{i}(t)$, $\mathbf{C}_\mathrm{ii}(t)$, $s(t)$, and $s_d(t)$

$$\dot{\mathbf{C}}_\mathrm{i} = 2\frac{\lambda_\mathrm{i}}{\mathfrak{F}}\Big(\mathbf{C}\tilde{\mathbf{T}} - \mathbf{C}_\mathrm{i}\tilde{\mathbf{X}}\Big)^\mathrm{D}\mathbf{C}_\mathrm{i}, \quad \mathbf{C}_\mathrm{i}|_{t=0} = \mathbf{C}_\mathrm{i}^0,\ \det \mathbf{C}_\mathrm{i}^0 = 1,\ \mathbf{C}_\mathrm{i}^0 = (\mathbf{C}_\mathrm{i}^0)^\mathrm{T} > 0, \tag{10.3}$$

$$\dot{\mathbf{C}}_\mathrm{ii} = 2\lambda_\mathrm{i}\varkappa(\mathbf{C}_\mathrm{i}\tilde{\mathbf{X}}\Big)^\mathrm{D}\mathbf{C}_\mathrm{ii}, \quad \mathbf{C}_\mathrm{ii}|_{t=0} = \mathbf{C}_\mathrm{ii}^0,\ \det \mathbf{C}_\mathrm{ii}^0 = 1,\ \mathbf{C}_\mathrm{ii}^0 = (\mathbf{C}_\mathrm{ii}^0)^\mathrm{T} > 0, \tag{10.4}$$

$$\dot{s} = \sqrt{\frac{2}{3}}\lambda_\mathrm{i}, \quad \dot{s}_\mathrm{d} = \frac{\beta}{\gamma}\dot{s}R, \quad s|_{t=0} = s^0,\ s_\mathrm{d}|_{t=0} = s_\mathrm{d}^0, \tag{10.5}$$

$$\tilde{\mathbf{T}} = 2\rho_\mathrm{R}\frac{\partial\psi_\mathrm{el}(\mathbf{C}{\mathbf{C}_\mathrm{i}}^{-1})}{\partial\mathbf{C}}\Big|_{\mathbf{C}_\mathrm{i}=\mathrm{const}}, \quad \tilde{\mathbf{X}} = 2\rho_\mathrm{R}\frac{\partial\psi_\mathrm{kin}(\mathbf{C}_\mathrm{i}{\mathbf{C}_\mathrm{ii}}^{-1})}{\partial\mathbf{C}_\mathrm{i}}\Big|_{\mathbf{C}_\mathrm{ii}=\mathrm{const}}, \tag{10.6}$$

$$R = \gamma s_\mathrm{e}, \quad s_\mathrm{e} = s - s_\mathrm{d}, \tag{10.7}$$

$$\lambda_\mathrm{i} = \frac{1}{\eta}\Big\langle\frac{1}{k_0}f\Big\rangle^m, \quad f = \mathfrak{F} - \sqrt{\frac{2}{3}}\Big[K + R\Big], \quad \mathfrak{F} = \sqrt{\mathrm{tr}\Big[\Big(\mathbf{C}\tilde{\mathbf{T}} - \mathbf{C}_\mathrm{i}\tilde{\mathbf{X}}\Big)^\mathrm{D}\Big]^2}. \tag{10.8}$$

The material parameters $\rho_\mathrm{R} > 0$, $\varkappa \geq 0$, $\beta \geq 0$, $\gamma \in \mathbb{R}$, $\eta \geq 0$, $m \geq 1$, $K > 0$, and the isotropic real-valued functions ψ_el, ψ_kin are assumed to be known; $k_0 > 0$ is used to obtain a dimensionless term in the bracket (it is not a material parameter). To be definite, we put $k_0 = 1$ MPa.

The notation λ_i stands for the inelastic multiplier which describes the rate of inelastic deformation. The quantities $\mathbf{C}$, $\mathbf{C}_\mathrm{i}$, $\mathbf{C}_\mathrm{ii}$, s, and s_d uniquely determine the 2nd Piola-Kirchhoff tensor $\tilde{\mathbf{T}}(t)$, the backstress tensor $\tilde{\mathbf{X}}(t)$, the isotropic hardening $R(t)$, the overstress $f(t)$, and the norm of the driving force $\mathfrak{F}(t)$. The presented material model is thermodynamically consistent [**25**].

In the current study, the elastic potential ψ_el corresponds to a compressible Neo-Hooke material with a bulk modulus k and a shear modulus μ, and ψ_kin to a Neo-Hooke material with a shear modulus $c/2$. We obtain in this special case for stresses and back stresses

$$\tilde{\mathbf{T}} = k\,\ln\sqrt{\det(\mathbf{C})}\ \mathbf{C}^{-1} + \mu\ \mathbf{C}^{-1}(\overline{\mathbf{C}}\mathbf{C}_\mathrm{i}^{-1})^\mathrm{D}, \qquad \tilde{\mathbf{X}} = \frac{c}{2}\ \mathbf{C}_\mathrm{i}^{-1}(\mathbf{C}_\mathrm{i}\mathbf{C}_\mathrm{ii}^{-1})^\mathrm{D}. \tag{10.9}$$

Note that the exact solution of the problem possesses the geometric property

$$\mathbf{C}_\mathrm{i}, \mathbf{C}_\mathrm{ii} \in M, \quad M := \Big\{\mathbf{B} \in Sym : \det\mathbf{B} = 1\Big\}. \tag{10.10}$$

Here, *Sym* is the set of symmetric tensors.

The constitutive equations presented in this section are discretized using an implicit time-stepping scheme which preserves the geometric property (10.10) [**26, 27**]. The material model was implemented in MSC.MARC using Hypela2 interface.

3. Isochoric change of the reference configuration

In this section we derive some transformation rules associated to the isochoric change of the reference configuration. The invariance of constitutive equations under such transformation is discussed in application to the material model presented in the previous section. Observe that the formal idea of isochoric configuration change was already utilized in order to simplify the mathematical treatment of material models within finite strain range [**27, 29**].

Recall that the constitutive equations of the previous section were formulated with respect to a certain fixed reference configuration $\widetilde{K}$. Let us rewrite the constitutive equations with respect to some new local reference configuration $\widetilde{K}^{\rm new} := \mathbf{F}_0\widetilde{K}$, where $\mathbf{F}_0$ is the deformation gradient from $\widetilde{K}$ to $\widetilde{K}^{\rm new}$ (see Fig. 10.1). The new deformation gradient $\mathbf{F}^{\rm new} := \mathbf{F}\mathbf{F}_0^{-1}$ is now a relative deformation gradient which operates on $\widetilde{K}^{\rm new}$ and transforms the line elements from $\widetilde{K}^{\rm new}$ to the current configuration K. This transformation gives rise to the new right Cauchy-Green tensor $\mathbf{C}^{\rm new} := \mathbf{F}_0^{-\rm T}\mathbf{C}\mathbf{F}_0^{-1}$ (cf. relation (13.170) in [**11**]). In other words, $\mathbf{C}^{\rm new}$ is obtained from $\mathbf{C}$ through a covariant push-forward operation. Next, suppose that the stress free configuration $\hat{K}$, the configuration of kinematic hardening $\check{K}$, and the current configuration K remain unaffected by the change of the reference configuration (see Fig. 10.1). In what follows, we suppose that the mapping $\mathbf{F}_0$ is isochoric, i.e. $\det \mathbf{F}_0 = 1$. We postulate the transformation rules for $\mathbf{F}$, $\mathbf{F}_{\rm i}$, $\mathbf{F}_{\rm ii}$, $\hat{\mathbf{F}}_{\rm e}$, $\check{\mathbf{F}}_{\rm ie}$, $\mathbf{C}$, $\mathbf{C}_{\rm i}$, $\mathbf{C}_{\rm ii}$

$$\mathbf{F}^{\rm new} = \mathbf{F}\mathbf{F}_0^{-1},\ \mathbf{F}_{\rm i}^{\rm new} = \mathbf{F}_{\rm i}\mathbf{F}_0^{-1},\ \mathbf{F}_{\rm ii}^{\rm new} = \mathbf{F}_{\rm ii}\mathbf{F}_0^{-1},\ \hat{\mathbf{F}}_{\rm e}^{\rm new} = \hat{\mathbf{F}}_{\rm e},\ \check{\mathbf{F}}_{\rm ie}^{\rm new} = \check{\mathbf{F}}_{\rm ie}, \tag{10.11}$$

$$\mathbf{C}^{\rm new} = \mathbf{F}_0^{-\rm T}\mathbf{C}\mathbf{F}_0^{-1},\ \mathbf{C}_{\rm i}^{\rm new} = \mathbf{F}_0^{-\rm T}\mathbf{C}_{\rm i}\mathbf{F}_0^{-1},\ \mathbf{C}_{\rm ii}^{\rm new} = \mathbf{F}_0^{-\rm T}\mathbf{C}_{\rm ii}\mathbf{F}_0^{-1}. \tag{10.12}$$

The scalar-valued internal variables s and s_d are unaffected by the transformation: $s^{\rm new} = s$, $s_{\rm d}^{\rm new} = s_{\rm d}$.[7] Observe that the conservative parts $\hat{\mathbf{F}}_{\rm e}$ and $\check{\mathbf{F}}_{\rm ie}$ which are associated to the distortion of the crystal lattice, remain unchanged during the configuration change. Thus, the stored energy should remain invariant, as well. Indeed, implementing relations (10.12), we arrive to

$$\psi_{\rm el}(\mathbf{C}^{\rm new}\ (\mathbf{C}_{\rm i}^{\rm new})^{-1}) = \psi_{\rm el}(\mathbf{C}\ \mathbf{C}_{\rm i}{}^{-1}), \quad \psi_{\rm kin}(\mathbf{C}_{\rm i}^{\rm new}(\mathbf{C}_{\rm ii}^{\rm new})^{-1}) = \psi_{\rm kin}(\mathbf{C}_{\rm i}\mathbf{C}_{\rm ii}{}^{-1}). \tag{10.13}$$

Next, since the elastic deformation gradient $\hat{\mathbf{F}}_{\rm e}$ remains unchanged during the transformation, the Cauchy stress $\mathbf{T}$ remains invariant, as well. Thus, the same mechanical response is predicted in terms of the Cauchy stresses. On the other hand, we obtain for the second Piola-Kirchhoff stresses $\tilde{\mathbf{T}} = (\det \mathbf{F})\ \mathbf{F}^{-1}\mathbf{T}\mathbf{F}^{-\rm T}$ operating on $\widetilde{K}$ and $\tilde{\mathbf{T}}^{\rm new} = (\det \mathbf{F}^{\rm new})\ (\mathbf{F}^{\rm new})^{-1}\mathbf{T}(\mathbf{F}^{\rm new})^{-\rm T}$ operating on $\widetilde{K}^{\rm new}$

$$\tilde{\mathbf{T}}^{\rm new} = \mathbf{F}_0\tilde{\mathbf{T}}\mathbf{F}_0^{\rm T}. \tag{10.14}$$

Analogously, due to the invariance of $\check{\mathbf{F}}_{\rm ie}$, we have for backstresses

$$\widetilde{\mathbf{X}}^{\rm new} = \mathbf{F}_0\widetilde{\mathbf{X}}\mathbf{F}_0^{\rm T}. \tag{10.15}$$

Combining these results with the potential relations (10.6), it can be easily shown that the same potential relations hold for new quantities (note that the mass density is preserved: $\rho_{\rm R}^{\rm new} = \rho_{\rm R}$). More precisely, the relations for stresses and back stresses with respect to the new configuration $\widetilde{K}^{\rm new}$ are obtained from (10.6) by formal replacement of $\tilde{\mathbf{T}}$, $\widetilde{\mathbf{X}}$, $\mathbf{C}$, $\mathbf{C}_{\rm i}$,

---

[7] In what follows it will be shown that the inelastic multiplier $\lambda_{\rm i}$ is independent of the choice of the reference configuration. Thus, it follows from (10.5) that the same holds for s and s_d.

and $\mathbf{C}_{\mathrm{ii}}$ with $\widetilde{\mathbf{T}}^{\mathrm{new}}$, $\widetilde{\mathbf{X}}^{\mathrm{new}}$, $\mathbf{C}^{\mathrm{new}}$, $\mathbf{C}_{\mathrm{i}}^{\mathrm{new}}$, and $\mathbf{C}_{\mathrm{ii}}^{\mathrm{new}}$. Taking (10.12), (10.14), and (10.15) into account, we obtain from (10.8)

$$\mathfrak{F}^{\mathrm{new}} := \sqrt{\mathrm{tr}\Big[\Big(\mathbf{C}^{\mathrm{new}}\tilde{\mathbf{T}}^{\mathrm{new}} - \mathbf{C}_{\mathrm{i}}^{\mathrm{new}}\tilde{\mathbf{X}}^{\mathrm{new}}\Big)^{\mathrm{D}}\Big]^2} = \sqrt{\mathrm{tr}\Big[\Big(\mathbf{C}\tilde{\mathbf{T}} - \mathbf{C}_{\mathrm{i}}\tilde{\mathbf{X}}\Big)^{\mathrm{D}}\Big]^2} = \mathfrak{F}, \tag{10.16}$$

$$f^{\mathrm{new}} = f, \quad \lambda_{\mathrm{i}}^{\mathrm{new}} = \lambda_{\mathrm{i}}.$$

In other words, the norm of the driving force, the overstress, and the inelastic multiplier remain invariant under the isochoric change of reference configuration. In particular, it follows that the evolution equations (10.5) for s and s_{d} remain invariant. Next, let us consider the evolution equations for internal variables $\mathbf{C}_{\mathrm{i}}$ and $\mathbf{C}_{\mathrm{ii}}$. Differentiating (10.12), and taking into account that the mapping $\mathbf{F}_0$ is fixed in time, we arrive at

$$\dot{\mathbf{C}}_{\mathrm{i}}^{\mathrm{new}} = \mathbf{F}_0^{-\mathrm{T}}\dot{\mathbf{C}}_{\mathrm{i}}\mathbf{F}_0^{-1}, \ \dot{\mathbf{C}}_{\mathrm{ii}}^{\mathrm{new}} = \mathbf{F}_0^{-\mathrm{T}}\dot{\mathbf{C}}_{\mathrm{ii}}\mathbf{F}_0^{-1}. \tag{10.17}$$

Substituting evolution equations (10.3) and (10.4) into this result, it can be shown after some computations that the evolution equations for the new quantities $\mathbf{C}_{\mathrm{i}}^{\mathrm{new}}$ and $\mathbf{C}_{\mathrm{ii}}^{\mathrm{new}}$ are obtained from (10.3) and (10.4), if the "old" quantities are formally replaced by their new counterparts. Summarizing this section we conclude that for any solution $\mathbf{C}_{\mathrm{i}}(t)$, $\mathbf{C}_{\mathrm{ii}}(t)$ of the problem (10.3)–(10.8) with a given local deformation history $\mathbf{C}(t)$, the corresponding solution with respect to a new reference configuration is given by the transformation rule (10.12) and it is governed by system (10.3)–(10.8) where all "old" quantities are formally replaced by their new counterparts. This useful property of the material model will be referred to as *invariance of constitutive equations under the change of reference configuration.*

4. Simulation results

The numerical results presented in this study were obtained using the commercial FEM code MSC.MARC. The material model is implemented as a user-defined subroutine using the Hypela2 interface in combination with the Total Lagrangian description. Since Total Lagrangian formulation is applied, the initial configuration is considered to be the reference configuration by default. The consistent material tangent which is required for implicit FEM computations is computed analytically according to [**26**]. Eight-node solid isoparametric elements with trilinear interpolation functions were used in this study, and a "constant dilatation" method is utilized in order to eliminate the element locking. All simulations were performed using the same set of material parameters, see table 10.1. The influence of the loading history on the material behavior is captured using the initial conditions imposed on the internal variables.

Table 10.1. Material parameters used for numerical simulations.
Tabelle 10.1. Materialparameter, die zur numerischen Simulation herangezogen wurden.

k [MPa]	μ [MPa]	c [MPa]	γ [MPa]
73500	28200	3500	460

K [MPa]	m [-]	η [s]	$\varkappa$ [MPa^{-1}]	β [-]
270	3.6	$4 \cdot 10^6$	0.005	5

4.1. Simulation of equal channel angular pressing: first pass. Let us consider a single ECAP pass of a cylindrical billet. The FEM-model of the workpiece consists of 2290 elements, as shown in Fig. 10.2a. The input channel of the die is oriented along the z-axis, and the output channel - along the y-axis. As it is common in the ECAP literature, we introduce the extrusion direction (ED), the normal direction (ND), and the transverse direction (TD) (Fig. 10.2a). Note that an L-shaped workpiece is considered in this simulation already at the beginning of the deformation process (at $t = 0$). This is done in order to shorten the transient stage of ECAP, since only the steady-state flow is to be analyzed in the current study. Due to this special choice of the initial configuration, the steady-state material flow can be observed already for relatively small punch displacements. Moreover, the use of L-shaped mesh in initial state allows to avoid severely distorted elements during the transient phase. Next, note that the die geometry is slightly smoothed in order to improve the convergence of the FEM solution. For the same reason, the problem is solved in a dynamic transient formulation with a fictitious mass density. Rayleigh damping is applied in order to suppress undesired oscillations.

Three common types of nonlinearities are encountered in the simulation of the extrusion: physical nonlinearity due to elastic-viscoplastic behavior of the billet material; geometric nonlinearity due to finite strains, displacements and rotations; and the nonlinearity due to the contact between the workpiece and the die. The die is assumed to be undeformable, and a frictionless contact is considered. The diameter of the billet d^{billet} is set to 50 mm. A no-slip contact between the punch and the workpiece is assumed. More precisely, the model is loaded by prescribing the displacements at the top surface of the billet: In order to mimic the motion of the punch, the axial displacements are prescribed as linear functions of time t, and the remaining nodal degrees of freedom are held zero. The overall pressing time was set to $T^{\text{ECAP}} = 100$ s, and the punch displacement $U_{\text{z}}^{\text{punch}}$ ranges up to 135 mm.[8] No back pressure was considered in the current study. The initial state is used as a reference configuration in this subsection. For the first ECAP pass, the material is assumed to be isotropic and stress free at the beginning of the process. Therefore, we put here the initial conditions as follows

$$\mathbf{C}_{\text{i}}|_{t=0} = \mathbf{C}_{\text{ii}}|_{t=0} = \mathbf{1}, \quad s|_{t=0} = s_{\text{d}}|_{t=0} = 0. \tag{10.18}$$

As expected, no rotation of the workpiece within the output channel was detected during the first pass. Next, the accumulated plastic deformation (plastic arc-length s) is not constant throughout the pressed workpiece. In particular, at final stage, the accumulated inelastic deformation ranges up to 0.719, 1.165, and 0.974 at certain Gauss points within elements O, M, I, respectively (see Fig. 10.2b).[9] Such heterogeneity of the steady-state flow was observed experimentally in numerous publications (see, for instance, [**34, 20, 13**] and references therein). Moreover, the effect of different process parameters like friction conditions, back-pressure and loading rate on the strain uniformity was numerically analyzed, as well (see [**6, 30**] and references therein). In the following, the plastic anisotropy accumulated within the central core region of the processed billet (corresponds to element M) will be analyzed, since this state is usually considered to be representative for the processed material.

---

[8] Note that in practical ECAP processes [**13**], a somewhat lower loading rate is typically used.

[9] The FEM animation of the first ECAP pass can be found at http://youtu.be/hf743Rd6b6I

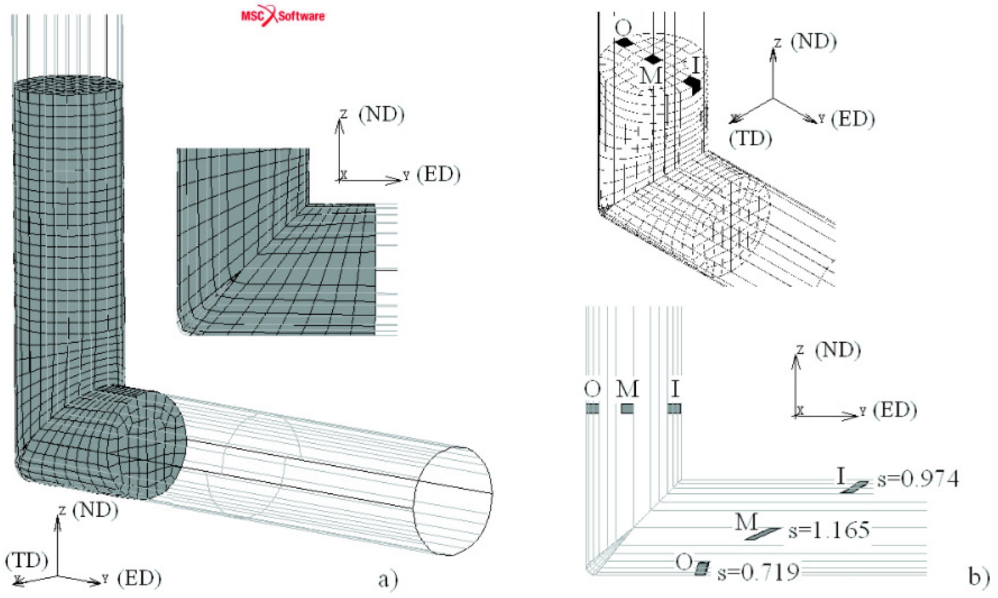

Figure 10.2. a) Undeformed finite element model of the cylindrical workpiece; b) Deformation of some representative elements within the billet.
Bild 10.2. a)Unverformte FEM-Vernetzung eines zylindrischen Halbzeugs; b)Verformung einzelner repräsentativer Elemente innerhalb des Halbzeugs.

At the time instance $t = T^{\text{ECAP}}$, the deformation gradient and the internal variables corresponding to a single Gauss point within the element M (see Fig. 10.2b) are as follows

$$\mathbf{F}|_{t=T^{\text{ECAP}}} = \mathbf{F}^{\text{ECAP}} \approx \begin{pmatrix} 1.0106 & 0.0027 & 0.0000 \\ 0.0096 & 2.1219 & -1.0185 \\ -0.0063 & 0.9828 & -0.0057 \end{pmatrix}, \tag{10.19}$$

$$\mathbf{C}_{\text{i}}|_{t=T^{\text{ECAP}}} = \mathbf{C}_{\text{i}}^{\text{ECAP}} \approx \begin{pmatrix} 1.0219 & 0.0166 & -0.0098 \\ 0.0166 & 5.4385 & -2.1540 \\ -0.0098 & -2.1540 & 1.0331 \end{pmatrix}, \quad s|_{t=T^{\text{ECAP}}} = s^{\text{ECAP}} \approx 1.1645, \tag{10.20}$$

$$\mathbf{C}_{\text{ii}}|_{t=T^{\text{ECAP}}} = \mathbf{C}_{\text{ii}}^{\text{ECAP}} \approx \begin{pmatrix} 1.0129 & 0.0099 & -0.0087 \\ 0.0099 & 5.1160 & -1.9815 \\ -0.0087 & -1.9815 & 0.9605 \end{pmatrix}, \quad s_{\text{d}}|_{t=T^{\text{ECAP}}} = s_{\text{d}}^{\text{ECAP}} \approx 0.9650. \tag{10.21}$$

These values will be used in the following to describe the induced plastic anisotropy of the billet material. Note that the final value of the deformation gradient deviates slightly from the theoretical result corresponding to homogeneous deformation. The value of the accumulated inelastic arc-length s^{ECAP} lies close to the theoretical estimation.

Finally, observe that the state after one ECAP pass is not exactly stress free, since no unloading stage was explicitly implemented in the simulation of the ECAP process. Let us consider such local elastic unloading.[10] First, note that the right stretch tensor $\mathbf{U} =$

---

[10] In general, the pure elastic unloading may become impossible for a given local state if the back stresses are too large. As it will be shown in the next subsection, that is not the case for the current simulation.

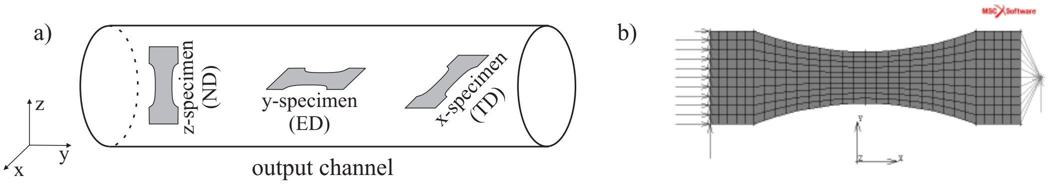

Figure 10.3. a) Orientation of the tension specimens with respect to the billet; b) FEM model of a tension specimen. Within the numerical simulation, the specimen is always oriented along the x-axis.
Bild 10.3. a) Ausrichtung der Zugprobekörper bezüglich des Halbzeugs; b) FEM-Modell eines Zugprobekörpers. Im Rahmen der numerischen Simulation ist der Probekörper entlang der x-Achse ausgerichtet.

$\mathbf{C}^{1/2}$ is uniquely determined for the stress-free state by the condition $\mathbf{C} = \mathbf{C}_{\mathrm{i}}$. In order to describe the kinematics upon unloading in a definite way, additional assumption concerning the rotation of the material particle is required. In this work we assume that the rotational part of the deformation gradient remains constant during stress release. More precisely, consider the polar decomposition of the deformation gradient

$$\mathbf{F}^{\mathrm{ECAP}} = \mathbf{R}^{\mathrm{ECAP}}\mathbf{U}^{\mathrm{ECAP}}, \quad (\mathbf{R}^{\mathrm{ECAP}})^{\mathrm{T}} = (\mathbf{R}^{\mathrm{ECAP}})^{-1}, \ \mathbf{U}^{\mathrm{ECAP}} = (\mathbf{U}^{\mathrm{ECAP}})^{\mathrm{T}} > 0. \qquad (10.22)$$

Since the internal variables remain unchanged during any elastic deformation, the deformation gradient after pure elastic unloading takes the form

$$\mathbf{F}^{\mathrm{unload}} = \mathbf{R}^{\mathrm{ECAP}}(\mathbf{C}_{\mathrm{i}}^{\mathrm{ECAP}})^{1/2}. \qquad (10.23)$$

Since elastic strains are relatively small in this case, the resulting deformation gradient $\mathbf{F}^{\mathrm{unload}}$ lies close to $\mathbf{F}^{\mathrm{ECAP}}$.

4.2. Tension tests. In order to estimate the plastic anisotropy induced by one ECAP pass at a certain material point, a series of virtual tension tests will be performed in this subsection. Toward that end, three tension samples are considered. Each sample is made of the material processed by a single ECAP pass and has its own orientation as shown in Fig. 10.3a. The same FEM model is used to mimic all tension tests, see Fig. 10.3b, and the same quasi-static loading rate is prescribed in all tests. The sample dimensions are 30 mm times 9 mm with 1mm thickness.

The concrete orientation of the samples is taken into account by the proper choice of initial conditions. For simplicity, the material of the tension samples is considered to be homogeneous, corresponding to the state which is described by relations (10.20), (10.21). As it can be seen from Fig. 10.3b, the sample is oriented along the x-axis within the FEM model of the tension test. Therefore, in general, a rigid-body rotation of the sample must be considered, which precedes the tension test: The specimens, which were cut from the workpiece along the y or z-axis must be oriented along the x-direction. For the y-specimen, the corresponding rotation can be described by

$$\mathbf{Q}^{\text{z-90}} = -\mathbf{e}_y \otimes \mathbf{e}_x + \mathbf{e}_x \otimes \mathbf{e}_y + \mathbf{e}_z \otimes \mathbf{e}_z. \qquad (10.24)$$

Analogously, for the z-specimen, we use the rotation tensor

$$\mathbf{Q}^{\text{y+90}} = -\mathbf{e}_z \otimes \mathbf{e}_x + \mathbf{e}_y \otimes \mathbf{e}_y + \mathbf{e}_x \otimes \mathbf{e}_z. \qquad (10.25)$$

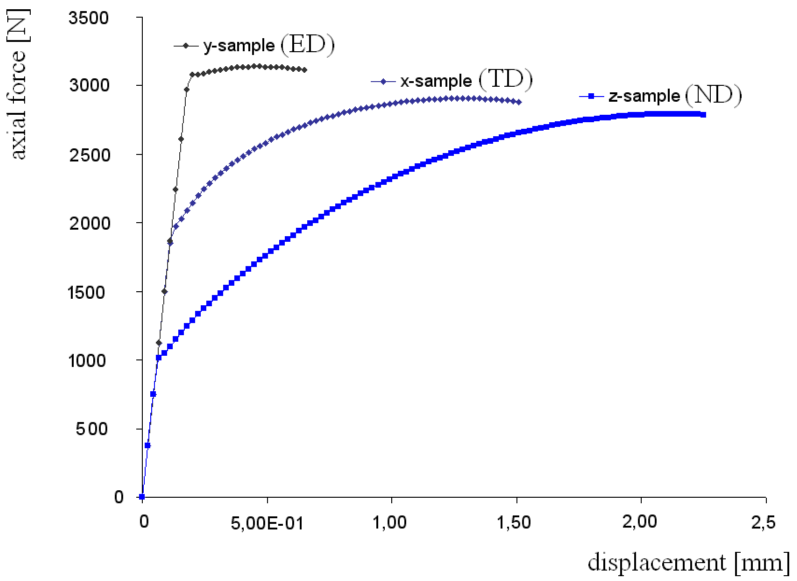

Figure 10.4. Simulation results of quasistatic tension concerning three different orientations of the specimen. The samples are cut from the billet material, processed by a single ECAP pass.

Bild 10.4. Simulationsergebnisse eines quasistatischen Zugversuchs unter Berücksichtigung der Ausrichtung der Probekörper. Die Probekörper wurden dem Halbzeug nach einem ECAP-Durchgang entnommen.

The state right before the tension is thus described by the following deformation gradients: $\mathbf{F}_0 = \mathbf{F}^{\text{unload}}$ for the x-specimen, $\mathbf{F}_0 = \mathbf{Q}^{\text{z-90}}\ \mathbf{F}^{\text{unload}}$ for the y-specimen, and $\mathbf{F}_0 = \mathbf{Q}^{\text{y+90}}\ \mathbf{F}^{\text{unload}}$ for the z-specimen. Since a new reference configuration $\widetilde{K}^{\text{new}} = \mathbf{F}_0 \widetilde{K}$ has to be introduced for the simulations of the tension test, the initial conditions imposed on the internal variables should be transformed according to $(10.12)_2$ and $(10.12)_3$:

$$\mathbf{C}_{\text{i}}|_{t=0} = \mathbf{F}_0^{-\text{T}} \mathbf{C}_{\text{i}}^{\text{ECAP}} \mathbf{F}_0^{-1} = \mathbf{1}, \ \mathbf{C}_{\text{ii}}|_{t=0} = \mathbf{F}_0^{-\text{T}} \mathbf{C}_{\text{ii}}^{\text{ECAP}} \mathbf{F}_0^{-1}, \ s|_{t=0} = s^{\text{ECAP}}, \ s_{\text{d}}|_{t=0} = s_{\text{d}}^{\text{ECAP}}. \tag{10.26}$$

Observe that, due to the special choice of $\mathbf{F}^{\text{unload}}$, the right Cauchy tensor of inelastic deformation is equal to the identity tensor at $t = 0$. Thus, the material state is stress free and the sample is unloaded at the beginning of the tension test.

The simulation results are presented in Fig. 10.4, showing the axial force as a function of the prescribed displacement. Due to the well-known mesh dependence of the FEM solution in the case of strain localization, the results obtained after the force maximum are not plotted. It follows from Fig. 10.4 that the material gets plasticized only if the external load exceeds a certain limit. Since pure elastic material response is observed at the beginning of the tension tests, the back stresses accumulated in the material are not sufficient to introduce the plastic flow in the fully unloaded state. Thus, the purely elastic unloading described in the previous section is indeed possible. As it can be seen from Fig. 10.4, an essential plastic anisotropy is introduced by a single ECAP pass. The highest flow stress under tension is observed for the y-specimen (cut in extrusion direction) in combination with a relatively low ductility due to a small hardening rate. The lowest yield stress is obtained during tension

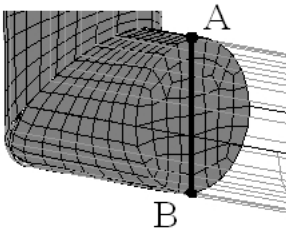

Figure 10.5. Material line $A-B$ used to estimate the rotation of the workpiece.
Bild 10.5. Materiallinie $A-B$, die zur Abschätzung der Halbzeugverdrehung herangezogen wurde.

of the z-sample (cut in normal direction), accompanied by a relatively high ductility with a high potential for hardening. Observe that these results correlate qualitatively with the experimental results presented in [**1**].[11] Due to the choice of the material parameters utilized in this study, the plastic anisotropy observed after one ECAP pass is much stronger than the anisotropy usually measured in real experiments (cf. [**1**]). Nevertheless, such strong accumulated anisotropy is advantageous for the estimation of the anisotropy effect on the material flow during the second ECAP pass, which will be simulated in the following.

4.3. Simulation of equal channel angular pressing: second pass. In this subsection we simulate numerically the material flow during the second ECAP pass following route B_C. The same FEM-model with the same loading conditions as the one used in subsection 4.1 is implemented now to simulate the second ECAP pass. The only difference between the simulations of both passes lies in the choice of initial conditions.

Let us recall the loading program which corresponds to route B_C. After the first pass the billet is rotated by 90° around the x-axis and after that it is rotated by 90° around its longitudinal axis (this axis coincides now with the axis of the input channel). More precisely, the deformation gradient characterizing the motion of the workpiece before the second ECAP pass is given by

$$\mathbf{F}_0 = \mathbf{Q}^{\text{z-90}}\ \mathbf{Q}^{\text{x-90}}\ \overline{\mathbf{F}}^{\text{ECAP}}, \quad \mathbf{Q}^{\text{x-90}} = \mathbf{e}_x \otimes \mathbf{e}_x - \mathbf{e}_z \otimes \mathbf{e}_y + \mathbf{e}_y \otimes \mathbf{e}_z. \tag{10.27}$$

Note that a simplified volumetric unloading is considered here instead of the total unloading, which leads to the use of $\overline{\mathbf{F}}^{\text{ECAP}}$ instead of $\mathbf{F}^{\text{unload}}$.[12] A new reference configuration $\widetilde{K}^{\text{new}} = \mathbf{F}_0 \widetilde{K}$ is introduced to simulate the second ECAP pass. This new reference configuration coincides with the initial configuration within the FEM simulation of the second pass. Thus, the initial conditions imposed on the internal variables are transformed according to (10.26).

The goal of this simulation is to estimate the influence of plastic anisotropy on the rotation of the billet within the output channel during the steady-state stage of the second ECAP pass. The rotation angle of the workpiece is defined as follows. The material line

---

[11] In [**1**], a series of upsetting tests can be found for samples cut from a billet after a single ECAP pass. The lowest compression yield stress was observed for the sample taken in the extrusion direction (y-sample in the current notation), which corresponds to the highest tension yield stress. On the other hand, in contrast to the simulation results presented in Fig. 10.4, the difference between the x and z-samples was negligible.

[12] This is done in order to demonstrate the applicability of the approach to the case of loaded initial configuration.

$A - B$, shown in Fig. 10.5, is projected along the y-axis onto the (x, z)-plane. The angle between the original and the final projections is considered to be the rotation angle. Such definition is reasonable, since the portion of the billet located behind the zone of severe plastic deformations performs nearly rigid body motion. Within the FEM simulation, the rotation angle ranges up to 0.9°, which corresponds to the maximum punch displacement of 135 mm (recall that the diameter of the billet d^{billet} was set to 50 mm). Note that the idealized pressing conditions which were utilized in this simulation are favorable for the rotation of the billet. Indeed, one expects even smaller rotations if the friction between the workpiece and the die is considered. Moreover, since a very strong plastic anisotropy is induced during the first ECAP pass (cf. Fig. 10.4), the rotation should be larger than for nearly isotropic billet material. On the other hand, the heterogeneity of the material properties distribution within the workpiece was not considered in this study, for a pure estimation of the *anisotropy effect*. Summarizing this subsection we conclude that the influence of the plastic anisotropy on the rotation of the workpiece is low.

5. Discussion and conclusion

A phenomenological model of finite-strain viscoplasticity proposed by Shutov and Kreißig is analyzed in this paper concerning the change of the reference configuration. This change is made according to the relation $\widetilde{K}^{\text{new}} = \mathbf{F}_0 \widetilde{K}$, with a unimodular $\mathbf{F}_0$ $(\det \mathbf{F}_0 = 1)$. For a given local strain-controlled process $\{\mathbf{F}(t)\}_{t \in [0,T]}$ and given initial conditions, a certain stress response is predicted by the model within the time interval $[0, T]$. It was shown that if the initial conditions imposed on the internal variables are transformed according to $(10.12)_2$, $(10.12)_3$ and if the prescribed deformation gradient is transformed according to $(10.11)_1$, then the same material response will be predicted by the model in terms of the Cauchy stresses. Observe that the form of the constitutive equations remains unchanged during that transformation. This invariance property is referred to as *invariance of constitutive equations under the change of the reference configuration.* Alternatively, this invariance property can be formulated as follows: For any modification of the local loading program according to $\mathbf{F}^{\text{new}}(t) = \mathbf{F}(t)\mathbf{F}_0^{-1}$ with a fixed $\mathbf{F}_0$ there is a corresponding modification of the initial conditions imposed on the internal variables such that the predicted stress response coincides with the stress response associated to $\mathbf{F}(t)$.

Note that such invariance is a strong assumption imposed on constitutive relations, and it can not be considered as a universal principle of material theory. Nevertheless, this assumption can be justified for materials without a preferred configuration.[13] Trivial examples of such materials are fluids (including idealized plastic materials). Moreover, in the general case of metal plasticity, a constitutive assumption can be introduced that the current deformation of the crystal lattice and not the deformation of the material determine the Cauchy stresses [**2, 4**]. If this assumption holds, then the absence of a preferred configuration can

---

[13] On the other hand, considering materials which posses a preferred configuration, it may be reasonable to use this certain configuration as a reference. For instance, the unstressed configuration is a natural reference configuration for hyperelastic constitutive relations. Thus, the invariance of the constitutive equations under the change of the reference configuration should not be expected in that case.

be expected and the corresponding constitutive equations should be invariant with respect to the configuration change.[14]

One important advantage of constitutive equations with such invariance property is that *the same numerical implementation can be used*, independently of the reference configuration: The change of the reference configuration leads solely to the modification of initial conditions. Some relevant numerical examples were presented in this paper dealing with multi-stage deformation processes.

Observe that the invariance requirement which is satisfied by the constitutive equations should be imposed on the numerical implementation, as well. The numerical schemes which exactly retain the invariance of the solution (even for large time steps) should be considered as advantageous over schemes which violate this property.

The proposed transformation rules were exemplified by the simulation of two ECAP passes following route B_C and a series of tension tests after a single pass. Although the model of viscoplasticity, which is utilized in the current study, tends to overestimate plastic anisotropy accumulated after one pass, this model still can be used to estimate the influence of this anisotropy on the material flow. Since isotropic homogeneous initial state was considered, no rotation of the workpiece within the output channel was observed during the first pass. Next, only a small rotation rate was observed during the steady-state phase of the second pass, even for a distinct plastic anisotropy which was confirmed by a series of tension tests. On the other hand, a somewhat larger rotation can occur within the steady-state phase of real ECAP due to the heterogeneously distributed plastic properties. Moreover, an essential workpiece rotation can occur within the transient stage of the second pass. These effects should be taken into account in the future work.

Acknowledgement

This research was supported by German Science Foundation (DFG) within SFB 692. The authors are grateful to Dr. M. Hockauf and to Dr. T. Halle for fruitful discussions. The help of C. Naumann with post processing of the simulation results is acknowledged.

---

[14] The invariance of constitutive equations with respect to the configuration change should not be confused with the concept of material isomorphism [**4, 5**]. Although this concept is based on similar assumptions, it represents an axiomatic framework for the description of material response.

Bibliography

[1] A. Agena, A study of flow characteristics of nanostructured Al-6082 alloy produced by ECAP under upsetting test, Journal of Materials Processing Technology. **209** 856–863 (2009).

[2] L. Anand, S. Brown, Constitutive equations for large deformations of metals at high temperatures. In: Chandra, J., Sri Vastav, R.P. (Eds.), Constitutive Models of Deformation. Siam, Philadelphia, 1–26 (1987).

[3] B. D. Annin, V. M. Zhigalkin. Material behaviour under complex loadings conditions (In Russian), Publishing House of Siberian Branch of the Russian Academy of Science (1999).

[4] A. Bertram, An alternative approach to finite plasticity based on material isomorphisms, International Journal of Plasticity **52**, 353–374 (1998).

[5] A. Bertram, Finite thermoplasticity based on isomorphisms, International Journal of Plasticity **19**, 2027–2050 (2003).

[6] J.R. Bowen, A. Gholinia, S.M. Roberts, P.B. Prangnell, Analysis of the billet deformation behaviour in equal channel angular extrusion, Materials Science and Engineering A287, 87–99 (2000).

[7] C. M. Dafermos, Hyperbolic Conservation Laws in Continuum Physics, Grundlehren der mathematischen Wissenschaften 325, Springer-Verlag Berlin Heidelberg (2010).

[8] S. Dannemeyer, Zur Veränderung der Fließfläche von Baustahl bei mehrachsiger plastischer Wechselbeanspruchung. Braunschweig (Carolo-Wilhelmina University) (1999).

[9] W. Dettmer, S. Reese, On the theoretical and numerical modelling of Armstrong–Frederick kinematic hardening in the finite strain regime, Computer Methods in Applied Mechanics and Engineering, **193**, 87–116 (2004).

[10] S. Hartmann, K.J. Quint, M. Arnold, On plastic incompressibility within time-adaptive finite elements combined with projection techniques, Computer Methods in Applied Mechanics and Engineering, **198**, 173–178 (2008).

[11] P. Haupt, Continuum Mechanics and Theory of Materials, 2nd edition, Springer, 2002.

[12] D. Helm, Formgedächtnislegierungen, experimentelle Untersuchung, phänomenologische Modellierung und numerische Simulation der thermomechanischen Materialeigenschaften, (Universitätsbibliothek Kassel, 2001).

[13] M. Hockauf, Fließspannungsverhalten ultrafeinkörniger Aluminiumwerkstoffe unter besonderer Berücksichtigung der Dehnrate, PhD, TU-Chemnitz (2009).

[14] M. Itskov, Tensor Algebra and Tensor Analysis for Engineers: With Applications to Continuum Mechanics (Springer, Berlin, Heidelberg) (2007).

[15] A. S. Khan, A. Pandey, T. Stoughton, Evolution of subsequent yield surfaces and elastic constants with finite plastic deformation. Part II: A very high work hardening aluminum alloy (annealed 1100 Al). International Journal of Plasticity **26**, 1421–1431 (2010).

[16] A. S. Khan, A. Pandey, T. Stoughton, Evolution of subsequent yield surfaces and elastic constants with finite plastic deformation. Part III: Yield surface in tension–tension stress space (Al 6061-T 6511 and annealed 1100 Al). International Journal of Plasticity **26**, 1432–1441 (2010).

[17] M. G. Lee, C. S. Han, K. Chung, J. R. Youn, T. J. Kang. Influence of back stresses in parts forming on crashworthiness. Journal of Material Processing Technology, **168**, 49–55 (2005).

[18] A. Lion, Constitutive modelling in finite thermoviscoplasticity: a physical approach based on nonlinear rheological elements, International Journal of Plasticity, **16**, 469–494 (2000).

[19] W. Noll, A mathematical theory of the mechanical behavior of continuous media, Archive for Rational Mechanics and Analysis, **2** 1, 197–226 (1958).

[20] M. Prell, C. Xu, T. G. Langdon, The evolution of homogeneity on longitudinal sections during processing by ECAP, Materials Science and Engineering, A 480, 449–455 (2008).

[21] Ch. Tsakmakis, A. Willuweit, A comparative study of kinematic hardening rules at finite deformations, International Journal of Non-Linear Mechanics, **39** 2, 539–554 (2004).

[22] V. M. Segal, V. I. Reznikov, A. E. Drobyshevskii, V. I. Kopylov, Plastic Metal Working by Simple Shear. Izvestia Akademii nauk SSSR. Metally, 115–123 (1981).

[23] V. M. Segal, Materials processing by simple shear, Materials Science and Engineering A197, 157–164 (1995).

[24] E. Steck, R. Ritter, U. Peil, A. Ziegenbein. Deutsche Forschungsgemeinschaft, Plasticity of Materials: Experiments, Models, Computation. (Wiley-VCH Verlag GmbH) (2001).

[25] A. V. Shutov, R. Kreißig, Finite strain viscoplasticity with nonlinear kinematic hardening: Phenomenological modeling and time integration, Computer Methods in Applied Mechanics and Engineering, **197**, 2015–2029 (2008).

[26] A. V. Shutov, R. Kreißig, Application of a coordinate-free tensor formalism to the numerical implementation of a material model. Zeitschrift für Angewandte Mathematik und Mechanik, **88** 11, 888–909 (2008).

[27] A. V. Shutov, R. Kreißig, Geometric integrators for multiplicative viscoplasticity: Analysis of error accumulation, Computer Methods in Applied Mechanics and Engineering, **199**, 700–711 (2010).

[28] A. V. Shutov, C. Kuprin, J. Ihlemann, M. F.-X. Wagner, C. Silbermann, Experimentelle Untersuchung und numerische Simulation des inkrementellen Umformverhaltens von Stahl 42CrMo4. Materialwissenschaft und Werkstofftechnik, **41**, 9, 765–775 (2010).

[29] A. V. Shutov, S. Panhans, R. Kreißig, A phenomenological model of finite strain viscoplasticity with distortional hardening. Zeitschrift für Angewandte Mathematik und Mechanik, **91** 8, 653–680 (2011).

[30] I.-H. Son, J.-H. Lee, Y.-T. Im, Finite element investigation of equal channel angular extrusion with back pressure, Journal of Materials Processing Technology, **171**, 480–487 (2006).

[31] I. N. Vladimirov, M. P. Pietryga, S. Reese, Anisotropic finite elastoplasticity with nonlinear kinematic and isotropic hardening and application to sheet metal forming, International Journal of Plasticity, **26**, 659–687 (2010).

[32] K. Wegener, M. Schlegel, Suitability of yield functions for the approximation of subsequent yield surfaces. International Journal of Plasticity, **12**, 1151–1177 (1996).

[33] B. W. Williams, C. H. M. Simha, N. Abedrabbo, R. Mayer, M.J. Worswick, Effect of anisotropy, kinematic hardening, and strain-rate sensitivity on the predicted axial crush response of hydroformed aluminium alloy tubes, International Journal of Impact Engineering, **37**, 652–661 (2010).

[34] C. Xu, M. Furukawa, Z. Horita, T. G. Langdon, The evolution of homogeneity and grain refinement during equal-channel angular pressing: A model for grain refinement in ECAP, Materials Science and Engineering A 398, 66–76 (2005).